VNIVERSITAT DE VALÈNCIA

Facultad de Farmacia y Ciencias de la Alimentación

Departamento de Medicina Preventiva y Salud Pública, Ciencias de la Alimentación, Toxicología y Medicina Legal

Programa de Doctorado con Mención hacia la Excelencia en Ciencias de la Alimentación

Mecanismos de acción tóxica producidos por la toxina T-2 y sus metabolitos en modelos de células hepáticas humanas 2D y 3D y mecanismos de defensa antioxidantes

Mechanisms of toxic action of T-2 toxin and its metabolites in 2D and 3D human liver cell models and antioxidant defense mechanisms

Tesis Doctoral Internacional

Valencia, julio 2024

Presentada por: **Mercedes Taroncher Ruiz**

Dirigida por: **Dra. María José Ruiz Leal**

Dr. Yelko Rodríguez Carrasco

La **Dra. María José Ruiz Leal,** Catedrática del Área de Toxicología y el **Dr. Yelko Rodríguez Carrasco**, Profesor Titular del Área de Nutrición y Bromatología, del Departamento de Medicina Preventiva y Salud Pública, Ciencias de la Alimentación, Toxicología y Medicina Legal, de la Universitat de València

CERTIFICAN QUE:

La graduada en Farmacia **Dña. Mercedes Taroncher Ruiz** ha realizado bajo su dirección el trabajo que lleva por título "Mecanismos de acción tóxica producidos por la toxina T-2 y sus metabolitos en modelos de células hepáticas humanas 2D y 3D y mecanismos de defensa antioxidantes" / "Mechanisms of toxic action of T-2 toxin and its metabolites in 2D and 3D human liver cell models and antioxidant defense mechanisms" y autorizan su presentación para optar al título de Doctora con Mención Internacional por la Universitat de València.

Y para que así conste, expiden y firman el presente certificado

Burjassot (Valencia), julio 2024

Firmado por MARIA JOSE RUIZ LEAL - NIF:***0541** el día 18/07/2024 con un certificado emitido por ACCVCA-120

YELKO| RODRIGUEZ| CARRASCO

Firmado digitalmente por YELKO|RODRIGUEZ| CARRASCO
Fecha: 2024.07.18 15:55:53 +02'00'

Dra. María José Ruiz Leal

Dr. Yelko Rodríguez Carrasco

La presente tesis doctoral ha dado lugar a 9 artículos publicados en las siguientes revistas:

1. *T-2 toxin and its metabolites: characterization, cytotoxic mechanisms and adaptive cellular response in human hepatocarcinoma (HepG2) cells. Food and Chemical Toxicology (2020), 145, 111654.*
   Índice de impacto JRC (2020): 6,025 (9/93) Q1, D1. Toxicology

2. *Interactions between T-2 toxin and its metabolites in HepG2 cells and in silico approach. Food and Chemical Toxicology (2020), 148, 111942.*
   Índice de impacto JRC (2020): 6,025 (9/93) Q1, D1. Toxicology

3. *Identification of biotransformation products of T-2 toxin in HepG2 cells using LC-Q-TOF MS. Foods (2024), 13 (10) 1501.*
   Índice de impacto JRC (2024): 4,7 (38/173) Q1. Food Science and Technology

4. *Stressful effects of T-2 metabolites and defense capability of HepG2 cells. Toxins (2022), 14 (12), 841.*
   Índice de impacto JRC (2022): 4,5 (45/142) Q2. Toxicology

5. *Effect of Phenolic Extract from Red Beans (Phaseolus vulgaris L.) on T-2 Toxin-Induced Cytotoxicity in HepG2 Cells. Foods (2022), 11 (7), 1033.*
   Índice de impacto JRC (2022): 5,2 (34/142) Q1. Food Science and Technology

6. *Evaluation of cytotoxicity, analysis of metals and cumulative risk assessment in microalgae. Toxicology Mechanisms and Methods (2023), 33 (5), 388-400.*
   Índice de impacto JRC (2023): 2,8 (52/106) Q2. Toxicology

7. *Cytoprotective Effects of Fish Protein Hydrolysates against H_2O_2-Induced Oxidative Stress and Mycotoxins in Caco-2/TC7 Cells. Antioxidants (2021), 10 (6), 975.*
   Índice de impacto JRC (2021): 7,675 (50/297) Q1. Food Science and Technology

8. *Assessment of the genotoxic and mutagenic effects induced by T-2 mycotoxin in HepG2 cells. Toxicology (2024), 501, 153712.*
   Índice de impacto JRC (2024): 4,8 (50/354) Q1. Toxicology

9. *Using microfluidic hepatic spheroid cultures to assess liver toxicity of T-2 mycotoxin. Cells (2024), 13 (11) 900.*
   Índice de impacto JRC (2024): 5,1 (63/205) Q2. Cell Biology

La doctoranda agradece al Ministerio de Ciencia e Innovación:

La beca de investigación de carácter predoctoral del Programa de Formación del Personal Investigador (F.P.I.), convocatoria 2021 PRE2021-096941.

La subvención para favorecer la movilidad de estudiantes en estudios de Doctorado con Mención hacia la Excelencia en el curso 2022-2023. Ministerio de Ciencia e Innovación.

La presente Tesis Doctoral Internacional se engloba dentro de los siguientes proyectos:

- GVPROMETEO2018-126, Estrategias biotecnológicas para reducir el crecimiento de hongos toxigénicos en alimentos. Financiado por la Conselleria de Educación, Investigación, Cultura y Deporte.
- GV/2020/020, Evaluation of the combined toxicity of mycotoxins and metabolites by *in vitro* and *in silico* and its characterization for the development of exposure biomarkers in humans. Financiado por Conselleria d'Innovació, Universitats, Ciència i Societat Digital, Generalitat Valenciana.
- BBI-JU through the H2020, Project AQUABIOPROFIT "Aquaculture and agriculture biomass side stream proteins and bioactives for feed, fitness and health promoting nutritional supplements" (Grant number 790956).
- Exposición combinada a micotoxinas y plaguicidas. Evaluación del riesgo, seguridad y estrategias de mitigación (PID2020-115871RB-I00, MCIN/AEI/10.13039/ 501100011033).

Ha contado con la participación y el apoyo de:

- Red Iberoamericana de Investigación de Valorización de Residuos y Subproductos de Origen Alimentario (VALORAL), auspiciada por la Asociación Universitaria Iberoamericana de Postgrado (AUIP).
- Red Nacional sobre las micotoxinas y hongos micotoxigenicos y de sus procesos de descontaminación (MYCOFOOD). Ministerio de Economía y Competitividad (AGL2017-90787-RET).
- Servei Central de Suport a la Investigació Experimental (SCSIE), Universitat de València, València.

IUF gGmbH ♦ Postfach 10 30 45 ♦ D-40021 Düsseldorf

Ms. Mercedes Taroncher Ruiz

IUF
LEIBNIZ-INSTITUT FÜR UMWELT-MEDIZINISCHE FORSCHUNG

July 11th 2022

Certificate of Research Stay for Mercedes Taroncher Ruiz

April 1st – June 30th, 2022

Stay at the IUF – Leibniz Research Institute for Environmental Medicine Düsseldorf, Germany

It is my great pleasure to confirm that Ms. Mercedes Taroncher Ruiz stayed as a visiting research student in my laboratory for a total of 3 month (01.04.2022 – 30.06.2022).

During the internship, she was trained on our protocols to induce human pluripotent stem cells (hiPSCs) into the neuronal lineage. Specifically, she analyzed the effect of the mycotoxin T-2 in brain cells of different developmental stages in 2D and 3D. The aims of her research project at the IUF were:

1. Generation of neural progenitor cells (NPCs) from human pluripotent stem cells (hiPSCs) in 2D according to protocols already established in our lab.
2. Differentiation of hiPSC-derived neural progenitor cells into neural effector cells in 2D (monolayer cultures) and 3D (BrainSpheres).
3. Study of the developmentally neurotoxic effects of T-2 toxin on 2D and 3D hiNPC and 2D and 3D differentiation in neurons and astrocytes.
4. To Analyze the effect of T-2 toxin on primary human neural progenitor cells (NPCs) of fetal origin to include a later developmental timepoint.

It was a pleasure to host Ms. Taroncher Ruiz as a visiting research student for a research visit at the IUF-Leibniz Research Institute for Environmental Medicine, in my group of Alternative Method Development for Environmental Toxicity Testing, University of Dusseldorf, Germany.

Ms. Taroncher Ruiz handled the very extensive and sophisticated work program with excellence. Her behavior towards her supervisors and colleagues was always exemplary. Her friendliness and obligingness was highly appreciated among colleagues. She impressed with her personal integrity and a high degree of reliability and team spirit.

IUF gGmbH
Auf'm Hennekamp 50
D-40225 Düsseldorf

Telefon: +49 (0)211-3389-217/389

ellen.fritsche@iuf-duesseldorf.de

http://www.iuf-duesseldorf.de

I am grateful to her for her outstanding work and wish her all the best for her future professional and personal life and look very much forward to publishing the excellent data with her in the near future.

IUF
LEIBNIZ-INSTITUT FÜR UMWELT-MEDIZINISCHE FORSCHUNG

Yours Sincerely,

IUF – Leibniz-Institut für
Umweltmedizinische Forschung GmbH
Auf'm Hennekamp 50 - 40225 Düsseldorf
Telefon +49-(0)211-33 89-0

Prof. Ellen Fritsche, M.D.
IUF - Leibniz Research Institute for Environmental Medicine
Group of Alternative Method Development for Environmental Toxicity Testing
Auf'm Hennekamp 50
40225 Düsseldorf
Germany

MAYO CLINIC

Mayo Clinic
200 First Street SW
Rochester, Minnesota 55905

August 14, 2023

Dear Sir or Madam,

This document is to confirm that Ms. Mercedes Taroncher-Ruiz was physically present and performing research in my laboratory at Mayo Clinic in Rochester, MN, USA from May 8, 2023 until July 31, 2023. Please feel free to reach out in case of additional questions.

Sincerely,

Alexander Revzin, Ph.D.
Professor
Department of Physiology and Biomedical Engineering

"Nada en este mundo debe ser temido...solo entendido. Ahora es el momento de comprender más, para que podamos temer menos."

Marie Curie

Agradecimientos

La realización de esta tesis ha sido un camino largo, acompañado de trabajo duro. No obstante, esta experiencia está llena de sonrisas, abrazos, alegría, alguna lágrima y amistad. Por ello, hay personas a las que les debo agradecer haber contribuido a formar parte de todos esos recuerdos inolvidables.

En primer lugar, a mis directores de tesis, por haberme guiado durante esta etapa. A la Dra. María José Ruiz Leal, por ser un referente para mí en todos los aspectos. Por tu apoyo, paciencia y comprensión. Gracias por la dedicación de tu tiempo y por tus innumerables consejos. Gracias por no dejarme caer nunca, ni en los días más grises. Al Dr. Yelko Rodríguez Carrasco, por la ayuda que me has brindado, tu dedicación y disponibilidad infinita. Gracias por tu sonrisa y generosidad constante. Tu pasión por tu profesión es inspiradora.

Al Dr. Francisco José Barba Orellana, por tu amabilidad y confianza depositada en mí. Gracias por ofrecerme una oportunidad laboral cuando más lo necesitaba.

Gracias a todos los profesores y al personal de secretaría del departamento, y en especial a Carmen Escrivá, por tu disponibilidad y gentileza.

A Vero, por ser la primera que conocí en esta etapa de mi vida y hacer que nuestra amistad sea tan especial. Gracias por enseñarme y ayudarme siempre, eres un gran ejemplo a seguir.

A Noe, Ale y Fran, gracias por ayudarme y escucharme siempre con una sonrisa. Juntos hemos compartido muchas horas de trabajo, perdiendo la noción del tiempo, pero también hemos disfrutado mucho durante estos años. Es un placer tener amigos como vosotros.

A Luna, gracias por transmitir esa luz única que tienes y que te hace tan especial. Tu energía de vivir es contagiosa y me ha ayudado en muchos momentos a seguir adelante. Gracias por estar siempre ahí, sin importar el tiempo o la distancia. Siempre tendrás un lugar muy especial en mi corazón.

A mis compañeros del laboratorio Fojan, Tiago, Alfonso, Bea, Cristina, Massi, Felipe, Raquel, Albert, Carmen, Mara, Sergio, Paula y Juan Manuel. Por haber vivido juntos esta experiencia y apoyarme siempre. Conoceros ha sido un regalo.

A Manolo, Alan, Sophia, y el Dr. Revzin, mi estancia con vosotros fue una de las experiencias más bonitas de mi vida, gracias por contribuir a hacerla tan especial.

A mis amigas de toda la vida, Idoia, Vicky y Majo, por ayudarme a desconectar y hacerme reír siempre, especialmente cuando más lo he necesitado. Porque aunque no tenéis muy claro que hago con unas células, siempre me escucháis con entusiasmo.

A Jose Antonio y Aurora, por la ilusión y el apoyo que me han transmitido durante todos estos años por esta tesis, tanto como unos padres a una hija.

A Jorge, por ser una fuente inagotable de ánimos, paciencia y comprensión. Gracias por ser mi fan número 1, mi incondicional. Te quiero.

A mi familia, en especial a las mujeres de mi vida, mi madre, mi hermana y mi tía, por ser un ejemplo constante de motivación, perseverancia y éxito. Mamá, gracias por haber creído siempre en mí.

Todos habéis dejado una huella imborrable en mi corazón.

Mercedes

ÍNDICE GENERAL / GENERAL INDEX

Índice de tablas/ Table index

Índice de figuras/ Figure index

ABREVIATURAS

15-ADON: 15-acetil deoxinivalenol
2D: células cultivadas en monocapa
3-ADON: 3-acetil deoxinivalenol
3D: modelos celulares tridimensionales
5-Fu: 5-fluorouracilo
ABTS: ácido 2,2'-azino-bis(3-etilbenzotiazolina-6-sulfónico)
ADME/t: absorción, distribución, metabolismo, excreción y transformación
AESAN: Agencia Española de Seguridad Alimentaria y Nutrición
AF: aflatoxina
AFB1: aflatoxina B1
ALT: alanina aminotransferasa
AME: metilalternariol
AOH: alternariol
AST: aspartato aminotransferasa
ATA: aleukia tóxica alimentaria
ATCC: colección americana de cultivo tipo
a_w: actividad del agua
BEA: beauvericina
BEAS-2B: células epiteliales bronquiales humanas
BHA: hidroxianisol butilato
BHE: barrera hematoencefálica
BHT: hidroxitolueno butilato
BOILED-Egg: distribución estimada intestinal o cerebral
BRL: células de hígado de rata
BSEP: bomba de exportación de sales biliares
BSO: D-L-butionina-(S, R)-sulfoximina
C28/I2: línea celular de condrocitos humanos
Caco-2: células de adenocarcinoma colorrectal humano
CAT: catalasa
CCK-8: cell counting kit-8
CFU-GM: unidad formadora de colonias: granulocitos y macrófagos;
CHO-K1: células de ovario de hámster chino

CI: índice de combinación
CIT: citrinina
CONTAM: Contaminantes de la Cadena Alimentaria
COX: ciclooxigenasa
CYP450: citocromo P450
DAS: diacetoxiscirpenol
DCF: 2,7-diclorofluoresceína
$DCFH_2$: 2,7-diclorodihidrofluoresceína
$DCFH_2$-DA: 2,7-diclorodihidrofluoresceína diacetato
DES: desmina
DMSO: dimetilsulfóxido
DON: deoxinivalenol
DPPH: 2,2-difenil-1-picrilhidracilo
DR: disrupción celular
EA: alcaloide ergótico
ECHA: Agencia Europea de Productos Químicos
EFSA: Autoridad Europea de Seguridad Alimentaria
EGF: factor de crecimiento epidérmico
ELISA: análisis de enzimoinmunoanálisis de adsorción
EMA: colorante de ácido nucleico A
EN: eniatina
ENB1: eniatina B1
EURL ECVAM: Laboratorio de referencia de la UE para alternativas a los ensayos con animales
FAO: Organización para la Agricultura y la Alimentación
FB: fumonisina
FITC: fluoresceína isotiocianato
FUS: fusaproliferina
FUS-X: fusarenona X
GC-1: células espermatogoniales
ɣ-GT: gamma-glutamil transferasa
GH3: células de pituitaria de rata
GM-CSF: factor estimulador de colonias de macrófagos y granulocitos
GPx: glutatión peroxidasa

GSH: glutatión reducido o glutatión
GSSG: glutatión oxidado
GST: glutatión-*S*-transferasa
HaCaT: células de queratinocitos humanos
HepG2: células de hepatocarcinoma humano
HGF: factor de crecimiento hepático
HIA: absorción gastrointestinal humana
HK-2: células epiteliales del túbulo proximal renal humano
HOB: biodisponibilidad oral humana
HRMS: espectrometría de masas de alta resolución
Hs68: células de fibroblastos de piel humana
HT-2: toxina HT-2
HT-29: línea celular de adenocarcinoma de colon humano
IARC: Agencia Internacional para la Investigación del Cáncer
IC_{50}: concentración inhibitoria del 50%
IDT: ingesta diaria tolerable
IEC-18: células derivadas del íleon de rata
IGF: factor de crecimiento insulinoide
IL: interleuquina
IMR-32: células de neuroblastoma humano
iNOS: óxido nítrico sintasa inducible
IPEC: enterocitos porcinos intestinales aislados del yeyuno de un lechón neonatal no amamantado
JAK/STAT: vía de señalización de citoquinas Janus cinasa/transductor de señal y activador de transcripción
JECFA: Comité Mixto FAO/OMS de Expertos en Aditivos Alimentarios
JNK: quinasa N terminal c-Jun
JRC: centro común de investigación
KBD: enfermedad de Kashin-Beck
L-02: línea de hepatocito fetal humano
LB: nivel más bajo o Lower Bound level
LC: cromatografía líquida
LD_{50}: dosis letal 50
LDH: lactato deshidrogenasa

LRMS: espectrometría de masas de baja resolución
LSEC: células endoteliales sinusoidales del hígado
LX2: células Lieming Xu-2
MAPK: protein quinasas activadas por mitógenos
MAPK/ERK: protein quinasas activadas por mitógenos/quinasa regulada por señales extracelulares
MATE: transportador de expulsión de multidrogas y toxinas
MCP-1: proteína 1 quimioatrayente de monocitos
MN: micronúcleos
MoA: mecanismo de acción
MON: moniliformina
MRC-5: línea celular de pulmón fetal similar a fibroblastos
MS: espectrometría de masas
MTT: sal de tetrazolio (bromuro de 3-(4,5-dimetiltiazol-2-il)-2,5-difeniltetrazolio
NAC: N-acetilcisteína
Neo: neosolaniol
NF-κβ: factor nuclear potenciador de las cadenas ligeras kappa de las células B activadas
NIV: nivalenol
Nrf2: factor nuclear eritroide 2
OATP: polipéptido transportador de aniones orgánicos
OCDE: Organización para la Cooperación y el Desarrollo Económico
ORAC: capacidad de absorción de radicales de oxígeno
OTA: ocratoxina A
p38: subfamilia de proteína quinasas activada por mitógeno
PAT: patulina
pc: peso corporal
PC: policarbonato
PT: proteínas totales
PC12: células neuronales
PCR: reacción en cadena de la polimerasa
PDMS polidimetilsiloxano
PE: polietileno
PEG: polietilenglicol

PETG: tereftalato de polietilenglicol
pGCs: células primarias de la granulosa de ovario porcino
P-gp: glicoproteína p
PI: yoduro de propidio
PK15: células epiteliales de riñón porcino
PLGA: poliácido láctico-co-glicólico
PMMA: polimetilmetacrilato
PPB: unión a proteínas plasmáticas
PS: poliestireno
PUFA: ácidos grasos poliinsaturados
PVC: cloruro de polivinilo
Q-Orbitrap: cuadrupolo-Orbitrap
QSAR: relación cuantitativa estructura química-actividad
Q-TOF: cuadrupolo de tiempo de vuelo
QuEChERS: Rápido, Fácil, Barato, Eficaz, Robusto, y Seguro; técnica de extracción
RASFF: Sistema de Alerta Rápida para Alimentos y Piensos
RAW264.7: línea celular de macrófagos de tumor en un ratón macho inducido con el virus de la leucemia murina de Abelson
RN: rojo neutro
ROO˙: radical peroxilo
ROS: especies reactivas de oxígeno
RPTEC: células epiteliales primarias del túbulo proximal renal humano
RT-qPCR: PCR cuantitativa en tiempo real
S9: fracción microsomal de roedor
SH-SY5Y: células de neuroblastoma humano
SOD: superóxido dismutasa
STE: esterigmatocistina
T-2: toxina T-2
TBHQ: terbutil hidroquinona
TEAC: capacidad antioxidante de equivalente a trolox
TGF-β1: factor de crecimiento transformante beta-1
TLR4: receptor tipo toll 4
TM4: células de Sertoli

TNF-α: factor de necrosis tumoral alfa
UB: nivel más alto o Upper Bound level
UE: Unión Europea
ULA: placas de ultrabaja fijación
Vero: células epiteliales de riñón de mono verde africano
WST-8: [2-(2-metoxi-4-nitrofenil)-3-(4-nitrofen-il)-5-(2,4disulfofenil)-2H-tetrazolio
X: xenobiótico
ZEA: zearalenona
α-SMA: α-actina del músculo liso
α-ZEL: α-zearalenol
β-ZEL: β-zearalenol

RESUMEN

En la presente Tesis Doctoral se ha llevado a cabo la evaluación de los efectos tóxicos producidos por la toxina T-2 y sus metabolitos HT-2, neosolaniol (Neo), T2-triol y T2-tetraol mediante métodos alternativos a la experimentación animal, concretamente modelos de predicción *in silico* y modelos *in vitro* en células de hepatocarcinoma humano (HepG2). Debido a que la T-2 es la micotoxina más citotóxica de los tricotecenos, los resultados obtenidos pueden contribuir a un mayor conocimiento de sus mecanismos de acción toxicológica. De esta manera se puede realizar una evaluación del riesgo más precisa, y adoptar medidas adecuadas para prevenir o mitigar el daño producido tras su exposición.

Para ello, se evalúan las propiedades toxicológicas y de los procesos ADME de la T-2, HT-2, Neo, T2-triol y T2-tetraol utilizando los métodos de predicción *in silico* AdmetSAR y SwissAdme. Tras observarse potenciales efectos tóxicos, se procede a la evaluación de la toxicidad de la T-2 y sus metabolitos HT-2, Neo, T2-triol y T2-tetraol en un modelo *in vitro*, con células HepG2 de forma individual y combinada, mostrando valores de IC_{50} entre 59,6 y 2770 nM. A continuación, se identifica y cuantifica la T-2 y sus principales productos de biotransformación en el medio extra e intracelular tras 24 h de exposición de la T-2 a las células HepG2, observándose la completa metabolización de T-2 y la fluctuación de los niveles de sus metabolitos tanto en la fracción celular como en el medio de cultivo, siendo HT-2 el mayoritario. Debido a la coexistencia de la T-2 y sus metabolitos, se determina el tipo de interacción entre ellos, y se evidencian diferentes efectos dependiendo de la combinación de micotoxinas y las concentraciones en la mezcla. Así, se observa efectos antagónicos en las combinaciones de T-2 + T2-triol, T-2 + Neo, Neo + T2-triol, Neo + T2-tretraol y Neo + HT-2, y efectos antagónicos a concentraciones bajas y aditivos a altas

en las combinaciones de T-2 + HT-2, T-2 + T2-tetraol, T2-triol + HT-2, T2-triol + T2-tretraol y T2-tetraol + HT-2.

Como posible mecanismo de acción tóxica, a continuación se evalúa la capacidad de la T-2 y sus metabolitos de generar especies reactivas de oxígeno (ROS) y el papel protector de los sistemas de defensa celular y enzimático. Respecto a la defensa celular, se observa una disminución general del glutatión (GSH) tras la exposición a las micotoxinas. Sin embargo, se observa una gran variedad de resultados, dependiendo de la micotoxina y de la concentración evaluada, en cuanto a la defensa enzimática (glutatión peroxidasa, GPx; glutatión transferasa, GST), catalasa (CAT) y superóxido dismutasa (SOD) en las células HepG2. El papel del GSH y las enzimas relacionadas (GPx y GST) en la defensa de las células HepG2 expuestas a la T-2 y sus metabolitos se confirma con el incremento de su actividad a nivel celular tras la adición de N-acetil-cisteína (NAC) y la reducción tras la adición de D-L-butionina-(S, R)-sulfoximina (BSO). Por otra parte, también se evalúa el efecto citoprotector de sustancias bioactivas presentes en legumbres (judías rojas), microalgas (*Tetraselmis chuii* y *Phaeodactylum tricornutum*) e hidrolizados de pescado, todos ellos componentes de la dieta Mediterránea y debido a su alto contenido en antioxidantes.

Por otra parte, la exposición de las células HepG2 a la T-2 pone de manifiesto una alteración de la proliferación celular observada con la disrupción del ciclo celular, que podría estar relacionado con los procesos de muerte celular apoptosis y necrosis. Además, se observa daño al ADN tras la exposición a T-2, el cual se determinó a través de ensayos de genotoxicidad, concretamente el ensayo de micronúcleos y el ensayo del cometa. No obstante, la exposición a T-

2 no causó efecto mutagénico mediante el ensayo de la mutación genética reversa bacteriana.

Finalmente, se aplica un modelo celular tridimensional (3D) de esferoides de células hepáticas en dispositivos microfluídicos para simular el entorno biológico *in vivo* y obtener resultados más precisos y relevantes para el estudio de la citotoxicidad de la T-2 en modelos hepáticos. Se estudian y comparan dos modelos de cultivo celular 3D en dispositivos microfluídicos: esferoides de monocultivo con células HepG2 y esferoides de co-cultivo con células HepG2 y LX2. Con estos modelos, se evalúan los efectos citotóxicos de la T-2 mediante diferentes procesos, tales como viabilidad celular, albúmina, enzimas metabólicas hepáticas y citoquinas inflamatorias. Los resultados obtenidos con los esferoides de co-cultivo en dispositivos microfluídicos confirman que los efectos observados tras la exposición de la T-2 presentan un enfoque más realista de las condiciones hepáticas que los obtenidos con esferoides de monocultivo o en placas estándar.

En resumen, los resultados obtenidos indican que la T-2 y sus metabolitos podrían suponer un riesgo para la salud humana. Por lo que sería necesario ampliar los conocimientos de los mecanismos de toxicidad para poder prevenir efectos adversos de la T-2 y sus metabolitos y reducir la exposición a través de la dieta para proteger la salud del consumidor.

SUMMARY

In this Doctoral Thesis, the evaluation of the toxic effects produced by the T-2 toxin and its metabolites HT-2, neosolaniol (Neo), T2-triol and T2-tetraol has been carried out using alternative methods to animal testing. Specifically, *in silico* predictive models and *in vitro* models using human hepatocellular carcinoma (HepG2) cells. Since T-2 is the most cytotoxic mycotoxin of the trichothecenes, the results obtained may contribute to a better understanding of its toxicological mechanisms of action. This will allow a more accurate risk assessment to be made and appropriate measures to be taken to prevent or mitigate harm following exposure.

For this purpose, the toxicological properties and ADME processes of T-2, HT-2, Neo, T2-triol and T2-tetraol were evaluated using the *in silico* predictive methods AdmetSAR and SwissAdme. After potential toxic effects were observed, the toxicity of T-2 and its metabolites HT-2, Neo, T2-triol and T2-tetraol was evaluated in an *in vitro* model using HepG2 cells individually and in combination. IC_{50} values ranging from 59.6 to 2770 nM were obtained. Next, T-2 and its main biotransformation products were identified and quantified in the extra- and intracellular medium after 24 h of T-2 exposure to HepG2 cells, showing complete metabolization of T-2 fluctuating levels of its metabolites both in the cellular fraction and in the culture medium, with HT-2 being the major one. Due to the coexistence of T-2 and its metabolites, the type of interaction between them was determined and different effects were found depending on the combination of mycotoxins and the concentrations in the mixture. Thus, antagonistic effects are observed for combinations of T-2 + T2-triol, T-2 + Neo, Neo + T2-triol, Neo + T2-tretraol and Neo + HT-2, and both antagonistic effects at low and additive effects at high concentrations for

combinations of T-2 + HT-2, T-2 + T2-tetraol, T2-triol + HT-2, T2-triol + T2-tretraol and T2-tetraol + HT-2.

As a possible mechanism of toxicological action, the ability of T-2 and its metabolites to generate reactive oxygen species (ROS) and the protective role of cellular and enzymatic defense systems were evaluated. In terms of cellular defense, a general decrease in glutathione (GSH) was observed after exposure to mycotoxins. However, depending on the mycotoxin and the concentration tested, a wide range of results were observed in terms of enzymatic defense (glutathione peroxidase, GPx; glutathione transferase, GST), catalase (CAT) and superoxide dismutase (SOD) in HepG2 cells. The role of GSH and related enzymes (GPx and GST) in the defense of HepG2 cells exposed to T-2 and its metabolites was confirmed by the increase in their activity at the cellular level after the addition of N-acetyl-cysteine (NAC) and the decrease after the addition of D-L-buthionine-(S, R)-sulfoximine (BSO). The cytoprotective effect of bioactive substances present in legumes (red beans), microalgae (*Tetraselmis chuii* and *Phaeodactylum tricornutum*) and fish hydrolysates, all of which are components of the Mediterranean diet and are known their high antioxidant content, was also evaluated.

Moreover, exposure of HepG2 cells to T-2 revealed an alteration in cell proliferation with cell cycle disruption, which could be related to the processes of cell death, apoptosis and necrosis. In addition, DNA damage was observed after T-2 exposure as determined by genotoxicity assays, namely the micronucleus assay and the comet assay. However, exposure to T-2 did not induce mutagenic effects using the bacterial reverse gene mutation assay.

Finally, a three-dimensional (3D) cellular model of liver cell spheroids was used in microfluidic devices to simulate the *in vivo* biological environment and to obtain more accurate and relevant results for the study of T-2 cytotoxicity in liver models. Two 3D cell culture models were investigated and compared in microfluidic devices: monoculture spheroids with HepG2 cells and co-culture spheroids with HepG2 and LX2 cells. The models were used to assess the cytotoxic effects of T-2 by different measures, such as cell viability, albumin, hepatic metabolic enzymes and inflammatory cytokines. The results obtained with co-culture spheroids in microfluidic devices confirmed that the effects observed after T-2 exposure represent a more realistic approach to liver conditions than those obtained with monoculture spheroids or in standard plates.

In conclusion, the results obtained indicate that T-2 and its metabolites could represent a risk to human health. Therefore, further knowledge of the mechanisms of toxicity would be necessary to prevent adverse effects of T-2 and its metabolites and to reduce dietary exposure in order to protect consumer health.

1. Introducción

Introduction

1. INTRODUCCIÓN

1.1. Micotoxinas

Las micotoxinas son metabolitos secundarios de bajo peso molecular producidos por hongos filamentosos. Las especies de los géneros *Aspergillus, Penicillium, Alternaria, Claviceps y Fusarium* producen una gran variedad de micotoxinas que pueden contaminar alimentos y piensos en todo el mundo, por lo que suponen un peligro para la salud humana y animal (Narváez et al., 2022).

La exposición a las micotoxinas es prácticamente inevitable debido a su ubicuidad, origen natural o producción durante los procesos de transformación de los alimentos. Las micotoxinas se generan en condiciones óptimas de crecimiento del hongo que dependen de factores físicos: humedad y actividad del agua (a_w), temperatura óptima entre 25-30 ºC (aunque el rango puede variar de 5-45 ºC) y la integridad física del alimento o grano; químicos: tipo de alimento, pH entre 2,5 y 7,5 y disponibilidad de oxígeno; y biológicos: como la presencia de invertebrados en el alimento (Eagles et al., 2019). Dependiendo del género productor, las micotoxinas pueden generarse en el campo durante la pre-cosecha, cosecha de cereales o durante el secado o almacenamiento. La contaminación de los alimentos por micotoxinas es un problema importante en Europa como lo demuestra el "Sistema de Alerta Rápida para Alimentos y Piensos" (RASFF) de la Autoridad Europea de Seguridad Alimentaria (EFSA). En el último informe (2022), las micotoxinas se clasifican según la categoría de peligro en tercer lugar en los productos alimenticios, con 534 notificaciones (RASFF, 2022). Estas micotoxinas se encuentran con frecuencia en los cereales de todo el mundo, en particular en el trigo, la cebada, el maíz, la avena, el centeno y el arroz (Fatima et al., 2018). Las micotoxinas producen importantes pérdidas económicas en todo el mundo porque el valor del cultivo se reduce cuando se

detectan altos niveles de micotoxinas en el grano (Pereira et al., 2014). Según la Organización para la Agricultura y la Alimentación (FAO), se han identificado varios cientos de micotoxinas diferentes en productos alimenticios y piensos para animales (Alshannaq and Yu, 2017). La exposición a micotoxinas puede darse directamente al ingerir alimentos infectados, o indirectamente a partir de animales alimentados con piensos contaminados (EFSA, 2017a; EFSA 2014).

Los principales hongos micotoxigénicos son capaces de producir un grupo de micotoxinas muy amplio y diverso desde un punto de vista químico y estructural. Las distintas especies del género *Fusarium* pueden producir la zearalenona (ZEA), fumonisinas (FBs), tricotecenos y micotoxinas emergentes como la beauvericina (BEA), eniatinas (ENs), moniliformina (MON) y fusaproliferina (FUS). Las distintas especies del género *Aspergillus* son capaces de producir micotoxinas como las aflatoxinas (AFs), esterigmatocistina (STE) y ocratoxinas (OTA). Las especies del género *Penicillium* pueden producir OTA, patulina (PAT) y citrinina (CIT). El alternariol (AOH) y metilalternariol (AME) son las principales micotoxinas producidas por varias especies del género *Alternaria*; mientras que determinadas especies de hongos del género *Claviceps* producen alcaloides ergóticos (EAs).

1.1.1. Toxicidad

Las micotoxinas pueden provocar efectos adversos a corto, medio y largo plazo en los consumidores dependiendo de la exposición y la concentración en el alimento. Los efectos tóxicos pueden variar desde leves hasta potencialmente tóxicos. Algunas micotoxinas han sido clasificadas por la Agencia Internacional para la Investigación del Cáncer (IARC) como cancerígenos. Este es el caso de las AFs que han sido clasificadas como cancerígenas para el ser humano (Grupo

1) y las fumonisinas B1 (FB_1) y B2 (FB_2), la fusarina C y la OTA, que han sido clasificadas como posiblemente cancerígenas para el ser humano (Grupo 2B) (IARC, 2024). La IARC clasifica a los tricotecenos producidos por el género *Fusarium* spp., tales como el deoxinivalenol (DON) o la toxina T-2 (T-2), así como a la ZEA en el grupo 3: "no clasificables en cuanto a su carcinogenicidad para humanos" debido a que los datos disponibles no tienen evidencia suficiente en animales de experimentación o estudios *in vitro* (IARC, 2024).

La toxicidad de las micotoxinas puede verse aumentada cuando varias micotoxinas están presentes en la dieta simultáneamente o como consecuencia de los metabolitos generados o de sus productos de degradación (EFSA, 2020). Las micotoxinas causan importantes efectos tóxicos a nivel celular y orgánico; por lo tanto, es importante conocer bien la toxicidad que generan para establecer con la mayor exactitud posible los niveles máximos permitidos en alimentos y piensos. En la Tabla 1 se muestran los efectos tóxicos de las principales micotoxinas.

Tabla 1. Hongos micotoxigénicos y efectos tóxicos de las principales micotoxinas.

Micotoxina	Hongos productores	Efectos tóxicos	Referencias
AFs y STE	*Aspergillus flavus, A. parasiticus, A. versicolor, A. venezuelensis*	Hepatotoxicidad, inmunotoxicidad, neurotoxicidad, nefrotoxicidad, genotoxicidad, carcinogenicidad	Navale et al., 2021
T-2, HT-2	*Fusarium sporotichioides, F. poae, F. equiseti* y *F. acuminatum*	Hepatotoxicidad, neurotoxicidad, inmunotoxicidad, hematotoxicidad, daño dermatológico, gastrointestinal, genotoxicidad	EFSA, 2017a; Dai et al., 2019; Sheng et al., 2019
DON	*Fusarium graminearum, F. culmorum*	Neurotoxicidad, dermotoxicidad, inmunotoxicidad, daño gastrointestinal, respiratorio,	Savard et al., 2014; Yang et al., 2014
ENs y BEA	*Fusarium proliferatum, F. subglutinans, F. poae, F. tricinctum, F. avenaceum*	Citotoxicidad, inmunotoxicidad, genotoxicidad	Urbaniak et al., 2020
FBs	*Fusarium proliferatum, F. verticillioides, F. nygamai, F. fujikuroi, Alternaria alternata*	Neurotoxicidad, hepatotoxicidad, daño cardiovascular y pulmonar	Chiotta et al., 2020

(Tabla 1, continuación)

Micotoxina	Hongos productores	Efectos tóxicos	Referencias
OTA	*Penicillium verrucosum, Aspergillus auricomus, A. alliaceus, A. carbonarius, A. niger*	Nefrotoxicidad, neurotoxicidad, hepatotoxicidad, inmunotoxicidad, genotoxicidad, teratogenicidad	Navale et al., 2021; Wang et al., 2019
PAT	*Aspergillus clavatus, Penicillium expansum, P. griseofulvum*	Hepatotoxicidad, neurotoxicidad, inmunotoxicidad, toxicidad gastrointestinal, mutagenicidad, genotoxicidad	Li et al., 2019
ZEA	*Fusarium cerealis, F. graminearum, F. culmorum, F. equiseti, F. semitectum, F. verticilloides, F. semitectum*	Hepatotoxicidad, inmunotoxicidad, daños al sistema reproductor y endocrino, genotoxicidad, carcinogenicidad	Rogowska et al., 2019
CIT	*Penicillium citrinum, P. expansum, P. verrucosum* y algunas especies de *Monascus* y *Aspergillus*	Hepatotoxicidad, nefrotoxicidad, teratogenicidad, mutagenicidad	Gu et al., 2021
EAs	*Claviceps purpurea, C. Africana y Epichloë sp.*	Vasoconstricción, neurotoxicidad, inmunotoxicidad, hepatotoxicidad	(Schrenk et al., 2024)

AFs: aflatoxinas; BEA: beauvericina; CIT: citrinina; DON: deoxinivalenol; EAs: alcaloides ergóticos; ENs: eniatinas; FBs: fumonisinas; HT-2: toxina HT-2; OTA: ocratoxina A; PAT: patulina; STE: esterigmatocistina; T-2: toxina T-2; ZEA: Zearalenona.

1.1.2. Legislación

Con el objetivo de evitar riesgos para la salud, la Unión Europea (UE) fija los límites máximos de determinados contaminantes en los alimentos, incluidas las micotoxinas. Estos límites quedan recogidos en el Reglamento (UE) 2023/915 de la Comisión de 25 de abril de 2023, que está en vigor desde mayo de 2023, derogando así el Reglamento (CE) nº 1881/2006. Recientemente, la Comisión Europea publicó el Reglamento (UE) 2024/1038 de la Comisión, de 9 de abril de 2024, por el que se modifica el Reglamento (UE) 2023/915 en lo que respecta a los límites máximos de las toxinas T-2 y HT-2 en los alimentos y que entró en vigor el 1 de julio de 2024. En la Tabla 2 se muestra de forma resumida los límites máximos de las micotoxinas legisladas y las matrices alimentarias a las que se refiere.

Por otra parte, desde el 1 de abril de 2024 es de aplicación el Reglamento de Ejecución (UE) 2024/885 de la Comisión, de 14 de diciembre de 2023, por el que se establecen los métodos de muestreo y análisis para el control del contenido de micotoxinas en los alimentos, derogando así el Reglamento (CE) nº 401/2006.

Tabla 2. Límites máximos de micotoxinas fijados en el Reglamento (UE) 2023/915 de la Comisión.

Micotoxina		Intervalo de límites máximos (µg/kg)	Matrices alimentarias contempladas en el Reglamento
AFs	Suma de B1, B2, G1 y G2	0,1 - 15	Frutas desecadas, higos secos, cacahuetes y otras semillas
	M1	0,025 – 0,050	Leche y preparados para lactantes
OTA		0,5 - 80	Pistachos, uvas pasas, hierbas secas, café soluble y otras frutas desecadas
PAT		10 - 50	Manzana, zumo de manzana y otras bebidas fermentadas elaboradas con manzana
DON		200 - 1750	Granos de cereales, pan, galletas y pastas alimenticias
ZEA		20 - 400	Maíz, harina de maíz, aceite de maíz refinado, granos de cereales, pan y galletas
FBs		200 - 4000	Granos de maíz, harina de maíz y cereales de desayuno
CIT		100	Complementos alimenticios a base de arroz fermentado con levadura roja *Monascus purpureus*
EAs		20 - 400	Cebada, trigo, espelta, avena, centeno, gluten de trigo
Suma de T-2 y HT-2*		10 - 1250	Granos de cereales sin transformar, productos de molienda de cereales, cereales comercializados y productos de panadería

* los niveles indicados para la suma de las toxinas T-2 y HT-2 se refieren a los límites máximos fijados en el Reglamento (UE) 2024/1038. AFs: aflatoxinas; CIT: citrinina; DON: deoxinivalenol; EAs: alcaloides ergóticos; FBs: fumonisinas; OTA: ocratoxina A; PAT: patulina; ZEA: zearalenona.

A nivel internacional, el Comité Mixto FAO/OMS de Expertos en Aditivos Alimentarios (JECFA) regula la evaluación de los riesgos asociados a toxinas naturales, como las micotoxinas, en alimentos para garantizar la inocuidad alimentaria.

1.1.3. Tricotecenos

Los tricotecenos son micotoxinas producidas por hongos toxigénicos del género *Fusarium*. Los tricotecenos son compuestos sesquiterpenoides tetracíclicos caracterizados por un grupo 12,13-epoxi y un grupo carbonilo funcional en C-8. El grupo de los tricotecenos se subdivide en cuatro tipos (A-D) según los sustituyentes en sus anillos tetracíclicos (Figura 1). El tipo A consta de la T-2, la toxina HT-2 (HT-2), neosolaniol (Neo), T2-triol, T2-tetraol y diacetoxiscirpenol (DAS); el tipo B consta del DON, y sus derivados acetilados 3-acetil y 15-acetil DON (3-ADON y 15-ADON), nivalenol (NIV), tricotecino y fusarenona-X (FUS-X); el tipo C lo forma la crotoxina y el tipo D la roridina A, verrucarina A y satratoxina H. Sin embargo, los más comunes son los que pertenecen a los tipos A y B.

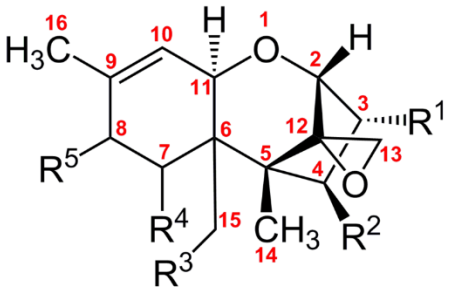

TIPO A

	R1	R2	R3	R4	R5
T-2	OH	OAc	OAc	H	$OCOCH_2CH(CH_2)_2$
HT-2	OH	OH	OH	H	OH
Neo	OH	OH	OAc	H	$OCOCH_2CH(CH_2)_2$
T2-tetraol	OH	OAc	OAc	H	H
DAS	OH	OAc	OAc	H	OH

TIPO B

	R1	R2	R3	R4	R5
DON	OH	H	OH	OH	= O
NIV	OH	OH	OH	OH	= O
Tricotecino	H	$OCOCH=CHCH_2$	H	H	= O
FUS-X	OH	OAc	OH	OH	= O

Figura 1. Estructura química de los tricotecenos más comunes.

1.1.3.1. Toxina T-2 y sus metabolitos

Entre los tricotecenos, se ha prestado considerable atención a la T-2, tricoteceno de tipo A, ya que es el compuesto que muestra mayor toxicidad en esta familia de micotoxinas (Dai et al., 2019; Fatima et al., 2018). La T-2 y su principal metabolito, la HT-2, son producidas por diversas especies del hongo Fusarium, como F. sporotichioides, F. poae, F. equiseti y F. acuminatum. Frecuentemente se reporta contaminación por T-2 y HT-2 en matrices alimentarias tales como trigo, maíz, cebada, avena y cereales procesados como

malta, cerveza, pan y piensos (Zhang et al., 2017). En un estudio de la EFSA, las concentraciones medias más altas de T-2 y HT-2 se midieron en granos de avena (LB = 127 μg/kg, UB = 128 μg/kg). Y, dentro de los cereales para el desayuno, en particular los copos de avena, tuvieron las concentraciones medias más altas de la suma de T-2 y HT-2 (LB = 13,9 μg/kg, UB = 16,5 μg/kg) (EFSA, 2017a). Debido a la alta toxicidad de la T-2, la EFSA estableció una ingesta diaria tolerable (IDT) para la T-2 y HT-2 de 0,02 μg/kg de peso corporal (pc) (EFSA, 2017b).

La T-2 también se ha detectado en el agua potable en zonas endémicas de China, como Qinghai, y en productos de la medicina tradicional china (Lei et al., 2016; Sun et al., 2012; Wang et al., 2012). Respecto al ganado, la Comisión Técnica de Contaminantes de la Cadena Alimentaria (Comisión CONTAM) de la EFSA concluyó que para los rumiantes, conejos y peces se considera poco probable que la exposición a la micotoxina plantee un riesgo. En el caso de los cerdos, las aves de corral, caballos y perros, la estimación de exposición a la T-2 indica que el riesgo de efectos nocivos es bajo. Sin embargo, los gatos son una de las especies más sensibles (EFSA, 2011).

La vía más común de exposición a la T-2 es a través del consumo de alimentos contaminados, aunque existen otras vías. Los agricultores pueden estar expuestos a través del contacto directo con el polvo de cereales y el heno contaminado. La T-2 es un factor predisponente en la enfermedad de Kashin-Beck (KBD), un tipo endémico crónico de osteocondropatía que se distribuyó principalmente desde el noreste hasta el suroeste de China (Deyu et al., 2018; Lei et al., 2016). Además, la T-2 se considera la principal causa de la enfermedad de aleukia tóxica alimentaria (ATA), un trastorno gastrointestinal que afectó a

soldados de la Segunda Guerra Mundial debido principalmente a la gran cantidad de T-2 ingerida a través de los cereales (Königs et al., 2009).

Tras la ingestión, la T-2 se metaboliza principalmente a HT-2 en el hígado a través de una reacción de desacetilación en la posición C-4 y, en concentraciones más bajas, en diversos metabolitos de fase I y II (EFSA, 2017b; Ling et al., 2020). Las principales vías metabólicas de T-2 son la hidrólisis, hidroxilación, deepoxilación y glucuronidación, aunque su principal biotransformación en el hígado es la hidrólisis (Wu et al., 2014; Yang et al., 2013). Algunas de las principales formas modificadas de la T-2 en mamíferos son la HT-2, Neo, T2-triol, T2-tetraol, 3-hidroxi-T-2 (3'-OH-T-2), 3-hidroxi-HT-2 (3'-OH-HT-2) y algunos productos C12,13-deepoxi (Wu et al., 2013, 2010; Figura 2). Todos ellos son metabolitos de fase I. La hidrólisis de T-2 conduce a una disminución de la actividad tóxica, por tanto, la toxicidad de los metabolitos es menor que la de T-2. No obstante, la toxicidad de HT-2 es similar a la de la T-2 y sus efectos no se pueden diferenciar (EFSA, 2017b; Ling et al., 2020). La T-2 y la HT-2 frecuentemente coexisten en altas concentraciones, sin embargo, sólo se han encontrado trazas de sus metabolitos en subproductos de avena, trigo y maíz (Chen et al., 2020; Ling et al., 2020). Tanto la T-2 como sus formas modificadas pueden aparecer en las mismas matrices alimentarias y pueden contribuir a la toxicidad general, por ello la Recomendación de la Comisión (2013/165/UE) sugiere un análisis completo que detecte la presencia simultánea de la T-2 y otras toxinas de Fusarium o sus propios metabolitos y la EFSA considera oportuno estudiar el efecto tóxico que genera su combinación (EFSA, 2017a; EFSA, 2017b).

Unos de los principales mecanismos de acción tóxica de la T-2 son la activación de las protein quinasas activadas por mitógenos (MAPK), apoptosis en varios tipos de células, necrosis, peroxidación lipídica, producción de especies reactivas de oxígeno e inhibición de la síntesis de proteínas, ADN y ARN, entre otros (Garreau De Loubresse et al., 2014; EFSA, 2017).

La amplia variación en la presencia de la T-2 de un año a otro y entre los diferentes alimentos analizados, ha abierto un nuevo debate sobre su importancia y la necesidad de una reevaluación de sus mecanismos de acción para una mejor comprensión de su toxicocinética, efectos adversos y riesgos toxicológicos.

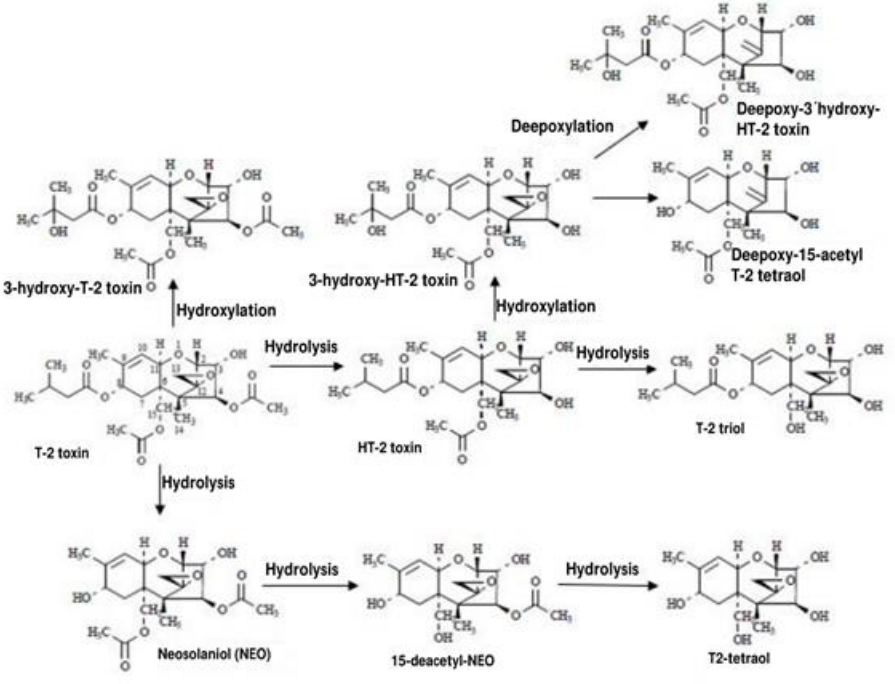

Figura 2. Principales vías metabólicas de biotransformación de fase I de T-2 en mamíferos.

1.2. Modelos alternativos a la experimentación *in vivo*

Aunque los modelos animales son los modelos de elección para el estudio de los efectos adversos que producen las sustancias tóxicas, éstos son complejos y pueden presentar problemas éticos (Kimura et al., 2018). Por ello, los cultivos celulares se han usado durante décadas sustituyendo a la experimentación animal con el fin de cumplir los principios básicos de las 3R: Reemplazo de los procedimientos o métodos que involucran el uso de animales; Reducción del número de animales utilizados para lograr el mismo objetivo; y Refinamiento de cualquier técnica o procedimiento desde el momento en que nace el animal hasta su muerte para minimizar su sufrimiento y mejorar su bienestar (Hampshire and Gilbert, 2019).

El Centro Común de Investigación (JRC) alberga la principal organización de la UE para la validación científica de métodos alternativos a los ensayos con animales: "EURL ECVAM", el Laboratorio de Referencia de la UE para alternativas a los ensayos con animales, establecido formalmente en 2011. El mandato y las actividades del EURL ECVAM (tal como se describen en la Directiva 2010/63/EC sobre la protección de los animales de experimentación) cubren todo el ciclo de vida de los métodos alternativos, es decir, desde el desarrollo y la validación hasta la aceptación regulatoria, el reconocimiento internacional y el uso científico adecuado. El EURL ECVAM participa activamente en la búsqueda de métodos que reemplacen, reduzcan o refinen (las "Tres R") el uso de animales de laboratorio. Los métodos desarrollados por los laboratorios de investigación se envían al EURL ECVAM, quien evalúa la solidez, confiabilidad y capacidad predictiva de los métodos alternativos (EURL ECVAM, 2023).

Por todo ello, el uso de experimentación alternativa in vitro, como los cultivos celulares, análisis computacional u organ-on-chip, ha sido ampliamente utilizado para investigaciones toxicológicas. Además, presentan un gran número de ventajas: se evitan las cuestiones éticas que conlleva el uso de animales, mayor control de las condiciones experimentales, mayor reproducibilidad y reducción de la variabilidad entre resultados, mayor rapidez de obtención de resultados y métodos más económicos (Díaz et al., 2020). Hoy en día, los modelos de predicción representan una estrategia fácil y rentable como alternativa a la experimentación animal. Los sistemas computacionales, simulaciones y modelos in silico proporcionan una base poderosa para abordar la predicción de interacciones biológicas, efectos tóxicos o bioactividad de moléculas, entre otros (Díaz et al., 2020; EFSA, 2014; EFSA, 2020).

Los chips son dispositivos microfluídicos de cultivo celular que contienen microcanales que pueden albergar células de diferentes linajes y orígenes, permitiéndoles interactuar compartiendo sus respectivos secretomas y características multicelulares, que en última instancia conforman una red celular viable. Este biosistema en un chip recrea la fisiología a nivel de órganos in vivo y la fisiopatología, simulando el tejido, estructuras y funciones a nivel de órganos in vitro. En lugar de animales, los chips se pueden utilizar en investigación fisiológica y ensayos de sustancias tóxicas (Ronaldson-Bouchard and Vunjak-Novakovic, 2018; Sontheimer-Phelps et al., 2019). Sin embargo, hay que tener en cuenta que aunque los modelos alternativos desempeñan un papel importante en la investigación, éstos no pueden sustituir completamente a los ensayos *in vivo.*

1.2.1. Modelos de predicción de la toxicocinética

Debido a las crecientes restricciones a nivel legislativo del uso de animales en experimentación, el enfoque alternativo basado en los métodos *in silico*, se considera una solución adecuada defendida por la Agencia Europea de Productos Químicos (ECHA) y la EFSA (EFSA, 2020). Según la opinión científica emitida por la EFSA, los métodos *in silico* han demostrado un poder predictivo cada vez mayor para realizar una correcta evaluación del riesgo, concretamente en lo referente al proceso ADME/t (absorción, distribución, metabolismo, excreción y toxicidad) predictivo (EFSA, 2014). Hasta la fecha, se han desarrollado diferentes herramientas *in silico* para predecir mecanismos de acción (MoA) y mecanismos por los cuales las sustancias químicas producen efectos adversos en diferentes órganos y tejidos tanto a nivel celular como molecular (Raies and Bajic, 2016).

Con los modelos *in silico*, los procesos ADME/t se pueden predecir utilizando diferentes softwares, algunos de ellos de acceso libre como los que se muestran a continuación:

- **AdmetSAR versión 2:** es una herramienta que utiliza las 5 reglas de Lipinski para posteriormente determinar parámetros como absorción gastrointestinal humana (HIA), biodisponibilidad oral humana (HOB), la unión a proteínas plasmáticas (PPB), sustratos de la glicoproteína p (P-gp) y penetración de la barrera hematoencefálica (BHE). También predice inhibidores de CYP450, transportadores farmacocinéticos como la P-gp, polipéptido transportador de aniones orgánicos (OATPs), transportador de expulsión de multidrogas y toxinas (MATE) y bomba de exportación de sales biliares (BSEP). Además, este modelo predice

efectos genotóxicos mediante el test de Ames y el ensayo de micronúcleos (Cheng et al., 2012; Yang et al., 2018).

- El software **SwissADME:** proporciona una gran variedad de parámetros similares al método AdmetSAR, y además incluye el método del BOILED-Egg (Brain Or Intestinal EstimateD), que genera una gráfica en 2D que discrimina entre moléculas con facilidad para la absorción gastrointestinal o facilidad para penetración a través de la BHE (Egan et al., 2000).
- **ProTox-III**: es un servidor web que predice la toxicidad oral de sustancias utilizando la estructura química de la molécula. Los resultados los expresa como la dosis letal 50 (LD_{50}), y clasifica las sustancias en función de su toxicidad prevista, otorgando valores de 1 a 5, siendo 1 las más tóxicas. También predice toxicidad específica como hepatotoxicidad o inmunotoxicidad, pero también la carcinogenicidad o mutagenicidad en general. Además, determina la presencia de receptores nucleares, alteración del potencial de membrana mitocondrial ($\Delta\Psi m$) o vías toxicológicas como la de respuesta al estrés del factor nuclear eritroide 2 (Nrf2).
- **DEREK Nexus®**: es un software que hace predicciones cualitativas de la toxicidad, basadas en reglas de conocimiento experto. Por ejemplo, usa toxicóforos (estructuras químicas responsables de las propiedades tóxicas de un compuesto) y está asociado con referencias bibliográficas y ejemplos de expertos toxicológicos. El resultado se expresa como el nivel de probabilidad de producir esa toxicidad en función de la similitud de la estructura química. Los resultados de la predicción van desde ciertos, plausibles, dudosos hasta inactivos (este último cuando la

estructura de la consulta no coincide con ninguna alerta estructural). Además, puede determinar entre otros efectos, la mutagenicidad y genotoxicidad de las sustancias.

- **VEGA QSAR©**: es un software similar al anterior, que predice la toxicidad de una sustancia mediante el uso de alertas estructurales proporcionadas por expertos. Es una plataforma que expresa resultados a nivel cuantitativo, usando relación cuantitativa estructura química-actividad (QSAR), y de forma cualitativa. Por ejemplo, establece si una sustancia es mutagénica, sospechosa de serlo o no lo es. Considera las propiedades fisicoquímicas fundamentales de los compuestos de la base de datos, así como sus características estructurales y MoA. En la resolución de la predicción, se evalúa también la similitud, precisión y concordancia de la sustancia a analizar con los dos o tres compuestos más similares en el conjunto de datos.
- **MycoCentral**: es una base de datos que alberga actualmente 904 micotoxinas y sus metabolitos. Contiene datos sobre la biosíntesis, vías metabólicas, fuentes de hongos productores, propiedades físico-químicas, los procesos ADME y predicción de toxicidad de cada micotoxina.
- **OpenFoodTox:** es una base de datos toxicológica que proporciona datos para todas las sustancias evaluadas por la EFSA. Se utiliza para la identificación y caracterización de peligros químicos, sobretodo de compuestos relacionados con alimentos, para evaluaciones ecológicas y de salud humana y animal. La base de datos se elaboró utilizando plantillas armonizadas de la Organización para la Cooperación y el Desarrollo Económico (OCDE).

- **Micotoxilico**: es una base de datos que contiene información sobre 4360 micotoxinas, clasificadas en 170 categorías en función de su estructura química. Por lo que concierne a su actividad, esta base de datos permite consultar el listado de aquellas micotoxinas clasificadas como mutágenas, carcinógenas o genotóxicas de acuerdo con las predicciones *in silico* llevadas a cabo con diferentes modelos QSAR y los datos disponibles en la literatura científica.
- **QSAR Toolbox:** es un software que combina varias herramientas de modelos *in silico* complementarias de QSAR para aumentar la predicción de la toxicidad. La QSAR Toolbox predice propiedades toxicológicas de sustancias químicas, donde se incluyen más de 900 micotoxinas. Informa sobre mutagenicidad y carcinogenicidad, y permite identificar las micotoxinas que deben priorizarse por su peligrosidad.

La predicción computacional de las micotoxinas es un campo recientemente en auge debido a su visión innovadora. Tolosa y colaboradores han evaluado la predicción de la hepatotoxicidad, carcinogenicidad, inmunotoxicidad y mutagenicidad de varias micotoxinas en salmón atlántico con la plataforma ProTox-III (Tolosa et al., 2020). De manera similar, Alonso-Jauregui y su equipo predijeron la mutagenicidad y el daño cromosómico de diversas micotoxinas (incluida la T-2), usando DEREK Nexus® y VEGA QSAR© (Alonso-Jauregui et al., 2021). Igualmente, Agahi y colaboradores y Pallarés y colaboradores utilizaron el software de SwissADME para predecir la toxicidad de la ZEA y sus metabolitos y ENB y sus metabolitos (Agahi et al., 2020; Pallarés et al., 2020). Otros autores, utilizaron el servidor AdmetSAR para predecir parámetros como la permeabilidad de la BHE, absorción intestinal, permeabilidad de las células Caco-2, sustrato/inhibidor de P-gp, sustrato/inhibidor del CYP45, el test de

Ames o la carcinogenicidad de antifúngicos que impidan el crecimiento de Fusarium graminearum (Joshi et al., 2021).

Habauzit y colaboradores crearon recientemente una base de datos (MycoCentral) para la cual hicieron uso de programas y softwares como PubChem, ChemSpider, PubChemPy, ChemSpiPy y estructuras SMILES (Habauzit et al., 2024). El "External Scientific Report" de la EFSA en 2022 describe el uso de metodologías de esta base datos, y las últimas actualizaciones (versión 2.0) de los datos de peligro de los compuestos químicos (Benfenati et al., 2022). Lemée y colaboradores recientemente han discutido como la herramienta QSAR Toolbox combina varios softwares como Vega QSAR, ADMETlab o LAZAR para evaluar la mutagenicidad de diversas micotoxinas (Lemée et al., 2023).

No obstante, aunque los enfoques predictivos no pueden reemplazar completamente los ensayos in vitro ni in vivo, pueden facilitar una toma de decisiones más temprana hasta que los resultados experimentales necesarios estén disponibles. Por este motivo, los modelos de predicción se consideran prometedores para mejorar la evaluación de riesgos de las micotoxinas.

1.2.2. Líneas celulares

Los efectos tóxicos de los xenobióticos han sido ampliamente estudiados en una gran variedad de líneas celulares, a diferentes tiempos de exposición y con diferentes concentraciones. Entre las líneas celulares más utilizadas en la última década se incluyen las células HepG2, Caco-2 o las LX2.

Células HepG2

Las células de hepatocarcinoma humano (HepG2; colección americana de cultivo tipo (ATCC): HB-8065) proceden de una línea hepática inmortalizada, que conserva el fenotipo hepático epitelial y sus funciones. Las células HepG2 han sido ampliamente utilizadas como sustitutos de estudios hepáticos y aceptadas para la evaluación de la toxicidad y el metabolismo inducidos por xenobióticos in vitro (Mulac et al., 2013). Dichas células se consideran apropiadas para la evaluación de la T-2, ya que son capaces de transformar la T-2 en sus metabolitos, y además, por ser el hígado el principal órgano metabolizador de T-2 y su principal órgano diana.

La bibliografía indica que las células HepG2 contienen enzimas de fase I como diversas isoenzimas del citocromo CYP450: CYP1A, CYP2C9, CYP2E1, CYP2D6, y de fase II como la glutatión-S-transferasa (Hewitt and Hewitt, 2004; Knasmüller et al., 2004). Además, Ye y sus colaboradores indican la gran relevancia de la isoenzima CYP1A1 en las células HepG2 (Ye et al., 2019), aunque la isoenzima más abundante en esta línea celular es la CYP3A4 (Lin et al., 2012).

Células Caco-2

La línea celular de adenocarcinoma colorrectal humano (Caco-2; ATCC: HTB-37) se usa como modelo validado internacionalmente para evaluar la absorción o permeabilidad intestinal de nutrientes (Yarnpakdee et al., 2015). Además, estas células son capaces de diferenciarse en cultivos in vitro a largo plazo, formando una monocapa continua con uniones estrechas que imitan la barrera intestinal (Yarnpakdee et al., 2015). Sin embargo, las células Caco-2 son heterogéneas y su rendimiento fisiológico depende en gran medida de las

condiciones de cultivo, lo que a menudo conduce a propiedades de transporte y permeabilidad variables. Para reducir la heterogeneidad de las células, se han aislado varios clones a partir de células Caco-2. El clon TC7 se caracteriza por su mayor capacidad para desarrollar uniones intracelulares, microvellosidades, transportadores de membrana típicos del intestino y enzimas metabólicas (Turco et al., 2011). Zucco y sus colaboradores, compararon las características de cuatro líneas celulares Caco-2 y concluyeron que el clon TC7 consistía en una población celular más homogénea, con funciones más representativas de los enterocitos del intestino delgado (Zucco et al., 2005). Muchos autores han utilizado esta línea celular para estudiar la permeabilidad y toxicidad de la T-2 (Lin et al., 2019; Martínez-Alonso et al., 2023; Tran et al., 2020).

Células LX2

En el hígado, aproximadamente el 20% de la masa celular son células no parenquimatosas hepáticas, como células sinusoidales, leucocitos y células estrelladas o Lieming Xu-2 (LX2). Las LX2 son células quiescentes en el hígado sano, con forma más redondeada y fenotipo fibrótico el cual se activa durante las lesiones, dando formas más alargadas fibroides (Friedman, 2008).

Para la caracterización de células LX2 se utilizan algunos marcadores como desmina (DES), que identifica su presencia o ausencia o el marcador α-actina del músculo liso (α-SMA), que indica la activación de dichas células. Se pueden analizar por diferentes técnicas como la reacción en cadena de la polimerasa cuantitativa en tiempo real (RT-qPCR) o por tinción de inmunofluorescencia (de Hoyos-Vega et al., 2023).

En los métodos in vitro se realizan co-cultivos de células LX2 (Sigma-Aldrich, SCC064) con otros tipos de células hepáticas, como las HepG2, para estabilizar

y mejorar la función hepática. Esta mejora puede atribuirse a que aumentan las interacciones yuxtacrinas y paracrinas entre los diferentes tipos de células (Kane et al., 2006; Khetani and Bhatia, 2008). Se ha demostrado que el co-cultivo de células endoteliales sinusoidales del hígado (LSEC), fibroblastos 3T3, células de Kupffer y LX2 mejora la secreción de albúmina de las células hepáticas en co-cultivo con células sembradas en placas estándar y en dispositivos microfluídicos (de Hoyos-Vega et al., 2023; Jang et al., 2019; Ukairo et al., 2013; Zhou et al., 2015).

1.2.3. Modelos 2D y 3D

Hay numerosos estudios que hacen uso de los modelos de cultivos celulares sembrando células en monocapa (2D) para realizar ensayos toxicológicos que determinen mecanismos de acción tóxica de diferentes compuestos químicos o tóxicos naturales, como las micotoxinas. Por ejemplo, las líneas celulares IPEC (enterocitos porcinos intestinales aislados del yeyuno de un lechón neonatal no amamantado), HepG2, C28/I2 (línea celular de condrocitos humanos), Caco-2 y HT-29 (línea celular de adenocarcinoma de colon humano) han sido utilizadas para evaluar los efectos citotóxicos de la micotoxina T-2 (Goossens et al., 2012; Jia et al., 2020; Martínez-Alonso et al., 2023; Mulac et al., 2013).

Sin embargo, en los cultivos 2D no se establecen interacciones apropiadas entre células ni entre las células y las matrices, y pueden no ser lo suficientemente estables para imitar la respuesta fisiológica frente a los compuestos tóxicos (Jensen and Teng, 2020). Por este motivo, en las últimas décadas se han descrito múltiples enfoques para promover la organización celular en modelos tridimensionales (3D), incluidos los esferoides y los organoides (de Hoyos-Vega et al., 2021; Mukundan et al., 2022). Por ejemplo, se ha demostrado que los

cultivos 3D de hepatocitos intercalados entre capas de gel (colágeno, heparina o matrigel) mejoran y estabilizan la función hepática (Foster et al., 2015; Vongchan et al., 2005).

Hay dos técnicas que se usan para generar esferoides:

- métodos con soporte (scaffold-based), que requieren material externo para que se agreguen las células, que imitan la matriz extracelular y el crecimiento celular;
- métodos sin soporte (scaffold free), que promueven la autoagregación celular sin añadir biomateriales y utilizando superficies de cultivo especializadas.

Las técnicas con soporte pueden diferenciarse según el material utilizado, que pueden ser soportes de polímeros sintéticos (como el polietilenglicol (PEG), poliácido láctico-co-glicólico (PLGA) y polidimetilsiloxano (PDMS)) y polímeros naturales (colágeno, alginatos, matrigel, gelatina, ácido hialurónico) y con estos métodos se usan frascos giratorios y/o microesferas portadoras. Entre las técnicas sin soporte para la generación de esferoides se pueden usar las placas de ultrabaja fijación (ULA), microplacas colgantes, gota colgante, biorreactores, microfluidos, recubrimiento líquido, placas de microondas o cultivo de pelets, entre otros, aprovechando factores como fuerzas magnéticas y gravitatorias (Zingales et al., 2023).

El empleo de esferoides de estructura regular y bien redondeados en ensayos in vitro garantiza una mayor reproducibilidad en los resultados. La caracterización de los esferoides se evalúa mediante los parámetros morfológicos como el área, perímetro, índice de esfericidad (circularidad) y solidez. La circularidad se utiliza para calcular la proximidad del esferoide a una geometría

esférica. Un valor próximo a 1 (100%) significa que el esferoide es un círculo (Amaral et al., 2017; Mora and Kwan, 2000). La circularidad del esferoide se calcula mediante la ecuación (1).

$$Circularidad = \frac{4\pi \cdot área}{perímetro^2} \qquad (1)$$

La solidez describe el grado en que una forma es convexa o cóncava. Un valor de 1 indica una forma completamente convexa. La solidez del esferoide se calcula mediante la ecuación (2).

$$Solidez = \frac{área}{área\ convexa} \qquad (2)$$

1.2.4. Nueva generación de modelos *in vitro*: Dispositivos microfluídicos

La microfluídica es una tecnología multidisciplinar que integra la nanotecnología, la biotecnología, la bioquímica, la física y la ingeniería (Damiati et al., 2018). Los dispositivos microfluídicos implementan los modelos de células y tejidos ya que representan modelos in vitro dinámicos y multiorgánicos, acercándose más al entorno biológico in vivo. Los dispositivos microfluídicos estan diseñados para cultivos celulares dinámicos interconectados, con entrada y salida de flujo para la perfusión de medios de cultivo celular. Estos dispositivos han ido ganando popularidad como plataformas de cultivo celular ya que ofrecen una serie de ventajas comparados con los modelos estándar y se pueden aplicar los métodos utilizados en placas convencionales con ligeras modificaciones. Entre las ventajas se incluye la utilización de cantidades menores de células, tejidos, de reactivos y de medio de cultivo; permite la integración de diferentes componentes del entorno celular (Park et al., 2019; Trujillo-de Santiago et al., 2019); permite un control preciso de la composición y la velocidad del flujo, la posibilidad de generar gradientes de oxígeno, hormonas o concentraciones de

compuestos a ensayar, y la oportunidad de realizar un muestreo durante la realización del ensayo (Bulutoglu et al., 2019; de Hoyos-Vega et al., 2021; McCarty et al., 2016). La capacidad de generar gradientes de oxígeno (colocando un canal aire-gas debajo de la membrana de PDMS), gradientes de nutrientes y de hormonas, permite que se obtengan niveles de actividad enzimática más fisiológicos que los obtenidos en las placas estándar (Kane et al., 2006; Lee et al., 2007).

Otra ventaja de estos dispositivos es la posibilidad de llevar a cabo una integración analítica en el dispositivo. Comúnmente, para evaluar la función de los cultivos en microfluídica se recolecta el medio y se analiza fuera del dispositivo. Este enfoque es útil, pero presenta la limitación de pérdida del analito en el proceso. Por ello, la integración analítica directamente en el dispositivo microfluídico elimina esta limitación. Con esta técnica se pueden determinar parámetros como la lactato deshidrogenasa (LDH), aspartato aminotransferasa (AST), alanina aminotransferasa (ALT), albúmina, factor de crecimiento hepático (HGF) y factor de crecimiento transformante beta-1 (TGF-β1) (Cedillo-Alcantar et al., 2019; Son et al., 2017).

Como se ha comentado previamente, los dispositivos microfluídicos permiten imitar algunas de las interconexiones fisiológicas o anatómicas entre órganos. Para ello, se siembran diferentes tipos de células (correspondientes a los órganos implicados) en diferentes dispositivos y, a continuación, se interconectan usando tubos y bombas peristálticas (Essaouiba et al., 2020); o cultivando diferentes células en diferentes cámaras de un único dispositivo y una posterior recirculación del medio de cultivo con una bomba peristáltica (Bauer et al., 2018).

Otra ventaja del uso de dispositivos microfluídicos, comparados con los modelos estándar, es la acumulación local de señales secretadas por las células, que actúan de manera autocrina y paracrina, para mejorar el fenotipo y la función de las células cultivadas. Esto se consigue porque las células se cultivan en condiciones estáticas y se confinan en pequeños volúmenes locales, recibiendo nutrientes de depósitos de medios de cultivo a través de canales de transporte. Como hay menos volumen en proporción que en las placas estándar, hay más exposición del tóxico al esferoide (Yazdi et al., 2015; Sabhachandani et al., 2016).

Por ejemplo, Choi y colaboradores determinaron una mejoría del fenotipo hepático en los dispositivos microfluídicos, debido a una mayor producción y acumulación de factores de crecimiento endógenos, como el HGF, factor de crecimiento epidérmico (EGF) y factor de crecimiento insulinoide (IGF). Además, observaron una mejora de la función de los esferoides hepáticos, medido con el aumento de la albúmina y la urea (Hoon Choi et al., 2020).

Los dispositivos microfluídicos pueden fabricarse mediante diversas metodologías y pueden estar formados por polímeros, vídrio, silicio, metales y cerámicas, entre otros materiales (Niculescu et al., 2021). Principalmente, se hacen de polímeros debido a su versatilidad, entre los que se incluyen el PDMS, polimetilmetacrilato (PMMA), policarbonato (PC), tereftalato de polietilenglicol (PETG), polietileno (PE), poliestireno (PS), cloruro de polivinilo (PVC), copolímero de estireno y siliconas (Becker and Locascio, 2002). Sin embargo, los más comúnmente utilizados son los de PDMS y PMMA, fabricados mediante litografía suave (Park et al., 2010). El PDMS se utiliza ampliamente debido a su excelente biocompatibilidad, presenta transparencia óptica, es fácil de moldear, tiene alta elasticidad, es barato y tiene una elevada permeabilidad al gas, siendo

esta última propiedad particularmente importante para el cultivo de células consumidoras de oxígeno, como pueden ser los hepatocitos (Nielsen et al., 2020; Pan et al., 2018).

Los esferoides se pueden formar en los dispositivos microfluídicos con micropocillos (cilíndricos o piramidales) utilizando los métodos descritos en el apartado 1.2.3. El uso de micropocillos es un método simple, que se basa en la sedimentación de células en espacios confinados (300 μm aproximadamente) que permite la formación de los esferoides (Chen et al., 2015). Los dispositivos microfluídicos con micropocillos son simples de fabricar y pueden sembrarse eficientemente con pocas células. En la Figura 3 se representa un dispositivo con micropocillos utilizado en esta tesis, y en la Figura 4 se muestra la formación de los esferoides en los micropocillos de dicho dispositivo.

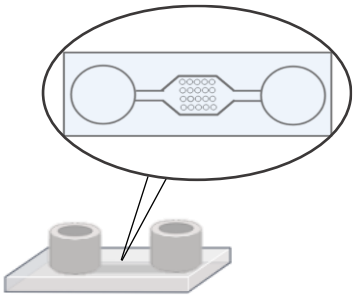

Figura 3: Esquema representativo de un tipo de dispositivo microfluídico con micropocillos fabricado con PDMS.

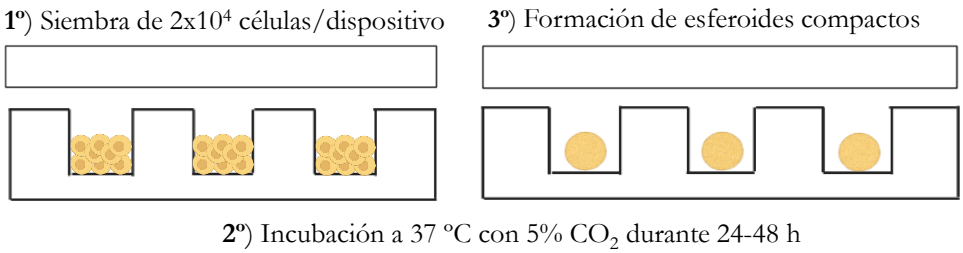

Figura 4: Esquema de la siembra de células y formación del esferoide en los dispositivos microfluídicos con micropocillos.

Este dispositivo ha sido usado previamente por otros autores. Entre ellos, Dadgar y colaboradores, quienes utilizaron dispositivos microfluídicos con micropocillos, multicámaras y microválvulas integradas, que permite la siembra en serie de esferoides en varias cámaras únicamente con 1x105 células por dispositivo (Dadgar et al., 2020). Por tanto, este tipo de plataformas también resultan adecuadas cuando el número de células es limitado.

Los dispositivos microfluídicos se han utilizado previamente para cultivar hepatocitos y otros tipos de células en modelos 3D y estudiar la toxicidad de una diversidad de compuestos (Adriani et al., 2016; Chen et al., 2019; Kang et al., 2020; Park et al., 2019). Sin embargo, hasta la fecha no se ha estudiado el potencial tóxico de la T-2 ni de otros tricotecenos en esferoides sembrados en estos dispositivos.

Por tanto, a pesar de los desafíos que supone la técnica microfluídica, ésta es una estrategia de cultivo muy prometedora, ya que pretende imitar la complejidad fisiológica de los modelos in vivo. Los dispositivos pueden utilizarse para el estudio de células de pacientes o tejido y pueden complementar modelos animales para hacer ensayos de toxicidad. Además, dado que pueden integrar varios tipos de tejidos orgánicos, por ejemplo, el hígado, el intestino y el

páncreas, se prevee un desarrollo continuo de sistemas multiorgánicos para evaluar los orígenes y la progresión de enfermedades hepáticas.

1.2.5. Ensayos toxicológicos *in vitro*

1.2.5.1. Viabilidad celular

El estudio *in vitro* de los efectos tóxicos de las sustancias se lleva a cabo mediante ensayos de citotoxicidad. La citotoxicidad es un mecanismo de toxicidad general, y un buen indicador de viabilidad celular. Estos ensayos permiten determinar de cada sustancia la concentración que inhibe el 50% de la viabilidad celular, es decir la IC50.

Algunos de los ensayos estandarizados para determinar la viabilidad celular son:

- Sal de tetrazolio (MTT): esta sal de color amarillo es soluble por lo que es captada por las células vivas y se convierte, debido a la acción de las enzimas succinato deshidrogenasa mitocondriales, en sal de formazán, que es insoluble y de tonalidad púrpura. El formazán queda retenido en las células vivas y puede liberarse al medio de cultivo extracelular mediante la acción del dimetilsulfóxido (DMSO). El color púrpura generado es proporcional a la cantidad de células viables.
- "Cell counting kit-8" (CCK-8): es un kit que realiza un ensayo colorimétrico para la determinación del número de células viables utilizando la sal de tetrazolio WST-8, similar a la del MTT. En este ensayo se utiliza una sal de tetrazolio, el [2-(2-metoxi-4-nitrofenil)-3-(4-nitrofenil)-5-(2,4-disulfofenil)-2H-tetrazolio, altamente soluble en agua, la cual se reduce por la deshidrogenasa a formazán en células vivas. La

cantidad de formazán está directamente relacionada con el número de células vivas.

- Contenido de Proteínas totales (PT): usa el azul de Comassie que se une a las proteínas celulares. El incremento de tonalidad azul será proporcional al número de células vivas.
- "Alamar Blue": la resazurina que tiene color azul atraviesa la membrana celular y se reduce a resofurina en las células vivas, que da una coloración roja fluorescente, la cual es directamente proporcional a la cantidad de células vivas.
- Rojo neutro (RN): es un colorante que penetra en los lisosomas y endosomas de células vivas. Por tanto, la concentración de RN será proporcional al número de células vivas.
- Lactato deshidrogenasa (LDH): la LDH es una enzima presente en el citosol de las células. Cuando las células sufren un daño que genera un aumento de permeabilidad en la membrana, se libera el contenido intracelular al exterior. Por tanto, el incremento de LDH en el medio de cultivo extracelular será proporcional al número de células muertas.
- Ensayo Live/Dead: es un kit con los fluorocromos calceína (de color verde) y homodímero de etidio (de color rojo). Tras la adición del fluorocromo se observa al microscopio de fluorescencia la intensidad de color verde, que es proporcional a la cantidad de células vivas, y la intensidad de color rojo, proporcional a las muertas.

En la Tabla 3 se describen algunos valores de IC50 de T-2 obtenidos con diferentes métodos de viabilidad en distintas líneas celulares.

Tabla 3. Valores de IC_{50} de T-2 obtenidos por diferentes ensayos de viabilidad celular.

Línea celular	Método	Tiempo de exposición (h)	IC_{50} (nM)	Referencia
HepG2	MTT	24	38± 0,12	Fernández-Blanco et al., 2018
		48	34± 7,00	
		72	44± 1,70	
	Alamar blue	24	8	Ivanova et al., 2006
TM4	CCK-8	24	8,10	Yang et al., 2021
PK15	MTT	24	1,17	Xiao et al., 2023
Células de Leydig	CCK-8	24	97,18	Sun et al., 2022
Células T jurkat	MTT	24	540	Wattanasuntorn et al., 2024
GH3	MTT	24	40	Fatima et al., 2018
	LDH		40	
CHO-K1	RN	24	52	Ruiz et al., 2011a
		48	50	
Vero	RN	24-72	4-5	Ruiz et al., 2011b
		24	4	Bouaziz et al., 2006
MRC-5	Alamar blue	24	3,41	Ivanova et al., 2006

CCK-8: cell counting kit-8; CHO-K1: células de ovario de hámster chino; GH3: células de pituitaria de rata; HepG2: células de hepatocarcinoma humano; IC_{50}: concentración que inhibe el 50% de la viabilidad celular; LDH: lactato deshidrogenasa; MRC-5: línea celular de pulmón fetal similar a fibroblastos; MTT: sal de tetrazolio; PK15: células epiteliales de riñón porcino; RN: rojo neutro; TM4: células de sertoli; Vero: células epiteliales de riñón de mono verde africano.

1.2.5.2 Interacción de micotoxinas

Las distintas especies de hongos micotoxigénicos pueden producir de forma simultánea diversas micotoxinas al colonizar los alimentos. De forma similar, una micotoxina determinada puede formarse por distintas especies de hongos. Por ello, la presencia de una o más micotoxinas de forma simultánea en los alimentos es muy frecuente. En base a lo anterior, el estudio del efecto tóxico de la mezcla de varias micotoxinas, así como la determinación del tipo de interacción que producen (sinérgicos, aditivos o antagónicos), son de gran importancia para realizar una adecuada evaluación del riesgo de la exposición a micotoxinas.

El efecto sinérgico consiste en la potenciación de los efectos tóxicos generados individualmente. El efecto aditivo cuando el efecto total de la combinación es igual a la suma de los efectos individuales; y el efecto antagónico ocurre cuando la combinación de las micotoxinas produce una toxicidad final menor de la que producirían las micotoxinas individualmente.

Uno de los métodos más utilizados para determinar el tipo de interacción entre micotoxinas, es el modelo matemático basado en el método de las isobolas o método de Chou (2006) y Chou y Talalay (1984). El método de las isobolas identifica el tipo de interacción entre diferentes micotoxinas mediante el índice de combinación (CI) según se muestra en la ecuación (3). El índice de combinación se utiliza para estudiar la influencia que tiene la presencia de dos o más sustancias. Los valores obtenidos mediante el CI indican si se produce un efecto sinérgico (CI< 1), aditivo (CI= 1) o antagónico (CI> 1). Este método demuestra que existe una relación entre la concentración de la sustancia de

estudio y el efecto producido, independientemente del número de sustancias en la mezcla y de sus mecanismos de acción.

$$^{n}(\mathrm{CI})_x = \sum_{J=1}^{n}(D)_j/(D_x)_j = \sum_{J=1}^{n}\frac{(D_x)_{1-n}\left\{[D]_j/\sum_{J=1}^{n}[D]\right\}}{(D_m)_j\left\{(f_{ax})_j/\left[1-(f_{ax})_j\right]\right\}^{1/mj}} \qquad (3)$$

Donde $^{n}(CI)_x$ es el índice de combinación para n compuestos (por ejemplo, micotoxinas) con un x% de inhibición (por ejemplo, inhibición de la proliferación); (Dx)1-n es la suma de la concentración de n compuestos que ejercen x% de inhibición en combinación; $\{[D]_j/\sum_{J=1}^{n}[D]\}$ es la proporcionalidad de la concentración de cada uno de los n compuestos que ejerce x% de inhibición en combinación; y (Dm)j {(fax)j/[1-(fax)j]}1/mj es la concentración de cada compuesto solo que ejerce x% de inhibición.

En la Tabla 4 se muestra el tipo de interacción obtenido con las combinaciones de algunas micotoxinas en cuya mezcla se incluye la T-2.

Tabla 4. Tipo de interacción producida tras la combinación de la T-2 con otras micotoxinas expuestas a diferentes tipos de células mediante el método de las isobolas.

Combinación de micotoxinas	Tipo de línea celular	Tipo de interacción	Referencia
BEA + T-2	CHO [illegible]	Sinergismo	Ruiz et al., 2011a
DON + T-2		Antagonismo	
T-2 + AFB_1	PK15	Sinergismo	Xiao et al., 2023
T-2+DON, T-2+PAT, T-2+DON+PAT	HepG2	Antagonismo y adición	Fernández-Blanco et al., 2018
T-2 + T2-triol	Células de Leydig	Sinergismo	Ling et al., 2020
T-2 + T2-tetraol			
HT-2 + Neo			Xu et al., 2022
T-2 + HT-2			
T-2 + Neo			
T-2 + BEA	IPEC	Antagonismo	Kolf-Clauw et al., 2013
T-2 + ENB_1		Adición	
T-2 + AFB_1	BEAS-2B	Sinergismo	McKean et al., 2006
	HepG2	Adición	
T-2 + NIV	Fibroblastos de ratón L929	Sinergismo	Tajima et al., 2002
DON + T-2	CFU-GM	Sinergismo y Adición	Ficheux et al., 2012
T-2 + ZEA		Adición	

AFB1: aflatoxina B1; BEA: beauvericina; BEAS-2B: células epiteliales bronquiales humanas; CFU-GM: unidad formadora de colonias: granulocitos y macrófagos; CHO-K1: células de ovario de hámster chino; DON: deoxinivalenol; ENB1: eniatina B1; HepG2: células de hepatocarcinoma humano; IPEC: enterocitos porcinos intestinales aislados del yeyuno de lechón neonatal no amamantado; Neo: neosolaniol; NIV: nivalenol; PAT: patulina; PK15: células epiteliales de riñón porcino; T-2: toxina T-2; ZEA: zearalenona.

1.2.5.3 Proliferación celular: Ciclo celular

La proliferación celular es un proceso biológico por el que tiene lugar una serie coordinada de acontecimientos para llevar a cabo el crecimiento celular, como la replicación del ADN, los orgánulos celulares y la división en dos células hijas. Este conjunto de eventos constituye el ciclo celular, y requiere diferentes fases (Figura 5) que se detallan a continuación:

- Fase G_0: es un estado de reposo en cuanto a la división, pero la célula sigue realizando sus funciones. Las células entran en esta fase normalmente cuando se ha detectado un daño en el ADN e intenta ser reparado para evitar replicarlo. Una vez en esta fase, las células pueden volver a entrar en el ciclo si el daño ha sido reparado y dividirse o seguir en la fase G_0 indefinidamente en estado quienescente.

- Fase G_1: es la primera fase de crecimiento, en la cual la célula se prepara para dividirse.

- Fase S: la célula sintetiza una copia completa del ADN en su núcleo, por tanto duplica su material genético. También duplica el centrosoma.

- Fase G_2: la célula condensa y organiza el material genético y se prepara para la división celular.

- Fase M: tiene lugar la división de una célula progenitora a dos células hijas.

El ciclo celular se controla mediante diferentes puntos de control clave, en los que se decide si la célula debería seguir dividiéndose o, por el contrario, retrasar la división o entrar en fase de reposo. Esto puede ocurrir al detectarse algún daño tanto interno como externo a la célula.

Se distinguen tres puntos de control clave:

- Entre la fase G_1 y la fase S: donde se identifica el daño al ADN. En este punto se puede inducir la parada del ciclo celular para intentar reparar el daño generado y no replicarlo y, si la lesión no puede ser reparada, conducir a apoptosis.
- En la fase G_2, donde se producen dos copias idénticas de ADN, para la posterior división celular en dos células idénticas. Si se detectan daños en el ADN, se evita la entrada en la fase M para no transmitirlos a las células hijas.
- En la fase M, donde se comprueba que los husos mitóticos o microtúbulos están unidos correctamente al cinetocoro. Si es así, las cromátidas se separan y acaban de completar la mitosis.

Estos puntos de control se usan normalmente como controles positivos en los ensayos *in vitro*. Así, el 5-Fluorouracilo (5-Fu) inhibe la timidilato sintasa, la cual bloquea la síntesis del nucleósido timidina, afectando así a la síntesis de ADN en la fase S. El etopósido inhibe la topoisomerasa II del ADN y ejerce sus efectos en el punto de control G_2/M.

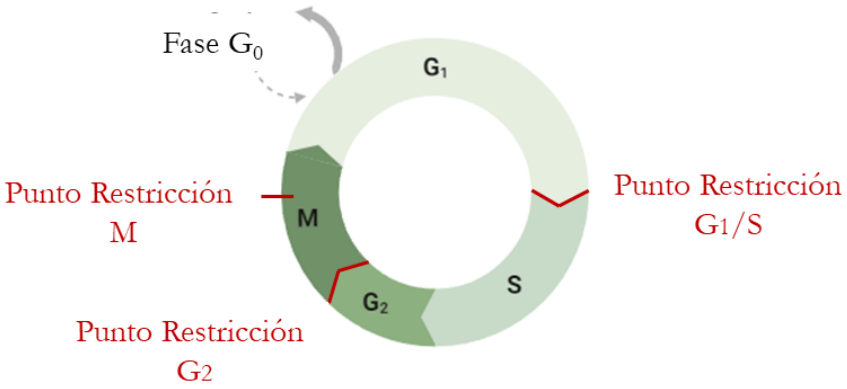

Figura 5. Representación de las fases del ciclo celular con los puntos de control.

La metodología más frecuente para analizar como una micotoxina afecta al ciclo celular es cuantificar el contenido de ADN en cada fase por citometría de flujo, clasificando a las células en las fases Sub G_0/G_1, G_0/G_1, S y G_2/M. Para ello, se utiliza el fluorocromo yoduro de propidio (PI) distinguiendo a las células en dichas fases. En la Tabla 5 se muestran algunos estudios que determinan el efecto de la T-2 y otros tricotecenos en las diferentes fases del ciclo celular en distintas líneas celulares.

Tabla 5. Alteración del ciclo celular tras la exposición de T-2 y otros tricotecenos en distintas líneas celulares.

Micotoxina	Línea celular	Parada del ciclo	Referencia
T-2	Células de Leydig	Fase G_1 y S	Sun et al., 2022
	GH3	Fase G_1	Fatima et al., 2018
	C28/I2	Fase G_0/G_1	Lei et al., 2017
	RPTEC	Sub G_1	Weidner et al., 2012
	pGCs	Fase G_0/G_1	Chen et al., 2024
	L-02	Fase G_0/G_1	Lei et al., 2017
	HK-2	Fase G_0/G_1	
	HaCaT	Fase G_0/G_1, S y G_2/M	Rachitha et al., 2023
	IMR-32	Fase G_1	Agrawal et al., 2015
DON	C28/I2	Fase G_2/M	Lei et al., 2017
	HK-2	Fase G_0/G_1	
	HepG2	Fase G_2/M	Yuan et al., 2018
	HepG2	Fase G_2	Domijan et al., 2023
HT-2	RPTEC	Sub G_1	Weidner et al., 2012
Neo	RPTEC	Sub G_1	

C28/I2: línea celular de condrocitos humanos; DON: deoxinivalenol; GH3: células de pituitaria de rata; HaCaT: células de queratinocitos humanos; HepG2: células de hepatocarcinoma humano; HK-2: células epiteliales del túbulo proximal renal humano; IMR-32: células de neuroblastoma humano; L-02: línea de hepatocitos fetales humanos; Neo: neosolaniol; pGCs: células primarias de la granulosa de ovario porcino; RPTEC: células epiteliales primarias del túbulo proximal renal humano; T-2: toxina T-2; HT-2: toxina HT-2.

1.2.5.4 Metodologías analíticas para la identificación y caracterización de micotoxinas y sus metabolitos

La contaminación de los alimentos por micotoxinas constituye un problema de salud mundial debido a los riesgos tóxicos asociados a la exposición humana a éstas a través de la dieta. En este sentido el establecimiento de límites reglamentarios ha impulsado el desarrollo y mejora de los procedimientos analíticos para la identificación y cuantificación de micotoxinas y sus

metabolitos, incluidas la T-2 y HT-2, en matrices alimentarias y biológicas (Meneely et al., 2023). Los procedimientos analíticos basados en técnicas cromatográficas o inmunoensayos normalmente requieren de una extracción con disolventes para liberar la micotoxina y/o sus metabolitos de la matriz a investigar, y de una posterior etapa de purificación del extracto. Como técnicas de extracción habituales se incluye la extracción en fase sólida, extracción con columnas de inmunoafinidad, extracción basada en QuEChERS (acrónimo de las palabras Quick, Easy, Cheap, Effective, Rudge, y Safe), extracción líquido-líquido o técnicas de microextracción, siendo éstas más comúnmente utilizadas con matrices biológicas por ser la cantidad de muestra a analizar el factor limitante (Iqbal, 2021).

Por otra parte, la determinación de los niveles de micotoxinas y/o sus metabolitos exige procedimientos analíticos suficientemente sensibles y selectivos para detectar estos componentes a niveles inferiores a los máximos permitidos. Las técnicas cromatográficas acopladas a la espectrometría de masas son las de elección para la identificación y cuantificación de micotoxinas. La cromatografía líquida (LC) es una de las técnicas de separación más ampliamente utilizada debido a su versatilidad y amplio campo de aplicación. Entre las ventajas más importantes que presenta la LC se encuentra la posibilidad de separar sustancias termolábiles, no volátiles, polares y apolares con aceptable resolución entre sustancias químicamente similares, de manera rápida y reproducible.

El alto poder de resolución aportado por las técnicas cromatográficas junto con la elevada selectividad y sensibilidad suministrada por el espectrómetro de masas (MS), convierte el acoplamiento de LC-MS en herramientas analíticas

altamente poderosas para la identificación y cuantificación de micotoxinas y sus metabolitos.

Para la distinción adecuada entre iones se ha ideado e introducido varios analizadores en plataformas de MS, pero, según el tipo analizador, las tecnologías de MS se pueden clasificar en MS de baja y alta resolución (LRMS y HRMS, respectivamente). Las principales diferencias entre los dos enfoques consisten en las mediciones de masa de un ion: la LRMS puede medir hasta dos cifras decimales, mientras que la HRMS puede llegar a cuatro o cinco, lo que tiene implicaciones cruciales en el procedimiento de identificación y cuantificación de analitos presentes en concentraciones muy bajas (del orden de pocos ng/g o inferior).

De acuerdo con el Reglamento de Ejecución (UE) 2024/885 de la Comisión que establece los métodos de muestreo y análisis para el control de los niveles de micotoxinas, la LRMS debe incluir un paso adicional de fragmentación del ion con el fin de generar dos iones productos característicos que deben ser monitorizados para tener una identificación y cuantificación confiable. Por el contrario, la HRMS no requiere de ese paso adicional, ya que un ion precursor puede identificarse adecuadamente a través de su medición exacta de masa, aunque la fragmentación también se puede aplicar en otro contexto para desarrollar enfoques no dirigidos.

En la tecnología de HRMS se utilizan principalmente dos analizadores: cuadrupolo-Orbitrap (Q-Orbitrap) y cuadrupolo - tiempo de vuelo (Q-TOF). El uso de la HRMS representa un paso adelante para el análisis de micotoxinas debido a varias ventajas en comparación con la LRMS. Ambos métodos proporcionan selectividad, precisión y sensibilidad similares cuando se trabaja

con enfoques dirigidos. No obstante, los espectrómetros HRMS pueden combinar dos modos de operación diferentes para adquirir la máxima información contenida en una muestra: escaneo completo (full scan) y fragmentación de todos los iones (all-ion fragmentation) (Medina et al., 2021). Esto significa que todos los iones precursores se registran y fragmentan, mientras que todos sus correspondientes iones producto también se registran simultáneamente. Esta poderosa característica permite el desarrollo de estrategias no dirigidas que no requieren de ningún estándar analítico para determinar la presencia de un determinado compuesto. Por lo general, este enfoque está respaldado por bases de datos que pueden hacer coincidir los datos espectrales con compuestos conocidos con una confianza determinada.

Esta característica de la HRMS se ha vuelto especialmente relevante para evaluar la exposición humana y animal a micotoxinas a través de la identificación de sus metabolitos en muestras biológicas. De hecho, los enfoques no dirigidos se están convirtiendo en una tendencia creciente para establecer perfiles metabólicos tentativos de micotoxinas (Arroyo-Manzanares et al., 2021).

Narváez y colaboradores evidenciaron la hidroxilación de la T-2 como la principal vía de biotransformación de esta micotoxina en humanos, mientras que las reacciones de conjugación parecieron ser residuales. Estos autores apuntan que dada la alta prevalencia del metabolito hidroxilado 3´-OH-T-2, éste podría representar una preocupación, teniendo en cuenta que no muestra una toxicidad significativamente menor, en comparación con su micotoxina original (Narváez et al., 2021).

1.2.5.5 Metabolismo celular

La biotransformación de la T-2 en mamíferos ocurre rápidamente. Se han descrito varios CYP450 involucrados en su metabolismo. Los principales metabolitos detectados corresponden a procesos de fase I y por tanto tienen una mayor polaridad y facilitan la excreción de dichos productos de biotransformación, reduciendo así la presencia en el organismo, y consecuentemente su toxicidad (Wu et al., 2020).

Los CYP450 son una superfamilia de enzimas monooxigenasas hemo ligadas a tiolato de cisteína, que catalizan la oxidación y el metabolismo de una gran cantidad de xenobióticos. Las isoenzimas CYP450 involucradas en el metabolismo de la T-2 difieren en función de la especie animal. Por ejemplo, las isoenzimas CYP3A22, CYP3A29 y CYP3A46 son comunes en cerdos, y las isoenzimas CYP1A5 y CYP3A37 en pollos, y todas ellas son capaces de catalizar la toxina T-2 y HT-2 para formar los metabolitos 3'-OH-T2 y 3'-OH-HT2. Además, la isoenzima CYP3A29 (en cerdos) y la carboxilesterasa (en humanos), hidroliza la T-2 a Neo. Otras enzimas que juegan un papel principal en el metabolismo de la T-2 en cerdos son las CYP3A39 y la CYP2C42, y en pollos la CYP1A4 y la CYP2C18. En cuanto a enzimas de fase II, en pollos tienen un papel fundamental la glutation transferasa (GST) y la gamma-glutamil transferasa (ɣ-GT), mientras que en ratas son importantes la aspartato aminotransferasa (AST), alanina aminotransferasa (ALT) y ɣ-GT. En humanos las que ejercen un papel más importante en la biotransformación de la T-2 son las isoenzimas CYP3A4 y CYP1A1 (Wu et al., 2014).

En la revisión de Bryla y colaboradores se habla de los principales metabolitos que se pueden identificar de la T-2 en las matrices alimentarias (Bryla et al.,

2018); mientras que Tran y colaboradores, revisan las rutas metabólicas de la T-2 y las posibles isoformas del CYP450 involucradas en su biotransformación en función de la especie animal (Tran et al., 2020).

1.2.5.6 Estrés oxidativo

Especies Reactivas de Oxígeno (ROS)

El estrés oxidativo es el resultado del desequilibrio entre las especies oxidantes y su sistema de defensa antioxidante, causado por un agente exógeno o endógeno, favoreciendo los procesos pro-oxidantes que dañan a las células y tejidos (Deyu et al., 2018).

Las especies reactivas de oxígeno (ROS) de manera endógena se pueden generar a través de la cadena de transporte de electrones mitocondrial o la fosforilación oxidativa. Entre las ROS se encuentran los radicales superperóxidos (O2-), el radical hidroxilo (HO.), el peróxido de hidrógeno (H2O2) y el radical peroxilo (ROO.) (Murphy et al., 2022). De manera exógena, las ROS pueden generarse por exposición a factores ambientales, como la radiación, o a contaminantes de origen alimentario, como los plaguicidas o las micotoxinas, entre otros. El estrés oxidativo puede intervenir produciendo cambios en el ciclo celular, en la reparación del ADN dañado, en la pérdida de la defensa enzimática, en la aparición de procesos inflamatorios, genotóxicos o mutagénicos, entre otros (Zhang et al., 2018).

La mayoría de métodos de cuantificación de las ROS intracelular se basan en el uso de sustancias no fluorescentes, que si sufren procesos oxidativos dan lugar a señales fluorescentes (Murphy et al., 2022). Uno de los más destacados para identificar las ROS intracelulares producido por las micotoxinas es la sonda 2,7-

diclorodihidrofluoresceína diacetato (DCFH2-DA) (Aranda et al., 2013). La DCFH2-DA difunde a través de la membrana celular, donde es desacetilada por las esterasas a un compuesto no fluorescente, la 2,7-diclorodihidrofluoresceína (DCFH2). En presencia de las ROS, la DCFH2 se oxida a 2,7-diclorofluoresceína (DCF), que es fluorescente. La intensidad de fluorescencia emitida es proporcional a la cantidad de ROS intracelulares. Se ha demostrado mediante este método que la exposición a la T-2 aumenta la producción de ROS intracelular de manera concentración-dependiente tras 24 h de exposición en diversas líneas celulares como las células de pituitaria de rata (GH3), en células epiteliales de riñón porcino (PK-15), en células de neuroblastoma-2a y en células espermatogoniales (GC-1) (Deyu et al., 2018; Fatima et al., 2018; Lee and Park, 2023; Li et al., 2021; Zhang et al., 2018).

Inflamación

Uno de los mecanismos de toxicidad que pueden generar las micotoxinas es la producción de factores inflamatorios. Normalmente las citoquinas proinflamatorias detectadas tras la exposición a micotoxinas son el factor de necrosis tumoral alfa (TNF-α), las interleuquinas (IL-1α, IL-1β, IL-6, IL-8, IL-10, IL-11) y las ciclooxigenasas (COX-2) (Bracarense et al., 2012; Huang et al., 2021; Liu et al., 2022; Sun et al., 2022). Otras citoquinas proinflamatorias no tan estudiadas son el factor estimulador de colonias de macrófagos y granulocitos (GM-CSF) y la proteína 1 quimioatrayente de monocitos (MCP-1). El GM-CSF es una citoquina proinflamatoria y reguladora asociada a la proliferación, diferenciación y quimiotaxis de las células inmunitarias, la regeneración epitelial y la fibrosis hepática (Karmacharya et al., 2022). Y la MCP-1 es una señal pleiotrópica que puede ser producida por células inmunitarias para promover la migración y la infiltración de otras células inmunitarias en el lugar lesionado

(Maher, 2001). Nagashima y colaboradores detectaron una inducción de la secreción de GM-CSF en cultivos hepáticos a consecuencia de una estimulación de las células por la micotoxina Rubratoxina B, sin embargo, no indujo la secreción de MCP-1 en células HepG2 (Nagashima et al., 2003).

La producción de citoquinas se puede analizar de numerosas maneras, como la técnica de la RT-qPCR, por citometría de flujo, con análisis de enzimoinmunoanálisis de adsorción (ELISA) o mediante paneles de inmunoensayos multiplex que permite cuantificar varias citoquinas en la misma muestra.

Algunas citoquinas proinflamatorias, como la IL-1β, la IL-6 y el factor nuclear potenciador de las cadenas ligeras kappa de las células B activadas (NF-ϰβ), están estrechamente relacionadas con el estrés oxidativo y con la inflamación porque se estimulan por las ROS que pueden generar las micotoxinas (Baker et al., 2021; Kamiya and Kim, 2021; Zingales et al., 2021). Algunos estudios han demostrado que la T-2 aumenta la expresión de citoquinas proinflamatorias y óxido nítrico sintasa inducible (iNOS). Esto potencia la síntesis de óxido nítrico (NO), y los niveles altos de NO conducen a un daño mitocondrial y desequilibrio redox, relacionado con la inducción de apoptosis en células GH3 (Li et al., 2008; Liu et al., 2017).

Liu y colaboradores demostraron que la T-2 induce la expresión de TNF-α en células de hígado de rata (BRL) (Liu et al., 2019). Dicha micotoxina produce también un aumento de expresión de las citoquinas TNF-α, IL-6 y IL-8 en células neuronales (PC12) (Pei et al., 2021). La T-2 aumenta la expresión de IL-6, IL-1β y TNF-α mediante la activación de la vía JAK/STAT, que está relacionado con la apoptosis (Wang et al., 2012). Otros autores indican que la T-

2 y el DON pueden aumentar los niveles de IL-1β, IL-6 y COX-2 y activar dos rutas de señalización inflamatoria, NF-ϰB y MAPK (incluye p38, ERK y JNK) las cuales desempeñan un papel fundamental en la regulación de expresión de genes inflamatorios (Pinton et al., 2010; Tian et al., 2012; Yi et al., 2018; Zhang et al., 2020). Un efecto similar se observó con el DON en hepatocitos porcinos y en co-cultivos de hepatocitos y células de Kupffer (Döll et al., 2009; Königs et al., 2008). Se ha demostrado que el DON aumenta la expresión de genes proinflamatorios (IL-6, IL-1β y TNF-α) mediante la activación de la vía JAK/STAT (Wang et al., 2012) y por inmunoestimulación de la vía TLR4/NF-ϰB (Liu et al., 2020).

Este mismo efecto se ha observado en micotoxinas producidas por otros géneros de hongos toxigénicos. Así, la AFB1 induce respuesta inflamatoria activando la vía del NF-ϰB (Chen et al., 2019) e induce daño inflamatorio hepático por la defosforilación de la COX-2 in vivo e in vitro (Zhang et al., 2019). Otros autores corroboran que la AFB1 y la OTA aumentan significativamente los niveles de citoquinas proinflamatorias, incluido el TNF-α e IL-6, mediante la activación de la vía NF-ϰB (Hou et al., 2018).

1.2.5.7 Sistemas de defensa antioxidante

Como se ha comentado previamente, en la célula pueden generarse ROS o radicales libres como consecuencia de procesos metabólicos. Sin embargo, hay compuestos antioxidantes que se encargan de contrarrestar estas moléculas con el fin de evitar un daño celular y contribuir a la homeostasis redox. Existen mecanismos antioxidantes endógenos y exógenos. En lo referente a los mecanismos endógenos se puede discernir entre enzimáticos (como la GST,

glutatión peroxidasa (GPx), catalasa (CAT) y superóxido dismutasa (SOD)) y los no enzimáticos como el glutatión (GSH) (Figura 6).

Los mecanismos de defensa antioxidante exógenos, se refiere a todos aquellos compuestos presentes en la dieta con poder antioxidante, como las vitaminas, los compuestos fenólicos, los hidrolizados de pescado, las legumbres o las microalgas, entre otros.

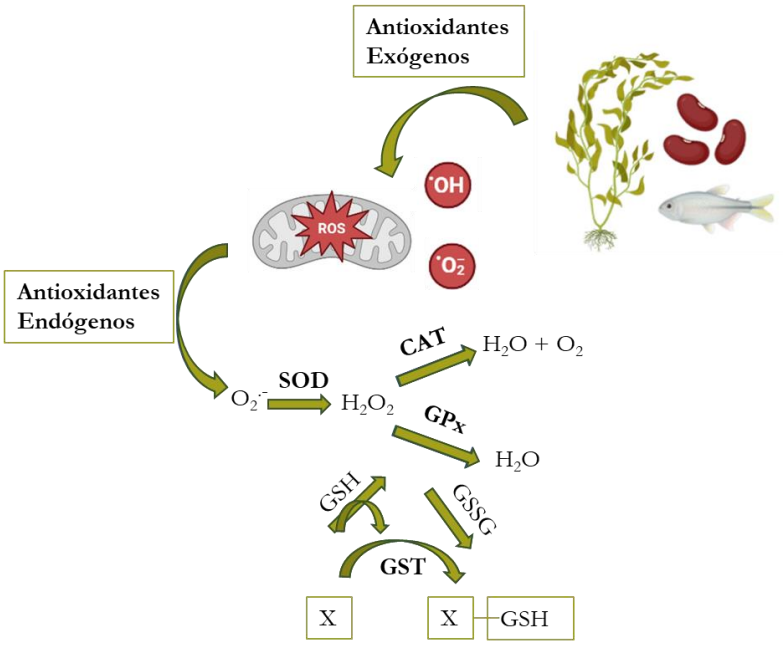

Figura 6: Esquema del sistema de defensa antioxidante endógeno y exógeno. X: xenobiótico; SOD: superóxido dismutasa; CAT: catalasa; GPx: glutatión peroxidasa; GST: Glutatión-S-transferasa; GSH: Glutatión reducido; GSSG: glutatión oxidado.

Sistemas de defensa antioxidante endógenos

El GSH es considerado uno de los antioxidantes endógenos más importantes. El GSH puede eliminar directamente los radicales libres o actuar como sustrato de la enzima GST (Figura 6) (Ali et al., 2020). El GSH es un tripéptido formado por el ácido glutámico (glutamato), glicina y cisteína. La función antioxidante la ejerce por la unión del grupo sulfhidrilo (-SH) de la cisteína al xenobiótico.

La N-acetilcisteína (NAC) es una fuente de grupos sulfhidrilo en las células, por tanto, es un precursor del GSH. Por otra parte, el D-L-butionina-(S, R)-sulfoximina (BSO) es un inhibidor de la ɤ-glutamilcisteína sintetasa, la enzima que desencadena la producción de GSH en el citosol. Por tanto, el BSO es un deplector del GSH (Zingales et al., 2020).

Respecto al sistema de defensa enzimático, la SOD convierte el anión superóxido (O_2^-) en oxígeno molecular (O_2) y H_2O_2. Este peróxido, puede ser eliminado por la GPx o la CAT (Ali et al., 2020). La GPx reduce los hidroperóxidos y el H_2O_2 a H_2O; y la CA cataliza el H_2O_2 a H_2O y O_2. Por otra parte, la GST responde al estrés oxidativo uniendo el GSH a compuestos oxidantes (Figura 6; Ali et al., 2020). Las principales técnicas de detección y cuantificación de las actividades enzimáticas son las espectrofotométricas.

En cuanto a las actividades enzimáticas en cultivos celulares expuestos a micotoxinas, hay una variedad de resultados (Tabla 6).

Tabla 6. Actividades enzimáticas en cultivos celulares expuestos a micotoxinas.

Micotoxina	Concentraciones (nM)	Línea celular	Sistema de defensa afectado	Referencias
ZEA, α-ZEL y β-ZEL	1560 – 12500	SH-SY5Y	↓ GSH, ↑GSSG, CAT y GST	Agahi et al., 2021
	6250 - 25000	HepG2	↓ GSH, CAT, ↑ SOD y GPx	Tatay et al., 2017
		CHO-K1	↓ GSH, CAT, ↑ SOD y GPx	Tatay et al., 2016
BEA	390 – 2500	SH-SY5Y	↑ GST	Agahi et al., 2021
	100 - 5000	CHO-K1	↑ SOD y CAT	Mallebrera et al., 2016
T-2	1000	Riñón porcino	↓ CAT	Li et al., 2021
	10 - 40	GH3	↓ GSH, ↑ SOD y GPx	Deyu et al., 2018
AOH	15000 - 60000	Caco-2	↓ GSH, GPx, GST	Fernández-Blanco et al., 2015

AOH: alternariol; BEA: beauvericina; Caco-2: células de adenocarcinoma colorrectal humano; CAT: catalasa; CHO-K1: células de ovario de hámster chino; GH3: células de pituitaria de rata; GPx: glutatión peroxidasa; GSH: glutatión reducido; GSSG: glutatión oxidado; GST: glutatión transferasa; HepG2: células de hepatocarcinoma humano; SH-SY5Y: células de neuroblastoma humano; SOD: superóxido dismutasa; T-2: toxina T-2; ZEA: zearalenona; α-ZEL: α-zearalenol; β-ZEL: β-zearalenol.

Por otra parte, Woelflingseder y colaboradores observaron que la adición previa de 1 mM de BSO en las células HepG2 y posterior tratamiento con DON, disminuyó la actividad del GSH y de las enzimas que requieren GSH (Woelflingseder et al., 2018). Se obtuvieron resultados similares con la micotoxina STE (micotoxina de Aspergillus) y los plaguicidas aldicarb, aldicarb sulfona, aldicarb sulfóxido y propoxur, tras la adición de BSO en las células SH-SY5Y y CHO-K1, respectivamente. Mientras que la adición de NAC aumentó su actividad (Maran et al., 2009; Zingales et al., 2020).

Sistemas de defensa antioxidante exógenos

Entre los antioxidantes sintéticos que se utilizan comúnmente para conservar productos alimenticios se incluyen el hidroxitolueno butilado (BHT), la terc-butilhidroquinona (TBHQ) y el hidroxianisol butilado (BHA), pero su uso es limitado debido a los posibles efectos tóxicos en los seres humanos (Kupfer et al., 2002). Hoy en día, existe una creciente demanda por parte de los consumidores del uso de antioxidantes naturales, tales como vitaminas, polifenoles, u otros compuestos, con el fin de disminuir el estrés oxidativo causado por la generación celular de ROS como consecuencia del metabolismo mitocondrial o de sustancias ingeridas en la dieta (como son las micotoxinas) (Granato et al., 2020; Wen et al., 2020). Entre los alimentos con propiedades antioxidantes se incluyen las legumbres, algunas microalgas y alimentos hidrolizados a partir de pescado.

Las legumbres, además de ser una gran fuente de proteína vegetal, fibra y ciertos micronutrientes, contienen una gran variedad de compuestos bioactivos y compuestos fenólicos (Rahate et al., 2021). Estos compuestos podrían desempeñar un papel bioactivo debido a su actividad antioxidante, pero también

antiinflamatoria, antimutagénica y antibacteriana. Dichas propiedades se han relacionado con la prevención de la obesidad, enfermedades cardiovasculares, neurodegenerativas y diabetes (Kimothi and Dhaliwal, 2020). Sin embargo, existe escasa información del efecto citoprotector de las legumbres frente a la exposición a micotoxinas. Vila-Donat y colaboradores demostraron el efecto citoprotector de un extracto obtenido de lentejas, por la presencia de la soyasaponina I, frente a la citotoxicidad producida por el AOH (micotoxina del género Alternaria) en células Caco-2 (Vila-Donat et al., 2015). De manera similar, Shia y colaboradores informaron del efecto citoprotector de los extractos de habas contra la apoptosis inducida por el H_2O_2 en células RAW264.7 (una línea celular de macrófagos que se estableció a partir de un tumor en un ratón macho inducido con el virus de la leucemia murina de Abelson) (Siah et al., 2012). Además, los extractos polifenólicos de la cáscara del cacahuete también mostraron efectos citoprotectores al eliminar radicales anión superóxido, así como la actividad de la SOD frente al estrés oxidativo inducido por la menadiona, un inductor de estrés oxidativo en células derivadas del íleon de rata (IEC-18) (Rossi et al., 2020).

Por otra parte, debido a la globalización se accede cada vez con mayor facilidad a una gran variedad de alimentos de diferente procedencia. Por ello, aunque en España no se consumen diariamente algas, éstas cada vez son más comunes en nuestra gastronomía. Además, las microalgas son una de las fuentes dietéticas más ricas en polifenoles y pigmentos que pueden utilizarse como alimento o complemento alimenticio (Postma et al., 2017, 2016). En este sentido, la EFSA y la Agencia Española de Seguridad Alimentaria y Nutrición (AESAN) en el ámbito del Reglamento (CE) nº 258/1997 sobre nuevos alimentos y nuevos ingredientes alimentarios, han autorizado la comercialización de la microalga

seca *Tetraselmis chuii* en complementos alimenticios en la UE. De manera similar, la microalga *Phaeodactylum tricornutum* y sus aceites derivados, también considerados un nuevo alimento, están permitidos para el consumo como complementos alimenticios en la UE (AESAN, 2017). Sin embargo, los compuestos antioxidantes, normalmente se encuentran en el citoplasma celular. Por ello, en ocasiones las células tienen que ser desintegradas por un proceso de disrupción celular (DR) para aprovechar al máximo su contenido.

Tetraselmis chuii es una microalga unicelular marina, verde, que pertenece a la familia *Chlorodendraceae*. *T. chuii* es ampliamente utilizada en acuicultura, por su alto contenido en ácidos grasos poliinsaturados (PUFAs), vitamina E, carotenoides, clorofilas y actividad antimicrobiana (Pérez-López et al., 2014). *Phaeodactylum triconutum* es una diatomea marina pinnada, unicelular, marrón, que pertenece a la familia *Phaeodactylaceae*. Sus células pueden sufrir transiciones morfológicas estimuladas por las condiciones ambientales y adaptar morfotipos fusiforme u ovalado. *P. triconutum* es rica en PUFAs y en el carotenoide fucoxantina, que es un pigmento con varias actividades biológicas (Gilbert-López et al., 2017). Khawli y colaboradores y Wang y colaboradores determinaron el efecto antioxidante de carotenoides y polifenoles de *P. triconutum*, a través del ensayo de capacidad de absorción de radicales de oxígeno (ORAC) y capacidad antioxidante de equivalente a trolox (TEAC) (Al Khawli et al., 2021; Wang et al., 2023). La actividad antioxidante de *T. chuii* a través del método del radical libre 2,2-difenil-1-picrilhidracilo (DPPH) y del ácido 2,2'-azino-bis(3-etilbenzotiazolina-6-sulfónico) (ABTS) fue confirmada por Moon & Cho y Widowati y colaboradores (Moon and Cho, 2023; Widowati et al., 2017).

Por lo que se refiere al pescado, es una gran fuente de proteínas y PUFAs en la dieta, y debido al crecimiento demográfico, su consumo aumenta anualmente. Sin embargo, entre un 20% y 80% del pescado se considera como desperdicio o subproducto por la industria pesquera, generando así un impacto en el medio ambiente (Caldeira et al., 2018). Estos residuos incluyen cabezas, vísceras, piel, espinas y escamas, que representan aproximadamente el 9-12%, 12-18%, 1-3%, 9-15% y 5% del peso total del pescado, respectivamente (Villamil et al., 2017). No obstante, estos residuos son ricos en proteínas, grasas, minerales y vitaminas, con uso potencial para el consumo humano cuando se manipula adecuadamente y de acuerdo con la legislación de calidad alimentaria. Por ejemplo, para utilizar estas proteínas de pescado, la producción de hidrolizados de proteínas de pescado es una opción prometedora, donde las proteínas se escinden en péptidos más pequeños y más solubles en agua en comparación con la proteína nativa, contribuyendo así a la sostenibilidad pesquera (Thuanthong et al., 2017). Por lo tanto, los hidrolizados de pescado se consideran productos de alto valor añadido que permiten aumentar los ingresos económicos de las industrias de transformación de los productos marinos. De esta manera, se reduce el impacto medioambiental de los residuos, contribuyendo a la sostenibilidad de la producción pesquera y la acuicultura. En los últimos años, el uso de este tipo de extractos se ha visto que mejora la funcionalidad de los productos alimenticios, en diferentes procesos como los organolépticos, sanitarios y tecnológicos (Poojary et al., 2016). Además, se ha observado que una de las causas por las que se utilizan es por su capacidad antioxidante.

En este sentido, Martí-Quijal y colaboradores estudiaron el efecto antioxidante de la cabeza, piel y vísceras de lubina (estómago, intestino y colon) mediante el ensayo del ORAC y TEAC (Martí-Quijal et al., 2023, 2020). Y

López-Medina y colaboradores evaluaron la capacidad antioxidante de hidrolizados de proteínas de músculo de calamar gigante, mediante el ensayo de DPPH y del ABTS (López-Medina et al., 2023).

Teniendo en cuenta los estudios recientes que demuestran los efectos beneficiosos de tomar antioxidantes en la dieta, resulta interesante conocer el efecto citoprotector de legumbres, microalgas e hidrolizados de pescado en células HepG2 y Caco-2 expuestas a T-2, ya que esto podría generar ideas sobre cómo complementar la dieta para contribuir a potenciar este efecto citoprotector. Además, podría considerarse una estrategia para mitigar o prevenir el daño producido por las micotoxinas que ingerimos a diario con la dieta.

1.2.5.8 Muerte celular: apoptosis y necrosis

Las células fisiológicamente intentan adaptarse a las condiciones externas y si sufren algún daño, intentan repararlo. Sin embargo, cuando ocurre un daño irreversible en la célula que la hace incapaz de llevar a cabo sus funciones se produce la muerte celular. La muerte celular puede ocurrir mediante dos procesos: apoptosis y necrosis.

La apoptosis es un proceso controlado genéticamente, que puede deberse a un estímulo fisiológico o patológico, en el cual la degradación del ADN es ordenada y no hay rotura de la membrana plasmática, por tanto, el contenido no se libera al exterior y únicamente afecta a células individuales, sin generar respuesta inflamatoria. La apoptosis se caracteriza por la externalización de los fosfolípidos de membrana, como la fosfatidilserina, los cuales son detectados y eliminados por las células fagocitarias, impidiendo así la inflamación (Sánchez and Arboleda, 2008). La apoptosis está controlada por el balance entre proteínas

proapoptóticas (como Bax, Bak y p53) y antiapoptóticas (como Bcl-2 y Bcl-x). El desequilibrio entre estas proteínas puede liberar el factor inductor de apoptosis al citosol activando la vía de las caspasas, que son unas enzimas que desencadenan una señal en cascada activando otras caspasas y son efectoras de la apoptosis, ya que inactivan proteínas estructurales, de señalización, reguladoras y del metabolismo de ácidos nucleicos (Logue and Martin, 2008). En lo referente a la necrosis, éste es un mecanismo de muerte celular no controlado, que se debe a un estímulo patológico donde la degradación del ADN es aleatoria e implica rotura de la membrana plasmática, por tanto, se libera el contenido intracelular al exterior, afectando así a las células vecinas y favoreciendo una respuesta inflamatoria.

La apoptosis y/o necrosis se puede evaluar por diferentes métodos, aunque la metodología de elección es la citometría de flujo con el método Annexina V-fluoresceína isotiocianato (FITC)/PI, que clasifica las poblaciones celulares en función de si son células sanas, necróticas, en apoptosis temprana o tardía (Figura 7). El FITC se une a la Anexina V, las células marcadas con FITC-Anexina V se encuentran en apoptosis. El yoduro de propidio (PI) es una molécula catiónica que no puede atravesar la membrana plasmática, por tanto sólo tiñe las células que han perdido la integridad de la membrana. Se intercala en los ácidos nucleicos de doble cadena de células necróticas o apoptóticas tardías, permitiendo identificarlas. La Anexina V es una proteína que tiene alta afinidad por la fosfatidilserina y no es capaz de penetrar las membranas, por tanto se une a las células que tienen expuesta la fosfatidilserina en el lado extracelular de la membrana plasmática. Teniendo esto en cuenta, como se muestra en la Figura 7, las células sanas serían Anexina V y PI negativas (Anexina V-FITC-/PI-), cuadrante inferior izquierdo), las células en apoptosis temprana

corresponderían con Anexina V-FITC+/PI- (cuadrante inferior derecho), las necróticas con Anexina V-FITC-/PI+ (cuadrante superior izquierdo) y las que están en apoptosis tardía serían Anexina V-FITC+/PI+ (cuadrante superior derecho) (Vermes et al., 1995).

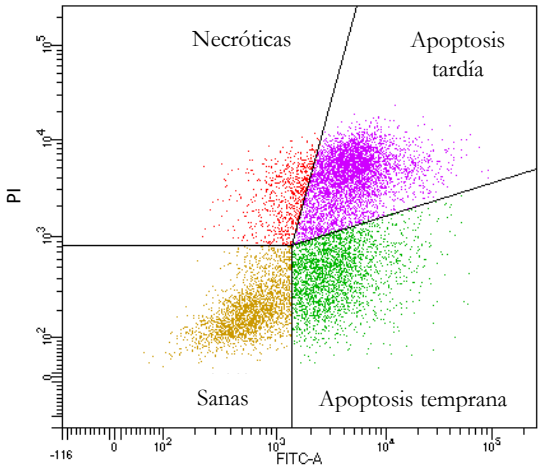

Figura 7. Distribución de poblaciones celulares obtenida mediante citometría de flujo. Células sanas (Anexina V-FITC$^-$/PI$^-$), células apoptóticas tempranas (Anexina V-FITC$^+$/PI$^-$), células apoptóticas tardías (Anexina V-FITC$^+$/PI$^+$) y células necróticas (Anexina V-FITC$^-$/PI$^+$).

La inducción de apoptosis por la T-2 ha sido confirmada por Lei y colaboradores en las células C28/I2, L-02 y HK-2 a la dosis de 0,02 nM de T-2 (Lei et al., 2017). De manera similar, Wu y colaboradores y Agrawal y sus coautores observaron un aumento de apoptosis temprana y tardía en las células L-02 y IMR-32 en un rango de 0,2 a 5 nM (Agrawal et al., 2015; Wu et al., 2019). Un ensayo reciente muestra como la T-2 a concentraciones de hasta 20 nM durante 24 h induce apoptosis en las células espermatogoniales GC-1 (Lee and

Park, 2023). También en ensayos *in vivo* se ha demostrado como la T-2 induce apoptosis en linfocitos de ratas, hipófisis de ratas y en células germinales de ratones macho, afectando su espermatogénesis (Guo et al., 2018; Rahman et al., 2021; Yang et al., 2019). Por tanto, la T-2 causa apoptosis en diferentes tipos de células, sin embargo, hay diferencias en función del tipo celular, tiempos de exposición de la micotoxina o sensibilidad de los ensayos aplicados, los cuales condicionan la respuesta.

1.2.5.9 Daño al ADN

Considerando que los mamíferos pueden estar continuamente expuestos a las micotoxinas a través de la dieta, resulta de gran interés el estudio de su potencial mutagénico y/o genotóxico. Según la EFSA, se recomienda el uso de una batería estándar de ensayos in vitro para las pruebas de genotoxicidad de contaminantes alimentarios (EFSA, 2011). Esta batería incluye pruebas para la detección de aberraciones cromosómicas, como la prueba de micronúcleos (MN) (TG OCDE 487) y el ensayo del cometa (TG OCDE 489), junto con un ensayo de mutación bacteriana para detectar mutaciones genéticas, como el test de Ames (OECD, 2020).

Mutaciones o aberraciones cromosómicas

Los fragmentos microscópicos de cromatina desprendidos del núcleo celular principal, llamados MN, son indicativos de rotura cromosómica o fallo del huso mitótico. La exposición a sustancias genotóxicas induce la formación de MN en las células en la interfase (Jakšić et al., 2012). Para detectarlos se usa la tinción EMA (colorante de ácido nucleico A), que atraviesa las membranas dañadas de células apoptóticas y necróticas y se une al ADN a través de fotoactivación. A continuación, una solución de lisis destruye la membrana citoplasmática con la

liberación de los MN, tanto de células vivas como muertas. Posteriormente se adiciona la tinción SYTOXTM green que se une a la cromatina de todas las células, quedando así diferente tinción en la cromatina de células sanas (únicamente teñidas con SYTOX green) y en las células muertas (teñidas con EMA y SYTOX green).

En la bibliografía disponible sobre la inducción de MN, sólo Somoskői y colaboradores estudiaron la respuesta genotóxica de la exposición a T-2 en blastocistos de embriones de ratón. Estos autores demostraron que a partir de 1,6 nM la T-2 aumenta la frecuencia de MN tras 96 h de exposición (Somoskői et al., 2018; Somoskői et al., 2016). Otros autores estudiaron la generación de MN en otros tricotecenos y sus combinaciones con otras micotoxinas de Fusarium. Juan-García y colaboradores estudiaron la frecuencia de MN que producen el DON y sus metabolitos (3-ADON y 15-ADON), de manera individual y combinada en las células HepG2. Individualmente, 3 μM de 3-ADON indujo MN, mientras que se observó un aumento de MN en todas las combinaciones de dichas micotoxinas a las concentraciones más bajas ensayadas (0,6 μM de DON y 0,2 μM del 3-ADON y 15-ADON) tras 48 h de exposición (Juan-García et al., 2018). Dichos autores reportaron que la BEA, también indujo MN a la concentración de 1,25 μM en las células HepG2 tras 48 h de exposición (Juan-García et al., 2019). De manera similar, Zingales y colaboradores confirmaron la aparición de MN tras la exposición de 0,70 – 3,12 μM de STE durante 48 h en las células SH-SY5Y (Zingales et al., 2021).

El ensayo del cometa es un método sensible para evaluar el daño del ADN, el cual determina la rotura en la doble cadena de ADN midiendo la migración electroforética del ADN a pH alcalino (pH=13). Las células se lisan y liberan el

ADN por la acción de detergentes y sales. Durante la electroforesis, el ADN dañado migra a una velocidad diferente a la del resto del material del núcleo formando colas en las células, simulando la forma de los cometas. Los tres parámetros más característicos de este ensayo son el "tail DNA %" (relacionado con la frecuencia de rupturas y se analiza en función de la intensidad de la fluorescencia de la cola), "tail length" (establece el grado de daño y se analiza en función de la longitud de la cola formada) y "olive tail moment" (considera tanto la longitud del cometa como la intensidad de la tinción) (Afanasieva and Sivolob, 2018).

Mamur y colaboradores, determinaron que la ENA, aumenta la intensidad de la cola del cometa en linfocitos humanos tras 1 h de exposición a concentraciones entre 0,14 y 1,15 μM de ENA (Mamur et al., 2018); de igual modo que el ácido fusárico (micotoxina de Fusarium) a la concentración de 3,12 a 12,50 μg/mL) en los mismos linfocitos tras 1 h de exposición, aunque la longitud de la cola del cometa no se vio afectada (Mamur et al., 2020). De manera similar, Jaksic y colaboradores estudiaron el efecto de FB1 y FB2, (micotoxinas de *Fusarium*), en células A549 y no observaron cambios significativos en la longitud de la cola del cometa a la concentración de 10 y 100 μM y tiempo de exposición 24 h (Jakšić et al., 2018). Además, Janik-Karpinska y colaboradores recientemente determinaron un aumento del daño al ADN de manera tiempo y concentración dependiente, debido a la acumulación de ADN encontrado en la cola del cometa tras la adición de 0,1 a 10 μM de T-2 durante 24 y 48 h de incubación en la línea celular Hs68 (fibroblastos de piel humana) (Janik-Karpinska et al., 2023). De manera similar, Zingales y colaboradores confirmaron el aumento de "tail DNA %", longitud de la cola y "olive tail moment" de manera concentración-dependiente tras la exposición de 0,70 a 3,12

μM de STE en las células SH-SY5Y durante 24 h (Zingales et al., 2021). Tatay y colaboradores evidenciaron el aumento del % de ADN en la cola del cometa tras la exposición de 0 a 25 μM de ZEA, α-ZEL y β-ZEL durante 24 h de incubación en HepG2, especialmente en los metabolitos (Tatay et al., 2017). También Mallebrera y colaboradores mostraron un aumento en el ADN de la cola tras exponer 1 μM 24 h de BEA en las células CHO-K1 (Mallebrera et al., 2016).

Mutaciones genéticas puntuales reversibles

Las lesiones tardías del ADN, como mutaciones, son el resultado de un equilibrio entre el daño inducido y la reparación del ADN. El ensayo de mutación genética reversa bacteriana es una prueba de mutagenicidad que permite la detección de mutaciones puntuales utilizando diferentes cepas bacterianas (5 en total) de *Salmonella typhimurium* y/o *Escherichia coli* (Mortelmans and Zeiger, 2000). Son cepas que tienen mutaciones en la ruta de biosíntesis de histidina, en el caso de *S. typhimurium*, o triptófano, en el caso de *E. coli*. Un compuesto mutagénico, revierte la mutación, y las cepas podrán sintetizar de nuevo el aminoácido y proliferar (a mayor potencial mutagénico, mayor crecimiento bacteriano). Al utilizar organismos procariotas (las bacterias) que carecen de sistemas de activación metabólica, requiere la adición de un sistema de activación metabólica exógena que contenga las enzimas necesarias para la biotransformación, imitando así las condiciones *in vivo* (Tejs, 2008). Por tanto, el efecto mutagénico de las sustancias evaluadas en las diferentes cepas bacterianas se realiza en presencia y en ausencia de fracción hepática microsomal de roedor (S9), que contiene isoenzimas de CYP450, según las directrices de la OCDE. En la Figura 8 se observa el crecimiento bacteriano de *S. typhimurium* cepa TA100 tras la exposición a la micotoxina T-2.

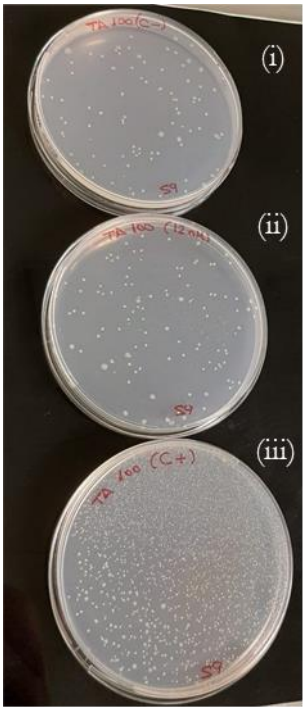

Figura 8. Representación del crecimiento bacteriano de *S. typhimurium* TA100 con S9 tras la exposición a 12 nM de T-2. (i) control negativo, (ii) concentración de 12 nM de T-2 y (iii) el control positivo para *S. typhimurium* TA100 con S9 (2-Aminoantraceno).

Alonso-Jauregui y colaboradores evaluaron la genotoxicidad de 12 micotoxinas, incluida la T-2, con la prueba SOS/umu, un método que muestra una fuerte correlación con el ensayo de mutación reversa bacteriana (Alonso-Jauregui et al., 2022). Estos autores compararon los resultados obtenidos para cada micotoxina entre la adición de una fracción microsomal S9 hepática y una alternativa procedente de riñón. Los resultados mostraron que el rango de 4 a 500 μg/mL de T-2 causa una respuesta mutagénica negativa con la fracción S9

hepática y una respuesta mutagénica positiva con la fracción S9 renal (Alonso-Jauregui et al., 2022).

Garofalo y colaboradores recientemente estudiaron la capacidad genotóxica de los tricotecenos en células intestinales IEC-6. La T-2 mostró la mayor exacerbación del daño al ADN respecto al resto de los tricotecenos estudiados (DAS, NIV, FUS-X y la toxina NX). Los autores demostraron además que la T-2 (10 nM) exacerbaba la genotoxicidad inducida por otras sustancias como fármacos (fleomicina), fungicidas (captan) y una toxina bacteriana (colibactina), todos ellos causantes de daño al ADN. Por tanto, demostraron que la T-2 causa daños al ADN y exacerban el fenotipo de genotoxinas con diversos mecanismos de acción (Garofalo et al., 2023).

1.3. Referencias

Adriani, G., Pavesi, A., Tan, A.T., Bertoletti, A., Thiery, J.P., Kamm, R.D., 2016. Microfluidic models for adoptive cell-mediated cancer immunotherapies. Drug Discov Today 21(9), 1472-1478. https://doi.org/10.1016/j.drudis.2016.05.006

AESAN, 2017. Leal, M. J. R., Daschner, Á., Oliag, P. T., & Marí, J. A. T. (2017). Informe del Comité Científico de la Agencia Española de Consumo, Seguridad Alimentaria y Nutrición (AECOSAN) en relación a una solicitud de evaluación inicial para la comercialización de un liofilizado de la microalga marina Tetraselmis chuii en complementos alimenticios en el marco del Reglamento (CE) Nº 258/97 sobre nuevos alimentos y nuevos ingredientes alimentarios. Rev Com Cient AESAN, (25), 11-22.

Afanasieva, K., Sivolob, A., 2018. Physical principles and new applications of comet assay. Biophys Chem 238, 1-7. https://doi.org/10.1016/j.bpc.2018.04.003

Agahi, F., Juan, C., Font, G., Juan-García, A., 2020. In silico methods for metabolomic and toxicity prediction of zearalenone, α-zearalenone and β-zearalenone. Food Chem Toxicol 146, 111818. https://doi.org/10.1016/j.fct.2020.111818

Agahi, F., Juan-García, A., Font, G., Juan, C., 2021. Study of enzymatic activity in human neuroblastoma cells SH-SY5Y exposed to zearalenone's derivates and beauvericin. Food Chem Toxicol 152, 112227. https://doi.org/10.1016/j.fct.2021.112227

Agrawal, M., Bhaskar, A.S.B., Rao, P.V.L., 2015. Involvement of Mitogen-Activated Protein Kinase Pathway in T-2 Toxin-Induced Cell Cycle Alteration and Apoptosis in Human Neuroblastoma Cells. Mol Neurobiol 51, 1379–1394. https://doi.org/10.1007/s12035-014-8816-4

Al Khawli, F., Martí-Quijal, F.J., Pallarés, N., Barba, F.J., Ferrer, E., 2021. Ultrasound extraction mediated recovery of nutrients and antioxidant bioactive compounds from phaeodactylum tricornutum microalgae. Appl Sci 11, 1–19. https://doi.org/10.3390/app11041701

Ali, S.S., Ahsan, H., Zia, M.K., Siddiqui, T., Khan, F.H., 2020. Understanding oxidants and antioxidants: Classical team with new players. J Food Biochem 44(3), e13145. https://doi.org/10.1111/jfbc.13145

Alonso-Jauregui, M., Font, M., González-Peñas, E., de Cerain, A.L., Vettorazzi, A., 2021. Prioritization of mycotoxins based on their genotoxic potential with an in silico-in vitro strategy. Toxins 13(10), 734. https://doi.org/10.3390/toxins13100734

Alonso-Jauregui, M., González-Peñas, E., López de Cerain, A., Vettorazzi, A., 2022. Genotoxicity of 12 Mycotoxins by the SOS/umu Test: Comparison of Liver and Kidney S9 Fraction. Toxins 14(6), 400. https://doi.org/10.3390/toxins14060400

Alshannaq, A., Yu, J.H., 2017. Occurrence, toxicity, and analysis of major mycotoxins in food. Int J Environ Res Public Health. 14(6), 632. https://doi.org/10.3390/ijerph14060632

Amaral, R.L.F., Miranda, M., Marcato, P.D., Swiech, K., 2017. Comparative analysis of 3D bladder tumor spheroids obtained by forced floating and hanging drop methods for drug screening. Front Physiol 8, 284532. https://doi.org/10.3389/fphys.2017.00605

Aranda, A., Sequedo, L., Tolosa, L., Quintas, G., Burello, E., Castell, J. V., Gombau, L., 2013. Dichloro-dihydro-fluorescein diacetate (DCFH-DA) assay: A quantitative method for oxidative stress assessment of nanoparticle-treated cells. Toxicol in Vitro 27, 954–963. https://doi.org/10.1016/j.tiv.2013.01.016

Arroyo-Manzanares, N., Campillo, N., López-García, I., Hernández-Córdoba, M., Viñas, P., 2021. High-resolution mass spectrometry for the determination of mycotoxins in biological samples. A review. Microchem J 166, 106197. https://doi.org/10.1016/j.microc.2021.106197

Baker, B.C., Heazell, A.E.P., Sibley, C., Wright, R., Bischof, H., Beards, F., Guevara, T., Girard, S., Jones, R.L., 2021. Hypoxia and oxidative stress induce sterile placental inflammation in vitro. Sci Rep 11(1), 7281. https://doi.org/10.1038/s41598-021-86268-1

Bauer, S., Wennberg Huldt, C., Kanebratt, K.P., Durieux, I., Gunne, D., Andersson, S., Ewart, L., Haynes, W.G., Maschmeyer, I., Winter, A., Ämmälä, C., Marx, U., Andersson, T.B., 2018. Erratum: Publisher Correction: Functional coupling of human pancreatic islets and liver spheroids on-a-chip: Towards a novel human ex vivo type 2 diabetes model. Sci Rep. 8. https://doi.org/10.1038/s41598-018-20340-1

Becker, H., Locascio, L.E., 2002. Polymer microfluidic devices. Talanta, 56(2), 267-287. https://doi.org/10.1016/S0039-9140(01)00594-X

Benfenati, E., Roncaglioni, A., Iovine, N., Mazzucotelli, M., Marzo, M., Toropov, A., Toropova, A., Baldin, R., Ciacci, A., Lettieri, M., Sartori, L., Yang, C., Magdziarz, T., Hobocienski, B., Mostrag, A., 2022. Maintenance, update and further development of EFSA's Chemical Hazards: OpenFoodTox 2.0. EFSA Supporting Publications 19(12), 7635E. https://doi.org/10.2903/sp.efsa.2022.en-7635

Bouaziz, C., Abid-Essefi, S., Bouslimi, A., El Golli, E., Bacha, H., 2006. Cytotoxicity and related effects of T-2 toxin on cultured Vero cells. Toxicon 48, 343–352. https://doi.org/10.1016/j.toxicon.2006.06.004

Bracarense, A.P.F.L., Lucioli, J., Grenier, B., Drociunas Pacheco, G., Moll, W.D., Schatzmayr, G., Oswald, I.P., 2012. Chronic ingestion of deoxynivalenol and fumonisin, alone or in interaction, induces morphological and immunological changes in the intestine of piglets. Br J Nutr 107, 1776–1786. https://doi.org/10.1017/S0007114511004946

Bryła, M., Wa´skiewicz, A., Ksieniewicz-Wo´zniak, E., Szymczyk, K., Edrzejczak, R.J., 2018. Modified fusarium mycotoxins in cereals and their products—Metabolism, occurrence, and toxicity: An updated review. Molecules 23(4), 963. https://doi.org/10.3390/molecules23040963

Bulutoglu, B., Rey-Bedón, C., Kang, Y.B., Mert, S., Yarmush, M.L., Usta, O.B., 2019. A microfluidic patterned model of non-alcoholic fatty liver disease: Applications to disease progression and zonation. Lab Chip 19, 3022–3031. https://doi.org/10.1039/c9lc00354a

Caldeira, M., Barreto, M.C., Barreto, C., Pestana, P., Cardoso, M.A.T., 2018. CODEN(USA): JSERBR Fish Residue Valorisation by the Production of Value-Added Compounds Towards a Sustainable Zero Waste Industry: A Critical Review. J Sci Eng Res 5, 418–447.

Cedillo-Alcantar, D.F., Han, Y.D., Choi, J., Garcia-Cordero, J.L., Revzin, A., 2019. Automated Droplet-Based Microfluidic Platform for Multiplexed Analysis of Biochemical Markers in Small Volumes. Anal Chem 91, 5133–5141. https://doi.org/10.1021/acs.analchem.8b05689

Chen, P., Xiang, B., Shi, H., Yu, P., Song, Y., Li, S., 2020. Recent advances on type A trichothecenes in food and feed: Analysis, prevalence, toxicity, and decontamination techniques. Food Control. 118, 107371. https://doi.org/10.1016/j.foodcont.2020.107371

Chen, Y., Gao, D., Liu, H., Lin, S., Jiang, Y., 2015. Drug cytotoxicity and signaling pathway analysis with three-dimensional tumor spheroids in a microwell-based microfluidic chip for drug screening. Anal Chim Acta 898, 85–92. https://doi.org/10.1016/j.aca.2015.10.006

Chen, Y., Sun, W., Kang, L., Wang, Y., Zhang, M., Zhang, H., Hu, P., 2019. Microfluidic co-culture of liver tumor spheroids with stellate cells for the investigation of drug resistance and intercellular interactions. Analyst 144, 4233–4240. https://doi.org/10.1039/c9an00612e

Chen, Y., Zheng, X., Zhou, R., Zhang, H., Liu, Y., Hu, X., Yin, Z., 2024. Mechanism of Apoptosis in Porcine Ovarian Granulosa Cells Triggered by T-2 Toxin. Genes 15, 579. https://doi.org/10.3390/genes15050579

Cheng, F., Li, W., Zhou, Y., Shen, J., Wu, Z., Liu, G., Lee, P.W., Tang, Y., 2012. AdmetSAR: A comprehensive source and free tool for assessment of chemical ADMET properties. J Chem Inf Model 52, 3099–3105. https://doi.org/10.1021/ci300367a

Chiotta, M.L., Fumero, M.V., Cendoya, E., Palazzini, J.M., Alaniz-Zanon, M.S., Ramirez, M.L., Chulze, S.N., 2020. Toxigenic fungal species and natural occurrence of mycotoxins in crops harvested in Argentina. Rev Argent Microbiol 52, 339–347. https://doi.org/10.1016/j.ram.2020.06.002

Choi, J., Loarca, L., De Hoyos-Vega, J.M., Neda Dadgar, X., Loutherback, K., Vijay Shah, X.H., Stybayeva, G., Revzin, A., Hoyos-Vega, D.J., 2020. Microfluidic confinement enhances phenotype and function of hepatocyte spheroids Microfluidic confinement enhances phenotype and function of hepatocyte spheroids. Am J Physiol Cell Physiol 319(3), C552-C560. https://doi.org/10.1152/ajpcell.00094.2020.-A

Chou, T.C., 2006. Theoretical basis, experimental design, and computerized simulation of synergism and antagonism in drug combination studies. Pharmacol Rev. 58(3), 621-681. https://doi.org/10.1124/pr.58.3.10

Chou, T. C., Talalayi, P., 1984. Quantitative analysis of dose-effect relationships: the combined effects of multiple drugs or enzyme inhibitors. Adv enzyme regul, 22, 27-55. https://doi.org/10.1016/0065-2571(84)90007-4

Dadgar, N., Gonzalez-Suarez, A.M., Fattahi, P., Hou, X., Weroha, J.S., Gaspar-Maia, A., Stybayeva, G., Revzin, A., 2020. A microfluidic platform for cultivating ovarian cancer spheroids and testing their responses to chemotherapies. Microsyst Nanoeng 6(1), 93. https://doi.org/10.1038/s41378-020-00201-6

Dai, C., Xiao, X., Sun, F., Zhang, Y., Hoyer, D., Shen, J., Tang, S., Velkov, T., 2019. T-2 toxin neurotoxicity: role of oxidative stress and mitochondrial dysfunction. Arch Toxicol. 93, 3041-3056. https://doi.org/10.1007/s00204-019-02577-5

Damiati, S., Kompella, U.B., Damiati, S.A., Kodzius, R., 2018. Microfluidic devices for drug delivery systems and drug screening. Genes 9(2), 103. https://doi.org/10.3390/genes9020103

de Hoyos-Vega, J.M., Hong, H.J., Loutherback, K., Stybayeva, G., Revzin, A., 2023. A Microfluidic Device for Long-Term Maintenance of Organotypic Liver Cultures. Adv Mater Technol 8(2), 2201121. https://doi.org/10.1002/admt.202201121

de Hoyos-Vega, J.M., Hong, H.J., Stybayeva, G., Revzin, A., 2021. Hepatocyte cultures: From collagen gel sandwiches to microfluidic devices with integrated biosensors. APL Bioeng. 5(4). https://doi.org/10.1063/5.0058798

Deyu, H., Luqing, C., Xianglian, L., Pu, G., Qirong, L., Xu, W., Zonghui, Y., 2018. Protective mechanisms involving enhanced mitochondrial functions and mitophagy against T-2 toxin-induced toxicities in GH3 cells. Toxicol Lett 295, 41–53. https://doi.org/10.1016/j.toxlet.2018.05.041

Díaz, L., Zambrano, E., Flores, M.E., Contreras, M., Crispín, J.C., Alemán, G., Bravo, C., Armenta, A., Valdés, V.J., Tovar, A., Gamba, G., Barrios-Payán, J., Bobadilla, N.A., 2020. Ethical Considerations in Animal Research: The Principle of 3R's. Rev Invest Clin 73, 199–209. https://doi.org/10.24875/RIC.20000380

Döll, S., Schrickx, J.A., Dänicke, S., Fink-Gremmels, J., 2009. Interactions of deoxynivalenol and lipopolysaccharides on cytokine excretion and mRNA expression in porcine hepatocytes and Kupffer cell enriched hepatocyte cultures. Toxicol Lett 190, 96–105. https://doi.org/10.1016/j.toxlet.2009.07.007

Domijan, A.M., Hercog, K., Štampar, M., Gajski, G., Gerić, M., Sokolović, M., Žegura, B., 2023. Impact of Deoxynivalenol and Zearalenone as Single and Combined Treatment on DNA, Cell Cycle and Cell Proliferation in HepG2 Cells. Int J Mol Sci 24(4), 4082. https://doi.org/10.3390/ijms24044082

Eagles, E.J., Benstead, R., MacDonald, S., Handy, R., Hutchinson, T.H., 2019. Impacts of the mycotoxin zearalenone on growth and photosynthetic responses in laboratory populations of freshwater macrophytes (Lemna minor) and microalgae (Pseudokirchneriella subcapitata). Ecotoxicol Environ Saf 169, 225–231. https://doi.org/10.1016/j.ecoenv.2018.10.101

EFSA, 2011. Scientific Opinion on the risks for animal and public health related to the presence of T-2 and HT-2 toxin in food and feed, 2011. EFSA J, 9 (12) 2481. https://doi.org/10.2903/j.efsa.2011.2481

EFSA 2014. Scientific Opinion on the risks for human and animal health related to the presence of modified forms of certain mycotoxins in food and feed. EFSA J, 12 (12) 3916. https://doi.org/10.2903/j.efsa.2014.3916

EFSA, 2017a. Human and animal dietary exposure to T-2 and HT-2 toxin. EFSA J, 15 (8) e04972. https://doi.org/10.2903/j.efsa.2017.4972

EFSA, 2017b. Appropriateness to set a group health based guidance value for T2 and HT2 toxin and its modified forms. EFSA J, 15 (1) e04655. https://doi.org/10.2903/j.efsa.2017.4655

EFSA, 2020. EFSA Panel on Contaminants in the Food Chain (CONTAM). Scientific Opinion on the risk assessment of ochratoxin A in food. EFSA J, 18(5), e06113. https://doi: 10.2903/j.efsa.2020.6113

EFSA, 2024. Risks for animal health related to the presence of ergot alkaloids in feed. EFSA J, 22 (1) e8496. https://doi.org/10.2903/j.efsa.2024.8496

Egan, W.J., Merz, K.M., Baldwin, J.J., 2000. Prediction of drug absorption using multivariate statistics. J Med Chem 43, 3867–3877. https://doi.org/10.1021/jm000292e

Essaouiba, A., Okitsu, T., Kinoshita, R., Jellali, R., Shinohara, M., Danoy, M., Legallais, C., Sakai, Y., Leclerc, E., 2020. Development of a pancreas-liver organ-on-chip coculture model for organ-to-organ interaction studies. Biochem Eng J 164, 107783. https://doi.org/10.1016/j.bej.2020.107783

EURL ECVAM, https://norecopa.no/3r-guide/eurl-ecvam/. Pagina actualizada el 19 de julio de 2023. Acceso el 21.05.2024

Fatima, Z., Guo, P., Huang, D., Lu, Q., Wu, Q., Dai, M., Cheng, G., Peng, D., Tao, Y., Ayub, M., ul Qamar, M.T., Ali, M.W., Wang, X., Yuan, Z., 2018. The critical role of p16/Rb pathway in the inhibition of GH3 cell cycle induced by T-2 toxin. Toxicology 400–401, 28–39. https://doi.org/10.1016/j.tox.2018.03.006

Fernández-Blanco, C., Elmo, L., Waldner, T., Ruiz, M.J., 2018. Cytotoxic effects induced by patulin, deoxynivalenol and toxin T2 individually and in combination in hepatic cells (HepG2). Food Chem Toxicol 120, 12–23. https://doi.org/10.1016/j.fct.2018.06.019

Fernández-Blanco, C., Font, G., Ruiz, M.J., 2015. Oxidative DNA damage and disturbance of antioxidant capacity by alternariol in Caco-2 cells. Toxicol Lett 235, 61–66. https://doi.org/10.1016/j.toxlet.2015.03.013

Ficheux, A.S., Sibiril, Y., Parent-Massin, D., 2012. Co-exposure of Fusarium mycotoxins: In vitro myelotoxicity assessment on human hematopoietic progenitors. Toxicon 60, 1171–1179. https://doi.org/10.1016/j.toxicon.2012.08.001

Foster, E., You, J., Siltanen, C., Patel, D., Haque, A., Anderson, L., Revzin, A., 2015. Heparin hydrogel sandwich cultures of primary hepatocytes. Eur Polym J 72, 726–735. https://doi.org/10.1016/j.eurpolymj.2014.12.033

Friedman, S.L., 2008. Hepatic Stellate Cells: Protean, Multifunctional, and Enigmatic Cells of the Liver. Physiol Rev 88(1), 125-172. https://doi.org/10.1152/physrev.00013.2007

Garofalo, M., Payros, D., Penary, M., Oswald, E., Nougayrède, J.P., Oswald, I.P., 2023. A novel toxic effect of foodborne trichothecenes: The exacerbation of genotoxicity. Environ Pollut 317, 120625. https://doi.org/10.1016/j.envpol.2022.120625

Garreau De Loubresse, N., Prokhorova, I., Holtkamp, W., Rodnina, M. V., Yusupova, G., Yusupov, M., 2014. Structural basis for the inhibition of the eukaryotic ribosome. Nature 513, 517–522. https://doi.org/10.1038/nature13737

Gilbert-López, B., Barranco, A., Herrero, M., Cifuentes, A., Ibáñez, E., 2017. Development of new green processes for the recovery of bioactives from Phaeodactylum tricornutum. Food Res Intern 99, 1056–1065. https://doi.org/10.1016/j.foodres.2016.04.022

Goossens, J., Pasmans, F., Verbrugghe, E., Vandenbroucke, V., De Baere, S., Meyer, E., Haesebrouck, F., De Backer, P., Croubels, S., 2012. Porcine intestinal epithelial barrier disruption by the Fusarium mycotoxins deoxynivalenol and T-2 toxin promotes transepithelial passage of doxycycline and paromomycin. BMC Vet Res 8, 1-10. https://doi.org/10.1186/1746-6148-8-245

Granato, D., Barba, F.J., Bursa´cbursa´c, D., Kovačevi´c, K., Lorenzo, J.M., Cruz, A.G., Putnik, P., 2020. Functional Foods: product development, technological trends, efficacy

testing, and safety. Annu Rev Food Sci Technol 11, 93-118. https://doi.org/10.1146/annurev-food-032519

Gu, S., Chen, Z., Wang, F., Wang, X., 2021. Characterization and inhibition of four fungi producing citrinin in various culture media. Biotechnol Lett 43, 701–710. https://doi.org/10.1007/s10529-020-03061-2

Guo, P., Liu, A., Huang, D., Wu, Q., Fatima, Z., Tao, Y., Cheng, G., Wang, X., Yuan, Z., 2018. Brain damage and neurological symptoms induced by T-2 toxin in rat brain. Toxicol Lett 286, 96–107. https://doi.org/10.1016/j.toxlet.2018.01.012

Habauzit, D., Lemée, P., Fessard, V., 2024. MycoCentral: An innovative database to compile information on mycotoxins and facilitate hazard prediction. Food Control 159, 110273. https://doi.org/10.1016/j.foodcont.2023.110273

Hampshire, V.A., Gilbert, S.H., 2019. Refinement, Reduction, and Replacement (3R) Strategies in Preclinical Testing of Medical Devices. Toxicol Pathol 47(3), 329-338. https://doi.org/10.1177/0192623318797289

Hewitt, N.J., Hewitt, P., 2004. Phase I and II enzyme characterization of two sources of HepG2 cell lines. Xenobiotica 34, 243–256. https://doi.org/10.1080/00498250310001657568

Hou, L., Gan, F., Zhou, X., Zhou, Y., Qian, G., Liu, Z., Huang, K., 2018. Immunotoxicity of ochratoxin A and aflatoxin B1 in combination is associated with the nuclear factor kappa B signaling pathway in 3D4/21 cells. Chemosphere 199, 718–727. https://doi.org/10.1016/j.chemosphere.2018.02.009

Huang, L., Zhu, L., Ou, Z., Ma, C., Kong, L., Huang, Y., Chen, Y., Zhao, H., Wen, L., Wu, J., Yuan, Z., Yi, J., 2021. Betulinic acid protects against renal damage by attenuation of oxidative stress and inflammation via Nrf2 signaling pathway in T-2 toxin-induced mice. Int Immunopharmacol 101, 108210. https://doi.org/10.1016/j.intimp.2021.108210

IARC, 2024: https://monographs.iarc.who.int/list-of-classifications. Acceso el 21.05.2024.

Iqbal, S.Z., 2021. Mycotoxins in food, recent development in food analysis and future challenges; a review. Curr Opin Food Sci 42, 237-247. https://doi.org/10.1016/j.cofs.2021.07.003

Ivanova, L., Skjerve, E., Eriksen, G.S., Uhlig, S., 2006. Cytotoxicity of enniatins A, A1, B, B1, B2 and B3 from Fusarium avenaceum. Toxicon 47, 868–876. https://doi.org/10.1016/j.toxicon.2006.02.012

Jakšić, D., Kocsubé, S., Bencsik, O., Kecskeméti, A., Szekeres, A., Jelić, D., Kopjar, N., Vágvölgyi, C., Varga, J., Šegvić Klarić, M., 2018. Fumonisin production and toxic capacity in airborne black Aspergilli. Toxicol in Vitro 53, 160–171. https://doi.org/10.1016/j.tiv.2018.08.006

Jakšić, D., Puel, O., Canlet, C., Kopjar, N., Kosalec, I., Klarić, M.S., 2012. Cytotoxicity and genotoxicity of versicolorins and 5- methoxysterigmatocystin in A549 cells. Arch Toxicol 86, 1583–1591. https://doi.org/10.1007/s00204-012-0871-x

Jang, K.-J., Otieno, M.A., Ronxhi, J., Lim, H.-K., Ewart, L., Kodella, K.R., Petropolis, D.B., Kulkarni, G., Rubins, J.E., Conegliano, D., Nawroth, J., Simic, D., Lam, W., Singer, M., Barale, E., Singh, B., Sonee, M., Streeter, A.J., Manthey, C., Jones, B., Srivastava, A., Andersson, L.C., Williams, D., Park, H., Barrile, R., Sliz, J., Herland, A., Haney, S., Karalis, K., Ingber, D.E., Hamilton, G.A., 2019. Reproducing human and cross-species drug toxicities using a Liver-Chip, Sci. Transl. Med 11(517), eaax5516. https://doi.org/10.1126/scitranslmed.aax5516

Janik-Karpinska, E., Ceremuga, M., Niemcewicz, M., Synowiec, E., Sliwinski, T., Stela, M., Bijak, M., 2023. DNA Damage Induced by T-2 Mycotoxin in Human Skin Fibroblast Cell Line—Hs68. Int J Mol Sci 24(19), 14458. https://doi.org/10.3390/ijms241914458

Jensen, C., Teng, Y., 2020. Is It Time to Start Transitioning From 2D to 3D Cell Culture? Front Mol Biosci 7, 33. https://doi.org/10.3389/fmolb.2020.00033

Jia, Z., Cheng, Y., Jiang, X., Zhang, C., Wang, G., Xu, J., Li, Y., Peng, Q., Gao, Y., 2020. 3D Culture System for Liver Tissue Mimicking Hepatic Plates for Improvement of Human Hepatocyte (C3A) Function and Polarity. Biomed Res Int 2020(1), 6354183. https://doi.org/10.1155/2020/6354183

Joshi, Tanuja, Joshi, Tushar, Sharma, P., Pundir, H., Chandra, S., 2021. In silico identification of natural fungicide from Melia azedarach against isocitrate lyase of Fusarium graminearum. J Biomol Struct Dyn 39, 4816–4834. https://doi.org/10.1080/07391102.2020.1780941

Juan-García, A., Taroncher, M., Font, G., Ruiz, M.J., 2018. Micronucleus induction and cell cycle alterations produced by deoxynivalenol and its acetylated derivatives in individual

and combined exposure on HepG2 cells. Food Chem Toxicol 118, 719–725. https://doi.org/10.1016/j.fct.2018.06.024

Juan-García, A., Tolosa, J., Juan, C., Ruiz, M.J., 2019. Cytotoxicity, genotoxicity and disturbance of cell cycle in hepg2 cells exposed to OTA and BEA: Single and combined actions. Toxins 11(6), 341. https://doi.org/10.3390/toxins11060341

Kamiya, N., Kim, H.K.W., 2021. Elevation of Proinflammatory Cytokine HMGB1 in the Synovial Fluid of Patients With Legg-Calvé-Perthes Disease and Correlation With IL-6. JBMR Plus 5(2), e10429. https://doi.org/10.1002/jbm4.10429

Kane, B.J., Zinner, M.J., Yarmush, M.L., Toner, M., 2006. Liver-specific functional studies in a microfluidic array of primary mammalian hepatocytes. Anal Chem 78, 4291–4298. https://doi.org/10.1021/ac051856v

Kang, Y.B., Eo, J., Bulutoglu, B., Yarmush, M.L., Usta, O.B., 2020. Progressive hypoxia-on-a-chip: An in vitro oxygen gradient model for capturing the effects of hypoxia on primary hepatocytes in health and disease. Biotechnol Bioeng 117, 763–775. https://doi.org/10.1002/bit.27225

Karmacharya, M.B., Hada, B., Park, S.R., Kim, K.H., Choi, B.H., 2022. Granulocyte-macrophage colony-stimulating factor (GM-CSF) shows therapeutic effect on dimethylnitrosamine (DMN)-induced liver fibrosis in rats. PLoS One 17(9), e0274126. https://doi.org/10.1371/journal.pone.0274126

Khetani, S.R., Bhatia, S.N., 2008. Microscale culture of human liver cells for drug development. Nat Biotechnol 26, 120–126. https://doi.org/10.1038/nbt1361

Kimothi, S., Dhaliwal, Y.S., 2020. Nutritional and Health Promoting Attribute of Kidney Beans (Phaseolus vulgaris L.): A Review. Int J Curr Microbiol Appl Sci 9, 1201–1209. https://doi.org/10.20546/ijcmas.2020.905.134

Kimura, H., Sakai, Y., Fujii, T., 2018. Organ/body-on-a-chip based on microfluidic technology for drug discovery. Drug Metab Pharmacokinet 33(1), 43-48. https://doi.org/10.1016/j.dmpk.2017.11.003

Knasmüller, S., Mersch-Sundermann, V., Kevekordes, S., Darroudi, F., Huber, W.W., Hoelzl, C., Bichler, J., Majer, B.J., 2004. Use of human-derived liver cell lines for the detection of environmental and dietary genotoxicants; Current state of knowledge. Toxicol 198(1-3),315–328. https://doi.org/10.1016/j.tox.2004.02.008

Kolf-Clauw, M., Sassahara, M., Lucioli, J., Rubira-Gerez, J., Alassane-Kpembi, I., Lyazhri, F., Borin, C., Oswald, I.P., 2013. The emerging mycotoxin, enniatin B1, down-modulates the gastrointestinal toxicity of T-2 toxin in vitro on intestinal epithelial cells and ex vivo on intestinal explants. Arch Toxicol 87, 2233–2241. https://doi.org/10.1007/s00204-013-1067-8

Königs, M., Mulac, D., Schwerdt, G., Gekle, M., Humpf, H.U., 2009. Metabolism and cytotoxic effects of T-2 toxin and its metabolites on human cells in primary culture. Toxicology 258, 106–115. https://doi.org/10.1016/j.tox.2009.01.012

Königs, M., Schwerdt, G., Gekle, M., Humpf, H.U., 2008. Effects of the mycotoxin deoxynivalenol on human primary hepatocytes. Mol Nutr Food Res 52, 830–839. https://doi.org/10.1002/mnfr.200700439

Kupfer, R., Dwyer-Nield, L.D., Malkinson, A.M., Thompson, J.A., 2002. Lung toxicity and tumor promotion by hydroxylated derivatives of 2,6-di-tert-butyl-4-methylphenol (BHT) and 2-tert-butyl-4-methyl-6-iso-propylphenol: Correlation with quinone methide reactivity. Chem Res Toxicol 15, 1106–1112. https://doi.org/10.1021/tx0255525

Lee, P.J., Hung, P.J., Lee, L.P., 2007. An artificial liver sinusoid with a microfluidic endothelial-like barrier for primary hepatocyte culture. Biotechnol Bioeng 97, 1340–1346. https://doi.org/10.1002/bit.21360

Lee, W.Y., Park, H.J., 2023. T-2 mycotoxin Induces male germ cell apoptosis by ROS-mediated JNK/p38 MAPK pathway. Ecotoxicol Environ Saf 262, 115323. https://doi.org/10.1016/j.ecoenv.2023.115323

Lei, R., Jiang, N., Zhang, Q., Hu, S., Dennis, B.S., He, S., Guo, X., 2016. Prevalence of Selenium, T-2 Toxin, and Deoxynivalenol in Kashin–Beck Disease Areas in Qinghai Province, Northwest China. Biol Trace Elem Res 171, 34–40. https://doi.org/10.1007/s12011-015-0495-0

Lei, Y., Guanghui, Z., Xi, W., Yingting, W., Xialu, L., Fangfang, Y., Goldring, M.B., Xiong, G., Lammi, M.J., 2017. Cellular responses to T-2 toxin and/or deoxynivalenol that induce cartilage damage are not specific to chondrocytes. Sci Rep 7(1), 2231. https://doi.org/10.1038/s41598-017-02568-5

Lemée, P., Fessard, V., Habauzit, D., 2023. Prioritization of mycotoxins based on mutagenicity and carcinogenicity evaluation using combined in silico QSAR methods. Environ Pollut 323, 121284. https://doi.org/10.1016/j.envpol.2023.121284

Li, B., Chen, Y., Zong, Y., Shang, Y., Zhang, Z., Xu, X., Wang, X., Long, M., Tian, S., 2019. Dissection of patulin biosynthesis, spatial control and regulation mechanism in Penicillium expansum. Environ Microbiol 21, 1124–1139. https://doi.org/10.1111/1462-2920.14542

Li, S.Y., Cao, J.L., Shi, Z.L., Chen, J.H., Zhang, Z.T., Hughes, C.E., Caterson, B., 2008. Promotion of the articular cartilage proteoglycan degradation by T-2 toxin and selenium protective effect. J Zhejiang Univ Sci B 9, 22–33. https://doi.org/10.1631/jzus.B071322

Li, X., Wang, X., Liu, S., Wang, J., Liu, X.Y., Zhu, Y., Zhang, L., Li, R., 2021. Betulinic acid attenuates T-2 toxin-induced cytotoxicity in porcine kidney cells by blocking oxidative stress and endoplasmic reticulum stress. Comparative Biochemistry and Physiology Part - C: Toxicol Pharmacol 249, 109124. https://doi.org/10.1016/j.cbpc.2021.109124

Lin, J., Schyschka, L., Mühl-Benninghaus, R., Neumann, J., Hao, L., Nussler, N., Dooley, S., Liu, L., Stöckle, U., Nussler, A.K., Ehnert, S., 2012. Comparative analysis of phase i and II enzyme activities in 5 hepatic cell lines identifies Huh-7 and HCC-T cells with the highest potential to study drug metabolism. Arch Toxicol 86, 87–95. https://doi.org/10.1007/s00204-011-0733-y

Lin, R., Sun, Y., Ye, W., Zheng, T., Wen, J., Deng, Y., 2019. T-2 toxin inhibits the production of mucin via activating the IRE1/XBP1 pathway. Toxicol 424, 152230. https://doi.org/10.1016/j.tox.2019.06.001

Ling, A., Sun, L., Guo, W., Sun, S., Yang, J., Zhao, Z., 2020. Individual and combined cytotoxic effects of T-2 toxin and its four metabolites on porcine Leydig cells. Food Chem Toxicol 139, 111277. https://doi.org/10.1016/j.fct.2020.111277

Liu, A., Guo, M., He, L., Martínez, M.A., Martínez, M., Lopez-Torres, B., Martínez-Larrañaga, M.R., Wang, X., Anadón, A., Ares, I., 2022. Nicotinamide N-methyltransferase protects against deoxynivalenol-induced growth inhibition by suppressing pro-inflammatory cytokine expression. Food Chem Toxicol 163, 112969. https://doi.org/10.1016/j.fct.2022.112969

Liu, D., Wang, Q., He, W., Chen, X., Wei, Z., Huang, K., 2020. Two-way immune effects of deoxynivalenol in weaned piglets and porcine alveolar macrophages: Due mainly to its exposure dosage. Chemosphere 249, 126464. https://doi.org/10.1016/j.chemosphere.2020.126464

Liu, X., Guo, P., Liu, A., Wu, Q., Xue, X., Dai, M., Hao, H., Qu, W., Xie, S., Wang, X., Yuan, Z., 2017. Nitric oxide (NO)-mediated mitochondrial damage plays a critical role in T-2 toxin-induced apoptosis and growth hormone deficiency in rat anterior pituitary GH3 cells. Food Chem Toxicol 102, 11–23. https://doi.org/10.1016/j.fct.2017.01.017

Liu, X., Pan, Z., Wang, Y., 2019. Ultrasound-assisted turbine bead milling for disintegration of Nannochloropsis oculata cells. J Appl Phycol 31, 1651–1659. https://doi.org/10.1007/s10811-018-1702-0

Logue, S.E., Martin, S.J., 2008. Caspase activation cascades in apoptosis. Biochem Soc Trans 36(1), 1-9. https://doi.org/10.1042/BST0360001

López-Medina, F.A., Dublán-García, O., Morachis-Valdez, A.G., López-Martínez, L.X., Gómez-Oliván, L.M., 2023. In vitro bioactive properties of protein hydrolysates from giant squid (Dosidicus gigas) by Bacillus subtilis. Food Res 7, 116–127. https://doi.org/10.26656/fr.2017.7(3).013

Maher, J.J., 2001. Interactions between Hepatic Stellate Cells and the Immune System, Seminars in Liver Disease (Vol. 21, No. 03, pp. 417-426). Copyright© 2001 by Thieme Medical Publishers, Inc., 333 Seventh Avenue, New York, NY 10001, USA. Tel.:+ 1 (212) 584-4662.

Mallebrera, B., Juan-Garcia, A., Font, G., Ruiz, M.J., 2016. Mechanisms of beauvericin toxicity and antioxidant cellular defense. Toxicol Lett 246, 28–34. https://doi.org/10.1016/j.toxlet.2016.01.013

Mamur, S., Ünal, F., Yılmaz, S., Erikel, E., Yüzbaşıoğlu, D., 2020. Evaluation of the cytotoxic and genotoxic effects of mycotoxin fusaric acid. Drug Chem Toxicol 43, 149–157. https://doi.org/10.1080/01480545.2018.1499772

Mamur, S., Yuzbasioglu, D., Yılmaz, S., Erikel, E., Unal, F., 2018. Assessment of cytotoxic and genotoxic effects of enniatin-A in vitro. Food Addit Contam Part A Chem Anal Control Expo Risk Assess 35, 1633–1644. https://doi.org/10.1080/19440049.2018.1486513

Maran, E., Fernández, M., Barbieri, P., Font, G., Ruiz, M.J., 2009. Effects of four carbamate compounds on antioxidant parameters. Ecotoxicol Environ Saf 72, 922–930. https://doi.org/10.1016/j.ecoenv.2008.01.018

Martínez-Alonso, C., Taroncher, M., Rodríguez-Carrasco, Y., Ruiz, M.J., 2023. Evaluation of the Bioaccessible Fraction of T-2 Toxin from Cereals and Its Effect on the Viability of Caco-2 Cells Exposed to Tyrosol. Toxins 15 (8), 493. https://doi.org/10.3390/toxins15080493

Martí-Quijal, F.J., Castagnini, J.M., Ruiz, M.J., Barba, F.J., 2023. Sea Bass Side Streams Extracts Obtained by Pulsed Electric Fields: Nutritional Characterization and Effect on SH-SY5Y Cells. Foods 12 (14), 2717. https://doi.org/10.3390/foods12142717

Martí-Quijal, F.J., Tornos, A., Príncep, A., Luz, C., Meca, G., Tedeschi, P., Ruiz, M.J., Barba, F.J., 2020. Impact of fermentation on the recovery of antioxidant bioactive compounds from sea bass byproducts. Antioxidants 9(3), 239. https://doi.org/10.3390/antiox9030239

McCarty, W.J., Usta, O.B., Yarmush, M.L., 2016. A microfabricated platform for generating physiologically-relevant hepatocyte zonation. Sci Rep 6(1), 26868. https://doi.org/10.1038/srep26868

McKean, C., Tang, L., Billam, M., Tang, M., Theodorakis, C.W., Kendall, R.J., Wang, J.S., 2006. Comparative acute and combinative toxicity of aflatoxin B1 and T-2 toxin in animals and immortalized human cell lines. J Appl Toxicol 26, 139–147. https://doi.org/10.1002/jat.1117

Meneely, J., Greer, B., Kolawole, O., Elliott, C., 2023. T-2 and HT-2 Toxins: Toxicity, Occurrence and Analysis: A Review. Toxins 15(8), 481. https://doi.org/10.3390/toxins15080481

Moon, S.H., Cho, S.J., 2023. Evaluation of the antioxidant activity of Tetraselmis chuii after in vitro gastrointestinal digestion and investigation of its antioxidant peptides. Algal Res 76, 103328. https://doi.org/10.1016/j.algal.2023.103328

Mora, C.F., Kwan, A.K.H., 2000. Sphericity, shape factor, and convexity measurement of coarse aggregate for concrete using digital image processing. Cement and concrete research 30(3), 351-358. https://doi.org/10.1016/S0008-8846(99)00259-8

Mortelmans, K., Zeiger, E., 2000. The Ames Salmonella/microsome mutagenicity assay, Mutation Research. 455(1-2), 29-60. https://doi.org/10.1016/S0027-5107(00)00064-6

Mukundan, S., Bell, J., Teryek, M., Hernandez, C., Love, A.C., Parekkadan, B., Chan, L.L.Y., 2022. Automated Assessment of Cancer Drug Efficacy On Breast Tumor Spheroids in Aggrewell™400 Plates Using Image Cytometry. J Fluoresc 32, 521–531. https://doi.org/10.1007/s10895-021-02881-3

Mulac, D., Lepski, S., Ebert, F., Schwerdtle, T., Humpf, H.U., 2013. Cytotoxicity and fluorescence visualization of ergot alkaloids in human cell lines. J Agric Food Chem 61, 462–471. https://doi.org/10.1021/jf304569q

Murphy, M.P., Bayir, H., Belousov, V., Chang, C.J., Davies, K.J.A., Davies, M.J., Dick, T.P., Finkel, T., Forman, H.J., Janssen-Heininger, Y., Gems, D., Kagan, V.E., Kalyanaraman, B., Larsson, N.G., Milne, G.L., Nyström, T., Poulsen, H.E., Radi, R., Van Remmen, H., Schumacker, P.T., Thornalley, P.J., Toyokuni, S., Winterbourn, C.C., Yin, H., Halliwell, B., 2022. Guidelines for measuring reactive oxygen species and oxidative damage in cells and in vivo. Nat Metab 4, 651–662. https://doi.org/10.1038/s42255-022-00591-z

Nagashima, H., Nakamura, K., Goto, T., 2003. Rubratoxin B induced the secretion of hepatic injury-related colony stimulating factors in human hepatoma cells. Toxicol Lett 145, 153–159. https://doi.org/10.1016/S0378-4274(03)00270-4

Narváez, A., Castaldo, L., Izzo, L., Pallarés, N., Rodríguez-Carrasco, Y., Ritieni, A., 2022. Deoxynivalenol contamination in cereal-based foodstuffs from Spain: Systematic review and meta-analysis approach for exposure assessment. Food Control 132, 108521. https://doi.org/10.1016/j.foodcont.2021.108521

Narváez, A., Izzo, L., Pallarés, N., Castaldo, L., Rodríguez-Carrasco, Y., Ritieni, A., 2021. Human biomonitoring of t-2 toxin, t-2 toxin-3-glucoside and their metabolites in urine through high-resolution mass spectrometry. Toxins 13(12), 869. https://doi.org/10.3390/toxins13120869

Navale, V., Vamkudoth, K.R., Ajmera, S., Dhuri, V., 2021. Aspergillus derived mycotoxins in food and the environment: Prevalence, detection, and toxicity. Toxicol Rep 8, 1008-1030. https://doi.org/10.1016/j.toxrep.2021.04.013

Niculescu, A.G., Chircov, C., Bîrcă, A.C., Grumezescu, A.M., 2021. Fabrication and applications of microfluidic devices: A review. Int J Mol Sci 22(4), 2011. https://doi.org/10.3390/ijms22042011

Nielsen, J.B., Hanson, R.L., Almughamsi, H.M., Pang, C., Fish, T.R., Woolley, A.T., 2020. Microfluidics: innovations in materials and their fabrication and functionalization. Anal Chem 92(1), 150-168. https://doi.org/10.1021/acs.analchem.9b04986

OECD Guideline for Testing of Chemicals Bacterial Reverse Mutation Test, 2020.

Pallarés, N., Righetti, L., Generotti, S., Cavanna, D., Ferrer, E., Dall'Asta, C., Suman, M., 2020. Investigating the in vitro catabolic fate of Enniatin B in a human gastrointestinal and colonic model. Food Chem Toxicol 137, 111166. https://doi.org/10.1016/j.fct.2020.111166

Pan, L.J., Tu, J.W., Ma, H.T., Yang, Y.J., Tian, Z.Q., Pang, D.W., Zhang, Z.L., 2018. Controllable synthesis of nanocrystals in droplet reactors. Lab Chip 18(1), 41-56. https://doi.org/10.1039/c7lc00800g

Park, D., Son, K., Hwang, Y., Ko, J., Lee, Y., Doh, J., Jeon, N.L., 2019. High-throughput microfluidic 3D cytotoxicity assay for cancer immunotherapy (CACI-ImpacT platform). Front Immunol 10, 1133. https://doi.org/10.3389/fimmu.2019.01133

Park, J., Li, J., Han, A., 2010. Micro-macro hybrid soft-lithography master (MMHSM) fabrication for lab-on-a-chip applications. Biomed Microdevices 12, 345–351. https://doi.org/10.1007/s10544-009-9390-9

Pei, X., Jiang, H., Liu, X., Li, L., Li, C., Xiao, X., Li, D., Tang, S., 2021. Targeting HMGB1 inhibits T-2 toxin-induced neurotoxicity via regulation of oxidative stress, neuroinflammation and neuronal apoptosis. Food Chem Toxicol 151, 112134. https://doi.org/10.1016/j.fct.2021.112134

Pereira, V.L., Fernandes, J.O., Cunha, S.C., 2014. Mycotoxins in cereals and related foodstuffs: A review on occurrence and recent methods of analysis. Trends Food Sci Technol 36(2), 96-136. https://doi.org/10.1016/j.tifs.2014.01.005

Pérez-López, P., González-García, S., Ulloa, R.G., Sineiro, J., Feijoo, G., Moreira, M.T., 2014. Life cycle assessment of the production of bioactive compounds from Tetraselmis suecica at pilot scale. J Clean Prod 64, 323–331. https://doi.org/10.1016/j.jclepro.2013.07.028

Pinton, P., Braicu, C., Nougayrede, J.P., Laffitte, J., Taranu, I., Oswald, I.P., 2010. Deoxynivalenol impairs porcine intestinal barrier function and decreases the protein

expression of claudin-4 through a mitogen-activated protein kinase-dependent mechanism. J Nutr 140, 1956–1962. https://doi.org/10.3945/jn.110.123919

Poojary, M.M., Barba, F.J., Aliakbarian, B., Donsì, F., Pataro, G., Dias, D.A., Juliano, P., 2016. Innovative alternative technologies to extract carotenoids from microalgae and seaweeds. Mar Drugs 14(11), 214. https://doi.org/10.3390/md14110214

Postma, P.R., Pataro, G., Capitoli, M., Barbosa, M.J., Wijffels, R.H., Eppink, M.H.M., Olivieri, G., Ferrari, G., 2016. Selective extraction of intracellular components from the microalga Chlorella vulgaris by combined pulsed electric field-temperature treatment. Bioresour Technol 203, 80–88. https://doi.org/10.1016/j.biortech.2015.12.012

Postma, P.R., Suarez-Garcia, E., Safi, C., Olivieri, G., Olivieri, G., Wijffels, R.H., Wijffels, R.H., 2017. Energy efficient bead milling of microalgae: Effect of bead size on disintegration and release of proteins and carbohydrates. Bioresour Technol 224, 670–679. https://doi.org/10.1016/j.biortech.2016.11.071

Rachitha, P., Krupashree, K., Brindhadevi, K., Pal, A., Chinnathambi, A., Alahmadi, T.A., Shanmuganathan, R., Karuppusamy, I., Raghavendra, V.B., 2023. Convalescent action of menthol against T-2 mycotoxin-induced toxicity: An in vitro study with HaCaT cells. Environ Res 227, 115690. https://doi.org/10.1016/j.envres.2023.115690

Rahate, K.A., Madhumita, M., Prabhakar, P.K., 2021. Nutritional composition, anti-nutritional factors, pretreatments-cum-processing impact and food formulation potential of faba bean (Vicia faba L.): A comprehensive review. LWT-Food Sci Technol 138, 110796. https://doi.org/10.1016/j.lwt.2020.110796

Rahman, S., Sharma, A.K., Singh, N.D., Prawez, S., 2021. Immunopathological effects of experimental T-2 mycotoxicosis in Wistar rats. Hum Exp Toxicol 40, 772–790. https://doi.org/10.1177/0960327120968852

Raies, A.B., Bajic, V.B., 2016. In silico toxicology: computational methods for the prediction of chemical toxicity. Wiley Interdiscip Rev Comput Mol Sci 6 (2), 147–172. https://doi.org/10.1002/wcms.1240

RASFF, 2022. Alert and Cooperation Network Health and Food Safety.

Reglamento (UE) 2023/915 de la comisión de 25 de abril de 2023 relativo a los límites máximos de determinados contaminantes en los alimentos (BOE núm. 119, de 5 de mayo de 2023).

Reglamento (UE) 2024/1038 de la comisión de 9 de abril de 2024 por el que se modifica el Reglamento (UE) 2023/915 en lo que respecta a los límites máximos de las toxinas T-2 y HT-2 en los alimentos (BOE núm. 1038, de 10 de abril de 2024).

Reglamento de ejecución (UE) 2024/885 de la comisión de 20 de marzo de 2024 que modifica el Reglamento de ejecución (UE) 2023/2782, por el que se establecen los métodos de muestreo y análisis para el control del contenido de micotoxinas en los alimentos (BOE núm. 885, de 21 de marzo de 2024).

Rogowska, A., Pomastowski, P., Sagandykova, G., Buszewski, B., 2019. Zearalenone and its metabolites: Effect on human health, metabolism and neutralisation methods. Toxicon 162, 46-56. https://doi.org/10.1016/j.toxicon.2019.03.004

Ronaldson-Bouchard, K., Vunjak-Novakovic, G., 2018. Organs-on-a-Chip: A Fast Track for Engineered Human Tissues in Drug Development. Cell Stem Cell 22(3), 310-324. https://doi.org/10.1016/j.stem.2018.02.011

Rossi, Y.E., Bohl, L.P., Vanden Braber, N.L., Ballatore, M.B., Escobar, F.M., Bodoira, R., Maestri, D.M., Porporatto, C., Cavaglieri, L.R., Montenegro, M.A., 2020. Polyphenols of peanut (Arachis hypogaea L.) skin as bioprotectors of normal cells. Studies of cytotoxicity, cytoprotection and interaction with ROS. J Funct Foods 67, 103862. https://doi.org/10.1016/j.jff.2020.103862

Ruiz, M. J., Franzova, P., Juan-García, A., Font, G., 2011a. Toxicological interactions between the mycotoxins beauvericin, deoxynivalenol and T-2 toxin in CHO-K1 cells in vitro. Toxicon 58, 315–326. https://doi.org/10.1016/j.toxicon.2011.07.015

Ruiz, M. J., Macáková, P., Juan-García, A., Font, G., 2011b. Cytotoxic effects of mycotoxin combinations in mammalian kidney cells. Food Chem Toxicol 49, 2718–2724. https://doi.org/10.1016/j.fct.2011.07.021

Sabhachandani, P., Motwani, V., Cohen, N., Sarkar, S., Torchilin, V., Konry, T., 2016. Generation and functional assessment of 3D multicellular spheroids in droplet based microfluidics platform. Lab Chip 16, 497–505. https://doi.org/10.1039/c5lc01139f

Sánchez, R., Arboleda, G., 2008. Mitocondria y muerte celular. Nova 6 (10). https://doi.org/10.22490/24629448.409

Savard, C., Pinilla, V., Provost, C., Segura, M., Gagnon, C.A., Chorfi, Y., 2014. In vitro effect of deoxynivalenol (DON) mycotoxin on porcine reproductive and respiratory

syndrome virus replication. Food Chem Toxicol 65, 219–226. https://doi.org/10.1016/j.fct.2013.12.043

Sheng, K., Lu, X., Yue, J., Gu, W., Gu, C., Zhang, H., Wu, W., 2019. Role of neurotransmitters 5-hydroxytryptamine and substance P in anorexia induction following oral exposure to the trichothecene T-2 toxin. Food Chem Toxicol 123, 1–8. https://doi.org/10.1016/j.fct.2018.10.041

Siah, S.D., Konczak, I., Agboola, S., Wood, J.A., Blanchard, C.L., 2012. In vitro investigations of the potential health benefits of Australian-grown faba beans (Vicia faba L.): Chemopreventative capacity and inhibitory effects on the angiotensin-converting enzyme, Î±- glucosidase and lipase. Br J Nutr 108(S1), S123-S134. https://doi.org/10.1017/S0007114512000803

Somoskői, B., Kovács, M., Cseh, S., 2018. Effects of T-2 and Fumonisin B1 combined treatment on in vitro mouse embryo development and blastocyst quality. Toxicol Ind Health 34, 353–360. https://doi.org/10.1177/0748233718764039

Somoskői, B., Kovács, M., Cseh, S., 2016. Effects of T-2 mycotoxin on in vitro development and chromatin status of mouse embryos in preimplantation stages. Toxicol Ind Health 32, 1260–1265. https://doi.org/10.1177/0748233714555394

Son, K.J., Gheibi, P., Stybayeva, G., Rahimian, A., Revzin, A., 2017. Detecting cell-secreted growth factors in microfluidic devices using bead-based biosensors. Microsyst Nanoeng 3(1), 1-9. https://doi.org/10.1038/micronano.2017.25

Sontheimer-Phelps, A., Hassell, B.A., Ingber, D.E., 2019. Modelling cancer in microfluidic human organs-on-chips. Nat Rev Cancer 19(2), 65-81. https://doi.org/10.1038/s41568-018-0104-6

Sun, L., Dai, J., Xu, J., Yang, J., Zhang, D., 2022. Comparative Cytotoxic Effects and Possible Mechanisms of Deoxynivalenol, Zearalenone and T-2 Toxin Exposure to Porcine Leydig Cells In Vitro. Toxins 14(2), 113. https://doi.org/10.3390/toxins14020113

Sun, L.Y., Li, Q., Meng, F.G., Fu, Y., Zhao, Z.J., Wang, L.H., 2012. T-2 toxin contamination in grains and selenium concentration in drinking water and grains in kaschin-beck disease endemic areas of Qinghai province. Biol Trace Elem Res 150, 371–375. https://doi.org/10.1007/s12011-012-9469-7

Tajima, O., Schoen, E.D., Feron, V.J., Groten, J.P. 2002. Statistically designed experiments in a tiered approach to screen mixtures of Fusarium mycotoxins for possible interactions. Food Chem Toxicol 40(5), 685-695. https://doi.org/10.1016/S0278-6915(01)00124-7

Tatay, E., Espín, S., García-Fernández, A.J., Ruiz, M.J., 2017. Oxidative damage and disturbance of antioxidant capacity by zearalenone and its metabolites in human cells. Toxicol in Vitro 45, 334–339. https://doi.org/10.1016/j.tiv.2017.04.026

Tatay, E., Font, G., Ruiz, M.J., 2016. Cytotoxic effects of zearalenone and its metabolites and antioxidant cell defense in CHO-K1 cells. Food Chem Toxicol 96, 43–49. https://doi.org/10.1016/j.fct.2016.07.027

Tejs, S., 2008. The Ames test: a methodological short review. Environ Biotech 4(1), 7-14.

Thuanthong, M., De Gobba, C., Sirinupong, N., Youravong, W., Otte, J., 2017. Purification and characterization of angiotensin-converting enzyme-inhibitory peptides from Nile tilapia (Oreochromis niloticus) skin gelatine produced by an enzymatic membrane reactor. J Funct Foods 36, 243–254. https://doi.org/10.1016/j.jff.2017.07.011

Tian, J., Yan, J., Wang, W., Zhong, N., Tian, L., Sun, J., Min, Z., Ma, J., Lu, S., 2012. T-2 toxin enhances catabolic activity of hypertrophic chondrocytes through ROS-NF-κB-HIF-2α pathway. Toxicol in Vitro 26, 1106–1113. https://doi.org/10.1016/j.tiv.2012.07.002

Tolosa, J., Barba, F.J., Pallarés, N., Ferrer, E., 2020. Mycotoxin Identification and In Silico Toxicity Assessment Prediction in Atlantic Salmon. Mar Drugs 18(12), 629. https://doi.org/10.3390/md18120629

Tran, V.N., Viktorová, J., Ruml, T., 2020. Mycotoxins: Biotransformation and bioavailability assessment using caco-2 cell monolayer. Toxins 12(10), 628. https://doi.org/10.3390/toxins12100628

Trujillo-de Santiago, G., Flores-Garza, B.G., Tavares-Negrete, J.A., Lara-Mayorga, I.M., González-Gamboa, I., Zhang, Y.S., Rojas-Martínez, A., Ortiz-López, R., Álvarez, M.M., 2019. The tumor-on-chip: Recent advances in the development of microfluidic systems to recapitulate the physiology of solid tumors. Materials 12(18), 2945. https://doi.org/10.3390/ma12182945

Turco, L., Catone, T., Caloni, F., Consiglio, E. Di, Testai, E., Stammati, A., 2011. Caco-2/TC7 cell line characterization for intestinal absorption: How reliable is this in vitro model for

the prediction of the oral dose fraction absorbed in human? Toxicol in Vitro 25, 13–20. https://doi.org/10.1016/j.tiv.2010.08.009

Ukairo, O., Kanchagar, C., Moore, A., Shi, J., Gaffney, J., Aoyama, S., Rose, K., Krzyzewski, S., Mcgeehan, J., Andersen, M.E., Khetani, S.R., Lecluyse, E.L., 2013. Long-term stability of primary rat hepatocytes in micropatterned cocultures. J Biochem Mol Toxicol 27, 204–212. https://doi.org/10.1002/jbt.21469

Urbaniak, M., Waskiewicz, A., Stepien, Ł., 2020. Fusarium cyclodepsipeptide mycotoxins: Chemistry, biosynthesis, and occurrence. Toxins 12(12), 765. https://doi.org/10.3390/toxins12120765

Medina, D.A.V, Bassolli Borsatto, J.V., Maciel, E.V.S., Lanças, F.M., 2021. Current role of modern chromatography and mass spectrometry in the analysis of mycotoxins in food. TRAC - Trend Anal Chem. 135, 116156. https://doi.org/10.1016/j.trac.2020.116156

Vermes, I., Haanen, C., Steffens-Nakken, H., Reutelingsperger, C., 1995. A novel assay for apoptosis Flow cytometric detection of phosphatidylserine early apoptotic cells using fluorescein labelled expression on Annexin V, J Immunol Methods, 184 (1) 39-51. https://doi.org/10.1016/0022-1759(95)00072-I

Vila-Donat, P., Fernández-Blanco, C., Sagratini, G., Font, G., Ruiz, M.J., 2015. Effects of soyasaponin I and soyasaponins-rich extract on the Alternariol-induced cytotoxicity on Caco-2 cells. Food Chem Toxicol 77, 44–49. https://doi.org/10.1016/j.fct.2014.12.016

Villamil, O., Váquiro, H., Solanilla, J.F., 2017. Fish viscera protein hydrolysates: Production, potential applications and functional and bioactive properties. Food Chem 224, 160-171. https://doi.org/10.1016/j.foodchem.2016.12.057

Vongchan, P., Warda, M., Toyoda, H., Toida, T., Marks, R.M., Linhardt, R.J., 2005. Structural characterization of human liver heparan sulfate. Biochim Biophys Acta Gen Subj 1721, 1–8. https://doi.org/10.1016/j.bbagen.2004.09.007

Wang, G., Zhang, H., Wang, Y., Liu, F., Li, E., Ma, J., Yang, B., Zhang, C., Li, L., Liu, Y., 2019. Requirement of LaeA, VeA, and VelB on Asexual Development, Ochratoxin A Biosynthesis, and Fungal Virulence in Aspergillus ochraceus. Front Microbiol 10, 2759. https://doi.org/10.3389/fmicb.2019.02759

Wang, M., Morón-Ortiz, Á., Zhou, J., Benítez-González, A., Mapelli-Brahm, P., Meléndez-Martínez, A.J., Barba, F.J., 2023. Effects of pressurized liquid extraction with dimethyl

sulfoxide on the recovery of carotenoids and other dietary valuable compounds from the microalgae Spirulina, Chlorella and Phaeodactylum tricornutum. Food Chem 405, 134885. https://doi.org/10.1016/j.foodchem.2022.134885

Wang, X., Liu, X., Liu, J., Wang, G., Wan, K., 2012. Contamination level of T-2 and HT-2 toxin in cereal crops from aba area in Sichuan Province, China. Bull Environ Contam Toxicol 88, 396–400. https://doi.org/10.1007/s00128-011-0478-6

Wattanasuntorn, P., Phuektes, P., Poapolathep, S., Mimapan, S., Tattiyapong, M., Fink-Gremmels, J., Oswald, I.P., Poapolathep, A., 2024. Individual cytotoxicity of three major type A trichothecene, T-2, HT-2, and diacetoxyscirpenol in human Jurkat T cells. Toxicon 243, 107718. https://doi.org/10.1016/j.toxicon.2024.107718

Weidner, M., Welsch, T., Hübner, F., Schwerdt, G., Gekle, M., Humpf, H.U., 2012. Identification and apoptotic potential of T-2 toxin metabolites in human cells. J Agric Food Chem 60, 5676–5684. https://doi.org/10.1021/jf300634k

Wen, C., Zhang, J., Feng, Y., Duan, Y., Ma, H., Zhang, H., 2020. Purification and identification of novel antioxidant peptides from watermelon seed protein hydrolysates and their cytoprotective effects on H2O2-induced oxidative stress. Food Chem 327, 127059. https://doi.org/10.1016/j.foodchem.2020.127059

Widowati, I., Zainuri, M., Kusumaningrum, H.P., Susilowati, R., Hardivillier, Y., Leignel, V., Bourgougnon, N., Mouget, J.L., 2017. Antioxidant activity of three microalgae Dunaliella salina, Tetraselmis chuii and Isochrysis galbana clone Tahiti. Earth Environ Sci 55, 1, 012067. IOP Publishing. https://doi.org/10.1088/1755-1315/55/1/012067

Woelflingseder, L., Del Favero, G., Blažević, T., Heiss, E.H., Haider, M., Warth, B., Adam, G., Marko, D., 2018. Impact of glutathione modulation on the toxicity of the Fusarium mycotoxins deoxynivalenol (DON), NX-3 and butenolide in human liver cells. Toxicol Lett 299, 104–117. https://doi.org/10.1016/j.toxlet.2018.09.007

Wu, J., Tu, D., Yuan, L.Y., Yuan, H., Wen, L.X., 2013. T-2 toxin exposure induces apoptosis in rat ovarian granulosa cells through oxidative stress. Environ Toxicol Pharmacol 36, 493–500. https://doi.org/10.1016/j.etap.2013.03.017

Wu, J., Zhou, Y., Yuan, Z., Yi, J., Chen, J., Wang, N., Tian, Y., 2019. Autophagy and apoptosis interact to modulate T-2 toxin-induced toxicity in liver cells. Toxins 11 (1) 45. https://doi.org/10.3390/toxins11010045

Wu, Q., Dohnal, V., Huang, L., Kuča, K., Yuan, Z., 2010. Metabolic pathways of trichothecenes. Drug Metab Rev 42 (2), 250-267. https://doi.org/10.3109/03602530903125807

Wu, Q., Qin, Z., Kuca, K., You, L., Zhao, Y., Liu, A., Musilek, K., Chrienova, Z., Nepovimova, E., Oleksak, P., Wu, W., Wang, X., 2020. An update on T-2 toxin and its modified forms: metabolism, immunotoxicity mechanism, and human exposure assessment. Arch Toxicol 94, 3645-3669. https://doi.org/10.1007/s00204-020-02899-9

Wu, Q.H., Wang, X., Yang, W., Nüssler, A.K., Xiong, L.Y., Kuča, K., Dohnal, V., Zhang, X.J., Yuan, Z.H., 2014. Oxidative stress-mediated cytotoxicity and metabolism of T-2 toxin and deoxynivalenol in animals and humans: An update. Arch Toxicol 88, 1309-1326. https://doi.org/10.1007/s00204-014-1280-0

Xiao, S., Wu, Y., Gao, S., Zhou, M., Liu, Z., Xiong, Q., Jiang, L., Yuan, G., Li, L., Yang, L., 2023. Deciphering the Hazardous Effects of AFB1 and T-2 Toxins: Unveiling Toxicity and Oxidative Stress Mechanisms in PK15 Cells and Mouse Kidneys. Toxins 15(8), 503. https://doi.org/10.3390/toxins15080503

Xu, J., Zhao, Z., Guo, W., Ling, A., Wang, J., Wang, X., Yang, J., 2022. Potential Role of Individual and Combined Effects of T-2 Toxin, HT-2 Toxin and Neosolaniol on the Apoptosis of Porcine Leydig Cells. Toxins 14 (2) 145. https://doi.org/10.3390/toxins14020145

Yang, D., Zhang, X., Yue, L., Hu, H., Wei, X., Guo, Q., Zhang, B., Fan, X., Xin, Y., Oh, Y., Gu, N., 2021. Thiamethoxam induces nonalcoholic fatty liver disease in mice via methionine metabolism disturb via nicotinamide N-methyltransferase overexpression. Chemosphere 273, 129727. https://doi.org/10.1016/j.chemosphere.2021.129727

Yang, L., Tu, D., Wang, N., Deng, Z., Zhan, Y., Liu, W., Hu, Y., Liu, T., Tan, L., Li, Y., Guo, S., Wang, A., 2019. The protective effects of DL-Selenomethionine against T-2/HT-2 toxins-induced cytotoxicity and oxidative stress in broiler hepatocytes. Toxicol in Vitro 54, 137–146. https://doi.org/10.1016/j.tiv.2018.09.016

Yang, S., Li, Y., Cao, X., Hu, D., Wang, Z., Wang, Y., Shen, J., Zhang, S., 2013. Metabolic pathways of T-2 toxin in in vivo and in vitro systems of Wistar rats. J Agric Food Chem 61, 9734–9743. https://doi.org/10.1021/jf4012054

Yang, S., Zhang, H., De Boevre, M., Zhang, J., Li, Yanshen, Zhang, S., De Saeger, S., Zhou, J., Li, Yi, Sun, F., 2018. Toxicokinetics of HT-2 Toxin in Rats and Its Metabolic Profile in Livestock and Human Liver Microsomes. J Agric Food Chem 66, 8160–8168. https://doi.org/10.1021/acs.jafc.8b02893

Yang, Z.B., Wan, X.L., Yang, W.R., Jiang, S.Z., Zhang, G.G., Johnston, S.L., Chi, F., 2014. Effects of naturally mycotoxin-contaminated corn on nutrient and energy utilization of ducks fed diets with or without Calibrin-A. Poult Sci 93, 2199–2209. https://doi.org/10.3382/ps.2013-03392

Yarnpakdee, S., Benjakul, S., Kristinsson, H.G., Bakken, H.E., 2015. Preventive effect of Nile tilapia hydrolysate against oxidative damage of HepG2 cells and DNA mediated by H2O2 and AAPH. J Food Sci Technol 52, 6194–6205. https://doi.org/10.1007/s13197-014-1672-4

Yazdi, S. R., Shadmani, A., Bürgel, S.C., Misun, P.M., Hierlemann, A., Frey, O., 2015. Adding the "heart" to hanging drop networks for microphysiological multi-tissue experiments. Lab Chip 15, 4138–4147. https://doi.org/10.1039/c5lc01000d

Ye, W., Lin, R., Chen, X., Chen, J., Chen, R., Xie, X., Deng, Y., Wen, J., 2019. T-2 toxin upregulates the expression of human cytochrome P450 1A1 (CYP1A1) by enhancing NRF1 and Sp1 interaction. Toxicol Lett 315, 77–86. https://doi.org/10.1016/j.toxlet.2019.08.021

Yi, Y., Zhao, F., Wang, N., Liu, H., Yu, L., Wang, A., Jin, Y., 2018. Endoplasmic reticulum stress is involved in the T-2 toxin-induced apoptosis in goat endometrium epithelial cells. J Appl Toxicol 38, 1492–1501. https://doi.org/10.1002/jat.3655

Yuan, L., Mu, P., Huang, B., Li, H., Mu, H., Deng, Y., 2018. EGR1 is essential for deoxynivalenol-induced G2/M cell cycle arrest in HepG2 cells via the ATF3ΔZip2a/2b-EGR1-p21 pathway. Toxicol Lett 299, 95–103. https://doi.org/10.1016/j.toxlet.2018.09.012

Zhang, Hua, Deng, X., Zhou, C., Wu, W., Zhang, Haibin, 2020. Deoxynivalenol induces inflammation in IPEC-J2 cells by activating p38 MAPK and ERK1/2. Toxins 12 (3) 180. https://doi.org/10.3390/toxins12030180

Zhang, L.Y., Zhan, D.L., Chen, Y.Y., Wang, W.H., He, C.Y., Lin, Y., Lin, Y.C., Lin, Z.N., 2019. Aflatoxin B1 enhances pyroptosis of hepatocytes and activation of Kupffer cells to promote liver inflammatory injury via dephosphorylation of cyclooxygenase-2: an in

vitro, ex vivo and in vivo study. Arch Toxicol 93, 3305–3320. https://doi.org/10.1007/s00204-019-02572-w

Zhang, X., Wang, Y., Velkov, T., Tang, S., Dai, C., 2018. T-2 toxin-induced toxicity in neuroblastoma-2a cells involves the generation of reactive oxygen, mitochondrial dysfunction and inhibition of Nrf2/HO-1 pathway. Food Chem Toxicol 114, 88–97. https://doi.org/10.1016/j.fct.2018.02.010

Zhang, Y.S., Zhang, Y.N., Zhang, W., 2017. Cancer-on-a-chip systems at the frontier of nanomedicine. Drug Discov Today 22(9), 1392-1399. https://doi.org/10.1016/j.drudis.2017.03.011

Zhou, Q., Patel, D., Kwa, T., Haque, A., Matharu, Z., Stybayeva, G., Gao, Y., Diehl, A.M., Revzin, A., 2015. Liver injury-on-a-chip: microfluidic co-cultures with integrated biosensors for monitoring liver cell signaling during injury. Lab Chip 15, 4467–4478. https://doi.org/10.1039/c5lc00874c

Zingales, V., Esposito, M.R., Torriero, N., Taroncher, M., Cimetta, E., Ruiz, M.J., 2023. The Growing Importance of Three-Dimensional Models and Microphysiological Systems in the Assessment of Mycotoxin Toxicity. Toxins 15(7), 422. https://doi.org/10.3390/toxins15070422

Zingales, V., Fernández-Franzón, M., Ruiz, M.J., 2021. Sterigmatocystin-induced DNA damage triggers cell-cycle arrest via MAPK in human neuroblastoma cells. Toxicol Mech Methods 31, 479–488. https://doi.org/10.1080/15376516.2021.1916801

Zingales, V., Fernández-Franzón, M., Ruiz, M.J., 2020. Sterigmatocystin-induced cytotoxicity via oxidative stress induction in human neuroblastoma cells. Food Chem Toxicol 136, 110956. https://doi.org/10.1016/j.fct.2019.110956

Zucco, F., Batto, A. F., Bises, G., Chambaz, J., Chiusolo, A., Consalvo, R., Stammati, A. (2005). An inter-laboratory study to evaluate the effects of medium composition on the differentiation and barrier function of Caco-2 cell lines. ATLA, 33(6), 603-618. https://doi.org/10.1177/026119290503300618

2. Objetivos

Objectives

2. OBJETIVOS

El objetivo general de la presente Tesis Doctoral es profundizar en el conocimiento de los mecanismos de acción toxicológica de la micotoxina T-2 mediante métodos alternativos, haciendo uso de modelos de predicción *in silico* e *in vitro*.

Para lograr este objetivo general se han planteado los siguientes objetivos específicos:

1. Realizar una búsqueda bibliográfica de la información toxicológica disponible sobre la micotoxina T-2 y sus principales metabolitos HT-2, Neo, T2-triol y T2-tetraol.
2. Determinar el perfil toxicológico y ADME de la T-2 y sus productos de biotransformación utilizando modelos de predicción *in silico*.
3. Determinar la citotoxicidad de la T-2 y sus metabolitos de forma individual y combinada, así como evaluar el tipo de interacción entre ellas en las células HepG2.
4. Identificar los productos de biotransformación de la T-2 intracelulares y en el medio extracelular durante un ciclo de 24 h en las células HepG2.
5. Analizar el estrés oxidativo mediante la determinación de la producción de especies reactivas de oxígeno (ROS) tras la exposición de T-2, Neo, T2-triol y T2-tetraol en células HepG2.
6. Estudiar los sistemas de defensa antioxidantes endógenos (enzimáticos y no enzimáticos) y exógenos presentes en la dieta (legumbres, microalgas e hidrolizados de pescado) frente al daño oxidativo producido por la T-2 y sus metabolitos en las células HepG2 y Caco-2.

7. Evaluar la proliferación, la muerte celular (apoptosis y necrosis) y el daño potencial al ADN (genotóxico y mutagénico), tras la exposición de la T-2 en las células HepG2.
8. Formar y caracterizar esferoides de células HepG2 en placas estándar y en dispositivos microfluídicos.
9. Comparar la citotoxicidad de la T-2 y los mecanismos de acción obtenidos en esferoides de células HepG2 y esferoides en co-cultivo de células HepG2 y LX2 en dispositivos microfluídicos.

2. OBJECTIVES

The general objective of this Doctoral Thesis is to improve the understanding of the mechanisms of toxicological action of mycotoxin T-2 through alternative methods, using *in silico* predictive models and *in vitro* methods.

In order to achieve this general goal, the following specific objectives have been set:

1. To review the available toxicological information on T-2 mycotoxin and its main metabolites HT-2, Neo, T2-triol and T2-tetraol.
2. To determine the toxicological and ADME profile of T-2 and its biotransformation products using *in silico* predictive models.
3. To determine the cytotoxicity of T-2 and its metabolites individually and in combination, and to assess the type of interaction between them in HepG2 cells.
4. To identify the biotransformation products of T-2 intracellularly and in the extracellular medium during a 24 h cycle in HepG2 cells.
5. To analyze oxidative stress by determining the production of reactive oxygen species (ROS) after exposure of T-2, Neo, T2-triol and T2-tetraol in HepG2 cells.
6. To study endogenous (enzymatic and non-enzymatic) and exogenous antioxidant defense systems present in the diet (legumes, microalgae and fish hydrolysates) against oxidative damage produced by T-2 and its metabolites in HepG2 and Caco-2 cells.
7. To assess the proliferation, cell death (apoptosis and necrosis) and potential DNA damage (genotoxic and mutagenic), after T-2 exposure in HepG2 cells.

8. To generate and to characterize HepG2 spheroids in both, standard plates and microfluidic devices.
9. To compare T-2 cytotoxicity and mechanisms of action obtained in HepG2 spheroids and co-culture spheroids of HepG2 and LX2 cells in microfluidic devices.

3. Resultados

Results

Food and Chemical Toxicology, 145 (2020), 111654

https://doi.org/10.1016/j.fct.2020.111654

3.1. T-2 toxin and its metabolites: characterization, cytotoxic mechanisms and adaptive cellular response in human hepatocarcinoma (HepG2) cells

Mercedes Taroncher*, Yelko Rodríguez-Carrasco, María-José Ruiz

Laboratory of Food Chemistry and Toxicology, Faculty of Pharmacy, University of Valencia, Av. Vicent Andrés Estellés s/n, 46100 Burjassot, Valencia, Spain

Abstract

The T-2 toxin (T-2) is a type A trichothecene produced by *Fusarium* species, and the most cytotoxic mycotoxin of the group. A study was made to determine T-2 cytotoxicity in human hepatocarcinoma (HepG2) cells; evaluate whether there is an adaptive response of HepG2 cells exposed to low concentrations of T-2; identify the T-2 metabolites by LC-Q-TOF MS; and determine whether T-2 disrupts cell proliferation in HepG2 cells. The IC_{50} values obtained ranged from 61.9 ± 2.4 nM to 70.7 ± 7.4 nM. No adaptive response was observed. There was no evidence of extra- or intracellular accumulation of T-2 after 24 h of exposure as determined by LC-Q-TOF MS. However, some T-2 metabolites such as HT-2 toxin, neosolaniol and T-2 triol showed important (>75%) intracellular accumulation. Cell distribution was significantly increased in $SubG_0/G_1$ phase (11.8-fold higher) and decreased (12%) in G_2/M phase at 60 nM T-2, versus the control. Simultaneously, increased necrosis (238%) and apoptosis/necrosis (up to 35.5%) were observed in HepG2 cells exposed to T-2. In conclusion, the results show that T-2 leads to loss of cell viability without an adaptive response, and that the metabolites generated play an important role in T-2 cytotoxicity, increasing HepG2 cell damage.

Key words: T-2 toxin; Metabolites; Adaptive response; Cell proliferation; Cellular damage; LC-Q-TOF MS.

* **Corresponding author**: Laboratory of Food Chemistry and Toxicology, Faculty of Pharmacy, University of Valencia, Av. Vicent Andrés Estellés, s/n, 46100, Burjassot, Valencia, Spain. E-mail address: Mercedes.taroncher@uv.es (M. Taroncher).

1. Introduction

Fusarium fungi produce various mycotoxins, including trichothecenes, with adverse effects upon humans and animals (Streit et al., 2012; van der Fels-Klerx et al., 2012). Trichothecenes are subdivided into four types (A-D) according to the substituents of the tetracyclic ring system. These mycotoxins frequently occur in cereals worldwide, notably in wheat, barley, maize, oats, rye and rice (Fatima et al., 2018). In such contaminated crops, mycotoxins and/or their metabolites can be found together, and their toxicological activities could result in cumulative additive or synergistic effects (EFSA, 2016, 2017). Considerable attention has been paid to T-2 toxin (T-2), a type A trichothecene, owing to its high toxicity (Fatima et al., 2018). According to the EFSA, T-2 and/or its metabolites were present in grains for human consumption in a significant number of collected samples from European countries, with oat being the food matrix showing the highest concentrations (41.7 μg/kg) (EFSA, 2017).

In vitro human liver microsomal incubations have been used in metabolic studies of mycotoxins, since liver microsomes contain a variety of enzymes that are involved in the formation of both phase I and phase II metabolites. Reactive metabolites can be broadly classified into electrophiles and radicals. Electrophilic reactive metabolites, formed in the presence of a toxic metabolizing system, are often able to form metabolites with small molecule trapping agents. In the scientific literature, several studies have revealed extensive metabolism of T-2 in the mammalian liver (Wu et al., 2014; Yang et al., 2017a, 2017b). Nowadays, state-of-the-art equipment such as liquid chromatography (LC) coupled to a tandem mass spectrometer (MS/MS) or a high-resolution mass spectrometer (HRMS) have become the standard in determining mycotoxins and/or their metabolites in biological matrices, and can provide indirect information on the

structure of the reactive species from which they are formed (Rodríguez-Carrasco et al., 2018). Nonetheless, few data are currently available regarding the detection of T-2 and its biotransformation products in tissues and biological fluids, thus complicating evaluation of the potential risks related to exposure to this mycotoxin (EFSA, 2017b). In this line, improved understanding of the metabolic fate of T-2 is of great interest from a toxicological point of view.

T-2 toxicity is related to food refusal, and increases the risk of septicemia and hemorrhage due to molecular effects such as apoptosis of leukocytes and thrombocytes (Steinkellner et al., 2019). Other cellular mechanisms observed are apoptosis, necrosis, lipid peroxidation and protein, DNA and RNA synthesis inhibition (Garreau De Loubresse et al., 2014; Fernández-Blanco et al., 2016). In line with the increased use and acceptance of non-animal testing worldwide, *in vitro* methods were selected in this work because they are suitable for determining mechanisms of toxicity of T-2, and are cheaper and briefer, and improve ethical aspects and the standardization and harmonization of results, compared to *in vivo* methods (EFSA, 2016).

On the other hand, some studies in various organisms suggest that biological systems may adapt to adverse effects of the environment. This adaptation is manifested by hormesis, and is based on the fact that chronic exposure to low levels of toxic agents may protect the organism against the negative effects of higher doses (Calabrese et al., 2007). Although T-2 has been tested for its cytotoxicity in different types of cell lines, no data are yet available on whether human cells are able to adapt to cellular damage secondary to continued exposure to T-2.

Knowledge about the toxicity of T-2 is crucial for risk assessment. Accordingy, the aims of the present study were to: (i) determine the cytotoxic

effect of T-2 in human hepatocarcinoma (HepG2) cells; (ii) identify the main T-2 metabolites using LC-Q-TOF MS; (iii) evaluate the adaptive response of HepG2 cells to adverse effects of T-2; and (iv) determine mechanisms of toxicity of T-2-induced cell damage.

2. Material and Methods

2.1 Reagents

The reagent grade chemicals and cell culture compounds used, namely Dulbecco's Modified Eagle's Medium (DMEM), penicillin, streptomycin, trypsin/EDTA solutions, phosphate buffered saline (PBS), HEPES, Newborn Calf Serum (NBCS), methylthiazoltetrazolium salt (MTT) dye, ribonuclease A from bovine pancreas (RNAase), annexin V-FITC, dimethyl sulfoxide (DMSO), t-octylphenoxypolyethoxyethanol (Triton-X 100), tris-hydroxymethyl aminomethane (Tris), propidium iodide (PI), formic acid (reagent grade, ≥95%) and ammonium formate (eluent additive for LC-MS, ≥99.0%) were acquired from Sigma-Aldrich (St. Louis, MO, USA). Methanol (MeOH) and ethyl acetate were purchased from Merck Life Science S.L. (Madrid, Spain). Deionized water (resistivity <18 MΩ cm) was obtained using a Milli-Q water purification system (Millipore, Bedford, MA, USA).

Standards of T-2 (MW: 466.52 g/mol), T-2 triol (MW: 382.45 g/mol), T-2 tetraol (MW: 298.33 g/mol), HT-2 toxin (HT-2; MW:424.48 g/mol), neosolaniol (NEO; MW: 382.40 g/mol), etoposide (MW: 588.56 g/mol) and 5-fluorouracil (5-Fu) (MW: 130.08 g/mol) were purchased from Sigma-Aldrich (St. Louis, MO, USA). Stock solutions of the mycotoxins were prepared in MeOH at appropriate working concentrations and maintained in the dark at -20 ºC.

2.2 Cell culture and treatment

Human hepatocarcinoma (HepG2) cells (ATCC: HB-8065) were cultured in DMEM medium supplemented with 10% NBCS, 100 U/ml penicillin and 100 mg/ml streptomycin. The incubation conditions were pH 7.4, 5% CO_2 at 37 °C and 95% air atmosphere at constant humidity. Cells were subcultured routinely twice a week with only a small number of sub-passages (< 40 subcultures) in order to maintain genetic homogeneity. The HepG2 cells were subcultured after trypsinization in 1:3 split ratio. The medium was changed every 2–3 days. The final mycotoxin concentrations tested were achieved by adding T-2 mycotoxin to the culture medium with a final MeOH concentration ≤1% (v/v). Appropriate controls containing the same amount of solvents were included in each experiment. Absence of mycoplasma was checked routinely using the MycoAlertTM PLUS Mycoplasma Kit (Lonza, Rockland, ME, USA).

2.3 *In vitro* cytotoxicity

Cytotoxic effects were determined in HepG2 cells by the MTT and Total Protein Content (PC) assays. They have been extensively used in *in vitro* toxicological studies for measuring cell proliferation and survival. The MTT assay determines the viability of cells by the reduction of soluble yellow tetrazolium salt, only in the metabolically active cells, via a mitochondrial-dependent reaction to an insoluble purple formazan crystal. The MTT viability assay was performed according to Ruiz et al. (2006). Briefly, the HepG2 cells were plated in 96-well culture plates at a density of 2×10^4 cells/well. After the cells reached 80% confluence, the culture medium was replaced with fresh medium containing serial dilutions of T-2. The range of T-2 concentrations was from 12.5 to 100 nM. The mycotoxin was exposed during 24 and 48 h. During

the exposure time, neither the medium nor the mycotoxin was replenished. After 24 and 48 h of exposure, the medium was removed and 200 µl of fresh medium was added to each well. Then, 50 µl of MTT was added per well, and the plates were returned to the incubator in the dark at 37 °C, 5% CO_2 during three hours. Then, the MTT solution was removed and 200 µl of DMSO was added followed by 25 µl of Sorensen´s glycine buffer. Plates were gently shaken for 5 min to achieve complete dissolution. Absorbance was measured at 540 nm using an automatic ELISA plate reader (MultiSkanEX, Thermo Scientific, MA, USA).

The PC method in turn is based on the increase in absorbance of Coomassie Brilliant Blue dye (Bio-Rad Laboratories, Madrid) when binding to proteins. The assay was performed in the same 96-well plates where the MTT test was carried out. First, the plates were washed with PBS, and each well received 200 µl of 0.1 N NaOH to dissolve the proteins. After 2 h of incubation at 37 °C and 5% CO_2, 170 µl of NaOH was removed from each well and 180 µl of diluted 22% Coomassie Brilliant Blue were added. The plates remained for 30 min at room temperature, and then absorbance was measured at 620 nm in an automatic ELISA plate reader (MultiSkanEX, Thermo Scientific, MA, USA).

For the MTT and PC assays, cell viability was expressed as a percentage relative to the control solvent (1% MeOH). Three independent experiments were conducted for each exposure time. The mean inhibition concentration (IC_{50}) values were calculated using SigmaPlot version 11 (Systat Software Inc., GmbH, Germany).

2.4 Adaptive response to mycotoxin exposure

In order to determine whether there is an adaptive response of HepG2 cells exposed to low concentrations of T-2, two assays (A and B) were simultaneously carried out. Assay A: The HepG2 cells were plated in 96-well culture plates at a density of 2×10^4 cells/well. After confluence, the culture medium was removed and replaced with fresh medium containing different concentrations of T-2 (10, 15 and 20 nM). Assay B: The HepG2 cells were plated in 96-well culture plates at a density of 2×10^4 cells/well. After confluence, the culture medium was replaced with fresh medium containing 0.25 or 2.5 nM T-2 during 2 h. Then, the culture medium was removed and replaced with fresh medium containing different concentrations of T-2 (10, 15 and 20 nM). This procedure is referred to as "pre-treatment assay" through the manuscript. In both assays, after 24 h of exposure, absorbance was measured at 540 nm using an automatic ELISA plate reader (MultiSkanEX, Thermo Scientific, MA, USA). Three independent experiments were performed, and the results were expressed as the mean ± standard error of the mean (SEM) of different independent experiments. Differences between control cells for each experiment (A and B) and cells not pretreated with T-2 mycotoxin were determined.

2.5. Concentration selection

General assays

The concentrations assayed in this study were selected considering that they were not cytotoxic for HepG2 cells and were below the IC_{50} values (from 61.9 ± 2.4 nM to 70.7 ± 7.4 nM). Three concentrations (15, 30 and 60 nM T-2) were tested in HepG-2 cells in this study.

Pre-treatment assays

The concentrations assayed in our study were selected considering two criteria. On one hand, they were required to represent levels of T-2 that could be reached through the diet, and on the other hand they were required to be non-cytotoxic for cells.

Different concentrations of T-2 toxin below IC_{50} (from 0.25 to 60 nM) were tested in HepG-2 cells; however, concentrations higher than 10 nM showed cytotoxicity (Figure 1S, supplementary data). To determine T-2 exposure in the population, the deterministic approach was used. In this approach, the estimated T-2 intake was calculated considering two factors: concentrations of T-2 reported in food (wheat and wheat-based products), and the average consumption of these food categories. The levels of T-2 exposure were calculated based on the occurrence of T-2 in wheat and wheat-based products reported in the latest scientific report of the EFSA (maximum level of T-2 found in breakfasts cereals for adults (4.47 μg/kg) and for infants and small children (0.11 μg/kg)) (EFSA, 2017), and the wheat and wheat-based products consumption data reported by the FAO for the Spanish population (0.27 kg/day) (FAOSTAT, 2020). According to the above, adults would be exposed to 2.59 nM T-2, whereas infants would be exposed to 0.064 nM T-2 through the consumption of this food category. The highest value selected in the pre-treatment assay (2.5 nM) is similar to that calculated using the deterministic approach. In addition, a lower T-2 concentration than the previously calculated concentration was also assayed in the pre-treatment assay, taking into account that infants and people sensitive to cereals (that is, gluten-free diets) could have significantly lower exposure to T-2. Hence, the T-2 concentrations tested in the pre-treatment assays were 0.25 and 2.5 nM.

2.6 Determination of T-2 and its metabolites by LC-Q-TOF MS

To determine the accumulation of T-2 and/or its metabolites or degradation products in culture medium, the extraction procedure described by Juan et al. (2014) was followed, with several modifications. First, the HepG2 cells were seeded in 6-well plates at a density of 47.2 x 10^4 cells/well until the cells reached confluence. Then, the culture medium was replaced with fresh medium containing 60 nM T-2. After 24 h of exposure, 0.5 mL of culture medium was collected from each well and transferred to a 4 mL Eppendorf Safe-Lock microcentrifuge tube. Three mL of ethyl acetate were added, and the mixture was shaken for 2 min with an Ultra-Turrax Ika T18 basic (Staufen, Germany) and centrifuged at 5600 × g for 5 min at 4 °C (Centrifuge 5810R, Eppendorf, Germany). The supernatant phase was collected and evaporated to dryness at 45 °C under a N_2 stream with a TurboVap-LV (Zymark, Allschwil, Switzerland) and then re-dissolved in 0.25 mL of a mixture of methanol:water (70:30, v/v) by vortexing vigorously (15 s), before transfer to a vial for analysis.

To determine the intracellular accumulation of T-2 and/or its metabolites or degradation products, 0.5 mL of culture medium containing cells was collected from the 6-well plates after 24 h of T-2 exposure at 60 nM, and allowed to proceed for the extraction procedure as described above. Simultaneously, the T-2 and the commercially available T-2 metabolites, namely T-2 triol, T-2 tetraol, HT-2 and NEO, were incubated in culture medium at the same concentrations and conditions (≤1% methanol). These samples were considered as controls and were used for recovery studies.

The analysis was performed using a liquid chromatography quadrupole time of flight mass spectrometry (LC-Q-TOF MS) system consisting of an LC Agilent 1200-LC system (Agilent Technologies, Palo Alto, CA, USA) equipped with a

vacuum degasser, an autosampler and a binary pump. The column was a Gemini NX-C18 (150 × 2 mm, i.d. 3 μm, Phenomenex, Torrance, CA, USA) with a guard column C18 (4 × 2 mm, i.d. 3 μM).

Mobile phases consisted of Milli-Q water with 0.1% formic acid and 5 nM ammonium formate as solvent system A, and methanol with 0.1% formic acid and 5 nM ammonium formate as solvent system B, with the following elution gradient: 0.5 min, 20% B; 0.5 min, 20–40% B; 5 min, 100% B; 2 min, decrease to 20% B, maintained 6 min. The flow rate used was 0.200 mL/min, and the total run time was 14 min. The sample volume injected was 20 μl.

The mass spectrometry (MS) analysis was carried out using a 6540 Agilent Ultra- High-Definition Accurate-Mass Q-TOF MS, equipped with an Agilent Dual Jet Stream electrospray ionization (Dual AJS ESI) interface in positive ionization mode. Operation conditions were as follows: sheath gas temperature 350 °C at a flow rate of 8 L/min, capillary voltage 3500 V, nebulizer pressure 45 psig, drying gas 10 L/min, gas temperature 300 °C, skimmer voltage 65 V, octopole RF peak 750 V, and fragmentor voltage 130 V. Analyses were performed using AutoMS/MS mode with fixed collision energy (10, 20 and 30) and in a mass range of 50–1000 *m/z*. The acquisition rate was 3 spectra/second. Acquisition data were processed with Agilent MassHunter Workstation software.

2.7 Measurement of necrosis-apoptosis by Annexin Y FITC-PI

Cell death generally proceeds through two molecular mechanisms: necrosis and apoptosis. During apoptosis, the externalization of phosphatidylserine (PS) to the outer layer of the plasma membrane occurs. The different populations of apoptotic cells (early or late), and necrotic and dead cells were identified by

Annexin V-FITC/PI double staining (Vermes et al., 1995). Annexin V is a Ca^{2+} -dependent phospholipid-binding protein with high affinity for PS, and binds to cells exposing PS to the extracellular side of the plasma membrane, whereas PI binds to the DNA of necrotic/dead cells. Viable cells with intact membranes exclude PI, whereas the membranes of dead and damaged cells are permeable to PI. Cells considered as viable are both Annexin V-FITC-/PI- negative; cells in early apoptosis (pro-apoptotic / apoptotic cells) are Annexin V-FITC+/PI-. Cells stained negative for Annexin V-FITC and positive for PI represented necrotic cells. Cells stained positive for both Annexin V-FITC and PI corresponded to late apoptotic/necrotic cells. For the Annexin V-FITC assay, 47.2 x 10^4 cells/well were seeded in 6-well plates. After 2 and 24 h of exposure at 15, 30 and 60 nM T-2, cells were trypsinized and resuspended in 360 µl of Hepes-Ca^{2+} buffer prepared as follows: 10 mM Hepes-NaOH (pH 7.4), 135 mM NaCl and 2.5 mM $CaCl_2$. After incubation at 4°C for 30 min in darkness, 10,000 cells were acquired and analyzed by BD LSRFortessa (BD Biosciences) flow cytometry. Quadrant statistics were performed to determine viable cells, early apoptotic cells, late apoptotic/necrotic cells and necrotic cells from the total population of cells. Three independent experiments were performed for each T-2 exposure time and concentration, and the results were expressed as the mean ± standard error of the mean (SEM) of different independent experiments.

2.8 Cell cycle distribution

Cell cycle analysis was performed using Vindelov's PI staining solution as described previously by Juan-García et al. (2013). The PI solution is a fluorescent DNA intercalating agent able to bind and label double-stranded nucleic acids, making it possible to achieve rapid and precise evaluation of cellular DNA

content by flow cytometric analysis. The cell cycle is monitored by different key checkpoints or decision points on whether the cell should divide, delay division, or enter a resting stage. 5-Fluorouracil (5-Fu) inhibits thymidylate synthase, which blocks synthesis of the nucleoside thymidine, and thus affects DNA synthesis in the S phase. The etoposide inhibits DNA topoisomerase II and exerts its effects at the G_2-M checkpoint. Etoposide and 5-Fu were used as positive control. A total of 47.2 x 10^4 cells/well were seeded in 6-well plates and exposed to 15, 30 and 60 nM T-2 during 24 h. Then, the cells were trypsinized and placed on ice for 30 min with 1 mL of fresh medium containing Vindelov's PI staining solution prepared as follows: 40 μg/mL RNAase, 0.1% Triton X-100, 10 mM Tris, 10 mM NaCl and 50 μg/ml of PI in PBS. Fifty thousand cells for each sample were analyzed using BD LSRFortessa (BD Biosciences) flow cytometry. The experiments were carried out in triplicate, and the results were expressed as the mean ± SEM of different independent experiments.

2.9 Statistical analysis

The statistical analysis of the data was carried out using the SPSS version 24.0 statistical package (IBM Corp., Armonk, NY, USA). Data were expressed as the mean ± SEM of different independent experiments. The statistical analysis of the results was performed using the Student *t*-test for paired samples. Differences between groups were analyzed using one-way analysis of variance (ANOVA) followed by the Tukey HDS post hoc test for multiple comparisons. Statistical significance was considered for $p \leq 0.05$.

3. Results

3.1 *In vitro* cytotoxicity

The cytotoxic effect of T-2 upon HepG2 cells was evaluated by the MTT and PC assays over 24 h and 48 h to determine the molar concentration of T-2 that reached 50% inhibition of cellular proliferation (IC_{50}). Cells exposed to T-2 revealed a decrease in cell viability in a time- and concentration-dependent manner by MTT and PC assay (Fig. 1). The IC_{50} values obtained by MTT assay were 68.6 ± 4.8 nM and 61.9 ± 2.4 nM at 24 h and 48 h, respectively. The IC_{50} values obtained by PC assay were 70.7 ± 7.4 nM and 65.0 ± 6.0 nM, respectively.

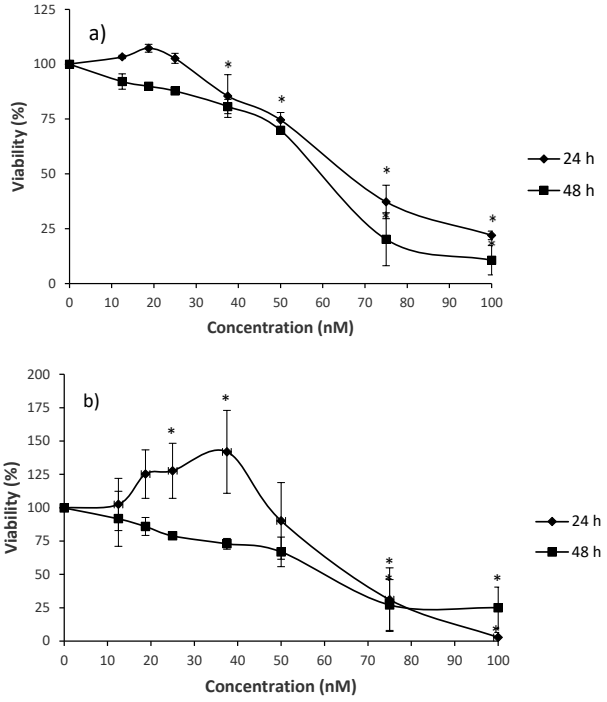

Figure 1. Concentration-effect curves of T-2 in HepG2 cells after 24 and 48 h of exposure by MTT assay a) and PC assay b). The concentrations of T-2 mycotoxin were from 0 to 100 nM. Data are expressed as the mean ± SEM (n=3). (*) $p \leq 0.05$ indicates significant differences compared to the control.

3.2. Cell adaption to T-2 exposure

To determine HepG2 cell adaptation to low T-2 concentrations, HepG2 cell viability after 2 h of pre-treatment (0.25 and 2.5 nM T-2) was compared against cell viability without pre-treatment (Figure 2). Figure 2 shows cell viability in the pre-treatment assays with MTT. The no pre-treatment assay showed a significant increase in cell viability of 48% and 10% after exposure to 15 and 20 nM T-2, respectively, compared to the control (Figure 2). The increase in cell viability can be due to the hormetic effect in HepG2 cells, which was observed with 15 and 20 nM (Figure 2) and 37.5 nM T-2 (Figure 1b). The pre-treatment assay with 0.25 nM T-2 showed a 20% increase in viability after exposure to 20 nM T-2 versus the control, whereas pre-treatment with 2.5 nM T-2 did not significantly increase cell viability versus the control. Moreover, the results in Figure 2 evidence a greater cytotoxic effect in pre-treated HepG2 cells than in cells without pre-treatment. Tukey's multiple comparison test showed pre-treatment of cells with 0.25 nM T-2 to result in a 24% decrease in cell viability, while pre-treatment with 2.5 nM T-2 reduced cell viability from 11% to 35% versus no T-2 pre-treatment (Figure 2).

3.3 Accumulation of T-2 and detection of putative metabolites in media and HepG2 cells

On one hand, the HepG2 cells were exposed to 60 nM for 24 h, and then the medium was removed and T-2 and/or its metabolites were determined according to section 2.6. On the other hand, the cells were re-dissolved in 0.5 mL of fresh medium, and the intracellular accumulation of T-2 and/or its metabolites was also determined according to section 2.6.

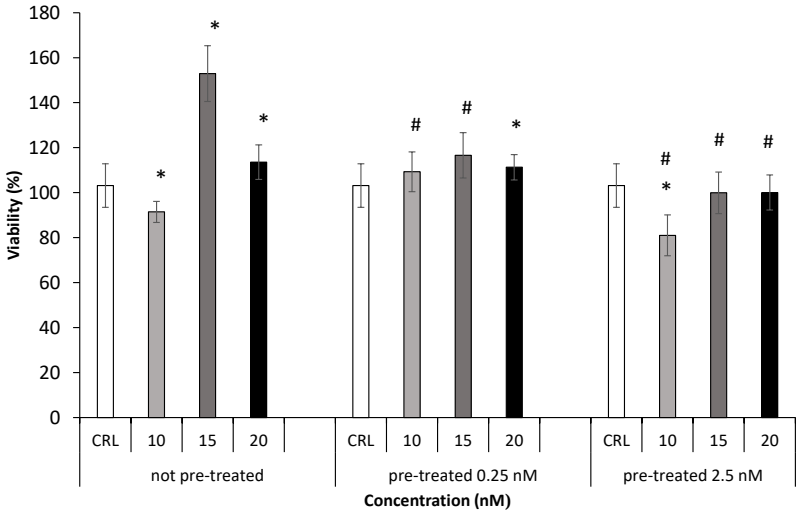

Figure 2. Viability (%) of HepG2 cells exposed during 24 h to 10, 15 and 20 nM T-2; and viability (%) of HepG2 cells after pre-treatment with different concentrations of T-2 (0.25 and 2.5 nM) during 2 h, and subsequent addition of fresh medium with serial dilutions of T-2 (10, 15 and 20 nM) for 24 h. Results were expressed as the mean ± SEM of three independent experiments. (*) $p \leq 0.05$ indicates a significant difference compared to control (CRL). (#) $p \leq 0.05$ indicates a significant difference compared to non-pre-treated assay.

Figure 3 shows the chromatograms obtained by LC-Q-TOF MS. Results from the control revealed a peak at 11.68 min which in full scan MS showed a stable and abundant ammonium adduct $[M+NH_4]^+$ at m/z 484.2541 corresponding to T-2 under positive electrospray ionization (ESI) mode (Fig. 3A). In addition, product ions (m/z 365, 305, 245 and 215) were generated by collision-induced dissociation of the T-2 ammonium adducts (Fig. 3B). These observed fragments corresponded to the loss of isovaleric acid chain at the C-8 position, acetic acid chains at positions C-4 and C-15, and loss of CO from the epoxy ring, in agreement with the literature (Yang et al., 2017a).

Nonetheless, results from cells exposed to T-2 revealed that there was no intracellular accumulation of this mycotoxin, since neither the characteristic ammonium adduct $[M+NH_4]^+$ nor the fragment ions were detected after 24 hours of T-2 exposure. Similar results were also found in the analyzed culture medium. However, several peaks were observed at different signal intensities in both culture medium and cells (Table 1). These peaks were also observed in the control and were identified as T-2 metabolites based on their mass spectra and retention times (R_t). The peak observed at Rt = 10.91 min was identified as HT-2, since it exhibited R_t and mass spectra consistent with the analytical standard of HT-2 (control), which showed a stable and abundant ammonium adduct $[M+NH_4]^+$ at m/z 442.2439 under ESI+ mode (Fig. 3C3). Other peaks with much weaker signal intensities (trace levels) than the HT-2 peak were observed at m/z 383.2064 and at m/z 400.1966, which corresponded to protonated T-2 triol (R_t = 9.70 min; Fig. 3C2) and ammonium adduct of NEO (R_t = 8.86 min; Fig. 3C1), respectively, since they exhibited the same physicochemical behaviour as the standards (control).

The different distributions of the detected mycotoxins in both the intracellular and the extracellular (culture medium) compartments are shown in Table 1. Results evidenced that T-2 is rapidly and completely metabolized by HepG2 cells, being mainly biotransformed into HT-2 toxin (94.1%), which was quantified at 56.40 nM. Other T-2 metabolites, namely NEO and T-2 triol, were also quantified but at significantly lower levels (NEO at 3.31 nM and T-2 triol at 0.15 nM). In all cases, intracellular accumulation of the detected T-2 metabolites was higher than (>75%) the levels observed in culture medium (Table 1).

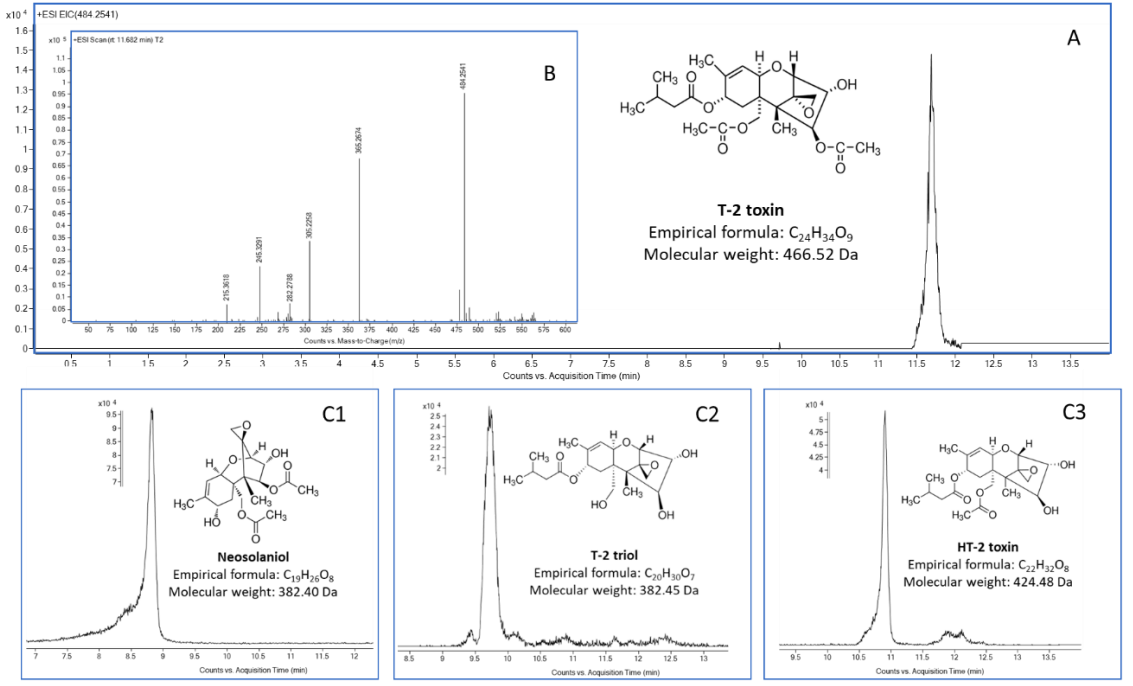

Figure 3. Extracted ion chromatogram (A) and the secondary mass (MS/MS) chromatogram (B) of T-2 in culture medium before HepG2 exposure, and extracted ion chromatograms of neosolaniol (C1), T-2 triol (C2) and HT-2 toxin (C3) detected at intracellular level after 24 h of exposure.

Table 1. Detection of T-2 and its metabolites in HepG2 cells after 24 h exposure to 60 nM T-2, and their distribution in the intracellular and extracellular compartments.

Mycotoxin	Intracellular concentration, nM (%)	Culture medium, nM (%)	Distribution in both compartments, nM (%)
T-2	*n.d.*	*n.d.*	*n.d.*
HT-2	44.27	12.13	56.40 (94.00)
NEO	2.95	0.36	3.31 (5.52)
T-2 triol	0.15	*n.d.*	0.15 (0.25)
Total	47.37 (78.95)	12.49 (20.82)	59.86 (99.77)

n.d.: not detected

3.4 Analysis of necrosis-apoptosis

The mechanism of induction of cell death was studied to determine the death pathway leading to the decline in cell proliferation. The early apoptotic, late apoptotic/necrotic and necrotic cells induced by the studied T-2 concentrations (15, 30 and 60 nM) after 2 h and 24 h of exposure in HepG2 cells are shown in Figures 5 and 6, respectively. No significant increase in early apoptotic, late apoptotic/necrotic or necrotic cells exposed to T-2 for 2 h was observed versus the control, indicating that under the studied conditions these death pathways are not activated in HepG2 cells (Fig. 4). However, after 24 h, a dose-dependent increase in early apoptotic, late apoptotic/necrotic and necrotic cells was observed (Fig. 5b-5d) with respect to the control cells (Fig. 5a). The early apoptotic cell population increased 18.97 ± 3.07% (30 nM T2) and 29.07 ± 3.25% (60 nM T2) with respect to the control (11.03 ± 1.31%) (Fig. 5e). Tukey's multiple comparison test indicated that significant differences between 15 and 30 nM (60%), between 15 and 60 nM (145%) and between 30 and 60 nM (53%) of T-2 were observed related to the early apoptotic cell population in HepG2

cells after 24 h of exposure. The apoptotic/necrotic (late apoptotic) cell population increased 12.27 ± 2.34% (30 nM) and 35.47 ± 8.24 % (60 nM) as compared with the control cells (5.30 ± 0.66%) (Fig. 5e). Moreover, according to Tukey's multiple comparison test, significant differences between 15 and 30 nM (105%), between 15 and 60 nM (approximately 495%) and between 30 and 60 nM (201%) of T-2 were observed related to the late apoptotic cell population in HepG2 cells after 24 h of exposure. Lastly, the necrotic cells increased at the highest concentration of 60 nM (5.43 ± 1.15%) versus the control (1.60 ± 0.69%) (Fig. 5e). The increase between the control and 60 nM was 238%. Tukey's multiple comparison test revealed significant differences between 30 and 60 nM (202%), but no differences between 15 and 30, and between 15 and 60 nM T-2 were observed related to necrotic cells after 24 h of exposure.

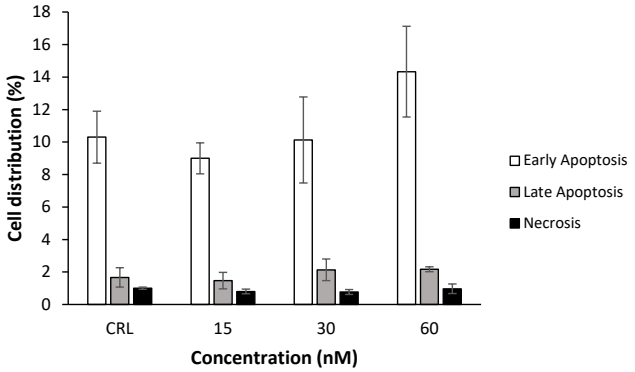

Figure 4. Analysis of apoptosis/necrosis induction in HepG2 cells after exposure to different T-2 concentrations (15, 30 and 60 nM) for 2 h. Cells were stained with Annexin V-FITC and PI to distinguish early apoptotic cells, late apoptotic/necrotic cells and necrotic cells. Data are expressed as the mean ± SEM of three independent experiments. No significant differences versus control (CRL) were observed.

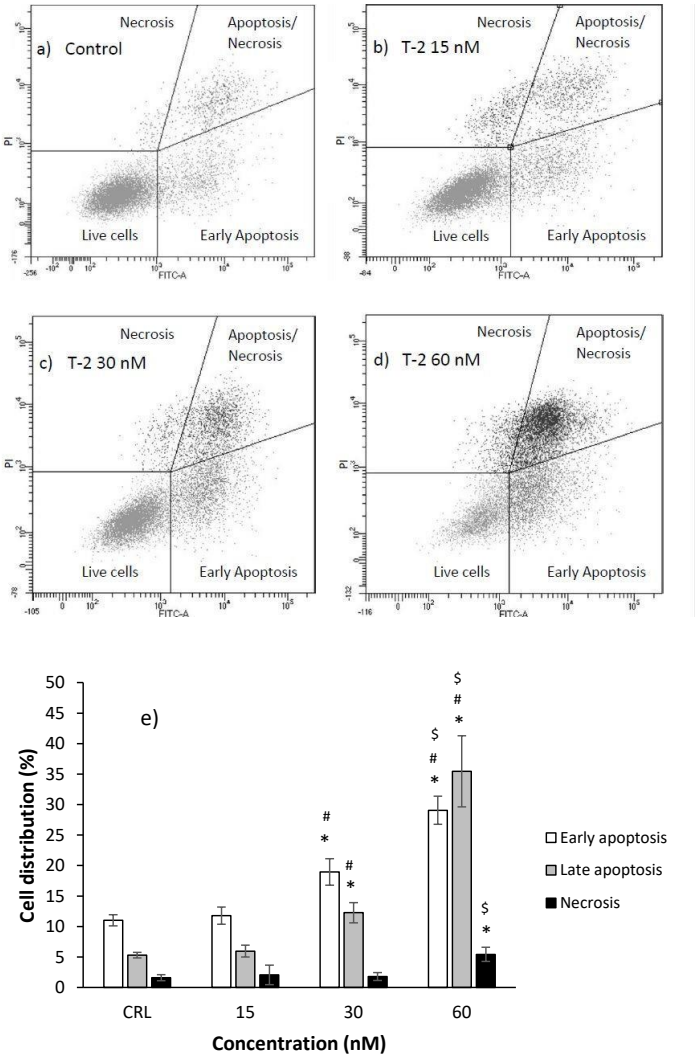

Figure 5. Analysis of apoptosis/necrosis induction in HepG2 cells after exposure to different T-2 concentrations (15, 30, and 60 nM) for 24 h. Cells were stained with Annexin V-FITC and PI to distinguish early apoptotic, apoptotic/necrotic (late apoptotic) and necrotic cells. a-d) Two-dimensional dot plots of FITC Annexin V versus PI through flow cytometry. e) Percentage of early apoptotic, apoptotic/necrotic (late apoptotic) and necrotic cells. Data are expressed as the mean ± SEM of three independent experiments. (*) $p \leq 0.05$ indicates a significant difference compared to control (CRL). (#) $p \leq 0.05$

indicates a significant difference compared to 15 nM T-2. (\$) $p \leq 0.05$ indicates a significant difference compared to 30 nM T-2.

3.5. Cell cycle distribution

Analysis of DNA content by flow cytometry provides a measure of cell cycle perturbation in HepG2 cells after T-2 exposure. Cells were incubated for 24 h with 15, 30 and 60 nM T-2 (Fig. 6). The G_2/M phase significantly increased (10.1%) at 15 nM T-2 versus the control. In contrast, a reduction of 12.5% in G_2/M phase was observed at 60 nM compared to the control (Fig. 6a). Tukey's multiple comparison test indicated that the percentage cell distribution in G_2/M phase was significantly lower ($p \leq 0.05$) after 60 nM T-2 compared to 15 nM T-2. The subG_0/G_1 phase showed a significant increase (11.8-fold higher) at the highest concentration assayed (60 nM) versus the control. Tukey's multiple comparison test showed the percentage cell distribution in subG_0/G_1 phase to be significantly higher ($p \leq 0.05$) after HepG2 cell exposure to 60 nM T-2 compared to 15 and 30 nM T-2. The G_0/G_1 phase evidenced a significant decrease (1.11-fold) at 30 nM T-2 with respect to the control. Tukey's multiple comparison test showed the percentage cell distribution in G_0/G_1 phase to be significantly lower ($p \leq 0.05$) after HepG2 cell treatment with 30 nM T-2 compared to 15 and 60 nM T-2.

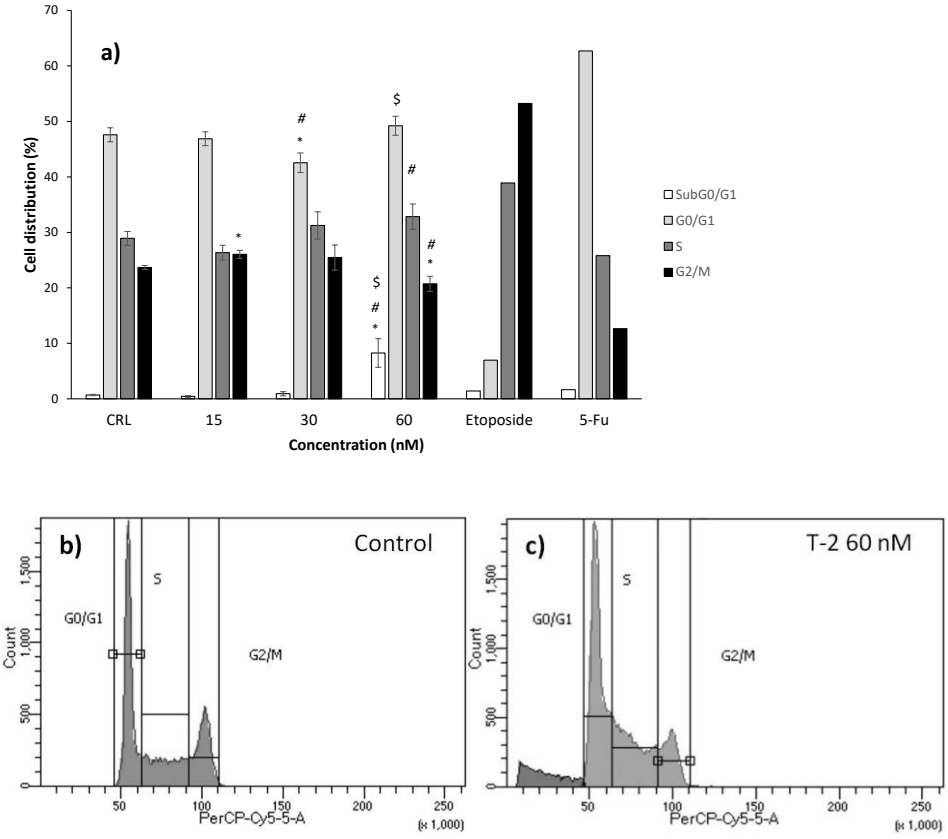

Figure 6. Analysis of cell cycle distribution of HepG2 cells after exposure to different T-2 concentrations (15, 30 and 60 nM) during 24 h. Cells were stained with Vindelov's PI solution and subjected to cell cycle analysis by flow cytometry. a) Percentage (%) of cell distribution in HepG2 cells. b) Histogram of control cells. c) Representative histogram of HepG2 cells exposed to 60 nM T-2 for 24 h. Data are expressed as the mean ± SEM of three independent experiments. Etoposide (2500 nM) and 5-Fu (15000 nM) were used as positive controls. (*) $p \leq 0.05$ indicates a significant difference compared to control (CRL). (#) $p \leq 0.05$ indicates a significant difference compared to 15 nM T-2. ($) $p \leq 0.05$ indicates a significant difference compared to 30 nM T-2.

4. Discussion

Over the years there have been many studies from different parts of the world describing the toxic effects of T-2 in different cell lines (Wu et al., 2014). The T-2 toxin has received much attention because it is the most toxic of all the trichothecenes, though it is less frequently detected compared to the rest of the trichothecenes (Taroncher et al., 2020). In the present study we assayed the effects of T-2 upon HepG2 cells, since liver cells could represent a possible target of exposure through either inhalation or ingestion, with subsequent systemic distribution (Dinu et al., 2011). Different IC_{50} values have been described for T-2 in various cell types of human and animal origin (Agrawal et al., 2015). The IC_{50} values obtained in the present study revealed that T-2 reduces cell viability in a dose- and time-dependent manner as determined by the MTT assay. Our results show that T-2 inhibits HepG2 cell proliferation at low nanomolar concentrations after 24 h of exposure, in concordance with the observations of other authors. The IC_{50} values for T-2 ranged from 38.0 ± 0.12 nM in HepG2 cells to 14,830 ± 4,440 nM in Caco-2 cells (Fernández-Blanco et al., 2018; Romero et al., 2016) after 24 h of exposure, and from 22.19 nM in L-02 cells to 230 ± 18 nM in RPTEC cells (Lei et al., 2017; Weidner et al., 2012). Differences between IC_{50} values obtained for T-2 could be explained by different cell sensitivities depending on the cell type and cytotoxic assay conditions, among other factors.

On the other hand, low cytotoxicity was observed with exposure to 50 nM T-2 during 24 h as determined by PC assay (Fig. 1b). Whereas higher cytotoxicity was observed at ≥ 75 nM T-2 concentration, at lower concentrations (≤ 37.5 nM) a hormetic effect was detected. The increase in cell viability at low concentrations could suggest an adaptive response to T-2 exposure. The cellular

behavior characterized by low concentration stimulation and high concentration inhibition of cell proliferation has been previously detected in other cells lines exposed to a wide variety of mycotoxins (Fernández-Blanco et al., 2016; Lombardi et al., 2012; Meca et al., 2011; Prosperini et al., 2014). Therefore, in order to determine whether HepG2 cells exhibit an adaptive effect, they were pre-treated with low T-2 concentrations prior to T-2 exposure during 24 hours. Contrary to expectations, our findings clearly suggested that low pre-treatment exposure did not have any adaptive effect in HepG2 cells. Therefore, further evaluation of T-2 and its metabolites was made to check whether the combination of them was able to increase the cytotoxic effects produced by T-2 in HepG2 cells.

Toxicological screening of degradation of T-2 in mammalian cell culture provides insights to the potential toxic effects in a target organ/system *in vivo*. In this way, in the regulatory context could be discussing the current status related to the safety assessment of T-2 and its metabolites. According to the literature, T-2 leads to the formation of a wide range of metabolites, with HT-2 being the predominant metabolite. This is in agreement with the results obtained our study (Figure 3). Other metabolites were also identified based on their mass spectra and R_t, but at lower concentrations, namely NEO and T-2 triol. These T-2 metabolites can be formed by deacetylation reactions or by removal of the C-8 isovaleryl groups, as reported in the literature (Knutsen et al., 2017). There were also other ions that could be putatively identified as minor oxidation products, but they showed very low intensities, and further identification was therefore not possible. The data reported herein confirm that T-2 is rapidly and completely metabolized, and results in the formation of much more polar compounds based on their R_t. The identified T-2 biotransformation products were found in

significantly greater amounts at intracellular level (Table 1). Furthermore, our results confirm that hydrolysis is the main pathway of T-2 metabolism, in concordance with the results recently reported by other authors (Knutsen et al., 2017; Wu et al., 2014). The metabolites generated in this study may be specific of HepG2 cells, though some may allow general predictions from the *in vitro* to the *in vivo* setting.

Therefore, in order to assess whether T-2 disrupts cell proliferation, cell cycle distribution and apoptosis were further studied. The cell cycle can be activated (proliferation) or inhibited (arrest) through different mechanisms according to the factors that act upon it. These mechanisms may exert beneficial effects in the case of cancer therapeutics or detrimental effects - often as a consequence of DNA damage. It has been reported that normal progression of the cell cycle could be affected by DNA damaging events particularly in the S or G_2/M phases, which are monitored by checkpoints that determine progression into the next stage if DNA damage is not detected (Prosperini et al., 2013). When DNA damage is irreparable, checkpoints eliminate such potentially hazardous cells through permanent cell-cycle arrest or cell death. In our study it has been observed that T-2 is able to disturb the normal progression of proliferating HepG2 cells. After 24 h, 15 nM T-2 caused a significant accumulation of cells in the G_2-M phase (Figure 6), which may indicate that a cell response to low doses inducing mitosis. This stimulation of mitosis may be an evolutionarily conserved process (Calabrese et al., 2007). However, cell cycle arrest is produced in G_2/M after the highest concentration of T-2 tested, which could be due to DNA damage (at a dose similar to its IC_{50}), suggesting that T-2 may impair mitosis (Fig. 6a). In this study, 60 nM T-2 resulted in G_2/M phase arrest, and the cells entered apoptosis. On the other hand, the reduction of cell distribution in the

G_0/G_1 phase observed with 30 nM T-2 corroborates the induction of apoptosis in HepG2 cells at 24 h of exposure (Fig 5a). The G_0/G_1 phase is a period when cells make critical decisions about their destiny, including the optional requirement to replicate DNA and complete the cell division cycle. Importantly, the checkpoints alarmed by genotoxic stress can delay cell-cycle progression even when cells have already passed this restriction point. Thus, depending on the nature of DNA damage, the cell cycle can maintain G_0/G_1 block (Bartek and Lukas, 2001; Fernández-Blanco et al., 2016). Behaviour similar to that recorded in the present study has been reported by Lei et al. (2017). These authors found that in C28/I2, L-02 and HK-2 cells, T-2 causes significant arrest in the G_0/G_1 phase, accompanied by a decreased accumulation of cells in the G_2/M phase when compared to untreated control cells. However, the tested doses (0.02 nM) were lower than in our study.

Moreover, a significant increase in the proportion of cells in the $SubG_0/G_1$ phase was seen with 60 nM T-2, which suggests that the cell cycle is arrested. This is also related to the fact that this T-2 concentration results in an increase in percentage cell early apoptosis, late apoptosis and necrosis (Fig. 5). These results are consistent with data found in the literature (Weidner et al., 2012; Agrawal et al., 2015). The mentioned increase in the proportion of cells in the $SubG_0/G_1$ phase could be a consequence of p21 protein, which comes into play as a result of DNA damage in IMR-32 cells. Moreover, G_0/G_1 phase arrest occurs to repair the damaged DNA through the activation of poly(ADP-ribose) polymerase (PARP) in order to avoid cell death by necrosis (Agrawal et al., 2015).

5-Fluorouracil disrupts DNA replication causing G_2/M phase arrest, DNA damage and cell death in the treated cells. The T-2 toxin showed behavior similar to that of 5-Fu in HepG2 cells. The cell cycle perturbation could be explained

by a checkpoint response to damaged DNA, or may represent an adaptive process in which a surveillance mechanism delays or arrests the cell cycle when DNA lesions occur in order to repair them (Abid-Essefi et al., 2003; Prosperini et al., 2013). If DNA damage is not repaired in the cells, the latter may experience apoptosis or necrosis. The results obtained in this study demonstrate that the apoptotic effect was maintained at all T-2 concentrations in a dose-dependent manner in HepG2 cells after 24 h of exposure. In contrast, necrosis was only induced at 60 nM T-2 (Fig. 5), which is consistent with arrest of the cell cycle at this concentration. The induction of apoptosis by T-2 has been confirmed by Lei et al. (2017) in C28/I2, L-02 and HK-2 cells; however, these authors tested lower doses (0.02 nM) than in our study. In the same manner, Wu et al. (2019) and Agrawal et al. (2014) reported an increase in total (early and late) apoptosis in L-02 and IMR-32 cells. Thus, in concordance with the results obtained in our study, T-2 is seen to cause apoptosis in various cell types. However, differences in the results of the abovementioned authors versus those obtained in our study could be explained by the different endpoints, exposure times and cell lines involved, and by the sensitivity of the applied tests, which could condition response.

According to data obtained in our study, potential DNA damaging activity has been evidenced after T-2 exposure in HepG2 cells. Several studies have shown that T-2 induces apoptosis through the reactive oxygen species-mediated mitochondrial pathway in different cell types (Wu et al., 2011; Fang et al., 2012; Ren et al., 2015). Also, it has been shown that oxidative stress is associated with p53-dependent cell cycle arrest, DNA repair and apoptosis (Agrawal et al., 2015; Liu et al., 2008). Moreover, Wu et al. (2019) determined that T-2 treated L-02 cells exhibited an increase in the cleavage of PARP-1 and the pro-apoptotic

factor Bax, causing activation of the caspase cascade, which is involved in apoptosis of the L-02 liver cell line. In conclusion, multiple pathways are involved in T-2 toxin-induced cellular damage, with mechanisms that generate a large number of T-2 metabolites. Further research is thus required, focusing on the mechanisms of toxicity of T-2 and its metabolites.

Acknowledgments

We are grateful for technical assistance from the SCSIE of the University of Valencia (Valencia, Spain). This research was funded by the Generalitat Valenciana (Project grant, PROMETEO 2018/216).

Conflicts of interest statement: The authors declare that they have no conflicts of interest. The funders had no role in the design of the study, in the analyses or interpretation of the data, in the writing of the manuscript, or in the decision to publish the results.

5. References

Abid-Essefi, S., Baudrimont, I., Hansen, W., Ouanes, Z., Mobio, TA., Anane, R., Creppy, EE., Bacha, H., 2003. DNA fragmentation, apoptosis and cell cycle arrest induced by zearalenone in cultured DOK, Vero and Caco-2 cells: prevention by Vitamin E. Toxicology 192, 237-248. https://doi.org/10.1016/S0300-483X(03)00329-9

Agrawal, M., Bhaskar, A.S.B., Rao, P.V.L., 2015. Involvement of Mitogen-Activated Protein Kinase Pathway in T-2 Toxin-Induced Cell Cycle Alteration and Apoptosis in Human Neuroblastoma Cells. Mol. Neurobiol. 51, 1379–1394. https://doi.org/10.1007/s12035-014-8816-4

Agrawal, YO., Sharma, PK., Shrivastava, B., Ojha, S., Upadhya, HM., Arya, DS., Goyal, SN., 2014. Hesperidin Produces Cardioprotective Activity via PPAR-gamma Pathway in Ischemic Heart Disease Model in Diabetic Rats. Plos One, 9 (11), e111212 https://doi.org/10.1371/journal.pone.0111212

Bartek, J., Lukas, J., 2001. Mammalian G1- and S-phase checkpoints in response to DNA damage. Curr. Opin. Cell. Biol. 13, 738-747. https://doi.org/10.1016/S0955-0674(00)00280-5

Bouaziz, C., Bouslimi, A., Kadri, R., Zaied, C., Hassen, B., Salwa, AE., 2013. The in vitro effects of zearalenone and T-2 toxins on Vero cells. Exp. Toxicol. Pathol. 65,497-501. https://doi.org/10.1016/j.etp.2012.02.005

Calabrese, E.J., Bachmann, K.A., Bailer, A.J., Bolger, P.M., Borak, J., Cai, L., Cedergreen, N., Cherian, M.G., Chiueh, C.C., Clarkson, T.W., Cook, R.R., Diamond, D.M., Doolittle, D.J., Dorato, M.A., Duke, S.O., Feinendegen, L., Gardner, D.E.,

Hart, R.W., Hastings, K.L., Hayes, A.W., et al., 2007. Biological stress response terminology: Integrating the concepts of adaptive response and preconditioning stress within a hormetic dose-response framework. Toxicol. Appl. Pharm. 222, 122–128. https://doi.org/10.1016/j.taap.2007.02.015

Dinu, D., Bodea, G.O., Ceapa, C.D., Munteanu, M.C., Roming, F.I., Serban, A.I., Hermenean, A., Costache, M., Zarnescu, O., Dinischiotu, A., 2011. Adapted response of the antioxidant defense system to oxidative stress induced by deoxynivalenol in Hek-293 cells. Toxicon 57, 1023–1032. https://doi.org/10.1016/j.toxicon.2011.04.006

EFSA, 2017a. Panel on Contaminants in the Food Chain (CONTAM); Scientific Opinion on Appropriateness to set a group health based guidance value for T2 and HT2 toxin and its modified forms. EFSA J. 15, 4655. https://doi.org/10.2903/j.efsa.2017.4655

EFSA, 2017b. Panel on Contaminants in the Food Chain (CONTAM); Scientific Report on Human and animal dietary exposure to T-2 and HT-2 toxin. EFSA J. 15, 4972. https://doi.org/10.2903/j.efsa.2017.4972

EFSA, 2016. Guidance on the establishment of the residue definition for dietary risk assessment. EFSA J. 14, 4549. https://doi.org/10.2903/j.efsa.2016.4549

EFSA, 2011. Panel on Contaminants in the Food Chain (CONTAM); Scientific Opinion on the risks for animal and public health related to the presence of Alternaria toxins in feed and food. EFSA J. 9, 2407. https://doi.org/10.2903/j.efsa.2011.2407

Fang, HQ., Wu, YL., Guo, JB., Rong, J., Ma, L., Zhao, ZM., Zuo, DY., Peng, Q., 2012. T-2 toxin induces apoptosis in differentiated murine embryonic stem cells through reactive oxygen species-mediated mitochondrial pathway. Apoptosis 17, 895-907. https://doi.org/10.1007/s10495-012-0724-3

Fatima, Z., Guo, P., Huang, D., Lu, Q., Wu, Q., Dai, M., Cheng, G., Peng, D., Tao, Y., Ayub, M., ul Qamar, M.T., Ali, M.W., Wang, X., Yuan, Z., 2018. The critical role of p16/Rb pathway in the inhibition of GH3 cell cycle induced by T-2 toxin. Toxicology 400–401, 28–39. https://doi.org/10.1016/j.tox.2018.03.006

Fernández-Blanco, C., Elmo, L., Waldner, T., Ruiz, M.J., 2018. Cytotoxic effects induced by patulin, deoxynivalenol and toxin T2 individually and in combination in hepatic cells (HepG2). Food Chem. Toxicol. 120, 12–23. https://doi.org/10.1016/j.fct.2018.06.019

Fernández-Blanco, C., Juan-García, A., Juan, C., Font, G., Ruiz, M.J., 2016. Alternariol induce toxicity via cell death and mitochondrial damage on Caco-2 cells. Food Chem. Toxicol. 88, 32–39. https://doi.org/10.1016/j.fct.2015.11.022

Food Balance Sheet, (2020, March 20). FAOSTAT, http://faostat.fao.org.

Garreau De Loubresse, N., Prokhorova, I., Holtkamp, W., Rodnina, M. V., Yusupova, G., Yusupov, M., 2014. Structural basis for the inhibition of the eukaryotic ribosome. Nature 513, 517–522. https://doi.org/10.1038/nature13737

Juan, C., Manyes, L., Font, G., Juan-García, A., 2014. Evaluation of immunologic effect of Enniatin A and quantitative determination in feces, urine and serum on treated Wistar rats. Toxicon 87, 45-53. https://doi.org/10.1016/j.toxicon.2014.05.005

Juan-García, A., Manyes, L., Ruiz, M.J., Font, G., 2013. Involvement of enniatins-induced cytotoxicity in human HepG2 cells. Toxicol. Lett. 218, 166-173. https://doi.org/10.1016/j.toxlet.2013.01.014

Knutsen, HK., Barregard, L., Bignami, M., Bruschweiler, B., Ceccatelli, S., Cottrill, B., Dinovi, M., Edler, L., Grasl-Kraupp, B., Hogstrand, C., Hoogenboom, L., Nebbia, C.S., Oswald, I., Petersen, A., Rose, M., Roudot, AC., Schwerdtle, T., Vleminckx, C., Vollmer, G., Wallace, H., et al., 2017. Appropriateness to set a group health based guidance value for T2 and HT2 toxin and its modified forms. EFSA J. 15, 1–53. https://doi.org/10.2903/j.efsa.2017.4655

Lei, Y., Guanghui, Z., Xi, W., Yingting, W., Xialu, L., Fangfang, Y., Goldring, M.B., Xiong, G., Lammi, M.J., 2017. Cellular responses to T-2 toxin and/or deoxynivalenol that induce cartilage damage are not specific to chondrocytes. Sci. Rep. 7, 2231. https://doi.org/10.1038/s41598-017-02568-5

Liu, YX., Wang, JL., Guo, JF., Wu, JJ., Lieberman, HB., Yin, YX., 2008. DUSP1 is controlled by p53 during the cellular response to oxidative stress. Mol. Cancer Res. 6, 624-633. https://doi.org/10.1158/1541-7786.MCR-07-2019

Lombardi, G., Prosperini, A., Font, G., Ruiz, M.J., 2012. Effect of polyphenols on enniatins-induced cytotoxic effects in mammalian cells. Toxicol. Mech. Meth. 22, 687–695. https://doi.org/10.3109/15376516.2012.717120

Meca, G., Font, G., Ruiz, M.J., 2011. Comparative cytotoxicity study of enniatins A, A 1, A 2, B, B 1, B 4 and J 3 on Caco-2 cells, Hep-G 2 and HT-29. Food Chem. Toxicol. 49, 2464–2469. https://doi.org/10.1016/j.fct.2011.05.020

Prosperini, A., Font, G., Ruiz, M.J., 2014. Interaction effects of Fusarium enniatins (A, A1, B and B1) combinations on in vitro cytotoxicity of Caco-2 cells. Toxicol. in Vitro 28, 88–94. https://doi.org/10.1016/j.tiv.2013.06.021

Prosperini, A., Juan-García, A., Font, G., Ruiz, M.J., 2013. Beauvericin-induced cytotoxicity via ROS production and mitochondrial damage in Caco-2 cells. Toxicol. Lett. 222, 204–211. https://doi.org/10.1016/j.toxlet.2013.07.005

Ren, ZH., Wang, YC., Deng, HD., Deng, YT., Deng, JL., Zuo, ZC., Wang, Y., Peng, X., Cui, HM., Shen, LH., 2015. Deoxynivalenol induces apoptosis in chicken splenic lymphocytes via the reactive oxygen species-mediated mitochondrial pathway. Environ. Toxicol. Pharmacol. 39, 339-346. https://doi.org/10.1016/j.etap.2014.11.028

Rodríguez-Carrasco, Y., Izzo, L., Gaspari, A., Graziani, G., Mañes, J., Ritieni, A., 2018. Urinary levels of enniatin B and its phase I metabolites: First human pilot biomonitoring study. Food Chem. Toxicol. 118, 454-459. https://doi.org/10.1016/j.fct.2018.05.052

Romero, A., Ares, I., Ramos, E., Castellano, V., Martínez, M., Martínez-Larrañaga, M-R., Anadón, A., Martínez, M-A., 2016. Mycotoxins modify the barrier function of Caco-2 cells through differential gene expression of specific claudin isoforms:

Protective effect of illite mineral clay. Toxicology 353-354, 21-33. https://doi.org/10.1016/j.tox.2016.05.003

Ruiz, M.J., Festila, L.E., Fernández, M., 2006. Comparison of basal cytotoxicity of seven carbamates in CHO-K1 cells. Environ. Toxicol. Chem. 88, 345–354. https://doi.org/10.1080/02772240600630622

Steinkellner, H., Binaglia, M., Dall'Asta, C., Gutleb, A.C., Metzler, M., Oswald, I.P., Parent-Massin, D., Alexander, J., 2019. Combined hazard assessment of mycotoxins and their modified forms applying relative potency factors: Zearalenone and T2/HT2 toxin. Food Chem. Toxicol. 131, 110599. https://doi.org/10.1016/j.fct.2019.110599

Streit, E., Schatzmayr, G., Tassis, P., Tzika, E., Marin, D., Taranu, I., Tabuc, C., Nicolau, A., Aprodu, I., Puel, O., Oswald, I.P., 2012. Current situation of mycotoxin contamination and co-occurrence in animal feed focus on Europe. Toxins (Basel). 4, 788–809. https://doi.org/10.3390/toxins4100788

Taroncher, M., Pigni, MC., Diana, MN., Juan-Garcia, A., Ruiz, MJ., 2020. Does low concentration mycotoxin exposure induce toxicity in HepG2 cells through oxidative stress?. Toxicol. Mech. Meth. 30, 417-426. https://doi.org/10.1080/15376516.2020.1757000

Van der Fels-Klerx, H.J., Klemsdal, S., Hietaniemi, V., Lindblad, M., Ioannou-Kakouri, E., van Asselt, E.D., 2012. Mycotoxin contamination of cereal grain commodities in relation to climate in North West Europe. Food Addit. Contam. 29, 1581–1592. https://doi.org/10.1080/19440049.2012.689996

Vermes, I., Haanen, C., Steffens-Nakken, H., Reutelingsperger, C., 1995. A novel assay for apoptosis - Flow cytometric detection of phosphatidylserine expression on early apoptotic cells using fluorescein labelled Annexin V. J. Immunol. Meth. 184, 39-51. https://doi.org/10.1016/0022-1759(95)00072-I

Weidner, M., Welsch, T., Hübner, F., Schwerdt, G., Gekle, M., Humpf, H-U., 2012. Identification and Apoptotic Potential of T-2 Toxin Metabolites in Human Cells. J. Agric. Food Chem. 60, 5676−5684. https://doi.org/10.1021/jf300634k

Wu, JZ., Qu, JW., Cao, HX., Jing, CW., Wang, Z., Xu, H., Ma, R., 2019. Monoclonal antibody AC10364 inhibits cell proliferation in 5-fluorouracil resistant hepatocellular carcinoma via apoptotic pathways. Onco. Targets Ther. 12, 5053-5067. https://doi.org/10.2147/OTT.S206517

Wu, Q-H., Wang, X., Yang, W., Nüssler, A.K., Xiong, L-Y., Kuca, K., Dohnal, V., Zhang, X-J., Yuan, Z-H., 2014. Oxidative stress-mediated cytotoxicity and metabolism of T-2 toxin and deoxynivalenol in animals and humans: an update. Arch. Toxicol. 88, 1309-1326. https://doi.org/10.1007/s00204-014-1280-0

Wu, J., Jing, L., Yuan, H., Peng, SQ., 2011. T-2 toxin induces apoptosis in ovarian granulosa cells of rats through reactive oxygen species-mediated mitochondrial pathway. Toxicol. Lett. 202, 168-177. https://doi.org/10.1016/j.toxlet.2011.01.029

Yang, S., De Boevre, M., Zhang, H., De Ruyck, K., Sun, F., Zhang, J., Jin, Y., Li, Y., Wang, Z., Zhang, S., Zhou, J., Li, Y., De Saeger, S., 2017a. Metabolism of T-2 Toxin in Farm Animals and Human In Vitro and in Chickens In Vivo Using Ultra High-

Performance Liquid Chromatography- Quadrupole/Time-of-Flight Hybrid Mass Spectrometry Along With Online Hydrogen/Deuterium Exchange Technique. J. Agric. Food Chem. 65, 7217-7227. https://doi.org/10.1021/acs.jafc.7b02575

Yang, S., Van Poucke, C., Wang, Z., Zhang, S., De Saeger, S., De Moevre, M., 2017b. Metabolic profile of the masked mycotoxin T-2 toxin-3-glucoside in rats (in vitro and in vivo) and humans (in vitro). World Mycotoxin J. 10, 349-362. https://doi.org/10.3920/WMJ2017.2224

SUPPLEMENTARY DATA

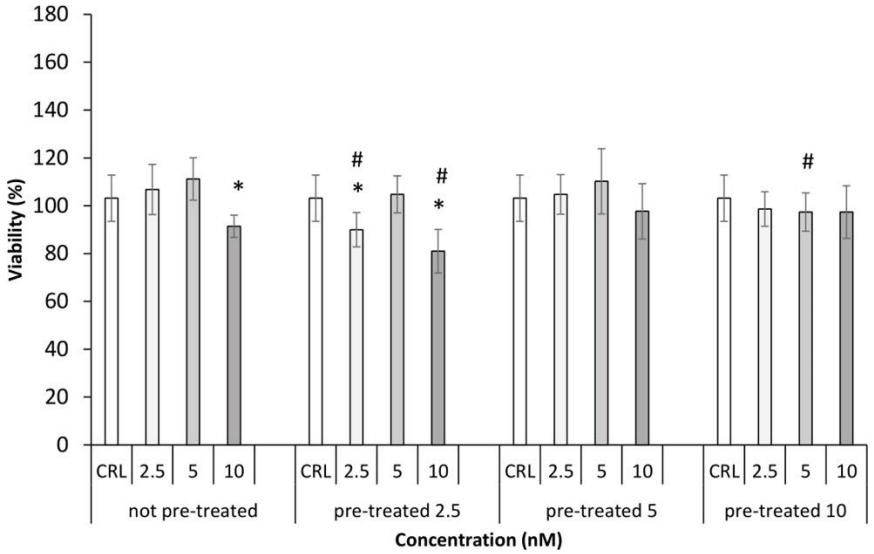

Figure S1. Viability (%) of HepG2 cells after pre-treatment with different T-2 concentrations (2.5 nM–10 nM) during 2 h, and subsequent addition of fresh medium with serial T-2 dilutions (2.5, 5 and 10 nM) for 24 h. Results are expressed as the mean ± SEM of three independent experiments. (*) $p \leq 0.05$ indicates a significant difference compared to control (CRL). (#) $p \leq 0.05$ indicates a significant difference compared to non-pre-treated cells.

Food and Chemical Toxicology, 148 (2021), 111942

https://doi.org/10.1016/j.fct.2020.111942

3.2. Interactions between T-2 toxin and its metabolites in HepG2 cells and *in silico* approach

Mercedes Taroncher, Yelko Rodríguez-Carrasco*, María-José Ruiz

Laboratory of Food Chemistry and Toxicology, Faculty of Pharmacy, University of Valencia, Av. Vicent Andrés Estellés s/n, 46100 Burjassot, Valencia, Spain

Abstract

The T-2 toxin (T-2) is commonly metabolized to HT-2 toxin (HT-2), Neosolaniol (NEO), T2-triol and T2-tetraol and they can modify the toxicity of T-2. In this study, T-2 and its modified forms were evaluated by *in vitro* and *in silico* methods. The *in vitro* cytotoxicity individually was evaluated by MTT and Total Protein Content (PC) assays in human hepatocarcinoma (HepG2) cells. The order of IC_{50} was T-2 tetraol>T-2 triol>NEO>T-2=HT-2. The T-2 and HT-2 evidenced the highest cytotoxic effect in HepG2 cells individually. No differences were observed in binary combinations tested and the two mycotoxins in the mixture tested individually. The T-2+HT-2 combination showed the highest toxic potential with the lowest IC_{50} value of 34.42 ± 0.58 nM at 24 h. All binary combinations exhibited antagonistic interactions. The ADME and toxicity profile of mycotoxins were obtained by the *in silico* admetSAR predictive model which determines the metabolic and toxicological approaches in order to know if these mycotoxins might be taken into consideration to support a more realistic and adequate risk assessment.

Keywords: T-2 toxin; cytotoxicity; metabolites; interaction; *in silico; in vitro.*

* **Corresponding author**: Laboratory of Food Chemistry and Toxicology, Faculty of Pharmacy, University of Valencia, Av. Vicent Andrés Estellés, s/n, 46100, Burjassot, Valencia, Spain. E-mail address: Yelko.Rodriguez@uv.es (Y. Rodríguez-Carrasco).

1. Introduction

Human beings are exposed to different mycotoxins through their daily diet. The exposure to these mycotoxins is practically unavoidable due to their ubiquity, natural origin or production during food transformation. Food contamination is a major problem in Europe as demonstrated by the notifications system issued by "Rapid Alert System for Food and Feed" (RASFF) of the European Food Safety Authority (EFSA). In the last report (2019), mycotoxins are classified according to the hazard category in the first place in food products, with 534 notifications (RASFF, 2020). The mycotoxins may cause adverse effects in the short, medium and long term for consumers depending on the concentrations in the food and the exposure time. Toxic effects can range from mild to potentially toxic such as cancer or mutations. However, their toxicity can be increased when they are present in the diet simultaneously or as a consequence of metabolism. In fact, synergistic toxic effects have been described *in vivo* and *in vitro* for some mixtures of mycotoxins or metabolites originated from a parent compound (EFSA, 2014a; 2020a; Sultana Shaik et al., 2016; Kar & Leszczynski, 2019). Hence, these aspects should be considered when dealing with contaminants ingested simultaneously in the diet.

Mycotoxins cause significant toxic effects at cellular and organic levels; therefore, it is important to know the toxicity of those that have not been studied or their toxicity data is absent. Currently, food safety agencies (EFSA; Food and Agriculture Organization, FAO; World Health Organization, WHO/OMS; Food and Drug Administration, FDA) have set as a new challenge, "to evaluate the possible cumulative and synergistic effects of the different chemical substances to which consumers are usually exposed through the diet", since to

date most of the published data are obtained from individual toxicity studies (unrealistic scenario) (EFSA, 2014b).

An additional challenge is to investigate the mechanisms of toxic action of alternative methods to animal experimentation for those substances whose mechanisms have not yet been fully elucidated (Directive 2010/63/EU). Given the increased requirements and restrictions at legislative level alternative approaches, such as *in vitro* and *in silico* methods, are a cost-effective solution because of saving time, money and minimizing animal testing, and are also encouraged and promoted by the European authorities (European Chemicals Agency (ECHA) and EFSA) (EFSA, 2020b). Computational approaches have already been proven as efficient alternatives for assessing the chemical toxicity by regulatory authorities. To date, different tools have been developed *in silico* to predict modes of action (MoA) and mechanisms by which Adverse Outcome Pathways (AOP) of known chemical substances occur in different organs and tissues at cellular and molecular level (Raies & Bajic, 2016).

In this sense, according to the scientific opinion issued by the EFSA in 2014, *in silico* methods have shown an increasing predictive power to carry out a correct risk assessment, specifically for predictive toxicology (EFSA, 2014a). Currently, there is a large number of toxicity data available, which are collected across several domains. *In silico* predictive approaches cannot completely replace standard bioassays or protocols, however, they can provide an earlier decision-making process until required data become available. This is an enormously promising area to improve the predictive accuracy for improving risk assessment of mycotoxins.

Fusarium fungi produce different mycotoxins of the class of trichothecenes (Streit et al., 2012; van der Fels-Klerx et al., 2012). The T-2 toxin (T-2) is a type

A trichothecene. These group of trichothecenes are tetracyclic sesquiterpenoid compounds characterized by a 12,13-epoxy group and a functional carbonyl group at C-8. The T-2 toxin is metabolized to modified forms through phase I and phase II metabolism (Dohnal et al., 2008; Knutsen et al., 2017). The mainly metabolites of T-2 in mammals are HT-2 toxin (HT-2), neosolaniol (NEO), T2-triol, T2-tetraol, 3'-OH-T-2, 3'-OH-HT-2, and some C12,13-deepoxy products (Wu et al., 2010, 2013; Figure 1). All of them are phase I metabolites. Hydrolysis and deepoxylation of T-2 lead to a decrease in toxic activity (Knutsen et al., 2017). Hydrolysis is the main metabolic fate of T-2 in the liver (Wu et al., 2014). Both, T-2 and its modified forms can occur together and may contribute to the overall toxicity (EFSA, 2016, 2017; Knutsen et al., 2017). The T-2 and HT-2 frequently co-occur at high concentrations; in contrast, trace levels of NEO, T2-triol and T2-tetraol have been detected in oat, wheat and corn bypoducts (Chen et al., 2020; Ling et al., 2020). The food matrix which showed the highest concentrations of T-2 was oat (41.7 μg/kg) (EFSA, 2017). The biochemical and cellular effects and potential modes of T-2 action are activation of the mitogen activated protein kinases (MAP kinases), apoptosis, necrosis, lipid peroxidation, reactive oxygen production, strong protein, DNA and RNA synthesis inhibition, among others (Garreau De Loubresse et al., 2014; Knutsen et al., 2017; Taroncher et al., 2020a, Taroncher et al., 2020b).

The simultaneous study of two or more *Fusarium* mycotoxins interaction has been initiated by our group (Ruiz et al., 2011a, 2011b; Lu et al., 2013; Tatay et al., 2014; Fernandez-Blanco et al., 2018; Taroncher et al., 2018; Zingales et al., 2020). However, there are still many mycotoxins to be evaluated and few studies have addressed to determine toxic effects of T-2 and its modified forms. It is

therefore needed to improve knowledge of the toxic effects of these mycotoxin combinations in order to better assess the risk.

Based on the above, the aims of this study were: (i) to determine the cytotoxic effect of individual and combined T-2 and its modified forms HT-2, NEO, T2-triol and T2-tetraol in the human hepatocarcinoma (HepG2) cells, which were selected due to the first passage through the liver markedly detoxifies T-2; (ii) to assess the interaction of mycotoxin combinations through toxicity studies based on computational models; and (iii) to predict the biological activities, toxicokinetic properties as well as physicochemical properties of mycotoxins by *in silico* approaches in order to know if these findings might be taken into consideration to support a more realistic and adequate risk assessment to the studied mycotoxins.

2. Material and Methods

2.1 Reagents

The reagent grade chemicals and cell culture compounds used, namely Dulbecco's Modified Eagle's Medium (DMEM), penicillin, streptomycin, trypsin/EDTA solutions, Phosphate Buffer Saline (PBS), Newborn Calf Serum (NBCS), methylthiazoltetrazolium salt (MTT) dye, dimethyl sulfoxide (DMSO), NaOH, NaCl, HEPES and $CaCl_2$ were purchased from Sigma-Aldrich (St Louis, USA). Methanol (MeOH) was from VWR International (LLC, Pennsylvania, USA). Deionised water (resistivity <18 MΩ cm) was obtained using a Milli-Q water purification system (Millipore, Bedford, MA, USA).

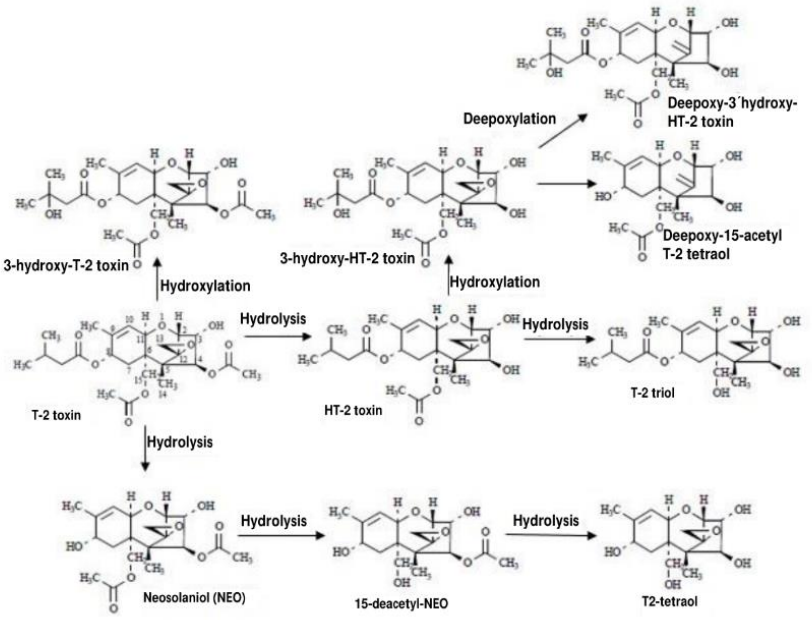

Figure 1. The major phase I metabolic pathways of T-2 bioactivation in animals are hydrolysis, hydroxylation and deepoxidation. The T-2 after being transformed to HT-2 (main metabolite in humans), it undergoes further hydroxylation at T-2 triol. The T-2 was hydrolyzed to give NEO, which was then metabolized to T-2 tetraol via 15-deacetyl-NEO.

Standard of mycotoxin T-2 (MW: 466.52 g/mol), HT-2 (MW: 424.48 g/mol), NEO (MW: 382.40 g/mol), T2-triol (MW: 382.45 g/mol) and T2-tetraol (MW: 298.33 g/mol), were purchased from Sigma-Aldrich (St. Louis Mo. USA). Chemicals structures of T-2 and its modified forms are shown in Figure 1. Stock solutions of the mycotoxins were prepared in methanol at appropriate working concentrations and maintained in the dark at -20 ºC.

2.2 Cell culture and treatment

Human hepatocarcinoma (HepG2) (ATCC: HB-8065) cells were cultured in DMEM medium supplemented with 10% NBCS, 100 U/ml penicillin and 100 mg/ml streptomycin. The incubation conditions were pH 7.4, 5% CO_2 at 37 °C and 95% air atmosphere at constant humidity. The medium was changed every 5 days. The final mycotoxin concentrations tested were achieved by adding each mycotoxin solution to the culture medium with a final MeOH concentration ≤1% (v/v). Appropriate controls containing the same amount of solvents were included in each experiment. Absence of mycoplasma was checked routinely using the MycoAlertTM PLUS Mycoplasma Kit (Lonza, Rockland, ME USA).

2.3 *In vitro* cytotoxicity

Cytotoxic effects were determined in HepG2 cells by the MTT and Total Protein Content (PC) assays. They have been extensively used in *in vitro* toxicological studies for measure cell proliferation and survival. The MTT assay determines the viability of cells by the reduction of yellow soluble tetrazolium salt (MTT), only in the metabolically active cells, via a mitochondrial-dependent reaction to an insoluble purple formazan crystal. The MTT viability assay was performed according to Ruiz et al. (2006).

Briefly: the HepG2 cells were plated in 96-well tissue culture plates at a density of 2×10^4 cells/well. After cells reached 80% of confluence, the culture medium was replaced with fresh medium containing serial dilutions of each mycotoxin. The range of mycotoxin concentration were: T-2 from 12.5 to 100 nM, HT-2 from 18.75 to 150 nM, NEO from 11 to 164 nM, T-2 triol from 164 to 2620 nM and T-2tetraol from 209 to 3350 nM. For each mycotoxin, the range of concentrations assayed were selected according to previous assays carried out with all the mycotoxins and considering the best concentration range to obtain the IC_{50} values. The mycotoxin was exposed during 24 h and 48 h. During the exposure time, neither the medium nor the mycotoxin was replenished. After 24 h and 48 h of exposure, the medium was removed and 200 µl of fresh medium was added to each well. Then, 50 µl/well of MTT were added and the plates returned to the incubator in the dark. After 3 h of incubation, the MTT solution was removed and 200 µl of DMSO were added followed by the addition of 25 µl Sorensen's glycine buffer. Plates were gently shaken for 5 min to achieve the complete dissolution. The absorbance was measured at 540 nm using an automatic ELISA plate reader (MultiSkanEX, Thermo Scientific, MA, USA).

The PC method is based on the increase of absorbance of Coomassie Brilliant Blue dye when binding to proteins. The assay was performed in the same 96-well plates where the MTT test was carry out. First, the plates were washed with PBS and then 200 µl of NaOH 0.1 N were added in each well to dissolve the proteins. After 2 h of incubation, 170 µl of NaOH were removed from each well and 180 µl of diluted 22% Coomassie Brilliant Blue were added. The plates remain for 30 min at room temperature and the absorbance was measured at 620 nm in an automatic ELISA plate reader (MultiSkanEX, Thermo Scientific, MA, USA).

For MTT and PC assays, cell viability was expressed as a percentage relative to the control solvent (≤1% MeOH). Three independent experiments were conducted for each exposure time. The mean inhibition concentration (IC_{50}) values were calculated using SigmaPlot version 11 (Systat Software Inc., GmbH, Germany).

2.4. Experimental design for mycotoxin mixtures

Cytotoxic effects in binary combinations were performed using the MTT assay after 24 h of exposure. The HepG2 cells were exposed to serial dilution factor of two of each individual mycotoxin and their binary mixtures. The mixtures were prepared with a different combination ratio starting from $IC_{50}/2$ to $IC_{50}/16$ based on the IC_{50} values of the mixture mycotoxins. For the highest concentrations of each combination, the sum of the $IC_{50}/2$ of each mycotoxin was chosen. The combination ratios were calculated on the basis of equipotent IC_{50} values obtained from the individual exposure experiments, so that the contribution to the effect of each mycotoxin would be equal (Chou, 2006). Four dilutions at 1:2 ratio of each mycotoxin combination with 8 replicates were performed and repeated in triplicate. Concentrations assayed with binary combinations of mycotoxins ranged from 4.38 to 35 nM for T-2 and HT-2, from 5.94 to 47.5 nM for NEO, from 70 to 560 nM for T-2 triol and from 155 to 1240 nM for T-2 tetraol. Combination ratios were 1:1 for T-2+HT-2, 1:16 for T-2+T-2 triol and HT-2+T-2 triol, 1:1.4 for T-2+NEO and HT-2+NEO, 1:2.2 for T-2 triol+T-2 tetraol, 1:11.8 for NEO+T-2 triol, 1:26.1 for NEO+T-2 tetraol and 1:35.4 for T-2+T-2 tetraol and HT-2+T-2 tetraol. Individual mycotoxin assays were tested simultaneously and they were compared with the data obtained in the binary combinations.

Cell viability was expressed as a percentage relative to the control solvent (≤1% MeOH). A triplicate of experiments was performed at each exposure time. The mean inhibition concentration (IC_{50}) values of binary combinations were calculated using SigmaPlot version 11 (Systat Software Inc., GmbH, Germany).

2.5 Computational tools in assessing the toxicological interactions in binary mixtures of T-2 and its modified forms

The isobologram method was used to determine the interactive effects that occurs when different compounds are in combination (Chou and Talalay, 1984; Chou, 2006). The median-effect/combination index (CI)-isobologram equation by Chou (2006) and Chou and Talalay (1984) was used to analyze the results. The equation is based on the median-effect equation of the mass-action law, which demonstrates that there is a univocal relationship between dose and effect independently of the number of substrates or products and of the mechanism of action or inhibition. The CI index was calculated by the equation:

$$^{n}(\mathrm{CI})_x = \sum_{J=1}^{n} (D)_j/(D_x)_j = \sum_{J=1}^{n} \frac{(D_x)_{1-n}\left\{[D]_j/\sum_{J=1}^{n}[D]\right\}}{(D_m)_j\left\{(f_{ax})_j/\left[1-(f_{ax})_j\right]\right\}^{1/mj}}$$

Where $^{n}(\mathrm{CI})_x$ is the combination index for n compounds (e.g., mycotoxins) at x% inhibition (e.g., proliferation inhibition); $(D_x)_{1\text{-}n}$ is the sum of the concentration of n compounds that exerts x% inhibition in combination; $\{[D]_j/\sum_{J=1}^{n}[D]\}$ is the proportionality of the concentration of each of n compounds that exerts x% inhibition in combination; and $(D_m)_j\ \{(fax)_j/[1\text{-}(fax)_j]\}^{1/mj}$ is the concentration of each compound alone that exerts x%

inhibition. From this equation, CI <1, =1, and >1 indicates synergism, additive effect and antagonism, respectively.

2.6 *In silico* prediction for toxicokinetics of T-2 and its modified forms in humans

Computational toxicology approaches can greatly enhance our understanding of the molecular and biological basis of toxicity and result in greater confidence in extrapolations, as well as critical factors to assess the risk, such as significant susceptibility factors, subpopulations at risk, and influences on the shape of the dose-response curve.

Variability in absorption, distribution, metabolism, excretion and toxicity (ADME/T) can have a dramatic impact on the toxicity of a substance (e.g. mycotoxin) with the metabolism playing the most important role. The *in silico* models allow to evaluate the reliability of the toxicokinetic prediction of T-2 and its modified forms. These models provide information to include in the assessment of the toxicological effect or mechanisms.

The individual consideration of ADME/T of T-2, HT-2, NEO, T-2 triol and T-2 tetraol was predicted using admetSAR version 2 (http://lmmd.ecust.edu.cn/admetsar2/), a comprehensive and free tool (Cheng et al., 2012; Yang et al., 2018). The admetSAR mainly focuses on *in silico* prediction for evaluating chemical ADME/T properties. In admetSAR (version 2) six physicochemical properties are used to define the applicability domain, which are molecular weight (MW), Log*P* (logarithm of the 1-octanol/water partition coefficient; CLog*P*), H-bond donors, H-bond acceptors, number of atoms and number of rings.

The main features of absorption are: human gastrointestinal absorption (HIA), human oral bioavailability (HOB) and Caco-2 cells permeability. The main features of distribution are: plasma protein bindings (PPB), targets of p-glycoprotein (P-gp) substrate and blood-brain barrier (BBB) penetration. Inhibitors of cytochrome P450 isoforms CYP1A2, CYP2C9, CYP2C19, CYP2D6 and CYP3A4 as well as substrates for the metabolism by isoforms CYP2C9, CYP2D6 and CYP3A4 were predicted. Some pharmacokinetics transporters in liver recommended in regulatory drug-drug interaction guidance are OATP1b1, OATP1b3, P-gP, MATE1 and BSEP, among others. These transporters are selected because they are the main drug transporters in hepatocytes and bile canaliculi and they can influence the permeability of mycotoxins into specific cells in hepatocytes and bile canaliculi. Moreover, this model anticipates toxicity of compounds on oral acute toxicity and genetic toxicity models of Ames test, rodent carcinogenicity (results are produced as positive or negative carcinogenicity on *in vivo* 2 year carcinogenicity tests of mice and rats) and micronucleus assay.

Besides, SwissADME (http://www.swissadme.ch/) predicts the HIA and BBB penetration by BOILED-Egg (Brain Or Intestinal EstimateD) method. BOILED-Egg method has a 2-D graphical nature which shows how a molecular structure is from the ideal physicochemical region for good absorption.

The BOILED-Egg method discriminates between well-absorbed and poorly absorbed molecules based on their lipophilicity and polarity described by the n-octanol/water partition coefficient ($\log P_{o/w}$) and the polar surface area (PSA), respectively (Egan et al., 2000). It is considered: TPSA<140 Å2 and $\log P_{o/w}$ between -2.3 and +6.8 a good intestinal absorption and TPSA<70 Å2 and

log$P_{o/w}$ from +0.4 to +6.0 a good brain penetration (Palm et al., 1997; Daina and Zoete, 2016).

2.7 Statistical analysis

The statistical analysis of the data was carried out using the SPSS version 24.0 statistical package (IBM Corp., Armonk, NY, USA). Data were expressed as mean ± standard error of the mean (SEM) of different independent experiments. The statistical analysis of the results was performed using the Student *t*- test for paired samples. Differences between groups were analyzed using one-way analysis of variance (ANOVA) followed by the Tukey HDS post-hoc test for multiple comparisons. Statistical significance was considered for $p \leq 0.05$.

3. Results

3.1 *In vitro* cytotoxicity of T-2 and its modified forms: individual and combined

The cytotoxic effect of T-2 and its modified forms on HepG2 cells was evaluated by MTT and PC assays over 24 h and 48 h. Cells exposed to T-2, HT-2, NEO, T-2 triol and T-2 tetraol revealed a decrease in cell viability in a time and concentration-dependent manner by MTT and PC assays (Figures 2 and 3).

Significant differences in cell viability at 24 h and 48 h were observed in cells exposed to T-2, HT-2, NEO, T-2 triol and T-2 tetraol by MTT assay. Cell viability decreased from 78% to 14% at 24 h of exposure and from 89% to 19% after 48 h for T-2 (Fig. 2a). Cell viability decreased from 37% to 76% and from 39% to 92% for HT-2 after 24 h and 48 h, respectively (Fig. 2b). Cell viability decreased from 23% to 77% and from 46% to 93% for NEO after 24 h and 48 h, respectively (Fig. 2c). Cell viability decreased from 23% to 77% and from 30%

to 88% for T-2 triol after 24 h and 48 h, respectively (Fig. 2d). And, cell viability decreased from 10% to 70% and from 23% to 89% for T-2 tetraol after 24 h and 48 h, respectively (Fig. 2e).

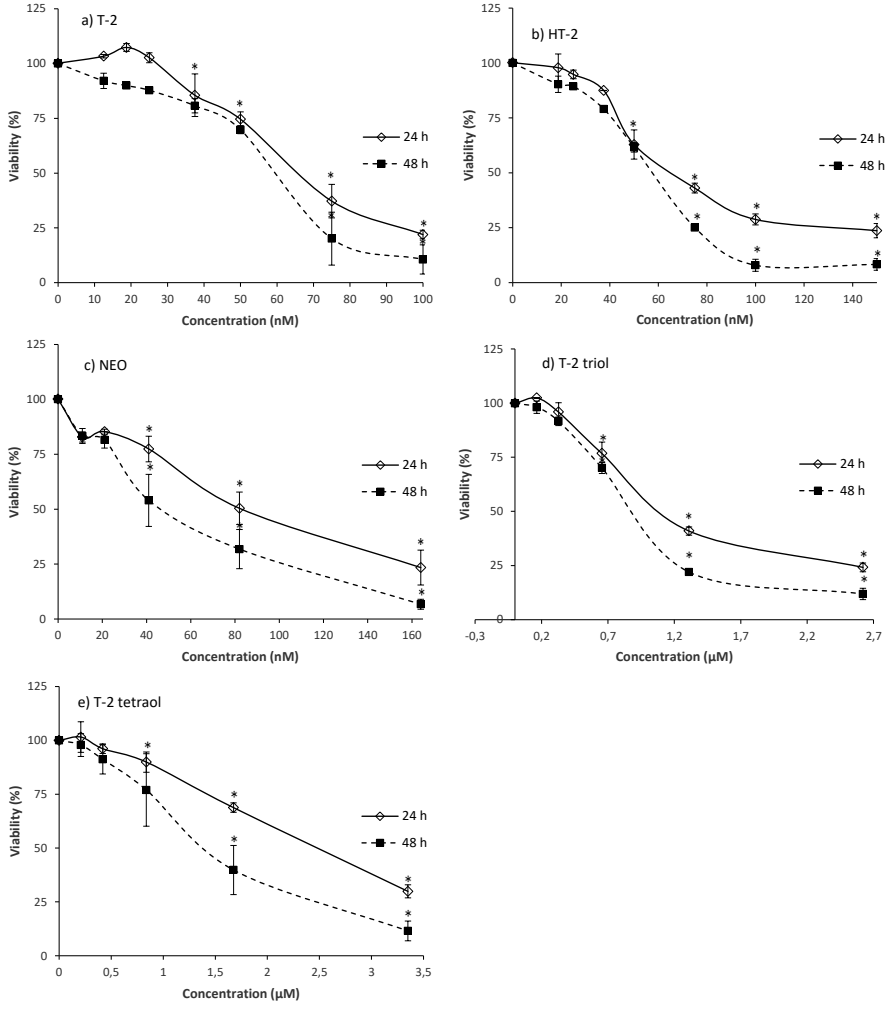

Figure 2. Dose response curves of a) T-2, b) HT-2, c) NEO, d) T-2 triol and e) T-2 tetraol on HepG2 cells after 24h (◊) and 48h (–■–) of exposure by the MTT assay. All values are expressed as mean ± SEM of 3 replicates. $p \leq 0.05$ (*) represents significant difference as compared to control values.

Figure 3 shows cell viability determined by the PC assay. It can be noticed that a significant increase in cell viability was observed in T-2 from 28% to 42% after 25 nM and 37.5 nM, HT-2 of 27% at 18.6 nM, NEO of 14% at 21 nM, and T-2 tetraol of 44% at 0.2 μM, compared to control (Figure 3). The increase in cell viability can be due to the hormetic effect in HepG2 cells. On the other hand, higher cytotoxic effect was observed in HepG2 cells exposed to T-2, HT-2, NEO, T-2 triol and T-2 tetraol by PC assay than MTT assay. Cell viability decreased from 69% to 97% and from 73% to 75% for T-2 after 24 h and 48 h of exposure, respectively (Fig. 3a). Cell viability decreased from 71% to 96% and from 58% to 93% for HT-2 after 24 h and 48 h, respectively (Fig. 3b). Cell viability decreased from 24% to 69% and from 41% to 83% for NEO after 24 h and 48 h, respectively (Fig. 3c). Cell viability decreased from 56% to 95% and from 66% to 79% for T-2 triol after 24 h and 48 h, respectively (Fig. 3d). And, cell viability decreased 62% and from 58% to 79% for T-2 tetraol after 24 h and 48 h, respectively (Fig. 3e).

As can be observed in Table 1, the IC_{50} values for each mycotoxin obtained from the two methods tested were similar. The order of IC_{50} decrease in HepG2 cells as follow at 24 h and 48 h: T-2 tetraol>T-2 triol>NEO>T-2=HT-2. The T-2 and HT-2 evidenced the highest cytotoxic effect in HepG2 cells. These results allowed setting the concentrations in the interaction assays.

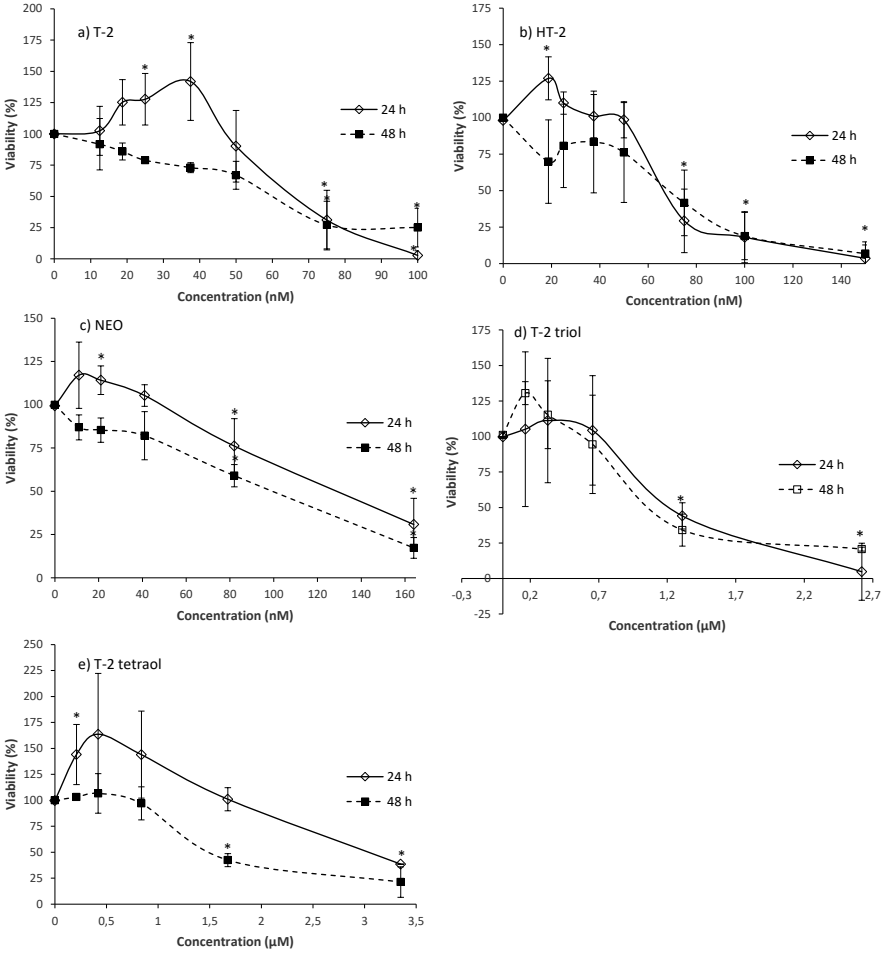

Figure 3. Dose response curves of a) T-2, b) HT-2, c) NEO, d) T-2 triol and e) T-2 tetraol on HepG2 cells after 24h (◊) and 48h (–■–) of exposure by the PC assay. All values are expressed as mean ± SEM of 3 replicates. $p \leq 0.05$ (*) represents significant difference as compared to control values.

Table 1. The medium inhibitory concentration (IC_{50}) of T-2, HT-2, NEO, T2-triol and T2-tetraol on HepG2 cells determined after 24 and 48 h of incubation by the MTT and PC assays.

Assay	IC_{50} (nM) ± SD									
	T-2		HT-2		NEO		T2-triol		T2-tetraol	
	24 h	48 h	24 h	48 h	24 h	48 h	24 h	48 h	24 h	48 h
MTT	68.6 ± 4.8	61.9 ± 2.4	68.2 ± 5.4	59.6 ± 1.1	95.6 ± 20	55.6 ± 13.7	1120 ± 20	890 ± 40	2480 ± 130	1380 ± 340
PC	70.7 ± 7.4	65.0 ± 6.0	66.1 ± 10.4	67.9 ± 19.3	121.1 ± 16	94.2 ± 8.6	1240 ± 310	870 ± 240	2770 ± 80	1480 ± 170

Results are mean ± SEM (n=3). The IC_{50} values were calculated using SigmaPlot version 11 (Systat Software Inc., GmbH, Germany).

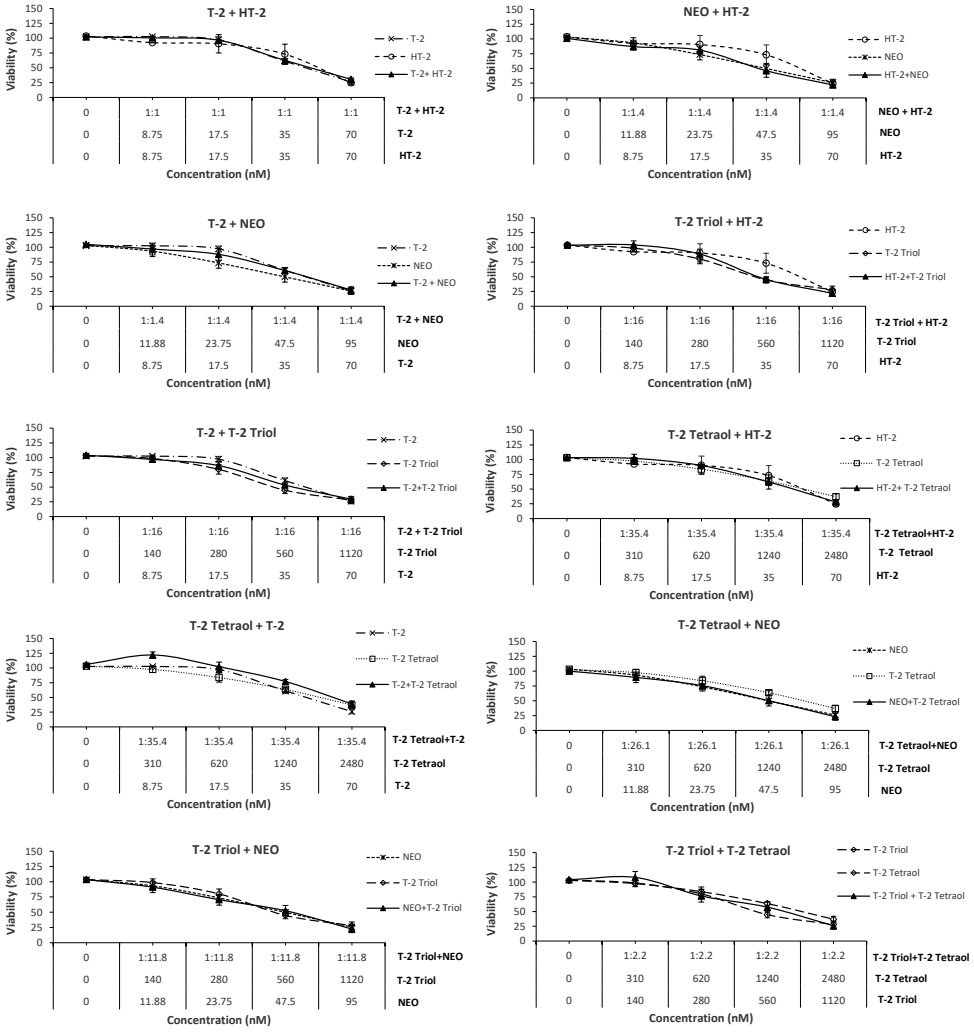

Figure 4. Cytotoxicity effects of individual T-2 (–·X–·–), HT-2 (–○–), NEO (--□ - -), T-2 triol (–◊– –), T-2 tetraol (···□··) and the binary combinations (–▲–) after 24 h of exposure by the MTT assay. All values are expressed as mean ± SEM (n=3).

Figure 4 shows dose-response (% viability) relationship curves of binary mixtures in HepG2 cells. No differences were observed in binary combinations

tested and the two mycotoxins in the mixture tested individually (Fig. 4). Table 2 shows the IC_{50} values of the mixtures. The order of IC_{50} values for these mixtures decrease in the following order: T-2 triol+T-2 tetraol > T-2 tetraol+T-2 > T-2 Tetraol+NEO = T-2 tetraol+HT-2 > T-2 triol+NEO > T-2 triol+T-2 = T-2 triol+HT-2> T-2+NEO > HT-2+NEO > T-2+HT-2. Among mycotoxin mixtures T-2+HT-2 showed the highest toxic potential with the lowest IC_{50} value of 34.42 ± 0.58 nM at 24 h. Whilst, the combinations that show the least cytotoxic effect are those containing T-2 tetraol in the mixture, followed by those containing T-2 triol and NEO (Table 2).

Table 2. The IC_{50} values obtained in an equipotent combinations of various concentrations of two mycotoxins of T-2 and its modified forms in HepG2 cells using MTT assay at 24 h of exposure.

Mycotoxin combination	**Ratio**	**IC_{50} (nM) ± SD**
T-2+HT-2	1:1	34.42 ± 0.58
T-2+NEO	1:1.36	55.04 ± 14.24
T-2+T-2 TRIOL	1:16	257.09 ± 25.21
NEO+HT-2	1:1.35	38.51 ± 16.83
T-2 TRIOL+HT-2	1:1.16	234.83 ± 8.65
T-2 TRIOL+NEO	1:11.8	460.77 ± 77.72
T-2 TRIOL+T-2 TETRAOL	1:2.2	816.96 ± 167.43
T-2 TETRAOL+T-2	1:35.4	713.66 ± 136.03
T-2 TETRAOL+HT-2	1:35.4	709.59 ± 61.63
T-2 TETRAOL+NEO	1:26.1	721.64 ±38.97

The IC_{50} values were calculated using SigmaPlot version 11 (Systat Software Inc., GmbH, Germany).

3.2 Toxicological interactions in binary mixtures of T-2 and its modified forms by computational tool

The isobologram analysis was used to determine the type of interaction between ten binary combinations, which include T-2+HT-2, T-2+NEO, T-2+T-2 triol, NEO+HT-2, T-2 triol+HT-2, T-2 triol+NEO, T-2 triol+T-2 tetraol, T-2 tetraol+T-2, T-2 tetraol+HT-2 and T-2 Tetraol+NEO at 24 h of exposure in HepG2 cells (Figure 5, Table 3). The CI values and types of action among mixtures are detailed in Table 3. As shown in Figure 5 and Table 3, all the binary combinations displayed an antagonistic effect (CI>1) at all the effect levels; the exception to this was the binary T-2 triol+HT-2, T-2+HT-2, T-2 triol+T-2 tetraol, T-2 tretaol+T-2 and T-2 tretaol+HT-2 combinations, which evidenced antagonistic effect (*fa*= 0.1, 0.25 and 0.50; CI>1) at low and moderate effect levels, but changed to addition at high effect levels (*fa*= 0.75 and 0.9; CI>0.9 and <1.1).

3.3 *In silico* prediction for toxicokinetics of T-2 and its modified forms in humans

Lipinski and coworkers predict that poor absorption or permeation is more likely when there are more than 5 H-bond donors, and more than 10 H-bond acceptors, the MW is over 500, and the calculated Log*P* is over 5. The basic physicochemical, pharmacological, and toxicological properties of the T-2 and its modified forms are summarized in Table 4. According to Lipinski's rule of five, both T-2 and its metabolites exhibit good absorption or permeation after oral exposure (Lipinski, 2004).

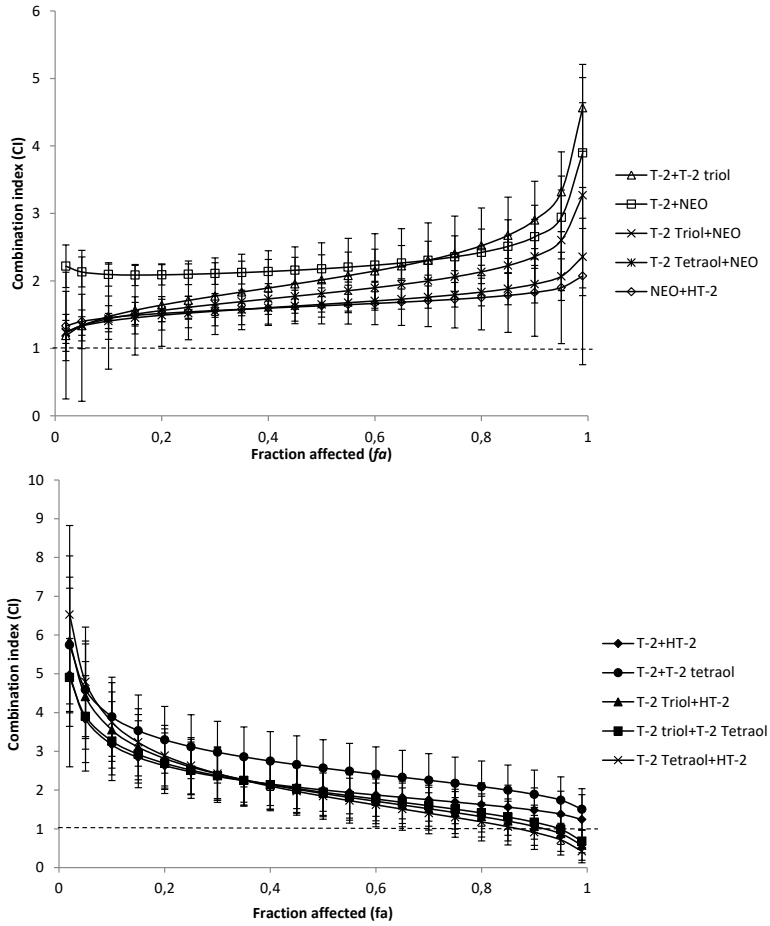

Figure 5. Combination index (CI) versus fraction affected (*fa*) curve as described by Chou and Talalay model on HepG2 cells exposed to a) T-2+T-2 triol, T-2+NEO, NEO-HT-2, T-2 triol+NEO, T-2 tetraol+NEO and b) T-2+HT-2, T-2 triol+HT-2, T-2 tetraol+HT-2, T-2 tetraol+T-2 and T-2 triol+T-2 tetraol in binary combinations. Each point represents the CI ± SD at a fractional affected (*fa*) as determined in our experiments. The striped line (CI=1) indicates additivity, the area under this line synergism and, the area above the line antagonism. All the binary combinations were at equimolar proportion.

Table 3. Dose–effect relationship parameters and mean combination index (CI) values (as a function of fractional inhibition of proliferation) of binary combinations of T-2 and its modified forms in HepG-2 cells after 24 h of exposure.

Mycotoxin	Ratio	Dm (nM)	m	r	CI Values at				
					CI_{10}	CI_{25}	CI_{50}	CI_{75}	CI_{90}
T-2	–	46.13	4.89	0.9642					
HT-2	–	47.88	1.76	0.9461					
NEO	–	48.60	1.74	0.9936					
T-2 TRIOL	–	621.34	2.45	0.9648					
T-2 TETRAOL	–	1721.80	1.97	0.9862					
T-2+HT-2	1:1	47.09	4.75	0.9542	3.17 ± 0.78 Ant	2.47 ± 0.58 Ant	2.00 ± 0.55 Ant	1.69 ± 0.56 Ant	1.48 ± 0.57 Add
T-2+NEO	1:1.36	43.88	2.15	0.9998	2.10 ± 0.17 Ant	2.10 ± 0.15 Ant	2.18 ± 0.21 Ant	2.36 ± 0.31 Ant	2.65 ± 0.47 Ant
T-2+T-2 TRIOL	1:16	42.49	2.13	0.9943	1.47 ± 0.21 Ant	1.71 ± 0.22 Ant	2.02 ± 0.30 Ant	2.40 ± 0.45 Ant	2.90 ± 0.69 Ant
NEO + HT-2	1:1.35	45.35	1.60	0.9807	1.46 ± 0.32 Ant	1.54 ± 0.23 Ant	1.63 ± 0.27 Ant	1.73 ± 0.42 Ant	1.83 ± 0.65 Ant
T-2 TRIOL + HT-2	1:16	41.01	4.85	0.9220	3.55 ± 0.98 Ant	2.60 ± 0.71 Ant	1.91 ± 0.60 Ant	1.42 ± 0.54 Add	1.06 ± 0.49 Add
T-2 TRIOL + NEO	1:11.8	45.83	1.65	0.9940	1.44 ± 0.19 Ant	1.61 ± 0.16 Ant	1.81 ± 0.20 Ant	2.06 ± 0.34 Ant	2.36 ± 0.55 Ant
T-2 TRIOL + T-2 TETRAOL	1:2.2	1487.01	4.57	0.8836	3.26 ± 1.02 Ant	2.52 ± 0.82 Ant	1.94 ± 0.73 Ant	1.51 ± 0.67 Add	1.17 ± 0.63 Add
T-2 TETRAOL + T-2	1:35.4	60.81	5.33	0.9282	3.89 ± 1.10 Ant	3.12 ± 0.97 Ant	2.57 ± 0.93 Ant	2.17 ± 0.91 Ant	1.89 ± 0.92 Add
T-2 TETRAOL + HT-2	1:35.4	1581.66	4.64	0.9226	3.76 ± 1.02 Ant	2.63 ± 0.73 Ant	1.84 ± 0.60 Ant	1.29 ± 0.51 Add	0.91 ± 0.44 Add
T-2 TETRAOL + NEO	1:26.1	46.22	1.61	0.9993	1.41 ± 0.11 Ant	1.52 ± 0.09 Ant	1.65 ± 0.11 Ant	1.79 ± 0.18 Ant	1.95 ± 0.28 Ant

The parameters *m*, *Dm* and *r* are the slope, antilog of x-intercept, and the linear correlation coefficient of the median-effect plot, which signifies the shape of the dose-effect curve, the potency (IC_{50}), and the conformity of the data to the mass-action law, respectively (Chou and Talalay, 1984; Chou, 2006). *Dm* and *m* values are used for calculating the CI values. CI < 1, CI=1 and, CI >1 indicate synergism (S), additive effect (Add), and antagonism (Ant), respectively. CI values at 10, 25, 50 75 and 90% inhibition of HepG2 cell growth are based on the combination index isobologram equations. HepG2 cells were exposed during 24h to equipotent combinations of four concentrations of two mycotoxins.

Most of mycotoxins are soluble in octanol rather than in water (high log*P* value); the only hydrophilic mycotoxin is T-2 tetraol. The aqueous solubility of these mycotoxins compromises bioavailability (HOB) manifested by their poor penetration through the blood–brain barrier (Figure 6). On the other hand, NEO, T-2 triol and T-2 tetraol are predicted as a good substrate of P-glycoprotein, a transmembrane efflux pump (Table 4, Figure 6). This means that, even though these mycotoxins are not able to penetrate through barriers by passive absorption, it uses P-gp pump as the transporter-mediated penetration pathway.

According to this predictive tool, all mycotoxins tested are substrate of CYP450 3A4 (CYP3A4) enzyme, involved in the Phase I oxidative metabolism. This finding is of great relevance, because 50% of the drugs cleared by metabolism are metabolized by CYP3A4 (Williams et al., 2014). Moreover, NEO, T-2 triol, T-2 tetraol are substrates for metabolic clearance mediated by enzymes other than CYPs, mainly UDP-glucoronosyl transferases (UGTs).

Respect to mycotoxin transporters, admetSAR tool indicates that transporter inhibition has been observed for T-2 and its modified forms (Table 4). In addition, genotoxic toxicity assays (Ames test, carcinogenicity and micronucleus test) were negative for all mycotoxins, with the exception of the Ames test for T-2 and HT-2. However, as expected T-2 and its modified forms induced liver injury and showed high toxicity (Table 4).

The BOILED-Egg method predicts highly intestinal absorption and poorly absorbed in brain (Figure 6).

Table 4. ADME and toxicity profile prediction of T-2 and its modified forms.

	T-2		HT-2		NEO		T2-triol		T2-tetraol	
	Result	Probability (%)	Result	Probability (%)	Result	Probability (%)	Result	Probability (%)	Result	Probability (%)
Lipinski molecular descriptors	*Yes; 0 violation*		*Yes; 0 violation*		*Yes; 0 violation*		*Yes; 0 violation*		*Yes; 0 violation*	
HBA (≤10)	9		8		8		7		6	
HBD (≤5)	1		2		2		3		4	
clogP (≤5)	2.04		1.57		0.79		1.05		−0.35	
MW (≤500 g/mol)	466.52		424.48		382.40		382.45		298.33	
n-ROTB (≤10)	6		5		3		4		1	
Boiled-Egg descriptors	*Yes; 0 violation*		*Yes; 0 violation*		*Yes; 0 violation*		*Yes; 0 violation*		*Yes; 0 violation*	
Lipophilicity: Log $P_{o/w}$ (WLOG)	1.69		1.12		0.10		0.55		−1.05	
Water solubility (TPSA/Å^2)	120.89		114.82		114.82		108.75		102.68	
Absorption										
HIA	(+)	96.75	(+)	93.82	(+)	95.19	(+)	91.03	(+)	91.21
HOB	(−)	70.00	(−)	65.71	(−)	61.68	(−)	68.88	(−)	64.29
Caco-2 permeability	(−)	66.60	(−)	69.00	(−)	61.68	(−)	68.88	(−)	82.50
Distribution										
BPB	0.957	100	0.98	100	0.652	100	0.924	100	0.636	100
P-gp substrate	(−)	55.36	(−)	56.84	(+)	71.17	(+)	59.33	(+)	71.50
BBB	(+)	98.35	(+)	95.12	(+)	96.26	(+)	95.12	(+)	95.21
Subcellular localization	Mitoch.	75.97	Mitoch.	77.34	Mitoch.	68.82	Mitoch.	74.89	Mitoch.	52.59
Metabolism										
CYP450 2C9 substrate	(−)	100	(−)	100	(−)	100	(−)	100	(−)	80.49
CYP450 2D6 substrate	(−)	84.08	(−)	84.54	(−)	83.58	(−)	85.02	(−)	75.62

	T-2		HT-2		NEO		T2-triol		T2-tetraol	
	Result	Probability (%)	Result	Probability (%)	Result	Probability (%)	Result	Probability (%)	Result	Probability (%)
CYP450 3A4 substrate	(+)	67.00	(+)	66.85	(+)	64.72	(+)	66.25	(+)	58.80
CYP450 1A2 inhibitor	(−)	86.65	(−)	84.38	(−)	88.74	(−)	83.14	(+)	86.22
CYP450 2C9 inhibitor	(−)	82.34	(−)	82.48	(−)	90.62	(−)	80.13	(−)	87.61
CYP450 2C19 inhibitor	(−)	83.54	(−)	81.89	(−)	88.30	(−)	80.78	(−)	81.50
CYP450 2D6 inhibitor	(−)	92.36	(−)	91.93	(−)	92.42	(−)	91.93	(−)	90.81
CYP450 3A4 inhibitor	(−)	93.61	(+)	95.81	(−)	93.59	(−)	95.17	(−)	94.26
UGT catalized	(−)	50.00	(−)	50.00	(+)	60.00	(+)	60.00	(+)	70.00
BSEP inhibitor	(+)	85.90	(+)	79.55	(−)	61.59	(+)	70.47	(−)	80.23
MATE1 inhibitor	(−)	96.00	(−)	96.00	(−)	96.00	(−)	96.00	(−)	98.00
OATP1b1 inhibitor	(+)	85.24	(+)	85.12	(+)	86.53	(+)	85.32	(+)	86.73
OATP1b3 inhibitor	(+)	89.47	(+)	91.41	(+)	94.25	(+)	87.17	(+)	96.19
Toxicity										
Mycotoxin-induced liver injury	(+)	62.50	(+)	55.00	(+)	55.00	(−)	57.50	(−)	60.00
Acute oral toxicity (category)	I	82.39	I	80.85	I	84.34	I	75.20	I	81.05
AMES mutagenesis	(+)	67.00	(+)	62.00	(−)	56.00	(−)	59.00	(−)	62.00
Carcinogenesis	(−)	100	(−)	100	(−)	90.00	(−)	100	(−)	94.29
Micronucleus assay	(−)	62.00	(−)	61.00	(−)	60.00	(−)	72.00	(−)	

BBB: blood-brain barrier; BBB (+): good penetrator of the BBB; BBB (-): poor penetrator of the BBB; BSEP: bile salt export pump pharmacokinetic transporter; Caco-2(-): poor permeability in an *in vitro* cellular permeability assay with Caco-2 cells. clog*P*: logarithm of compound partition coefficient between n-octanol and water; HBA: number of hydrogen bond acceptors; HBD: number of hydrogen bond donors; HIA: human gastrointestinal absorption; HOB: human oral bioavailability; I: Toxicity category I is Highly toxic and Severely irritating; Mitoch: mitochondria; n-ROTB: number of rotatable bounds; OATP1B1(organic anion transporting polypeptide 1B1 pharmacokinetic transporter; OATP 1B3:organic anion transporting polypeptide1B3 pharmacokinetic transporter; PPB: plasma protein binding; P-gp: P-glycoprotein; PK: pharmacokinetic transporter; $P_{o/w}$: n-octanol/water partition coefficient; TPSA: polar surface area obtained from admetSAR version 2.

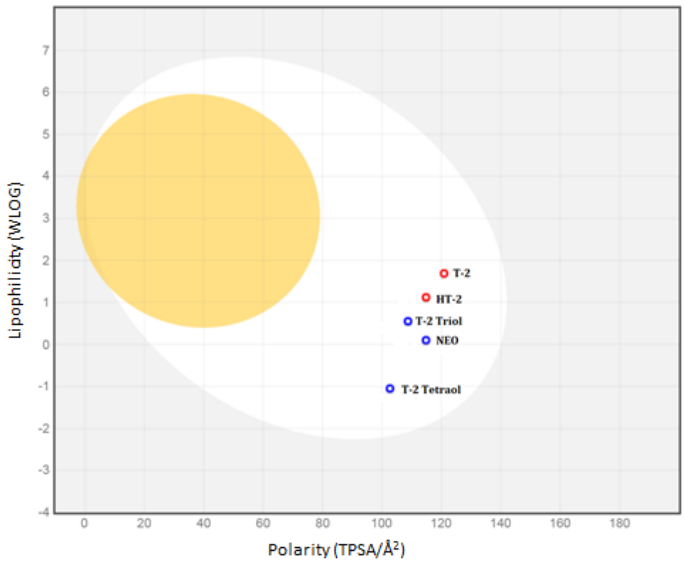

Figure 6. BOILED-Egg predictive model. The passive gastrointestinal absorption (HIA) and brain access (BBB) of T-2 and its modified forms. The region (yolk) is the physicochemical space of mycotoxins with highest probability to permeate the brain, and the white region is the physicochemical space of mycotoxins with highest probability of being absorbed by the gastrointestinal tract. The gray region represents an area of low permeability and absorption; blue circle represents positive P-gp; red circle represents negative P-gp.

4. Discussion

The T-2 is the most toxic of the type A trichothecene which is rapidly absorbed after ingestion, distributed without accumulation in any specific organs and rapidly metabolized by deacetylation resulting in the formation of HT-2, which is its major metabolite *in vivo*. Therefore, traditionally, toxicity studies are performed considering these two chemical forms. However, other reactions are involved during T-2 metabolism in mammals, which produce a great variety of

chemical forms, whose implication in the toxic effects of T-2 is the aim of this study. The hydrolysis is one reaction and, among others, the main modified forms obtained are NEO, T2-triol, and T2-tetraol (Figure 1; Nathanail et al., 2015).

The T-2 has been widely studied due to its high toxicity. However, there are few studies about the cytotoxicity of its metabolites, and even less studies on the interaction among them. In this study, cytotoxic effect of T-2 and its modified forms has been determined by *in vitro* assay in HepG2 cells. All individual mycotoxins showed a dose-dependent cytotoxicity respect to HepG2 cells proliferation. The cytotoxicity of T-2 and HT-2 observed in HepG2 cells are within the same range. It could be attributed to quickly biotransformation of T-2 into HT-2. Respect to the PC assay, an increase in cell viability was observed after low concentration of mycotoxins exposure in HepG2 cells. The increase in cell viability at low concentrations could suggest an adaptive response to T-2, HT-2, NEO and T-2 tetraol exposure. The cellular behavior characterized by low-concentration stimulation and high concentration inhibition of cell proliferation has been previously observed in HepG2 cells exposed to T-2 toxin (Fernández-Blanco et al., 2018; Taroncher et al., 2020a, Taroncher et al., 2020b). In this study, the order of cytotoxicity decreases in the following order: T-2 = HT-2 > NEO > T-2 triol > T-2 tetraol. Similar results to those reported in this study, were obtained by Ling et al. (2020) and Königs et al. (2009) on hepatic (HepG2) cells, renal (RPTEC) cells and lung fibroblasts (NHLF) exposed to equivalent doses of T-2 and its metabolites. Nevertheless, IC_{50} values differ from the values obtained in our study.

Cytotoxic differences among T-2 and its modified forms may be attributed to the increase of hydroxyl groups in structures as a consequence of hydrolysis,

leading to reduce the potency of the toxic effects. Wu et al. (2010) reported that hydrolysed metabolites of T-2 are less cytotoxic than the parent molecule, referring to hydrolysis and hydroxylation of the parent molecule as the major pathways involved in metabolism of T-2 (Figure 1). Moreover, these biotransformation pathways are the principal detoxification mechanisms associated with trichothecenes in mammalian cells (Wu et al., 2010; Li et al., 2011; Ling et al., 2020). On the other hand, the lower cytotoxic effect of NEO respect to T-2 and HT-2 can be due to the absence of lateral chain at C-8 which allows binding more easily to the ribosome causing saturation and consequently antagonistic effect at low doses (Ling et al., 2020). This hypothesis is supported by our results since antagonistic effect has been evidenced in all binary combination with NEO (Table 3).

Mycotoxin toxicity cannot always be predicted based on individual mycotoxins exposure. Evaluation of mycotoxin-mycotoxin interaction risk is an important part of food safety. To assess human exposure to metabolites of mycotoxins, in addition to the parent compounds, it should be considered that sometimes biotransformation leads to less toxic products that decrease the risk to exposed individuals. This fact is because many modified forms are hydrolysed into the parent compounds or released from the matrix during digestion. For this purpose, the interaction type should be characterized, in order to understand the potential for mycotoxin-mycotoxin interactions due to inhibition or induction of mechanisms dictating its toxicokinetics. So, it is necessary to carry out assays on mixture toxicity studies to simulate a real scenario of T-2 exposure. Respect to T-2 and its modified forms, the type of interaction varies depending on the mixture tested and their concentrations. As expected, in our study the order of cytotoxicity in the binary combinations correlates with the IC_{50} of the

individual mycotoxins (Table 2). The highest cytotoxic mixture was T-2+HT-2. The T-2 and HT-2 have similar and the highest individual cytotoxic effects (Table 1). On the other hand, the least cytotoxic combinations are those with T-2 triol or T-2 tetraol in the mixture (Table 2). The results obtained by Ling et al. (2020) were similar to ours results. These authors studied the effects of T-2 and its four metabolites in combination on porcine Leydig cells and they also observed that the most cytotoxic combinations are those containing T-2 in the mixture.

Respect to the interaction type, binary combinations of T-2+HT-2, T-2+T-2 tetraol, T-2 triol+HT-2, T-2 triol+T-2 tetraol and T-2 tetraol+HT-2 exerted an antagonistic effect at low fraction affect in the mixture ($\leq CI_{75}$ values) and an additive effect at higher one ($\geq CI_{75}$ values) (Table 3 and Figure 5). Whereas binary combinations of T-2+T-2 triol, T-2+NEO, T-2 triol+NEO, T-2 tetraol+NEO and NEO+HT-2 showed antagonistic effect at all concentrations tested in a concentration-dependent manner (Figure 5). The antagonistic effect at the high dose of combinations may be justified by their similar chemical structure and therefore they could compete for binding the same receptor. Thus, because of its minor steric hindrance the T-2 metabolites can bind to the receptor easier than T-2 and HT-2, and decrease the toxic response. These findings contribute significantly to the risk assessment, as it is demonstrated that T-2 biotransformation *in vivo* decreases the potential cytotoxic effect of T-2 in mammalian cells (Ling et al., 2020). Similar results were also recently observed by Ling et al. (2020), who reported antagonism at high concentrations in T-2+NEO and HT-2+NEO combinations. However, T-2+HT-2 displayed synergism at low fraction affected (*fa*) and antagonistic effect at high fraction affected in the mixture on porcine Leydig cells. Ruiz and co-workers (2011a,

2011b) evaluated the interactions among three *Fusarium* mycotoxins namely deoxynivalenol (DON), T-2 and beauvericin (BEA) in CHO-K1 and Vero cells. In all combinations with T-2 an antagonistic effect was observed, and the highest antagonistic effect was observed with the binary DON+T-2 combination. However, the binary combination T-2+BEA showed synergism. The difference between the type of interaction, as previously mentioned, is due to the similarity of the chemical structure between both trichothecenes DON and T-2, which favors competition for the same receptors. On the other hand, differences in both chemical structures and mechanism of action of T-2 and BEA, allowed to observe a synergistic effect result.

Other data in literature regarding to interaction types about mycotoxins' combinations differ from those tested in our study depending on the type of cells, the type of mycotoxin' mixtures and the concentrations chosen in the mixture. Fernández-Blanco et al. (2018) reported additive effect at high fraction affected (*fa*) in the T-2+patulin (PAT) combination. In that study, mycotoxins produced by different type of fungi were selected. These mycotoxins have different mechanism of action which may be the cause of the different behavior of the mycotoxins in the mixture. So, as previously mentioned, the type of mycotoxins present in the samples determine the type of occurring interaction.

As mentioned above, simultaneous presence of multiple mycotoxins could be harmful to cells, therefore, to know the potential risk of mycotoxins, it is really important to know their absorption and fate in organisms. In recent years, with the rapid development of computational toxicology, *in silico* methods has been widely used to predict the relevant properties of mycotoxins and other substances. During this period, there has been produced many software programs and computational methods which share the objective of predicting

ADME (absorption, distribution, metabolism and excretion) and toxicology approaches across different institutions (Myatt et al., 2018). Several guidance documents have been drafted to improve standardization, harmonization and update of *in silico* methods by regulatory authorities including EFSA (EFSA, 2016). The *in silico* toxicology methods are computational approaches that analyze, simulate, visualize or predict the toxicity of chemical products. These computational models deliver a rapid, intuitive and descriptive, easily reproducible, robust method to predict toxicokinetics of mycotoxins. These methods are usually used together with other toxicity tests and are based on experimental data, quantitative structure-activity relationship and scientific data. The predictive SwissADME computer model is considered as a valid alternative to experimental procedures (Daina & Zoete, 2016; Zoete et al., 2016; Daina et al, 2017).

Exposure to T-2 occurs primarily through ingestion. Oral absorption is affected by chemical structure of the mycotoxin, stability, contents of the gastrointestinal tract, residence time in the intestine, aqueous solubility, the rate of passive intestinal permeability or between tight intestinal cellular junctions, intestinal metabolism, carrier-mediate influx via active transport mechanism, and active efflux via transporters such as P-gp. The mycotoxins NEO, T-2 triol and T-2 tetraol have a strong affinity for the P-gp transporter (Figure 6; Table 4); so, this union could prevent the greater human gastrointestinal absorption compared to the other mycotoxins (T-2 and HT-2). However, on the other hand, T-2 showed the highest intestinal permeability due to it is highly soluble and high lipophilic to pass through the cell membrane (Table 4). Moreover, the presence of significant quantities of the CYP450 3A4 isozyme in the smaller intestine, which has substrate specificity similar to P-gp, could contribute to this effect.

The P-gp has a significant influence on substances absorption (by transporting molecules back into the gastrointestinal lumen), distribution (by preventing xenobiotics into important tissues like brain), metabolism (acting synergistically with CYP450 3A4), and excretion (by affecting both biliary and renal tubular function). Therefore, the action of P-gp could contribute to reach the target of mycotoxins or to remove the mycotoxins from cells before they exert the toxic effect (Wang et al., 2011). The T-2 and its four main metabolites exert passive gastrointestinal absorption (Table 4; Figure 6), but according to its affinity to P-gp, mycotoxins could be expelled from cells or absorbed.

On the other hand, mycotoxin-mycotoxin interactions are possible due to competition for the efflux transporter. As shown in the results of Table 4, the T-2 and its major metabolites inhibit relevant hepatocyte transports (OATP1b1 and OATP1b3) of each other concomitant mycotoxin. Inhibition of BSEP has also been observed. It is important when elevated bile acids levels are observed; due to the inhibition of this process may lead to cholestasis and potential hepatotoxicity in *in vivo* systems.

These results played an important role in clarifying how T-2 and its modified forms jointly impaired the HepG2 cells proliferation. However, more *in vivo* studies are required to verify our results. The toxicity of T-2 and its modified forms can either result from the parent T-2, or from potentially reactive or toxic metabolites which are formed during their biotransformation. In this study, all binary combinations of T-2 and its metabolites showed antagonism, which implies that the combination of T-2 metabolites provide a novel strategy for detoxification of T-2 and it may give a new insight on risk assessment strategies for the combination of mycotoxins and their modified forms. Furthermore, although SwissADME, admetSAR and BOILED-Egg models are a good

computational approach to mimic the behavior of the mycotoxins studied, further toxicological studies are needed to verify the prediction of the toxicity profile of T-2 and its metabolites.

CRediT authorship contribution statement

Mercedes Taroncher: Data curation, Formal analysis, Investigation, Methodology, Writing - original draft, Writing - review & editing. Yelko Rodríguez-Carrasco: Formal analysis, Project administration, Supervision, Writing - review & editing. María-Jos´e Ruiz: Conceptualization, Data curation, Investigation, Methodology, Supervision, Writing – review & editing.

Declaration of competing interest

The authors declare that they have no known competing financial interests or personal relationships that could have appeared to influence the work reported in this paper.

Acknowledgments

We are grateful for technical assistance from the SCSIE of the University of Valencia (Valencia, Spain). This research was funded by the project grant given by the Generalitat Valenciana (Spain) GV/2020/020 (Conselleria d'Innovacio, Universitats, Ciencia i Societat Digital, Generalitat Valenciana).

5. References

Chen, P., Xiang, B., Shi, H., Yu, P., Song, Y., Li, S., 2020. Recent advances on type A trichothecenes in food and feed: Analysis, prevalence, toxicity, and decontamination techniques. Food Control 118, 107371. https://doi.org/10.1016/j.foodcont.2020.107371

Cheng, F., Li, W., Zhou, Y., Shen, J., Wu, Z., Liu, G., Lee, P.W., Tang, Y., 2012. admetSAR: a comprehensive source and free tool for evaluating chemical ADMET properties. J. Chem. Inf. Model. 52, 3099-3105. https://doi.org/10.1021/ci300367a

Chou, T.C., 2006. Theoretical basis, experimental design, and computerized simulation of synergism and antagonism in drug combination studies. Pharmacol. Rev. 58, 621–681. https://doi.org/10.1124/pr.58.3.10

Chou, T.C., Talalay, P., 1984. Quantitative analysis of dose-effect relationships: the combined effects of multiple drugs or enzyme inhibitors. Adv. Enzym. Regul. 22, 27–55. https://doi.org/10.1016/0065-2571(84)90007-4

Daina, A., Zoete, V., 2016. A boiled-egg to predict gastrointestinal absorption and brain penetration of small molecules. Chem. Med. Chem. 11(11), 1117. https://doi.org/ 10.1002/cmdc.201600182

Daina A, Michielin O, Zoete V., 2017. SwissADME: a free web tool to evaluate pharmacokinetics, drug-likeness and medicinal chemistry friendliness of small molecules. Sci. Rep. 7, 42717. https://doi.org/10.1038/srep42717

Directive 2010/63/EU of the European Parliament and of the Council of 22 September 2010 on the protection of animals used for scientific purposes. DOUE L 276/33.

Dohnal, V., Jezkova, A., Jun, D., Kuca, K., 2008. Metabolic pathways of T-2 toxin. Curr. Drug Metab. 9, 77-82. https://doi.org/10.2174/138920008783331176

EFSA, 2014a. Modern methodologies and tools for human hazard assessment of chemicals. EFSA J. 12(4), 3638. https://doi.org/10.2903/j.efsa.2014.3638

EFSA, 2014b. CONTAM Panel (EFSA Panel on Contaminants in the Food Chain). Scientific opinion on the risks to human and animal health related to the presence of beauvericin and enniatins in food and feed. EFSA J. 12, 3802. https://doi.org/10.2903/j.efsa.2014.3802

EFSA, 2016. Setting of maximum residue levels for amitraz, coumaphos, flumequine, oxytetracycline, permethrin and streptomycin in certain products of animal origin. EFSA J. 14, e04570. https://efsa.onlinelibrary.wiley.com/doi/abs/10.2903/j.efsa.2016.4570D

EFSA, 2017. Panel on Contaminants in the Food Chain (CONTAM); Scientific Opinion on Appropriateness to set a group health based guidance value for T2 and HT2 toxin and its modified forms. EFSA J. 15, 4655. https://doi.org/10.2903/j.efsa.2017.4655.

EFSA, 2020a. European Food Safety Authority (EFSA), Craig, P. S., Dujardin, B., Hart, A., Hernandez-Jerez, A. F., Hougaard Bennekou, S., Kneuer, C., Ossendorp, B., Pedersen, R., olterink, G., Mohimont, L. Cumulative dietary risk characterisation of pesticides that have chronic effects on the thyroid. EFSA J. 18(4), e06088. https://doi.org/10.2903/j.efsa.2020.6088

EFSA, 2020b. Food Standards Agency (FSA), Animal and Plant Health Agency (APHA), Lorenzoni A, Tsoulli C, McCarthy C and Adkin A, 2020. Integration of computational tools, data analysis and social science into food safety risk assessment. EFSA J.18(S1):e181108, 12 pp. https://doi.org/10.2903/j.efsa.2020.e181108

Egan, W.J., Merz, K. M., Baldwin, J.J., 2000. Prediction of drug absorption using multivariate statistics. J. Med. Chem. 43, 3867-3877. https://doi.org/10.1021/jm000292e

Fernández-Blanco, C., Elmo, L., Waldner, T., Ruiz, M.J., 2018. Cytotoxic effects induced by patulin, deoxynivalenol and toxin T2 individually and in combination in hepatic cells (HepG2). Food Chem. Toxicol. 120, 12-23. https://doi.org/10.1016/j.fct.2018.06.019

Garreau De Loubresse, N., Prokhorova, I., Holtkamp, W., Rodnina, M.V., Yusupova, G., Yusupov, M., 2014. Structural basis for the inhibition of the eukaryotic ribosome. Nature 513, 517–522. https://doi.org/10.1038/nature13737.

Kar, S., Leszczynski, J., 2019. Exploration of computational approaches to predict the toxicity of chemical mixtures. Toxics 7(1), 15. https://doi.org/10.3390/toxics7010015

Knutsen, H.K., Barregard, L., Bignami, M., Bruschweiler, B., Ceccatelli, S., Cottrill, B., et al., 2017. Appropriateness to set a group health based guidance value for T2 and HT2 toxin and its modified forms. EFSA J. 15, 1–53. https://doi.org/10.2903/j.efsa.2017.4655.

Königs, M., Mulac, D., Schwerdt, G., Gekle, M., Humpf, H.U., 2009. Metabolism and cytotoxic effects of T-2 toxin and its metabolites on human cells in primary culture. Toxicology 258(2-3), 106-115. https://doi.org/10.1016/j.tox.2009.01.012

Li, Y., Wang, Z., Beier, R.C., Shen, J., Smet, D.D., De Saeger, S., Zhang, S., 2011. T-2 toxin, a trichothecene mycotoxin: review of toxicity, metabolism, and analytical methods. J. Agric. Food Chem. 59(8), 3441-3453. https://doi.org/10.1021/jf200767q

Ling, A., Sun, L., Guo, W., Sun, S., Yang, J., Zhao, Z., 2020. Individual and combined cytotoxic effects of T-2 toxin and its four metabolites on porcine Leydig cells. Food Chem. Toxicol. 139, 111277. https://doi.org/10.1016/j.fct.2020.111277

Lipinski, C.A., 2004. Lead- and drug-like compounds: the rule-of-five revolution. Drug Discov. Today Technol, 1(4), 337-341

Lu, H., Fernández-Franzón, M., Font, G., Ruiz, M.J., 2013. Toxicity evaluation of individual and mixed enniatins using an in vitro method with CHO-K1 cells. Toxicol in Vitro, 27, 672-680. https://doi.org/10.1016/j.tiv.2012.11.009

Myatt, G.J., Ahlberg, E., Akahori, Y., Allen, D., Amberg, A., Anger, LT., et al., 2018. In silico toxicology protocols. Regul. Toxicol. Pharmacol. 96, 1–17. http://www.sciencedirect.com/science/article/pii/S0273230018301144

Nathanail, A.V., Varga, E., Meng-Reiterer, J., Bueschl, C., Michlmayr, H., Malachova, A., et al., 2015. Metabolism of the Fusarium mycotoxins T-2 toxin and HT-2 toxin in wheat. J. Agricult. Food Chem. 63, 7862-7872. http:// doi.org/10.1021/acs.jafc.5b02697

Palm, K., Stenberg, P., Luthman, K., Artursson, P., 1997. Polar molecular surface properties predict the intestinal absorption of drugs in humans. Pharm. Res. 14(5), 568-571. http:// doi.org/10.1023/A:1012188625088

Raies, A.B., Bajic, V.B., 2016. In silico toxicology: computational methods for the prediction of chemical toxicity. WIREs Comput. Mol. Sci. 6, 147–172. http://doi.org/10.1002/wcms.1240

RASFF, 2020. Rapid Alert System for Food and feed. Annual Report. 2019. https://ec.europa.eu/food/safety/docs/rasff_annual_report_2019.pdf (Accessed October 16, 2020).

Ruiz, M.J., Festila, L.E., Fernández, M., 2006. Comparison of basal cytotoxicity of seven carbamates in CHO-K1 cells. Environ. Toxicol. Chem. 88, 345–354. https://doi.org/ 10.1080/02772240600630622.

Ruiz, M.J., Franzova, P., Juan-García, A., Font, G., 2011a. Toxicological interactions between the mycotoxins beauvericin, deoxynivalenol and T-2 toxin in CHO-K1 cells in vitro. Toxicon 58, 315-326. http://doi.org/10.1016/j.toxicon.2011.07.015

Ruiz, M.J., Macáková, P., Juan-García, A., Font, G., 2011b. Cytotoxic effects of mycotoxin combinations in mammalian kidney cells. Food Chem. Toxicol. 49, 2718-2724. http://doi.org/10.1016/j.fct.2011.07.021

Streit, E., Schatzmayr, G., Tassis, P., Tzika, E., Marin, D., Taranu, I., et al., 2012. Current situation of mycotoxin contamination and co-occurrence in animal feed focus on Europe. Toxins 4, 788–809. https://doi.org/10.3390/toxins4100788.

Sultana Shaik, A., Shaik, A. P., Jamil, K., Alsaeed, A.H., 2016. Evaluation of cytotoxicity and genotoxicity of pesticide mixtures on lymphocytes. Toxicol. Mech. Meth., 26, 588-594. https://doi.org/10.1080/15376516.2016.1218577

Taroncher, M., Tolosa, J., Prosperini, A., Ruiz, M.J., 2018. In silico and in vitro prediction of the toxicological effects of individual and combined mycotoxins. Food Chem. Toxicol. 122, 194-202. https://doi.org/10.1016/j.fct.2018.09.055

Taroncher, M., Rodríguez-Carrasco, Y., Ruiz, M.J., 2020a. T-2 toxin and its metabolites: Characterization, cytotoxic mechanisms and adaptive cellular response in human hepatocarcinoma (HepG2) cells. Food Chem. Toxicol. 145, 111654. https://doi.org/10.1016/j.fct.2020.111654

Taroncher, M., Pigni, M. C., Diana, M.N., Juan-García, A., Ruiz, M.J., 2020b. Does low concentration mycotoxin exposure induce toxicity in HepG2 cells through oxidative stress?. Toxicol Mech Meth, 1-10. https://doi.org/10.1080/15376516.2020.1757000

Tatay, E., Meca, G., Font, G., Ruiz, M.J., 2014. Interactive effects of zearalenone and its metabolites on cytotoxicity and metabolization in ovarian CHO-K1 cells. Toxicol. in Vitro 28, 95-103. https://doi.org/10.1016/j.tiv.2013.06.025

Van der Fels-Klerx, H.J., Klemsdal, S., Hietaniemi, V., Lindblad, M., Ioannou-Kakouri, E., van Asselt, E.D., 2012. Mycotoxin contamination of cereal grain commodities in relation to climate in North West Europe. Food Addit. Contam. 29, 1581–1592. https://doi.org/10.1080/19440049.2012.689996.

Wang, Z., Chen, Y., Liang, H., Bender, A., Glen, R.C., Yan, A., 2011. P-glycoprotein Substrate Models Using Support Vector Machines Based on a Comprehensive Data set. J. Chem. Inf. Model. 51, 1447–1456 doi.org/10.1021/ci2001583

Williams, J.A., Hyland, R., Jones, B.C., Smith, D.A., Hurst, S., Goosen, T.C., et al., 2014. Drug-drug interactions for UDP-glucuronosyltransferase substrates: a pharmacokinetic explanation for typically observed low exposure (AUCi/AUC) ratios. Drug Metab. Dispos. 32(11), 1201-1208

Wu, Q.H., Dohnal, V., Huang, L.L., Kuka, K., Yuan, Z.H., 2010. Metabolic pathways of trichothecenes. Drug Metab. Rev. 42, 250-267. https://doi.org/10.3109/03602530903125807

Wu, J., Tu, D., Yuan, L. Y., Yuan, H., & Wen, L. X., 2013. T-2 toxin exposure induces apoptosis in rat ovarian granulosa cells through oxidative stress. Environmental toxicology and pharmacology, 36(2), 493-500. https://doi.org/10.1016/j.etap.2013.03.017

Wu, Q.H., Wang, X., Yang, W., Nüssler, A.K., Xiong, L.Y., Kuca, K., et al., 2014. Oxidative stress-mediated cytotoxicity and metabolism of T-2 toxin and

deoxynivalenol in animals and humans: an update. Arch. Toxicol. 88, 1309–1326. https://doi.org/10.1007/s00204-014-1280-0.

Yang, H., Lou, Ch., Sun, L., Li, J., Cai, Y., Wang, Z.,et al., 2018. admetSAR 2.0: web-service for prediction and optimization of chemical ADMET properties. Bioinformatics bty707. https://doi.org/10.1093/bioinformatics/bty707

Zingales, V., Fedeli, C., Fernández-Franzón, M., Ruiz, M.J., 2020. Cytotoxic effects of individual and combined sterigmatocystin and nivalenol on liver hepatocellular carcinoma cells. Food Chem. Toxicol. 143, 111473. https://doi.org/10.1016/j.fct.2020.111473

Zoete, V., Daina, A., Bovigny, C., Michielin, O., 2016. SwissSimilarity: A Web Tool for Low to Ultra High Throughput Ligand-Based Virtual Screening J. Chem. Inf. Model. 56, 1399−1404. http://doi.org/10.1021/acs.jcim.6b00174

Foods, 13 (2024), 1501

https://doi.org/10.3390/foods13101501

3.3. Identification of biotransformation products of T-2 toxin in HepG2 cells using LC-Q-TOF MS

Mercedes Taroncher [1,2], Veronica Zingales [1,2], Yelko Rodríguez-Carrasco [1,2,*] and María-José Ruiz[1,2]

[1] Laboratory of Food Chemistry and Toxicology, Faculty of Pharmacy and Food Science, University of Valencia, av. Vicent Andrés Estellés s/n, Burjassot 46100, Spain.

[2] University of Valencia research group Alternative methods for determining toxic effects and risk assessment of contaminants and mixtures (RiskTox; GIUV2021-513).

Abstract

The T-2 toxin (T-2) is a type A trichothecene found in cereals. The formation of metabolites is a frequent cause of mycotoxin-induced toxicity. In this work, the conversion of T-2 during bio-transformation reactions in HepG2 cells was evaluated. For this, HepG2 cells were exposed to 30 ($IC_{50}/2$) and 60 (IC_{50}) nM of T-2 for 0, 1, 2, 3, 6, 8 and 24h, and the concentration of T-2 and its metabolites HT-2, T2-triol, T2-tetraol and neosolaniol were determined in both cell fraction and the culture medium, through liquid chromatography coupled to high-resolution mass spectrometry-time of flight (LC-Q-TOF MS). Results showed a fast metabolization of T-2 (>90%) during the first 2h, being the HT-2 its main (>95%) biotransformation product. The cell fraction showed higher levels ($p < 0.05$) of HT-2 (39.9 ± 2.1 nM) compared to the culture medium (12.53 ± 2.4 nM). This trend was also observed for the identified metabolites. T2-triol reached its maximum concentration (1.7 ± 0.4 nM) at 2h, and at later times, a time-dependent increase in the T2-tetraol and neosolaniol concentrations was observed. The identification of T-2 metabolites shows the need to continue combined toxicity studies of mycotoxins for a correct risk characterization to these natural contaminants.

Key words: T-2 toxin; biotransformation; HepG2; in vitro; LC-Q-TOF MS

Key Contribution: In this work, the biotransformation that occurs in the T-2 toxin, a mycotoxin that may be found in foods, was evaluated and its main metabolites were determined through confirmation methods both in the cellular fraction (HepG2 cells) and in the culture medium.

---

* **Corresponding author**: Laboratory of Food Chemistry and Toxicology, Faculty of Pharmacy and Food Science, University of Valencia, av. Vicent Andrés Estellés s/n, Burjassot 46100, Spain. E-mail address: Yelko.rodriguez@uv.es (Y. Rodríguez-Carrasco). Tel.: +34-96-3544-228; Fax: +34-96-3544-228.

1. Introduction

Field crops are naturally contaminated by several species of *Fusarium* fungi, which produce trichothecene mycotoxins. The mycotoxins have been frequently evaluated and, the European Food Safety Authority (EFSA) considers that due to the toxicity following dietary exposure, there is a potential risk for acute and chronic adverse effects in humans and animals [1]. Therefore, it is needed to identify and quantify their levels in cereals to monitor and verify that the established maximum levels are not exceeded. The T-2 toxin (T-2) is one of the most common mycotoxins of the trichothecenes found mainly in oat, wheat and wheat byproducts [2]. The exposure of T-2 in the population was calculated considering the concentration reported in wheat and wheat-based products and the average consumption of cereals. The maximum level of T-2 found in breakfast cereals for adults and infants was 4.47 μg/kg and 0.11 μg/kg, respectively [1]. Moreover, the wheat and wheat-based products consumption data reported by the Food Agriculture Organization was 0.27 kg/day [3]. According to the above, adults would be exposed to 2.59 nM T-2, whereas infants would be exposed to 0.064 nM T-2 .

As the most toxic trichothecene, the T-2 is regarded as the main cause of alimentary toxic aleukia disease (ATA), a gastrointestinal disorder, that affected World War II soldiers and people around the world after ingesting moldy food [4]. The ATA is characterized by vomiting, diarrhea, gastroenteritis, leukopenia (aleukia), hemorrhages, skin inflammation and in severe cases death due to asphyxia [5]. The ATA affected some people, especially those between the ages of 10 and 40, with a mortality rate of 60% in the former URSS from 1932 to 1947, mainly due to the large amount of T-2 ingested through grain. However, since then, more analysis on the levels of this mycotoxin in cereals have been

carried out and, the maximum levels established for the intake of grain without food risk have been determined. Since then, no further cases of ATA have been reported [6,7].

Rapidly after ingestion, the T-2 is mainly metabolized into HT-2 toxin (HT-2) in the liver, through a deacetylation reaction at C-4 position by intestinal microflora, and, in lower concentrations, various phase I and phase II metabolites [8]. It has been previously reported that the main metabolic pathways of T-2 in animals and humans are hydrolysis, hydroxylation, deepoxilation and glucuronidation [9–11]. Furthermore, animal species and gender may affect the metabolic pathway of T-2 [12]. Some of the main T-2 modified forms are HT-2, Neosolaniol (Neo), T2-triol, T2-tetraol, 3´-OH-HT-2, 3´-OH-T-2, deepoxy-3´hydroxy-HT-2, deepoxy-3´hydroxy-T-2 triol, deepoxy-15-acetyl-T-2 tetraol and deepoxy T-2 tetraol [13,14]. The main metabolic pathway of T-2 for humans, mice and rats is hydrolysis, and the HT-2 is the main metabolite [11]. The toxicity of the metabolites of T-2 is lower than that of T-2 [8,15]. Although, the toxicity of HT-2 is very similar to T-2, and their effects cannot be differentiated. The same modified forms were obtained after the metabolism of T-2 and HT-2 [14].

Biotransformation of T-2 results in increased solubility and facilitates excretion of the modified forms, thus reducing the mycotoxin-induced toxicity [12]. However, it should be taken into account that phase II metabolites of T-2 could be hydrolyzed to their parent compounds after intake [16]. Recently, the natural contamination and toxicity of mycotoxin metabolites found in cereals constitute a global health concern. Therefore, is of great interest to evaluate the biotransformation kinetics and identify the main products of T-2, to make a more accurate evaluation of real toxicity of the mycotoxin ingestion. Hepatic cell

lines such as human hepatocarcinoma (HepG2) cells are very appropriate for this evaluation, since they are sensitive to T-2 induced trans-formation into its modified forms. Moreover, the HepG2 cells have been widely accepted for assessment of xenobiotic induced toxicity and metabolism. It has been reported that HepG2 cells contain phase I and phase II enzymes such as CYP1A, CYP2C9, CYP2E1, CYP2D6 and glutathione-*S*-transferases [17,18]. Also, Ye and co-authors reported the presence of CYP1A1 in HepG2 cells [19]. Although the most abundant CYP isoenzyme in HepG2 cells is CYP3A4 [20]. Indeed, Tatay et al., reported that the HepG2 cells were able to biotransform some mycotoxins, such as the zearalenone (ZEA), to its metabolites [21]. And, the metabolic profiling of up to 20 mycotoxins was evaluated in HepG2 cells by Gerdermann et al., [22].

The application of liquid chromatography coupled to high-resolution mass spectrometry-time of flight (LC-Q-TOF MS) system, allows the identification and quantification of the metabolites in a very accurate manner. This structural elucidation of T-2 and its metabolites HT-2, Neo, T2-triol and T2-tetraol was possible by this combined method. To clarify the metabolism of T-2, in the present study we used HepG2 cells to evaluate the biotransformation products in a cycle of 24 h by identifying and quantifying the T-2 and its main metabolites in both, cell fraction and culture medium. The mycotoxins were selectively detected by LC-Q-TOF MS.

2. Material and Methods

2.1 Reagents

The reagent chemicals and cell culture compounds used: Dulbecco's Modified Eagle's Medium (DMEM), trypsin/EDTA solutions, Phosphate

Buffer Saline (PBS), penicillin, streptomycin and Newborn Calf Serum (NBCS) were purchased from Sigma-Aldrich (St Louis, USA). Methanol (MeOH) was acquired from Merck Life Science S.L. (Madrid, Spain). Deionised water (resistivity <18 MΩ cm) was obtained using a Milli-Q water purification system (Millipore, Bedford, MA, USA).

Standards of T-2 (MW:466.52 g/mol), HT-2 (MW:424.48 g/mol) and Neo (MW:382.40 g/mol) were purchased from Sigma-Aldrich and T2-triol (MW:382.45 g/mol) and T2-tetraol (MW:298.33 g/mol) were acquired from Cayman Chemical Company (St. Louis, MO, USA). Stock solutions of the mycotoxins were prepared in MeOH at appropriate working concentrations and maintained in the dark at -20 ºC.

On the other hand, a working standard solution at 10 μM T-2 was prepared to spike the culture medium (3 mL) and reaching final mycotoxin concentrations of 30 nM and 60 nM to incubate the cells. All standard solutions were kept in the darkness and stored at -20 ºC.

2.2. Cell culture and treatment

The HepG2 cells (ATCC: HB-8065) were seeded in DMEM medium supplemented with 100 U/mL penicillin, 10% NBCS and 100 mg/mL streptomycin. The pH 7.4, 5% CO_2 at 37 ºC and 95% air atmosphere at constant humidity were the incubation conditions. Cells were passaged twice a week with a small number of sub-passages (<20 subcultures) to maintain genetic homogeneity. The final mycotoxin concentrations assayed were achieved by adding T-2 to the culture medium with a final MeOH concentration ≤ 1% (v/v). Every experiment has appropriate controls with the same volume of solvent.

The T-2 concentrations selected in this study were IC_{50} (60 nM) and $IC_{50}/2$ (30 nM) obtained in previous assays carried out after 24 h of T-2 exposure in HepG2 cells by the methylthiazoltetrazolium salt (MTT) [23].

2.3. Experimental design for T-2 biotransformation study

HepG2 cells were cultured in 6-well tissue culture plates with 47.2×10^4 cells/well. After 80% of confluence of cells, the medium was replaced with fresh medium containing T-2 at 30 and 60 nM. Cells were exposed to the mycotoxin during 0, 1, 2, 3, 6, 8 and 24 h. A triplicate of experiments was performed at each exposure time. Neither the medium nor the mycotoxin were replaced during the exposure period. After each exposure time, the medium was collected in 15 mL Falcon tubes and 500 µL of trypsin were added to each well and the plates incubated for 1 min. Then, trypsin containing cells was transferred to a 5 mL Eppendorf Safe-Lock Microcentrifuge Tube.

2.4. Sample preparation

The extraction of T-2 and its biotransformation products from the medium was carried out following the protocol described by Taroncher et al., 2020. In summary, a 0.5 mL aliquot of medium was transferred to a 5 mL Eppendorf Safe-Lock Microcentrifuge Tube. Next, 3 mL of ethyl acetate were added, and the mixture was vortexed for 2 min and then centrifuged at 5600 × g at 4 °C for 5 min (Centrifuge 5810R, Eppendorf, Germany). The collected supernatant was dried under N_2 stream at 45ºC with a TurboVap-LV (Zymark, Allschwil, Switzerland). Subsequently, the residue was resuspended in a mixture of 140 µL of MeOH:water (70:30, v/v) and vortexed 1 min again before being filtered through a 0.22-µm filter and vialized for analysis.

On the other hand, extraction of the intracellular accumulation of T-2 and/or its biotransformation products was carried out as follows: the medium in the well was removed and 0.5 mL of trypsin was added to the cells. After that, trypsin containing cells was transferred to a 5 mL Eppendorf Safe-Lock Microcentrifuge Tube. Next, 3 mL of ethyl acetate were added, and the mixture was homogenized with an Ultra-Turrax Ika T18 basic (Staufen, Germany) for 2 min and subsequently centrifuged at 5600 × g at 4 °C for 5 min (Centrifuge 5810R, Eppendorf, Germany). The collected supernatant was dried under a nitrogen stream with a TurboVap-LV (Zymark, Allschwil, Switzerland) at 45 °C and resuspended in 140 μL of MeOH:water mixture (70:30, v/v) and 1 min vortexed. Finally, after extracting, it was filtered and vialized for subsequent analysis.

In parallel, the T-2 and its metabolites T2-triol, T2-tetraol, HT-2 and Neo, were incubated in growth media for 24 h at the same concentrations (30 and 60 nM) and conditions (≤1% MeOH in the medium). The extraction of the analytes was carried out as previously described. These samples were considered as control and used for recovery studies.

2.5. Determination of T-2 and its biotransform products by LC-Q-TOF MS

The analytical determination was carried out through LC-Q-TOF MS instrument equipped with a LC Agilent 1200-LC system (Agilent Technologies, Palo Alto, CA, USA) containing a vacuum degasser, an autosampler, a binary pump and a thermostatically controlled column chamber. The chromatographic column was a Gemini NX-C_{18} column (150 × 2 mm, i.d. 3 μm, Phenomenex, Torrance, California) and a guard column C_{18} (4 × 2 mm, i.d. 3 μM) kept at 30 ºC. The mobile phases were 0.1% formic acid aqueous solution and 5 mM

ammonium formate (A) and MeOH with 0.1% of formic acid and 5 mM ammonium formate (B) at a flow rate of 0.200 mL/min. The gradient elution program was: 0-0.5 min, 20% B; 0.5-1min, 20%~40% B; 1-6 min, 40%~100% B; 6-8 min, 100%~20% B; 8-14 min, 20% B. The injection volume was set to 20 µL.

Mass spectrometry was performed on a 6540 Agilent Ultra High Definition Accurate-Mass Quadrupole time-of-flight (Q-TOF) MS. The electrospray interface (DUAL AJS ESI) source was operated in positive (ESI+) mode. The following were the MS parameters set: seath gas temperature 350 ºC at a flow rate of 8 L/min, nebulizer pressure 45 psi, capillary voltage 3.5 kV, drying gas 10 L/min, skimmer voltage 65 V, gas temperature 300 ºC, octupole RF peak 750 V and fragmentor voltage 130 V. The scanning range was m/z 50~1000. The acquisition rate was 3 scans/s for the following collision energies: 10, 20 and 40 eV. Internal mass correction was enabled throughout two reference masses: m/z 121.050873 and 922.009798. Instrument control and data acquisition were performed using Agilent MassHunter Workstation software B.08.00. Potential analytes were identified by the MassHunter METLIN Metabolite PCD (Personal Compound Database) and PCDL (Personal Compound Database and Library) from Agilent Technologies.

The analyte identification in the target analysis was performed by comparing the retention times of peaks in positive samples with those provided by analytical standards. A strict mass error of 5 ppm was applied to each sample's matching theoretical mass. Identification points were achieved for suitable confirmatory methods as indicated the Commission Decision 2002/657/EC. On the other hand, for a retrospective analysis characteristics were first extracted from total ion chromatograms using the batch recursive feature extraction algorithm for

small molecules using Agilent MassHunter Profinder (Agilent Technologies). The settings for this algorithm were as follows: retention time filter, 1-14 min; ion intensity filter, 600 counts; retention time tolerance, ± 0.3 min; mass tolerance, ± 5 ppm; Q-score > 80. Following peak deconvolution and chromatographic peak alignment, the MassHunter Mass Profiler software and the Agilent Mycotoxins and Related Metabolites PCDL were used to identify the extracted features. The following criteria were used to identify the features: mass tolerance ± 5 ppm; positive ions included H+, NH4+; mass score, 100; isotope abundance score, 60; isotope spacing score, 50.

2.6. Method validation

For the quantitative analysis of T-2 and its biotransformation products, the method was fully validated according to Commission Decision 2002/657/EC concerning the performance of analytical methods. Selectivity was evaluated by using blank culture medium samples. Responses attributable to interfering components should not be more than 20% of the analyte's response at the limit of quantification (LOQ). The LOQ was defined as the lowest concentration within the linear range at which the instrument was capable to quantify the analyte with a mass error below 5 ppm. Carryover effect was evaluated by injecting blank samples after the highest calibration points of the calibration curves. The calibration curves were constructed by a linear regression model in a linear range from LOQ to 120 ng/mL and at least six calibration standard levels should meet the acceptance criteria. The concentration levels of the calibration curves were analyzed to evaluate the accuracy and precision in five replicates within three validation batches. The signal suppression-enhancement (SSE) was evaluated by comparing signal intensities from blank samples spiked

at 30 nM after extraction with those obtained from injection of neat standard solutions at same concentration dissolved in the injection solvent. A SSE value of 100% indicates that no matrix effect was present. SSE values below 100% indicate signal suppression and values above 100% indicate signal enhancement. The accuracy and precision were assessed in triplicate (repeatability, RSDr) on three different days (reproducibility, RSDR). The recovery was determined by comparing the analytes responses in blank and spiked samples at 30 and 60 nM of each mycotoxin. The precision was assessed by calculating the relative standard deviation (RSD).

Data from mass spectrometry and chromatographic were used to confirm the presence of analytes in the samples. Therefore, mycotoxin identification was carried out at each of the following identification points: the exact mass set to five decimal places and the retention time from extracted ion chromatogram of the peak in samples compared with those of standard solutions at a tolerance of ± 2.5% were used to confirm the peaks for the mycotoxins included in this study. The mass accuracy (Δ) for a measured ion was calculated according to the following formula and reported as part-per-million (ppm):

$$\Delta(ppm) = 1 \times 10^6 \frac{(m/z_{\text{measured}} - m/z_{\text{theoretical}})}{m/z_{\text{theoretical}}}$$

The effectiveness of the validated method was demonstrated by including a blank sample, a reagent blank, a replicate sample, and the lowest calibration point at the beginning and at the end of each group of samples for quality assurance/quality control (QA/QC) analysis. Samples were analyzed in duplicate and quantifiable values of mycotoxins should be identified in both replicates for confirmatory purposes.

2.7. Statistical analysis

The statistical software Statgraphics version 16.01.03 (IBM Corp., Armonk, NY, USA) was used to analyze the data statistically. Three independent experiments´mean ± standard error of the mean (SEM) was used to express the data. The Student t-test for paired samples was used to statistically analyze the data. The one-way analysis of variance (ANOVA), followed by Tukey HDS *post-hoc* test for multiple comparisons was used for analyze differences between groups. Statistical significance was considered as $p \leq 0.05$.

3. Results and Discussion

3.1. Optimization of Q-TOF HRMS parameters

By injecting the analytical standards of T-2, HT-2, T2-triol, T2-tetraol and Neo at a concentration of 1 μg/mL, the compound-dependent MS parameters were optimized. The instrument operated in both ionization modes in order to determine the ionization mode that generated better ionization of the analytes under study. To evaluate the accuracy of the mass measurements, they were also compared to the theoretical masses. The studied mycotoxins formed stable ammonium and protonated adducts and therefore they were monitored to evaluate the fragments that generated greater intensity for subsequent analysis. Table 1 shows the analytical parameters of the studied compounds referring to elemental composition, retention time, adduct ion, measured mass, mass accuracy and fragmentation pattern. Analytes eluted from 8.84 to 11.62 min. As expected, T-2 metabolites eluted first meaning they showed a more polar character, and they are considered as a detoxification products of parent compound being in agreement with previous studies [10]. When compared to the theoretical masses, the chosen ions showed excellent accuracy, with mass

errors within a strict range (< 2 ppm). For T-2, HT-2 and Neo the characteristic ammonium adducts $[M + NH4]^+$ showed the highest intensity whereas the protonated ions $[M + H]^+$ for T2-triol and T2-tetraol were chosen based in the displayed intensities.

Table 1. LC-Q-TOF MS parameters for the target mycotoxins

Compound	Retention time (min)	Molecular formula	Measured mass (*m/z*)	Adduct	Mass accuarcy (Δ ppm)	Major fragments
T-2	11.62	$C_{24}H_{34}O_9$	484.2541	$[M+NH_4]^+$	-0.81	365[a], 305
HT-2	10.87	$C_{22}H_{32}O_8$	442.2435	$[M+NH_4]^+$	-1.26	263[a], 323
T2-triol	9.75	$C_{20}H_{30}O_7$	383.2064	$[M+H]^+$	-1.02	303[a], 125
T2-tetraol	9.91	$C_{15}H_{22}O_6$	299.1495	$[M+H]^+$	-0.54	285[a], 102
Neo	8.84	$C_{19}H_{26}O_8$	400.1966	$[M+NH_4]^+$	-1.21	215[a], 245

[a]The base peak in the MS/MS spectra

3.2. Method performance

Table 2 summarizes the results of the method validation. The signal response of the investigated MS, in an interval of 6 points between the LOQ and 120 ng/mL, was linear for all analytes, obtaining a correlation coefficient greater than 0.990 for the evaluated mycotoxins. Regarding the matrix effect, all analytes showed an absolute value of matrix effect greater than 90%. These results indicated that the culture medium barely influenced the response of the analytes and these could be quantified through a calibration curve built in solvent. The accuracy results showed that the extraction of the analytes was optimal at the two concentration levels tested, obtaining a recovery range from 80.4 to 84.1%

at 30 nM and from 87.3 to 94.6% at 60 nM. Likewise, the method was repeatable and reproducible, showing RSDr and RSDR values lower than 10% and 12%, respectively, in all cases. The LOQs obtained showed good sensitivity, being able to quantify concentrations of the assayed mycotoxins between 0.02 and 0.2 ng/mL.

Table 2. Method performance.

Analyte	SSE[a] (%)	Recovery (%)		Precision (%) [RSD_r[b], (RSD_R[c])]		LOQ[d] (ng/mL)
		30 nM	60 nM	30 nM	60 nM	
T-2	95	84.1	94.6	6.3 (9.2)	5.4 (8.2)	0.05
HT-2	97	82.0	90.8	7.2 (9.5)	6.3 (7.6)	0.10
T2-triol	91	83.1	90.3	6.7 (10.3)	7.2 (9.7)	0.04
T2-tetraol	90	80.9	89.7	6.4 (10.5)	8.6 (10.8)	0.02
Neo	94	80.4	87.3	9.1 (11.7)	5.9 (9.4)	0.20

[a]SSE: signal suppression-enhancement; bRSDr: repeatability; cRSDR: reproducibility; dLOQ: limit of quantification.

3.3. Identification of T-2 and its metabolites

To study the biotransformation of T-2 by HepG2 cells, the cells were exposed to 30 and 60 nM of T-2 for a time of 0, 1, 2, 3, 6, 8 and 24 h. Each assay was carried out in triplicate and after each exposure time the culture medium was collected. Similarly, the cells contained in the wells were redissolved in 0.5 mL of trypsin and these cell fractions were taken to evaluate the intracellular accumulation of T-2 and/or its bio-transformation products. The extraction and

determination of T-2 and its metabolites in both the culture medium and the cells were carried out as previously mentioned.

The results revealed a rapid and complete T-2 biotransformation based on the mass shift of metabolites obtained from MS full scan and MS/MS. Metabolites are typically slightly different from those of the parent compound due to metabolic transformation pathways known as oxidation by enzymes in microsomal cytochromes P450, reduction by epoxide-hydrolases and hydrolysis by non-specific esterases and amidases. Hydroxylation has been well characterized, which is catalyzed by CYP450 enzymes [24].

Despite these modifications, during collision-induced dissociation they still retain a common skeleton, resulting in similar fragmentation patterns. Consequently, the chemical structures of T-2 metabolites were evaluated by analyzing the mass change and fragmentation pattern obtained from the full MS scan and MS/MS analysis. Figures 1 and 2 and tables S1 and S2 show the evolution of T-2 levels (60 nM) and its bio-transformation products in both, the HepG2 cellular fraction and the cultured medium, respectively, collected at different assayed times.

At time 0 h, after comparing the signal obtained from the MS full scan and MS/MS analysis with the mycotoxin standards, it was found that the observed peak had the same retention time (Rt=11.62 min), accurate MS value (ammonium adduct $[M+NH4]^+$ at m/z 484.2539, −0.81 ppm), and MS/MS fragmentation pattern than T-2 standard. In fact, the MS/MS spectra of the observed peak generated product ions at m/z 305 due to the elimination of the acetic acid side chain (42 Da) in position C-4 and at m/z 365 because of the breakage of the isovaleric acid side chain at the C-8 position and a neutral loss of $NH_3 \cdot H_2O$ (119 Da) (Figure 3). Therefore, T-2 was the only mycotoxin

identified at 0 h in the culture medium and quantified at 58.7 ± 1.7 nM, and none of its metabolites were detected in the medium or inside the cell, probably due to the short exposure time that was not sufficient for its metabolization.

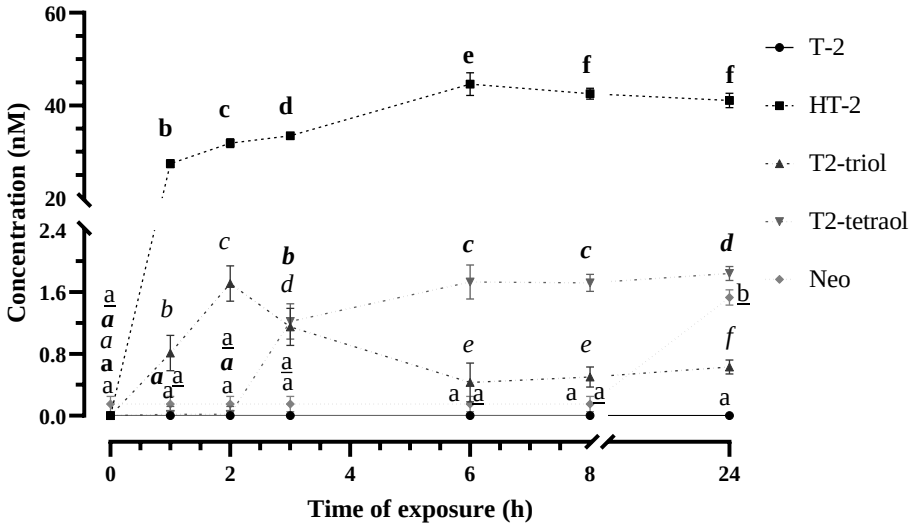

Figure 1. Concentration of T-2, HT-2, T2-triol, T2-tetraol and Neo identified and quantified by LC-Q-TOF MS in the cell fraction of HepG2 cells after 0, 1, 2, 3, 6, 8 and 24 h of 60 nM of T-2 exposure. Values are expressed as mean ± SEM (n = 3). Values with different superscript letter for each metabolite are significantly different ($p \leq 0.05$). The black superscript letter indicates the statistic of T-2. The bold superscript letter indicates the statistic of HT-2. The cursiva superscript letter indicates the statistic of T2-triol. The bold cursiva superscript letter indicates the statistic of T2-tetraol. The underlined superscript letter indicates the statistic of Neo.

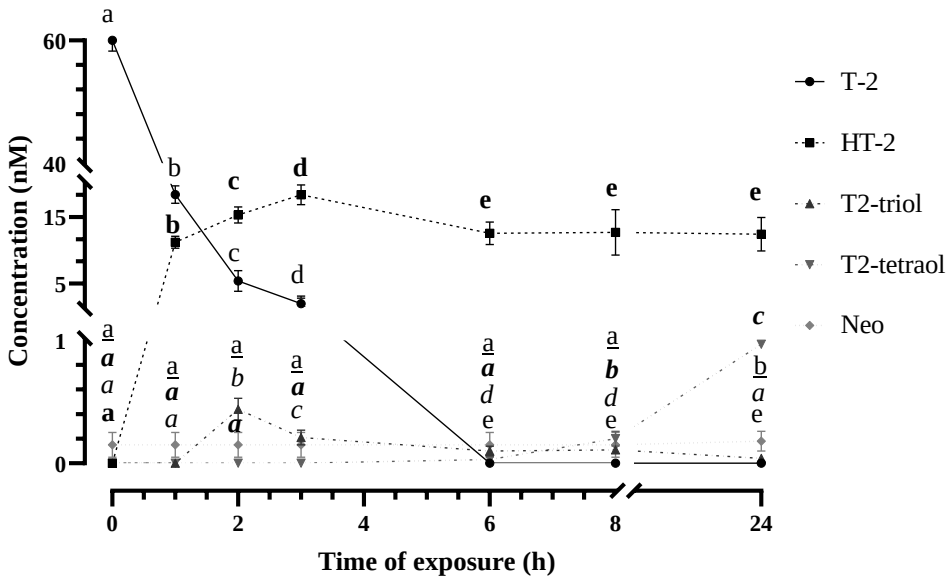

Figure 2. Concentration of T-2, HT-2, T2-triol, T2-tetraol and Neo identified and quantified by LC-Q-TOF MS in the culture medium of HepG2 cells after 0, 1, 2, 3, 6, 8 and 24 h of 60 nM of T-2 exposure. Values are expressed as mean ± SEM (n = 3). Values with different superscript letter for each metabolite are significantly different ($p \leq 0.05$). The black superscript letter indicates the statistic of T-2. The bold superscript letter indicates the statistic of HT-2. The cursiva superscript letter indicates the statistic of T2-triol. The bold cursiva superscript letter indicates the statistic of T2-tetraol. The underlined superscript letter indicates the statistic of Neo.

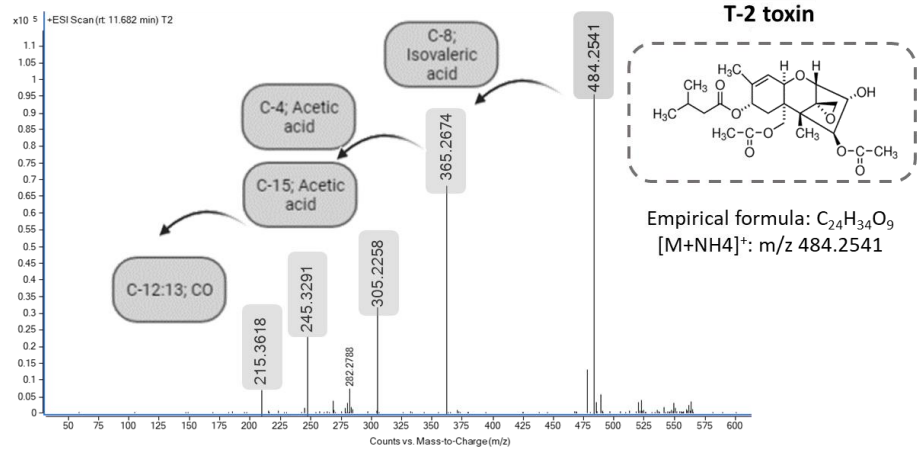

Figure 3. Mass spectra of T-2 standard. Precursor ion at *m/z* 484.2541 ($[H+NH4]^+$) and major product ions at *m/z* 365.2674 and *m/z* 205.2258.

Nonetheless, after 1 h of exposure, the T-2 concentration found in the culture medium was significantly lower (18.3 ± 1.3 nM) compared to the initial time, being the T-2 not detected in the cell fraction. In addition, at this exposure time, another signal was detected at 10.87 min (ammonium adduct $[M+NH4]^+$ at *m/z* 442.2435, −1.26 ppm) both in the culture medium and in the cell fraction. The MS/MS spectra of this signal generated fragment ions at *m/z* 323 by the cleavage of the isovaleric acid side chain at the C-8 position and the C-3 or -4 position (H_2O), and at *m/z* 263, which is formed from *m/z* 323 by the loss of the acetyl group and H_2O (60 Da) at C-15 position. Hence, this mycotoxin was identified as HT-2 being the above-mentioned data similar when compared with the HT-2 analytical standard. HT-2 was quantified at 11.2 ± 2.1 nM and 27.4 ± 3.5 nM in culture medium and cell fraction, respectively, after 1 h of exposure. In addition, a weak signal was also detected at 9.75 min, being its accurate MS value (protonated adduct $[M+H]^+$ at *m/z* 383.2064, −1.02 ppm), and MS/MS fragmentation pattern similar than T2-triol analytical standard (Figure 4). Hence,

T2-triol (also known as deacetyl HT-2 toxin) was only detected at 0.82 ± 0.2 nM in cell fraction after 1h of T-2 exposure.

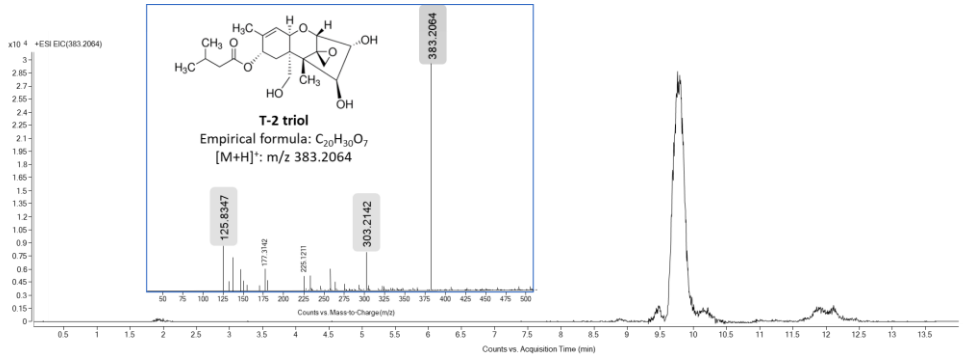

Figure 4. Total ion chromatogram (*m/z* 383.2064 $[M+H]^+$) and mass spectra of T2-triol standard. The major product ion peak was obtained at *m/z* 303.2142.

Following 2 and 3 h of T-2 exposure to HepG2 cells, a significant decrease in the mycotoxin concentration in the culture medium was again observed (5.5 ± 0.9 nM after 2 h and 1.9 ± 0.3 nM after 3 h of exposure). This reduction evidenced the biotransformation of T-2 into its metabolites HT-2 and T2-triol. In detail, an increase ($p < 0.05$) in the concentration of HT-2 was observed in both the cell fraction (32.5 ± 2.8 nM at 2h and 36.0 ± 3.1 nM at 3h) and in the culture medium (15.6 ± 2.0 nM at 2h and 18.2 ± 3.4 nM at 3h). About T2-triol, a significant reduction in the concentration of this metabolite was observed in both the cell fraction and in the culture medium between these investigated times (1.7 ± 0.4 nM versus 1.1 ± 0.3 nM in cell fraction and 0.5 ± 0.1 nM vs 0.2 ± 0.03 nM in culture medium at 2 and 3h, respectively). It is noteworthy that after 3 h of exposure, a slight signal was additionally detected at 9.91 min in samples from cell fraction, being its accurate MS value (protonated adduct $[M+H]^+$ at

m/z 299.1495, −0.54 ppm), and MS/MS fragmentation pattern coincident with the values obtained from the T2-tetraol analytical standard (Figure 5). Thus, the reduction in T2-triol levels could be due to its biotransformation to T2-tetraol since this can be formed after dealkylation of T2-triol or deacetylation of neosolaniol-derived metabolites, as previously reported by Yang et al. [13].

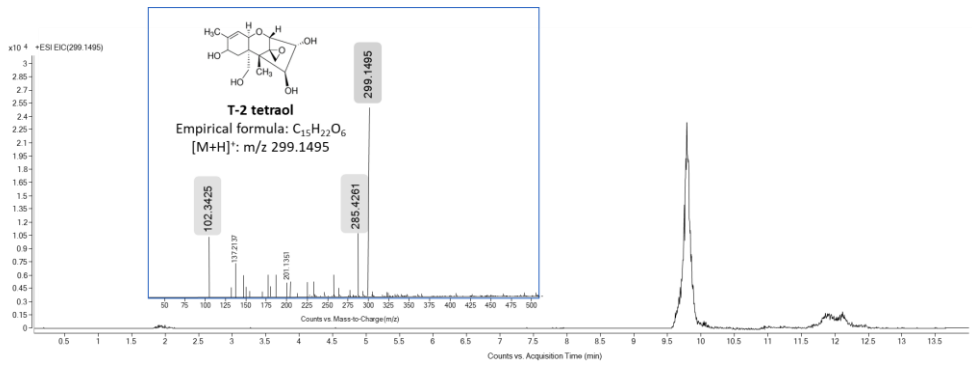

Figure 5. Total ion chromatogram (m/z 299.1495 $[M+H]^+$) and mass spectra of T2-tretraol standard. The major product ion peak was obtained at m/z 285.4261.

After 6 hours of exposure, T-2 is no longer detected in the culture medium. As far as its main metabolite is concerned, a reduction ($p < 0.05$) in HT-2 concentration was quantified, with no significant changes observed in its levels between 6 h and 24 h (12.53 ± 2.4 nM) of exposure. In parallel, a significant increase in HT-2 levels was observed in the cell fraction at 6 h (44.4 ± 3.9 nM) and subsequently a reduction, with no differences ($p < 0.05$) between 8 h and 24 h (39.9 ± 2.1 nM). Concerning T2-triol, the levels found in the culture medium were significantly reduced throughout the exposure time and were not detected after 24 h. Similarly, in the cell fraction, a reduction ($p < 0.05$) in levels of this

metabolite was observed between 3 h (1.1 ± 0.6 nM) and 6h (0.4 ± 0.07 nM) of exposure, and subsequently the levels fluctuated up to a concentration of 0.64 ± 0.12 nM at 24 h of exposure. These fluctuations could be justified considering the results observed for the toxin T2-tetraol, since a significant increase in its concentration was observed as the exposure time increased from 3 h (1.20 ± 0.3 nM) to 24 h in the cell fraction (1.8 ± 0.7 nM). Regarding the culture medium, T2-tetraol was detected for the first time at 6 h of exposure (0.03 ± 0.01 nM) and its concentration increased significantly until 24 h (1.05 ± 0.03 nM).

Finally, after 24 h of exposure, a new but weak signal was detected in both, the culture medium and the cell fraction. This metabolite was eluted at 8.84 min and showed an $[M+NH4]^+$ ion at m/z 400.1966 (−1.21 ppm) with the elemental composition of $C_{19}H_{30}NO_8$, suggesting that it was a metabolite of T-2 with the cleavage of an isovaleryl at the C-8 position. The MS/MS spectra of this signal generated fragment ions at m/z 245 and 215, which correspond to [T2 – isoval acid – 2 acetic acid+H]$^+$ (sum formula neutral compound $C_{15}H_{16}O_3$) and [T2 – isoval acid – 2 acetic acid – CH_2O+H]$^+$ (sum formula neutral compound $C_{14}H_{14}O_2$), respectively (Figure 6). These MS and MS/MS values were coincident with the values of the Neo analytical standard. Hence, Neo was quantified at 0.2 ± 0.02 nM and at 1.54 ± 0.61 nM in culture medium and cell fraction, respectively, after 24 h of T-2 exposure in HepG2 cells. This metabolite could be further metabolized to 4-deacetyl-neosolaniol and 15-deacetyl-neosolaniol and then to T2-tetraol after deacetylation, as also evidenced Yang et al. [25].

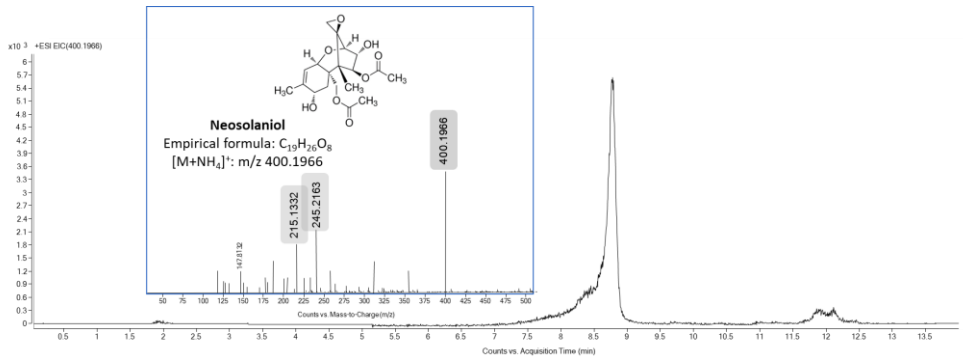

Figure 6. Total ion chromatogram (m/z 400.1966 $[M+NH4]^+$) and mass spectra of Neo standard. The major product ion peak was obtained at m/z 245.2163.

On the other hand, after total ion chromatograms were properly processed to eliminate unnecessary information and produce accurate findings, a retrospective analysis of samples based on the Related Metabolites PCDL and the spectrum library Agilent Mycotoxins was carried out. The results showed that additional metabolites were putatively identified in both, culture medium and cell fraction samples, collected after 6 hours of exposure to T-2. In detail, weak signals produced peaks at 9.45 min (m/z 500.2487) and at 9.21 min (m/z 458.2371). These ions were observed to have a mass 16 Da higher than T-2 and HT-2, respectively. This suggests that they were monohydroxylated forms of T-2 ($C_{24}H_{38}NO_{10}^+$) and HT-2 ($C_{22}H_{36}NO_9^+$). Based on previous research on T-2 biotransform products, these metabolites were identified to be 3'-OH-T-2 and 3'-OH-HT-2, respectively [13,26]. However, these signals were weak in the detected samples and could not be confirmed due to the lack of analytical standards.

T-2 metabolism is very complex because there are many metabolites detected and the CYPs involved depend on the species. According to Lootens et al., during the hydroxylation of T-2 toxin in liver, the CYP450s plays an important

role in the process of T-2 biotransformation and the CYPs involved differ among different species of animals. The main CYP-enzymes involved in the metabolism of T-2 would be CYP3A22, CYP3A29 and CYP3A46 in pigs [27], CYP1A4, CYP1A5, CYP2C18 and CYP3A37 in chicken [28] and CYP1A1, CYP1A2, CYP2A1 and CYP2B4 in rabbits [29]. On the other hand, Lin et al. reported that the contributions of the CYP450 enzyme family to T-2 metabolism in vitro followed the descending order CYP3A4, CYP2E1, CYP1A2, CYP2B6 or CYP2D6 or CYP2C19 [30]. However, it has been reported also a variety of results depending on the cell species. For example, the enzyme that plays the main role in the metabolism of T-2 is the CYP1A1 in Caco-2 cells [31], the CYP3A4 and CYP1A1 in HepG2 cells [15,32–34] and the CYP3A46 in porcine primary hepatocytes [35].

Regarding the results obtained after exposing HepG2 cells to 30 nM of T-2 and studying their biotransformation from 0 to 24h, it should be noted that only HT-2 was detected in quantifiable amounts (from LOQ to 17.9 ± 2.3 nM) (Figure 7). The evolution of HT-2 levels reproduces the trend observed in the study carried out with 60 nM of T-2 (data not shown). The rest of the metabolites identified in the targeted and retrospective study at the 60 nM of T-2 were not detected at 30 nM of T-2. Probably due to the low levels that would be below the LOQ of the method, despite showing good sensitivity. This T-2 concentration corresponds to the $IC_{50}/2$ value according to other studies [15]. Conducting studies at low doses of T-2 is appropriate given the levels of mycotoxin contamination that typically appear in foods. Even at these doses, the toxic effects are notable, which could involve activation of oxidative stress, mitochondrial damage, abnormal DNA methylation, autophagy and apoptosis as recently reviewed in literature [36,37]. This is also highlighted by the results

of a study carried out at low doses of T-2 (50% LOAEL), they published that T-2 reduces the synthesis of the anti-inflammatory cytokines such as TGF-β and increases the secretion of proinflammatory cytokines, compromisings the integrity of the intestinal mucosal barrier [38]. Furthermore, combined toxic effects due to the co-exposure of T-2 and its metabolites should be also considered, because of combinations exhibit varying degrees of cytotoxicity compared to the mycotoxins ingestion individually, with stronger cytotoxicity as recently reviewed by Skrzydlewski and colleagues [39].

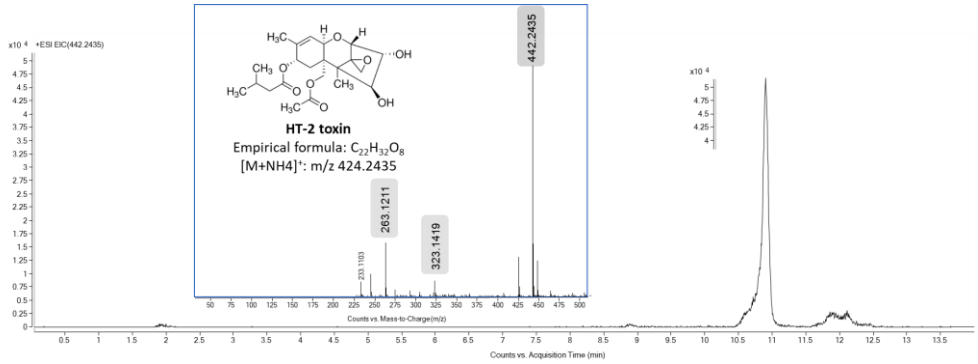

Figure 7. Total ion chromatogram (m/z 442.2435 $[M+NH4]^+$) and mass spectra of HT-2 standard. The major production peak was obtained at m/z 263.1211.

The findings on the T-2 biotransformation products over 24 h would help to fill the gap on the field of trichothecenes. They contribute to providing further information needed to update the established maximum levels of T-2 exposure based on the expected toxicity of this mycotoxin and its metabolites and the possible effects of synergism or interaction between them. In this way, a better risk assessment is carried out, given that in recent years the EFSA has considered that the T-2 toxicity was dismissed and it has been reassessed.

4. Conclusions

A sensitive LC-QTOF MS method was applied for the structural elucidation of T-2 biotransformation products formation along 24 h in *in vitro* system. The T-2 was rapidly metabolized by HepG2 cells and its hydroxilation metabolites were quantified being HT-2, T2-triol, T2-tetraol and Neo the main metabolites. Through the combination of the accurate mass measurements providing qualitative information of TOF and the MassHunter Mass Profiler software additional metabolites were putatively identified. Additional investigation is required to comprehend the molecular processes behind the cytotoxicity of several mycotoxins in animals and humans. This includes to deep into the whole route and alterations of important enzymes in the mycotoxins pathway.

The next step in the research would be to study the toxicity produced by the mixture of these mycotoxins. In the future, it is intended to make binary and tertiary combinations and to test the possible synergistic, additive or antagonistic effects. Furthermore, with *in silico* computational methods, it is pretended to establish which are the target organs of these mycotoxins, to orientate the possible toxicity in 3D to carry out assays in hepatic spheroids.

Author Contributions: Conceptualization, M.T., Y.R.-C. and M.-J.R.; methodology, M.T. V.Z. and Y.R.-C.; software, MT.T. and Y.R.-C.; validation, M.T., Y.R.-C. and M.-J.R.; formal analysis, M.T., V.Z. and Y.R.-C.; investigation, M.T. and Y.R.-C.; resources, M.T. and Y.R.-C.; data curation, M.T., and Y.R.-C.; writing—original draft preparation, M.T., V.Z. Y.R.-C. and M.-J.R.; writing—review and editing, M.T., V.Z., Y.R.-C. and M.-J.R.; visualization, M.T., V.Z., Y.R.-C. and M.-J.R.; super-vision, Y.R.-C. and M.-J.R.; project administration, M.-J.R.; funding acquisition, M.-J.R.. All authors have read and agreed to the published version of the manuscript.

Funding: This research was funded by the Spanish Ministry of Science and Innovation PID2020-115871RB-I00, MCIN/AEI/ 10.13039/501100011033.

Informed Consent Statement: Not applicable.

Data Availability Statement: Data is contained within the article.

Acknowledgments: M. Taroncher is grateful for the predoctoral grant PRE2021-096941 provided by the Spanish Ministry of Science and Innovation project. Veronica Zingales was supported by a Generalitat Valenciana grant with number APOSTD/CIAPOS2021.

Conflicts of Interest: The authors declare no conflicts of interest.

5. References

1. EFSA, 2017. Human and Animal Dietary Exposure to T-2 and HT-2 Toxin. EFSA Journal 2017, 15, doi:10.2903/j.efsa.2017.4972.
2. Chen, P.; Xiang, B.; Shi, H.; Yu, P.; Song, Y.; Li, S. Recent Advances on Type A Trichothecenes in Food and Feed: Analysis, Prevalence, Toxicity, and Decontamination Techniques. Food Control 2020, 118.
3.Food Balance Sheet, 2020, March 20. FAOSTAT. Http://Faostat.Fao.Org.
4. Königs, M.; Mulac, D.; Schwerdt, G.; Gekle, M.; Humpf, H.U. Metabolism and Cytotoxic Effects of T-2 Toxin and Its Metabolites on Human Cells in Primary Culture. Toxicology 2009, 258, 106–115, doi:10.1016/j.tox.2009.01.012.
5. Yagen, B.; Joffe, A.Z. Screening of Toxic Isolates of Fusarium Poae and Fusarium Sporotrichioides Involved in Causing Alimentary Toxic Aleukia; 1976, 32 (3), 423-427.
6. Peraica, M.; Radic, B.; Lucic, A.; Pavlovic, & M. Toxic Effects of Mycotoxins in Humans; 1999, 77(9), 754.
7. Peraica, M.; Richter, D.; Rašić, D. Mycotoxicoses in Children. Arh Hig Rada Toksikol 2014, 65, 347–363.
8. Ling, A.; Sun, L.; Guo, W.; Sun, S.; Yang, J.; Zhao, Z. Individual and Combined Cytotoxic Effects of T-2 Toxin and Its Four Metabolites on Porcine Leydig Cells. Food and Chemical Toxicology 2020, 139, 111277. doi:10.1016/j.fct.2020.111277.
9. Welsch, T.; Humpf, H.U. HT-2 Toxin 4-Glucuronide as New T-2 Toxin Metabolite: Enzymatic Synthesis, Analysis, and Species Specific Formation of T-2 and HT-2 Toxin Glucuronides by Rat, Mouse, Pig, and Human Liver Microsomes. J Agric Food Chem 2012, 60, 10170–10178, doi:10.1021/jf302571y.
10. Wu, Q.H.; Wang, X.; Yang, W.; Nüssler, A.K.; Xiong, L.Y.; Kuča, K.; Dohnal, V.; Zhang, X.J.; Yuan, Z.H. Oxidative Stress-Mediated Cytotoxicity and Metabolism of T-2 Toxin and Deoxynivalenol in Animals and Humans: An Update. Arch Toxicol 2014, 88, 1309–1326.
11. Yang, S.; Li, Y.; Cao, X.; Hu, D.; Wang, Z.; Wang, Y.; Shen, J.; Zhang, S. Metabolic Pathways of T-2 Toxin in in Vivo and in Vitro Systems of Wistar Rats. J Agric Food Chem 2013, 61, 9734–9743, doi:10.1021/jf4012054.
12. Wu, Q.; Qin, Z.; Kuca, K.; You, L.; Zhao, Y.; Liu, A.; Musilek, K.; Chrienova, Z.; Nepovimova, E.; Oleksak, P.; et al. An Update on T-2 Toxin and Its Modified

Forms: Metabolism, Immunotoxicity Mechanism, and Human Exposure Assessment. Arch Toxicol 2020, 94, 3645–3669.
13. Yang, S.; De Boevre, M.; Zhang, H.; De Ruyck, K.; Sun, F.; Zhang, J.; Jin, Y.; Li, Y.; Wang, Z.; Zhang, S.; et al. Metabolism of T-2 Toxin in Farm Animals and Human in Vitro and in Chickens in Vivo Using Ultra High-Performance Liquid Chromatography- Quadrupole/Time-of-Flight Hybrid Mass Spectrometry Along with Online Hydrogen/Deuterium Exchange Technique. J Agric Food Chem 2017, 65, 7217–7227, doi:10.1021/acs.jafc.7b02575.
14. Wu, Q.; Dohnal, V.; Huang, L.; Kuča, K.; Yuan, Z. Metabolic Pathways of Trichothecenes. Drug Metab Rev 2010, 42, 250–267.
15. Taroncher, M.; Rodríguez-Carrasco, Y.; Ruiz, M.J. Interactions between T-2 Toxin and Its Metabolites in HepG2 Cells and in Silico Approach. Food and Chemical Toxicology 2021, 148, 111942. doi:10.1016/j.fct.2020.111942.
16. Steinkellner, H.; Binaglia, M.; Dall'Asta, C.; Gutleb, A.C.; Metzler, M.; Oswald, I.P.; Parent-Massin, D.; Alexander, J. Combined Hazard Assessment of Mycotoxins and Their Modified Forms Applying Relative Potency Factors: Zearalenone and T2/HT2 Toxin. Food and Chemical Toxicology 2019, 131, 110599.
17. Hewitt, N.J.; Hewitt, P. Phase I and II Enzyme Characterization of Two Sources of HepG2 Cell Lines. Xenobiotica 2004, 34, 243–256, doi:10.1080/00498250310001657568.
18. Knasmüller, S.; Mersch-Sundermann, V.; Kevekordes, S.; Darroudi, F.; Huber, W.W.; Hoelzl, C.; Bichler, J.; Majer, B.J. Use of Human-Derived Liver Cell Lines for the Detection of Environmental and Dietary Genotoxicants; Current State of Knowledge. In Proceedings of the Toxicology; May 20 2004, (198) 315–328.
19. Ye, W.; Lin, R.; Chen, X.; Chen, J.; Chen, R.; Xie, X.; Deng, Y.; Wen, J. T-2 Toxin Upregulates the Expression of Human Cytochrome P450 1A1 (CYP1A1) by Enhancing NRF1 and Sp1 Interaction. Toxicol Lett 2019, 315, 77–86, doi:10.1016/j.toxlet.2019.08.021.
20. Lin, J.; Schyschka, L.; Mühl-Benninghaus, R.; Neumann, J.; Hao, L.; Nussler, N.; Dooley, S.; Liu, L.; Stöckle, U.; Nussler, A.K.; et al. Comparative Analysis of Phase i and II Enzyme Activities in 5 Hepatic Cell Lines Identifies Huh-7 and HCC-T Cells with the Highest Potential to Study Drug Metabolism. Arch Toxicol 2012, 86, 87–95, doi:10.1007/s00204-011-0733-y.
21. Tatay E, M.G.F.G.R.M. Cytotoxic and Interactive Effects of Zearalenone, α-Zearalenol and β-Zearalenol and Formation of Metabolites in HepG2 Cells. Toxicol 2014, 31, 187–195.
22. Gerdemann, A.; Behrens, M.; Esselen, M.; Humpf, H.U. Metabolic Profiling as a Powerful Tool for the Analysis of Cellular Alterations Caused by 20 Mycotoxins in HepG2 Cells. Arch Toxicol 2022, 96, 2983–2998, doi:10.1007/s00204-022-03348-5.
23. Taroncher, M.; Rodríguez-Carrasco, Y.; Ruiz, M.J. T-2 Toxin and Its Metabolites: Characterization, Cytotoxic Mechanisms and Adaptive Cellular Response in Human

Hepatocarcinoma (HepG2) Cells. Food and Chemical Toxicology 2020, 145, 111654. doi:10.1016/j.fct.2020.111654.
24.Wen, J.; Mu, P.; Deng, Y. Mycotoxins: Cytotoxicity and Biotransformation in Animal Cells. Toxicol Res (Camb) 2016, 5, 377–387.
25. Yang, S.; Zhang, H.; De Boevre, M.; Zhang, J.; Li, Y.; Zhang, S.; De Saeger, S.; Zhou, J.; Li, Y.; Sun, F. Toxicokinetics of HT-2 Toxin in Rats and Its Metabolic Profile in Livestock and Human Liver Microsomes. J Agric Food Chem 2018, 66, 8160–8168, doi:10.1021/acs.jafc.8b02893.
26. Narváez, A.; Izzo, L.; Pallarés, N.; Castaldo, L.; Rodríguez-Carrasco, Y.; Ritieni, A. Human Biomonitoring of T-2 Toxin, t-2 Toxin-3-Glucoside and Their Metabolites in Urine through High-Resolution Mass Spectrometry. Toxins (Basel) 2021, 13(12) 869, doi:10.3390/toxins13120869.
27. Lootens, O.; Vermeulen, A.; Croubels, S.; De Saeger, S.; Van Bocxlaer, J.; De Boevre, M. Possible Mechanisms of the Interplay between Drugs and Mycotoxins—Is There a Possible Impact? Toxins (Basel) 2022, 14(12), 873.
28. Osselaere, A.; Li, S.J.; De Bock, L.; Devreese, M.; Goossens, J.; Vandenbroucke, V.; Van Bocxlaer, J.; Boussery, K.; Pasmans, F.; Martel, A.; et al. Toxic Effects of Dietary Exposure to T-2 Toxin on Intestinal and Hepatic Biotransformation Enzymes and Drug Transporter Systems in Broiler Chickens. Food and Chemical Toxicology 2013, 55, 150–155, doi:10.1016/j.fct.2012.12.055.
29. Guerre, P.; Eeckhoutte, C.; Burgat, V.; Galtier, P. The Effects of T-2 Toxin Exposure on Liver Drug Metabolizing Enzymes in Rabbit. Food Addit Contam 2000, 17, 1019–1026, doi:10.1080/02652030050207819.
30. Lin, N.N.; Chen, J.; Xu, B.; Wei, X.; Guo, L.; Xie, J.W. The Roles of Carboxylesterase and CYP Isozymes on the in Vitro Metabolism of T-2 Toxin. Mil Med Res 2015, 2, 1-7, doi:10.1186/s40779-015-0041-6.
31. Kruber, P.; Trump, S.; Behrens, J.; Lehmann, I. T-2 Toxin Is a Cytochrome P450 1A1 Inducer and Leads to MAPK/P38- but Not Aryl Hydrocarbon Receptor-Dependent Interleukin-8 Secretion in the Human Intestinal Epithelial Cell Line Caco-2. Toxicology 2011, 284, 34–41, doi:10.1016/j.tox.2011.03.012.
32. Zhu, J.; Li, G.; Huang, Q.; Wen, J.; Deng, Y.; Jiang, J. TET3-Mediated DNA Demethylation and Chromatin Remodeling Regulate T-2 Toxin-Induced Human CYP1A1 Expression and Cytotoxicity in HepG2 Cells. Biochem Pharmacol 2023, 211, 115506, doi:10.1016/j.bcp.2023.115506.
33.Wen, J.; Mu, P.; Deng, Y. Mycotoxins: Cytotoxicity and Biotransformation in Animal Cells. Toxicol Res (Camb) 2016, 5, 377–387.
34. Song, W.; Wang, Y.; Huang, T.; Liu, Y.; Chen, F.; Chen, Y.; Jiang, Y.; Zhang, C.; Yang, X. T-2 Toxin Metabolism and Its Hepatotoxicity: New Insights on the Molecular Mechanism and Detoxification. Environmental Pollution 2023, 330, 121784.
35. Wang, J.; Jiang, J.; Zhang, H.; Wang, J.; Cai, H.; Li, C.; Li, K.; Liu, J.; Guo, X.; Zou, G.; et al. Integrated Transcriptional and Proteomic Analysis with in Vitro Biochemical Assay Reveal the Important Role of CYP3A46 in T-2 Toxin

Hydroxylation in Porcine Primary Hepatocytes. Molecular and Cellular Proteomics 2011, 10(9), doi:10.1074/mcp.M111.008748.
36. Janik, E.; Niemcewicz, M.; Podogrocki, M.; Ceremuga, M.; Stela, M.; Bijak, M. T-2 Toxin—the Most Toxic Trichothecene Mycotoxin: Metabolism, Toxicity, and Decontamination Strategies. Molecules 2021, 26(22) 6868.
37. Song, W.; Wang, Y.; Huang, T.; Liu, Y.; Chen, F.; Chen, Y.; Jiang, Y.; Zhang, C.; Yang, X. T-2 Toxin Metabolism and Its Hepatotoxicity: New Insights on the Molecular Mechanism and Detoxification. Environmental Pollution 2023, 330, 121784.
38. Wojtacha, P.; Trybowski, W.; Podlasz, P.; Żmigrodzka, M.; Tyburski, J.; Polak-śliwińska, M.; Jakimiuk, E.; Bakuła, T.; Baranowski, M.; Żuk-Gołaszewska, K.; et al. Effects of a Low Dose of T-2 Toxin on the Percentage of T and B Lymphocytes and Cytokine Secretion in the Porcine Ileal Wall. Toxins (Basel) 2021, 13(4) 277, doi:10.3390/TOXINS13040277.
39. Skrzydlewski, P.; Twarużek, M.; Grajewski, J. Cytotoxicity of Mycotoxins and Their Combinations on Different Cell Lines: A Review. Toxins (Basel) 2022, 14(4) 244.

Toxins, 14 (2022), 841

https://doi.org/10.3390/toxins14120841

3.4. Stressful effects of T-2 metabolites and defense capability of HepG2 cells

Mercedes Taroncher [1], Fiona Halbig [2], Yelko Rodríguez-Carrasco [1,*] and María-José Ruiz[1]

[1] Department of Preventive Medicine and Public Health, Food Science, Toxicology and Forensic Medicine, Faculty of Pharmacy, University of Valencia, 46100 Burjassot, Valencia, Spain.

[2] Rheinische Friedrich-Wilhelms-Universität Bonn, 53115 Bonn, Germany; Fionahalbig@web.de

Abstract

The T-2 toxin (T-2), a mycotoxin produced by several species of *Fusarium* which belongs to group A of trichothecenes, is rapidly metabolized, and its main metabolites are HT-2, Neosolaniol (Neo), T2-triol and T2-tetraol. In this work, the antioxidant defense system of HepG2 cells against oxidative stress induced by T-2 and its metabolites was evaluated. The results obtained demonstrated that there is an overall decrease of glutathione (GSH) levels after all mycotoxins exposure. Moreover, the GSH levels and the enzymatic activities related to GSH (GPx and GST) increased with NAC pre-treatment (glutathione precursor) and decreased with BSO pre-treatment (glutathione inhibitor). The GPx activity is increased by T2-tetraol. The GST activity increased after T-2 and T2-triol exposure; however, T2-tetraol decreases its activity. Furthermore, CAT activity increased after T-2 and T2-triol; nevertheless, Neo decreases its activity. Finally, SOD activity is increased by all mycotoxins, except after T-2 exposure. So, the damage associated to oxidative stress by T-2 and its metabolites is relieved by antioxidant enzymes system on HepG2 cells.

Key words: T-2 toxin; metabolites; glutathione; antioxidant enzymes.

Key Contribution: the role played by oxidative stress of T-2 and mainly its metabolites Neo, T2-triol and T2-tetraol on HepG2 cells.

* **Corresponding author**: Department of Preventive Medicine and Public Health, Food Science, Toxicology and Forensic Medicine, Faculty of Pharmacy, University of Valencia, 46100 Burjassot, Valencia, Spain. E-mail address: Yelko.rodriguez@uv.es

1. Introduction

Mycotoxins are toxic secondary metabolites produced under favorable conditions by fungi which grow on food and feed worldwide [1]. Mycotoxin contamination is an aggravated problem in developing countries. The most detected mycotoxins in food are aflatoxins (AFs), fumonisins (FBs), ochratoxin A (OTA), patulin (PAT), zearalenone (ZEA) and trichotecenes. Among the trichotecenes, the T-2 toxin (T-2) is the most cytotoxic compound [1,2]. The T-2 is produced by various species of *Fusarium*, such as *F. sporotichioides*, *F. poae*, *F. equiseti* and *F. acuminatum*. It is detected in field crops such as wheat, maize, barley, oats and processed grains such as malt, beer and bread [3]. Furthermore, the T-2 has also been detected in drinking water in endemic areas of China such as Qinghai and in traditional Chinese medicines [4–6]. The most common rout of T-2 exposure is through ingestion, although there are other routes. Farmers may be exposed via direct contact with contaminated grain dust and hay, and it could cause organ damage to the kidney, liver, skin, brain and gut [7,8].

The T-2 is rapidly metabolized to the HT-2, Neosolaniol (Neo), T2-triol and T2-tetraol, [1,9] consequently, the cytotoxic mechanism of T-2 *in vivo* and *in vitro* might be partly attributable to its metabolites [10]. Previously, the cytotoxicity of T-2 metabolites was studied individually and in combinations in various *in vitro* studies and it was observed that T-2 showed the highest cytotoxic effect [9]. The T-2 is a predisposing factor in the Kashin-Beck disease (KBD), a chronic endemic type of osteochondropathy that was mainly distributed from northeastern to southwestern China [4,11]. Moreover, the T-2 induces neurotoxicity, emesis, cardiovascular alterations, immunodepression, muscular weakness, ataxia anorectic responses, hepatotoxicity and bone marrow damage [1,12,13]. The T-2 decrease the levels of antibodies, immunoglobulins as well as

diverse cytokines [12]. An important toxicity of T-2 is the mitochondrial toxicity. The T-2 may induce the collapse of mitochondrial membrane potential and promote the production of mitochondrial reactive oxygen species (ROS). Mu et al. suggested that alterations in mitochondrial gene expression could alter the coupling of mitochondrial oxidative phosphorylation leading to ROS generation [14].

Oxidative metabolites can be scavenged by GSH. The function of GSH may be evaluated in vitro adding exogenous compounds capable of decrease or increase the GSH synthesis. For instance, N-Acetyl-cysteine (NAC) is an effective source of sulfhydryl groups in cells and a scavenger of free radicals because it may interact with ROS, so it is a precursor of GSH. On the other hand, D-L-buthionine-(S, R)-sulfoximine (BSO) is an inhibitor of γ-glutamylcysteine synthetase, the enzyme that triggers the cytosol´s production of GSH.

There are a variety of studies reporting the effects of oxidative stress damage generated by mycotoxins in different cell lines [15–17]. However, there are few reports in the literature concerning the effects of T-2 and its metabolites on enzymatic and no-enzimatic antioxidant defense. We selected the HepG2 cells due to it is a hepatic cell line and the liver is the main drug metabolizing organ and the main T-2 target organ [12,18]. In this study, the GSH levels and the antioxidant defense system (GPx, GST, SOD and CAT activities) of HepG2 cells exposed to T-2, Neo, T2-triol and T2-tetraol were evaluated. Moreover, to demonstrate the role of GSH in T-2 and its metabolites detoxification, the effect of pre-treatments with NAC or BSO was also assayed.

2. Results

2.1. *In vitro* cytotoxicity

The MTT assay was used to assess the cytotoxicity of T-2 and its modified forms on HepG2 cells after 24 h and the results were published in our previous work [9]. The results demonstrated that T-2, Neo, T2-triol and T2-tetraol exposure reduced cell viability in a manner that was dependent on both time and concentration. This decrease of cell viability is of the same order for all mycotoxins, being between 10 and 70% for T-2 and T2-tetraol, and between 23 and 77% for Neo and T2-triol.

In this study, we have selected the $IC_{50}/2$, $IC_{50}/4$, $IC_{50}/8$ values for each mycotoxin obtained from the MTT assay, that were 7.5, 15 and 30 nM for T-2, 12.5, 25 and 50 nM for Neo, 0.12, 0.25 and 0.45 μM for T2-triol and 0.45, 0.9 and 1.7 μM for T2-tetraol.

2.2. Intracellular ROS generation

Due to the cytotoxic effect observed of T-2 and its metabolites on HepG2 cells, we studied the generation of ROS to test if oxidative stress is one of the mechanisms by which these mycotoxins exert their cytotoxicity. As it can be observed in Figure 1, there was an increase of ROS production after T-2, T2-triol and T2-tetraol exposure. The increases of ROS production were from 17.79 to 27.92% for T-2, 21.75 for T2-triol and from 23.09 to 40.81% for T2-tetraol.

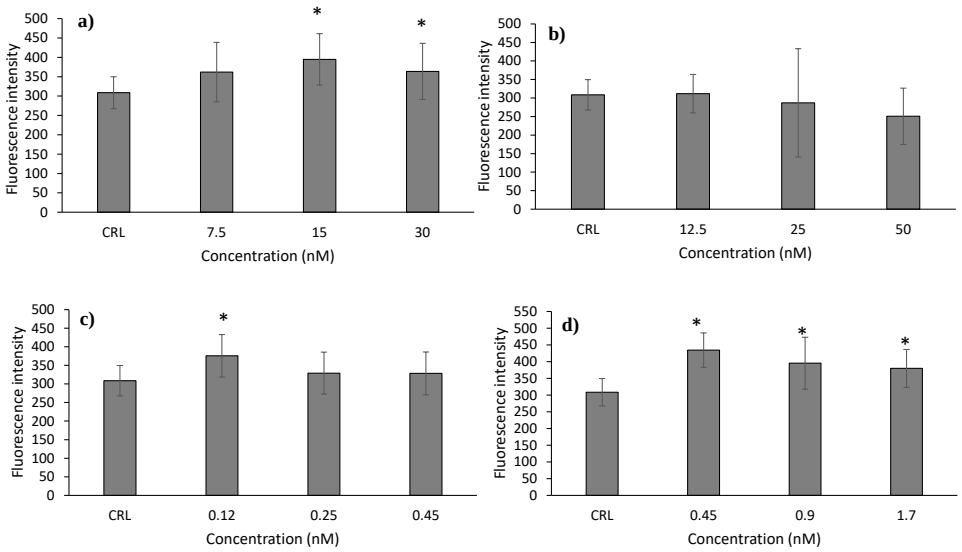

Figure 1. The ROS-induced fluorescence in HepG2 cells exposed to T-2 (7.5, 15 and 30 nM) (a), Neo (12.5, 25 and 50 nM) (b), T2-triol (0.12, 0.25 and 0.45 μM) (c) and T2-tetraol (0.45, 0.9 and 1.7 μM) (d) during 24 h. Results are expressed as mean ± SEM (n=2). Student's t-test for paired samples was used to statistical analysis of results. * $p \leq 0.05$ indicates a significant difference from the control (CRL; fresh medium).

2.3. GSH determination

As far as the GSH determination after T-2 exposure is concerned, the GSH levels and GSH/GSSG ratio significantly decreased ($p \leq 0.05$) at 7.5 nM by 50.6 and 52.7% and at 15 nM by 25.8 and 18.7%, respectively, compared to control (Figs. 2a and 2c). And, the GSSG levels decreased at all the assayed concentrations respect to control cells (Fig. 2b).

Regarding to NAC pre-treatment, a significant increase on GSH levels (30.1%) in control cells was observed respect to control without NAC pre-treatment, (Fig. 2). Also, at 7.5 and 30 nM T-2, NAC pre-treatment led to an

increase in GSH level (68.3 and 19.3%, respectively), GSSG content (45.7 and 14.7%, respectively), and the GSH/GSSG ratio (112.4 and 13.9%, respectively) respect to cells in fresh medium, showing a NAC protective effect in HepG2 cells. Furthermore, an increase of GSH (13.3%) and GSH/GSSG (10%) at 30 nM was observed, corresponding with a decrease (12.3%) of GSSG levels, compared to control with NAC pre-treatment.

Concerning the BSO pre-treatment, a decrease in GSH level (57.6%), GSSG level (37.4%) and GSH/GSSG ratio (35.2%) was obtained in their own controls compared to controls without pre-treatment. In this respect, a significant decrease of GSH levels was determined of 47.2 and 88.5% at 15 and 30 nM, respectively. And the GSH/GSSG ratio decreased from 17.6 to 81.4% (Fig. 2c). On the other hand, a significant decrease of GSH levels (66.6%) was also obtained after the exposure of T-2 at the highest con-centration (30 nM) compared to their own control. Whereas a significant decrease in GSH/GSSG ratio (from 26.9 to 70.5%) was obtained respect to control with BSO pre-treatment.

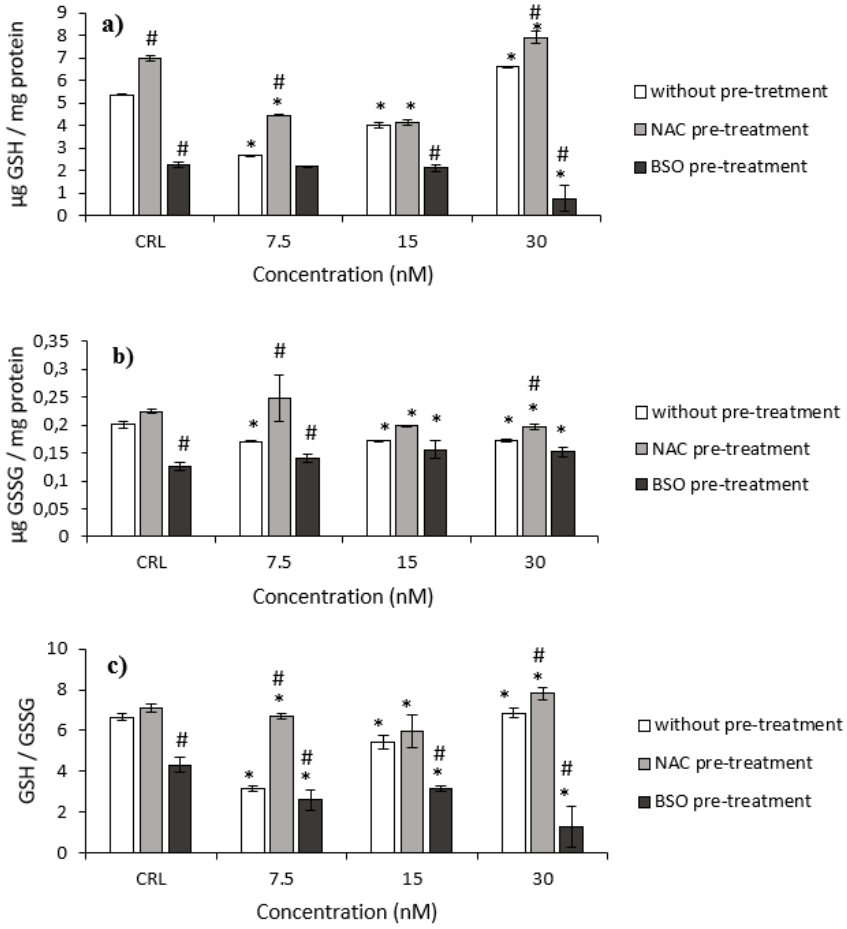

Figure 2. Effect of T-2 (7.5, 15 and 30 nM) with and without NAC or BSO pre-treatment on GSH levels (a), GSSG levels (b), and on the GSH/GSSG ratio (c) after 24 h of exposure. Data are expressed as mean values ± SEM of three independent experiments. One-way ANOVA followed by the Turkey HDS *post-hoc* test for multiple comparisons was used to analyzed difference between groups. * $p \leq 0.05$ indicates a significant difference from the respective control (CRL; fresh medium or without pre-treatment, NAC pre-treatment and BSO pre-treatment); # $p \leq 0.05$ indicates a significant difference respect to the fresh medium.

Regarding to Neo (Fig. 3), in fresh medium, the GSH levels and GSH/GSSG ratio significantly decreased from 56.2 to 73.3%, and from 48.6 to 70.4%, after Neo exposure, respectively, compared to control cells (Figs 3a and 3c). On contrary, the GSSG content significantly increased from 13.2 to 37.1% (Fig 3b).

Concerning the NAC pre-treatment, an increase of GSH and GSSG levels, and GSH/GSSG ratio (by 16.9, 22.4 and 26.8%, respectively) in control cells was observed respect to control in fresh medium (Fig. 3). Similarly, the pre-treatment with NAC produced an increase of GSH levels (from 137.4 to 197.6%) and GSH/GSSG ratio (from 102.3 to 159.9%) in cells exposed to Neo, respect to cells in fresh medium, which showed a cytoprotecting effect of NAC in these cells.

Respect to BSO pre-treatment, a decrease in the GSH levels and GSH/GSSG ratio (47.4 and 26.4%, respectively) was obtained in controls compared to controls without BSO. And, the GSSG levels significantly decreased by 18.3% at the highest Neo concentration. Additionally, a significant decrease of GSH levels (by 32.9 and 55.9%) and GSH/GSSG ratio (by 49.4 and 62.6%) and a significant increase of GSSG levels (by 17.6 and 18.6%) were also obtained after 12.5 and 50 nM of Neo exposure, respectively, compared to BSO pre-treated controls.

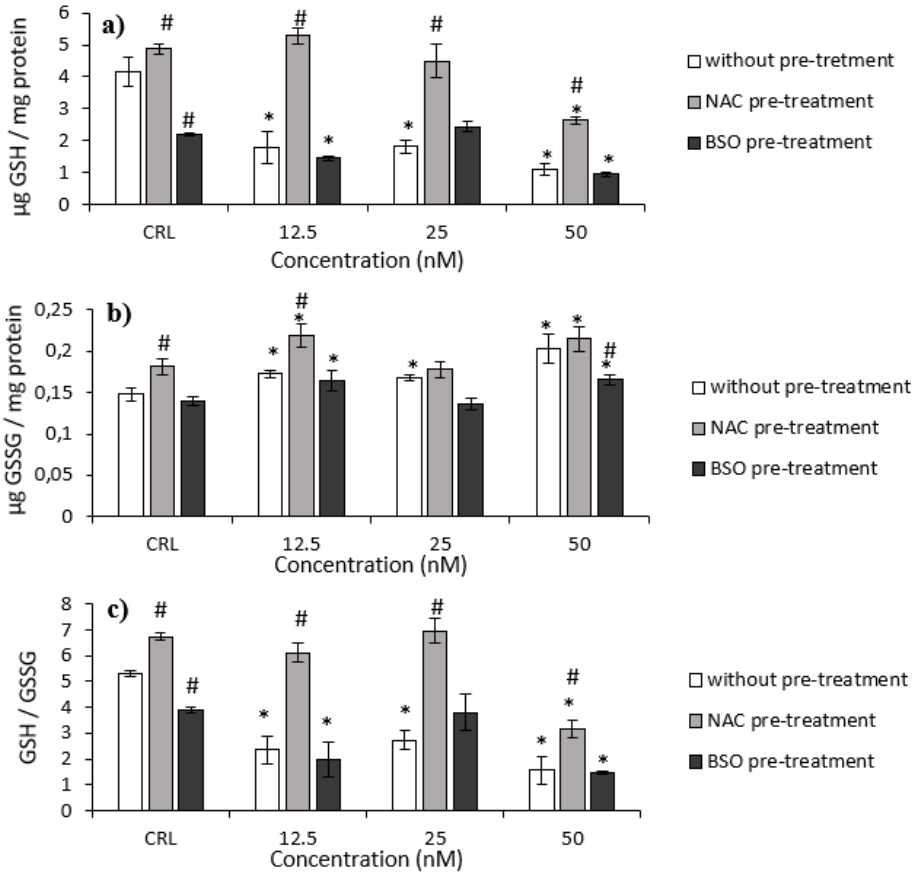

Figure 3. Effect of Neo (12.5, 25 and 50 nM) with and without NAC or BSO pre-treatment on GSH levels (a), GSSG levels (b), and on the GSH/GSSG ratio (c) after 24 h of exposure. Data are expressed as mean values ± SEM of three independent experiments. One-way ANOVA followed by the Turkey HDS *post-hoc* test for multiple comparisons was used to analyzed difference between groups. * $p \leq 0.05$ indicates a significant difference from the respective control (CRL; fresh medium or without pre-treatment, NAC pre-treatment and BSO pre-treatment); # $p \leq 0.05$ indicates a significant difference respect to the fresh medium.

Regarding T2-triol (Fig. 4), the GSH levels and GSH/GSSG ratio decrease after 0.45 μM T2-triol exposure (57.9 and 53.3%, respectively) in fresh medium, whereas the GSSG content significantly increased (34.2%) compared to control cells.

Concerning the effects of NAC pre-treatment, a significant increase of GSH and GSSG levels was determined in control cells by 14 and 28.8%, respectively, compared to controls without NAC pre-treatment (Fig. 4). Additionally, NAC pre-treatment induced an increase of GSH level (from 26.8 to 34.7%), GSSG levels (15.7%) and GSH/GSSG ratio (20.1%) in cells exposed to T2-triol compared to cells in fresh medium (Fig. 4).

Regarding the BSO pre-treatment, a significant decrease in the GSH levels (up to 60.3%) and GSH/GSSG ratio (up to 59.9%) were also obtained after T2-triol exposure compared to its own control. Finally, a decrease up to 38.7% of GSSG content of T2-triol was observed compared to cells without BSO pre-treatment (Fig. 4b).

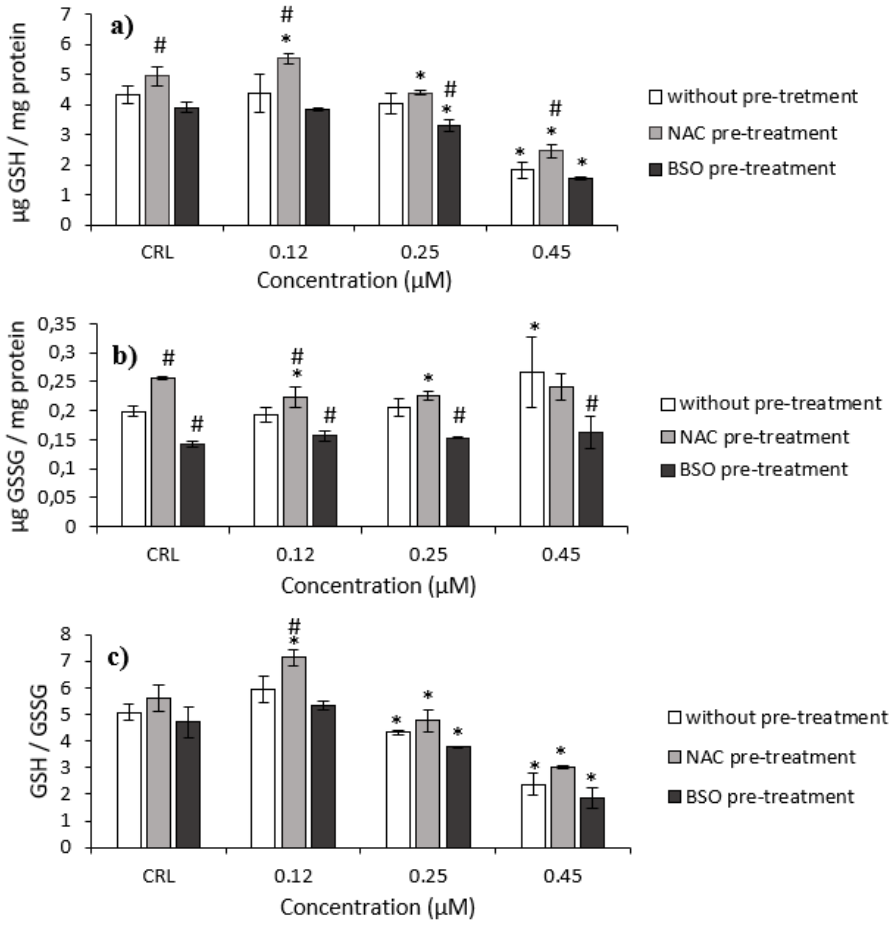

Figure 4. Effect of T2-triol (0.12, 0.25 and 0.45 µM) with and without NAC or BSO pre-treatment on GSH levels (a), GSSG levels (b), and on the GSH/GSSG ratio (c) after 24 h of exposure. Data are expressed as mean values ± SEM of three independent experiments. One-way ANOVA followed by the Turkey HDS *post-hoc* test for multiple comparisons was used to analyzed difference between groups. * $p \leq 0.05$ indicates a significant difference from the respective control (CRL; fresh medium or without pre-treatment, NAC pre-treatment and BSO pre-treatment); # $p \leq 0.05$ indicates a significant difference respect to the fresh medium.

Similar results were obtained with T2-tetraol, the GSH levels and GSH/GSSG ratio increased (15.3 and 13.7%, respectively) at 0.45 μM and decreased (31.1 and 22.4%, respectively) at 1.7 μM respect to the control cells. (Fig. 5).

The NAC pre-treatment produced an increase of GSH levels (30.9%), GSSG levels (15.6%) and GSH/GSSG ratio (15.2%,) in controls compared to controls without NAC. When cells exposed to NAC pre-treatment were compared to cells exposed to fresh medium, an increase of GSH, GSSG levels and GSH/GSSG ratio was observed. These values increased up to 66.8%, 32.9% and 26.4%, respectively.

Concerning the BSO pre-treatment, a significant decrease in the GSH, GSSG levels and GSH/GSSG ratio was observed (Fig. 5). The BSO pre-treatment showed a decrease from 47.1 to 58.9% of GSH levels, from 23.3 to 27.1% of GSSG levels and from 30 to 51.6% of GSH/GSSG ratio, respect to cells without BSO. Finally, with BSO pre-treatment, a significant decrease up to 31.9% was observed in the GSH/GSSG ratio respect to its own control.

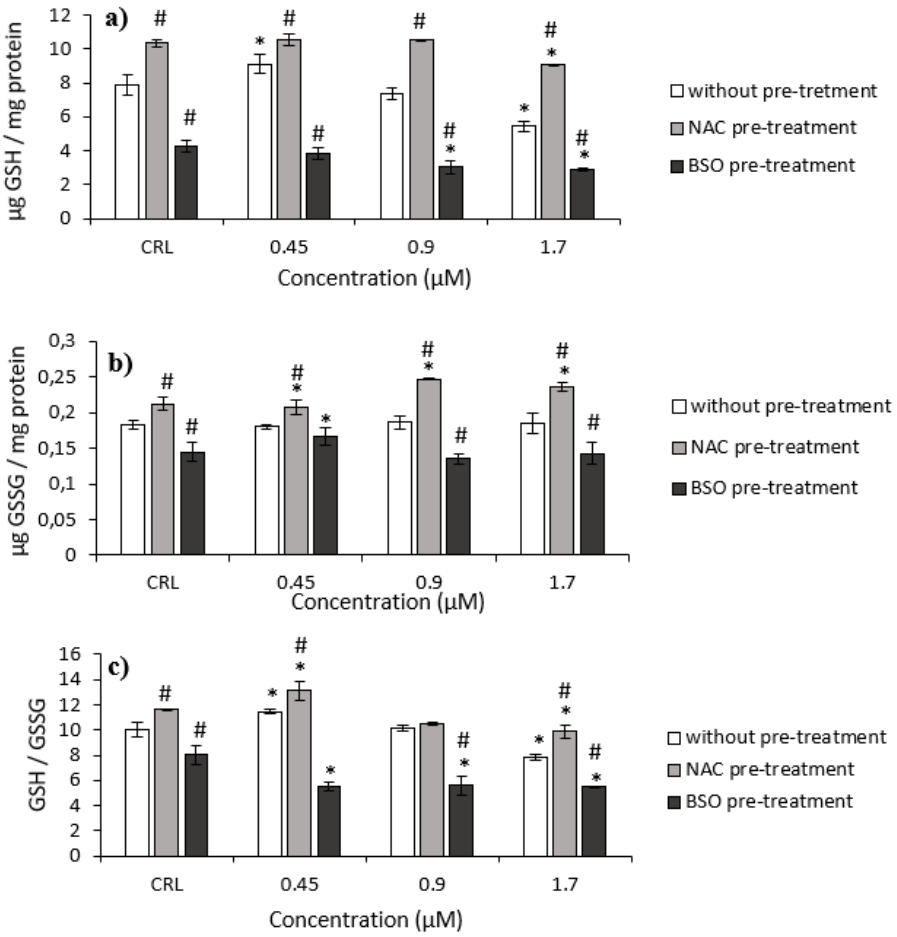

Figure 5. Effect of T2-tetraol (0.45, 0.9 and 1.7 µM) with and without NAC or BSO pre-treatment on GSH levels (a), GSSG levels (b), and on the GSH/GSSG ratio (c) after 24 h of exposure. Data are expressed as mean values ± SEM of three independent experiments. One-way ANOVA followed by the Turkey HDS post-hoc test for multiple comparisons was used to analyzed difference between groups. * $p \leq 0.05$ indicates a significant difference from the respective control (CRL; fresh medium or without pre-treatment, NAC pre-treatment and BSO pre-treatment); # $p \leq 0.05$ indicates a significant difference respect to the fresh medium.

2.4. Enzymatic activity

The GPx, GST, CAT and SOD activities were assessed in HepG2 cells after 24 h of incubation with T-2 (7.5, 15 and 30 nM) and its modified forms, Neo (12.5, 25 and 50 nM), T2-triol (0.12, 0.25 and 0.45 μM) and T2-tetraol (0.45, 0.9 and 1.7 μM).

Concerning GPx activity, a significant decrease (67.9%) was obtained after 30 nM T-2 exposure in fresh medium as shown in Fig. 6a, whereas, a significant increase was observed at this concentration in cells pre-treated with NAC (326.4%) pre-treatment, compared to cells in fresh medium. Regarding to Neo exposure, an increase by 249.2% at 25 nM was determined in NAC pre-treated cells compared to its own control, while an increase (from 242.9 to 548.3%) were observed at all concentrations tested compared to cells in fresh medium (Fig. 6b).

Respect to T2-triol, control NAC pre-treated increased (77.9%) the GPx activity while control BSO pre-treated significantly decreased (23.2%) respect to fresh medium control cells. Cells NAC pre-treated increased the GPx activity from 37.2 to 68.8% compared to its own control. And it increased (from 104.5 to 223.7%) respect to fresh medium cells (Fig. 6c). Finally, regarding to T2-tetraol, an increase in GPx activity by 77.9% was shown in control NAC pre-treatment compared to control without pre-treatment, while a decrease by 23.2% in control BSO pre-treatment was observed. The GPx activity increased by 39.2%, from 18 to 51.2% and by 79.8 to 108.4%, in HepG2 cells exposed to T2-tetraol in fresh medium and in cells pre-treated with NAC respect to its own control and respect to the corresponding cells in fresh medium, respectively.

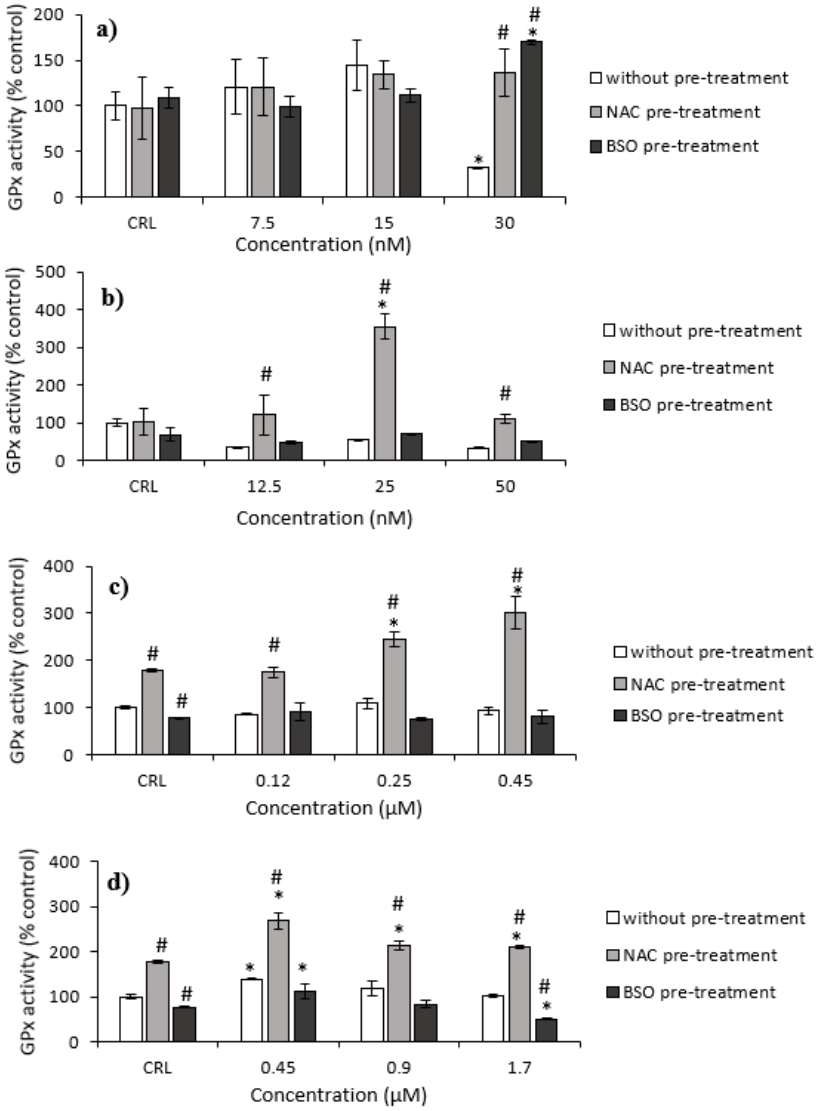

Figure 6. Effect of T-2 (7.5, 15 and 30 nM) (a), Neo (12.5, 25, 50 nM) (b), T2-triol (0.12, 0.25, 0.45 μM) (c) and T2-tetraol (0.45, 0.9, 1.7 μM) (d) with and without NAC or BSO pre-treatment on glutathione peroxidase activity after 24 h of exposure. Data are ex-pressed in % of the unexposed control (CRL). In terms of μmol of NADPH oxidized/min/mg of protein, the GPx activity is expressed; mean ± SEM (n = 3). One-way ANOVA followed by the Turkey HDS *post-hoc* test for multiple comparisons was used to analyzed difference

between groups. * $p \leq 0.05$ indicates a significant difference from the respective control (fresh medium or without pre-treatment, NAC pre-treatment and BSO pre-treatment); # $p \leq 0.05$ indicates a significant difference respect to the fresh medium.

On the other hand, with BSO pre-treatment, the GPx activity decreased respect to cells in fresh medium (50.7%) and respect to its own control (35.3%) after the highest con-centration of T2-tetraol (Fig. 6d).

As shown in Fig. 7a, the GST activity increased significantly in HepG2 cells from 49.8% to 115.7% after T-2 exposure in fresh medium. After NAC pre-treatment, the highest increase in GST activity was observed at 15 nM T-2 compared to its own con-trol cells (by 102.3%) and respect to cells in fresh medium (by 38.2%). Regarding to Neo exposure, only was observed in cells with NAC pre-treatment, an increase up to 221.8% (50 nM) and 39.8% (25 nM) compared to cells without pre-treatment and to control with NAC pre-treatment, respectively (Fig. 7b).

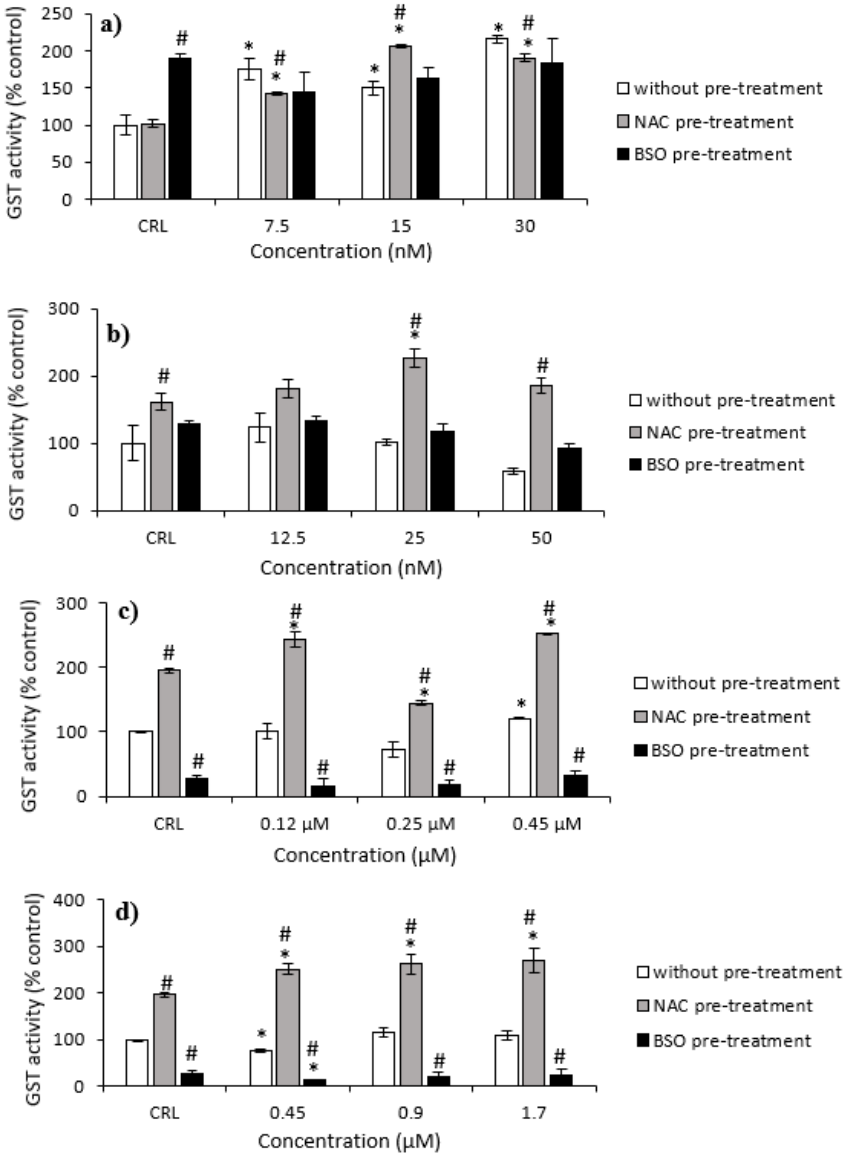

Figure 7. Effect of T-2 (7.5, 15 and 30 nM) (a), Neo (12.5, 25, 50 nM) (b), T2-triol (0.12, 0.25, 0.45 µM) (c) and T2-tetraol (0.45, 0.9, 1.7 µM) (d) with and without NAC or BSO pre-treatment on glutathione *S*-transferase activity after 24 h of exposure. Data are expressed in % of the unexposed control (CRL). In terms of mol of product formed/min/mg of protein, the GST activity is expressed; mean ± SEM (n = 3). One-way ANOVA followed by the Turkey

HDS *post-hoc* test for multiple comparisons was used to analyzed difference between groups. * $p \leq 0.05$ indicates a significant difference from the respective control (fresh medium or without pre-treatment, NAC pre-treatment and BSO pre-treatment); # $p \leq 0.05$ indicates a significant difference respect to the fresh medium.

With regard to T2-triol exposure, a significant increase (20.9%) at 0.45 μM was shown in cells with fresh medium compared to the control. Regarding the effects of NAC pre-treatment, an increase of 95.6% in control NAC pre-treated cells compared to control no pre-treated was obtained. Moreover, an increase of GST activity after T2-triol exposure up to 29% compared to control cells with NAC pre-treatment was observed as well as an increase from 97.5 to 140.6% compared to cells without pre-treatment. Conversely, a decrease of 72.6% in control BSO pre-treated compared to control cells no pre-treated was shown. Similarly, a decrease up to 83.7% after T2-triol exposure was observed compared to cells without BSO pre-treatment (Fig. 7c). Finally, regarding to T2-tetraol exposure, an increase of 95.6% was shown in control cells NAC pre-treated compared to control no pre-treated, whereas BSO pre-treated showed a decrease of 72.6%. Furthermore, a significant increase was obtained at all concentrations tested in cells pre-treated with NAC respect to its own control cells (from 28.3 to 37.2%) and also to the corresponding cells in fresh medium (from 146.5 to 227.7%). On the other hand, the GST activity decreased in cells BSO pre-treated exposed to 0.45 μM by 45.8% compared to control BSO pre-treated. Whilst, a decrease at all concentrations tested in cells pre-treated with BSO respect to cells without pre-treatment from 80.6 to 76.9% was also observed (Fig. 7d).

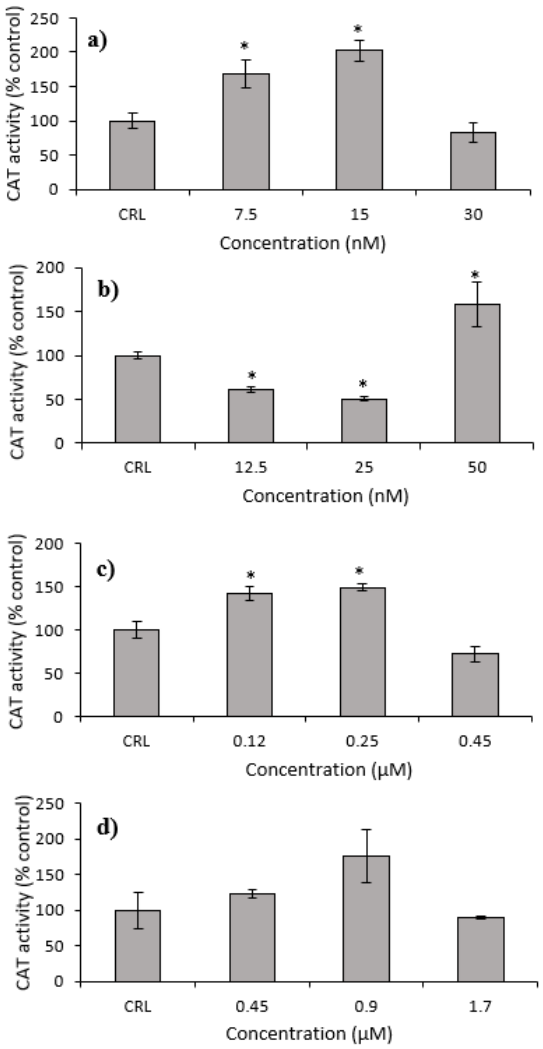

Figure 8. Effect of T-2 (7.5, 15 and 30 nM) (a), Neo (12.5, 25, 50 nM) (b), T2-triol (0.12, 0.25, 0.45 μM) (c) and T2-tetraol (0.45, 0.9, 1.7 μM) (d) on catalase activity after 24 h of exposure. Data are expressed in % of the unexposed control (CRL). The CAT activity is expressed as μmol of H_2O_2/min/mg of protein; mean ± SEM (n = 3). Student's t-test for paired samples was used to statistical analysis of results. * $p \leq 0.05$ indicates a significant difference respect to the control.

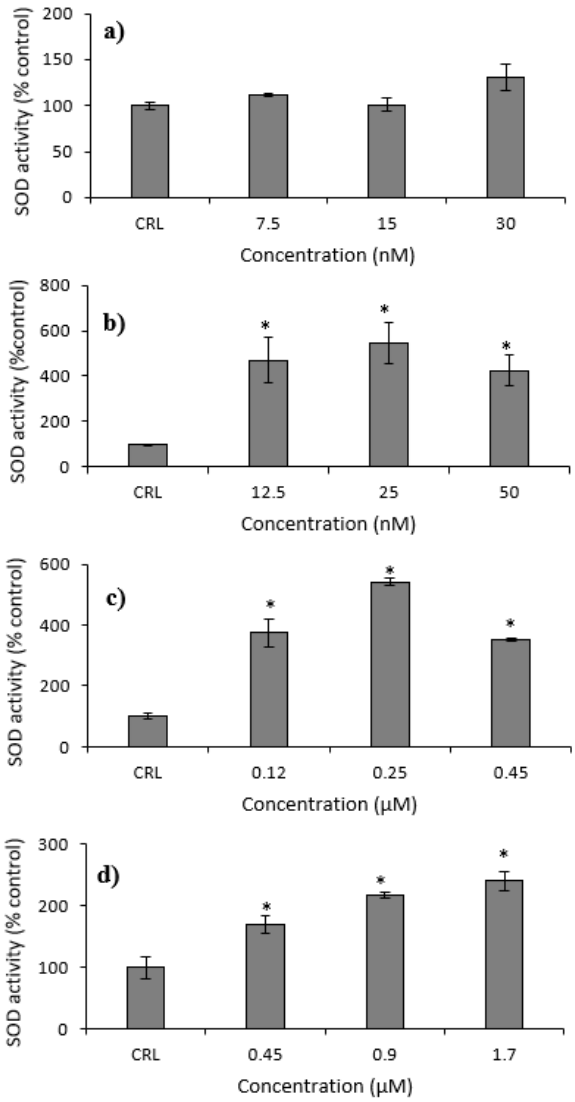

Figure. 9. Effect of T-2 (7.5, 15 and 30 nM) (a), Neo (12.5, 25, 50 nM) (b), T2-triol (0.12, 0.25, 0.45 µM) (c) and T2-tetraol (0.45, 0.9, 1.7 µM) (d) on superoxide dismutase activity after 24 h of exposure. Data are expressed in % of the unexposed control (CRL); mean ± SEM (n = 3). Student's t-test for paired samples was used to statistical analysis of results. * $p \leq 0.05$ indicates a significant difference respect to the control.

The Fig. 8a shows that the CAT activity increased at the lower T-2 and T2-triol concentrations from 68.9 to 102.2% and from 41.9 to 48.6%, respectively, respect to control cells (Fig. 8c). Conversely, at the lower Neo concentrations, the CAT activity significantly decreased from 38.9 to 49.3%, while an increase of 58.2% was detected at the highest Neo concentration respect to control (Fig. 8b). (Fig. 8d).

Finally, respect to SOD activity in HepG2 cells, an increase at all concentrations tested of Neo (from 325.3 to 445.9%), T2-triol (from 250.65 to 441.2%) and T2-tetraol (from 70.4 to 140.2%) compared to their respective controls was obtained (Figs. 9b, c and d).

3. Discussion

This study showed that in HepG2 cells T-2, T2-triol and T2-tetraol triggered an increase of intracellular ROS levels after 24 h of exposure (Fig. 1), demonstrating that oxidative stress plays a role in cellular toxicity.

The induction of oxidative stress by T-2 has been previously demonstrated by other authors [3,10,11,21–29]. The results obtained for T-2 in HepG2 cells grown in medium, showed a decrease in GSH levels at 7.5 and 15 nM compared to control cells. However, intracellular GSH increases at 30 nM and it may be to keep the cells in a reduced state and to avoid oxidative stress to high doses (Figs. 1a and 2a).

In our results, correlated with the decrease in GSH levels, an increase of GST activity was observed. However, GPx activity remained unchanged (Fig. 7a, 6a). According to Gouze et al. [30], the 12,13-epoxide group, which characterizes all epoxy-trichothecene toxins, could be a substrate for GST conjugation, as GST is active on epoxides group. These authors demonstrated that deoxynivalenol

(DON) trichothecene has the ability to conjugate to GST as DON is a substrate of GST [30]. Therefore, in this work the increase of GST enzymatic activity after T-2 exposure leads us to speculated that this mycotoxin could be a substrate for GST due to the structural similarity of both trichothecenes. So, the GST-mediated conjugation could represent a detoxification pathway in protecting cells from injury by T-2. On the other hand, GPx activity in HepG2 is not the main implicated enzyme in detoxifying against cytotoxicity of T-2. Also, it is possible that GPx inactivates itself by the decrease of its own substrate. Similarly, SOD activity remains unchanged after T-2 exposure, nevertheless, CAT activity increased (Fig. 8a, 9a). This can be due to the fact that T-2 increases ROS (Fig. 1a), including H_2O_2, and it is transformed rapidly to H_2O and O_2 by CAT. Thus, our results suggest that the mainly enzymes involved in detoxifying T-2 in HepG2 cells are GST and CAT. Therefore, GST activity remains high, since this enzyme is important to protect against oxidative stress to which the HepG2 cells is submitted, as shown by the equally high CAT activity and GSH content at the highest T-2 concentration tested.

Similar results to our SOD activity were reported in HepG2 cells exposed to OTA, in Hek-293 cells after DON exposure, and in SH-SY5Y cells after beauvericin (BEA), α-ZEL and β-ZEL exposure. These authors demonstrated that the activity of SOD tended to the control levels, that are cells exposed to culture medium only, without mycotoxins [31–33]. Regarding to enzymatic activities in cell culture exposed to mycotoxin, there is a variety of results. According to our results, Yang et al. [10,18] observed an increase in CAT, SOD and GPx activity after T-2 exposure (from 10 to 100 nM) in broiler hepatocytes. Conversely, Li et al. [21] and Zhang et al. [3] reported a de-crease in CAT activity after T-2 exposure on porcine kidney and Leydig cells. The in-crease of CAT,

GPx and SOD activities suggests that in hepatocytes, the T-2 increases ROS which are catalyzed by SOD, and the high levels of H_2O_2 as a result of the reaction is detoxified by CAT and GPx decreasing the GSH levels. On the contrary, the SOD, GPx and CAT enzymes do not seem to be the main enzymes responsible for the detoxification in Leydig or porcine kidney cells in response to T-2 exposure. So, these enzymes are not activated by the cells to prevent from oxidative stress.

The mechanism of toxicity of T-2 modified forms are the innovative part of this study, as little or no information is available. Regarding to Neo, a significant decrease of GSH and increase of GSSG levels at all concentrations tested were determined in HepG2 cells (Fig. 3a, b). These results are similar to the effects of T-2 in this work. Nevertheless, the depletion in GSH levels seems is not related to its involvement through the activity of GPx, due to its activity remain unchanged (Fig. 6b, 7b). So, cell enzymatic system no related to GSH is the most important enzymatic defense system in HepG2 cells exposed to Neo. The increase of SOD activity has also been observed in GH3 and broiler hepatocytes [10,11,18] after T-2 exposure. Other authors reported differences in the results of the CAT activity depending on the range of concentration tested in different cell types exposed to T-2 [3,21,31,34]. However, no data were reported about Neo.

A significant decrease of GSH and an increase of GSSG levels at the highest concentration of T2-triol (0.45μM) tested were found in HepG2 cells (Fig. 4a, b). Similar effects were observed with ZEA and its metabolites on CHO-K1, HepG2 and SH-SY5Y cells [31,34,35], BEA in CHO-K1 cells [36] and OTA in HepG2 cells [33]. The decrease in GSH levels is accompanied by an increase in

GST at 0.45μM. However, GPx activity remains unchanged (Fig. 7c, 6c). This indicate that the T2-triol detoxifying enzyme is mainly GST.

On the other hand, the increase of ROS after T2-triol exposure (Fig 1c) provide the stimulus for increasing the CAT and SOD activities at all concentrations (Fig. 8c, 9c). Many research has been carried out to assess the impact of different mycotoxins on the antioxidant defense system have been very studied by different authors. However, as far as author´s knowledge, no data about the effects of T-2 metabolites on the enzymatic antioxidant protective system is found in the literature yet.

On HepG2 cells, intracellular GSH increased immediately at the lowest concentration (0.45 μM) of T2-tetraol, acting as a major thiol-disulfide redox buffer as a response of oxidative damage to keep the cells in a reduced state (Fig. 5a). However, with the higher concentration (1.7 μM), GSH is deplected due to high levels of oxidative stress. On the other hand, the increase in GSH content was accompanied by an increase in GPx activity at 0.45 μM. Nonetheless, the GST activity decreased (Fig. 6d, 7d). So, regarding to T2-tetraol, the main enzymatic detoxifying mechanism involved was GPx. On the other hand, the oxidizing compounds produced by T2-tetraol were catalyzed by SOD enzyme, because its activity increased at all concentrations tested. The increase of ROS after T2-tretraol exposure (Fig. 1d) leads to GSH action (Fig. 5a) and also to the SOD activity (fig. 9d). On the contrary, the T2-tetraol did not stimulate CAT activity; so, we can conclude that T2-tetraol was detoxified by GPx and SOD enzymatic activities (Fig 8d, 9d). In a previous work, we demonstrated that the T-2 is converted by hydrolysis to Neo and T2-triol, but all three metabolites end up as T2-tetraol [9], and it is known that the GPx is the most important enzyme for the extra peroxisomal inactivation of H_2O_2, particularly in liver cells. So, this

is related with our results, which show that in HepG2 cells the final metabolite T2-tetraol is detoxified mainly by GPx enzyme. According to our results, the increase in GPx and SOD enzymatic activities were previously reported for T-2 [10,11,18] and for DON [38]. Furthermore, similar to our results, the tendency of CAT to basal rate levels [17,32,33] and the decrease in GST [17,31] was previously observed after OTA, DON and STE exposure in cell cultures.

The role of the pre-treatment with NAC and BSO, a GSH promoter and a GSH depletory, respectively, was also evaluated. For T-2, Neo, T2-triol and T2-tetraol, the GSH levels were increased in cells with NAC pre-treatment because the GSH is involved in the cellular defense mechanism when HepG2 cells were exposed to these mycotoxins. It was evidenced by the increase in GPx and GST activities after NAC-pretreatment in all mycotoxin treatments. We determined that pre-treatment with the antioxidant NAC suppressed oxidative damage induced by T-2 and its metabolites on HepG2 cells. On the contrary, overall, BSO showed a significant decrease in GSH levels in cells ex-posed to T-2, T2-triol and T2-tetraol. However, no effects were observed after Neo exposure compared to cells without BSO pre-treatment. This can be because the GPx and GST enzymes (depend on GSH levels) are not involved in the Neo detoxification mechanism. In fact, no changes were observed in GPx (after Neo and T2-triol exposure) and GST (after Neo exposure) activities after BSO pre-treatment compared to cells without pre-treatment. On the contrary, GST activity after BSO exposure is highly suppressed because of the GSH levels decrease and GST is an enzyme GSH-related. Similar results related to the antioxidant defense system after NAC and BSO pre-treatment have already been described on HepG2 [39,40] and SH-SY5Y cells [17]. According to these authors, the NAC blocks ROS induced by STE on SH-SY5Y cells because the

GSH levels and GPx and GST activity increased compared to cells without NAC pre-treatment [17]. And, the same cells have more predisposition to oxidative damage induced by STE after BSO pre-treatment, because GSH levels decreased in cells treated with STE at all concentrations tested further than in cells without pre-treatment, leading to a decrease in GPx and GST activities. The results obtained in this work are similar to those obtained by these authors and confirm that GSH was involved in defense mechanism of the HepG2 cells after trichothecenes exposure.

4. Conclusions

In conclusion, our results suggest that T-2, Neo, T2-triol and T2-tetraol lead to the actuation of the GSH redox system in HepG2 cells, because the decrease of intracellular GSH levels was observed after all mycotoxins and the stimulation of GSH dependent enzyme system. So, the GSH depletion confirmed oxidative stress as an underlying mechanism involved in the cytotoxicity of T-2 and its metabolites. Nevertheless, regarding to antioxidant enzymes, each mycotoxin acts in a different way. Furthermore, the GSH levels and the enzymatic activities related to GSH increased in NAC pre-treated and decreased in BSO pre-treated cells. So, the damage associated to oxidative stress by T-2 and its metabolites is relieved by antioxidant enzymes system on HepG2 cells.

5. Materials and Methods

5.1. Reagents

The substances utilized for cell culture and reagent grade chemicals include Dulbecco's Modified Eagle's Medium (DMEM), streptomycin, penicillin, phosphate buffered saline (PBS), trypsin/EDTA solutions, newborn calf serum

(NBCS), sodium azide (NaN3), β–nicotinamide adenine dinucleotide phosphate (β-NADPH), GSH, GSSG, NAC, BSO, N-ethylmaleimide (NEM), o-phtaldialdehyde (OPT), t-octylphenoxypolyethoxyethanol (Triton-X100), 1-chloro-2,4-dinitrobenzene (CDNB), tris hydroxymethyl aminomethane (Tris), ethylenediaminetetraacetic acid (EDTA), and H_2O_2 were purchased from Sigma-Aldrich (St. Louis, MO, USA). Methanol (MeOH) were acquired from Merck Life Science S.L. (Madrid, Spain). A Milli-Q water purification system (Millipore, Bedford, MA, USA) was used to produce deionized water (resistivity <18 MΩ cm). Standards of T-2 (MW: 466.52 g/mol), Neosolaniol (Neo; MW: 382.40 g/mol), T-2 triol (MW: 382.45 g/mol) and T-2 tetraol (MW: 298.33 g/mol) were purchased from Sigma-Aldrich (St. Louis, MO, USA). Stock solutions of the mycotoxins were made in MeOH at the proper working concentrations and kept at a constant temperature of - 20 ºC in the dark.

5.2. Cell culture and treatment

Human hepatocarcinoma (HepG2) cells (ATCC: HB-8065) were grown in DMEM medium with 10% NBCS, 100 U/ml penicillin and 100 mg/mL streptomycin. The pH 7.4, 5% CO_2 at 37 ºC and 95% air atmosphere at constant humidity were the conditions used for incubation. In order to maintain genetic homogeneity, cells were sub-cultivated twice a week with only a small number of sub-passages. After trypsinization, the HepG2 cells were sub-cultivated in a 1:3 split ratio. The final mycotoxin concentrations assayed were obtained by adding each mycotoxin to the culture medium with a final MeOH concentration ≤1% (v/v). Controls containing the same amount of solvents were used in each experiment.

5.3. *In vitro* cytotoxicity

Cytotoxic effects were determined in HepG2 cells by the MTT assay. In this test, only metabolically active cells are used to evaluate whether a cell is viable by reducing soluble yellow tetrazolium salt to an insoluble purple formazan crystal through a mitochondrial-dependent reaction. The MTT viability assay was carried out as described by Ruiz et al. [41]. Briefly, at a density of 2×10^4 cells/well, the HepG2 cells were seeded in 96-well tissue culture plates. After cells reached 80% of confluence, serial dilutions of T-2, Neo, T2-triol and T2-tetraol in fresh medium were added. Mycotoxin concentrations ranged from: 12.5 to 100 nM for T-2, 11 to 164 nM for Neo, 164 to 2620 nM for T2-triol and 209 to 3350 nM for T2-tetraol. The range of concentrations tested for each mycotoxin was chosen based on assays done previously with all the mycotoxins. The mycotoxin was exposed for 24 h. After that, 200 µL of fresh medium was added to each well after the medium was removed. Then, 50 µL/well of MTT were added and the plates were put back into the incubator in the dark. The MTT solution was removed after 3 h of incubation, and 200 µL of DMSO and 25 µL Sorensen's glycine buffer were added. To achieve the complete dissolution, plates were shaken during 5 min. Using an automatic ELISA plate reader (MultiSkanEX, Thermo Scientific, MA, USA) the absorbance was determined at 540 nm.

Cell viability was expressed as a percentage relative to the control solvent (1% MeOH). Determinations were performed in three independent experiments. The mean inhibition concentration (IC_{50}) values were obtained using SigmaPlot version 11 (Systat Software Inc., GmbH, Germany).

5.4. Intracellular ROS generation

Adding H_2-DCFDA allowed researchers to observe intracellular ROS generation in HepG2 cells after 24 h. Intracellular esterases deacetylate the H_2-DCFDA after it has been absorbed by cells, and the non-fluorescent 2', 7'-dichlorodihydrofluorescein (H_2-DCF) that results is converted by ROS into the highly fluorescent dichlorofluorescein (DCF). Briefly, a 96-well black culture microplate was seeded with 2×10^4 cells/well. After cells reached 80% of confluence, the culture medium was changed to fresh medium containing different concentrations of T-2 (7.5, 15, 30 nM), Neo (12.5, 25, 50 nM), T2-triol (0.12, 0.25, 0.45 μM) and T2-tetraol (0.45, 0.9, 1.70 μM) for 24 h of incubation. The range of concentrations tested for each mycotoxin was chosen in accordance with earlier research done in our laboratory based on the IC_{50} values, and considering the best concentration range for each mycotoxin $IC_{50}/2$, $IC_{50}/4$, $IC_{50}/8$ values [9]. Afterwards, the culture medium was removed and cells were incubated with 50 μM H_2-DCFDA/well in fresh medium during 30 min. Later, the H_2-DCFDA was removed and cells were washed with PBS and after adding 200 μL PBS/well, in-creases in fluorescence were measured on a Wallace Victor2, model 1420 multilabel counter (PerkinElmer, Turku, Finland), at excitation/emission wavelengths of 485/535 nm. Results are expressed as increase in fluorescence respect to solvent control. Determinations were performed in two independent experiments with 12 replicates each.

5.5. GSH determination

Determination of GSH and GSSG was evaluated according to Maran et al. [42]. Briefly, a six-well plate was seeded with 2.25×10^5 cells/well. The cells were exposed to different treatments: (a) fresh medium (DMEM medium), (b) NAC

pre-treatment (DMEM medium plus 1mM NAC) and (c) BSO pre-treatment (DMEM medium plus 60 μM BSO). Once the cells reached 80% confluence, the culture medium was replaced with fresh medium containing different concentrations of T-2 (7.5, 15, 30 nM), Neo (12.5, 25, 50 nM), T2-triol (0.12, 0.25, 0.45 μM) and T2-tetraol (0.45, 0.9, 1.70 μM) incubated for 24 h. Following removal of the medium, the cells were washed with PBS and homogenized in 0.25 mL of 20 mM Tris and 0.1% Triton. The microplate reader Wallace Victor^2, model 1420 multilabel counter (PerkinElmer, Turku, Finland) with excitation and emission wavelength of 345 and 424 nm, was used to measure the concentrations of GSH and GSSG, respectively. The level of GSH and GSSG was represented in μg/mg proteins. Determinations were performed in three independent experiments.

5.6. Determination of enzymatic activities

To determine the scavenging procedures in HepG2 cells exposed to T-2 and its metabolites, the G*S*T, GPx, CAT and SOD activities were determined at the concentrations previously selected. For these assays, 2.25×10^5 cells/well were seeded in six-well plates. The cells were exposed to different treatments: (a) fresh medium (DMEM medium), (b) NAC pre-treatment (DMEM medium plus 1mM NAC) and (c) BSO pre-treatment (DMEM medium plus 60 μM BSO). After cells achieved the 80% confluence, cells were treated with the T-2, Neo, T2-triol and T2-tetraol for 24 h. Then, cells were homogenized in 0.1M phosphate buffer pH 7.5 with 2mM EDTA after the medium was eliminated. All the enzyme determinations were performed in triplicate.

Following the conjugation of GSH with CDNB for 5 min, the G*S*T activity was assessed using the method of [42]. The reaction mixture contained in a final

volume of 1 mL: 100 µL of 20 mM GSH, 825 µL of 0.1M Na/K phosphate buffer at pH 6.5, 25 µL of 50 mM CDNB dissolved in ethanol and 50 µL of homogenized cell sample. The G*S*T activity was expressed as mol of product formed/min/mg of protein using a molar absorptivity of CDNB (9.6 mM^{-1} cm^{-1}). Enzymatic activity was evaluated in a thermocirculator of PerkinElmer UV/vis spectrometer Lambda 2 version 5.1 (PerkinElmer, Turku, Finland). The absorbance was measured at 340 nm.

According to Maran et al. (2009), the GPx activity was measured spectrophotometrically utilizing H_2O_2 as substrate for Se-dependent peroxidase activity of GPx by following oxidation of NADPH during the first five min in a coupled reaction with GR, as described by Maran et al. (2009). In 1mL final volume, the reaction mixture contained 4mM NaN_3 with 500 µL of 0.1M phosphate buffer, pH 7.5 and 2 mM EDTA, 250 µL of ultrapure water, 100 µL of 20 mM GSH, 2U GR, 50 µL of 5 mM H_2O_2 and 20 µL of 10 mM NADPH. Fifty microliter of homogenized cell sample were added to the reaction mixture. At pH 7.5, one unit of GPx will reduce 1 µmol of GSSG per min. Using a molar absorptivity of NADPH (6.22 mM^{-1} cm^{-1}), the enzymatic activity of the GPx enzyme was determined and expressed as µmol of NADPH oxidized/min/mg of protein. Assays were carried out at 25 °C in a thermocirculator of PerkinElmer UV/vis spectrometer Lambda 2 version 5.1 (PerkinElmer, Turku, Finland). At 340 nM, the absorbance was measured.

According to Zingales et al. [17] the CAT activity was measured. Briefly, 100 µL of homogenized cell sample were combined with 400 µL of 40 mM H_2O_2 and 500 µL of 0.5 M potassium phosphate buffer at pH 7.2. Using a spectrophotometer (Super Aquarius CECIL 9500 CE), the rate of enzymatic decomposition of H_2O_2 was measured as decreases in absorbance at 240 nm for

3 min at 30 °C. The molar absorptivity of H_2O_2 (43.6 mM^{-1} cm^{-1}) was used to calculate the CAT activity, which is represented as μmol H_2O_2/min/mg of protein.

The Ransod kit (Randox Laboratories, United Kingdom) modified for 1.5 mL cuvettes was used to measure the SOD activity. The free radical superoxide is destroyed by the SOD by being changed into peroxide. A spectrophotometer of PerkinElmer UV/Vis Lambda 2 version 5.1 (PerkinElmer, Turku, Finland) was used to measure the SOD activity at 505 nm for 3 min at 37 °C. Units of SOD/mg protein were used to express the SOD values.

5.7. Determination of protein content

The Bio-Rad DC Protein Assay, with the catalogue number 5000116, was used to determine the protein content. Using an automatic ELISA plate reader (MultiSkanEX, Labsystem, Helsinki, Finland), the concentration of protein (μg/ml) was measured at 690 nm.

5.8. Pre-treatment with BSO or NAC

Cells were pretreated with NAC or BSO prior to the mycotoxin exposure to examine the effects of these compounds on the modulation of intracellular GSH content and on the enzymatic activities related to GSH content. Approximately, 2.25×10^5 cells/well were exposed to 1mM NAC or 60 μM BSO dissolved in medium during 24 h, after that, the cells were treated with fresh medium containing T-2, Neo, T2-triol and T2-tetraol at the designated concentrations during 24 h. As control, cells with 1% MeOH in the medium were used. The GSH content and enzymatic activities were evaluated after 24 h of exposure as previously mentioned. Comparison between cells exposed to different

concentration of each mycotoxin in fresh medium and NAC or BSO pre-treatment were performed.

5.9. Statistical analysis

Data of various independent experiments were expressed as mean ± SEM. Stu-dent's t-test for paired samples was used to statistical analysis of results. One-way ANOVA followed by the Turkey HDS *post-hoc* test for multiple comparisons was used to analyzed difference between groups. Statistically significant was considered the difference level of $p \leq 0.05$.

Author contributions: Conceptualization, M.T. and M.-J.R.; methodology, M.T. and F.H.; software, M.T.; validation, M.T. and M.-J.R.; formal analysis, M.T. and F.H.; research, M.T.; resources, M.T.; data curation, M.T. and F.H.; writing: preparation of original draft, M.T.; Writing: review and edition, M.-J.R. and Y.R.-C.; visualization, M.-J.R. and Y.R.-C.; supervision, M.-J.R. and Y.R.-C.; project administration, M.-J.R.; acquisition financing, M.-J.R. All authors have read and agreed to the published version of the manuscript.

Funding: This research was funded by the Ministry of Science and Innovation (Spain) (PID2020-115871RB-I00). M. Taroncher thanks the Ministerio de Ciencia e Innovación for providing the Ph.D. grant (PRE2021-096941).

Institutional Review Board Statement: Not applicable.

Informed Consent Statement: Not applicable.

Data Availability Statement: Data is contained within the article.

Conflicts of interest: The authors declare no conflict of interest.

6. References

1. Dai, C.; Xiao, X.; Sun, F.; Zhang, Y.; Hoyer, D.; Shen, J.; Tang, S.; Velkov, T. T-2 Toxin Neurotoxicity: Role of Oxidative Stress and Mitochondrial Dysfunction. Arch Toxicol 2019, 93, 3041–3056.
2. Wild, C.P.; Gong, Y.Y. Mycotoxins and Human Disease: A Largely Ignored Global Health Issue. Carcinog 2009, 31, 71–82, doi:10.1093/carcin/bgp264.

3. Zhang, Y.F.; Yang, J.Y.; Li, Y.K.; Zhou, W. Toxicity and Oxidative Stress Induced by T-2 Toxin in Cultured Mouse Leydig Cells. Toxicol Mech Methods 2017, 27, 100–106, doi:10.1080/15376516.2016.1258747.
4. Lei, R.; Jiang, N.; Zhang, Q.; Hu, S.; Dennis, B.S.; He, S.; Guo, X. Prevalence of Selenium, T-2 Toxin, and Deoxynivalenol in Kashin–Beck Disease Areas in Qinghai Province, Northwest China. Biol Trace Elem Res 2016, 171, 34–40, doi:10.1007/s12011-015-0495-0.
5. Sun, L.-Y.; Li, Q.; Meng, F.-G.; Fu, Y.; Zhao, Z.-J.; Wang, L.-H. T-2 Toxin Contamination in Grains and Selenium Concentration in Drinking Water and Grains in Kaschin-Beck Disease Endemic Areas of Qinghai Province. Biol Trace Elem Res 2012, 150, 371–375, doi:10.1007/s12011-012-9469-7.
6. Wang, X.; Liu, X.; Liu, J.; Wang, G.; Wan, K. Contamination Level of T-2 and HT-2 Toxin in Cereal Crops from Aba Area in Sichuan Province, China. Bull Environ Contam Toxicol 2012, 88, 396–400, doi:10.1007/s00128-011-0478-6.
7. Arcella, D.; Gergelova, P.; Innocenti, M.L.; Steinkellner, H. Human and Animal Dietary Exposure to T-2 and HT-2 Toxin. EFSA J 2017, 15, doi:10.2903/j.efsa.2017.4972.
8. Máté, M.; Gábor, M.; Zsuzsanna, N. The Effects of T-2 Toxin on Animal Health, Focusing Especially on Poultry: literature review. Magy Allatorvosok Lapja 2018, 140, 475–483.
9. Taroncher, M.; Rodríguez-Carrasco, Y.; Ruiz, M.J. Interactions between T-2 Toxin and Its Metabolites in HepG2 Cells and in Silico Approach. Food Chem Toxicol 2021, 148, 111942, doi:10.1016/j.fct.2020.111942.
10. Yang, L.; Yu, Z.; Hou, J.; Deng, Y.; Zhou, Z.; Zhao, Z.; Cui, J. Toxicity and Oxidative Stress Induced by T-2 Toxin and HT-2 Toxin in Broilers and Broiler Hepatocytes. Food Chem Toxicol 2016, 87, 128–137, doi:10.1016/j.fct.2015.12.003.
11. Deyu, H.; Luqing, C.; Xianglian, L.; Pu, G.; Qirong, L.; Xu, W.; Zonghui, Y. Protective Mechanisms Involving Enhanced Mitochondrial Functions and Mitophagy against T-2 Toxin-Induced Toxicities in GH3 Cells. Toxicol Lett 2018, 295, 41–53, doi:10.1016/j.toxlet.2018.05.041.
12. Petruška, P.; Latacz, A.; Kolesárová, A.; Capcarová, M. Effect of quercetin and T-2 toxin on antioxidant parameters of porcine blood in vitro. Microbiol, Biotech Food Sci 2012; Vol. 2, 510-516.
13. Sheng, K.; Lu, X.; Yue, J.; Gu, W.; Gu, C.; Zhang, H.; Wu, W. Role of Neurotransmitters 5-Hydroxytryptamine and Substance P in Anorexia Induction Following Oral Exposure to the Trichothecene T-2 Toxin. Food Chem Toxicol 2019, 123, 1–8, doi:10.1016/j.fct.2018.10.041.
14. Mu, P.; Xu, M.; Zhang, L.; Wu, K.; Wu, J.; Jiang, J.; Chen, Q.; Wang, L.; Tang, X.; Deng, Y. Proteomic Changes in Chicken Primary Hepatocytes Exposed to T-2 Toxin Are Associated with Oxidative Stress and Mitochondrial Enhancement. Proteomics 2013, 13, 3175–3188, doi:10.1002/pmic.201300015.

15. Juan-García, A.; Bind, M.-A.; Engert, F. Larval Zebrafish as an in Vitro Model for Evaluating Toxicological Effects of Mycotoxins. Ecotoxicol Environ Saf 2020, 202, 110909, doi:10.1016/j.ecoenv.2020.110909.
16. Taroncher, M.; Rodríguez-Carrasco, Y.; Ruiz, M.J. T-2 Toxin and Its Metabolites: Characterization, Cytotoxic Mechanisms and Adaptive Cellular Response in Human Hepatocarcinoma (HepG2) Cells. Food Chem Toxicol 2020, 145, 111654, doi:10.1016/j.fct.2020.111654.
17. Zingales, V.; Fernández-Franzón, M.; Ruiz, M.J. Sterigmatocystin-Induced Cytotoxicity via Oxidative Stress Induction in Human Neuroblastoma Cells. Food Chem Toxicol 2020, 136, 110956, doi:10.1016/j.fct.2019.110956.
18. Yang, L.; Tu, D.; Wang, N.; Deng, Z.; Zhan, Y.; Liu, W.; Hu, Y.; Liu, T.; Tan, L.; Li, Y.; et al. The Protective Effects of DL-Selenomethionine against T-2/HT-2 Toxins-Induced Cytotoxicity and Oxidative Stress in Broiler Hepatocytes. Toxicol in Vitro 2019, 54, 137–146, doi:10.1016/j.tiv.2018.09.016.
19. Li, X.; Wang, X.; Liu, S.; Wang, J.; Liu, X.Y.; Zhu, Y.; Zhang, L.; Li, R. Betulinic Acid Attenuates T-2 Toxin-Induced Cytotoxicity in Porcine Kidney Cells by Blocking Oxidative Stress and Endoplasmic Reticulum Stress. Comp Biochem Physiol Part C: Toxicol Pharmacol 2021, 249, 109124, doi:10.1016/j.cbpc.2021.109124.
20. Gaigé, S.; Djelloul, M.; Tardivel, C.; Airault, C.; Félix, B.; Jean, A.; Lebrun, B.; Troadec, J.D.; Dallaporta, M. Modification of Energy Balance Induced by the Food Contaminant T-2 Toxin: A Multimodal Gut-to-Brain Connection. Brain Behav Immun 2014, 37, 54–72, doi:10.1016/j.bbi.2013.12.008.
21. Wu, J.; Jing, L.; Yuan, H.; Peng, S. qing T-2 Toxin Induces Apoptosis in Ovarian Granulosa Cells of Rats through Reactive Oxygen Species-Mediated Mitochondrial Pathway. Toxicol Lett 2011, 202, 168–177, doi:10.1016/j.toxlet.2011.01.029.
22. He, S. jun; Hou, J. fa; Dai, Y. yi; Zhou, Z. lei; Deng, Y. feng N-Acetyl-Cysteine Protects Chicken Growth Plate Chondrocytes from T-2 Toxin-Induced Oxidative Stress. J Appl Toxicol 2012, 32, 980–985, doi:10.1002/jat.1697.
23. Agrawal, M.; Bhaskar, A.S.B.; Rao, P.V.L. Involvement of Mitogen-Activated Protein Kinase Pathway in T-2 Toxin-Induced Cell Cycle Alteration and Apoptosis in Human Neuroblastoma Cells. Mol Neurobiol 2015, 51, 1379–1394, doi:10.1007/s12035-014-8816-4.
24. Zhang, X.; Wang, Y.; Velkov, T.; Tang, S.; Dai, C. T-2 Toxin-Induced Toxicity in Neuroblastoma-2a Cells Involves the Generation of Reactive Oxygen, Mitochondrial Dysfunction and Inhibition of Nrf2/HO-1 Pathway. Food Chem Toxicol 2018, 114, 88–97, doi:10.1016/j.fct.2018.02.010.
25. Fatima, Z.; Guo, P.; Huang, D.; Lu, Q.; Wu, Q.; Dai, M.; Cheng, G.; Peng, D.; Tao, Y.; Ayub, M.; et al. The Critical Role of P16/Rb Pathway in the Inhibition of GH3 Cell Cycle Induced by T-2 Toxin. Toxicol 2018, 400–401, 28–39, doi:10.1016/j.tox.2018.03.006.

26. Guo, P.; Liu, A.; Huang, D.; Wu, Q.; Fatima, Z.; Tao, Y.; Cheng, G.; Wang, X.; Yuan, Z. Brain Damage and Neurological Symptoms Induced by T-2 Toxin in Rat Brain. Toxicol Lett 2018, 286, 96–107, doi:10.1016/j.toxlet.2018.01.012.
27. Liu, X.; Guo, P.; Liu, A.; Wu, Q.; Xue, X.; Dai, M.; Hao, H.; Qu, W.; Xie, S.; Wang, X.; et al. Nitric Oxide (NO)-Mediated Mitochondrial Damage Plays a Critical Role in T-2 Toxin-Induced Apoptosis and Growth Hormone Deficiency in Rat Anterior Pituitary GH3 Cells. Food Chem Toxicol 2017, 102, 11–23, doi:10.1016/j.fct.2017.01.017.
28. Gouze, M.E.; Laffitte, J.; Rouimi, P.; Loiseau, N.; Oswald, I.P.; Galtier, P. Effect of Various Doses of Deoxynivalenol on Liver Xenobiotic Metabolizing Enzymes in Mice. Food Chem Toxicol 2006, 44, 476–483, doi:10.1016/j.fct.2005.08.020.
29. Agahi, F.; Juan-García, A.; Font, G.; Juan, C. Study of Enzymatic Activity in Human Neuroblastoma Cells SH-SY5Y Exposed to Zearalenone's Derivates and Beauvericin. Food Chem Toxicol 2021, 152, 112227, doi:10.1016/j.fct.2021.112227.
30. Dinu, D.; Bodea, G.O.; Ceapa, C.D.; Munteanu, M.C.; Roming, F.I.; Serban, A.I.; Hermenean, A.; Costache, M.; Zarnescu, O.; Dinischiotu, A. Adapted Response of the Antioxidant Defense System to Oxidative Stress Induced by Deoxynivalenol in Hek-293 Cells. Toxicon 2011, 57, 1023–1032, doi:10.1016/j.toxicon.2011.04.006.
31. Ramyaa, P.; Krishnaswamy, R.; Padma, V.V. Quercetin Modulates OTA-Induced Oxidative Stress and Redox Signalling in HepG2 Cells - Up Regulation of Nrf2 Expression and down Regulation of NF-KB and COX-2. Biochim Biophys Acta Gen Subj 2014, 1840, 681–692, doi:10.1016/j.bbagen.2013.10.024.
32. Tatay, E.; Espín, S.; García-Fernández, A.J.; Ruiz, M.J. Oxidative Damage and Disturbance of Antioxidant Capacity by Zearalenone and Its Metabolites in Human Cells. Toxicol in Vitro 2017, 45, 334–339, doi:10.1016/j.tiv.2017.04.026.
33. Tatay, E.; Font, G.; Ruiz, M.J. Cytotoxic Effects of Zearalenone and Its Metabolites and Antioxidant Cell Defense in CHO-K1 Cells. Food Chem Toxicol 2016, 96, 43–49, doi:10.1016/j.fct.2016.07.027.
34. Mallebrera, B.; Font, G.; Ruiz, M.J. Disturbance of Antioxidant Capacity Produced by Beauvericin in CHO-K1 Cells. Toxicol Lett 2014, 226, 337–342, doi:10.1016/j.toxlet.2014.02.023.
35. Krishnaswamy, R.; Devaraj, S.N.; Padma, V.V. Lutein Protects HT-29 Cells against Deoxynivalenol-Induced Oxidative Stress and Apoptosis: Prevention of NF-KB Nuclear Localization and down Regulation of NF-KB and Cyclo-Oxygenase - 2 Expression. Free Radic Biol Med 2010, 49, 50–60, doi:10.1016/j.freeradbiomed.2010.03.016.
36. Gao, W.; Jiang, L.; Ge, L.; Chen, M.; Geng, C.; Yang, G.; Li, Q.; Ji, F.; Yan, Q.; Zou, Y.; et al. Sterigmatocystin-Induced Oxidative DNA Damage in Human Liver-Derived Cell Line through Lysosomal Damage. Toxicol in Vitro 2015, 29, 1–7, doi:10.1016/j.tiv.2014.08.007.
37. Woelflingseder, L.; del Favero, G.; Blažević, T.; Heiss, E.H.; Haider, M.; Warth, B.; Adam, G.; Marko, D. Impact of Glutathione Modulation on the Toxicity of the

Fusarium Mycotoxins Deoxynivalenol (DON), NX-3 and Butenolide in Human Liver Cells. Toxicol Lett 2018, 299, 104–117, doi:10.1016/j.toxlet.2018.09.007.
38. Ruiz, MJ.; Festila, L.E.; Fernández, M. Comparison of Basal Cytotoxicity of Seven Carbamates in CHO-K1 Cells. Toxicol Environ Chem 2006, 88, 345–354, doi:10.1080/02772240600630622.
39. Maran, E.; Fernández, M.; Barbieri, P.; Font, G.; Ruiz, M.J. Effects of Four Carbamate Compounds on Antioxidant Parameters. Ecotoxicol Environ Saf 2009, 7

Foods, 11 (2022), 1033

https://doi.org/10.3390/foods11071033

3.5. Effect of Phenolic Extract from Red Beans (*Phaseolus vulgaris* L.) on T-2 Toxin-Induced Cytotoxicity in HepG2 Cells

Carmen Martínez-Alonso [1,†], Mercedes Taroncher [1,†], Luigi Castaldo [2], Luana Izzo [2], Yelko Rodríguez-Carrasco [1,*], Alberto Ritieni [2] and María-José Ruiz[1,2]

[1] Department of Preventive Medicine and Public Health, Food Science, Toxicology and Forensic Medicine, Faculty of Pharmacy, University of Valencia, Burjassot, 46100 Valencia, Spain; Carmar36@alumni.uv.es (C.M.-A.); Mercedes.Taroncher@uv.es (M.T.); M.Jose.Ruiz@uv.es (M.-J.R.)

[2] Department of Pharmacy, Faculty of Pharmacy, University of Naples "Federico II", Via Domenico Montesano 49, 80131 Naples, Italy; luana.izzo@unina.it (L.I.); luigi.castaldo2@unina.it (L.C.); alberto.ritieni@unina.it (A.R.).

† These authors contributed equally to this work.

Abstract

Red beans contain human bioactive compounds such as polyphenols. Several *in vitro* studies have proposed the natural compounds as an innovative strategy to modify the toxic effects produced by mycotoxins. Hence, in this work, a complete investigation of the polyphenolic fraction of red beans was performed using a Q-Orbitrap high-resolution mass spectrometry analysis. Notably, epicatechin and delphinidin were the most detected polyphenols found in red bean extracts (3.297 and 3.108 mg/Kg, respectively). Moreover, the red bean extract was evaluated against the T-2 toxin (T-2) induced cytotoxicity in hepatocarcinoma cells (HepG2) by direct treatment, simultaneous treatment, and pre-treatment assays. These data showed that T-2 affected the cell viability in a dose-dependent manner, as well as observing a cytotoxic effect and a significant increase in ROS production at 30 nM. The simultaneous treatment and the pre-treatment of HepG2 cells with red bean extract was not able to modify the cytotoxic T-2 effect. However, the simultaneous treatment of T-2 at 7.5 nM with the red bean extract showed a significant decrease in ROS production, with respect to the control. These results suggest that the red bean extract could modulate oxidative stress on HepG2 cells.

Key words: Beans; phenolic compounds; T-2 toxin; HepG2 cells; reactive oxygen species.

---

* **Corresponding author**: Department of Preventive Medicine and Public Health, Food Science, Toxicology and Forensic Medicine, Faculty of Pharmacy, University of Valencia, Burjassot, 46100 Valencia, Spain. E-mail address: Yelko.rodriguez@uv.es

1. Introduction

Red beans (*Phaseolus vulgaris* L.), in addition to being a great source of vegetable protein, fiber, and certain micronutrients in the human diet, contain a great variety of bioactive compounds. Bioactive compounds are simple substances that have biological activity, associated with their ability to modulate one or more metabolic processes, which results in the promotion of better health conditions. Different bioactive compounds have been studied for their positive effect on human health, such as the following: enzymes, probiotics, prebiotics, fibers, phytosterols, peptides, proteins, saponins, unsatured fatty acids, and phenolic compounds, among others [1]. Particularly, colored beans have significant amounts of phenolic compounds. Phenolic compounds are classified as flavonoids (flavones, flavonols, flavanones, isoflavones, anthocyanins, chalcones, dihydrochalcones, and catechins), phenolic acids (hydroxybenzoic, hydroxyphenyl acetic, hydroxyphenyl pentanoic, and cinnamic hydroxyl acids), tannins, stilbenes, and lignans. Phenolic acids, flavonoids, and anthocyanidins are the main phenolic compounds identified and characterized in beans [2,3]. Phenolic compounds determine the color of the seeds of these legumes; hence, in general, a higher phenolic content is observed in more pigmented beans [4]. Phenolic compounds, besides from contributing to the smell, taste, and color of food, have a long-term intake that could play a bioactive role due to their antioxidant activity, which has been related to the prevention of obesity, cardiovascular and neurodegenerative diseases, cancer, and diabetes, as well as exhibiting antiinflammatory, antimutagenic, and antibacterial properties [5,6]. Madhujith et al. demonstrated that beans, especially those with colored skins, possess strong antioxidant activity as measured by different model systems [7]. Epidemiological studies correlated the consumption of procyanidin-rich foods

with a lower incidence of inflammatory disease and diseases of multifactorial pathogenesis [8]. Similarly, the transcription and secretion of proinflammatory cytokines, including IL-1β, IL-2, IL-6, TNF-α, and interferon- γ, could be down-regulated by procyanidins, as reported in some *in vitro* and *in vivo* studies [9,10].

Despite the fact that legumes are protein rich foods, they are lacking in sulphur-containing amino acids. On the other hand, cereals contain sulphur amino acids but are limited in the essential amino acid lysine. Hence, a combination of legumes and cereals would improve the protein and nutrient density of the subsequent food products. However, the resulting high nutritional value food products could be susceptible to deterioration by fungal contamination, accompanied by the production of mycotoxins [11].

Mycotoxins are the secondary metabolites produced by filamentous fungi. The species assigned to the *Aspergillus*, *Penicillium*, *Alternaria*, *Claviceps*, and *Fusarium* genera produce a wide range of mycotoxins, which can contaminate food and feed, resulting in a significant threat to human and animal health [12]. Trichothecenes are a complex group of tetracyclic sesquiterpenoids produced by several *Fusarium* spp. Type A and B trichothecenes are the most relevant mycotoxins reported in food and feed regarding their incidence and concentration [13]. Among the trichothecenes, T-2 toxin (T-2) is the compound that shows the highest toxicity. Several studies have reported that T-2 toxin causes multiple damages to organs such as the kidney, liver, brain, gastrointestinal tract, and bone marrow [14]. Similarly, the toxic effects derived from repeated exposure to T-2 include genotoxicity, immunotoxicity, neurotoxicity, and reproductive toxicity [15,16]. Therefore, the European Food Safety Authority (EFSA) established a tolerable daily intake (TDI) for T-2 and

its main metabolite HT-2 of 0.02 μg/Kg body weight (bw) to limit their exposure [13].

Based on the abovementioned information, the aims of this work are as follows: (i) to evaluate the total phenolic content (TPC), the phenolic profile, using ultra-high-performance liquid chromatography coupled with high-resolution mass spectrometry (UHPLC-Q-Orbitrap HRMS), and the antiradical activity of red bean extracts, and (ii) to assess the effect of the red bean extract on T-2 toxin-induced cytotoxicity in human hepatocarcinoma (HepG2) cells.

2. Material and Methods

2.1 Chemical and Reagents

Methanol (MeOH) and ethanol (EtOH) of HPLC grade were acquired from Merck (Darmstadt, Germany). Formic acid and ammonium formate were obtained from Fluka (Milan, Italy). Ethyl acetate was purchased from Merck Life Science S.L. (Madrid, Spain). Deionized water (resistivity < 18 MΩ cm) was obtained using a Milli-Q water purification system (Millipore, Bedford, MA, USA).

The chemical reagents and cell culture components used, namely Dulbecco's Modified Eagle's Medium (DMEM), penicillin, streptomycin, trypsin/EDTA solutions, phosphate buffered saline (PBS), Newborn Calf Serum (NBCS), methylthiazoltetrazolium salt (MTT) dye, dimethyl sulfoxide (DMSO), Sorensen's glycine buffer, dichlorodihydrofluorescein diacetate (H_2-DCFDA), 2,2-diphenyl-1-picrylhydrazyl (DPPH), Folin–Ciocalteu's phenol reagent, gallic acid ($C_7H_6O_5$), potassium chloride (KCl), sodium hydroxide (NaOH), hydrochloric acid (HCl), sodium chloride (NaCl), sodium phosphate dibasic

(Na_2HPO_4), potassium phosphate monobasic (KH_2PO_4), and sodium carbonate (Na_2CO_3), were acquired from Sigma-Aldrich (Barcelona, Spain).

The standard of T-2 (MW: 466.52 g/mol) was purchased from Sigma-Aldrich (Barcelona, Spain). Standards of polyphenols (purity > 98%), namely protocatechuic acid, cyanidin 3,5-diglucoside, epicatechin, chlorogenic acid, cyanidin 3-galactoside, caffeic acid, catechin, *p*-cumaric acid, apigenin 7-glucoside, genistein, delphinidin, naringin, cyanidin, rosmarinic acid, myricitrin, diosmin, isoquercetin, rutin, kaempferol 3-glucoside, vitexin, ellagic acid, luteolin 7-glucoside, myricetin, diadzein, quercetin, delphinidin 3,5-diglucoside, naringenin, luteolin, kaempferol, and apigenin, were acquired from Sigma-Aldrich (Milan, Italy). Stock solutions of T-2 were prepared in MeOH at appropriate working concentrations and maintained in the dark at -20 °C.

2.2. Preparation of Red Bean Extract

The polyphenols were extracted from red beans according to the procedure reported in the literature with some modifications [17]. In summary, 0.5 g of ground beans was extracted with 10 mL of a solution MeOH:H_2O. The assayed mixtures were 20:80, 30:70, 50:50, 70:30, and 80:20 (*v*/*v*). Hydrochloric acid 2N was added to the sample until a pH adjustment to 2, to avoid the protonated forms of carboxylic groups present in polyphenols. Then, the mixture was subjected to a horizontal shaker (250 rpm) at room temperature for 3 h and centrifuged for 3 min at 3500 rpm. Finally, MeOH was evaporated from the acidified sample extract under reduced pressure (250 mbar) at 50 °C for 15 min by Buchi Rotavapor R-200 (Buchi, Postfach, Switzerland) and the aqueous extract containing polyphenols was filtered with a 0.2 μm polytetrafluoroethylene (PTFE) filter and stored in amber glass flask at 4 °C.

2.3. Determination of Total Phenolic Content (TPC)

The Folin–Ciocalteu assay was used to determine the total phenolic content in accordance with the procedure reported by Izzo et al. [18]. Briefly, 0.5 mL of red bean extract or blank (deionized water) was diluted with deionized water (4.5 mL) and 0.25 mL of Folin–Ciocalteu reagent 1 N was added. Then, 1 mL of 2% sodium carbonate solution was added and the mixture was allowed to stand at room temperature for 1 h in dark conditions. Finally, the absorbance was measured with a spectrophotometer at 765 nm against a reagent blank. The analysis was carried out in triplicate and the results were expressed as mg of gallic acid equivalents (GAE) per Kg of sample.

2.4. Determination of Polyphenolic Profile

The polyphenolic profile of the red bean extracts was carried out on a UHPLC-Q Exactive Orbitrap-HRMS system (Thermo Fisher Scientific, Waltham, MA, USA), composed of a Dionex Ultimate 3000 liquid chromatograph equipped with a solvent rack compartment (SRD-3x00), a quaternary rapid separation pump (LPG-3400RS), a rapid separation autosampler (WPS-3000RS), and a temperature-controlled column compartment (TCC-3000SD). The chromatographic separation was performed on a Kinetex F5 (50 × 2.1 mm; 1.7 μm) reverse-phase column (Phenomenex, Milan, Italy) at 25 °C. The mobile phase consisted of water containing 0.1% formic acid (A) and MeOH containing 0.1% formic acid (B). The separation gradient consisted of an initial 0% of phase B, increasing to 40% B in 1 min, 80% B in a further 1 min, and 100% B in 3 min. Then, the gradient was held at 100% B for 4 min and reduced to 0% B in 2 min, followed by 2 min of column

reequilibration at 0% B. The total run time was 13 min. The flow rate was 0.5 mL/min and the injection volume was 1 μL.

The mass spectrometer was equipped with an electrospray (ESI) source that simultaneously operates in positive and negative ion switching mode. Full ion MS and all–ion fragmentation (AIF) were set as scan events. The following settings were used in full MS mode: resolution power of 70,000 Full Width at Half Maximum (FWHM) (defined for m/z 200); automatic gain control (AGC) target: 1×10^6; scan range: 80–1200 m/z; injection time set to 200 ms; scan rate set at 2 scan/s. The ion source parameters were as follows: sheath gas pressure: 18; auxiliary gas: 3; spray voltage: 3.5 kV; capillary temperature: 320 °C; S-lens RF level: 60; auxiliary gas heater temperature: 350°C. For the scan event of AIF, the parameters in the negative and positive mode were set as follows: mass resolving power = 17,500 FWHM; ACG target = 1×10^5; maximum injection time = 200 ms; scan time = 0.10 s; scan range = 80–1200 m/z; isolation window to 5.0 m/z; retention time to 30 s. The collision energy was varied between 10 and 60 eV to acquire representative product ion spectra.

For the identification and confirmation of the molecular ion and fragments, a mass tolerance below 5 ppm was set. Data analysis and processing were performed using Xcalibur software, v. 3.1.66.10 (Xcalibur, Thermo Fisher Scientific, Waltham, MA, USA).

2.5. Determination of Antiradical Activity (DPPH)

The total free radical scavenging activity of the red bean extracts was determined using the method reported in the literature with modifications [19]. Briefly, DPPH (4 mg) was solubilized in 10 mL of MeOH and then diluted to reach an absorbance value of 0.90 (± 0.05) at 517 nm. This solution was used to

perform the assay and 200 μL of red bean extract was added to 1 mL of working solution. The mixture was vortexed, kept for 90 min in the dark, and centrifuged for 5 min at 11,000 rpm. Finally, the decreased absorbance was measured at 517 nm. The analysis was carried out in triplicate and the results were expressed as mmol Trolox Equivalents (TE) per Kg of sample.

2.6. Cell Culture

Human hepatocarcinoma (HepG2) cells (ATCC: HB-8065) were cultured in DMEM medium supplemented with 10% NBCS, 100 U/mL penicillin, and 100 mg/mL streptomycin. The cells were maintained at pH 7.4, 5% CO_2 at 37 °C, and 95% air atmosphere at constant humidity. The cells were subcultured routinely twice a week with only a small number of sub-passages (<20 passages) in order to maintain genetic homogeneity. HepG2 cells were subcultured after trypsinization in a 1:3 split ratio. The medium was changed every 5 days. The final mycotoxin concentrations tested were achieved by adding T-2 mycotoxin to the culture medium, with a final MeOH concentration ≤ 1% (*v*/*v*).

2.7. HepG2 Cells Treatment

The HepG2 cells were cultured in 96-well tissue culture plates by adding 200 μL/well of density at 2×10^4 cells/well. After the cells reached 80% confluence, the culture medium was replaced with a fresh medium containing different concentrations of T-2 (7.5, 15, and 30 nM) and serial dilutions of red bean extracts (from 1:32 to 1) buffered to pH 7.4. Then, the plates were incubated in the dark at 37 °C and 5% CO_2 for 24 h. The assayed T-2 concentrations correspond to sublethal T-2 concentrations for HepG2 cells (<IC_{50}), based on

previous studies carried out in our laboratory [20], and they were $IC_{50}/2$, $IC_{50}/4$, and $IC_{50}/8$, respectively.

The following two more assays were performed: simultaneous treatment and pretreatment. On one hand, for pretreatment studies, HepG2 cells were exposed to one red bean extract dilution according to previous cell proliferation assays (red bean extract 1:8 dilution) for 1 and 24 h. Then, the medium containing the red bean extract was removed and cells were exposed at the T-2 concentrations described above for 24 h. On the other hand, to conduct studies of simultaneous treatment, HepG2 cells were exposed to the assayed T-2 concentrations and the 1:8 diluted red bean extract for 24 h.

Appropriate controls containing the same amount of solvent were included in each experiment.

2.8. Determination of Cell Viability

Cell viability was determined in HepG2 cells by the MTT assay. The MTT assay is based on the capacity of viable cells to metabolize, via a mitochondrial-dependent reaction, specifically, the reduction of yellow tetrazolium salt to an insoluble purple formazan crystal. The MTT assay was carried out according to the procedure reported by Ruiz et al. [21]. In summary, after treatment studies, the medium containing the compounds was removed and each well received 200 µL of fresh medium containing 50 µL of MTT. The plates were returned to the incubator in the dark at 37 °C and 5% CO_2 for 3 h. Then, the MTT solution was removed and 200 µL of DMSO was added, followed by 25 µL of Sorensen's glycine buffer. The absorbance was measured at 620 nm on a Wallace Victor2, model 1420 multilabel counter (PerkinElmer, Turku, Finland). The blank

absorbance value (from wells without cells but treated with MTT) was subtracted from all absorbance values.

Cell viability was expressed as a percentage relative to control cells (≤1% MeOH). Three independent experiments were conducted with eight replicates each, and the results were expressed as the mean ± standard error of the mean (SEM) of different independent experiments.

2.9. Determination of Reactive Oxygen Species (ROS)

Intracellular ROS production was monitored in HepG2 cells by adding H_2-DCFDA [22]. H_2-DCFDA is taken up by cells and then deacetylated by intracellular esterases; the resulting non-fluorescent 2',7'-dichlorodihydrofluorescein (H_2-DCF) is converted to greatly fluorescent dichlorofluorescein (DCF) when oxidized by ROS. Briefly, 2×10^4 cells/well were seeded in a 96-well black polystyrene culture microplate. Once cells exhibited 80% confluence, the culture medium was replaced and cells were loaded with 20 μM H_2-DCFDA in a fresh medium for 20 min in darkness. Then, H_2-DCFDA was removed and replaced by a fresh medium containing 1:8 diluted red bean extract, T-2 (30, 15, and 7.5 nM), and the combination of diluted red bean extract with T-2 at the different concentrations assayed. Finally, the fluorescence emitted by the DCF was monitored at different times (0, 5, 15, 30, 45, 60, 90, and 120 min) on a Wallace Victor2, model 1420 multilabel counter (PerkinElmer, Turku, Finland), at excitation/emission wavelengths of 485/535 nm, respectively. The blank absorbance value (from wells without cells but treated with H_2-DCFDA) was subtracted from all absorbance values.

The determinations were performed in three independent experiments with 24 replicates each and the results are expressed as an increase (%) in fluorescence in respect to control cells.

2.10. Statistical Analysis

Statistical analysis of data was carried out using the Statgraphics version 16.01.03 statistical package (IBM Corp., Armonk, NY, USA). Data are expressed as mean ± SEM of different independent experiments. The statistical analysis of the results was performed by Student's *t*-test for paired samples. The differences between groups were analyzed by employing one-way analysis of variance (ANOVA) continued by the Tukey HDS post-hoc test for multiple comparisons. Statistical significance was considered for $p \leq 0.05$.

3. Results and Discussion

3.1. Total Phenolic Content and Antiradical Activity of Red Bean Extract

The extraction of phenolic compounds from red beans was optimized by testing different mixtures of MeOH:H_2O and further determined through the Folin–Ciocalteu assay. The results are shown in Table 1. Based on the results obtained, the mixture 70:30 was optimal to extract phenolic compounds from red beans. The obtained TPC content (2325 ± 98 mg GAE/Kg) was in the same range to that of other studies performed on similar food matrices with values of 1230 mg/Kg [23], 1205 mg/Kg [24], 1690–4850 mg/Kg [25], and 3450 mg/Kg [26]. The TPC and DPPH data of undiluted red bean extracts are shown in Table S1.

The total free radical scavenging activity of the red bean extract was evaluated through the DPPH assay. The results are in agreement with the previous assay being the highest antioxidant activity obtained with the mixture MeOH:H_2O (70:30, *v/v*) (Table 1). In addition, it was observed that the larger the phenolic content, the better the free radical scavenging activity. Significant differences in the phenolic content and the antioxidant activity among legume extracts were also reported by Zhao et al. [27]. Similarly, the values of antiradical activity obtained from red bean extract (49.2 ± 4.6 mmol TE/Kg) were comparable to those reported in other studies [28,29]. Besides, the antioxidant properties shown by the phenolic compounds, the antiinflammatory activity by different mechanisms, including modulation of the inflammatory cascade, has also been reported in the literature [30]. García-Lafunete et al. reported that the phenolic rich extracts from beans inhibited the expression of IL-1β, IL-6, and TNF-α genes of stimulated macrophages RAW 246.7, with colored beans showing more activity than white beans [31].

Table 1. Total phenolic content (TPC) and antiradical activity (DPPH) of dry red beans using different mixtures of MeOH:H_2O. Values are reported as mean ± SD of independent experiments performed in triplicate.

MeOH:H_2O (*v/v*)	**TPC (mg GAE/Kg ± SD)**	**DPPH (mmol TE/Kg ± SD)**
80:20	1892 ± 237	42.3 ± 5.8
70:30	2325 ± 98	49.2 ± 4.6
50:50	1348 ± 24	30.4 ± 6.1
30:70	1272 ± 8	29.2 ± 8.7
20:80	1287 ± 28	27.5 ± 7.3

PC: total phenolic content; GAE: gallic acid equivalents; DPPH: antiradical activity; TE: Trolox equivalents.

3.2. Identification and Quantification of Active Compounds in Red Bean Extract

A total of 30 polyphenols were investigated in the red beans by using UHPLC-Q-Orbitrap HRMS analysis. The chromatographic and spectrometric parameters are shown in Table 2. The results showed a good chromatographic shape and separation of all studied compounds through the UHPLC gradient system employed within a 13 min run. Four different structural isomers, namely genistein and apigenin (m/z 269.0455), and vitexin and apigenin 7-glucoside (m/z 431.0983), were found. Compound identification was conducted by comparing the retention times of the standards with the peaks observed in sample extracts. For quantification purposes, calibration curves at eight concentration levels were built in triplicate. All regression coefficients were greater than 0.990.

Table 2. Chromatographic and spectrometric parameters, including retention time, adduct ion, theoretical and measured mass (*m*/*z*), accuracy, and sensibility, for the investigated bioactive compounds (n = 30).

Compound	RT (min)	Chemical Formula	Adduct Ion	Theoretical Mass (*m*/*z*)	Measured Mass (*m*/*z*)	Product Ion	Mass Accuracy (Δ ppm)	LOD (mg/Kg)	LOQ (mg/Kg)
Protocatechuic acid	1.60	$C_7H_6O_4$	$[M-H]^-$	153.01930	153.01857	109.02840	−4.771	0.026	0.078
Cyanidin 3,5-diglucoside	3.03	$C_{27}H_{31}O_{16}$	$[M+H]^+$	611.16066	611.16022	449.19708–287.06469	−0.719	0.026	0.078
Epicatechin	3.08	$C_{15}H_{14}O_7$	$[M-H]^-$	289.07176	289.07202	221.94647–203.09201–161.04478	0.890	0.013	0.039
Chlorogenic acid	3.20	$C_{16}H_{18}O_9$	$[M-H]^-$	353.08780	353.08798	191.05594–84.98998	0.509	0.013	0.039
Cyanidin 3-galactoside	3.23	$C_{21}H_{21}O_{11}$	$[M+H]^+$	449.10784	449.10654	287.05576	−2.894	0.026	0.078
Caffeic acid	3.25	$C_9H_8O_4$	$[M-H]^-$	179.03498	179.03455	134.99960	−2.401	0.013	0.039
Catechin	3.27	$C_{15}H_{14}O_6$	$[M-H]^-$	289.07175	289.07205	247.02241–205.10712–151.03923–125.02335	1.037	0.026	0.078
p-cumaric acid	3.39	$C_9H_8O_3$	$[M-H]^-$	163.04001	163.03937	119.04917	−3.925	0.026	0.078
Apigenin 7-glucoside	3.45	$C_{21}H_{20}O_{10}$	$[M-H]^-$	431.09837	431.09875	341.10919–283.26419	0.881	0.013	0.039
Genistein	3.47	$C_{15}H_{10}O_5$	$[M-H]^-$	269.04554	269.04562	241.14435–213.14908–151.03935	0.297	0.013	0.039

Table 2. Cont.

Delphinidin	3.48	$C_{15}H_{11}O_7$	$[M-H]^+$	303.04992	303.04993	257.12119–137.05981	0.033	0.026	0.078
Naringin	3.54	$C_{27}H_{32}O_{14}$	$[M-H]^-$	579.17193	579.17185	271.15524–227.12846–161.04475	−0.138	0.013	0.039
Cyanidin	3.57	$C_{15}H_{11}O_6$	$[M+H]^+$	287.05501	287.05472	207.05879–147.07649	−0.611	0.013	0.039
Rosmarinic acid	3.58	$C_{18}H_{16}O_8$	$[M-H]^-$	359.07724	359.07742	179.05537	0.501	0.013	0.039
Myricitrin	3.59	$C_{21}H_{20}O_{12}$	$[M-H]^-$	463.08820	463.08701	316.02126–178.97646	−2.57	0.013	0.039
Diosmin	3.64	$C_{28}H_{32}O_{15}$	$[M-H]^-$	607.16684	607.16534	300.99796–284.03838	−2.471	0.013	0.039
Isoquercetin	3.65	$C_{21}H_{20}O_{12}$	$[M-H]^-$	463.08820	463.08853	431.09848–187.09698–174.95542	0.712	0.013	0.039
Rutin	3.65	$C_{27}H_{30}O_{16}$	$[M-H]^-$	609.14611	609.14673	300.99911–271.05026–255.12390	1.017	0.013	0.039
Kaempferol 3-glucoside	3.66	$C_{21}H_{20}O_{11}$	$[M-H]^-$	447.09195	447.09329	284.03079–255.02881–227.07033	3.000	0.013	0.039
Vitexin	3.67	$C_{21}H_{20}O_{10}$	$[M-H]^-$	431.09837	431.09711	341.10803–311.05457–269.13815	−2.921	0.013	0.039
Ellagic acid	3.67	$C_{14}H_6O_8$	$[M-H]^-$	300.99899	300.99911	245.91669–229.93712–185.01208–117.00336	0.398	0.013	0.039

Table 2. Cont.

Luteolin 7-glucoside	3.68	$C_{21}H_{20}O_{11}$	$[M-H]^-$	447.09328	447.09381	285.04028	1.185	0.013	0.039
Myricetin	3.73	$C_{15}H_{10}O_8$	$[M-H]^-$	317.03029	317.02924	178.87917–151.00217–137.02290	−3.310	0.013	0.039
Daidzein	3.75	$C_{15}H_9O_4$	$[M-H]^-$	253.05063	253.04977	209.96429–225.00984	−3.398	0.013	0.039
Quercetin	3.86	$C_{15}H_{10}O_7$	$[M-H]^-$	301.03538	301.03508	174.95551	−0.996	0.013	0.039
Delphinidin 3,5-diglucoside	3.87	$C_{27}H_{31}O_{17}$	$[M+H]^+$	628.16340	628.16385	465.10339–303.04987	0.716	0.026	0.078
Naringenin	3.91	$C_{15}H_{12}O_5$	$[M-H]^-$	271.06120	271.06110	235.92595–151.03917	−0.368	0.013	0.039
Luteolin	3.94	$C_{15}H_{10}O_6$	$[M-H]^-$	285.04046	285.04086	174.95486–89.02095	1.401	0.013	0.039
Kaempferol	4.00	$C_{15}H_{10}O_6$	$[M-H]^-$	285.04046	285.04086	93.00679	1.403	0.013	0.039
Apigenin	4.08	$C_{15}H_{10}O_5$	$[M-H]^-$	269.04554	269.04541	225.06136–117.01828	−0.483	0.013	0.039

RT: retention time; LOD: limit of detection; LOQ: limit of quantification.

The quantification of the main phenolic acids and flavonoids in red beans was performed by using a UHPLC-Q-Orbitrap HRMS method. The results are shown in Table 3. Up to 22 polyphenols were detected. Among the quantified polyphenols, epicatechin was the major flavanol (3.297 ± 0.119 mg/Kg). The delphinidin, an important anthocyanidin of pigmented beans, was quantified at 3.108 ± 0.023 mg/Kg. Flavanols and anthocyanidins represented 36% and 24.5% of total polyphenolic compounds in red bean samples, respectively. The other important polyphenols quantified in samples were p-coumaric acid, isoquercetin, and kaempferol 3-O-glucoside. The polyphenols content of undiluted red bean extracts is shown in Table S2.

3.3. Effects of Red Bean Extract on the Cell Viability by Individual Exposure

The HepG2 cell viability evaluated by the MTT assay after 24 h of exposure with red bean extract dilutions, from 1 to 1:32, is shown in Figure 1. The results clearly indicated that the viability of HepG2 cells was affected by the more concentrated red bean extracts. In particular, the undiluted (1) and diluted (1:2 and 1:4) red bean extracts significantly decreased HepG2 cell viability from 83% to 23%. Nonetheless, the red bean extract diluted 1:8 significantly increased the cell viability (20%) compared to the control.

The reduction in cell viability caused by the more concentrated or undiluted extracts has also been observed in other studies. Recently, Ziemlewska et al. [32] indicated that high concentrations of the bioactive compounds contained in red fruits inhibited the cell cycle in the G_2/M phase and caused cell death, exerting a negative impact on cell viability. These authors demonstrated that high

concentrations of phenolic extracts from berries induced apoptosis due to the activation of the caspases.

Table 3. Polyphenols content in dry red beans. Results are expressed as mean ± SD from three independent determinations.

Compound	**Content (mg/Kg) ± SD**
Apigenin 7-O-glucoside	<LOQ
Catechin	<LOQ
Chlorogenic acid	0.045 ± 0.002
Cyanidin	0.677 ± 0.046
Cyanidin 3-glucoside	<LOQ
Cyanidin 3,5-diglucoside	0.171 ± 0.015
Daidzein	<LOQ
Delphinidin	3.108 ± 0.023
Delphinidin 3,5-diglucoside	0.210 ± 0.020
Ellagic acid	0.045 ± 0.001
Epicatechin	3.297 ± 0.119
Genistin	<LOQ
Isoquercetin	1.039 ± 0.119
kaempferol 3-O-glucoside	0.803 ± 0.026
Luteolin	0.021 ± 0.001
Naringenin	<LOQ
Naringin	<LOQ
p-coumaric acid	1.929 ± 0.106
Protocatechiuc acid	0.532 ± 0.016
Quercetin	0.292 ± 0.026
Rosmarinic acid	<LOQ
Rutin	0.479 ± 0.037

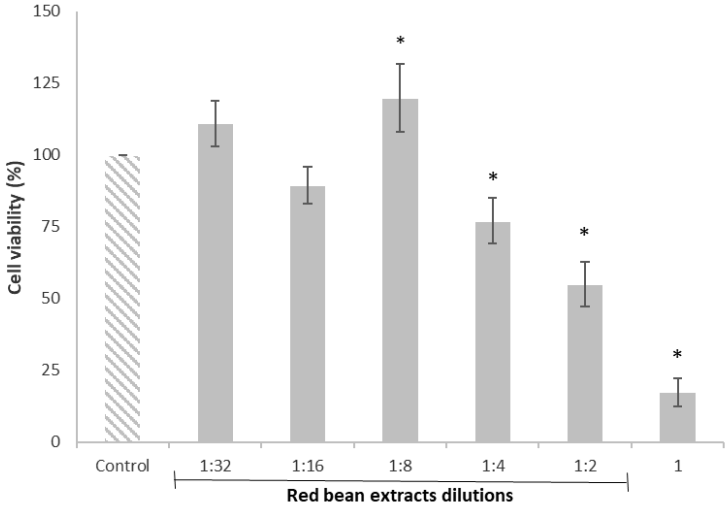

Figure 1. HepG2 cell viability after 24 h of treatment with red bean extracts (undiluted extract (1) and dilutions from 1:2 to 1:32). All values are expressed as mean ± SEM of 3 replicates. (*) $p \leq 0.05$ indicates significant differences compared to control.

3.4. Effects of Simultaneous Treatment in HepG2 Cell Viability Exposed to T-2 and Red Bean Extract

The effect in HepG2 cells simultaneously exposed to T-2 (7.5, 15 and 30 nM) and 1:8 diluted red bean extract is described in Figure 2. The HepG2 cell viability was affected in a concentration-dependent manner. Cytotoxic effects were observed in the cells exposed to 30 nM T-2 alone and in combination with the extract, with a significant reduction in cell viability compared to the control cells by 32% and 56%, respectively. This could be due to the fact that the diluted red bean extract did not completely prevent T-2 cytotoxicity. The diluted red bean extract slightly lowered HepG2 cell viability, which was a statistically significant decrease only in cells exposed to the highest T-2 concentration; whereas it did not completely prevent T-2 cytotoxicity.

On the other hand, cells exposed to the lowest T-2 concentration tested (7.5 nM) showed a significant increase in cell viability (11%) compared to the control; cell viability was slightly higher (13%) in cells simultaneously treated with T-2 and the diluted red bean extract.

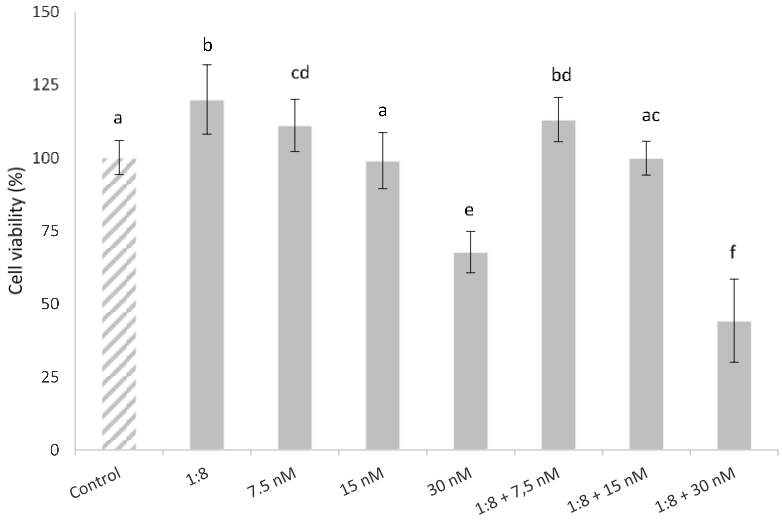

Figure 2. HepG2 cell viability (%) during 24 h of exposure to T-2 (7.5, 15 and 30 nM) and 1:8 diluted red bean extract alone and in combination. All values are expressed as mean ± SEM of 3 replicates. Values in the same figure with different superscript letters are significantly different ($p \leq 0.05$). 1:8 = 1:8 diluted red bean extract.

3.5. Effects of Pretreatment in HepG2 Cell Viability Exposed to T-2 and Red Bean Extract

The effects of cell pretreatment with red bean extract for 1 h and 24 h before the T-2 addition are shown in Figure 3. The results indicated that the pre-treatment with red bean extract was not able to protect or ameliorate the cytotoxic T-2 effect in HepG2 cells in all T-2 concentrations tested. This effect

was increased at 24 h of exposure. Similar results were reported by Kössler et al. [33], who showed that curcumin (phenolic compound) reduced cell viability and induced apoptosis in human embryonic kidney cells (HEK293) in a dose-dependent manner at 22 h of exposure. There are no other data from *in vitro* studies by other authors with bean extracts. However, Vila-Donat et al. [34] reported synergistic cytoprotective effects against cytotoxicity induced by alternariol on Caco-2 cells exposed to an extract obtained from other types of legumes, such as lentils.

3.6. Reactive Oxygen Species

The intracellular accumulation of ROS in HepG2 cells exposed to T-2 toxin was analyzed using the dichlorofluorescein assay (DCFH-DA). The cells were exposed to T-2 (7.5, 15, and 30 nM) and 1:8 diluted red bean extract for different exposure times (0, 5, 15, 30, 45, 60, 90, and 120 min), and the results are expressed as an increase in fluorescence (%) with respect to the control (Figure 4). The simultaneous exposure to T-2 at the lowest concentration tested (7.5 nM) and the red bean extract showed a significant reduction ($p \leq 0.05$) in ROS production after 120 min of exposure with respect to control cells (Figure 4A); whereas there were no significant differences in ROS production at 15 nM with respect to control cells (Figure 4B). On the contrary, a significant increase ($p \leq 0.05$) in ROS production with respect to controls was observed in the case of the simultaneous exposure to T-2 at 30 nM alone and in combination with the red bean extract at 60 min of exposure (Figure 4C).

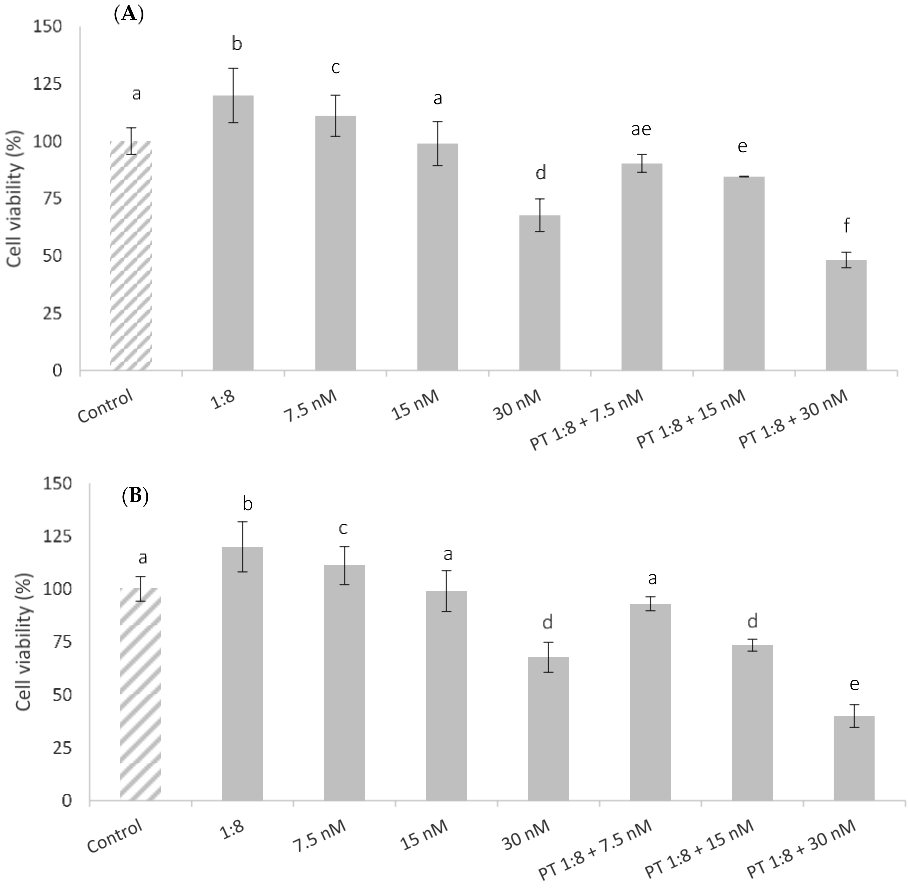

Figure 3. HepG2 cell viability (%) of pretreated cells (PT) with 1:8 red bean extract for 1 h (A) and 24 h (B) and afterward exposed to T-2 (7.5, 15, and 30 nM) during 24 h. All values are expressed as mean ± SEM of 3 replicates. Values in the same figure with different superscript letters are significantly different ($p \leq 0.05$).

Data reported by Lee et al. [35] demonstrated that the treatment of HepG2 cells with extracts obtained from different types of beans (black, red, and green) against the Tert Butyl Hydroperoxide (TBHP) agent significantly decreased the production of ROS. On the other hand, Yang et al. [3] showed that the level of

intracellular ROS production in HCT116 cells decreased significantly in cells treated with phenolic extracts of beans compared to untreated cells.

The abovementioned results can demonstrate the ability of phenolic extracts to modulate oxidative stress. However, further studies with regard to biological activity, including studies into the mechanisms of action and structure-activity relationships, are necessary to fully understand the modes of action of these bioactive compounds and to fully exploit their cytoprotective potential effect, as highlighted in the literature [36].

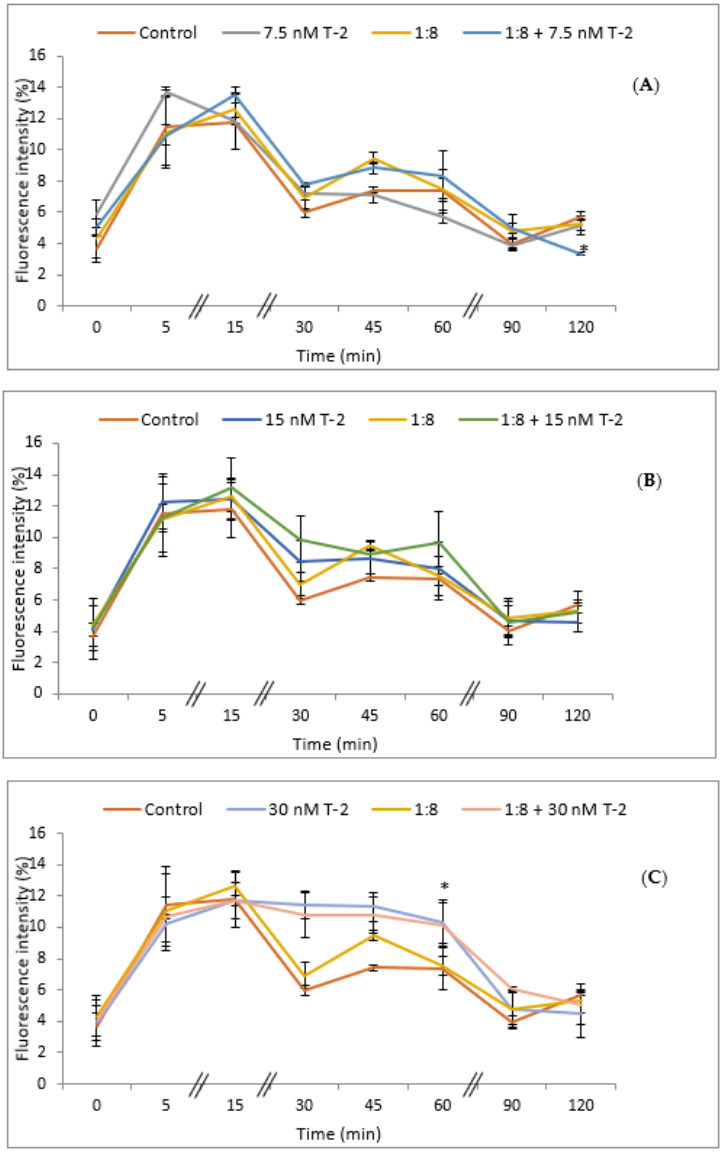

Figure 4. Intracellular ROS production in HepG2 cells exposed to: (A) 7.5 nM T-2; (B) 15 nM T-2; (C) 30 nM T-2; and 1:8 diluted red bean extract, alone or in combination, after 0, 5, 15, 30, 45, 60, 90, and 120 min. All values are expressed as mean ± SEM of 4 replicates. (*) $p \leq 0.05$ represents significant difference as compared to control values.

4. Conclusions

The chemical profile obtained from this study evidenced that red beans are a rich source of bioactive compounds such as flavanols and anthocyanidins, which confers antiradical activity and human health benefits. On the other hand, red bean extract (diluted 1:8) showed a significant increase in HepG2 cell proliferation after 24 h of exposure. Similar results were observed after HepG2 cell exposure to T-2 toxin at the lowest concentration assayed (7.5 nM) corresponding to its $IC_{50}/8$, which could indicate a probable adaptative response of HepG2 cells. However, higher T-2 concentrations showed cytotoxic effects and ROS production on HepG2 cells. The results from the simultaneous and pretreatment assays indicated that the 1:8 diluted red bean extract did not prevent T-2 cytotoxicity neither in simultaneous exposures nor with the pre-treatment. Finally, the combination of T-2 at 7.5 nM with the diluted red bean extract showed a decrease in ROS production compared to the control at the longest exposure time tested (120 min). The antioxidant activity or the possible T-2 hormetic effect observed in simultaneous treatment could be responsible for the latter result, suggesting that the red bean extract could modulate oxidative stress on HepG2 cells.

Supplementary Materials: The following supporting information can be downloaded at: www.mdpi.com/xxx/s1, Table S1: Total phenolic content (TPC) and antiradical activity (DPPH) of undiluted red bean extracts using different mixtures of MeOH:H_2O. Values are reported as mean ± SD of independent experiments performed in triplicate; Table S2. Polyphenols content in undiluted red bean extracts. Results are expressed as mean ± SD from three independent determinations.

Author Contributions: Conceptualization, Y.R.-C., M.-J.R. and A.R.; methodology, C.M.-A., M.T. and L.C.; software, M.T. and L.I.; validation, M.T., L.I. and Y.R.-C.; formal analysis, C.M.-A., M.T. L.C., L.I.; writing—original draft preparation, C.M.-A., L.I., Y.R.-C.; writing—review and editing, M.-J.R., A.R. and Y.R.-C.; supervision, A.R.

and M.-J.R.; project administration, M.-J.R.; funding acquisition, M.-J.R. All authors have read and agreed to the published version of the manuscript.

Funding: This research was funded by the Spanish Ministry of Science and Innovation Project (PID2020-115871RB-I00).

Institutional Review Board Statement: Not applicable

Informed Consent Statement: Not applicable

Data Availability Statement: The data presented in this study are available on request from the corresponding author. The data are not publicly available to preserve the privacy of the volunteers that participated in the present study.

Conflicts of Interest: The authors declare no conflict of interest.

5. References

1. Rahate, K.; Madhumita, M.; Prabhakar, P. Nutritional composition, anti-nutritional factors, pretreatments-cum-processing impact and food formulation potential of faba bean (Vicia faba L.): A comprehensive review. LWT-Food Sci. Technol. 2021, 138, 110796.
2. Angiolillo, L.; Del Nobile, M.A.; Conte, A. The extraction of bioactive compounds from food residues using microwaves. Curr. Opin. Food Sci. 2015, 5, 93–98.
3. Yang, Q.; Gan, R.; Ge, Y.; Zhang, D.; Corke, H. Polyphenols in Common Beans (Phaseolus vulgaris L.): Chemistry, Analysis, and Factors Affecting Composition. Compr. Rev. Food Sci. Food Saf. 2018, 17, 1518–1539.
4. Gan, R.; Deng, Z.; Yan, A.; Shah, N.; Lui, W.; Chan, C.; Corke, H. Pigmented edible bean coats as natural sources of polyphenols with antioxidant and antibacterial effects. LWT-Food Sci. Technol. 2016, 73, 168–177.
5. Kimothi, S.; Dhaliwal, Y. Nutritional and Health Promoting Attribute of Kidney Beans (Phaseolus vulgaris L.): A Review. Int. J. Curr. Microbiol. Appl. Sci. 2020, 9, 1201–1209.
6. Taroncher, M.; Vila-Donat, P.; Tolosa, J.; Ruiz, M.J.; Rodríguez-Carrasco, Y. Biological activity and toxicity of plant nutraceuticals: An overview. Curr. Opin. Food Sci. 2021, 42, 113–118.
7. Madhujith, T.; Naczk, M.; Shahidi, F. Antioxidant activity of common beans (Phaseolus vulgaris L.). J. Food Lipids 2004, 11, 220–233.
8. Khan, N.; Monagas, M.; Llorach, R.; Urpi-Sarda, M.; Rabassa, M.; Estruch, R.; Andrés-Lacueva, C. Targeted and metabolomic study of biomarkers of cocoa powder consumption effects on inflammatory biomarkers in patients at high risk of cardiovascular disease. Agro Food Ind. Hi Tech. 2010, 21, 51–54.
9. Terra, X.; Montagut, G.; Bustos, M.; Llopiz, N.; Ardèvol, A.; Bladé, C.; Fernández-Larrea, J.; Pujadas, G.; Salvadó, J.; Arola, L.; Blay, M. Grape-seed procyanidins

prevent low-grade inflammation by modulating cytokine expression in rats fed a high-fat diet. J. Nutr. Biochem. 2009, 20, 210–218.
10. Al-Hanbali, M.; Ali, D.; Bustami, M.; Abdel-Malek, S.; Al-Hanbali, R.; Alhussainy, T.; Qadan, F.; Matalka, K.Z. Epicatechin suppresses IL-6, IL-8 and enhances IL-10 production with NF-kappaB nuclear translocation in whole blood stimulated system. Neuro Endocrinol. Lett. 2009, 30, 131–138.
11. RASFF (Rapid Alert for Food and Feed). RASFF Annual Report 2020. Available online: https://ec.europa.eu/food/safety/rasff-food-and-feed-safety-alerts/reports-and-publications_es (accessed on 2 February 2022).
12. Narváez, A.; Castaldo, L.; Izzo, L.; Pallarés, N.; Rodríguez-Carrasco, Y.; Ritieni, A. Deoxynivalenol contamination in cere-al-based foodstuffs from Spain: Systematic review and meta-analysis approach for exposure assessment. Food Control 2021, 132, 108521.
13. EFSA (European Food Safety Authority). Scientific report on Human and animals dietary exposure to T-2 and HT-2 toxin. EFSA J. 2017, 15, 4972.
14. Dai, C.; Xiao, X.; Sun, F.; Zhang, Y.; Hoyer, D.; Shen, J.; Tang, S.; Velkov, T. T-2 toxin neurotoxicity: Role of oxidative stress and mitochondrial dysfunction. Arch. Toxicol. 2019, 93, 3041–3056.
15. You, L.; Zhao, Y.; Kuca, K.; Wang, X.; Oleksak, P.; Chrienova, Z.; Nepovimova, E.; Jaćević, V.; Wu, Q.; Wu, W. Hypoxia, oxidative stress, and immune evasion: A trinity of the trichothecenes T-2 toxin and deoxynivalenol (DON). Arch. Toxicol. 2021, 95, 1899–1915.
16. Taroncher, M.; Rodríguez-Carrasco, Y.; Ruiz, M. Interactions between T-2 toxin and its metabolites in HepG2 cells and in silico approach. Food Chem. Toxicol. 2021, 148, 111942.
17. Vila-Donat, P.; Fernández-Blanco, C.; Sagratini, G.; Font, G.; Ruiz, M.J. Effects of soyasaponin I and soyasaponins-rich extract on the alternariol-induced cytotoxicity on Caco-2 cells. Food Chem. Toxicol. 2015, 77, 44–49.
18. Izzo, L.; Rodríguez-Carrasco, Y.; Pacifico, S.; Castaldo, L.; Narváez, A.; Ritieni, A. Colon Bioaccessibility under *In Vitro* Gastrointestinal Digestion of a Red Cabbage Extract Chemically Profiled through UHPLC-Q-Orbitrap HRMS. Antioxidants 2020, 9, 955.
19. Castaldo, L.; Izzo, L.; Gaspari, A.; Lombardi, S.; Rodríguez-Carrasco, Y.; Narváez, A.; Grosso, M.; Ritieni, A. Chemical Composition of Green Pea (Pisum sativum L.) Pods Extracts and Their Potential Exploitation as Ingredients in Nutraceutical Formulations. Antioxidants 2022, 11, 105.
20. Taroncher, M.; Rodríguez-Carrasco, Y.; Ruiz, M. T-2 toxin and its metabolites: Characterization, cytotoxic mechanisms and adaptive cellular response in human hepatocarcinoma (HepG2) cells. Food Chem. Toxicol. 2021, 145, 111654.
21. Ruiz, M.J.; Festila, L.E.; Fernández, M. Comparison of basal cytotoxicity of seven carbamates in CHO-K1 cells. Toxicol. Environ. Chem. 2006, 88, 345–354.

22. Ruiz-Leal, M.; George, S. An *in vitro* procedure for evaluation of early stage oxidative stress in an established fish cell line applied to investigation of PHAH and pesticide toxicity. Mar. Environ. Res. 2004, 58, 631–635.
23. Soriano Sancho, R.; Pavan, V.; Pastore, G. Effect of *in vitro* digestion on bioactive compounds and antioxidant activity of common bean seed coats. Food Res. Int. 2015, 76, 74–78.
24. Ombra, M.N.; d'Acierno, A.; Nazzaro, F.; Riccardi, R.; Spigno, P.; Zaccardelli, M.; Pane, C.; Maione, M.; Fratanni, F. Phenolic Composition and Antioxidant and Antiproliferative Activities of the Extracts of Twelve Common Bean (Phaseolus vulgaris L.) Endemic Ecotypes of Southern Italy before and after Cooking. Oxid. Med. Cell. Longev. 2016, 12, 1398298.
25. Orak, H.H.; Karamać, M.; Amarowicz, R. Antioxidant activity of phenolic compounds of red bean (Phaseolus vulgaris L). Oxid. Commun. 2015, 38, 67–76.
26. Ross, K.; Beta, T.; Arntfield, S. A comparative study on the phenolic acids identified and quantified in dry beans using HPLC as affected by different extraction and hydrolysis methods. Food Chem. 2009, 113, 336–344.
27. Zhao, Y.; Du, S.; Wang, H.; Cai, M. *In vitro* antioxidant activity of extracts from common legumes. Food Chem. 2014, 152, 462–466.
28. Korus, J.; Gumul, D.; Folta, M.; Bartoń, H. Antioxidant and antiradical activity of raw and extruded common beans. Electron. J. Pol. Agric. Univ. 2007, 10, 6.
29. Doğan Cömert, E.; Ataç Mogol, B.; Gökmen, V. Relationship between color and antioxidant capacity of fruits and vegetables. Curr. Res. Food Sci. 2020, 2, 1–10.
30. García-Lafuente, A.; Guillamón, E.; Villares, A.; Rostagno, M.; Martínez, J.A. Flavonoids as anti-inflammatory agents: Implications in cancer and cardiovascular disease. Inflamm. Res. 2009, 58, 537–552.
31. García-Lafuente, A.; Moro, C.; Manchón, N.; Gonzalo-Ruiz, A.; Villares, A.; Guillamón, E.; Rostagno, M.; Mateo-Vivaracho, L. *In vitro* anti-inflammatory activity of phenolic rich extracts from white and red common beans. Food Chem. 2014, 161, 216–223.
32. Ziemlewska, A.; Zagórska-Dziok, M.; Nizioł-Łukaszewska, Z. Assessment of cytotoxicity and antioxidant properties of berry leaves as by-products with potential application in cosmetic and pharmaceutical products. Sci. Rep. 2021, 11, 3240.
33. Kössler, S.; Nofziger, C.; Jakab, M.; Dossena, S.; Paulmichl, M. Curcumin affects cell survival and cell volume regulation in human renal and intestinal cells. Toxicology 2012, 292, 123–135.
34. Vila-Donat, P.; Fernández-Blanco, C.; Sagratini, G.; Font, G.; Ruiz, M. Effects of soyasaponin I and soyasaponins-rich extract on the Alternariol-induced cytotoxicity on Caco-2 cells. Food Chem. Toxicol. 2015, 77, 44–49.
35. Lee, J.H.; Ham, H.; Kim, M.Y.; Ko, J.Y.; Sim, E.; Kim, H.; Lee, C.K.; Jeon, Y.H.; Jeong, H.S.; Woo, K.S. Phenolic compounds and antioxidant activity of adzuki bean cultivars. Legume Res. 2018, 41, 681–688.

36. Zhu, F.; Du, B.; Xu, B. Anti-inflammatory effects of phytochemicals from fruits, vegetables, and food legumes: A review. Crit Rev. Food Sci. Nutr. 2018, 58, 1260–1270.

SUPPLEMENTARY MATERIAL

Table S1. Total phenolic content (TPC) and antiradical activity (DPPH) of undiluted red bean extracts using different mixtures of MeOH:H_2O. Values are reported as mean ± SD of independent experiments performed in triplicate.

Mixture (v/v)	TPC (mg/mL undiluted extract)	DPPH (mmol TE/mL undiluted extract)
20:80	0.0171	7.6×10^{-4}
70:30	0.0169	8.1×10^{-4}
50:50	0.0179	8.4×10^{-4}
30:70	0.0310	1.37×10^{-3}
80:20	0.0252	1.17×10^{-3}

TPC: total phenolic content; GAE: gallic acid equivalents; DPPH: antiradical activity; TE: Trolox equivalents.

Table S2. Polyphenols content in undiluted red bean extracts. Results are expressed as mean ± SD from three independent determinations.

Compound	**Content (mg/mL undiluted extract)**
Apigenin 7-O-glucoside	<LOQ
Catechin	<LOQ
Chlorogenic acid	7.5×10^{-6}
Cyanidin	1.1×10^{-4}
Cyanidin 3-glucoside	<LOQ
Cyanidin 3,5-diglucoside	2.8×10^{-5}
Daidzein	<LOQ
Delphinidin	5.1×10^{-4}
Delphinidin 3,5-diglucoside	3.5×10^{-5}
Ellagic acid	7.5×10^{-6}
Epicatechin	5.4×10^{-4}
Genistin	<LOQ
Isoquercetrin	1.7×10^{-4}
kaempferol 3-O-glucoside	1.3×10^{-4}
Luteolin	3.5×10^{-6}
Naringenin	<LOQ
Naringin	<LOQ
p-coumaric acid	3.2×10^{-4}
Protocatechiuc acid	8.8×10^{-5}
Quercetin	4.9×10^{-5}
Rosmarinic acid	<LOQ
Rutin	7.9×10^{-5}

Toxicology Mechanisms and Methods, 33 (2022), 388-400

https://doi.org/10.1080/15376516.2022.2152514

3.6. Evaluation of cytotoxicity, analysis of metals and cumulative risk assessment in microalgae

Mercedes Taroncher [a], Yelko Rodríguez-Carrasco [a,*], Francisco J. Barba [a] and María-José Ruiz[a]

[a] Department of Preventive Medicine and Public Health, Food science, Toxicology and Forensic Medicine, Faculty of Pharmacy, University of Valencia, Valencia, Spain

Abstract

Microalgae are one promising source for the production of bioactive compounds. However, microalgae can accumulate harmful substances. So, our objectives were (i) to evaluate cell viability after *Phaeodactylum triconutum* (0% and 65% cell disruption, DR) and *Tetraselmis chuii* (0% and 67% DR) freeze-dried exposure in HepG2 cells by MTT assay; (ii) to evaluate cell viability after *P. triconutum* and *T. chuii* extract exposure; (iii) to assess the effect in cell viability when they were simultaneously exposed to T-2 toxin and, (iv) to evaluate if inflammatory response is related to the mechanism of toxicity of these microalgae by qPCR assays. Results demonstrated that cell viability did not increase after freeze-dried microalgae exposure in HepG2 cells. And, no IC_{50} values were observed. However, an increase in HepG2 cell viability after exposure of *T. chuii* 0% DR extract at 5, 25 and 100 μg/mL was observed. Additionally, 1:64 diluted *T. chuii* 0% DR with $IC_{50}/4$ T-2 and with $IC_{50}/2$ T-2 and 1:32 diluted *T. chuii* 0% DR with $IC_{50}/4$ T-2 showed an increase in cell viability. Both microalgae increased the relative TNF-α, IL-1β and IL-6 mRNA expression. Concluding, no cytotoxic effect was evidenced but, it was noted up-regulation of inflammatory genes after *T. chuii* exposure in HepG2 cell. Thus, more studies related the mechanistic toxicity of microalgae are needed to evaluate the potential toxicological risk of inflammation of these novel foods.

Key words: microalgae; T-2 toxin; HepG2 cells; cytotoxicity; inflammation

* **Corresponding author**: Department of Preventive Medicine and Public Health, Food science, Toxicology and Forensic Medicine, Faculty of Pharmacy, University of Valencia, Valencia, Spain. E-mail address: Yelko.rodriguez@uv.es

1. Introduction

There is a growing demand for renewable high value carbohydrates, proteins, lipids, polyphenols and pigments as an alternative for traditional agricultural crops. Microalgae are one of the most promising sources for producing these biomolecules (Postma et al. 2016) which can be used as supplementary food or feed (Postma et al. 2017). In this sense, the European Food Safety Authority (EFSA) and the Spanish Agency for Consumer Affairs, Food Safety and Nutrition (AECOSAN) within the scope of Regulation (EC) No 258/1997 on novel foods and novel food ingredients have authorized to market dried microalgae *Tetraselmis chuii* in food supplements in the European Union. And the microalgae *Phaeodactylum tricornutum* and its derived oils, also considered a novel food, are permitted for consumption as food supplements by the general population in the European Union (EU). These microalgae consumption under the conditions proposed by the company reveals that no adverse effects on human health are produced (AECOSAN 2017). For instance, natural carotenoids are more easily absorbed by animals than those obtained via chemical, that is because there is an increase demand for carotenoids obtained from natural sources such as microalgae (Martínez et al. 2018). Such products are normally located intracellular, in the cytoplasm, in internal organelles or bound to cell membranes, so the cells need to be disintegrated before extraction. Thus, the evaluation of the cell disruption (DR) yield is therefore of great importance.

The bead milling is a mechanical DR method less expensive whose ability to extract valuable compounds from microalgae, including lipids, carbohydrates and proteins has been widely demonstrated (Safi et al. 2017; Postma et al. 2017; Alavijeh et al. 2020). Bead milling has been applied in the chemical industry for

the release of intracellular products of yeast (Imatoukene et al. 2020), cyanobacteria (Geada et al. 2019) and microalgae (Safi et al. 2017).

Phaeodactylum triconutum is a marine pennate diatom, unicellular brown microalga, which belongs to family *Phaeodactylaceae*. Its cells can undergo morphological transitions stimulated by environmental conditions between fusiform, triradiate and oval morphotypes. *P. triconutum* is rich in polyunsaturated fatty acids (PUFAs) and carotenoid fucoxanthin, which is a pigment with several biological activities (Gilbert-López et al. 2017). *Tetraselmis chuii* is a green marine unicellular microalga which belongs to family *Chlorodendraceae*. *T. chuii* is extensively used in aquaculture which presents high content of lipids such as PUFAs, vitamin E, carotenoids, chlorophylls and antimicrobial activity (Pérez-López et al. 2014).

On the other hand, microalgae constitute the first level of aquatic trophic chains. Because of their short generation times, microalgae can accumulate potentially harmful substances, and any effect on them will affect to higher trophic levels, ultimately humans. Potential hazards may include a range of contaminants, like metals, cyanotoxins, mycotoxins, pesticide residues, as well as pathogens. High industrial activity and transport have contributed to the wide distribution of metals in the aquatic environment. Thus, co-occurrence of metals in aquatic plants due to aquatic pollution and bioaccumulation has been observed. Therefore, metals find their way into the food chain and pose serious health problems for consumers (Hui et al., 2021).

Mycotoxins are an important class of contaminants of emerging concern which growing in warm and humid environments, chemically stable and persist also in aquatic environments, potentially reflecting the influence of fungicide resistance and climatic factors on fungal diseases in agricultural crops (Eagles et

al. 2019). Much researchers have explored the use of natural resources, such as microalgae, to prevent or mitigate the consequences of fungal contamination and consequently, the mycotoxins release. The T-2 toxin (T-2) is a mycotoxin produced by fungi of the *Fusarium* genus, specifically it belongs to group A of trichothecenes and it is the most toxic of this group. In this sense, effective methods for assessing cytotoxic effect of accumulating contaminants on microalgae is required in food safety to protect the consumers. *In vitro* cytotoxicity of microalgae has been extensively studied. A wide variety of assays, from cell proliferation (Abolhasani et al. 2018; Parra-Riofrío et al. 2020) to inflammatory response (Sasaki et al. 2019; Neumann et al. 2019) has been evaluated. High concentration of tumor necrosis factor alpha (TNF-α) is usually associated with cell death, cardiovascular disseases, inflammation and other health problems (Gerosa-Neto et al. 2016). The TNF-α stimulates production of reactive oxygen species (ROS) in cellular lines, and ROS can act as signalling molecules that facilitate activation of nuclear factor-ϰB (NF-ϰB). Since NF-ϰB plays an ubiquitous role in the pathogenesis of inflammatory gene expression, the cytokine is a current target for the treatment of various diseases. So, NF-ϰB is an important transcription factor to regulate pro-inflammatory mediators such as TNF-α and interleukin-6 (IL-6) (Kim and Kim 2014). Also, IL-1β and IL-6, are closely related to oxidative stress *in vitro* (Kamiya and Kim 2021; Baker et al. 2021). However, there are few reports about the biological molecular mechanisms through they exert their cytotoxicity.

In view of this, and taking into account the increasing use of microalgae as novel food in the agricultural food industry, this work assesses toxic effects after microalgae exposure by an *in vitro* toxicity method using HepG2 cells. The aims of this study were: i) to evaluate the cell viability after the exposure of *P.*

triconutum (0% and 65% DR) and *T. chuii* (0% and 67% DR) freeze-dried microalgae (from 1 to 1/32 dilutions) in HepG2 cells by the MTT assay; (ii) to evaluate the cell viability after *P. triconutum* (at increasing concentrations from 0.1 to 100 mg/ml) and *T. chuii* (from 2 to 400 mg/ml) extracts exposure in HepG2 cells by the MTT assay; (iii) to assess the effect in cell viability of microalgae extracts when they were simultaneously exposed to T-2 at 7.5, 15 and 30 nM in HepG2 cells by MTT assay and, (iv) to evaluate if inflammatory response in HepG2 cells is related to the microalgae's mechanism of toxicity.

2. Material and methods

2.1. Reagents

The reagent grade chemicals and cell culture compounds used, namely Dulbecco's Modified Eagle's Medium (DMEM), penicillin, streptomycin, trypsin/EDTA solutions, Phosphate Buffered Saline (PBS), NewBorn Calf Serum (NBCS), methylthiazoltetrazolium salt (MTT) dye and DiMethyl SulfOxide (DMSO) were acquired from Sigma-Aldrich (St. Louis, MO, USA). Methanol (MeOH) was purchased from Merck Life Science S.L. (Madrid, Spain). Deionized water (resistivity <18 MΩ cm) was obtained using a Milli-Q water purification system (Millipore, Bedford, MA, USA). Standard of T-2 toxin (MW: 466.52 g/mol) was purchased from Sigma-Aldrich (St. Louis, MO, USA). Stock solution of the mycotoxin was prepared in MeOH at appropriate working concentrations and maintained in darkness at -20 ºC. Freeze-dried of *P. triconutum* and *T. chuii* were gently provided by NOFIMA (Norway).

2.2. Cell culture and treatment

Human hepatocarcinoma (HepG2) cells (ATCC: HB-8065) were cultured in DMEM medium supplemented with 10% NBCS, 100 U/mL penicillin and 100 mg/mL streptomycin. The incubation conditions were pH 7.4, 5% CO_2 at 37 °C and 95% air atmosphere at constant humidity. The medium was changed every 2-3 days.

2.3. Disruption percentage selection

Although there are many studies evaluating microalgae bioactivities, there is limited information comparing the effects of microalgae on different percentages of DR. So, in order to bring new insights into the different effects according to their percentage of DR, different disruption percentage were applied to know the most effective. The cell membrane of microalgae was disrupted by bead milling in previous studies developed in our laboratory. The percentages of disruption of each microalga were selected considering those that produced highest liberation of antioxidant compounds. The highest analyzed total antioxidant capacity (TAC) was detected in the samples with 65% and 67% DR for *P. triconutum* and *T. chuii*, respectively (data no shown). So, the percentages of DR selected were 0% and 65% DR for *P. triconutum* and 0% and 67% DR for *T. chuii*, in order to compare the different effects in cell viability of HepG2 cells between the percentage of disruption that releases the most antioxidant compounds and that which releases the least (0% DR).

2.4. Preparation of ethanolic extract from *P. triconutum* and *T. chuii*

Extraction was performed according to Sansone et al. (2017) with slight modifications. In order to avoid oxidation of the samples, extraction procedure

was conducted in darkness, at room temperature under nitrogen atmosphere. Briefly: freeze-dried microalgae (1 g) of *P. triconutum* 0% DR*, P. triconutum* 65% DR, *T. chuii* 0% DR and *T. chuii* 67% DR was extracted twice with 10 mL of ethanol. The mixture was subjected to stir bar agitation at room temperature for 30 min, and then centrifuged at 4000 × g for 10 min, at 20 °C. The upper ethanolic phases were combined and concentrated in a rotary evaporator (Büchi Rotavapor R-200, Postfach, Switzerland). Dry extract was stored under nitrogen atmosphere at -20 °C prior to the analysis. For the *in vitro* cytotoxicity assays, dry extracts were resuspended in DMSO.

2.5. *In vitro* cytotoxicity assay

Cytotoxic effects of samples were determined in HepG2 cells by the MTT assay. The MTT assay determines the viability of cells by the reduction of soluble yellow tetrazolium salt, only in the metabolically active cells, via a mitochondrial-dependent reaction to an insoluble purple formazan crystal. The MTT viability assay was performed according to Ruiz et al. (Ruiz et al., 2006). Briefly, the HepG2 cells were plated in 96-well culture plates at a density of 2×10^4 cells/well. After the cells reached 80% confluence, different assays were carried out. Assay A: the culture medium was replaced with fresh medium containing serial dilutions of each freeze-dried microalga (*P. triconutum* 0% DR, *P. triconutum* 65% DR, *T. chuii* 0% DR or *T. chuii* 67% DR). The amount of 5 mg of freeze-dried microalgae was resuspended in 5 mL of fresh medium and filtered. Then, 1:2 dilutions were carried out using fresh medium to obtain 1, 1:2, 1:4, 1:8, 1:16 and 1:32 dilutions. Assay B: HepG2 cells were exposed to 2, 5, 10, 25, 50, 100, 200 and 400 μg/mL of *T. chuii* extract and 0.1, 1, 10, 50 and 100 μg/mL of *P. triconutum* extract during 24 h. Microalgae extracts were diluted in complete cell

medium. Assay C: cytotoxic effect of T-2 was also evaluated in HepG2 cells after confluence by MTT assay. In this assay, HepG2 cells were exposed to T-2 (7.5, 15 and 30 nM) for 24 h, which are the $IC_{50}/8$, $IC_{50}/4$ and $IC_{50}/2$ of T-2. The IC_{50} value was previously determined in our laboratory (Taroncher et al., 2020). In all assays (A, B and C), after 24 h of exposure, the medium was removed and 200 µL of fresh medium were added to each well. Then, 50 µL of MTT were added per well, and the plates were returned to the incubator in the dark at 37 °C, 5% CO_2 during 3 h. Then, the MTT solution was removed and 200 µL of DMSO were added followed by 25 µL of Sorensen's glycine buffer. Absorbance was measured at 540 nm using an automatic ELISA plate reader (MultiSkanEX, Thermo Scientific, MA, USA). Cell viability was expressed as a percentage relative to the control solvent (≤1% DMSO). Assays were performed in three independent experiments and in quadruplicate per concentration. The results were expressed as the mean ± standard error of the mean (SEM) of different independent experiments.

2.6. Effect in cell viability of microalgae exposed simultaneously with T-2

The effect of microalgae against T-2 effect on HepG2 cells was evaluated by MTT assay. Two assays were performed after cell confluence. Assay A: simultaneous treatment with freeze-dried microalgae and T-2. In this assay, after confluence the culture medium was removed and HepG2 cells were simultaneously exposed to fresh medium containing dilutions (1:64 and 1:32) of freeze-dried of *P. triconutum* (0% and 65% DR), *T. chuii* (0% and 67% DR) and T-2 at $IC_{50}/2$ (30 nM), $IC_{50}/4$ (15 nM) and $IC_{50}/8$ (7.5 nM) concentrations for 24 h. Assay B: simultaneous treatment with extracts of microalgae and T-2. After

cell confluence, the culture medium was removed and HepG2 cells were simultaneously exposed to extracts of *P. triconutum* (0% and 65% DR) at 0.1, 1, 10, 50 and 100 μg/mL, *T. chuii* (0% and 67% DR) at 2, 5, 10, 25, 50, 100, 200 and 400 μg/mL and 7.5 nM T-2 for 24 h.

In the assay A, the results obtained were compared with cells exposed to T-2 (7.5, 15 and 30 nM) and 1:64 and 1:32 of *P. triconutum* (0% and 65% DR) freeze-dried microalgae and *T. chuii* (0% and 67% DR) freeze-dried microalgae, individually. The high dilutions were selected because they present the highest cell viability values (Fig. 1). The concentrations 7.5, 15 and 30 nM T-2 were chosen to test microalgae response when they were exposed at a T-2 concentration range in which from non-toxic to toxic effect is observed.

In assay B, the results obtained were compared with cells exposed to 7.5 nM T-2 and 0.1, 1, 10, 50 and 100 μg/mL extracts of *P. triconutum* (0% and 65% DR) and 2, 5, 10, 25, 50, 100, 200 and 400 μg/mL *T. chuii* (0% and 67% DR). The concentration of 7.5 nM T-2 was chosen because it showed a cytoprotective effect in HepG2 cells in previous studies carried out in our laboratory (Martínez-Alonso et al. 2022). Three independent experiments were carried out with four replicates each, and the results were expressed as the mean ± standard error of the mean (SEM) of different independent experiments.

2.7. RNA extraction and quantification

The total RNA of cells was isolated using ReliaPrep™ RNA Cell Miniprep System kit and treated with RNase free DNase (Promega) to remove genomic DNA contamination, according to the manufacturer's instructions. The extracted RNA of each sample was firstly checked for quantity and quality using Nanodrop 2000 (Thermo Scientific), showing concentrations between 339.8 and

113.4 ng/µL and appropriate 260/280 and 260/230 ratios both ≥ 2. The RNA samples were stored at -20 ºC and after that, the samples were diluted to 100 ng/µL with pure Milli-Q H_2O until their reverse transcription to complementary DNA (cDNA).

2.8. Reverse transcription and qPCR reaction

First, synthesis of cDNA was carried out using 5 µL of total RNA (500 ng) according to the instructions of TaqMan™ MicroRNA Reverse Transcription Kit protocol (Thermo Fisher Scientific, Madrid, Spain). The qPCR was performed for all primer pairs and a single amplification product was obtained for each gene by the melting curve assay. Primer pairs for each gene were designed based on the entire coding region of the candidate genes using Primer-BLAST (Ye et al., 2012), according to the following parameters: primer length of about 20 bases, GC content of 45–60 %, melting temperature (Tm value) between 58 and 60 ºC, and amplicon product size ranging from 50 to 150 base pair. Primer amplification efficiency was determined from standard curve generated by cDNA serial dilution (serial dilution factor = 2) for each gene in triplicate. The gene-specific primers used in the present study are listed in Table 1. Real-time amplification reactions were performed in 96 well plates using SYBR Green detection reactive and run with the StepOne Plus Real-time PCR instrument (Applied Biosystems). Reactions were prepared in a total volume of 10 µL containing: 3 µL of 1:2 diluted templates, 2 µL of amplification primer mix (forward/reverse of each gene; 2.5 µM) and 5 µL of SYBR Green (Applied Biosystems). Non-template controls (NTC) were also included for each primer pair, replacing the template by DNAse and RNAse free water. The cycling conditions were set as default: initial denaturation step of 95 ºC for 5 min to

activate the Taq DNA polymerase, followed by 40 cycles of denaturation at 95 ºC for 15 s, annealing temperatures ranging from 58 to 60 ºC (depending on the primers) for 15 s and elongation at 72 ºC for 45 s. The melting curve was generated by heating the amplicon from 60 to 90 ºC. Baseline, threshold cycles (Ct) and primer parameters analysis were automatically determined using the StepOne Plus Software version 2.3 (Applied Biosystems).

Table 1. Gene-specific primers for qPCR assays

Gene symbol	**Gene name**	**Optimum T^a (ºC)**	**Forward primer/ Revers primer**
IL-1β	Interleukin-1 β	60	GGAGAATGACCTGAGCACCT/ GGAGGTGGAGAGCTTTCAGT
IL-6	Interleukin-6	60	AGTCCTGATCCAGTTCCTGC/ CTACATTTGCCGAAGAGCCC
TNF-α	Tumor Necrosis Factor-α	58	CCGACTATCTCGACTTTGCC/ ACAGGGCAATGATCCCAAAG

2.9. Inflammatory activity assay

In order to know if cytotoxic effect is mediated by inflammatory activity, the evaluation of inflammatory genes expression was carried out. HepG2 cells were seeded at a density of 47.2×10^4 cells/well in a 6 well plate. Once cells reached 80% confluence, the culture medium was removed and replaced with fresh medium containing 0.1, 10 and 50 μg/mL of extract of *P. triconutum* 0% DR and 5, 25 and 100 μg/ml of ethanolic extract of *T. chuii* 0% DR during 24 h. The

selection of the concentrations of the extracts assayed is correlated with those which showed significant changes in cell viability assays. The relative IL-1β, IL-6 and TNF-α mRNA expression was measured in HepG2 cells according to the manufacturer´s instructions and according to 2.8 section. Assays were performed in three independent experiments and in triplicate per concentration. The results were expressed as the mean ± SEM of different independent experiments.

2.10. Analysis of metals in microalgae

The presence and content of As, Hg, Cd, and Pb in freeze-dried microalgae was evaluated. A microwave accelerated reaction system (MARS, CEM, Vertex, Spain) was used for the acid mineralization of samples. Briefly, 10 mg of sample were placed in a Teflon vessel. Then, 500 μL of HNO_3 (69% v/v) were added to the samples and the digestion was carried out in the microwave system at 800 W and 180 °C for 15 min. After cooling and eliminating the nitrogen vapors, the digested samples were filtered through Whatman No. 1 filter paper and brought up to 5 mL with distilled water. Then, an inductively coupled plasma spectrometer mass detector (ICP MS, Agilent model 7900) was employed to identify and quantify the metals. The operating conditions were as follows: Ar plasma gas flow (15.0 L/min), carrier gas (1.0 L/min), reaction gas (He), nebulizer pump speed (0.30 rps), RF power (1550 W), and RF matching (1.80 V). Internal standard solutions of 72Ge, 103Rh, and 193Ir (ISC Science) at 20 μg/g were used to correct signal fluctuations and instrumental drift.

A standard calibration curve with concentrations ranging from 0-1000 μg/L was used for the quantification of As, Cd, and Pb and while a standard calibration curve between 0 and 100 μg/L was used for Hg. Distilled water was

used as a blank and the metal concentrations in the digested blank were subtracted from the sample values. The results were expressed as μg of each element/Kg of microalgae in wet weight.

2.11. Risk assessment evaluation

In order to calculate inorganic As (iAs) data and methyl Hg (MeHg) or inorganic Hg (iHg) from the total Hg data, conversion factors were applied. The conversion factor for total As to iAs ranges from 2% to 4%, according to a Joint FAO/WHO Expert Committee on Food Additives (JECFA) report (EFSA, 2014). In this study, a conversion factor of 4% was selected to be conservative. On the other hand, it was assumed that MeHg accounted for 100% of the total Hg in order to quantify the exposure to MeHg. Otherwise, to assess iHg nephrotoxicity, a cautiously 30% threshold was selected (EFSA, 2015).

The single metal exposure assessment was calculated through a semi-probabilistic method by taking into consideration the minimum (lower-bound) and maximum (upper-bound) metal content in microalgae. Those values were multiplied by the average aquatic plants mean consumption and divided by the body weight (bw). Since the consumption of microalgae in Spain is not established, the latest consumption data of aquatic plants in China reported by FAO, which is 12.26 Kg/capita/year, was considered (FAO, 2019). And, 70 Kg bw was assumed as a default value for risk assessment studies as established by EFSA (2012) (EFSA, 2012).

The cumulative exposures of iAs, Cd, Hg, and Pb in microalgae were estimated throughout the relative potency factors (RPF) model. The exposure to each of the four metals was calibrated using RPF based on one indicator chemical:

$$Exp_{cum} = \sum_{i=1}^{n} Exp_i \ x \ RPF_i$$

Where Exp_{cum} (μg/Kg bw per day) indicates cumulative exposure of Pb, Cd, Hg, and iAs; Exp_i (μg/Kg bw per day) denotes the exposure of one of the four metals; and RPF_i is the relative potency factor of the corresponding metal. The RPFs were determined by comparing the No Observed Adverse Effect Level (NOAEL) or lower confidence limit of Benchmark dose (BMDL) on the neurotoxicity or nephrotoxicity of a specific metal to that of an index metal. The RPF were calculated by directly comparing the derived BMDL where human data were available. The NOAEL or BMDL obtained from data from animal experiments were used in the absence of human values. The animal-to-human conversion was carried out using an uncertainty factor of 100 (Suomi et al. 2017). Pb was selected as indicator chemical for neurotoxicity because its toxicological data were obtained from a population epidemiological data and due to Pb had the highest potential for neurotoxicity of the four metals (Dongre, 2020). The dose-response values of the other three metals were used to determine the RPFs for each one, with Pb having a RPF of 1 (Table 2).

The RPF values for nephrotoxicity were obtained using the same principle. The RPFs were determined in accordance with their respective toxic potentials, with Cd, which had the highest potential for nephrotoxicity, as the indicator chemical (Table 3).

Table 2. Relative potency factor (RPF) values of studied metals for neurotoxicity.

Metal	Toxicological parameter (µg/Kg bw per day)	RPF
iAs	NOAEL, human = 30	0.020
Cd	NOAEL, rats = 2	0.250
MeHg	$BMDL_{05}$, human = 1.2	0.420
Pb	$BMDL_{01}$, human = 0.5	1

BMDL: Benchmark dose limit; bw: body weight; iAS: inorganic arsenic; MeHg: methyl mercury; NOAEL: no observed adverse effect level; RPF: relative potency factor.

Table 3. Relative potency factor (RPF) values of studied metals for nephrotoxicity.

Metal	Toxicological parameter (µg/Kg bw per day)	RPF
iAs	$BMDL_{10}$, human = 50	0.008
Cd	$BMDL_{10}$, human = 0.41	1
iHg	NOAEL, rat = 6	0.068
Pb	$BMDL_{10}$, human = 0.63	0.646

BMDL: Benchmark dose limit; bw: body weight; iAS: inorganic arsenic; iHg: inorganic mercury; NOAEL: no observed adverse effect level; RPF: relative potency factor.

2.12. Statistical analysis

The statistical analysis of the data was carried out using the Statgraphics version 16.01.03 statistical package (IBM Corp., Armonk, NY, USA). The statistical analysis of the results was performed using the student t-test for paired samples. Differences between groups were analyzed using the one-way analysis

of variance (ANOVA), followed by a Tukey HDS *post-hoc* test for multiple comparisons. Differences were considered significant from $p \leq 0.05$.

3. Results

3.1. Cytotoxic effect of freeze-dried microalgae

The cytotoxic effect of *P. triconutum* 0% DR, *P. triconutum* 65% DR, *T. chuii* 0% DR and *T. chuii* 67% DR freeze-dried microalgae in HepG2 cells were evaluated by MTT assay after 24 h. The range of diluted freeze-dried microalgae were: 1, 1:2, 1:4, 1:8, 1:16 and 1:32. After 24 h of treatment, all freeze-dried microalgae significantly decreased HepG2 cell viability (Fig. 1). Undiluted *P. triconutum* 0% DR decreased 14.2% cell viability respect to control whereas freeze-dried of *P. triconutum* 65% DR (from 1:16 to 1) decreased cell viability from 14.5% to 42.8% (Figs. 1A and 1B). Similarly, *T. chuii* 0% DR (from 1:8 to 1) decreased cell viability from 15.4% to 24.5%, and 1:4 diluted and undiluted *T. chuii* 67% DR freeze-dried microalgae decreased cell viability approximately 20% respect to control (Figs. 1C and 1D). So, the higher decrease in cell viability was observed with undiluted *P. triconutum* 65% DR. On the other hand, none of the freeze-dried microalgae tested increased the mitochondrial function of HepG2 cells. So, freeze-dried microalgae not provide cytoprotection to HepG2 cells.

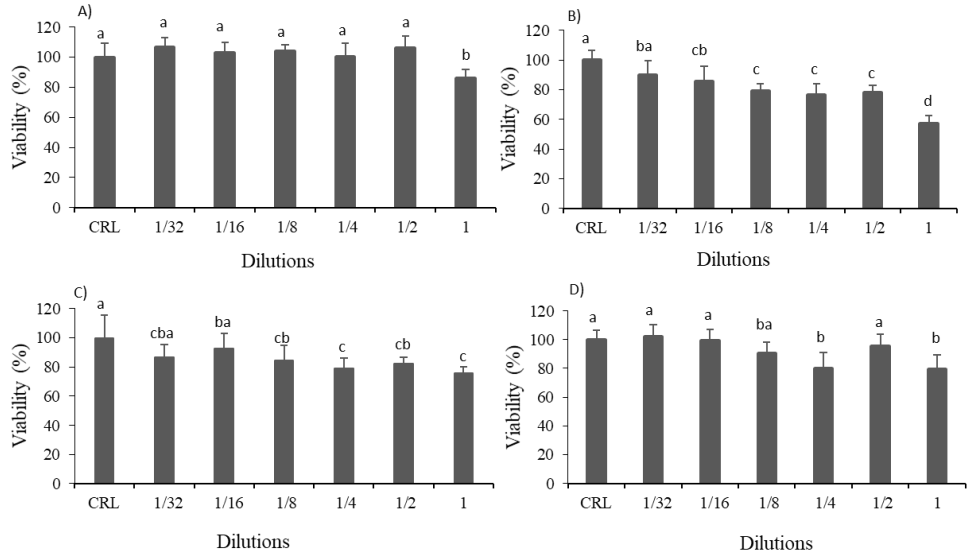

Figure 1. Effect of freeze-dried of *P. triconutum* 0% DR (A); *P. triconutum* 65% DR (B); *T. chuii* 0% DR (C) and *T. chuii* 67% DR (D) in HepG2 cell viability (MTT assay) after 24 h of exposure at increasing dilutions (from 1 to 1/32). Values are expressed as mean ± SEM (n = 3). Values in the same figure with different superscript letter are significantly different ($p \leq 0.05$). CRL: control.

3.2. Cytotoxic effect of microalgae extracts

After the exposure of *P. triconutum* (0% and 65% DR) and *T. chuii* (0% and 67% DR) extracts on HepG2 cells, the potential cytotoxic effect was evaluated (Figure 2). The *P. triconutum* 0% DR decreased cell viability 23.1% and 14.9% at 50 and 100 μg/mL, respectively, respect to control (Fig. 2A). Furthermore, *T. chuii* 0% DR increased cell viability 12.7%, 12.8% and 14.9% at 5, 25 and 100 μg/mL, respectively, respect to control (Fig. 2C). So, *T. chuii* 0% DR extract provide an increase in viability of HepG2 cells. Nevertheless, no significant effects on cell viability were observed after *P. triconutum* 65% DR (Fig. 2B) and *T. chuii* 67% DR (Fig. 2D) extracts exposure in HepG2 cells.

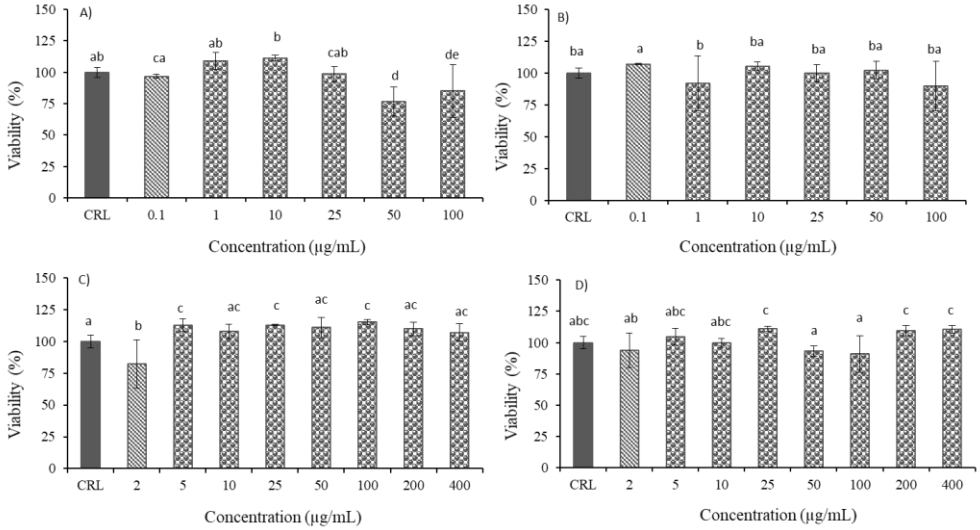

Figure 2. Effect of extracts of *P. triconutum* 0% DR (A); *P. triconutum* 65% DR (B); *T. chuii* 0% DR (C) and *T. chuii* 67% DR (D) in HepG2 cell viability by MTT assay after 24 h of exposure at increasing concentrations of *P. triconutum* (from 0.1 to 100 µg/mL) and *T. chuii* (from 0 to 400 mg/mL). Values are expressed as mean ± SEM (n = 3). Values in the same figure with different superscript letter are significantly different ($p \leq 0.05$). CRL: control.

3.3. Effect in cell viability of simultaneous exposure of freeze-dried microalgae and T-2 toxin

Figure 3 shows that $IC_{50}/4$ T-2 and $IC_{50}/8$ T-2 not affected HepG2 cell viability. However, the $IC_{50}/2$ T-2 decreased 30.45% HepG2 cell viability respect to control. Moreover, the results in Figure 3 shows the effect in HepG2 cells simultaneously exposed to diluted (1:64 and 1:32) freeze-dried microalgae and T-2 ($IC_{50}/2$ T-2, $IC_{50}/4$ T-2 and $IC_{50}/8$ T-2) in order to determine the freeze-dried microalgae protection against T-2 mycotoxin in HepG2 cells when both of them are exposed simultaneously.

Figure 3 clearly demonstrated that almost all freeze-dried microalgae simultaneous exposed to T-2 decreased HepG2 cell viability. In particular, in Fig. 3A is shown that *P. triconutum* 0% DR (1:64) simultaneously exposed to IC_{50}/2 T-2 decreased (30,5%) cell viability, and the 1:32 diluted *P. triconutum* 0% DR simultaneously exposed to IC_{50}/2 T-2 and IC_{50}/4 T-2 decreased cell viability by 20.2% and 12.2%, respectively, compared to control. On the other hand, there were no significant differences between the different concentrations of T-2 simultaneously exposed to diluted *P. triconutum* 0% DR and T-2 tested alone. However, a significant decrease of cell viability (22.1%) was observed between IC_{50}/2 T-2 simultaneously exposed to 1:64 diluted *P. triconutum* 0% DR freeze-dried and *P. triconutum* (1:64) tested individually. And, between IC_{50}/4 T-2 (17.6%) and IC_{50}/2 T-2 (25.1%) simultaneously exposed to 1:32 diluted *P. triconutum* 0% DR compared to *P. triconutum* (1:32) tested individually. In Fig. 3B, after the exposure of *P. triconutum* 65% DR, a significant decrease in cell viability was observed after simultaneous exposure of *P. triconutum* (1:64 dilution) and IC_{50}/2 T-2 (23.6%) or IC_{50}/8 T-2 (18.8%) and, *P. triconutum* (1:32 dilution) and IC_{50}/2 T-2 (23.3%) compared to control. There was observed a decrease in cell viability at IC_{50}/2 T-2 (30.2%) and IC_{50}/8 T-2 (25.8%) simultaneously exposed to 1:64 diluted *P. triconutum* 65% DR compared to *P. triconutum* (1:64) individually. Moreover, a significant decrease in cell viability was observed between IC50/8 T-2 simultaneously exposed to *P. triconutum* diluted 1:64 (19.8%) compared to IC_{50}/8 T-2 tested individually. And, a significant decrease in cell viability was observed between IC_{50}/8 T-2 simultaneously exposed to *P. triconutum* diluted 1:32 (12.5%) compared to IC_{50}/8 T-2 tested individually. In Figure 3D, the reduction in cell viability was observed after simultaneous exposure of IC_{50}/2 T-2 and 1:64 dilution of *T. chuii* 67% DR (34.5%) or 1:32 dilution of *T. chuii* 67%

DR (58.1 %), compared to control. Moreover, a significant decrease of cell viability (30.1%) was observed between IC_{50}/2 T-2 simultaneously exposed to 1:64 diluted *T. chuii* 67% DR freeze-dried microalgae and *T. chuii* 67% DR (1:64) tested individually. Respect to 1:32 diluted *T. chuii* 67% DR simultaneously exposed with IC_{50}/2 T-2 cell viability significantly decreased compared to the IC_{50}/2 T-2 (39.7%) and to 1:32 dilution of *T. chuii* 67% DR (58.9%) tested individually. However, an increase in cell viability was observed after simultaneous exposure of IC_{50}/4 T-2 and 1:32 dilution of *T. chuii* 67% DR compared to IC_{50}/4 T-2 (20%) and the control (17.2%). On the other hand, as shown in Figure 3C, *T. chuii* 0% DR significantly increased cell viability. As it is shown in Fig. 3C, 1:64 diluted *T. chuii* 0% DR simultaneously exposed with IC_{50}/4 T-2 significantly increased the cell viability compared to the IC_{50}/4 T-2 (52.2%), 1:64 dilution of *T. chuii* (53.3%) and the control (48.6%), all of them tested individually. Respect to 1:64 diluted *T. chuii* 0% DR simultaneously exposed with IC_{50}/2 T-2 was observed an increase in cell viability compared to the IC_{50}/2 T-2 (81.6%), 1:64 dilution of *T. chuii* (30.3%) and the control (26.3%), all of them tested individually. Similarly, 1:32 diluted *T. chuii* 0% DR simultaneously exposed with IC_{50}/4 T-2 increased the cell viability compared to the IC_{50}/4 T-2 (35.8%), 1:32 dilution of *T. chuii* (52.6%), and the control (32.6%) all of them tested individually. Nevertheless, 1:32 diluted *T. chuii* 0% DR simultaneously exposed with IC_{50}/2 T-2 significantly decreased the cell viability (30.6%) compared to the control.

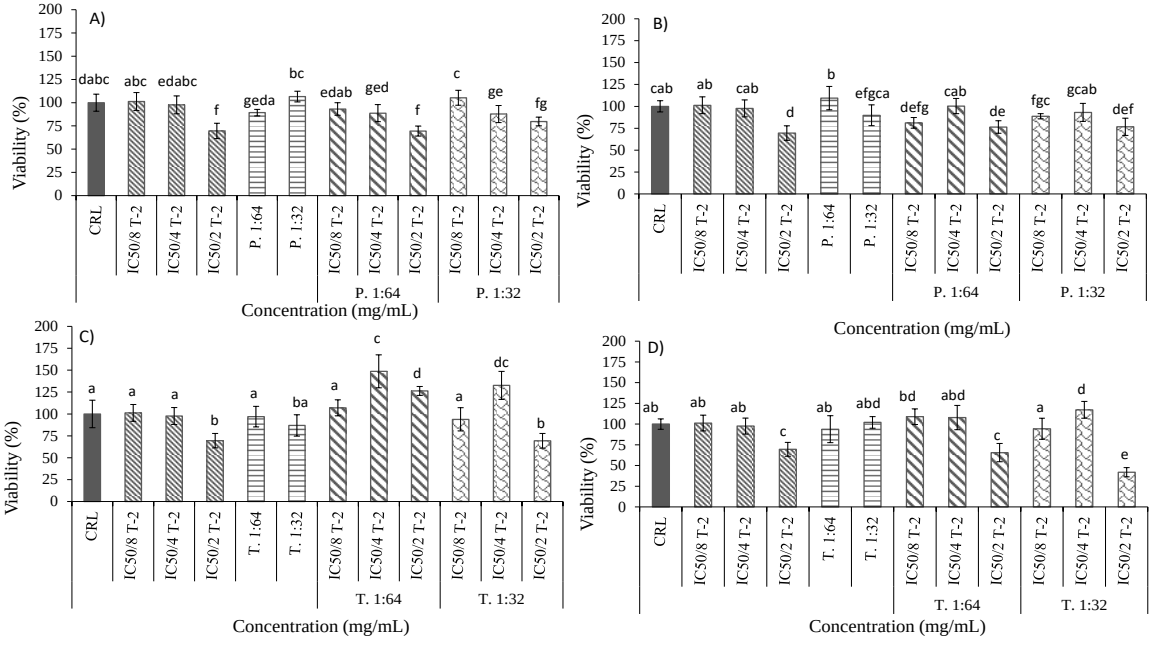

Figure 3. Cell viability (%) after 24 h of simultaneous exposure of 7.5 (IC50/8), 15 (IC50/4) and 30 (IC50/2) nM T-2 and diluted 1:32 and 1:64 freeze-dried of *P. triconutum* 0% DR (A); *P. triconutum* 65% DR (B); *T. chuii* 0% DR (C) and *T. chuii* 67% DR (D) alone and in combination by MTT assay. Values are expressed as mean ± SEM (n = 3). Values in the same figure with different superscript letter are significantly different ($p \leq 0.05$). CRL: control; P.: *P. triconutum*; T.: *T. chuii*; T-2: T-2 toxin.

3.4. Effect in cell viability of simultaneous exposure of microalgae extracts and T-2 toxin

In Fig. 4A, after 100 μg/mL *P. triconutum* 0% DR extract simultaneously exposed with 7.5 nM T-2 a decrease in cell viability was observed compared to control (18%) and T-2 (19%), both tested individually. No changes were observed after simultaneous exposure of 7.5 nM T-2 and *P. triconutum* 65% DR extract (Fig. 4B). However, 50 μg/mL *P. triconutum* 0% DR extract (Fig. 4A), 2 μg/mL *T. chuii* 0% DR extract (Fig. 4C) and 2 μg/mL *T. chuii* 67% DR extract (Fig. 4D) simultaneously exposed with T-2 significantly increased the cell viability compared their extracts tested individually by 31.2%, 26.5% and 18.26%, respectively. Differences between each microalgae extracts and their controls were described in 3.2 section.

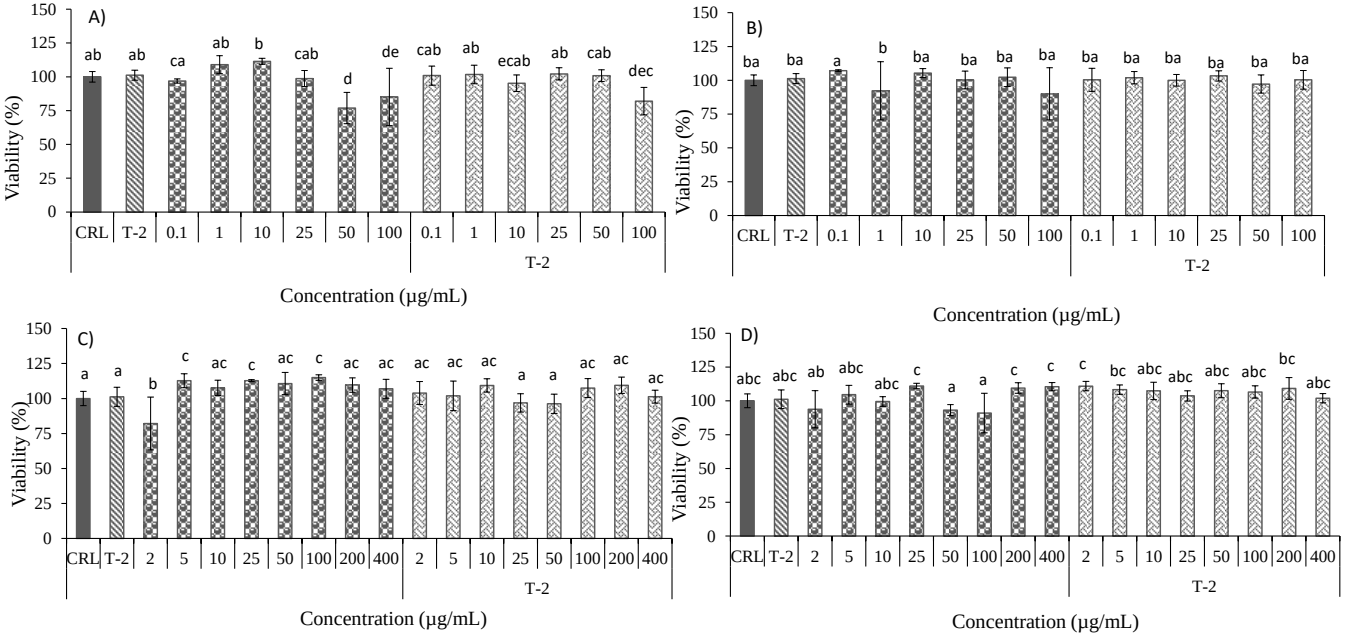

Figure 4. HepG2 cell viability (%) after 24 h of simultaneous exposure of 7.5 nM T-2 and *P. triconutum* 0% DR (A); *P. triconutum* 65% DR (B); *T. chuii* 0% DR (C); and *T. chuii* 67% DR (D) extracts by MTT assay. The concentrations increasing from 0 to 100 µg/mL for *P. triconutum* and from 0 to 400 µg/mL for *T. chuii*. Values are expressed as mean ± SEM (n = 3). Values in the same figure with different superscript letter are significantly different ($p \leq 0.05$). CRL: control; T-2: T-2 toxin.

3.5. Inflammatory response of *P. triconutum* and *T. chuii* extracts

To evaluate whether the cytotoxic effect of microalgae extracts was involved in the inflammatory response, the effect of *P. triconutum* 0% DR and *T. chuii* 0% DR extracts on the expression of the pro-inflammatory cytokines interleukin-1β (IL-1β), interleukin-6 (IL-6) and tumour necrosis factor-α (TNF-α) in HepG2 cells was evaluated. *P. triconutum* 0% DR and *T. chuii* 0% DR extracts were selected in this assay according to their different response in HepG2 cells. *T. chuii* 0% DR extracts was selected because it is the only one that produce an increase in viability of HepG2 cells and *P. triconutum* 0% DR as having similar % DR.

The analysis of the relative mRNA expression levels of inflammatory genes IL-1β, IL-6 and TNF-α in HepG2 cells exposed to 0.1, 10 and 50 μg/mL *P. triconutum* 0% DR and 5, 25 and 100 μg/mL *T. chuii* 0% DR extracts indicated that a proinflammatory effect was induced after 24 h of exposure (Fig. 5). The IL-1β mRNA was up-regulated by *P. triconutum* 0% DR extract at all concentrations tested, except at 10 μg/mL, compared to control. And, *T. chuii* 0% DR extract showed that IL-1β mRNA was up-regulated in a concentration-dependent manner (Fig 5A). The IL-6 mRNA was up-regulated by *P. triconutum* 0% DR and *T. chuii* 0% DR extracts at all concentrations tested except at 50 μg/mL *P. triconutum* 0% DR (Fig. 5B). Finally, an up-regulation of TNF-α mRNA was obtained after *P. triconutum* 0% DR extract except after the lower concentration tested (0.1 μg/mL) compared to control, whereas after *T. chuii* 0% DR extract exposure, the TNF-α mRNA was only up-regulated at the lowest concentration, 5 μg/mL *T. chuii* 0% DR extract.

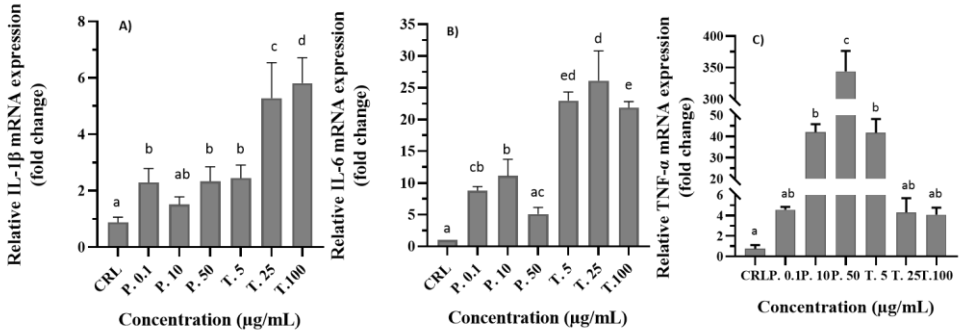

Figure 5. Effect of *P. triconutum* 0% DR and *T. chuii* 0% DR on IL-1β (A), IL-6 (B) and TNF-α (C) expression in HepG2 cells. Cells were treated with *P. triconutum* 0% DR (0.1, 10 and 50 µg/mL) and *T. chuii* 0% DR (5, 25 and 100 µg/mL) for 24 h. The relative mRNA expression levels were measured by real-time PCR. The average of the target gene values was normalized to the corresponding 18S rRNA value and expressed as fold change compared with the solvent control. Data are expressed as mean ± SEM of three independent experiments (n = 3) with 3 replicates each. Values in the same figure with different superscript letter are significantly different ($p \leq 0.05$). CRL: control, P.: *P. triconutum*, T.: *T. chuii*.

3.6. Content of metals in analyzed microalgae

The content of the metals found in analysed microalgae samples is reported in Table 4. All microalgae samples were contaminated with iAs and Pb at a mean content of 3.37 µg/Kg (range: 1.6 – 7.1 µg/Kg) and 692.4 µg/Kg (range: 43 – 2005 µg/Kg), respectively. In addition, contamination of Hg (MeHg average content = 889 µg/Kg; iHg average content = 2.6 µg/Kg) and Cd (average content = 9.9 µg/Kg) was also found in 25.0 % and 37.5% of microalgae samples, respectively. The single metal exposure (Exp_i) was calculated taken into consideration the here reported metal data, with the minimum and maximum

content being used as an assumption to calculate lower-bound (LB) and upper-bound (UP) scenarios of exposure (Table 4).

It has to be highlighted that co-contamination of several metals were detected in 100% of analysed samples. Up to 50% of samples showed co-contamination of two metals, and 37.5% of samples with three metals. And, As, Cd, Hg and Pb were detected in one sample. The significant co-contamination of samples indicated that joint effects need to be considered when conducting exposure assessment studies. A thorough evaluation of the potential health effects of concurrent exposure to various substances is known as cumulative risk assessment. Hence, taken into consideration the Exp_i and the RPF_i, the cumulative exposure (Exp_{cum}) for neurotoxicity and nephrotoxicity in both LB and UB scenarios was calculated and reported in Table 4.

The renal toxicity of Cd led to the establishment of a tolerable weekly intake (TWI) of 2.5 μg/Kg bw (EFSA, 2011). Therefore, the ratio of the estimated cumulative exposure to the TWI (divided by 7 to convert to daily value) of Cd was used to calculate the health risk of nephrotoxicity. The results showed that a 4.4% TWI was reached considering the LB exposure, while an UB exposure could pose a risk given that the ratio exceeded the 100%.

For neurotoxicity evaluation, the margin of exposure (MOE) method was used, by which the BMDL01 of Pb as an indicator chemical was divided by the estimated cumulative exposure of the four chemicals. The results showed that a MOE value of 22.1 was obtained considering the LB exposure. However, under an UB exposure scenarios the calculated risk should be of concern given that the MOE value was lower than 1.

Table 4. Cumulative exposure levels of iAs, Cd, MeHg, iHg and Pb in different microalgae for neurotoxicity and nephrotoxicity.

Metal	Range (μg/kg)	Exp_i (μg/kg bw per day)		Exp_{cum} for neurotoxicity (μg/kg bw per day)		Exp_{cum} for nephrotoxicity (μg/kg bw per day)	
		LB exposure	UB exposure	LB exposure	UB exposure	LB exposure	UB exposure
iAs	1.6–7.1	0.0008	0.0034	0.0227	0.9660	0.0158	0.6282
Cd	5–13.7	0.0024	0.0066				
MeHg	7–10.8	0.0034	0.0052				
iHg	1.5–3.2	0.0007	0.0015				
Pb	43–2005	0.0206	0.9621				

Exp_i: individual exposure; Exp_{cum}: cumulative exposure; iAs: inorganic arsenic; iHg: inorganic mercury; LB: lower-bound; MeHg: methyl mercury; UP: upper-bound.

However, although the MOE value indicates that metals are potential toxicological risk for consumers when they are chronically exposed to the contaminated food, due to the population consumes microalgae sporadically, the concentration of metals in these foods is not a potential concern for the consumer.

4. Discussion

Commercial production of microalgae biomass for food and feed is a recent worldwide trend. Microalgae *Phaeodactylum* and *Tetraselmis sp.* are authorized in EU for placing on the market as novel food. According to the Scientific report of AECOSAN, the recommended intake of the dried microalgae *T. chuii* per person/day is 250 mg (sauce or power) or 50 mg/day (salt prepared). In this report, the AECOSAN calculates the Acceptable Daily Intake (ADI) for dried *T. chuii* to be 25 mg/kg body weight/day, that is 1,750 mg/day for a 70 kg adult (AECOSAN, 2017). Stiefvatter et al (2020) developed a study with the microalgae *P. tricornutum* and its derived oils, also considered a novel food intended as food supplements to be consumed by the general population in the EU. These authors administered 3.5 g/day of the microalgae *P. tricornutum* for two weeks to healthy young adults and concluded that the microalgae are safety to consume for human.

The *T. chuii* has a strong scavenging activity against 2,2-difenyl-1-picrylhydrazyl (DPPH) and peroxyl radicals and it stimulates a response to cell damage and activates a repairing mechanism in human epidermal cells (Jo et al. 2012). These microalgae are gained increasing interest due to various valuable constituents. Gille et al. made lipophilic fractions of *P. tricornutum* and detected carotenoids, α-tocopherol, fatty acids and lipophilic peroxides (Gille et al. 2020).

And, Hernández-López et al. made ethanolic extracts of *Tetraselmis sp.* and analysed polyphenols, carotenoids and chlorophylls (Hernández-López et al. 2021). In this study, we assess the effect of the *P. triconutum* and *T. chuii* extracts on mitochondrial metabolic activity, as an indicator of cell viability. We evaluated the potential cytotoxic of ethanolic extracts at increasing concentrations after 24 h of exposure in HepG2 cells by MTT assay. We observed a decreased cell viability after *P. triconutum* 0% DR exposure at 50 and 100 μg/mL, respect to control. Similarly, Koo and coworkers evaluated the cytotoxic effect of fucoxanthin (a marine carotenoid found in *P. triconutum*) and *P. triconutum* extract in 3T3-L1 cells (Koo et al. 2019). They observed that fucoxanthin was cytotoxic to cells at concentrations above 80 μM, and *P. triconutum* extract at 1000 μg/mL. Moreover, Neumann and coworkers observed a decrease in metabolic activity of RAW 264.7 cells exposed to 50 μg/mL fucoxanthin (Neumann et al. 2019). Also, fucoxanthin was also able to reduce the metabolic activity of HepG2, HeLa and Caco-2 cells in a dose-dependent manner. An inhibitory effect of up to 58% at 50 μg/mL was observed in HepG2 cells, whereas in HeLa and Caco-2 cells, the cytotoxic effect was stronger (Neumann et al. 2019). Furthermore, the cytotoxic effect of the ethanolic and hexane *P. tricornutum* extracts on peripheral blood mononuclear (PBMCs) cells was evaluated using the MTT assay. The PBMCs cells were exposed to different concentrations of the *P. tricornutum* extracts (0.01, 0.1, and 1%) for 24 h. Only 1% ethanolic extract decreased the cell viability by 76% (Neumann et al. 2018). In the same way, the cytotoxicity of a chrysolaminarin-enriched extract (0.01, 0.1, 1% w/v) obtained from *P. tricornutum* was evaluated and the results demonstrated that all concentrations impair cell viability of primary dermal cell (NHDF) in a concentration-dependent manner (Carballo et al. 2018). According to Samarakoon and

coworkers, inhibitory viability effect of hexane, chloroform, ethyl acetate and aqueous *P. tricornutum* extracts (in a range of concentration from 6.25 to 50 μg/mL) was reported in RAW 264.7 macrophages (Samarakoon et al. 2013). Also, 25 and 50 μg/mL of *P. tricornutum* extracts decreased viability of endothelial HMEC-1 cells (le Goff et al. 2020).

Regarding to *T. chuii*, in our study we observed an increase in cell viability after *T. chuii* 0% DR exposure at 5, 25 and 100 μg/mL, respect to control. However, this effect was not observed previously by other authors. In Lung adenocarcinoma (A549) cells exposed to 400 μg/mL *T. chuii* extract a reduction in cell viability was observed by 80% after 24 and 48 h of exposure (Sansone et al. 2017). And, 125 μg/mL hexane extract of *Tetraselmis sp.* reduced HepG2 cell viability down to 10.8 % after 72 h of exposure (Custódio et al. 2014). The cytotoxicity of the *T. suecica* extracts in MCF-7 and 4 T1 cells was evidenced from 24 to 72 h by Hussein et al. (2020). *T. suecica*–methanol and *T. suecica*–chloroform extracts exhibited an IC_{50} value of 100 and 69.2 μg/mL in MCF-7 cells after 24 h, respectively (Hussein et al. 2020). Parra-Riofrío and coworkers (2020) studied the exopolysaccharides (EPS) obtained from *T. suecica* and reported that they have high cytotoxic effects on gingival fibroblast (HGF-1) with IC_{50} values from 165 to 61 μg/mL (Parra-Riofrío et al. 2020). Finally, Guzmán and coworkers demonstrated that 25 - 100 μM of peptides from the microalgae *T. suecica* AQ-1756, AQ-1757 and AQ-1766 decreased HEK293 cell viability in a concentration-dependent manner, after 24 of exposure (Guzmán et al. 2019).

Moreover, microalgae phenolic extracts have the ability to inhibit trichothecene production by *Fusarium* fungi (Scaglioni et al. 2019). In our results we observed that 50 μg/mL *P. triconutum* 0% DR extract (Fig. 4A), 2 μg/mL *T. chuii* 0% DR extract (Fig. 4C) and 2 μg/mL *T. chuii* 67% DR extract (Fig. 4D)

simultaneously exposed with T-2 increased the cell viability compared to their extracts tested individually by 31.2%, 26.5% and 18.26%, respectively. This may suggest that even if T-2 occurs in these microalgae, the mycotoxin could not induce cytotoxicity in HepG2 cells. So, these results suggest an increase in cell viability when the mycotoxin T-2 is exposed with *P. triconutum* and *T. chuii* extracts. Similar results were obtained by other authors. The crude phenolic extracts from natural resources of the Southern Brazilian region are proposed such as strategies to scale up their application in food industries because they have demonstrated an ability to inhibit fungal development without promoting stress and consequent mycotoxin production. They have found the possibility of applying these compounds as natural fungicides in the coastal ecosystem of Southern Brazil (Badiale Furlong et al. 2021). Souza et al., demonstrated the antifungal activity of 54 μg/mL phenolic extracts from *Spirulina platensis* (1.15 mg phenolic compound/g) against *A. flavus* (Souza et al., 2011). Phenolic extracts of commercial *Chlorella sp.* were also able to inhibit *A. flavus* and *R. oryzae* growth and, the production of aflatoxins by *A. flavus* was inhibited by 100% (Souza et al., 2011). Moreover, Pagnussatt et al. (2014) showed the antifungal activity of phenolic extracts from *Spirulina sp.* against *Fusarium* fungi. And, Pagnussatt et al. (2016) showed the antifungal and antimycotoxigenic effect of *S. platensis* LEB 18 phenolic extracts in free and encapsulated form on *F. graminearum* complex. Scaglioni et al. (2018) showed the inhibitory effect of phenolic extracts from *Nannochloropsis sp.* and *S. platensis* LEB 18 in maize culture media under field conditions. In corn fields, the authors found a minor contamination by *F. verticillioides* and its main mycotoxin, the fumonisin B1. In fact, phenolic extracts from *S. platensis* LEB 18 were used to formulate cereal mix for institutional food for children.

On the other hand, the antimycotoxigenic effect of the *Nannochloropsis* and *Spirulina* extracts on the isolate of *F. graminearum* species complex was demonstrated mainly against the NIV synthesis (Scaglioni et al. 2019). The extracts of both microalgae also had a promising effect on DON production, reaching no detection (with *Nannochloropsis sp.* extract) and 62% reduction (with *Spirulina sp.* extract) on fungal biomass developed with grains (Scaglioni et al. 2019). According to Shi and coworkers, the crude extract of marine red alga *Chondria tenuissima* exhibited antifungal activities (Shi et al. 2020).

In order to clarify the biological mechanism of these microalgae at the molecular level, we studied the difference in pro-inflammatory gene expression patterns in HepG2 cells treated with *P. triconutum* 0% DR and *T. chuii* 0% DR extracts. The genes involved in inflammatory responses TNF-α, IL-1β and IL-6, were all significantly up-regulated after extract exposure. The up-regulation of the pro-inflammatory biomarkers TNF-α, IL-1β and IL-6 genes after *P. triconutum* 0% DR and *T. chuii* 0% DR extracts exposure indicates that HepG2 cells were unable to defend themselves against inflammatory response of these microalgae. The up-regulation of TNF-α, IL-1β and IL-6 genes by these extracts may therefore be considered as there are potential inflammatory agent. To our knowledge, this is the first report that an ethanol extract from *P. triconutum* and *T. chuii* releases an inflammatory response. Carballo et al. (2019) found that *P. triconutum* significantly up-regulated the expression of IL-1 β mRNA levels in spleen of fish. On the other hand, Neumann et al. (2019) reported that fucoxanthin induced no changes in pro-inflammatory genes TNF-α, IL-1β and IL-6 in PBMCs cells, whereas different *P. tricornutum* extracts showed anti-inflammatory mRNA genes expression of PBMCs cells (Neumann et al. 2018).

The high up-regulation of TNF-α, IL-1β and IL-6 found in our study could be linked to the detection of metals (Pb, As, Hg and Cd) in these microalgae. Sabeti et al. (2021) observed that exposure to metals, As, Pb, Cd and Hg among others, in the highly polluted region is correlated with an increase of TNF-α and IL-6 in exhaled breath condensates (EBC) of population. Similarly, other authors reported a positive correlation between EBC TNF-α (Vossoughi et al. 2014) and EBC IL-1β (de Prins et al. 2014) with air pollutants, such as metals, in healthy subjects. Some authors evaluate methods of metal mitigation using nanoparticles. Ahamed et al. proved that the addition to $nTiO_2$ nanoparticles in human lung epithelial (A549) cells decreased the bioavailability of metals, such as Pb, due to the strong absorption of Pb on the surface area of $nTiO_2$, reducing the free Pb ions in culture medium (Ahamed et al. 2019). However, further studied in *in vivo* models are needed to assess nanoparticles effectiveness and safety for the consumer. As microalgae is a novel food, the toxicological risk assessment is needed as evidenced by the exposure to metals through the microalgae intake calculated here.

5. Conclusion

In summary, only an increase in cell viability was observed after exposure of *T. chuii* 0% DR extract. However, with a co-exposure of T-2, it was observed an increase in cell viability of freeze-dried of *T. chuii* 0% DR and *T. chuii* 67% DR and extracts of *P. triconutum* 0% DR, *T. chuii* 0% DR and *T. chuii* 67% DR. Moreover, the extracts of these microalgae produced an up-regulation of TNF-α, IL-1β and IL-6 genes, which could be related with the metals detected in the samples. We are aware that these microalgae are used as food supplement and additive in the food industry. However, there is an increasing awareness of the

importance of establishing the potential toxicological risk associated to the consume of microalgae or their application in food industry. So, further studies are required to assess food safety. It is important that the novel food, e.g. ethanol extract of *P. triconutum* and *T. chuii*, meets the acceptance criteria stablished by Regulation (EC) No 258/1997 concerning novel foods and novel food ingredients to ensure consumer safety.

Funding: This research was funded by Ministry of Science and Innovation Project (PID2020-115871RB-I00. M. Taroncher thanks the FPI grant (PRE2021-096941) provided by Spanish Ministry of Science and Innovation Project. The authors are thankful to Katerina Kousoulaki (NOFIMA, Norway), Marielena Kokkali (NOFIMA, Norway), Dorinde Kleingris and her team at the National Algae pilot plant in Mongstad (NAM) in Norway for cultivating and providing the microalgal biomass samples to carry out the experiments. Finally, the authors also acknowledge the Research Council of Norway, which provided funding through the A2F (Algae 2 Future) project (Project No. 267872/E50) for the production of the microalgae biomass used in this study.

6. References

Abolhasani MH, Safavi M, Goodarzi MT, Kassaee SM, Azin M. 2018. Identification and anti-cancer activity in 2D and 3D cell culture evaluation of an Iranian isolated marine microalgae Picochlorum sp. RCC486. DARU, Journal of Pharmaceutical Sciences. 26(2):105–116. https://doi.org/10.1007/s40199-018-0213-5

Ahamed M, Akhtar MJ, Alhadlaq HA. 2019. Preventive effect of TiO 2 nanoparticles on heavy metal Pb-induced toxicity in human lung epithelial (A549) cells. Toxicology in Vitro. 57:18–27. https://doi.org/10.1016/j.tiv.2019.02.004

Alavijeh RS, Karimi K, Wijffels RH, van den Berg C, Eppink M. 2020. Combined bead milling and enzymatic hydrolysis for efficient fractionation of lipids, proteins, and carbohydrates of Chlorella vulgaris microalgae. Bioresour Technol. 309. https://doi.org/10.1016/j.biortech.2020.123321

Badiale Furlong E, Badiale Furlong V, Kupski L, Scaglioni PT, Denardi de Souza T, Christ-Ribeiro A. 2021. Use of natural resources from Southern Brazil as a strategy to mitigate fungal contamination. Crit Rev Food Sci Nutr. 61(2):275–282. https://doi.org/10.1080/10408398.2020.1726868

Baker BC, Heazell AEP, Sibley C, Wright R, Bischof H, Beards F, Guevara T, Girard S, Jones RL. 2021. Hypoxia and oxidative stress induce sterile placental inflammation in vitro. Sci Rep. 11(1). https://doi.org/10.1038/s41598-021-86268-1

Calderon Pascual, V., Ruiz Leal, M.J., Daschner, Á., Talens Oliag, P., Tur Marí, J.A. (2017). Report of the Scientific Committee of the Spanish Agency for Consumer Affairs, Food Safety and Nutrition (AECOSAN) on a request for initial assessment

for marketing of the dried marine microalgae Tetraselmis chuii in food supplements under Regulation (EC) No 258/97 on novel foods and novel food ingredients. https://www.aesan.gob.es/AECOSAN/docs/documentos/seguridad_alimentaria/evaluacion_riesgos/informes_cc_ingles/HIDROXITIROSOL INGLES.pdf

Carballo C, Chronopoulou EG, Letsiou S, Maya C, Labrou NE, Infante C, Power DM, Manchado M. 2018. Antioxidant capacity and immunomodulatory effects of a chrysolaminarin-enriched extract in Senegalese sole. Fish Shellfish Immunol. 82:1–8. https://doi.org/10.1016/j.fsi.2018.07.052

Carballo C, Pinto PIS, Mateus AP, Berbel C, Guerreiro CC, Martinez-Blanch JF, Codoñer FM, Mantecon L, Power DM, Manchado M. 2019. Yeast β-glucans and microalgal extracts modulate the immune response and gut microbiome in Senegalese sole (Solea senegalensis). Fish Shellfish Immunol. 92:31–39. https://doi.org/10.1016/j.fsi.2019.05.044

Custódio L, Soares F, Pereira H, Barreira L, Vizetto-Duarte C, Rodrigues MJ, Rauter AP, Alberício F, Varela J. 2014. Fatty acid composition and biological activities of Isochrysis galbana T-ISO, Tetraselmis sp. and Scenedesmus sp.: Possible application in the pharmaceutical and functional food industries. J Appl Phycol. 26(1):151–161. https://doi.org/10.1007/s10811-013-0098-0

De Prins S, Dons E, van Poppel M, Int Panis L, de Mieroop E van, Nelen V, Cox B, Nawrot TS, Teughels C, Schoeters G, Koppen G. 2014. Airway oxidative stress and inflammation markers in exhaled breath from children are linked with exposure to black carbon. Environ Int. 73:440–446. https://doi.org/10.1016/j.envint.2014.06.017

Dietary exposure to inorganic arsenic in the European population. 2014. EFSA Journal. 12(3). https://doi.org/10.2903/j.efsa.2014.3597

Dongre RS. 2020. Lead: toxicological profile, pollution aspects and remedial solutions. In Lead Chemistry. IntechOpen.

Eagles EJ, Benstead R, MacDonald S, Handy R, Hutchinson TH. 2019. Impacts of the mycotoxin zearalenone on growth and photosynthetic responses in laboratory populations of freshwater macrophytes (Lemna minor) and microalgae (Pseudokirchneriella subcapitata). Ecotoxicol Environ Saf. 169:225–231. https://doi.org/10.1016/j.ecoenv.2018.10.101

EFSA Panel on Contaminants in the Food Chain (CONTAM); Scientific Opinion on tolerable weekly intake for cadmium. EFSA Journal 2011. 9(2):1975. [19 pp.] https://doi:10.2903/j.efsa.2011.1975. Available online: www.efsa.europa.eu/efsajournal

EFSA Scientific Committe Committee; Guidance on selected default values to be used by the EFSA Scientific Committee, Scientific Panels and Units in the absence of actual measured data. EFSA Journal 2012. 10(3):2579. 32 pp. https://doi:10.2903/j.efsa.2012.2579. Available online: www.efsa.europa.eu

EFSA Scientific Committee. 2015. Statement on the benefits of fish/seafood consumption compared to the risks of methylmercury in fish/seafood. EFSA Journal 2015:13(1):3982, 36 pp. https://doi:10.2903/j.efsa.2015.3982.

European Food Safety Authority. 2014. Dietary exposure to inorganic arsenic in the European population. EFSA Journal 2014;12(3):3597, 68 pp. https://doi:10.2903/j.efsa.2014.3597.

FAO. 2019. www.fao.org/faostat (Accessed 20 July 2022).

Geada P, Loureiro L, Teixeira JA, Vasconcelos V, Vicente AA, Fernandes BD. 2019. Evaluation of disruption/permeabilization methodologies for Microcystis aeruginosa as alternatives to obtain high yields of microcystin release. Algal Res. 42. https://doi.org/10.1016/j.algal.2019.101611

Gerosa-Neto J, Antunes BMM, Campos EZ, Rodrigues J, Ferrari GD, Neto JCR, Bueno Junior CR, Lira FS. 2016. Impact of long-term high-intensity interval and moderate-intensity continuous training on subclinical inflammation in overweight/obese adults. J Exerc Rehabil. 12(6):575–580. https://doi.org/10.12965/jer.1632770.385

Gilbert-López B, Barranco A, Herrero M, Cifuentes A, Ibáñez E. 2017. Development of new green processes for the recovery of bioactives from Phaeodactylum tricornutum. Food Research International. 99:1056–1065. https://doi.org/10.1016/j.foodres.2016.04.022

Gille A, Hollenbach R, Trautmann A, Gomez MR, Krüger R, Bischoff SC, Posten C, Briviba K. 2020. Lipophilic compounds, but not fucoxanthin, mediate the genotoxic effect of photoautotrophic grown Phaeodactylum tricornutum in Caco-2 and HT-29 cells. J Funct Foods. 64. https://doi.org/10.1016/j.jff.2019.103671

Guidance on selected default values to be used by the EFSA Scientific Committee, Scientific Panels and Units in the absence of actual measured data. 2012. EFSA Journal. 10(3):2579. https://doi.org/10.2903/j.efsa.2012.2579

Guzmán F, Wong G, Román T, Cárdenas C, Alvárez C, Schmitt P, Albericio F, Rojas V. 2019. Identification of Antimicrobial Peptides from the Microalgae Tetraselmis suecica (Kylin) Butcher and Bactericidal Activity Improvement. Mar Drugs. 17(8). https://doi.org/10.3390/md17080453

Hernández-López I, Benavente Valdés JR, Castellari M, Aguiló-Aguayo I, Morillas-España A, Sánchez-Zurano A, Acién-Fernández FG, Lafarga T. 2021. Utilisation of the marine microalgae Nannochloropsis sp. and Tetraselmis sp. as innovative ingredients in the formulation of wheat tortillas. Algal Res. 58. https://doi.org/10.1016/j.algal.2021.102361

Hussein HA, Mohamad H, Ghazaly MM, Laith AA, Abdullah MA. 2020. Cytotoxic effects of Tetraselmis suecica chloroform extracts with silver nanoparticle co-application on MCF-7, 4 T1, and Vero cell lines. J Appl Phycol. 32(1):127–143. https://doi.org/10.1007/s10811-019-01905-7

Imatoukene N, Koubaa M, Perdrix E, Benali M, Vorobiev E. 2020. Combination of cell disruption technologies for lipid recovery from dry and wet biomass of Yarrowia lipolytica and using green solvents. Process Biochemistry. 90:139–147. https://doi.org/10.1016/j.procbio.2019.11.011

Jo WS, Yang KM, Park HS, Kim GY, Nam BH, Jeong MH, Choi YJ. 2012. Effect of microalgal extracts of tetraselmis suecica against uvb-induced photoaging in human

skin fibroblasts. Toxicol Res. 28(4):241–248. https://doi.org/10.5487/TR.2012.28.4.241

Kamiya N, Kim HKW. 2021. Elevation of Proinflammatory Cytokine HMGB1 in the Synovial Fluid of Patients With Legg-Calvé-Perthes Disease and Correlation With IL-6. JBMR Plus. 5(2). https://doi.org/10.1002/jbm4.10429

Kim B, Kim HS. 2014. Chrysanthemum zawadskii extract activates peroxisome proliferator-activated receptor-α and has an anti-inflammatory activity : Potential interest for the skin barrier function. Korean Journal of Chemical Engineering. 31(10):1831–1838. https://doi.org/10.1007/s11814-014-0109-0

Koo SY, Hwang JH, Yang SH, Um JI, Hong KW, Kang K, Pan CH, Hwang KT, Kim SM. 2019. Anti-obesity effect of standardized extract of microalga phaeodactylum tricornutum containing fucoxanthin. Mar Drugs. 17(5). https://doi.org/10.3390/md17050311

Le Goff M, Delbrut A, Quinton M, Pradelles R, Bescher M, Burel A, Schoefs B, Sergent O, Lagadic-Gossmann D, le Ferrec E, Ulmann L. 2020. Protective action of ostreococcus tauri and phaeodactylum tricornutum extracts towards benzo[a]pyrene-induced cytotoxicity in endothelial cells. Mar Drugs. 18(1). https://doi.org/10.3390/md18010003

Martínez JM, Delso C, Angulo J, Álvarez I, Raso J. 2018. Pulsed electric field-assisted extraction of carotenoids from fresh biomass of Rhodotorula glutinis. Innovative Food Science and Emerging Technologies. 47:421–427. https://doi.org/10.1016/j.ifset.2018.04.012

Martínez-Alonso C, Taroncher M, Castaldo L, Izzo L, Rodríguez-Carrasco Y, Ritieni A, Ruiz M-J. 2022. Effect of Phenolic Extract from Red Beans (Phaseolus vulgaris L.) on T-2 Toxin-Induced Cytotoxicity in HepG2 Cells [Internet]. https://doi.org/10.3390/foods

Neumann U, Derwenskus F, Flister VF, Schmid-Staiger U, Hirth T, Bischoff SC. 2019. Fucoxanthin, a carotenoid derived from Phaeodactylum tricornutum exerts antiproliferative and antioxidant activities in vitro. Antioxidants. 8(6). https://doi.org/10.3390/antiox8060183

Neumann U, Louis S, Gille A, Derwenskus F, Schmid-Staiger U, Briviba K, Bischoff SC. 2018. Anti-inflammatory effects of Phaeodactylum tricornutum extracts on human blood mononuclear cells and murine macrophages. J Appl Phycol. 30(5):2837–2846. https://doi.org/10.1007/s10811-017-1352-7

Pagnussatt FA, de Lima VR, Dora CL, Costa JAV, Putaux JL, Badiale-Furlong E. 2016. Assessment of the encapsulation effect of phenolic compounds from Spirulina sp. LEB-18 on their antifusarium activities. Food Chem. 211:616–623. https://doi.org/10.1016/j.foodchem.2016.05.098

Pagnussatt FA, del Ponte EM, Garda-Buffon J, Badiale-Furlong E. 2014. Inhibition of Fusarium graminearum growth and mycotoxin production by phenolic extract from Spirulina sp. Pestic Biochem Physiol. 108(1):21–26. https://doi.org/10.1016/j.pestbp.2013.11.002

Parra-Riofrío G, García-Márquez J, Casas-Arrojo V, Uribe-Tapia E, Abdala-Díaz RT. 2020. Antioxidant and Cytotoxic Effects on Tumor Cells of Exopolysaccharides From Tetraselmis suecica (Kylin) Butcher Grown Under Autotrophic and Heterotrophic Conditions. Mar Drugs. 18(11). https://doi.org/10.3390/md18110534

Pérez-López P, González-García S, Ulloa RG, Sineiro J, Feijoo G, Moreira MT. 2014. Life cycle assessment of the production of bioactive compounds from Tetraselmis suecica at pilot scale. J Clean Prod. 64:323–331. https://doi.org/10.1016/j.jclepro.2013.07.028

Postma PR, Pataro G, Capitoli M, Barbosa MJ, Wijffels RH, Eppink MHM, Olivieri G, Ferrari G. 2016. Selective extraction of intracellular components from the microalga Chlorella vulgaris by combined pulsed electric field-temperature treatment. Bioresour Technol. 203:80–88. https://doi.org/10.1016/j.biortech.2015.12.012

Postma PR, Suarez-Garcia E, Safi C, Olivieri G, Olivieri G, Wijffels RH, Wijffels RH. 2017. Energy efficient bead milling of microalgae: Effect of bead size on disintegration and release of proteins and carbohydrates. Bioresour Technol. 224:670–679. https://doi.org/10.1016/j.biortech.2016.11.071

de Prins S, Dons E, van Poppel M, Int Panis L, de Mieroop E van, Nelen V, Cox B, Nawrot TS, Teughels C, Schoeters G, Koppen G. 2014. Airway oxidative stress and inflammation markers in exhaled breath from children are linked with exposure to black carbon. Environ Int. 73:440–446. https://doi.org/10.1016/j.envint.2014.06.017

Regulation (EC) No 258/97 of the European Parliament and of the Council of 27 January 1997 concerning novel foods and novel food ingredients. Off. J. Eur. Communities, 40 (1997), 1-7

Ruiz M, Festila LE, Fernández M. 2006. Comparison of basal cytotoxicity of seven carbamates in CHO-K1 cells. Toxicol Environ Chem. 88(2):345–354. https://doi.org/10.1080/02772240600630622

Sabeti Z, Ansarin K, Seyedrezazadeh E, Jafarabadi MA, Zafari V, Dastgiri S, Shakerkhatibi M, Gholampour A, Khamnian Z, Sepehri M, et al. 2021. Acute responses of airway oxidative stress, inflammation, and hemodynamic markers to ambient PM2.5 and their trace metal contents among healthy adolescences: A panel study in highly polluted versus low polluted regions. Environmental Pollution. 288. https://doi.org/10.1016/j.envpol.2021.117797

Safi C, Cabas Rodriguez L, Mulder WJ, Engelen-Smit N, Spekking W, van den Broek LAM, Olivieri G, Sijtsma L. 2017. Energy consumption and water-soluble protein release by cell wall disruption of Nannochloropsis gaditana. Bioresour Technol. 239:204–210.

Samarakoon KW, Ko JY, Shah MMR, Lee JH, Kang MC, O-Nam K, Lee JB, Jeon YJ. 2013. In vitro studies of anti-inflammatory and anticancer activities of organic solvent extracts from cultured marine microalgae. Algae. 28(1):111–119. https://doi.org/10.4490/algae.2013.28.1.111

Sansone C, Galasso C, Orefice I, Nuzzo G, Luongo E, Cutignano A, Romano G, Brunet C, Fontana A, Esposito F, Ianora A. 2017. The green microalga Tetraselmis suecica reduces oxidative stress and induces repairing mechanisms in human cells. Sci Rep. 7. https://doi.org/10.1038/srep41215

Sasaki K, Othman M ben, Ferdousi F, Yoshida M, Watanabe M, Tominaga K, Isoda H. 2019. Modulation of the neurotransmitter systems through the anti-inflammatory and antidepressant-like effects of squalene from Aurantiochytrium sp. PLoS One. 14(6). https://doi.org/10.1371/journal.pone.0218923

Scaglioni PT, Blandino M, Scarpino V, Giordano D, Testa G, Badiale-Furlong E. 2018. Application of Fungicides and Microalgal Phenolic Extracts for the Direct Control of Fumonisin Contamination in Maize. J Agric Food Chem. 66(19):4835–4841. https://doi.org/10.1021/acs.jafc.8b00540

Scaglioni PT, de Oliveira Garcia S, Badiale-Furlong E. 2019. Inhibition of in vitro trichothecenes production by microalgae phenolic extracts. Food Research International. 124:175–180. https://doi.org/10.1016/j.foodres.2018.07.008

Shi ZZ, Liu XH, Li XN, Ji NY. 2020. Antifungal and Antimicroalgal Trichothecene Sesquiterpenes from the Marine Algicolous Fungus Trichoderma brevicompactum A-DL-9-2. J Agric Food Chem. 68(52):15440–15448. https://doi.org/10.1021/acs.jafc.0c05586

Souza M, Prietto L, Christ Ribeiro A, Denardi de Souza T, Badiale-Furlong E. 1050. Assessment of the antifungal activity of Spirulina platensis phenolic extract against Aspergillus flavus.

Stiefvatter, L., Neumann, U., Rings, A., Frick, K., Schmid-Staiger, U., & Bischoff, S. C. (2022). The Microalgae Phaeodactylum tricornutum Is Well Suited as a Food with Positive Effects on the Intestinal Microbiota and the Generation of SCFA: Results from a Pre-Clinical Study. Nutrients, 14(12), 2504. https://doi.org/10.3390/nu14122504

Suomi J, Tuominen P, Savela K. 2017. Dietary exposure of Finnish children to heavy metal mixture–a cumulative assessment. Human and Ecological Risk Assessment.23(5):1234–1248.

Taroncher M, Rodríguez-Carrasco Y, & Ruiz MJ. 2020. T-2 toxin and its metabolites: Characterization, cytotoxic mechanisms and adaptive cellular response in human hepatocarcinoma (HepG2) cells. Food and Chemical Toxicology, 145, 111654.

Vossoughi M, Schikowski T, Vierkötter A, Sugiri D, Hoffmann B, Teichert T, Herder C, Schulte T, Luckhaus C, Raulf-Heimsoth M, et al. 2014. Air pollution and subclinical airway inflammation in the SALIA cohort study. Immunity and Ageing. 11(1). https://doi.org/10.1186/17

Antioxidants, 10 (2021), 975

https://doi.org/10.3390/antiox10060975

3.7. Cytoprotective effects of fish protein hydrolysates against H_2O_2-induced oxidative stress and mycotoxins in Caco-2/TC7 cells

Mercedes Taroncher[1], Yelko Rodríguez-Carrasco[1], Tone Aspevik[2], Katerina Kousoulaki[2], Francisco J. Barba[1]* and María-José Ruiz[1]

[1] Department of Preventive Medicine and Public Health, Food Science, Toxicology and Forensic Medicine, Faculty of Pharmacy, University of Valencia, Avda. Vicent Andrés Estellés, s/n. 46100, Burjassot, València, Spain; mercedes.taroncher@uv.es (M.T.); yelko.rodriguez@uv.es (Y.R-C); M.jose.ruiz@uv.es (M-J.R.)

[2] Department of Nutrition and Feed Technology, Nofima AS, 5141 Bergen, Norway; Tone.Aspevik@Nofima.no (T.A.); katerina.Kousoulaki@Nofima.no (K.K.)

Abstract

Many studies report the potent antioxidant capacity of fish protein hydrolysates, including radical scavenging activity and inhibition ability on lipid peroxidation (LPO). In this study, the *in vitro* cytotoxicity of protein hydrolysates from different salmon, mackerel and herring side streams fractions was evaluated in the concentration range from 1 to 1:32 dilution using Human colon adeno-carcinoma cells TC7 clone (Caco-2/TC7) by MTT and PT assays. The protein hydrolysates' antioxidant capacity and oxidative stress effects were evaluated by LPO and reactive oxygen species (ROS) generation, respectively. The antioxidant capacity of pure and bioavailable hydrolysate fraction were also evaluated and compared. Additionally, mycotoxin levels were determined in the fish protein hydrolysates and their cytoprotective effect against T-2 toxin was evaluated. Both hydrolysates and their bioavailable fraction induced similar cell viability rates. The highest cytoprotective effect was obtained for the salmon viscera protein hydrolysate (HSV), which increased the cell viability by 51.2%. ROS accumulation induced by H_2O_2 and LPO was suppressed by all pure hydrolysates. The cytoprotective effect of hydrolysates was observed against T-2. Moreover, the different fish fraction protein hydrolysates contain variable

nutrients and unique bioactive peptide composition showing variable bioactivity which could be a useful tool in developing dietary supplements with different target functional properties.

Keywords: Fish hydrolysates; cytotoxicity; oxidative stress; cytoprotective effect; bioavailability

---

* **Corresponding author**: Department of Preventive Medicine and Public Health, Food Science, Toxicology and Forensic Medicine, Faculty of Pharmacy, University of Valencia, Avda. Vicent Andrés Estellés, s/n. 46100, Burjassot, València, Spain; E-mail address: francisco.barba@uv.es (F.J.B); Tel.: +34-963544972 (F.J.B.)

1. Introduction

Synthetic antioxidants are commonly used to preserve food products, including butylated hydroxytoluene (BHT), tert-butyl hydroquinone (TBHQ) and butylated hydroxyanisole (BHA), but their use is limited due to the potential toxic effects in humans [1–3]. Therefore, nowadays there is an increasing consumer´s demand for natural antioxidants in order to delay food deterioration caused by oxidation as well as to alleviate the oxidative stress caused by mitochondrial generation of reactive oxygen species (ROS) [4–7], being of a great interest proteins and peptides [8–10].

Protein hydrolysates and peptides exhibit multiple physiological functionalities such as antimicrobial, antioxidant, antihypertensive, cholesterol-lowering effects and immunomodulatory activities [11–13]. Moreover, in some recent studies the ability of fish protein hydrolysates to suppress DSS-Induced colitis by modulating intestinal inflammation in mice as well as to suppresses diabetes and modulates intestinal microbiome in a murine model of diet-induced obesity has been observed [14,15].

Filleting of fish generates large amounts of protein-rich side stream materials, such as heads, backbones, viscera, and trimmings, with potential use for human consumption when handled properly and according to food-grade regulations. In order to use side stream fish proteins directly, the production of fish protein hydrolysates is a promising option, where the proteins are cleaved into smaller and more water-soluble peptides compared with the native protein [16].

Fish protein hydrolysates can have great application potential in the food, medical and cosmetic industries [17]. An example is collagen, abundant in connective tissue rich fish fractions, such as skin and bones [18]. Marine collagen has shown promising activities such as antioxidant, wound healing, anti-aging,

the adipogenic differentiation inhibition and anti-freezing, among others [13,19–22]. Numerous studies have reported that peptides derived from fish collagen and protein hydrolysates of a variety of fish species such as tuna, salmon, cuttlefish, sardinella, tilapia and shrimp showed potent antioxidant activities including radical scavenging activity, reducing power, and inhibition ability on lipid and protein oxidation [23,24]. Moreover, Zhao et al. [25] and Wong et al. [26] reported that protein hydrolysates of miiuy croaker swim bladders and hydrolysate of blue-spotted stingray could scavenge radicals and inhibit lipid peroxidation. Yarnpakdee et al. [27] studied lipid oxidation in protein hydrolysates from the muscle of Indian mackerel. Sheriff et al. [28] reported powerful antioxidant, lipid peroxidation inhibition and free radical scavenging activity of hydrolysate from backbones of Indian mackerel. Kumar et al. [29] found a good ability to scavenge hydroxyl radicals from antioxidant peptides obtained from horse mackerel viscera protein.

The bioavailability of fish protein hydrolysates has been evaluated in several studies [30–34] using the *in vitro* digestion technique. The human colorectal adenocarcinoma (Caco-2) cell line is the international validated model used for evaluating the intestinal absorption of food nutrients, also recognized as a reliable cell model for cell-based bioassays of food antioxidant activity [35]. These cells are able to differentiate in long-term culture and to polarize, when seeded on semipermeable membranes, on which they form a continuous monolayer with tight junctions mimicking the intestinal barrier [36]. Nevertheless, Caco-2 cells are heterogeneous and their physiological performance highly dependent on culture conditions, often leading to variable transport properties and permeability. In order to reduce the heterogeneity of the cells, several clones have been isolated from Caco-2 cells. The TC7 clone

was obtained from a late passage of the parental Caco-2 cell line and characterized for its ability to transport [36]. Zucco et al. [37] compared the characteristics of four Caco-2 cell lines and concluded that TC7 clone consisted of a more homogeneous cell population, with more representative functions of the small intestinal enterocytes. Thus, in our study we evaluated the suitability of Caco-2/TC7 as a predictive *in vitro* model for intestinal transport of fish protein hydrolysate compounds.

Mycotoxins are secondary toxic metabolites produced by fungi found in cereals and their side streams, monitored in both food and feed by national and international public health programs to evaluate compliance with the current regulations [38,39]. Aquaculture fish are commonly exposed to feed borne mycotoxins, especially from wheat and maize derived raw materials largely used in aquafeed formulations due to their favorable availability, price and protein content [40]. There are severable studies evaluating the presence of mycotoxins in terrestrial animals, whereas the data on the occurrence of mycotoxins in farmed fish is limited [41].

The aims of this study were: (i) to evaluate the viability of Caco-2/TC7 cells after 24 h exposure of protein hydrolysates based on heads, backbones and viscera from salmon, mackerel and herring (only viscera), and fish collagen based on flounder skin before and after an *in vitro* digestion process; (ii) to determine the cytoprotective/cytotoxic effects of these protein hydrolysates against oxidative stress-induction in Caco-2/TC7 cells; (iii) to identify possible fungal metabolites in these hydrolysates using a liquid chromatography high resolution mass spectrometry technique and to evaluate the cytoprotective effect of hydrolysates in co-exposure with T-2 toxin.

2. Materials and Methods

2.1 Reagents

The reagent grade chemicals and cell culture compounds used, namely Dulbecco's Modified Eagle's Medium (DMEM + GlutaMAX™), antibiotic solution (penicillin-streptomycin), non-essential amino acids (NEAA), 4-(2-hydroxyethyl)-1-piperazineethanesulfonic acid (HEPES), fungizone, trypsin/EDTA solutions, Phosphate Buffer Saline (PBS), Fetal Bovine Serum (FBS), methylthiazoltetrazolium salt (MTT) dye, dimethyl sulfoxide (DMSO), thiobarbituric acid (TBA), deferoxamine mesylate salt (DFA), di-ter-butylmethylphenol (BHT), 1,3,3,3 tetramethoxipropan (TMP), 2',7'-dichlorodihydrofluorescein diacetate (H_2-DCFDA), t-octylphenoxypolyethoxyethanol, glacial acetic acid, H_2O_2, NaOH, NaCl, glycine, Coomassie Brilliant Blue, ethyl acetate and $CaCl_2$, were purchased from Sigma-Aldrich (St Louis, USA). Methanol (MeOH) was purchased from VWR International (LLC, Pennsylvania, USA). Deionized water (resistivity <18 MΩ cm) was obtained filtering tap water through a Milli-Q water purification system (Millipore, Bedford, MA, USA). Standards of mycotoxins were purchased from Sigma-Aldrich (St Louis, USA).

Enzymatic protein hydrolysates based on mackerel heads (HMH), mackerel back-bones (HMB), mackerel viscera (HMV), salmon heads (HSH), salmon backbones (HSB), salmon viscera (HSV) and herring viscera (HHV) were produced according to Aspevik et al. [42]. In brief, the raw materials were mixed with tap water (1:1) and subjected to enzymatic hydrolysis for 50 min at 55 °C using the protease Food Pro PNL (DuPont Wilmington, DE). After thermal inactivation of the enzyme (> 90 °C, 10 min), the water phase (hydrolysate) was separated from the insoluble fraction and lipids and further purified using a 0.1

μm ceramic membrane filter before spray drying to a light-yellow powder. The chemical properties of protein hydrolysates of mackerel and salmon are shown in Aspevik et al. [42]. Flounder skin collagen was kindly provided by Seagarden (Karmøy, Norway).

2.2 Cell culture and treatment

The Caco-2/TC7 cells were cultured in DMEM medium supplemented with 10% FBS, 1% HEPES, 1% NEAA, 0.2% fungizone, 100 U/ml penicillin and 100 mg/ml streptomycin. The incubation conditions were pH 7.4, 5% CO_2 at 37 °C and 95% air atmosphere at constant humidity. The medium was changed every 2-3 days. All experiments were carried out 7 days post-seeding, when the integrity of the Caco-2/TC7 cell mono-layers had a measure of transepithelial electrical resistance (TEER) above 300 Ω/cm2. The clonal line Caco-2/TC7 cells were kindly provided by Central Service for Experimental Research (SCSIE) of the University of Valencia (Valencia, Spain).

2.3 *In vitro* cytotoxicity

Cytotoxic effects were determined in Caco-2/TC7 cells by the MTT and total protein content (PC) assays. The two assays have been extensively used for *in vitro* toxicological studies used to measure cell proliferation and survival. The MTT assay determines the viability of cells by the reduction of yellow soluble MTT, only in the metabolically active cells, via a mitochondrial-dependent reaction to an insoluble purple formazan crystal. The MTT viability assay was performed according to Ruiz et al. [43].

Briefly, the Caco-2/TC7 cells were plated in 96-well tissue culture plates at a density of 2×10^4 cells/well. In Caco-2/TC7, the culture medium was replaced

with fresh medium containing serial dilutions of each hydrolysate. The amount of 1 mg of the powdered hydrolysates was resuspended in 1 ml of fresh medium. Following, 1:2 dilutions were carried out using fresh medium. The range of concentrations of the hydrolysates was: 1 (mg/ml), 1:2 (0.5 mg/ml), 1:4 (0.25 mg/ml), 1:8 (0.125 mg/ml), 1:16 (0.0625mg/ml), 1:32 (0.03125mg/ml). The hydrolysates were exposed during 24 h. During the exposure time, neither the medium nor the hydrolysate was replenished. After 24 h of exposure, the medium was removed and 200 µl of fresh medium were added to each well. Then, 50 µl/well of MTT were added and the plates returned to the incubator in the dark. After 3 h of incubation, the MTT solution was removed and 200 µl of DMSO were added followed by 25 µl Sorensen's glycine buffer. Plates were gently shaken for 5 min to achieve the complete dissolution. The absorbance was measured at 540 nm using an automatic ELISA plate reader (MultiSkanEX, Thermo Scientific, MA, USA).

The PC method is based on the increase of absorbance of Coomassie Brilliant Blue dye when binding to proteins. The assay was performed in the same 96-well plates where the MTT test was carry out. First, the plates were washed with PBS and each well received 200 µl of NaOH 0.1 N to dissolve the proteins. After 2 h of incubation, 170 µl of NaOH were removed of each well and 180 µl of diluted 22% Coomassie Brilliant Blue were added. The plates remain for 30 min at room temperature and the absorbance was measured at 620 nm in an automatic ELISA plate reader (MultiSkanEX, Thermo Scientific, MA, USA).

For MTT and PC assays, cell viability was expressed as a percentage relative to the control solvent (medium DMEM + GlutaMAX™). Determinations were performed in three independent experiments with 4 replicates for each one. The

mean inhibition concentration (IC_{50}) values were calculated using SigmaPlot version 11 (Systat Soft-ware Inc., GmbH, Germany).

2.4 Intracellular ROS generation

Early intracellular ROS production was monitored in Caco-2/TC7 cells by adding H_2-DCFDA. The H_2-DCFDA is taken up by cells and then deacetylated by intracellular esterase's; the resulting non-fluorescent 2',7'-dichlorodihydrofluorescein (H_2-DCF) is switched to highly fluorescent dichlorofluorescein (DCF) when oxidized by ROS. The generation of ROS was monitored according to Ruiz-Leal and George [44]. Briefly, 2×10^4 cells/well were seeded in a 96-well black culture microplate. In Caco-2/TC7 cells the culture medium was replaced, and cells were loaded with 20 μM H_2-DCFDA in fresh medium for 20 min. Then two assays (A and B) were simultaneously carried out. Assay A: H_2-DCFDA was removed and 200 μl/well of fresh medium or medium with hydrolysates 1 mg/ml were added. Assay B: H_2-DCFDA was removed and 200 μl/well of fresh medium or medium with hydrolysates (1 mg/ml) and 5 mM H_2O_2 were added. In both assays, the ROS level was monitored by measuring the increase in fluorescence on a Wallace Victor2, model 1420 multilabel counter (PerkinElmer, Turku, Finland), at intervals up to 2 h at excitation/emission wavelengths of 485/535 nm, respectively. Results were expressed as fluorescence intensity. Determinations were performed in three independent experiments with 16 replicates each.

2.5 Lipid peroxidation assay

Lipid peroxidation (LPO) assay was carried out by determining the formation of reactive thiobarbituric acid reactive substances (TBARS), according to Ferrer

et al. [45]. The TBARS allows to determine the production of a red adduct between TBA and malondialdehyde (MDA), which is a biomarker used to prove that the LPO process has occurred. Briefly, 2.25×10^5 cells/well were seeded in six-well plates. In Caco-2/TC7 cells two assays (A and B) were simultaneously carried out after confluence. Assay A: the culture medium was replaced for fresh medium with hydrolysates 1 mg/ml. Assay B: the culture medium was replaced for fresh medium with 5 mM H_2O_2 for 5 minutes, except the control. After that, the culture medium with H_2O_2 was replaced for fresh medium with hydrolysates (1 mg/ml). In both assays, the Caco-2/TC7 cells were exposed to 1 mg/ml of hydrolysates for 24 h. Then, the medium was removed, and cells were washed with PBS, homogenized in 150 mM sodium phosphate buffer (NaH_2PO_4) pH 7.4 and lysate with the Ultra-Turrax T8 IKA®-WERKE. Immediately, cells were boiled at 100 °C in a water bath for 20 min under acidic condition in the presence of 0.5% TBA, 1.5 mM DFA and 3.75% BHT. After that, the samples were placed on ice for 5 min and centrifuged at 2880×g for 15 min. The absorbance was measured at 532 nm. Three independent experiments were conducted with three replicates each. Results were expressed as ng of MDA/mg of protein measured by the Lowry method.

2.6 Comparison of cytotoxicity between pure hydrolysates and their bioavailable fraction

The Caco-2/TC7 were exposed to 0.0625 mg/ml of bioaccessible fraction of each hydrolysate. To obtain the bioaccessible fraction, the standardized method INFOGEST was applied. Simulated Salivary Fluid (SSF), Simulated Gastric Fluid (SGF), Simulated Intestinal Fluid (SIF) and enzymatic activity assays were prepared according to Minekus et al. [46]. Because of the high percentage of

proteins in the hydrolysate samples, the salivary step was carried out without amylase enzyme. Briefly, 2.5 ml of hydrolysate solution, 2 ml of SSF, 12.5 µl of 0.3 M $CaCl_2$ and deionized water to a final volume of 5 ml were mixed for 2 min. Afterwards, to simulate the gastric phase, 3.75 ml of SGF, 0.8 ml of pepsin solution (25.000 U/ml) and 2.5 µl of 0.3 M $CaCl_2$ were add-ed. Then, the pH was adjusted at 3.0, deionized water was added up to a final volume of 10 ml. This gastric mixture was incubated for 2 h. Subsequently, 5.5 ml of SIF containing pancreatin (100 U trypsin activity/ml) and bile salts (10 mmol/l), and 20 µl of 0.3 M $CaCl_2$ were added. The pH was adjusted at 7.0, deionized water was added up to a final volume of 20 ml, and the intestinal mixture was incubated for 2 h. The oral, gastric, and intestinal steps were performed by mechanical shaking at 95×rpm and 37 °C. At the end of the *in vitro* digestive process, samples were cooled in an ice bath and centrifuged at 3100×g and 4 °C for 60 min to obtain the bioaccessible fraction.

The Caco-2/TC7 cells were seeded at a density of 2.25×10^5 cells in inserts 6-well Transwell Permeable Supports, 12 mm diameter (Corning, NY, USA) and 0.4 mm of pore size, and grown for 7 days. The culture medium in the apical and basolateral sides was replaced every 2–3 days. The integrity of the Caco-2/TC7 cell monolayers was confirmed by measuring the transepithelial electrical resistance (TEER) using an electric resistance device (Millicell-ERS, Millipore Corp), and monolayers with TEER above 300 Ω/cm^2 were used for the bioavailability assay. Medium of apical (upper compartment) and basolateral side (lower compartment) was removed and transport was assessed by paracellular passage of bioaccessible fraction of hydrolysates (0.0625 mg/ml) in apical side to the basolateral side. So, 1,5 ml of bioaccessible fraction of digested hydrolysates was added to the apical side and 2 ml of medium without serum

was added to the basolateral side. Control samples composed by transport medium without serum were also evaluated. The medium of the basolateral side, which is the bioavailable fraction, is collected. Then, with the bioavailable fraction, the MTT assay was carried out to determine the cytotoxicity of bioavailable fraction of hydrolysates at 0.0625 mg/ml. The results obtained were compared with the pure hydrolysates at 0.0625 mg/ml. The concentration 0.0625 mg/ml was chosen because it is one of the ones which exerted the highest cytoprotective effect in Caco-2/TC7 cells by the MTT assay (Fig. 1). Determinations were performed in three independent experiments with 4 replicates each.

2.7 Cytoprotective effect of hydrolysates exposed together with T-2 toxin

The T-2 toxin (T-2) is a *Fusarium* mycotoxin frequently occurring in cereals worldwide and the most toxic fusariotoxin. The recent animal dietary exposure to T-2 conducted by EFSA, reported the occurrence of T-2 in feed in concentrations of up to 405 μg/kg [47]. Hence, cytoprotective effect of hydrolysates in Caco-2/TC7 cells was evaluated by MTT assay, exposing 60 nM T-2 to each hydrolysate at 0.0625 mg/ml. to develop the MTT assay 2×10^4 cells/well were plated in 96-well tissue culture plate and the assay was performed as described in 2.3 *In vitro* cytotoxicity section. The results obtained were compared with cells exposed to 60 nM T-2 and pure hydrolysates at 0.0625 mg/ml individually. The concentration of 60 nM was chosen because it showed a cytotoxic effect in previous studies in our laboratory [48]. Determinations were performed in three independent experiments with 4 replicates each.

2.8 Determination of fungal metabolites in fish hydrolysates through liquid chromatography quadrupole time of flight mass spectrometry

The extraction of mycotoxins from hydrolysates of fish samples was performed according to the sample preparation procedure described by Taroncher et al. [48] slightly modified. In brief, 0.5 ml of hydrolysate fish sample was collected and transferred to a 4 ml Eppendorf Safe-Lock microcentrifuge tube. Then, 3 ml of ethyl acetate were added, and the mixture was shaken for 2 min with an Ultra-Turrax Ika T18 basic (Staufen, Germany) and centrifuged at 5600×g for 3 min (Centrifuge 5910R, Eppendorf, Germany). The supernatant phase was collected and evaporated under gentle N_2 stream at 45 ºC to dryness with a TurboVap-LV (Zymark, Allschwil, Switzerland), redissolved in 0.14 ml of a mixture methanol:water (70:30, *v/v*) and then filtered through a 0.2 μm filter prior to the analysis.

The analysis was performed using a liquid chromatography quadrupole time of flight mass spectrometry (LC-Q-TOF MS) system consisting of an LC Agilent 1200-LC system (Agilent Technologies, Palo Alto, CA, USA) equipped with a vacuum degasser, an autosampler and a binary pump. The column was a Gemini NX-C18 (150 × 2 mm, i.d. 3 μm, Phenomenex, Torrance, CA, USA) with a guard column C18 (4 × 2mm, i.d. 3 μm). Mobile phases consisted of Milli-Q water with 0.1% formic acid and 5 nM ammonium formate as solvent system A, and methanol with 0.1% formic acid and 5 nM ammonium formate as solvent system B, with the following elution gradient: 0.2 min, 20% B; 0.5 min, 20-40% B; 5 min, 100% B; 2 min, decrease to 20% B, maintained 6 min. The flow rate used was 0.200 ml/min, and the total run time was 14 min. The sample volume injected was 20 μl.

The mass spectrometry (MS) analysis was carried out using a 6540 Agilent Ultra-High Definition Accurate-Mass Q-TOF MS, equipped with an Agilent Dual jet Stream electrospray ionization (Dual AJS ESI) interface in both positive and negative ionization modes. The conditions were as follows: sheath gas temperature 350 °C at a flow rate of 8 l/min, capillary voltage 3500 V, nebulizer pressure 45 psig, drying gas 10 l/min, gas temperature 300 °C, skimmer voltage 65 V, octopole RF peak 750 V, and fragmentor voltage 130 V. Analyses were performed using AutoMS/MS mode in a mass range of 50-1200 m/z. The acquisition rate was 3 scans/s for three different collision energies (10, 20 and 40 eV). Internal mass correction was enabled by using two reference masses in positive mode (121.050873 and 922.009798 m/z) and two reference masses in negative mode (112.985587 and 1033.988109 m/z). Instrument control and data acquisition were performed using Agilent MassHunter Workstation software B.08.00. Potential analytes were identified by the MassHunter METLIN Metabolite PCD (Personal Compound Database) and PCDL (Personal Compound Database and Library) from Agilent Technologies.

2.9 Statistical analysis

The statistical analysis of the data was carried out using the Statgraphics version 16.01.03 statistical package (IBM Corp., Armonk, NY, USA). Data were expressed as mean ± standard error of the mean (SEM) of different independent experiments. The statistical analysis of the results was performed using the Student *t*-test for paired samples. Differences between groups were analyzed using one-way analysis of variance (ANOVA) followed by Tukey HDS post-hoc test for multiple comparisons. Statistical significance was considered for $p \leq 0.05$ and tendencies for $0.1 < p < 0.05$.

3. Results

3.1 *In vitro* cytotoxicity

The safe supplementation level of hydrolysates HSV, HSB, HSH, HMH, HMB, HMV, HHV and Collagen based on evaluation of cytotoxic effect in Caco-2/TC7 cells was evaluated by MTT and PC assays over 24 h. The concentration range of the hydrolysates selected to study the potential cytotoxic/cytoprotective effects on these cells was: 1, 0.5, 0.25, 0.125, 0.0625, 0.03125 mg/ml.

After 24 h of treatment, most hydrolysates did not show significant effects on the mitochondrial function of Caco-2/TC7 cells at any of the concentrations tested, except HSB at 0.125mg/ml and HSV at 0.0625 mg/ml and 0.25 mg/ml (Figure 1). The maximum measured MTT increase was 27% for HSB and 51.2% for HSV. The increase in cell viability can be due to the hormetic effect of the test hydrolysates in Caco-2/TC7 cells.

In the PC assay (Fig. 2) all hydrolysates except HSB and HMV, showed a hormetic effect when the cells were exposed to specific dilutions, including 0.0625mg/ml. The maximum measured PC increase was 18% for HMB, 19% for HSV, 69% for collagen, 139% for HHV, 140% for HSH and 214% for HMH. At 0.0625mg/ml used in the subsequent tests, the PC increasing effect of the different hydrolysates was as following: HSV = HMB < collagen < HSH < HHV < HMH (p=0.000).

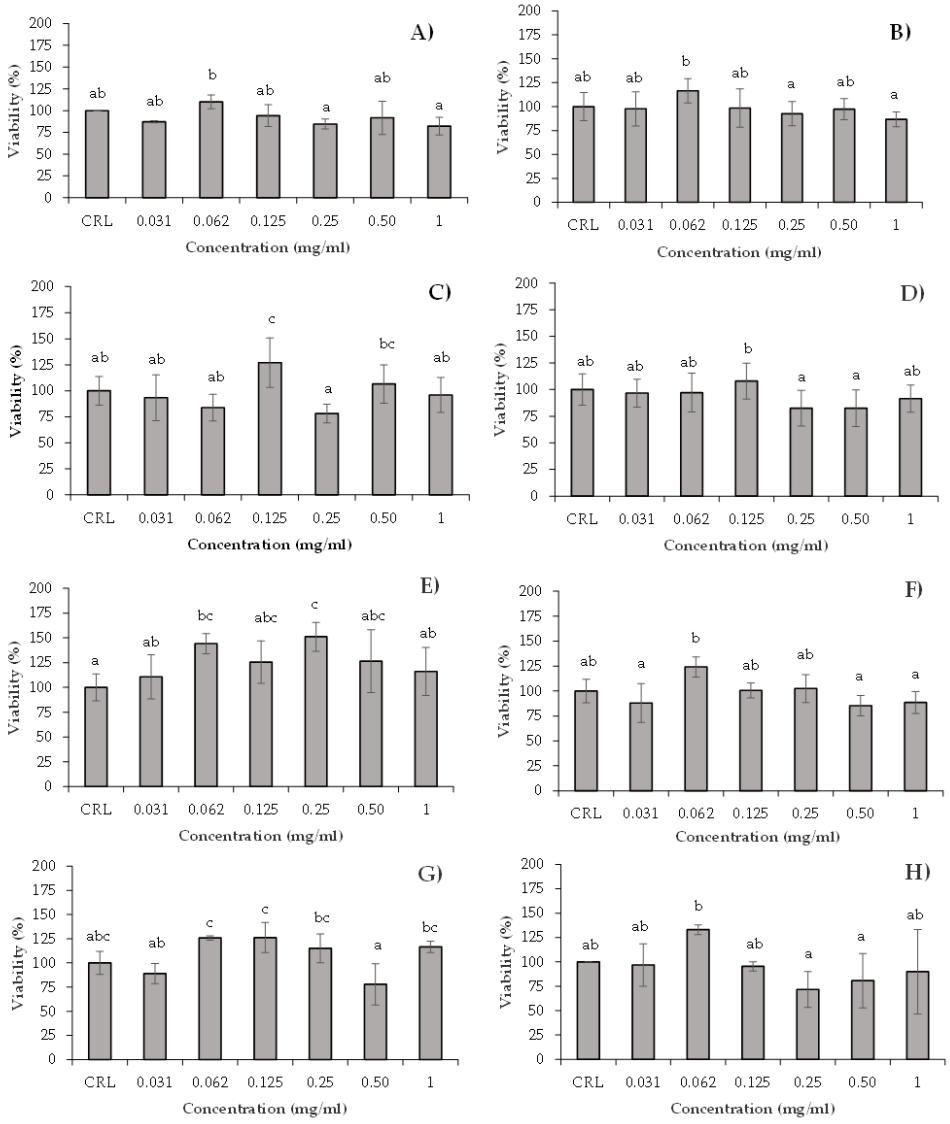

Figure 1. Effect of HSH (A), HMH (B), HSB (C), HMB (D), HSV (E), HMV (F), HHV (G) and Collagen (H) on cell viability (MTT assay) in Caco-2/TC7 cells after 24 h of exposure at increasing concentrations from 0 to 1 mg/mL. Values are expressed as mean ± SEM (n=3). Values in the same figure with different superscript letter are significantly different ($p< 0.05$). CRL: control.

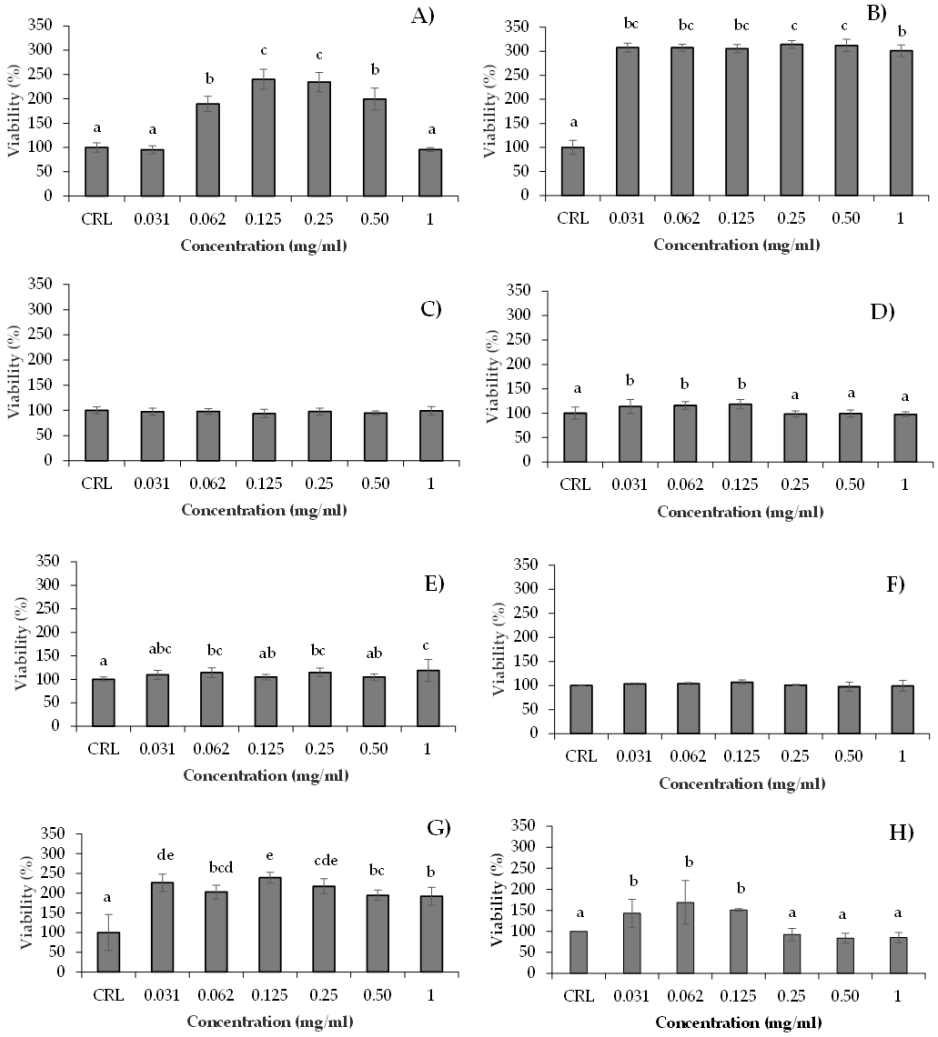

Figure 2. Effect of HSH (A), HMH (B), HSB (C), HMB (D), HSV (E), HMV (F), HHV (G) and Collagen (H) on cell viability (PC assay) in Caco-2/TC7 cells after 24 h of exposure at increasing concentrations from 0 to 1 mg/mL. Values are expressed as mean ± SEM (n=3). Values in the same figure with different superscript letter are significantly different ($p < 0.05$). CRL: control.

3.2 Intracellular ROS generation

The intracellular accumulation of ROS in Caco-2/TC7 cells exposed to hydrolysates (HSV, HSB, HSH, HMH, HMB, HMV, HHV and Collagen) (1 mg/ml) without (Fig. 3) and with (Fig. 4) H_2O_2 was analyzed using H_2-DCFDA. Figure 3 shows ROS generation grouped by type of fish hydrolysate. Figure 3 shows differences between ROS generation of hydrolysates respect to control. In general, ROS production increased slightly at 5 min and then decreased and stabilized 60 min after exposure, at lower levels than at trial start, but without significant differences respect to the control. Only significant differences of HMH and collagen at 90 and 15 min respectively, respect to the control were determined (Fig. 3; Table 1). The production of ROS in Caco-2/TC7 cells treated with salmon heads hydrolysate (HSH) and collagen was lower, whereas in those treated with HSB, HSV, HMH and HMB was higher as compared to the control (Table 1). No differences were found between HMV, HHV and control (Table 1). Among the different hydrolysates, lowest ROS accumulation in Caco-2/TC7 cells was observed by exposure with HSH followed and at increasing ROS accumulation levels by collagen, then HMV, HHV, HMB, HSB, HMH and last HSV at 120 min, but not all differences were statistically significant (Table 1). Significant differences appeared at 15 min exposure, when higher ROS accumulation was found in the HMH and HSV as compared to the HSH treatment (p=0.003; Tukey HSD), and again at 90 min exposure when ROS accumulation was significantly higher in HSB as compared to the collagen treatment (p=0.001; Tukey HSD).

Figure 4 shows ROS generation of hydrolysates exposed simultaneously to H_2O_2 grouped by type of fish hydrolysate. The ROS generation of hydrolysates with H_2O_2 was compared with H_2O_2 tested alone. When Caco-2/TC7 cells were

exposed to oxidative stress induced by H_2O_2, showed an increase in ROS levels which ranged from 1.9-fold to 17.2-fold at 0 and 45 min, respectively, compared to the control. Nevertheless, at 5 min Collagen and most fish hydrolysates except HMB induced lower ROS accumulation as compared to H_2O_2 treatment alone, statistically significant only for HSH, HSV and HMV (p=0.000; Tukey HSD). After 5 min, the strongest antioxidant effect was induced by HMV. The antioxidant effect of fish hydrolysates was maintained until 45 min following exposure and gradually disappeared as compared to the H_2O_2 treatment at 60 min following exposure, when there were analyzed higher ROS levels in HSV, HSB, HMH and HMB treatments as compared to both the control and the H_2O_2 treatment (Fig. 4). Considering the whole trial period, it was Collagen which induced significant antioxidant effect against H_2O_2 exposure and HHV which induced the highest ROS accumulation, not significantly as compared to all treatments (Table 2).

3.3 Lipid peroxidation assay

The LPO on Caco-2/TC7 cells was determined by the TBARS method in the presence of hydrolysates HSV, HSB, HSH, HMH, HMB, HMV, HHV and Collagen (1 mg/ml) with and without H_2O_2. As it is shown in Figure 5, the incubation for 24 h in the absence of oxidative stress significantly decreased the LPO production in Caco-2/TC7 cells ($p \leq 0.05$). Cells treated with H_2O_2 alone showed significant LPO increase compared to the control, whereas all the hydrolysate treated cells showed similar LPO levels to that of the control, though there was an overall increase of LPO in the combined hydrolysate / H_2O_2 treatments, compared to the non-pretreated cells of a magnitude between 40.2 and 146.3%.

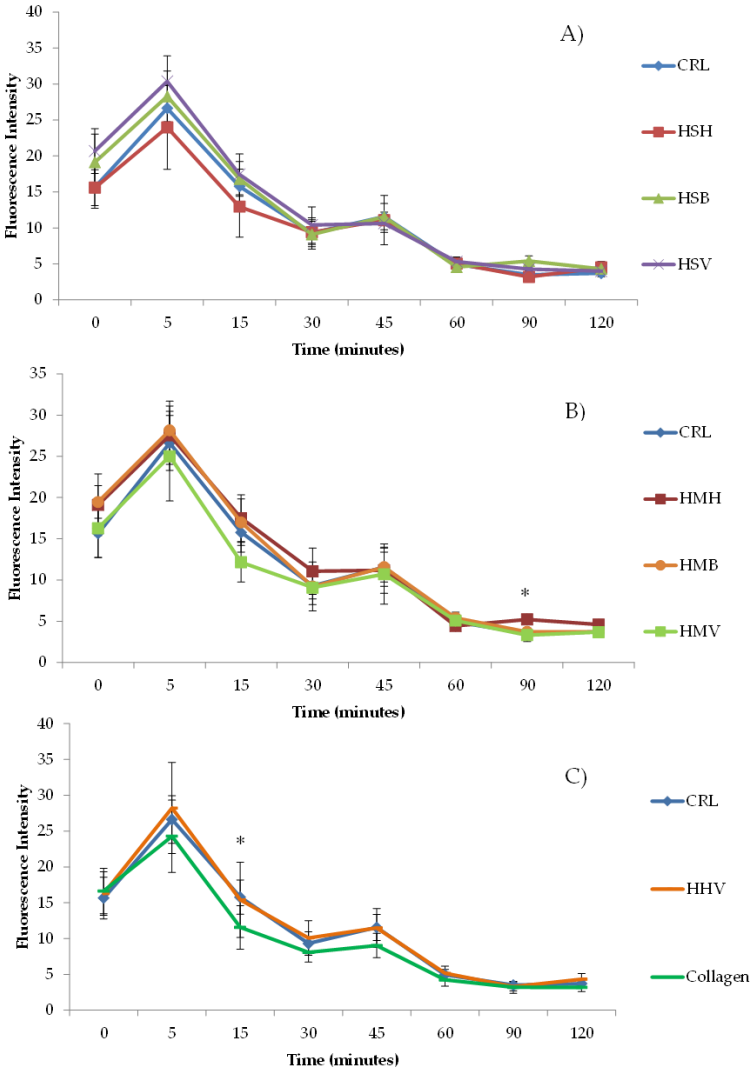

Figure 3. Time dependence of ROS-induced fluorescence in Caco-2/TC7 cells exposed to (A) salmon hydrolysates, (B) mackerel hydrolysates and (C) herring hydrolysates and fish collagen at 1 mg/ml without oxidative stress induced by H_2O_2. Results are expresses as mean ± SEM (n=3). (*) $p \leq 0.05$ indicates significant differences compared to the control (CRL).

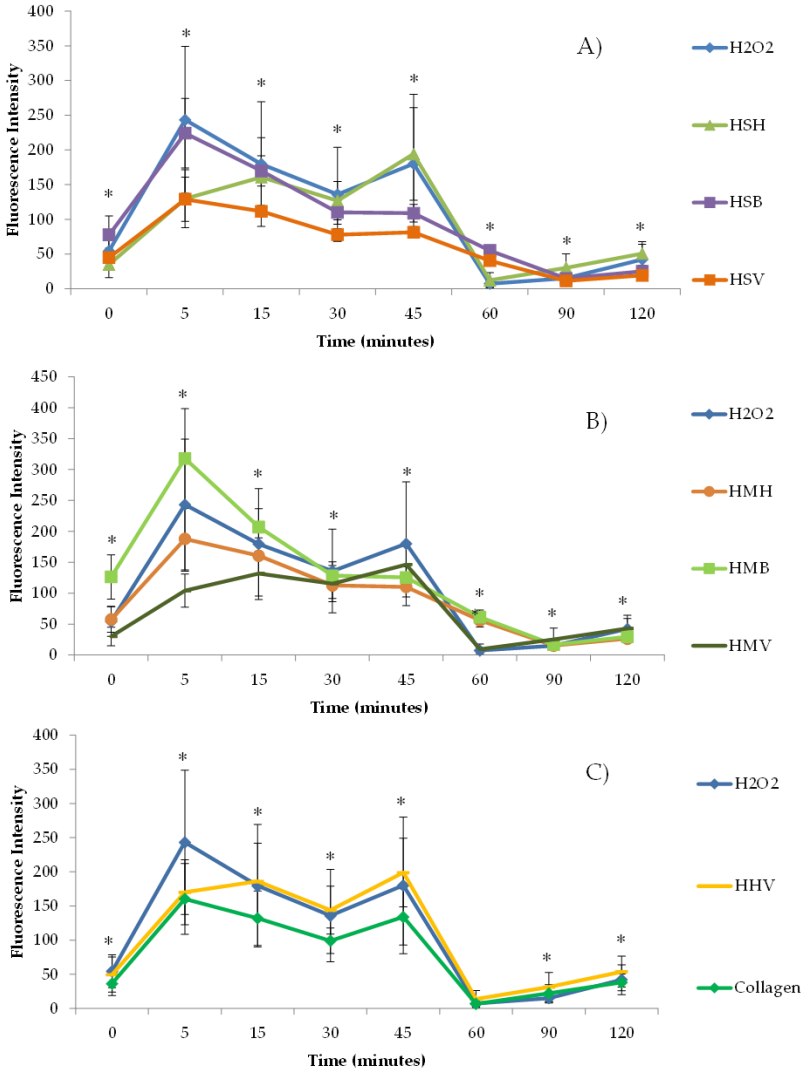

Figure 4. Time dependence of ROS-induced fluorescence in Caco-2/TC7 cells exposed to (A) salmon hydrolysates, (B) mackerel hydrolysates and (C) herring hydrolysates and fish collagen at 1 mg/ml with oxidative stress induced by H_2O_2. Results are expresses as mean ± SEM (n=3). (*) $p \leq 0.05$ indicates significant differences compared to the H_2O_2.

Table 1. Outcomes of the differences between hydrolysates and collagen without H_2O_2 and control from 0 to 120 min of exposure using ANOVA followed by Tukey HDS post-hoc test for multiple comparison

			SALMON			MACKEREL			HERRING
		CTR	HSH	HSB	HSV	HMH	HMB	HMV	HHV
SALMON	HSH	*HSH<CTR (0.1> p>0.05)*							
	HSB	*HSB>CTR (0.1> p>0.05)*	*HSB>HSH (p≤0.05)*						
	HSV	*HSV>CTR (0.1> p>0.05)*	*HSV>HSH (p≤0.05)*	*NS*					
MACKEREL	HMH	*HMH>CTR (p≤0.05)*	*HMH>HSH (p≤0.05)*	*NS*	*NS*				
	HMB	*HMB>CTR (0.1> p>0.05)*	*HMB>HSH (0.1> p>0.05)*	*NS*	*NS*	*NS*			
	HMV	*NS*	*NS*	*HMV<HSB (p≤0.05)*	*HMV<HSV (p≤0.05)*	*HMV<HMH (p≤0.05)*	*HMV<HMB (p≤0.05)*		
HERRING	HHV	*NS*	*HHV>HSH (0.1> p>0.05)*	*HHV<HSB (0.1> p>0.05)*	*HHV<HSV (0.1> p>0.05)*	*HHV<HMH (p≤0.05)*	*HHV<HMB (0.1> p>0.05)*	*HMV<HHV (0.1> p>0.05)*	
FLOWNDER	Collagen	*Collagen<CTR (p≤0.05)*	*NS*	*Collagen<HSB (p≤0.05)*	*Collagen<HSV (p≤0.05)*	*Collagen<HMH (p≤0.05)*	*Collagen<HMB (p≤0.05)*	*Collagen<HMV (p≤0.05)*	*Collagen<HHV (p≤0.05)*

NS: non-significant.

Table 2. Outcomes of the differences between hydrolysates and collagen with H_2O_2 and control from 0 to 120 min of exposure using ANOVA followed by Tukey HDS post-hoc test for multiple comparison.

				SALMON			MACKEREL			HERRING
		CTR	H_2O_2	HSH_{H2O2}	HSB_{H2O2}	HSV_{H2O2}	HMH_{H2O2}	HMB_{H2O2}	HMV_{H2O2}	HHV_{H2O2}
	H_2O_2	*H_2O_2>CTR ($p \leq 0.05$)*								
SALMON	HSH_{H2O2}	*HSH>CTR ($p \leq 0.05$)*	*NS*							
	HSB_{H2O2}	*HSB>CTR ($p \leq 0.05$)*	*NS*	*NS*						
	HSV_{H2O2}	*HSV>CTR ($p \leq 0.05$)*	*HSV<H_2O_2 (0.1> p>0.05)*	*NS*	*HSV<HSB ($p \leq 0.05$)*					
MACKEREL	HMH_{H2O2}	*HMH>CTR ($p \leq 0.05$)*	*NS*	*NS*	*NS*	*HMH>HSV ($p \leq 0.05$)*				
	HMB_{H2O2}	*HMB>CTR ($p \leq 0.05$)*	*NS*	*NS*	*HMB>HSB ($p \leq 0.05$)*	*HMB>HSV ($p \leq 0.05$)*	*HMB>HMH (0.1> p>0.05)*			
	HMV_{H2O2}	*HMV>CTR ($p \leq 0.05$)*	*NS*	*HMV<HSH ($p \leq 0.05$)*	*NS*	*NS*	*NS*	*NS*		
HERRING	HHV_{H2O2}	*HHV>CTR ($p \leq 0.05$)*	*NS*	*HHV>HSH ($p \leq 0.05$)*	*NS*	*HHV>HSV ($p \leq 0.05$)*	*NS*	*NS*	*HHV>HMV ($p \leq 0.05$)*	
FLOWNDER	Collagen $_{H2O2}$	*Collaben>CTR ($p \leq 0.05$)*	*Collagen<H_2O_2 ($p \leq 0.05$)*	*NS*	*Collagen<HSB ($p \leq 0.05$)*	*NS*	*Collagen>HMH (0.1> p>0.05)*	*Collagen<HMB ($p \leq 0.05$)*	*NS*	*Collagen<HHV ($p \leq 0.05$)*

NS: non-significant.

Respect to hydrolysates simultaneously exposed to H_2O_2, HSB, HMH and HMV showed cytotoxic protection respect to H_2O_2 exposure. The highest cytoprotective effect was obtained for HMV, significantly only as compared to HSV, collagen and H_2O_2 treatments. In cells without H_2O_2 pretreatment, HSV offered highest antioxidant effect, and HSH the lowest.

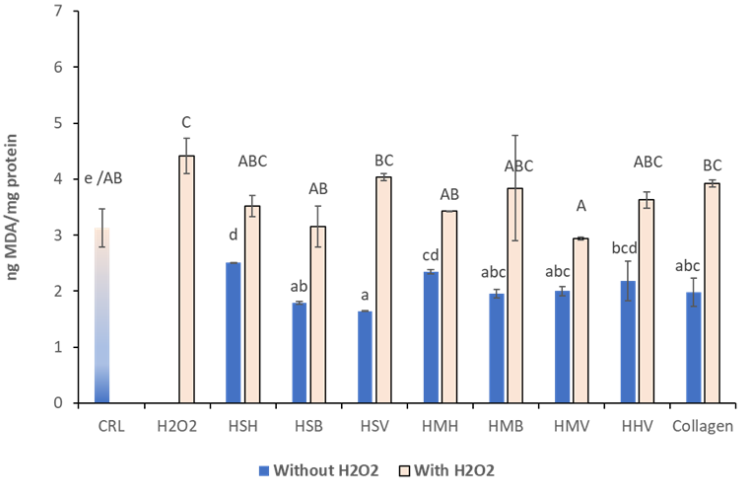

Figure 5. The LPO measured by MDA production in Caco-2/TC7 cells incubated with hydrolysates HMH, HSV, HSB, HMB, HHV, HSH, HMV and Collagen (1 mg/ml) with and without oxidative stress (H_2O_2). Results are expressed as mean ± SEM (n=3) in ng of MDA/mg of protein measured by Lowry method. Values with common small or capital letters, for the treatment without or with H_2O_2 induced stress, respectively, are not significantly different (p<0.05; Tukey HSD). CRL: control.

3.4 Comparison of cytotoxicity between pure hydrolysates and their bioavailable fraction

In general terms, the bioavailable fraction of the tested fish hydrolysates showed similar effects as the respective pure hydrolysates. There were no significant differences in the cytoprotective effect of pure fish hydrolysates as

compared to their bioavailable extracts (p>0.1), with the exception of the bioavailable fraction of herring viscera hydrolysate (HHV) which increased cell viability significantly as compared to the respective pure hydrolysate (Fig. 6) (p<0.001; Tukey HSD).

Comparing the three salmon and three mackerel fraction hydrolysates together, the ANOVA analysis did not show significant species effects. On the other hand, significant differences were observed between the different side stream fractions. The backbone hydrolysate fractions did not inducing cytoprotective effect (-10.47% viability as compared to the pure hydrolysates). Head hydrolysates induced 10.98% increase in cell viability, and the viscera induced significantly higher cell viability (28,78%) as compared to the other two fractions (HBa<HHb<HVc; p<0.001; Tukey HSD). Comparing the visceral hydrolysate fraction effects, HMV (mackerel) induced significantly lower viability improvement (12.8% increased viability as compared to the pure hydrolysates) as compared to HSV (salmon) (39.72%) and HHV (herring) (50.70%) (p<0.001; Tukey HSD).

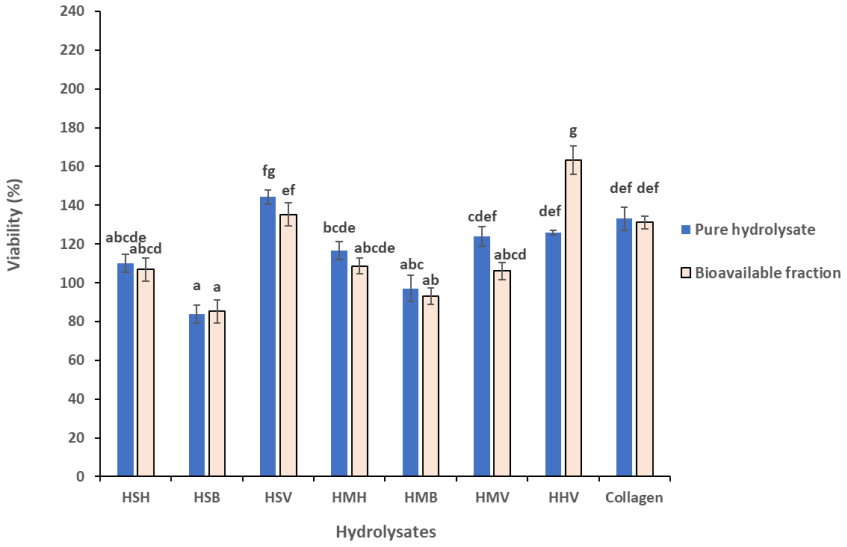

Figure 6. Viability (%) of the fish-based protein hydrolysates compared with the bioavailable fraction of the same protein hydrolysate at 1:16 dilution in Caco-2/TC7 cells after 24 h of exposure by MTT. Values are expressed as mean ± SEM (n=3). Values with common letters are not significantly different (p<0.001; Tukey HSD).

3.5 Cytoprotective effect of hydrolysates against T-2 mycotoxin

Exposing Caco-2/TC7 cells to T-2 mycotoxin significantly reduced their viability. All tested fish side stream hydrolysates exerted cytoprotective effect against T-2 mycotoxin, not statistically significantly though for the backbone hydrolysates HSB and HMB and collagen as observed in Figure 7.

As seen in the viability trial without exposure to T-2 mycotoxin, the cytoprotective effect of salmon hydrolysates was higher than that of mackerel in cells exposed to T-2, this time species factor showed tendency for effect (p=0.1). Likewise, the side stream fraction induced statistically significant effects, with the backbone fractions inducing the lowest cytoprotective effect (19.16%

increased viability as compared to the T-2 treated cells), followed by the heads (43.46% increase in cell viability), and the viscera, which induced significantly higher cell viability (69.92%) as compared to the other two fractions (HBa<HHb<HVc; $p<0.001$; Tukey HSD). Comparing the visceral hydrolysate fraction effects, it was HSV (salmon) which induced the highest cytoprotective effect against T-2 mycotoxin exposure (76.18% increased viability as compared to the T-2 treated cells), significantly higher as compared to HHV (herring) (62.47%) and HMV (mackerel) (60.80%) ($p<0.01$; Tukey HSD).

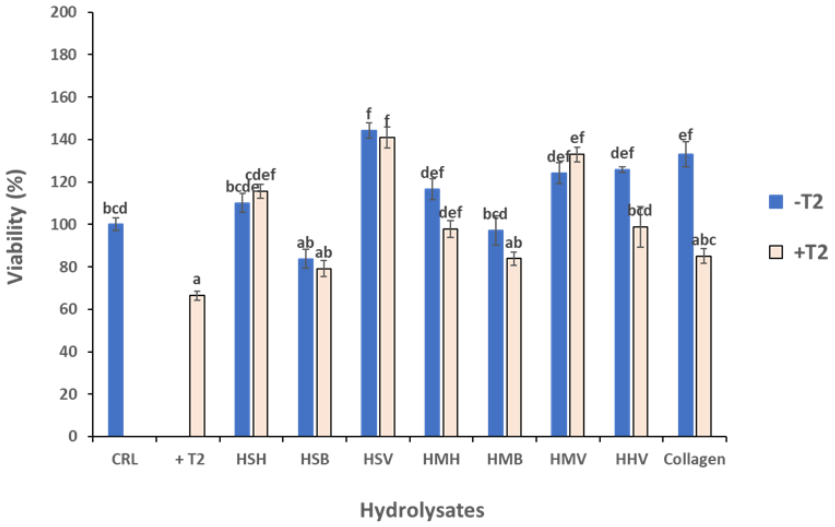

Figure 7. Viability (%) of T-2 toxin, pure hydrolysates and hydrolysates combined with T-2 in Caco-2/TC7 cells after 24 h of exposure by MTT. All hydrolysates were added at 1:16 dilution and T-2 at 60 nM. Values are expressed as mean ± SEM (n=2). Values with common letters are not significantly different ($p<0.001$; Tukey HSD). CRL: control.

3.6 Identification of fungal metabolites in fish hydrolysates

The retrospective screening was applied to high resolution mass spectrometry data acquired in AutoMS/MS mode using a Q-TOF MS system. The screening of suspected fungal metabolites was performed using the MassHunter METLIN Metabolite PCD and PCDL. No fungal metabolites were identified in analyzed fish hydrolysates. To guarantee the quality control and quality assurance of the results, a pool sample of fish hydrolysates spiked with a mixture of mycotoxins at instrumental detection limit was performed and included in the same batch (Fig. 8).

4. Discussion

Fish filleting side stream materials contain high levels of structural and bioactive proteins and smaller peptides, and lower levels of lipids containing long chain ω-3 polyunsaturated fatty acids (ω-3-PUFAs), phospholipids, bioactive nitrogenous compounds, organic minerals, and vitamins, among others. Most of fish side streams are considered waste, though highly nutritious, contain among other significant amounts of protein [49]. Effective use of fish side stream raw materials reduces the environmental impact of aquaculture and fisheries and could provide high-added-value products to increase economical income for the marine product processing industries. Over the last years, the use of extracts and compounds obtained from marine side stream biomass to improve the functionality of food products from different points of view such as organoleptic, health and technological, has attracted much interest [50]. Among different applications, extracts and compounds obtained from fish side streams can be used as colorants, antimicrobials, antioxidant compounds, PUFAS, essential amino acids and emulsifiers. These properties allow them to act as

preservatives, to improve the nutritional and health profile of foods, as well as to improve the technological characteristics of the products. On the other hand, the use of these products may also have a great interest from the pharmaceutical point of view such as nutraceuticals, biorefinery or development of new packaging systems [51].

In the present study, protein hydrolysates based on different side stream fractions from salmon, mackerel and herring, and flounder skin collagen have been selected to evaluate their potential use as functional food ingredients. Serial dilutions of each hydrolysate were chosen to study the potential cytotoxic/cytoprotective effects of the hydrolysates in Caco-2/TC7 cells. The hydrolysates did not show cytotoxic effects, however, a cytoprotective effect when Caco-2/TC7 cells where exposed to HSB at 0.125 mg/ml and HSV at 0.0625 mg/ml and 0.25 mg/ml by MTT assay was observed (Fig. 1). The increase in cell viability at lower concentrations can be due to the hormetic effect. It can be observed either a xenobiotic or an antioxidant substance, a hormone or a metabolite in several studies [52–54].

By the PC assay, all hydrolysates except HSB and HMV, showed an increase in cell viability when Caco-2/TC7 cells were exposed to specific dilutions, including 0.0625 mg/ml (Fig. 2). Wiriyaphan et al. [55] reported that hydrolysate of side streams of *Nemipterus* spp. did not have cytotoxic effects on Caco-2 cells. Further, several studies on fish-based protein hydrolysates on multiple human cell lines have shown low toxicity and high cell viability [51,52]. Gómez et al. [56] showed a cytoprotective effect after 24 h of treatment with red tilapia side streams in Caco-2 cells, demonstrating increase of cell viability in a dose-dependent manner.

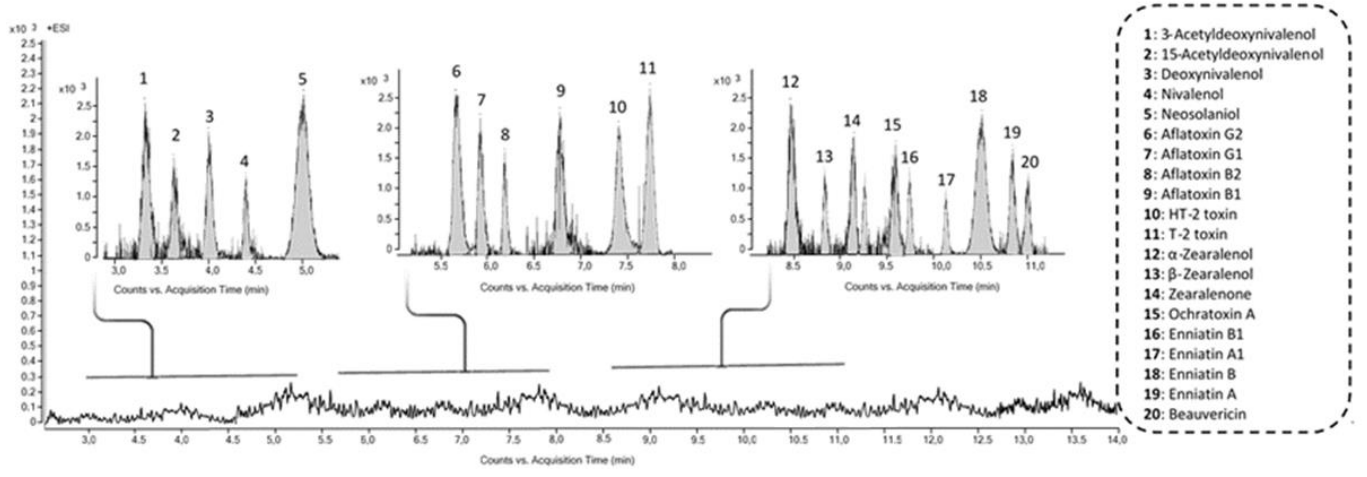

Figure 8. LC-Q-TOF MS extracted ion chromatogram of a pool sample of fish protein hydrolysates spiked with a mixture of mycotoxins.

Similarly to our results, in which the viscera hydrolysate showed highest cytoprotective effect, these authors demonstrated that the highest protection was achieved at 0.1 and 0.25 mg/ml for RTVH-A (red tilapia viscera hydrolysate with higher antioxidant activity) and FRTVH-V (red tilapia viscera hydrolysate with molecular weight cut-offs of <1 kDa fraction), respectively. In this line, Zhong et al. [57], found that protein hydrolysates isolated from silver carp by-products showed cytoprotective effect on Caco-2 cells exposed to low concentrations of H_2O_2 and the highest capacity to neutralize radicals. Hu et al. [58] did not observe any significant cytotoxic effects on HepG2 cells after exposure of hydrolysate of monkfish (*Lophius litulon*) muscle during 24 h, by MTT assay. However, it was reported an increase in a concentration-dependent manner of cell viability compared with control when the cells were exposed to peptides with antioxidant activity with H_2O_2-induced oxidative damage. For instance, the peptide MMP-12 increased the HepG2 cell viability from 48.85% ± 1.68% to 63.28% ± 2.06%, to 79.35% ± 2.85%, and to 88.65% ± 3.42% at the concentrations of 10, 50, and 100 μM, respectively. Those findings suggested that the peptides from hydrolysate of monkfish muscle could strongly protect H_2O_2-induced oxidative damage HepG2 cells, especially at high concentrations. These results were consistent with the data presented by Zheng et al. [59], who showed that hydrolysate of swim bladders of *Nibea japonica* exposed to human umbilical vein endothelial (HU-VECs) cells during 24 h did not decrease cell viability. Indeed, a collagen peptide of the swim bladders named SNNH-1, promoted the growth of these cells. Moreover, Yang et al. [60] evidenced that marine collagen peptides from *Nibea japonica* skin have the potential to promote NIH-3T3 fibroblasts cells.

Reactive oxygen species (ROS) are generated in aerobic organisms during mitochondrial respiration to detoxify substances, chemical defense, cell signaling and biosynthetic reactions [35,61]. When the elimination of ROS is inadequate or their generation exceeds their elimination, ROS are accumulated in cells and oxidative stress occurs. Excess of ROS alters the normal cell metabolism oxidizing cell membrane phospholipids, proteins, lipids, DNA and enzymes, among others [62]. Oxidative stress contributes to many noncommunicable disease pathologies such as neurodegenerative conditions, cardiovascular and inflammatory diseases, emphysema and certain types of cancer [63]. Therefore, there is a significant interest in the development and application of functional food supplements with antioxidant properties to promote disease prevention and protect human health. The maintenance and proliferation of cell viability by a treatment with salmon, mackerel and herring hydrolysates could be related to the fact that these hydrolysates do not produce more ROS at cellular level than cells not exposed to these hydrolysates. The ROS are generated by different physiological oxidative processes in the organisms and associated with pathogenesis of various human diseases [64]. The overproduction of ROS culminates in oxidative damage to some key biological macromolecules which leads to significantly reduced cell viability [58]. In our study, none of the tested hydrolysates at 1 mg/ml concentration leads to significant increase in the intracellular ROS levels in Caco-2 cells ($p > 0.05$) except HMH and collagen at 90 and 15 min respectively, compared to the control (Fig. 3; Table 1). However, cells pretreated with H_2O_2 showed an increase of ROS generation at all times of exposure compared to the control (Fig. 4). The decrease in intracellular ROS levels using a pretreatment with these hydrolysates suggested that sequestration or neutralization of free radicals is a possible mechanism of action in the

antioxidant peptides found in hydrolysates. Similar results were obtained by Zhen et al. [59] who studied the effect of SNNH-1 on ROS levels in HUVECs cells. After H_2O_2 treatment, the fluorescence intensity in HUVECs cells was significantly higher compared to the control. However, SNNH-1 pretreatment reduced ROS levels at concentration-dependent manner on HUVECs cells. These results were in agreement with the data presented by Li et al. [65], who found that collagen peptides from sea cucumbers (*Acaudina molpadioides*) could protect RAW264.7 cells from H_2O_2-induced damage. Hu et al. [58] observed the effects of MMP-4, MMP-7, and MMP-12 (three peptides of hydrolysate of monkfish, *Lophius litulon*, muscle), on the level of ROS in oxidative damage HepG2 cells. The level of ROS observed in HepG2 cells exposed to only H_2O_2 was 231.7% ± 13.5%, which was significantly higher than the control (100%). The intracellular ROS levels were significantly attenuated by MMP-4, MMP-7, and MMP-12 pretreatment in a dose-dependent manner. Among them, MMP-7 showed the strongest scavenging effect of ROS and decreased the ROS level from 229.5% ± 16.8% to 165.2% ± 11.9%, to 137.3% ± 14.3%, and to 129.1% ± 8.6% at the concentrations of 10, 50, and 100 μM, respectively. Chen et al. [12] reported that the exposure of HepG2 cells with tilapia fish skin gelatin hydrolysates for 24 h decreased the level of ROS in a dose-dependent manner. Similarly, according to Wang et al. [32], the HepG2 cells caused significant inhibition of oxidative damage compared with cells treated only with H_2O_2, after pretreatment with mackerel proteins hydrolysate (5 mg/ml). Gómez et al. [56] determined that Caco-2 cells treated with H2O2 showed a 5 times increase in intracellular ROS levels compared to untreated cells, but these levels decreased by approximately 40% by pretreatment with red tilapia viscera hydrolysates RTVH-A and FRTVH-V. Other antioxidant peptides with high cellular

antioxidant activity via neutralization of intracellular ROS, have been identified in different sources of proteins such as tilapia muscle [35] and tilapia scale gelatin [66].

Antioxidant collagen peptides are also known to provide cell protect from oxidative stress damage through scavenging ROS and increasing the levels of intracellular antioxidant enzymes [67]. This work shows that flounder skin collagen protects cells from oxidative stress decreasing ROS level and MDA. Moreover, comparing with hydrolysates, it is one of the ones which exerts the most protective effect. These finding are corroborated with the results obtained by other authors. Collagen peptides from crimson snapper (*Lutianus erythroptrus*) scales [12] and royal jelly [64] could prolong the average life of Drosophila treated with H_2O_2 by decreasing the contents of peroxide products, such as MDA and protein carbonylation. Moreover, Wang et al. [68] determined that collagen of red lip croaker could protect H_2O_2-damaged HepG2 cells from oxidative stress by decreasing ROS and MDA levels and enhancing endogenous antioxidant enzyme defense system, so it could serve as antioxidant used in food and healthy products. Moreover, collagen peptides are popular in cosmetics because, for example, they can protect the skin from ultraviolet (UV) radiation injuries [68].

The LPO occurs as a non-specific process secondary to initial cell damage, which can be blocked by antioxidants. The MDA is the oxidative metabolite of cell lipid oxidation and can attack unsaturated fatty acids in the cell membrane, which causes cell damage. Therefore, the degree of LPO and cell damage can be evaluated according to the MDA content in cells [30]. Our results showed that salmon, mackerel, and herring hydrolysates prevented the propagation of LPO decreasing the MDA levels in Caco-2/TC7 cells. These results demonstrated

that salmon (HSB) and mackerel (HMH and HMV) hydrolysates may protect Caco-2/TC7 cells from oxidative damage. Similar results were obtained by Zheng et al. [59], who reported that MDA content in HUVEC cells was significantly higher after H_2O_2 treatment compared to the control, however, pretreatment of HUVECs with SNNH-1 decreased the amount of MDA in a dose-dependent manner. In addition, Cai et al. [69] reported that FPYLRH (S8) from the swim bladders of miiuy croaker (*Miichthys miiuy*) could down-regulate the contents of MDA, suggesting that it plays a protective role in the antioxidant effects on HUVECs cells against H_2O_2-induced damage. According to that, Zhen et al. [59] determined the effect of SNNH-1 pretreatment on the levels of MDA after oxidative damage of HU-VECs induced by H_2O_2. The results concluded that SNNH-1 inhibited intracellular LPO and enhanced the cell´s antioxidant defense system. Hu et al. [58] studied the effects of protein hydrolysate of monkfish on MDA levels in H_2O_2-induced HepG2 cells. The MDA content (21.63 ± 0.81 nM/mg protein) in HepG2 cells exposed to H_2O_2 was significantly increased compared with the control group (9.32 ± 0.35 nM/mg protein). At the 10, 50, and 100 μM concentration, the MDA content of MMP-12 peptide was 18.8 ± 0.56, 16.46 ± 0.74, and 12.43 ± 0.62 nM/mg protein, which was lower than those of MMP-4 and MMP-7 peptides, and the H_2O_2 treated group. Therefore, MMP-4, MMP-7 and MMP-12 peptides could reduce the oxidative stress injury by the decrease of LPO.

The results obtained in this study indicate that fish protein hydrolysates represent great candidate molecules for the development of antioxidant dietary supplements. However, peptides are often chemically and physically unstable, display rapid clearance, and are quickly degraded by enzymes [70]. Therefore, ensuring the bioaccessibility of peptides should be evaluated. Thus, the

bioavailable fraction of the different protein hydrolysates was achieved and a comparison between cell viability of pure hydrolysates and their bioavailable fraction was carried out. These results revealed the same trend as the as the pure hydrolysates. This indicates that there were no statistically significant differences, in terms of toxicity or antioxidant capability, of the protein hydrolysates once the digestion process has been carried out.

Additionally, the viability of cells exposed to pure hydrolysates and to hydrolysates combined with T-2 was compared to corroborate the cytoprotective effect of fish hydrolysates. The results evidenced that almost all the hydrolysates combined with T-2 showed an increase in viability compared to cell exposure to T-2 alone. This may be due to the fact that these hydrolysates counteract the cytotoxic effect of T-2 and they act as if the cell were only exposed to the hydrolysate. Hydrolysates based on viscera, regardless of the specie, combined with T-2, exercised the same effect on cell viability than if they were not exposed to T-2, so viscera hydrolysate exert the most protective effect. As it can be observed in Figure 7 and according to MTT assay (Figure 1), 1:16 dilution of HSV exercised the most cytoprotective effect compared with the rest of hydrolysates. Moreover, when hydrolysates were combined with T-2, HSV also exercised the most cytoprotective effect. However, when Collagen was combined with T-2 significantly decreased cell viability respect to its corresponding pure hydrolysates. That could be because of collagen evidenced the highest bacterial content of all hydrolysates analyzed (data not shown), which may be related with conditions of degradation or breakdown of the fish. Furthermore, Collagen evidenced higher levels of trimethylamine-N (TMA; 66 mg N/100 g) [42], which is indicator of poor product quality. That fact could explain that a co-exposure of Collagen with T-2 decreased the viability, because

of collagen did not have the necessary quality parameters to protect the cell against this damage.

Finally, it is important to know whether the feedstuffs used for farmed fish are contaminated. Fish from aquaculture is fed using different feeds and raw materials from vegetal origin and plant products, which could be contaminated by mycotoxins [71]. Different studies have shown that some mycotoxins carry-over from feed into edible tissues or fluids from animals [72–74]. As far as the foodstuffs from aquaculture industries is concerned, the occurrence of aflatoxins, ochratoxin A, and *Fusarium* mycotoxins such as thrichotecenes and the emerging fusariotoxins have been reported in literature [75–79]. Tolosa et al. [76] determined the occurrence of enniatins (ENs) in feed for farmed fish and in fish samples of sea bass and sea bream. They reported an occurrence of ENs in up to 25% of analyzed samples (n=20) at levels from 1.01 to 119.0 μg/Kg and revealed higher average concentrations of EN A1 (11.1 μg/Kg), EN B (13.0 μg/Kg) and EN B1 (19.0 μg/Kg) in head than in liver (5.1, 12.6 and 5.3 μg/Kg for EN A1, EN B and EN B1, respectively). Those findings corroborate the ability of ENs to distribute and persist into tissues and even penetrate different barriers, including blood-brain barrier, in higher organisms as previously evidenced in literature [80,81]. However, mycotoxins were not detected in the protein hydrolysates, suggesting that the fish had not been exposed to mycotoxins.

To summarize, HSV showed the highest cytoprotective effect in Caco-2/TC7 as evidenced by MTT, ROS and LPO assays. HMV treatment also showed a reduction in ROS values when compared to H_2O_2. On the other hand, the HHV bioavailable fraction showed the highest percentage of cell viability in Caco-

2/TC7 cells compared to the rest of hydrolysates. Moreover, HSV presented the highest cytoprotective effect when hydrolysates are combined with T-2 toxin.

5. Conclusions

Taken all together, findings from this study suggest that heads, backbones and viscera from salmon, mackerel and herring could be utilized as valuable raw materials in the development of health-promoting functional foods with potential antioxidant capacities. Both hydrolysates and their bioavailable fraction induced similar cell viability rates. Moreover, from the results obtained it can be concluded that the highest cytoprotective effect was obtained for the salmon viscera protein hydrolysate. In addition, ROS accumulation induced by H_2O_2 and LPO was suppressed by all pure hydrolysates and the cytoprotective effect of all hydrolysates was observed against T-2. This scientific basis may provide a solution for dealing the high cost and environmental problems associated with disposal of such waste material. However, more studies are needed to investigate the biological effects of fish hydrolysate in order to transform protein rich side stream products into valuable products as well as to ensure food safety.

Author Contributions: Conceptualization, M.T. and M.-J.R.; methodology, M.T. and T.A.; software, M.T.; validation, M.T. and M.-J.R.; formal analysis, M.T.; investigation, M.T.; resources, M.T.; data curation, M.T.; K.K.; writing—original draft preparation, M.T.; writing—review and editing, M.-J.R.; Y.R.; F.J.B.; K.K. and T.A.; visualization, M.-J.R.; Y.R.; F.J.B. and K.K.; supervision, M.-J.R.; Y.R.; F.J.B. and K.K.; project administration, F.J.B.; funding acquisition, F.J.B. and Y.R. All authors have read and agreed to the published version of the manuscript.

Funding: This research was funded by the EU Commission and BBI-JU Horizon H2020, through AQUABIOPRO-FIT project (Aquaculture and agriculture biomass side stream proteins and bioactives for feed, fitness and health promoting nutritional supplements) grant number 790956, and the project grant given by the Generalitat Valenciana (Spain) GV/2020/020 (Conselleria d'Innovacio, Universitats, Ciencia i Societat Digital Generalitat Valenciana).

Acknowledgments: M.T. acknowledges the research contract (CPI-20-031) within the AQUABI-OPROFIT project. We are grateful for technical assistance from the SCSIE of the University of Valencia (Valencia, Spain).

Conflicts of Interest: The authors declare no conflict of interest.

6. References

1. Lanigan, R. S.; Yamarik, T. A. Final report on the safety assessment of BHT. Int. J. Toxicol. 2002, 21, 19–94.
2. Nagai, F.; Ushiyama, K.; Kano, I. DNA cleavage by metabolites of butylated hydroxytoluene. Arch. Toxicol. 1993, 67, 552–557.
3. Kupfer, R.; Dwyer-Nield, L. D.; Malkinson, A. M.; Thompson, J. A. Lung toxicity and tumor promotion by hydroxylated derivatives of 2,6-di-tert-butyl-4-methylphenol (BHT) and 2-tert-butyl-4-methyl-6-iso-propylphenol: Correlation with quinone methide reactivity. Chem. Res. Toxicol. 2002, 15, 1106–1112.
4. Wen, C.; Zhang, J.; Feng, Y.; Duan, Y.; Ma, H.; Zhang, H. Purification and identification of novel antioxidant peptides from watermelon seed protein hydrolysates and their cytoprotective effects on H2O2-induced oxidative stress. Food Chem. 2020, 327, 127059.
5. Ganesan, K.; Xu, B. A critical review on phytochemical profile and health promoting effects of mung bean (Vigna radiata). Food Sci. Hum. Wellness 2018, 7, 11–33.
6. Granato, D.; Nunes, D. S.; Barba, F. J. An integrated strategy between food chemistry, biology, nutrition, pharmacology, and statistics in the development of functional foods: A proposal. Trends Food Sci. Technol. 2017, 62, 13–22.
7. Granato, D.; Barba, F. J.; Bursać Kovacević, D.; Lorenzo, J. M.; Cruz, A. G.; Putnik, P. Functional foods: Product development, technological trends, efficacy testing, and safety. Annu. Rev. Food Sci. Technol. 2020, 11, 93–118.
8. Ucak, I.; Afreen, M.; Montesano, D.; Carrillo, C.; Tomasevic, I.; Simal-Gandara, J.; Barba, F. J. Functional and bioactive properties of peptides derived from marine side streams. Mar. Drugs 2021, 19.
9. Agrawal, H.; Joshi, R.; Gupta, M. Purification, identification and characterization of two novel antioxidant peptides from finger millet (Eleusine coracana) protein hydrolysate. Food Res. Int. 2019, 120, 697–707.
10. Ballatore, M. B.; Bettiol, M. del R.; Vanden Braber, N. L.; Aminahuel, C. A.; Rossi, Y. E.; Petroselli, G.; Erra-Balsells, R.; Cavaglieri, L. R.; Montenegro, M. A. Antioxidant and cytoprotective effect of peptides produced by hydrolysis of whey protein concentrate with trypsin. Food Chem. 2020, 319, 126472.
11. Lorenzo, J. M.; Munekata, P. E. S.; Gómez, B.; Barba, F. J.; Mora, L.; Pérez-Santaescolástica, C.; Toldrá, F. Bioactive peptides as natural antioxidants in food products – A review. Trends Food Sci. Technol. 2018, 79, 136–147.

12. Chen, S.; Yang, Q.; Chen, X.; Tian, Y.; Liu, Z.; Wang, S. Bioactive peptides derived from crimson snapper and in vivo anti-aging effects on fat diet-induced high fat Drosophila melanogaster. Food Funct. 2020, 11, 524–533.
13. Wu, R.; Wu, C.; Liu, D.; Yang, X.; Huang, J.; Zhang, J.; Liao, B.; He, H. Antioxidant and anti-freezing peptides from salmon collagen hydrolysate prepared by bacterial extracellular protease. Food Chem. 2018, 248, 346–352.
14. Axarlis, K.; Daskalaki, M. G.; Michailidou, S.; Androulaki, N.; Tsoureki, A.; Mouchtaropoulou, E.; Kolliniati, O.; Lapi, I.; Dermitzaki, E.; Venihaki, M.; Kousoulaki, K.; Argiriou, A.; Marsni, Z. E.; Tsatsanis, C. Diet supplementation with fish-derived extracts suppresses diabetes and modulates intestinal microbiome in a murine model of diet-induced obesity. Mar. Drugs 2021, 19.
15. Daskalaki, M. G.; Axarlis, K.; Aspevik, T.; Orfanakis, M.; Kolliniati, O.; Lapi, I.; Tzardi, M.; Dermitzaki, E.; Venihaki, M.; Kousoulaki, K.; Tsatsanis, C. Fish side stream-derived protein hydrolysates suppress DSS-induced colitis by modulating intestinal inflammation in mice. Mar. Drugs 2021, 19.
16. Aspevik, T.; Oterhals, Å.; Rønning, S. B.; Altintzoglou, T.; Wubshet, S. G.; Gildberg, A.; Afseth, N. K.; Whitaker, R. D.; Lindberg, D. Valorization of proteins from co- and by-products from the fish and meat industry. Chem. Chem. Technol. Waste Valorization 2017, 123–150.
17. Liu, Z.; Li, Y.; Song, H.; He, J.; Li, G.; Zheng, Y.; Li, B. Collagen peptides promote photoaging skin cell repair by activating the TGF-β/Smad pathway and depressing collagen degradation. Food Funct. 2019, 10, 6121–6134.
18. Gu, L.; Shan, T.; Ma, Y.; Tay, F. R.; Niu, L. Novel Biomedical Applications of Crosslinked Collagen. Trends Biotechnol. 2019, 37, 464–491.
19. Chi, C.-F.; Cao, Z.-H.; Wang, B.; Hu, F.-Y.; Li, Z.-R.; Zhang, B. Antioxidant and functional properties of collagen hydrolysates from Spanish mackerel skin as influenced by average molecular weight. Molecules 2014, 19, 11211–11230.
20. Lee, E. J.; Hur, J.; Ham, S. A.; Jo, Y.; Lee, S.; Choi, M.-J.; Seo, H. G. Fish collagen peptide inhibits the adipogenic differentiation of preadipocytes and ameliorates obesity in high fat diet-fed mice. Int. J. Biol. Macromol. 2017, 104, 281–286.
21. Felician, F. F.; Yu, R.-H.; Li, M.-Z.; Li, C.-J.; Chen, H.-Q.; Jiang, Y.; Tang, T.; Qi, W.-Y.; Xu, H.-M. The wound healing potential of collagen peptides derived from the jellyfish Rhopilema esculentum. Chinese J. Traumatol. 2019, 22, 12–20.
22. Park, S. H.; Jo, Y.-J. Static hydrothermal processing and fractionation for production of a collagen peptide with anti-oxidative and anti-aging properties. Process Biochem. 2019, 83, 176–182.
23. Jin, J.-E.; Ahn, C.-B.; Je, J.-Y. Purification and characterization of antioxidant peptides from enzymatically hydrolyzed ark shell (Scapharca subcrenata). Process Biochem. 2018, 72, 170–176.
24. Sila, A.; Bougatef, A. Antioxidant peptides from marine by-products: Isolation, identification and application in food systems. A review. J. Funct. Foods 2016, 21, 10–26.

25. Zhao, W.-H.; Chi, C.-F.; Zhao, Y.-Q.; Wang, B. Preparation, physicochemical and antioxidant properties of acid-and pepsin-soluble collagens from the swim bladders of miiuy croaker (Miichthys miiuy). Mar. Drugs 2018, 16, 161.
26. Wong, F.-C.; Xiao, J.; Ong, M. G.-L.; Pang, M.-J.; Wong, S.-J.; Teh, L.-K.; Chai, T.-T. Identification and characterization of antioxidant peptides from hydrolysate of blue-spotted stingray and their stability against thermal, pH and simulated gastrointestinal digestion treatments. Food Chem. 2019, 271, 614–622.
27. Yarnpakdee, S.; Benjakul, S.; Kristinsson, H. G.; Maqsood, S. Effect of pretreatment on lipid oxidation and fishy odour development in protein hydrolysates from the muscle of Indian mackerel. Food Chem. 2012, 135, 2474–2482.
28. Sheriff, S. A.; Sundaram, B.; Ramamoorthy, B.; Ponnusamy, P. Synthesis and in vitro antioxidant functions of protein hydrolysate from backbones of Rastrelliger kanagurta by proteolytic enzymes. Saudi J. Biol. Sci. 2014, 21, 19–26.
29. Sampath Kumar, N. S.; Nazeer, R. A.; Jaiganesh, R. Purification and biochemical characterization of antioxidant peptide from horse mackerel (Magalaspis cordyla) viscera protein. Peptides 2011, 32, 1496–1501.
30. Wang, B.; Xie, N.; Li, B. Charge properties of peptides derived from casein affect their bioavailability and cytoprotection against H2O2-induced oxidative stress. J. Dairy Sci. 2016, 99, 2468–2479.
31. Abdelhedi, O.; Nasri, M. Basic and recent advances in marine antihypertensive peptides: Production, structure-activity relationship and bioavailability. Trends Food Sci. Technol. 2019, 88, 543–557.
32. Wang, L.; Wang, X.; Bai, F.; Fang, Y.; Wang, J.; Gao, R. The anti-skin-aging effect of oral administration of gelatin from the swim bladder of Amur sturgeon (Acipenser schrenckii). Food Funct. 2019, 10, 3890–3897.
33. Gómez, L. J.; Gómez, N. A.; Zapata, J. E.; López-García, G.; Cilla, A.; Alegría, A. Optimization of the red tilapia (Oreochromis spp.) viscera hydrolysis for obtaining iron-binding peptides and evaluation of in vitro iron bioavailability. Foods 2020, 9, 883.
34. Liao, W.; Chen, H.; Jin, W.; Yang, Z.; Cao, Y.; Miao, J. Three newly isolated calcium-chelating peptides from tilapia bone collagen hydrolysate enhance calcium absorption activity in intestinal Caco-2 Cells. J. Agric. Food Chem. 2020, 68, 2091–2098.
35. Yarnpakdee, S.; Benjakul, S.; Kristinsson, H. G.; Bakken, H. E. Preventive effect of Nile tilapia hydrolysate against oxidative damage of HepG2 cells and DNA mediated by H2O2 and AAPH. J. Food Sci. Technol. 2015, 52, 6194–6205.
36. Turco, L.; Catone, T.; Caloni, F.; Consiglio, E. Di; Testai, E.; Stammati, A. Caco-2/TC7 cell line characterization for intestinal absorption: How reliable is this in vitro model for the prediction of the oral dose fraction absorbed in human? Toxicol. Vitr. 2011, 25, 13–20.
37. Zucco, F.; Batto, A.-F.; Bises, G.; Chambaz, J.; Chiusolo, A.; Consalvo, R.; Cross, H.; Dal Negro, G.; de Angelis, I.; Fabre, G. An inter-laboratory study to evaluate

the effects of medium composition on the differentiation and barrier function of Caco-2 cell lines. Altern. to Lab. Anim. 2005, 33, 603–618.
38. Decastelli, L.; Lai, J.; Gramaglia, M.; Monaco, A.; Nachtmann, C.; Oldano, F.; Ruffier, M.; Sezian, A.; Bandirola, C. Aflatoxins occurrence in milk and feed in Northern Italy during 2004–2005. Food Control 2007, 18, 1263–1266.
39. Commission Regulation (EC) No 1881/2006 of 19 December 2006 setting maximum levels for certain contaminants in foodstuffs. Off J Eur Union 2006, 364.
40. Hashem, M. Isolation of mycotoxin-producing fungi from fishes growing in aquacultures. Res. J. Microbiol. 2011, 6, 862.
41. Pietsch, C.; Kersten, S.; Burkhardt-Holm, P.; Valenta, H.; Dänicke, S. Occurrence of deoxynivalenol and zearalenone in commercial fish feed: An initial study. Toxins (Basel). 2013, 5, 184–192.
42. Aspevik, T.; Thoresen, L.; Steinsholm, S.; Carlehög, M.; Kousoulaki, K. Sensory and chemical properties of protein hydrolysates based on mackerel (Scomber scombrus) and salmon (Salmo salar) side stream materials. J. Aquat. Food Prod. Technol. 2021, 1–12.
43. Ruiz, M.J.; Festila, L. E.; Fernández, M. Comparison of basal cytotoxicity of seven carbamates in CHO-K1 cells. Toxicol. Environ. Chem. 2006, 88, 345–354.
44. Ruiz-Leal, M.; George, S. An in vitro procedure for evaluation of early stage oxidative stress in an established fish cell line applied to investigation of PHAH and pesticide toxicity. Twelfth Int. Symp. Pollut. Responses Mar. Org. 2004, 58, 631–635.
45. Ferrer, E.; Juan-García, A.; Font, G.; Ruiz, M. J. Reactive oxygen species induced by beauvericin, patulin and zearalenone in CHO-K1 cells. Proc. Estiv 2008, 15th Int. Congr. Vitr. Toxicol. 25 to 28 Sept 2008 Stock. Sweden 2009, 23, 1504–1509.
46. Minekus, M.; Alminger, M.; Alvito, P.; Ballance, S.; Bohn, T.; Bourlieu, C.; Carriere, F.; Boutrou, R.; Corredig, M.; Dupont, D. A standardised static in vitro digestion method suitable for food–an international consensus. Food Funct. 2014, 5, 1113–1124.
47. Arcella, D.; Gergelova, P.; Innocenti, M. L.; Steinkellner, H. Human and animal dietary exposure to T-2 and HT-2 toxin. EFSA J. 2017, 15, e04972.
48. Taroncher, M.; Rodríguez-Carrasco, Y.; Ruiz, M.-J. T-2 toxin and its metabolites: Characterization, cytotoxic mechanisms and adaptive cellular response in human hepatocarcinoma (HepG2) cells. Food Chem. Toxicol. 2020, 145, 111654.
49. Thuanthong, M.; De Gobba, C.; Sirinupong, N.; Youravong, W.; Otte, J. Purification and characterization of angiotensin-converting enzyme-inhibitory peptides from Nile tilapia (Oreochromis niloticus) skin gelatine produced by an enzymatic membrane reactor. J. Funct. Foods 2017, 36, 243–254.
50. Poojary, M.; Barba, F.; Aliakbarian, B.; Donsì, F.; Pataro, G.; Dias, D.; Juliano, P. Innovative alternative technologies to extract carotenoids from microalgae and seaweeds. Mar. Drugs 2016, 14, 214.

51. Barba, F. J.; Grimi, N.; Vorobiev, E. Evaluating the potential of cell disruption technologies for green selective extraction of antioxidant compounds from Stevia rebaudiana Bertoni leaves. J. Food Eng. 2015, 149, 222–228.
52. Meiliana, A.; Wijaya, A. Hormesis in Health and Disease: Molecular Mechanisms. Indones. Biomed. J. 2020, 12, 288–303.
53. Rainey, N. E.; Moustapha, A.; Petit, P. X. Curcumin, a multifaceted hormetic agent, mediates an intricate crosstalk between mitochondrial turnover, autophagy, and apoptosis. Oxid. Med. Cell. Longev. 2020, 2020, 1–23.
54. Karbarz, M.; Mytych, J.; Solek, P.; Stawarczyk, K.; Tabecka-Lonczynska, A.; Koziorowski, M.; Luczaj, L. Cereal grass juice in wound healing: hormesis and cell-survival in normal fibroblasts, in contrast to toxic events in cancer cells. J. Physiol. Pharmacol. , 70(4). doi: 10.26402/jpp.2019.4.10.
55. Wiriyaphan, C.; Xiao, H.; Decker, E. A.; Yongsawatdigul, J. Chemical and cellular antioxidative properties of threadfin bream (Nemipterus spp.) surimi byproduct hydrolysates fractionated by ultrafiltration. Food Chem. 2015, 167, 7–15.
56. Gómez, L. J.; Gómez, N. A.; Zapata, J. E.; López-García, G.; Cilla, A.; Alegría, A. In-vitro antioxidant capacity and cytoprotective/cytotoxic effects upon Caco-2 cells of red tilapia (Oreochromis spp.) viscera hydrolysates. Food Res. Int. 2019, 120, 52–61.
57. Zhong, S.; Ma, C.; Lin, Y. C.; Luo, Y. Antioxidant properties of peptide fractions from silver carp (Hypophthalmichthys molitrix) processing by-product protein hydrolysates evaluated by electron spin resonance spectrometry. Food Chem. 2011, 126, 1636–1642.
58. Hu, X.-M.; Wang, Y.-M.; Zhao, Y.-Q.; Chi, C.-F.; Wang, B. Antioxidant peptides from the protein hydrolysate of monkfish (Lophius litulon) muscle: Purification, identification, and cytoprotective function on HepG2 cells damage by H2O2. Mar. Drugs 2020, 18, 153.
59. Zheng, J.; Tian, X.; Xu, B.; Yuan, F.; Gong, J.; Yang, Z. Collagen peptides from swim bladders of giant croaker (Nibea japonica) and their protective effects against H2O2-induced oxidative damage toward human umbilical vein endothelial cells. Mar. Drugs 2020, 18, 430.
60. Yang, F.; Jin, S.; Tang, Y. Marine collagen peptides promote cell proliferation of NIH-3T3 fibroblasts via NF-κB signaling pathway. Molecules 2019, 24, 4201.
61. Muinde, K. B.; Donglu, F.; Zhao, L.; Qiuhui, H. Agaricus bisporus peptide fractions confer cytoprotective ability against hydrogen peroxide-induced oxidative stress in HepG2 and Caco-2 cells. J. Food Meas. Charact. 2020, 14, 2503–2519.
62. Benzie, I. F. F.; Choi, S.-W. Chapter One - Antioxidants in food: Content, measurement, significance, action, cautions, caveats, and research needs. In Advances in Food and Nutrition Research; Henry, J., Ed.; Academic Press, 2014; Vol. 71, pp. 1–53.
63. Pisoschi, A. M.; Pop, A. The role of antioxidants in the chemistry of oxidative stress: A review. Eur. J. Med. Chem. 2015, 97, 55–74.

64. Qiu, W.; Chen, X.; Tian, Y.; Wu, D.; Du, M.; Wang, S. Protection against oxidative stress and anti-aging effect in Drosophila of royal jelly-collagen peptide. Food Chem. Toxicol. 2020, 135, 110881.
65. Li, Y.; Li, J.; Lin, S.-J.; Yang, Z.-S.; Jin, H.-X. Preparation of antioxidant peptide by microwave-assisted hydrolysis of collagen and its protective effect against H2O2-induced damage of RAW264. 7 Cells. Mar. Drugs 2019, 17, 642.
66. Ngo, D.-H.; Qian, Z.-J.; Ryu, B.; Park, J. W.; Kim, S.-K. In vitro antioxidant activity of a peptide isolated from Nile tilapia (Oreochromis niloticus) scale gelatin in free radical-mediated oxidative systems. J. Funct. Foods 2010, 2, 107–117.
67. Hong, H.; Fan, H.; Chalamaiah, M.; Wu, J. Preparation of low-molecular-weight, collagen hydrolysates (peptides): Current progress, challenges, and future perspectives. Food Chem. 2019, 301, 125222.
68. Wang, W.-Y.; Zhao, Y.-Q.; Zhao, G.-X.; Chi, C.-F.; Wang, B. Antioxidant peptides from collagen hydrolysate of redlip croaker (Pseudosciaena polyactis) scales: Preparation, characterization, and cytoprotective effects on H2O2-damaged HepG2 cells. Mar. Drugs 2020, 18, 156.
69. Cai, S.-Y.; Wang, Y.-M.; Zhao, Y.-Q.; Chi, C.-F.; Wang, B. Cytoprotective effect of antioxidant pentapeptides from the protein hydrolysate of swim bladders of miiuy croaker (Miichthys miiuy) against H2O2-mediated human umbilical vein endothelial cell (HUVEC) injury. Int. J. Mol. Sci. 2019, 20, 5425.
70. Erak, M.; Bellmann-Sickert, K.; Els-Heindl, S.; Beck-Sickinger, A. G. Peptide chemistry toolbox–Transforming natural peptides into peptide therapeutics. Bioorg. Med. Chem. 2018, 26, 2759–2765.
71. Matejova, I.; Svobodova, Z.; Vakula, J.; Mares, J.; Modra, H. Impact of mycotoxins on aquaculture fish species: A review. J. world Aquac. Soc. 2017, 48, 186–200.
72. Mahmoud, A. F.; Escrivá, L.; Rodríguez-Carrasco, Y.; Moltó, J. C.; Berrada, H. Determination of trichothecenes in chicken liver using gas chromatography coupled with triple-quadrupole mass spectrometry. LWT 2018, 93, 237–242.
73. Rodríguez-Carrasco, Y.; Izzo, L.; Gaspari, A.; Graziani, G.; Mañes, J.; Ritieni, A. Simultaneous determination of AFB1 and AFM1 in milk samples by ultra high performance liquid chromatography coupled to quadrupole orbitrap mass spectrometry. Beverages 2018, 4, 43.
74. Adegbeye, M. J.; Reddy, P. R. K.; Chilaka, C. A.; Balogun, O. B.; Elghandour, M. M.; Rivas-Caceres, R. R.; Salem, A. Z. Mycotoxin toxicity and residue in animal products: Prevalence, consumer exposure and reduction strategies–A review. Toxicon 2020, 177, 96–108.
75. Tolosa, J.; Barba, F. J.; Pallarés, N.; Ferrer, E. Mycotoxin Identification and In Silico Toxicity Assessment Prediction in Atlantic Salmon. Mar. Drugs 2020, 18, 629.
76. Tolosa, J.; Font, G.; Mañes, J.; Ferrer, E. Natural occurrence of emerging Fusarium mycotoxins in feed and fish from aquaculture. J. Agric. Food Chem. 2014, 62.
77. Tolosa, J.; Barba, F. J.; Font, G.; Ferrer, E. Mycotoxin incidence in some fish products: QuEChERS methodology and liquid chromatography linear ion trap tandem mass spectrometry approach. Molecules 2019, 24.

78. Nogueira, W. V.; de Oliveira, F. K.; Marimón Sibaja, K. V.; Garcia, S. de O.; Kupski, L.; de Souza, M. M.; Tesser, M. B.; Garda-Buffon, J. Occurrence and bioacessibility of mycotoxins in fish feed. Food Addit. Contam. Part B 2020, 13, 244–251.
79. Meucci, V.; Armani, A.; Tinacci, L.; Guardone, L.; Battaglia, F.; Intorre, L. Natural occurrence of ochratoxin A (OTA) in edible and not edible tissue of farmed gilthead seabream (Sparus aurata) and European seabass (Dicentrarchus labrax) sold on the Italian market. Food Control 2020, 120, 107537.
80. Rodríguez-Carrasco, Y.; Heilos, D.; Richter, L.; Süssmuth, R. D.; Heffeter, P.; Sulyok, M.; Kenner, L.; Berger, W.; Dornetshuber-Fleiss, R. Mouse tissue distribution and persistence of the food-born fusariotoxins Enniatin B and Beauvericin. Toxicol. Lett. 2016, 247, 35–44.
81. Krug, I.; Behrens, M.; Esselen, M.; Humpf, H.-U. Transport of enniatin B and enniatin B1 across the blood-brain barrier and hints for neurotoxic effects in cerebral cells. PLoS One 2018, 13, e0197406.

Toxicology, 501 (2024), 153712

https://doi.org/10.1016/j.tox.2023.153712

3.8. Assessment of the genotoxic and mutagenic effects induced by T-2 mycotoxin in HepG2 cells

Mercedes Taroncher [a], Cristina Fuentes [a,b,1], Yelko Rodríguez-Carrasco [a] and María-José Ruiz [a]

[a] Research group in Alternative methods for determining toxic effects and risk assessment of contaminants and mixtures (RiskTox). Laboratory of Food Chemistry and Toxicology, Faculty of Pharmacy and Food Sciences, Universitat de València, Av. Vicent Andrés Estellés s/n, 46100 Burjassot, València, Spain

[b] Department of Food Technology, Universitat Politècnica de València. Camino de Vera s/n, 46022, València, Spain

Abstract

The T-2 toxin is a mycotoxin produced by molds belonging to *Fusarium*. Among the *Fusarium* mycotoxins, trichothecenes are frequently reported in food and feed, being the T-2 toxin (T-2) the mycotoxin which possesses the highest toxicity. According to EFSA, T-2 is found in various cereal grains used in food and feed products, mainly in oats, and it has a high environmental impact due to its mechanisms of toxicity. However, recent information on its genotoxic and mutagenic effects is lacking. This work aimed to evaluate the genotoxic and mutagenic potential of T-2 *in vitro*. For this purpose, HepG2 cells were exposed to 15, 30, and 60 nM T-2 for 24 h, then the DNA damage was evaluated by the micronucleus and the comet assays. In addition, point mutation analysis was performed by the bacterial reverse mutation test using 0.15-60 nM of T-2 concentrations. The results showed chromosomal damage at 60 nM T-2 since significantly more MN appeared at this concentration than in the control samples. Regarding the comet assay, DNA double helix breaks appeared at all concentrations tested and, in a concentration-dependent manner. However, no mutagenic effects were observed at any of the concentrations tested for the *Salmonella typhimurium* (*S. typhimurium*) strains TA98, TA100, TA1535, TA1537, or the *Escherichia coli* (*E. coli*) WP2 strain in the absence or presence of a metabolic activation system. Therefore, these results showed that T-2 mycotoxin produced

genotoxic effects by MN and comet assay, while no mutagenicity was observed. However, further research simulating different metabolic activation pathways and the combined exposure of this mycotoxin with other mutagenic chemicals that could be present in the diet is necessary to discard the mutagenic potential of T-2 fully. These results highlight the carcinogenic potential and danger associated with T-2 exposure and should be considered to prevent associated food risks for the human population.

Key words: HepG2 cells, micronucleus, comet assay, mutagenicity, genotoxicity

---

[1] **Corresponding author**: Cristina Fuentes. Department of Food Technology, Universitat Politècnica de València. Camino de Vera s/n, 46022, València, Spain. crifuelp@upvnet.upv.es

Abbreviations

2-AA, 2-aminoanthracene; 9-AC, 9-aminoacridine; 2-NF, 2-Nitrofluorene; AFB1, Aflatoxin B1; BEA, Beauvericin; CECT, Spanish Collection of Culture Strains; CRL, control; DMEM, Dulbecco´s Modified Eagle´s Medium; DMSO, Dimethyl sulfoxide; DON, Deoxynivalenol; EDTA, Ethylenediaminetetraacetic acid; EFSA, European Food Safety Agency; EMA, nucleic acid dye A; EtOH, ethanol; IARC, International Agency for Research on Cancer; IC_{50}, Mean inhibition concentration; LMA, Low Melting point Agarose; MeOH, methanol; MN, micronucleus; MTT, methylthiazol tetrazolium salt; NADP, Nicotinamide Adenine Dinucleotide Phosphate; NaN3, sodium azide; NBCS, Newborn Calf Serum; OECD, Organisation for Economic Cooperation and Development; OTA, Ochratoxin A; PBS, Phosphate Buffered Saline; PI, Propidium Iodide; RNase A, ribonuclease A; S9, metabolic activation system fraction; SEM, Standard Error of the Mean; Trp, tryptophan.

1. Introduction

The increasing incidence of cancer is a public health concern and may be attributed to changes in the environment and lifestyle exposures, including diet (Lécuyer et al., 2022). During the last decades, several investigations have been carried out to study how the whole diet may cause point mutations, thus, increasing the risk of developing cancer (Agudo et al., 2018; Shivappa et al., 2014; Van Woudenbergh et al., 2013). Several dietary factors such as nitrites, coffee, tea, processed meat, or alcohol have been associated with cancer risk (IARC, 2023). Although the role of these factors in carcinogenesis is not clearly understood, evidence suggests that chronic diseases and carcinogenesis are promoted by inflammatory processes (Lécuyer et al., 2022; Mantovani et al., 2008). Some food contaminants, such as mycotoxins, to which we could be exposed through our daily diet have been classified by the International Agency for Research on Cancer (IARC) as carcinogenic. This is the case of aflatoxins that have been classified as carcinogenic to humans (Group 1) and fumonisin B1 and B2, fusarin C, and ochratoxin A (OTA), which have been classified as possibly carcinogenic to humans (Group 2B) (IARC, 2023).

The T-2 toxin (T-2) belongs to the large group of mycotoxins called trichothecenes, which represent the main group of *Fusarium* toxins, and the trichothecene that possesses the highest toxicity. The T-2 is mainly found in grain cereals (EFSA, 2011a). The T-2 may cause adverse effects at the cellular and organ levels, such as hepatotoxicity, neurotoxicity, immunodepression, and bone marrow injury (Dai et al., 2019). Regarding its carcinogenicity potential, the IARC classifies toxins derived from *Fusarium sporotrichioides*, including T-2, as "not classifiable as to its carcinogenicity to humans" (Group 3) due to the available data do not support an evaluation of sufficient evidence in experimental

animals or mechanistic studies (IARC, 2023). However, no recent information on *in vitro* mutagenic properties of T-2 has been published and no further conclusions have been formulated yet (EFSA, 2011a).

Considering that humans and animals could be continuously exposed to T-2 through diet, the analysis of the mutagenic and genotoxic potential of this mycotoxin results in great interest. According to the European Food Safety Agency (EFSA), a standard *in vitro* battery is recommended for the genotoxicity testing of food contaminants (EFSA, 2011b). This battery includes *in vitro* tests for detecting chromosomal aberrations, such as the micronucleus (MN) test (TG OECD 487) and the comet assay (TG OECD 489), together with a bacterial mutation assay for detecting gene mutations, such as the Ames test (TG OECD 471).

Microscopic chromatin fragments detached from the main cell nucleus, called micronuclei, are indicative of chromosome breakage or mitotic spindle failure. Exposure to genotoxic substances induces the formation of MN in interphase cells. In the MN test, dyes that bind to DNA through photoactivation are used in interphase cells that are analyzed microscopically for the presence of micronuclei (Jaksic et al., 2012). Similarly, the comet assay is a sensitive method to assess DNA damage in single cells. This method determines the frequency of DNA breakage by measuring the electrophoretic migration of DNA from nucleoids obtained after cell lysis in a thin layer of agarose (Afanasieva et al., 2018). In contrast to the MN test and the comet assay, which are both tests for genotoxicity testing, the bacterial reverse mutation assay is a mutagenicity test that allows the detection of point mutations using different bacterial strains of *Salmonella typhimurium* and/or *Escherichia coli* (Mortelmans and Zeiger, 2000). This assay detects late DNA lesions, such as mutations, which are the result of a

balance between induced DNA damage and DNA repair. However, unlike the comet assay that determines premutagenic lesions, providing very important information on the mechanism of action of chemical compounds; the bacterial reverse mutation assay does not provide information on the mechanism of action of the compounds, which is crucial for a correct characterization of risk assessment (Hansen et al., 2009). Importantly, many chemicals are biologically inactive unless they are biotransformed to more reactive intermediate metabolites. Cytochromes P450 is a superfamily of cysteine thiolate-ligated heme-containing monooxygenase enzymes that catalyze the oxidation and metabolism of a large number of xenobiotics and endogenous compounds. Cytochrome P450 enzymes are mainly present in liver cells and also to a lesser extent in other parts of the body such as the lung and kidney cells (Cook et al., 2016). Since the bacterial reverse mutation assay employs prokaryotic cells, it requires the addition of an exogenous metabolic activation system that contains the necessary enzymes for biotransformation and mimics mammalian *in vivo* conditions (Tejs, 2008).

Some studies have evaluated the genotoxicity by the MN and comet assays after mycotoxin exposure in different cell lines (Horvatovich et al., 2013; Rakkestad et al., 2010; Zhang et al., 2017). However, in human hepatocarcinoma (HepG2) cells, there is no literature regarding the evaluation of the genotoxicity of T-2. Accordingly, the objective of this study was to evaluate the *in vitro* genotoxicity and mutagenic potential of T-2 mycotoxin. For this purpose, we developed an *in vitro* genotoxicity strategy, according to EFSA recommendations, in which we integrated validated assays that detect different premutagenic DNA lesions in HepG2 cells (comet assay and MN determination), and point mutations in five selected bacterial strains (bacterial

reverse mutation assay). The HepG2 cells were selected because the liver is the main T-2 metabolizing organ, but also because the liver is the main target organ for T-2. The mutagenic effect of T-2 in the different bacterial strains was performed in the presence and absence of a commercial cofactor-supplemented post-mitochondrial fraction (S9) prepared from rodent livers, according to OECD guidelines. The S9 fraction is responsible for carrying out the T-2 metabolization, in case it occurs via CYP450.

2. Materials and methods

2.1. Reagents, Media, and Test Strains

The reagent grade chemicals and cell culture compounds used, namely Dulbecco´s Modified Eagle´s Medium (DMEM), penicillin, streptomycin, trypsin/EDTA solutions, Phosphate Buffered Saline (PBS), newborn calf serum (NBCS), dimethyl sulfoxide (DMSO), agarose, low melting temperature agarose (LMA), disodium ethylenediaminetetraacetate dihydrate (Na_2-EDTA), sodium dihydrogen phosphate (NaH_2PO_4), disodium hydrogen phosphate (Na_2HPO_4), ribonuclease A (RNase), paraformaldehyde, histidine, biotin, tryptophan, D-glucose 6-phosphate, nicotinamide adenine dinucleotide phosphate (NADP), 2-aminoanthracene (2-AA), mitomycin C, sodium azide (NaN_3), 2-nitrofluorene (2-NF), 9-aminoacridine (9-AC), Nutrient Broth No. 2, KCl and $MgCl_2$, were acquired from Sigma-Aldrich (St. Louis, MO, USA). Methanol (MeOH), ethanol (EtOH), sodium chloride (NaCl), propidium iodide (PI), and sodium hydroxide (NaOH) were purchased from Merck Life Science S.L. (Madrid, Spain). The Litron *In Vitro* Microflow Kit for the MN assay by flow cytometry was purchased from Litron Laboratories (Litron Laboratories, Rochester, NY). Rat liver (Sprague Dawley) S9 fraction was acquired from Fisher Scientific

(Waltham, MA, USA). Tryptone Soy Agar and bacteriological agar were purchased from Scharlab (Barcelona, Spain). The S9 mix for the bacterial reverse mutation assay consisted of 100 mM phosphate buffer (pH 7.4), 4 mM NADP, 5 mM D-glucose-6-phosphate, 33 mM KCl, 8 mM $MgCl_2$ and 10% (v/v) S9 liver fraction. Deionized water (resistivity < 18 MΩ cm) was obtained using a Milli-Q water purification system (Millipore, Bedford, MA, USA).

The standard of T-2 (MW: 466.52 g/mol) was purchased from Sigma-Aldrich (St. Louis, MO, USA). Stock solutions of the mycotoxin were prepared in MeOH at the appropriate working solution and maintained in the darkness at -20 ºC.

The *Salmonella typhimurium* strains TA98, TA100, TA1535, and TA1537, and *Escherichia coli* WP2 were supplied by the Spanish Collection of Culture Strains (CECT, Valencia, Spain).

2.2 Cell culture and treatment

The HepG2 cells (ATCC: HB-8065) were cultured in DMEM medium supplemented with 10% NBCS, 100 U/mL penicillin, and 100 mg/mL streptomycin. The incubation conditions were pH 7.4, 5% CO_2 at 37 ºC, and 95% air atmosphere at constant humidity. The HepG2 cells were subcultured after trypsinization in a 1:3 split ratio twice a week. The T-2 concentrations selected in the present study were IC_{50} (60 nM), $IC_{50}/2$ (30 nM), and $IC_{50}/4$ (15 nM). The IC_{50} value was obtained according to previous assays carried out after 24 h of T-2 exposure in HepG2 cells by the tetrazolium salt (MTT) (Taroncher et al., 2020). Final mycotoxin concentrations tested were achieved by adding T-2 mycotoxin to the culture medium with a final MeOH concentration ≤ 1%

(v/v). Appropriate controls containing the same quantity of solvents were included in each experiment.

2.3. Alkaline Comet assay

The DNA strand break induction was determined by alkaline comet assay (pH > 13), as described by Mallebrera et al. (2016). Briefly, HepG2 cells were seeded in six-well plates. Once the cells reached 80% confluence, cells were exposed to 15, 30, and 60 nM T-2 for 24 h. Then, cells were suspended in LMA (1% PBS, 37 ºC), and 70 μL of the suspension were transferred to agarose pre-coated slides (1% H_2O) and covered with a coverslip (24 x 24 cm). After gelling for 10 min at 4 ºC, the coverslip was gently removed and the slides were immersed in lysis solution for at least 1 h at 4 ºC in the darkness. After lysis, the slides were covered by electrophoresis buffer for 40 min at room temperature to allow the DNA to unroll. Electrophoresis was run in the same solution for 20 min at 1 V/cm and 300 mA. When an electric field was applied, intact DNA strands remained in the head, while the broken pieces of DNA migrated toward the anode forming a typical comet tail. After electrophoresis, the slides were dried in 96% EtOH (-20 ºC, 5 min) and left to dry completely at room temperature overnight. Cells were stained with 500 μL of PI (20 μg/mL) and analyzed using a Leica DM-4500B microscope (Leica Microsystems, Wetzlar, Germany) at 20x magnification. Two slides were prepared for each treatment condition and three independent replicates were performed. Fifty randomly selected individual cells per slide were analyzed by using Comet Assay Software Project Lab (CaspLab) 1.2.3b1 version. The results were expressed in terms of three comet assay parameters, namely the percentage of DNA in the tail (% tail DNA), tail length, and olive tail moment.

2.4. Micronucleus assay

Micronucleus assay was carried out using the Litron *In Vitro* Microflow kit (Litron Laboratories, Rochester, NY). This assay should be performed by exposing logarithmically dividing cells to the toxicant for 1.5-2 normal cell cycles. At this time, cells must be harvested and processed for MN scoring. The assay was performed according to the manufacturer´s instructions based on previous reports (Bryce et al., 2008). Briefly, $47.2x10^4$ cells/well were seeded in six-well plates and exposed to 15, 30, and 60 nM T-2 for 48 h, which is equal to 1.5-2 doubling times for this cell line. On the day of the experiment, cells were stained with the nucleic acid dye A (EMA) solution and placed on the ice near a light source for 30 min, to induce its photoactivation. The EMA fluorochrome dye is a reagent that crosses the compromised outer membrane of apoptotic and necrotic cells and binds to DNA through photoactivation. Then, cells were washed, lysed with the Litron Lysis kit solution, and preserved from light for 60 min. During the lysis step, cytoplasmic membranes were digested to liberate nuclei and MN. Finally, a lysis solution containing SYTOX fluorochrome, which labels all chromatin, was added and cells were incubated for 30 min at room temperature in darkness. The differential staining allows the distinction between healthy chromatin and dead/dying cells. Analysis was performed by using a BD FACSVerse (BD Biosciences, Franklin Lakes, NJ, USA) flow cytometry, following the instructions and templates provided by the Litron *In Vitro* Microflow Kit manual and as described by Bryce et al. (2008). Three independent experiments were performed. The results were expressed as a percentage of MN per 20,000 cells.

2.5. Bacterial reverse mutation assay

The mutagenic effect of T-2 mycotoxin was evaluated by the bacterial reverse mutation assay according to the preincubation method described by the Organisation for Economic Cooperation and Development (OECD) test guideline (TG) 471 (OECD, 2020). The tester strains utilized were *S. typhimurium* TA98, TA100, TA1535 and TA1537, and *E. coli* WP2. A total of 7 concentrations of T-2 toxin were analyzed (from 0.15 to 60 nM). Preliminary experiments with each strain were performed to confirm that the T-2 mycotoxin concentrations used in this study were not toxic for the bacteria. The test was conducted in the absence, or presence, of a metabolic activation system derived from a rat liver extract (S9 fraction). In the experiments, the bacterial cultures were grown in 20 mL of Nutrient Broth nº 2 for 10–12 h at 37 °C to an approximate density of 10^9 cells/mL. Then, 100 μL of the tester strains were mixed with 100 μL of each concentration of the test solution and 500 μL of buffer or S9 mix, and preincubated at 37 °C for 20 min. After the incubation period, 2 mL of melted top agar containing 0.05 mM of biotin/histidine or tryptophan was added, and the entire mixture was rapidly poured onto minimal agar plates. The plates were incubated at 37 °C for 72 h and then the number of the revertant colonies were counted. Negative (1% DMSO) and positive mutagenesis controls were included in each experiment. In the absence of S9 fraction, positive controls were 1 μg/plate 2-NF for TA98, 1 μg/plate NaN_3 for TA100 and TA1535, 50 μg/plate 9-aminoacridine for TA1537, and 1 μg/plate mitomycin C for *E. coli* WP2. For the metabolic activation experiments, 2.5 and 20 μg/plate 2-AA were used for *S. typhimurium* strains and *E. coli* WP2, respectively. Three replicate plates were performed in each treatment condition. Results were expressed as the mean number of revertants per plate. According

to this assay, a substance is considered mutagenic if the number of mean revertant colonies at two consecutive concentrations is at least two-fold higher than the number of revertants in the corresponding negative control (Dolan et al., 2021).

2.6. Statistical analysis

Data were expressed as mean ± SEM of different independent experiments. The statistical analysis of the results was performed by Students t-test for paired samples. The difference level of $p \leq 0.05$ was considered statistically significant.

3. Results

3.1. Alkaline Comet assay

In this study, the DNA strand breakage was analyzed by the comet assay. The comet tails after the exposure of all T-2 concentrations tested (15, 30, and 60 nM) in HepG2 evidenced the DNA strand breakage (Figs. 1b-d). No comet tail was observed in the control group, indicating no DNA damage in cells not exposed to the mycotoxin (Fig. 1a).

For the T-2 concentrations tested, an increase in tail DNA %, tail length, and olive tail moment in a concentration-dependent manner was observed (Table 1). According to these results, the increase in tail DNA% ranged from 13.94 to 52.57%, for tail length from 9.98 to 80.83%, and for olive tail moment from 1.90 to 23.22%.

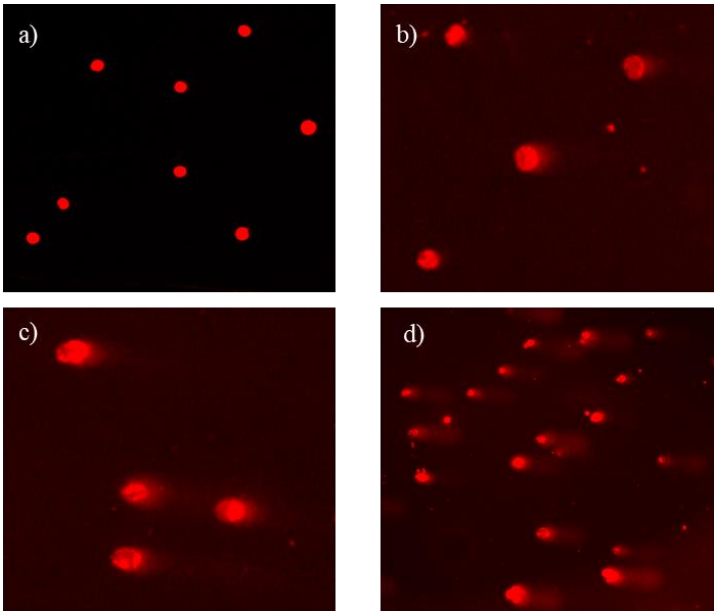

Figure 1. Effects of T-2 on DNA damage in HepG2 cells measured by alkaline comet assay. The cells were treated with 0 (control) (a), 15 (b), 30 (c), and 60 (d) nM T-2 for 24 h. Cells were observed under a fluorescent microscope with 20x magnification and quantified.

3.2. Micronucleus assay

Figure 2 shows the MN detected in HepG2 cells after T-2 exposure for 48 h. The results demonstrated that only at 60 nM T-2, a significant increase in MN (12.1 ± 1.2 %) was produced, compared to the control (6.9 ± 0.9 %). So, T-2 exhibits genotoxicity at the highest concentration tested in HepG2 cells.

Table 1. The tail DNA %, tail length, and olive tail moment in HepG2 cells exposed to 15, 30, and 60 nM T-2 for 24 h. Data represent the mean ± SEM. (*) $p \leq 0.05$ indicates a significant difference compared to the control.

Samples	Tail DNA (%)	Tail length	Olive tail moment
Control	3.74 ± 3.21	4.27 ± 1.21	0.53 ± 0.44
15 nM T-2	13.94 ± 7.98*	9.98 ± 3.46*	1.90 ± 1.05*
30 nM T-2	19.52 ± 7.33*	30.91 ± 14.38*	5.14 ± 3.85*
60 nM T-2	52.57 ± 12.08*	80.83 ± 19.94*	23.22 ± 9.36*

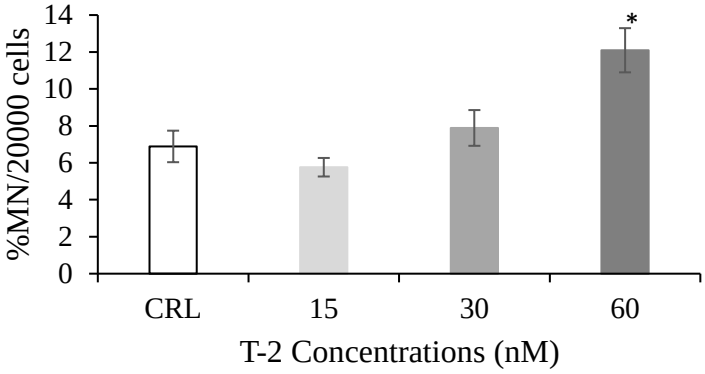

Figure 2. Genotoxicity assessment by micronucleus assay in HepG2 cells exposed to 15, 30, and 60 nM T-2 for 48h. Data are expressed as a percentage of MN per 20,000 cells ± SEM (n=3). (*) $p \leq 0.05$ indicates a significant difference compared to the control (CRL).

3.3. Bacterial reverse mutation assay

The results for the bacterial reverse mutation assay in the five selected bacterial strains after T-2 exposure are shown in Table 2. The different positive controls used in the absence or presence of the S9 fraction significantly increased the mutant frequencies for all the strains over the negative controls, indicating that experimental conditions were correct. Moreover, the mutant frequencies in the positive and negative controls were similar to those found in other studies in all the five strains used (Levy et al., 2019). As can be observed in Table 2, when bacteria were treated with the different T-2 concentrations, no significant differences were observed in the number of revertant colonies with those obtained in the negative controls for all the strains. Therefore, our results show that T-2 does not induce point mutations by base pair substitutions or frameshifts in either the genome of *S. typhimurium* or *E. coli* under the experimental conditions used. These results were observed in both, in the absence or presence of the S9 metabolic system, indicating that either T-2 or its metabolites do not induce a mutagenic response in the bacterial reverse mutation assay at the tested concentrations.

4. Discussion

The genotoxicity induced by T-2 is one mechanism of action that has not been widely understood yet. Moreover, there is scarce information about the effects produced by the T-2. Thus, more information would be useful to food safety agencies to facilitate the establishment of a more accurate T-2 concentration so that the population can be safely exposed.

Table 2. Results in the bacterial reverse mutation assay after the exposure of T-2 (0.15-60 nM) to *Salmonella typhimurium* and *Escherichia coli* WP2 strains, in the absence or presence of S9 fraction in the growth medium.

Concentration (nM)	TA98		TA100		TA1535		TA1537		WP2	
	-S9	+S9	-S9	+S9	-S9	+S9	-S9	+S9	-S9	+S9
0.15	34	34	118	104	24	31	9	8	18	18
0.3	29	32	127	116	34	30	10	8	14	18
1.5	30	33	121	122	28	29	9	6	14	18
3	30	32	125	124	30	30	7	5	16	8
15	35	29	146	98	26	28	10	7	12	20
30	26	32	117	125	34	28	7	7	12	12
60	28	22	124	118	33	28	7	6	10	12
Negative control[a]	30	32	118	112	34	30	8	6	14	15
Positive control	161[b]	1275[c]	799[d]	2827[c]	760[d]	158[c]	341[e]	170[c]	135[f]	40[c]

Values are the mean number of revertants per plate of three replicates. a: 1% DMSO; b: 2-Nitrofluorene (2-NF); c: 2-Aminoanthracene (2-AA); d: NaN_3; e: 9-aminoacridine (9-AC); f: mitomycin C.

The genotoxic effect of T-2 was evaluated by the comet and MN assays according to the methods described in TG OECD 489 and 487, respectively. Regarding the comet assay, our results showed that after 15, 30, and 60 nM T-2 exposure, DNA strand breakage was observed in a concentration-dependent manner. Similarly, Zingales et al. analyzed the genotoxic potential of sterigmatocystin produced by *Aspergillus* fungi in SH-SY5Y cells and reported increasing values of tail DNA %, tail length, and olive tail moment with increasing concentrations (IC_{50}, $IC_{50}/2$, and $IC_{50}/4$) of sterigmatocystin. However, they obtained lower values respect those obtained in this study regarding the tail DNA % (10.09% *vs* 52.57%), tail length (32.94% *vs* 80.83%), and olive tail moment (4.69% *vs* 23.22%) (Zingales et al., 2021). Mamur et al.

reported that fusaric acid, which is a mycotoxin less toxic than T-2, induced comet tail intensity at 3.12 (7.18), 6.25 (6.40), and 12.50 (6.69) μg/mL in a concentration-dependent manner, respect to control (4.22) in isolated human lymphocytes after 1 h of exposure. Nevertheless, comet tail length was not affected (Mamur et al., 2020). Also, these authors described a significant increase in comet tail intensity at 0.14, 0.29, and 1.15 μM Enniatin A regarding the control after 1 h of exposure in isolated human lymphocytes (Mamur et al., 2018). On the other hand, significant DNA damage was detected by comet assay at 1 and 12 μM beauvericin (BEA) in CHO-K1 and Caco-2 cells after 24 h of exposure (Mallebrera et al., 2016; Prosperini et al., 2013). However, Takakura et al. studied the genotoxicity of deoxynivalenol (DON), the main type B trichothecene mycotoxin produced by *Fusarium* fungi, in TK6 and HepaRG cells; and they evidenced that this mycotoxin did not induce primary DNA damage by the comet assay (Takakura et al., 2014). In addition, the DNA damage observed in HepG2 cells after T-2 exposure may lead to genomic instability and the development of chronic alterations. Therefore, it is crucial to reach more mechanisms of genotoxicity. In our work, we decided to continue by evaluating the possible generation of MN after T-2 exposure, to gauge the severity of cell damage and to achieve a better understanding of the molecular mechanisms of toxicity at the cellular level.

Assessing MN is a useful tool to measure the rate of chromatin damage. The results that we obtained in this work at the concentrations tested, evidenced that only at the IC_{50} of T-2 an increase of MN was observed compared to the control. Limited literature about the induction of micronuclei produced by T-2 is available. Only Somoskői et al. investigated the genotoxic response of T-2 exposure in blastocysts of mouse embryos. These authors reported that 0.75

ng/mL (1.6 nM) T-2 increased MN up to 33.3% after 96 h of exposure (Somoskői et al., 2016). However, no significant differences were found between control and treated blastocysts at 0.5 ng/mL (1.1 nM) T-2 (Somoskői et al., 2018). The MN induction after exposure to other mycotoxins has been studied in different cell lines. Takakura et al. reported that a short treatment (3h) of 25 μM DON and other trichothecene from *Fusarium* genera with a similar mechanism of action to T-2, produced 9.8% more MN than the solvent control in human TK6 cells. Moreover, after 24 h of exposure, 3.2 μM DON produced an increase of up to 17.4% MN compared to the control (Takakura et al., 2014). Juan-García et al. evaluated the induction of MN by the main metabolite of DON, the 3-ADON, in HepG2 cells. These authors evidenced that 3 μM of 3-ADON produced an increase of 13.1% MN in HepG2 cells after 48 h of exposure compared to the control (Juan-García et al., 2018). Similarly, an increase of 14% of MN compared to the solvent was found after 0.5 μg/mL (637.8 nM) BEA exposure in PK15 cells (Klarić et al., 2008). On the other hand, Juan-García et al. showed that BEA and OTA caused a strong induction of MN at 1.25 and 25 μM, respectively, compared to control in HepG2 cells (Juan-García et al., 2019). Induced MN frequencies above the solvent control of citrinin (50 to 100 μM) and OTA (20 to 30 μM) were reported after 24 h in V79 cells (Föllmann et al., 2014). Regarding aflatoxin B1 (AFB1), one of the most toxic mycotoxins, Singto et al. reported that HepG2 treatment with 3 μg/mL (9.6 μM) of AFB1, significantly increased (1.8-fold respect to control) the number of micronucleated cells (Singto et al., 2020). Accordingly, Tadee et al. also showed that 5 μg/mL (16 μM) AFB1 induced genotoxicity in HepG2 cells increasing MN after 24 h of exposure (Tadee et al., 2020).

Undoubtedly, scientific research has demonstrated that a high proportion of MN is associated with apoptosis. In the last decade, important research has been carried out on apoptosis as one of the main mechanisms of action of this mycotoxin (Agrawal et al., 2015; Lei et al., 2017; Wu et al., 2019). Apoptosis could also be related to cell cycle arrest, especially when it is produced by a genotoxicant, to prevent the transmission of damaged genetic information and the promotion of DNA repair. Also, the apoptosis could be related to the generation of reactive oxygen species, or different signaling pathways, such as the MAP Kinase pathway (Wada and Penninger, 2004). Thus, it is necessary to continue studying this signaling pathway, such as the expression of C-Jun N-terminal kinase (JNK), ERK, or p38, to confirm whether this mycotoxin affects this path in hepatic cells and how it regulates the expression of apoptotic genes cell survival.

The mutagenic effect of T-2 was evaluated by the bacterial reverse mutation assay. This test is the most widely used method to assess the potential of chemical agents to produce gene mutations such as substitution, addition, or deletion of one or a few DNA base pairs (Press et al., 1983). The method is based on the ability of different strains of *S. typhimurium* and *E. coli* to reverse mutations in the histidine (his-) and tryptophan (trp-) operon genes in the presence of mutagenic agents, respectively.

Our results showed that T-2 exposure at the range of concentrations tested in this study does not produce point mutations in the absence or presence of the S9 metabolic system. The absence of mutagenicity of T-2 has been previously described on the *S. typhimurium* histidine-requiring strains TA 98, TA 100, TA 1535, TA 1537, and TA 1538 and *Saccharomyces cerevisiae* with and without metabolic activation system (EFSA, 2011a). In our study, an *E. coli* WP2

tryptophan-dependent strain was included. The use of this strain detects trp− to trp+ reversion at a site blocking a step in the biosynthesis of tryptophan before the formation of anthranilic acid. The target site for a specific back mutation consists of an ochre (UAA) nonsense mutation located in the trpE gene. This can be reverted to wild type by any type of base change (base pair substitution mutation, i.e., transversions and transitions) in the original alteration site or elsewhere in the chromosome, suppressing the original defect (Mortelmans and Zeiger, 2000). The use of *E. coli* WP2 allows the detection of certain oxidizing and cross-linking mutagens not observable by using the above-mentioned *S. typhimurium* strains (OECD, 2020). Our results confirmed that T-2 does not induce mutations according to these mechanisms at the concentrations tested, supporting the lack of mutagenic activity of this mycotoxin observed for S. *typhimurium* strains.

As previously mentioned, a rat liver S9 fraction was employed as a source of metabolic activation in this study. Liver S9 fraction is standardly used in mutagenic *in vitro* assays such as the bacterial reverse mutation assay. However, some mutagenic compounds may need another type of bioactivation since different metabolic transformations occur in the cells of different tissues (Jeong, 2017). Moreover, variability in genotoxic responses can occur due to differences in the metabolic fraction properties, including enzyme concentration, induction treatment or rat strain, and even production batches and suppliers (Brendt et al., 2021; Stott et al., 2004). Consequently, the inclusion of alternative *in vitro* metabolic activation systems in genotoxicity and carcinogenicity testing has been proposed (Ku et al., 2007). In this context, Alonso-Jauregui and colleagues performed the genotoxicity assessment of 12 mycotoxins, including the T-2, with the SOS/umu test, a method that shows a strong correlation with the

bacterial reverse mutation assay (Alonso-Jauregui et al., 2022). These authors compared the results obtained for each mycotoxin with a liver S9 fraction and an alternative S9 fraction from the kidneys. They found that T-2 displayed a negative mutagenic response without metabolic activation and with liver S9. However, in the presence of the kidney S9 activation system, a positive mutagenic response was observed in three out of four experiments at concentrations higher than 31 μg/mL, even if not a clear concentration–response was obtained in any of the experiments. The results obtained by these authors confirm that the organ used for the S9 fraction preparation influences the genotoxic activity of some mycotoxins, including the T-2. Moreover, the same authors, detected the presence of an epoxide alert in the common scaffold of trichothecenes such as T-2, by using the expert knowledge-based platform DEREK Nexus® (Alonso-Jauregui et al., 2022) which predicts a plausible mutagenicity and chromosomal damage *in vitro* and *in vivo*. Hence, this information suggests that further mutagenic studies employing different types of S9 fractions should be performed to discard the mutagenic potential of this mycotoxin.

Several mycotoxins, either from the same or from different fungal species, may occur simultaneously in feed and food products. For this reason, Smerák et al. (2001) studied the mutagenicity of the combination of selected trichothecenes such as T-2 and the well-known mutagen AFB1, using the Ames test on the strains TA98 and TA100. These authors found that 0.1, 0.25, and 1 μg/dish T-2 concentrations did not produce any mutagenic effect when administered alone. However, when bacteria were exposed to T-2 (0.1 μg/dish) in combination with AFB1, the mixture produced a significantly stronger mutagenic effect than AFB1 alone (Smerák et al., 2001). Similarly, Garofalo et al. (2023) studied the

capability of trichothecenes to increase the genotoxicity induced by various genotoxins in proliferating intestinal IEC-6 cells using DNA damage quantification by in-cell-western. The T-2 showed the strongest DNA damage exacerbation effect of all the trichothecenes studied, higher than diacetoxyscirpenol, nivalenol, fusarenon-X, and NX toxin. The authors reported that T-2 exacerbated the genotoxicity induced by the radiomimetic drug, phleomycin, which causes the oxidation of bases and strand breaks; the dietary fungicide captan that induces oxidative DNA damage and strand breaks; and colibactin, a bacterial genotoxin produced in the gut, that induces DNA inter-strand crosslinks. Thus, these results demonstrated that T-2 causes DNA damage exacerbating the phenotype of genotoxins with diverse mechanisms of action. In addition, the absence of a mutagenic response in the bacterial reverse mutation assay observed for T-2 in this study is consistent with the results previously reported by other authors. However, further research simulating different metabolic activation pathways and the combined exposure of this mycotoxin with other mutagenic chemicals that can be present in the diet is necessary, to prevent food risks to the human population.

5. Conclusion

This research analyzed the genotoxicity and mutagenicity potential of T-2 toxin *in vitro*. Our results suggest that this mycotoxin is genotoxic but not mutagenic based on the determination of DNA damage formation, single-stranded DNA breaks, MN formation, and non-growth of revertant bacterial colonies. These findings contribute to defining the toxicological profile of the mycotoxin by *in vitro* methods and should be considered for evaluating the impact of T-2 during risk assessment. Nonetheless, studies simulating different

metabolic activation pathways, chemical mixtures, and in vivo conditions should be performed to corroborate these results and confirm food safety.

CRediT Authorship Contribution Statement: Cristina Fuentes: Formal analysis, Research, Methodology, Writing – original draft. Mercedes Taroncher: Conceptualization, Formal analysis, Research, Methodology, Writing – original draft. María-José Ruiz: Conceptualization, Acquisition of financing, Resources, Supervision, Validation, Visualization, Writing – review and editing. Yelko Rodríguez-Carrasco: Supervision, Visualization, Writing – review and editing.

Declaration of competing interests: The authors declare that they have no known competing financial interests or personal relationships that could have appeared to influence the work reported in this paper.

Data availability: Data will be made available on request.

Acknowledgments: This work is part of a research project funded by the Spanish Ministry of Science and Innovation PID2020-115871RB-I00, MCIN/AEI/10.13039/501100011033. Mercedes Taroncher is grateful for the pre-doctoral grant PRE2021-096941 provided by the Spanish Ministry of Science and Innovation project. Cristina Fuentes was supported by a Margarita Salas Postdoctoral Fellowship from Universitat Politècnica de València funded by Ministerio de Universidades and the European Union-NextGeneration EU. Funding for open access charge: CRUEUniversitat Politècnica de València.

6. References

Afanasieva, K., & Sivolob, A. (2018). Physical principles and new applications of comet assay. Biophysical chemistry, 238, 1-7. https://doi.org/10.1016/j.bpc.2018.04.003

Agrawal, M., Bhaskar, A.S.B., Rao, P.V.L., 2015. Involvement of Mitogen-Activated Protein Kinase Pathway in T-2 Toxin-Induced Cell Cycle Alteration and Apoptosis in Human Neuroblastoma Cells. Mol. Neurobiol. 51, 1379–1394. https://doi.org/10.1007/s12035-014-8816-4

Agudo, A., Cayssials, V., Bonet, C., Tjønneland, A., Overvad, K., Boutron-Ruault, M.C., Affret, A., Fagherazzi, G., Katzke, V., Schübel, R., Trichopoulou, A., Karakatsani, A., La Vecchia, C., Palli, D., Grioni, S., Tumino, R., Ricceri, F., Panico, S., Bueno-De-Mesquita, B., Peeters, P.H., Weiderpass, E., Skeie, G., Nøst, T.H., Lasheras, C., Rodríguez-Barranco, M., Amiano, P., Chirlaque, M.D., Ardanaz, E., Ohlsson, B., Dias, J.A., Nilsson, L.M., Myte, R., Khaw, K.T., Perez-Cornago, A., Gunter, M., Huybrechts, I., Cross, A.J., Tsilidis, K., Riboli, E., Jakszyn, P., 2018. Inflammatory potential of the diet and risk of gastric cancer in the European Prospective

Investigation into Cancer and Nutrition (EPIC) study. Am. J. Clin. Nutr. 107, 607–616. https://doi.org/10.1093/ajcn/nqy002

Alonso-Jauregui, M., González-Peñas, E., López de Cerain, A., Vettorazzi, A., 2022. Genotoxicity of 12 Mycotoxins by the SOS/umu Test: Comparison of Liver and Kidney S9 Fraction. Toxins, 14 (6), 400. https://doi.org/10.3390/toxins14060400

Brendt, J., Lackmann, C., Heger, S., Velki, M., Crawford, S.E., Xiao, H., Thalmann, B., Schiwy, A., Hollert, H., 2021. Using a high-throughput method in the micronucleus assay to compare animal-free with rat-derived S9. Sci. Total Environ. 751,142269. https://doi.org/10.1016/j.scitotenv.2020.142269

Bryce, S.M., Avlasevich, S.L., Bemis, J.C., Lukamowicz, M., Elhajouji, A., Van Goethem, F., De Boeck, M., Beerens, D., Aerts, H., Van Gompel, J., Collins, J.E., Ellis, P.C., White, A.T., Lynch, A.M., Dertinger, S.D., 2008. Interlaboratory evaluation of a flow cytometric, high content in vitro micronucleus assay. Mutat. Res. Genet. Toxicol. Environ. Mutagen. 650, 181–195. https://doi.org/10.1016/j.mrgentox.2007.11.006

Cook, D.J., Finnigan, J.D., Cook, K., Black, G.W., Charnock, S.J., 2016. Cytochromes P450: History, Classes, Catalytic Mechanism, and Industrial Application, in Advances in Protein Chemistry and Structural Biology. Academic Press Inc., pp. 105–126. https://doi.org/10.1016/bs.apcsb.2016.07.003

Dai, C., Xiao, X., Sun, F., Zhang, Y., Hoyer, D., Shen, J., Tang, S., Velkov, T., 2019. T-2 toxin neurotoxicity: role of oxidative stress and mitochondrial dysfunction. Arch. Toxicol. 93, 3041-3056. https://doi.org/10.1007/s00204-019-02577-5

Dolan, L.C., Ciliutti, P., Bisini, L., Marabottini, C., Curtin, B., 2021. Genotoxicity evaluation of magnesium salts of isobutyrate and 2-methylbutyrate. Toxicol. Rep. 8, 1814–1818. https://doi.org/10.1016/j.toxrep.2021.10.012

EFSA. Scientific Opinion on the risks for animal and public health related to the presence of T-2 and HT-2 toxin in food and feed, 2011a. EFSA J. 9, 2481. https://doi.org/10.2903/j.efsa.2011.2481

EFSA. Scientific opinion on genotoxicity testing strategies applicable to food and feed safety assessment, 2011b. EFSA J. https://doi.org/10.2903/j.efsa.2011.2379

Föllmann, W., Behm, C., Degen, G.H., 2014. Toxicity of the mycotoxin citrinin and its metabolite dihydrocitrinone and of mixtures of citrinin and ochratoxin A in vitro. Arch. Toxicol. 88, 1097–1107. https://doi.org/10.1007/s00204-014-1216-8

Garofalo, M., Payros, D., Penary, M., Oswald, E., Nougayrède, J.P., Oswald, I.P., 2023. A novel toxic effect of foodborne trichothecenes: The exacerbation of genotoxicity. Environ. Pollut. 317,120625. https://doi.org/10.1016/j.envpol.2022.120625

Hansen, K., Mika, S., Schroeter, T., Sutter, A., Ter Laak, A., Steger-Hartmann, T., Heinrich, N. & Muller, K. R. (2009). Benchmark data set for in silico prediction of Ames mutagenicity. J. Chem. Inf. Model., 49(9), 2077-2081. https://doi.org/10.1021/ci900161g

Horvatovich, K., Hafner, D., Bodnár, Z., Berta, G., Hancz, C., Dutton, M., Kovács, M., 2013. Dose-related genotoxic effect of T-2 toxin measured by comet assay using

peripheral blood mononuclear cells of healthy pigs. Acta Vet. Hung. 61, 175–186. https://doi.org/10.1556/AVet.2013.010

IARC (2023). Monographs on the evaluation of carcinogenic risks to humans. International Agency for Research on Cancer, World Health Organization (16 September 2023) https://monographs.iarc.who.int/list-of-classifications

Jakšić, D., Puel, O., Canlet, C., Kopjar, N., Kosalec, I., & Klarić, M. Š. (2012). Cytotoxicity and genotoxicity of versicolorins and 5-methoxysterigmatocystin in A549 cells. Arch. Toxicol., 86, 1583-1591. https://doi.org/10.1007/s00204-012-0871-x

Jeong, T.C., 2017. Biotransformation of toxicants, in Lu's Basic Toxicology: Fundamentals, Target Organs, and Risk Assessment, Seventh Edition. https://doi.org/10.4324/9781315391700-4

Juan-García, A., Taroncher, M., Font, G., Ruiz, M.J., 2018. Micronucleus induction and cell cycle alterations produced by deoxynivalenol and its acetylated derivatives in individual and combined exposure on HepG2 cells. Food Chem. Toxicol. 118, 719–725. https://doi.org/10.1016/j.fct.2018.06.024

Juan-García, A., Tolosa, J., Juan, C., & Ruiz, M. J. (2019). Cytotoxicity, genotoxicity and disturbance of cell cycle in HepG2 cells exposed to OTA and BEA: single and combined actions. Toxins, 11(6), 341. https://doi.org/10.3390/toxins11060341

Klarić, Š., egvi Klari, M., Pepeljnjak, S., Rozgaj, and Rùica (2008) Genotoxicity of fumonisin B1, beauvericin and ochratoxin A in porcine kidney PK15 cells: effects of individual and combined treatment. Croat. Chem. Acta. 81 (1), 139-146.

Ku, W.W., Bigger, A., Brambilla, G., Glatt, H., Gocke, E., Guzzie, P.J., Hakura, A., Honma, M., Martus, H.J., Obach, R.S., Roberts, S., 2007. Strategy for genotoxicity testing-Metabolic considerations. Mutat. Res. Genet. Toxicol. Environ. Mutagen. 627, 59–77. https://doi.org/10.1016/j.mrgentox.2006.10.004

Lécuyer, L., Laouali, N., Dossus, L., Shivappa, N., Hébert, J.R., Agudo, A., Tjonneland, A., Halkjaer, J., Overvad, K., Katzke, V.A., Le Cornet, C., Schulze, M.B., Jannasch, F., Palli, D., Agnoli, C., Tumino, R., Dragna, L., Iannuzzo, G., Jensen, T.E., Brustad, M., Skeie, G., Zamora-Ros, R., Rodriguez-Barranco, M., Amiano, P., Chirlaque, M.D., Ardanaz, E., Almquist, M., Sonestedt, E., Sandström, M., Nilsson, L.M., Weiderpass, E., Huybrechts, I., Rinaldi, S., Boutron-Ruault, M.C., Truong, T., 2022. Inflammatory potential of the diet and association with risk of differentiated thyroid cancer in the European Prospective Investigation into Cancer and Nutrition (EPIC) cohort. Eur. J. Nutr. 61 (7), 625 – 3635. https://doi.org/10.1007/s00394-022-02897-w

Lei, Y., Guanghui, Z., Xi, W., Yingting, W., Xialu, L., Fangfang, Y., Goldring, M.B., Xiong, G., Lammi, M.J., 2017. Cellular responses to T-2 toxin and/or deoxynivalenol that induce cartilage damage are not specific to chondrocytes. Sci. Rep 7. 7 (1), 2231. https://doi.org/10.1038/s41598-017-02568-5

Levy, D.D., Zeiger, E., Escobar, P.A., Hakura, A., van der Leede, B. jan M., Kato, M., Moore, M.M., Sugiyama, K. ichi, 2019. Recommended criteria for the evaluation of

bacterial mutagenicity data (Ames test). Mutat. Res. Genet. Toxicol. Environ. Mutagen. 848, 403074. https://doi.org/10.1016/j.mrgentox.2019.07.004

Mallebrera, B., Juan-Garcia, A., Font, G., Ruiz, M.J., 2016. Mechanisms of beauvericin toxicity and antioxidant cellular defense. Toxicol. Lett. 246, 28–34. https://doi.org/10.1016/j.toxlet.2016.01.013

Mamur, S., Ünal, F., Yılmaz, S., Erikel, E., Yüzbaşıoğlu, D., 2020. Evaluation of the cytotoxic and genotoxic effects of mycotoxin fusaric acid. Drug. Chem. Toxicol. 43, 149–157. https://doi.org/10.1080/01480545.2018.1499772

Mamur, S., Yuzbasioglu, D., Yılmaz, S., Erikel, E., & Unal, F. (2018). Assessment of cytotoxic and genotoxic effects of enniatin-A in vitro. Food Addit. Contam.: Part A, 35(8), 1633-1644. https://doi.org/10.1080/19440049.2018.1486513

Mantovani, A., Allavena, P., Sica, A., Balkwill, F., 2008. Cancer-related inflammation. Nature. 454, 436-444. https://doi.org/10.1038/nature07205

Mcdaniels, A.E., Reyes, A.L., Wymer, L.J., Rankin, C.C., Stelma, G.N., 1990. Chromotests for Detecting Genotoxins. Environ. Mol. Mutagen. 16 (3), 204-215. https://doi.org/10.1002/em.2850160308

Mortelmans, K., Zeiger, E., 2000. The Ames Salmonella/microsome mutagenicity assay. Mutat. Res. 455, 29-60. https://doi.org/10.1016/S0027-5107(00)00064-6

OECD GUIDELINE FOR TESTING OF CHEMICALS Bacterial Reverse Mutation Test, 2020.

Press, E.B., Maron, D.M., Ames, B.N., 1983. Revised methods for the Salmonella mutagenicity test. Mutat. Res. 113, 173-215. https://doi.org/10.1016/0165-1161(83)90010-9

Prosperini, A., Juan-García, A., Font, G., Ruiz, M.J., 2013. Beauvericin-induced cytotoxicity via ROS production and mitochondrial damage in Caco-2 cells. Toxicol. Lett. 222, 204–211. https://doi.org/10.1016/j.toxlet.2013.07.005

Rakkestad, K.E., Skaar, I., Ansteinsson, V.E., Solhaug, A., Holme, J.A., Pestka, J.J., Samuelsen, J.T., Dahlman, H.J., Hongslo, J.K., Becher, R., 2010. DNA damage and DNA damage responses in THP-1 Monocytes after exposure to spores of either Stachybotrys chartarum or Aspergillus versicolor or to T-2 toxin. Toxicol. Sci. 115, 140–155. https://doi.org/10.1093/toxsci/kfq045

Shivappa, N., Steck, S.E., Hurley, T.G., Hussey, J.R., Hébert, J.R., 2014. Designing and developing a literature-derived, population-based dietary inflammatory index. Public Health Nutr. 17, 1689–1696. https://doi.org/10.1017/S1368980013002115

Singto, T., Tassaneeyakul, W., Porasuphatana, S., 2020. Research Paper Protective Effects of Purple Waxy Corn on Aflatoxin B1-induced Oxidative Stress and Micronucleus in HepG2 Cells. Indian J. Pharm. Sci. 82 (3):506-513. https://doi.org/10.36468/pharmaceutical-sciences.674

Smerák, P., Bárta, I., Polívková, Z., Bártová, J., Sedmíková, M., 2001. Mutagenic effects of selected trichothecene Mycotoxins and their combinations with Aflatoxin B1. Czech. J. Food. Sci. https://doi.org/19, 90–96. 10.17221/6583-CJFS

Somoskői, B., Kovács, M., Cseh, S., 2018. Effects of T-2 and Fumonisin B1 combined treatment on in vitro mouse embryo development and blastocyst quality. Toxicol. Ind. Health 34, 353–360. https://doi.org/10.1177/0748233718764039

Somoskői, B., Kovács, M., Cseh, S., 2016. Effects of T-2 mycotoxin on in vitro development and chromatin status of mouse embryos in preimplantation stages. Toxicol. Ind. Health 32, 1260–1265. https://doi.org/10.1177/0748233714555394

Stott, W.T., Kan, H.L., McFadden, L.G., Sparrow, B.R., Gollapudi, B.B., 2004. Effect of strain and diet upon constitutive and chemically induced activities of several xenobiotic-metabolizing enzymes in rats. Reg. Tox. Pharmacol. 39, 325–333. https://doi.org/10.1016/j.yrtph.2004.02.007

Tadee, A., Mahakunakorn, P., Porasuphatana, S., 2020. Oxidative stress and genotoxicity of co-exposure to chlorpyrifos and aflatoxin B1 in HepG2 cells. Toxicol. Ind. Health 36, 336–345. https://doi.org/10.1177/0748233720928169

Takakura, N., Nesslany, F., Fessard, V., Le Hegarat, L., 2014. Absence of in vitro genotoxicity potential of the mycotoxin deoxynivalenol in bacteria and in human TK6 and HepaRG cell lines. Food Chem. Toxicol. 66, 113–121. https://doi.org/10.1016/j.fct.2014.01.029

Taroncher, M., Rodríguez-Carrasco, Y., Ruiz, M.J., 2020. T-2 toxin and its metabolites: Characterization, cytotoxic mechanisms and adaptive cellular response in human hepatocarcinoma (HepG2) cells. Food Chem. Toxicol. 145. https://doi.org/10.1016/j.fct.2020.111654

Tejs, S., 2008. The Ames test: a methodological short review, Environ. Biotech. 4 (1), 7-14

Van Woudenbergh, G.J., Theofylaktopoulou, D., Kuijsten, A., Ferreira, I., Van Greevenbroek, M.M., Van Der Kallen, C.J., Schalkwijk, C.G., Stehouwer, C.D.A., Ocké, M.C., Nijpels, G., Dekker, J.M., Blaak, E.E., Feskens, E.J.M., 2013. Adapted dietary inflammatory index and its association with a summary score for low-grade inflammation and markers of glucose metabolism: The cohort study on diabetes and atherosclerosis maastricht (CODAM) and the hoorn study 1-4. Am. J. Clin. Nutr. 98, 1533–1542. https://doi.org/10.3945/ajcn.112.056333

Wada, T., Penninger, J.M., 2004. Mitogen-activated protein kinases in apoptosis regulation. Oncogene. 23, 2838- 2849. https://doi.org/10.1038/sj.onc.1207556

Wu, J., Zhou, Y., Yuan, Z., Yi, J., Chen, J., Wang, N., Tian, Y., 2019. Autophagy and apoptosis interact to modulate T-2 toxin-induced toxicity in liver cells. Toxins, 11 (1), 45. https://doi.org/10.3390/toxins11010045

Zhang, Y.F., Yang, J.Y., Li, Y.K., Zhou, W., 2017. Toxicity and oxidative stress induced by T-2 toxin in cultured mouse Leydig cells. Toxicol. Mech. Methods 27, 100–106. https://doi.org/10.1080/15376516.2016.1258747

Zingales, V., Fernández-Franzón, M., Ruiz, M.J., 2021. Sterigmatocystin-induced DNA damage triggers cell-cycle arrest via MAPK in human neuroblastoma cells. Toxicol. Mech. Methods 31, 479–488. https://doi.org/10.1080/15376516.2021.1916801

Cells, 13 (2024), 900

3.9. Using microfluidic hepatic spheroid cultures to assess liver toxicity of T-2 mycotoxin

Mercedes Taroncher[1,2], Alan M. Gonzalez-Suarez[1], Kihak Gwon[1], Samuel Romero[3], Angel D. Reyes-Figueroa[3,4], Yelko Rodríguez-Carrasco[2], María-José Ruiz[2], Gulnaz Stybayeva[1], Alexander Revzin[1,*], Jose M. de Hoyos-Vega[1,*]

[1] Department of Physiology and Biomedical Engineering, Mayo Clinic, Rochester, MN, USA 55901

[2] Research Group in Alternative Methods for Determining Toxics Effects and Risk Assessment of Contaminants and Mixtures (RiskTox). Laboratory of Food Chemistry and Toxicology, Faculty of Pharmacy, University of Valencia, Av. Vicent Andrés Estellés s/n, 46100, Valencia, SPAIN

[3] Centro de Investigación en Matemáticas Unidad Monterrey, Apodaca, NL, MEXICO 66628

[4] Consejo Nacional de Ciencia y Tecnología, CDMX, MEXICO 03940

Abstract

The *Fusarium* fungi is found in cereals and feedstuffs and may produce mycotoxins, which are secondary metabolites, such as the T-2 toxin (T-2). In this work, we explored the hepatotoxicity of T-2 using microfluidic 3D hepatic cultures. The objectives were: (i) exploring the benefits of microfluidic 3D cultures compared to conventional 3D cultures available commercially (Aggrewell plates), (ii) establishing 3D co-cultures of hepatic cells (HepG2) and stellate cells (LX2) and assessing T-2 exposure in this model, (iii) characterizing the induction of metabolizing enzymes, and (iv) evaluating inflammatory markers upon T-2 exposure in microfluidic hepatic cultures. Our results demonstrated that, in comparison to commercial (large-volume) 3D cultures, spheroids formed faster and were more functional in microfluidic devices. The viability and hepatic function decreased with increasing T-2 concentrations in both monoculture and co-cultures. The RT-PCR analysis revealed that exposure to T-2 upregulate expression of multiple Phase I and Phase II hepatic enzymes. In addition, several pro- and anti-inflammatory proteins were increased in co-cultures after exposure to T-2.

Key words: T-2; HepG2 cells, microfluidic devices; spheroids; cytotoxicity.

* **Correspondence**: Department of Physiology and Biomedical Engineering, Mayo Clinic, Rochester, MN, USA 55901. E-mail address: dehoyos-vega.jose@mayo.edu; revzin.alexander@mayo.edu

1. Introduction

Mycotoxins are secondary metabolites of low-molecular weight produced by filamentous fungi that are often present in food. They may cause adverse effects in the short and long term for consumers depending on the concentrations present in aliments and the exposure time [1]. Mycotoxins are present worldwide in cereals –notably in wheat, barley, maize, oats, rye and rice– and in animal feed [2]. Mycotoxins represent one of the most important categories of natural toxins relative to human and animal health. Mycotoxins produce significant economic losses around the world be-cause the value of the crop is reduced when high levels of mycotoxins are detected in the grain [2]. According to the Food and Agriculture Organization (FAO), more than 300 different mycotoxins have been identified in food commodities and animal feed [3]. Among these, the T-2 toxin (T-2) is found in several cereals, but more predominantly in oats [1]. The T-2 is a type A trichothecene (tetracyclic sesquiterpenoid compounds characterized by a 12,13-epoxy group and a functional carbonyl group at C-8) produced by several species of *Fusarium* fungi [4]. Some of the described mechanisms of action of this toxin are inhibition of protein synthesis, activation of the mitogen-activated protein kinase (MAPK), apoptosis in various cell types, and inhibition of DNA and RNA synthesis [5]. Studies revealed that T-2 can induce apoptosis of hematopoietic progenitors, blocking the renewal of blood cells in the bone marrow, which leads to a decrease in the number of leukocytes and thrombocytes, and increases the risk of septicemia and hemorrhage [6]. It has been pointed out that after ingestion of T-2, its detoxification may not always be completed, producing more adverse effects than expected [7]. Therefore, the European Commission requested that the European Food Safety Authority (EFSA) review the information regarding the toxicity of T-2 and the levels of

this mycotoxin that produce adverse effects in humans and livestock [7]. This mandate has opened a new debate regarding the importance of the T-2 toxin and the need for a re-evaluation of its mechanisms of action for a better understanding of its toxicokinetics, adverse effects, and present and future risks.

While animal models may be preferred for the study of T-2 toxin, they are complex, making it challenging to study mechanisms; they also present ethical issues and may not accurately recapitulate human physiology [8]. As a result, there have been extensive studies on T-2 cytotoxicity *in vitro* in a variety of cell lines such as IPEC, HepG2, C28/I2, Caco-2, and HT-29 cells [9–12]. Given the reported adverse effects of T-2 on the liver [13], there is considerable interest in modeling liver toxicity and metabolism of T-2 *in vitro.* HepG2 cells were derived from hepatocellular carcinoma but retain epithelial hepatic phenotype and are used widely as surrogates for liver studies. These cells have been used by us and others previously to assess the toxicity of T-2 [12,14], however, these past studies utilized 2D cultures. For example, Ruiz's team recently revealed an antioxidant defense system of HepG2 cells against the oxidative stress induced by T-2 [15,16]. However, compared to 3D (spheroid) cultures, 2D cultures lack appropriate cell-cell and cell-matrix interactions and may not be sufficiently stable to mimic the physiologic response to toxic compounds [17].

Multiple approaches have been reported to promote organization of hepatocytes and other liver cells into 3D constructs including spheroids [18,19]. For example, 3D cultures of hepatocytes sandwiched between layers of gel (collagen, heparin, or Matrigel) have been shown to enhance and stabilize hepatic function [20–23]. Another approach is to use 3D plates (e.g., AggreWell plates) to aggregate cells into uniform spheroids in the absence of the exogenous ECM [19]. Each of these approaches has limitations: use of gel sandwiches may be

costly while spheroids in conventional 3D plates may have a limited window of hepatic function and phenotype maintenance [24].

Microfluidic devices have been used extensively for culturing hepatocytes and other cell types in 3D [25,26]. Microfluidic devices may be used to apply physiological forces as well as to conserve cells and reagents required for testing. Our team has a long-standing interest in using microfluidic devices where cells are cultured under static conditions while confined to small local volumes and receive nutrients from media reservoirs via transport channels. We showed in several publications that such an arrangement results in local accumulation of secreted signals that act in an autocrine and paracrine manner to enhance phenotype of cultured cells [27–30].

Another strategy employed commonly both in standard and microfluidic hepatic cultures is to introduce nonparenchymal cells to stabilize and enhance hepatic function. This enhancement may be attributed to the increase of juxtacrine and paracrine interactions between both cell types [31–33]. For example, it has been shown that the co-culture of liver sinusoidal endothelial cells (LSECs), 3T3 fibroblasts, Kupffer and LX2 cells, enhanced the albumin secretion of hepatic cells in standard and microfluidic devices [29,34–36].

In this study, we wanted to evaluate whether microfluidic 3D hepatic cultures, either alone or in co-cultures with nonparenchymal cells, were suitable for assessing toxicity of T-2. To the best of our knowledge, this is the first effort to evaluate T-2 toxicity in 3D hepatic cultures, microfluidic or otherwise.

2. Material and Methods

2.1 Reagents

The following reagents were purchased from Sigma Aldrich: Pluronic F-127 (P2443), Tween 20 (P9416), and primer sequences of CYP1A1 and CYP2E1. The primer sequences of GAPDH, CYP1A2, CYP3A4, UGT1A1, MDR1 and MDR2 were purchased from Integrated DNA technologies (IDT). The following reagents were purchased from Thermo Fisher scientific: Dublecco´s Modified Eagle Medium (DMEM, MT-10-013-CV), penicillin-streptomycin (15140122), Gibco Fetal Bovine Serum (FBS, 10437028), Calcein, Ethidium homodimer (Live/Dead Viability/Cytotoxicity kit, L3224), Hoechst 33342 and Vybrant DiD (V22889), Human albumin kit (E110-125) was purchased from Bethyl Laboratories, Inc. Standard T-2 toxin (MW: 466.6 g/mol, 21259-20-1) was purchased from Cayman chemical company (Ann Arbor, Michigan, USA). Polydimethylsiloxane (PDMS, Sylgard 184 Silicone Elastomer Kit kit, 2065622) and SU-8 2100 were purchased from Ellsworth and Kayaku Advanced Materials, respectively.

2.2 Fabrication of microfluidic devices

The microfluidic devices were comprised of two polydimethylsiloxane (PDMS) layers: 1) the top layer consisting of a flow channel with a culture chamber of 100 μm in height, and 2) the bottom layer that contained an array of 84 microwells of 250×300 μm (diameter ×depth). The top and bottom layer master molds were fabricated using standard photolithography techniques. First, 4-inch silicon wafers (University Wafer) were cleaned using oxygen plasma. Next, the wafers were spin-coated using SU-8 2100 negative photoresist to create a 100 μm and 300 μm thickness film for the top and bot-tom master

molds, respectively, as recommended by the manufacturer. Followed by a soft bake step, the design was micropatterned into the resist using a Micro Pattern Generator (μPG 101, Heidelberg, Germany). After a postexposure bake, the mold was developed in SU-8 developer and hard-baked for 2 h at 135 ºC. Afterwards, both molds were exposed to chlorotrimethylsilane for 30 min.

Microfluidic devices were fabricated using standard soft-lithography. A mixture of 10:1 weight ratio of PDMS base to curing agent was poured onto the master molds. After degassing for 10 min, the mixture was baked at 80 ºC for 20 min. Next, the partially cured PDMS was cast out from the master mold and cut, and the inlet and outlet holes were punched at the most distal part of the flow channel. The top and bottom PDMS layers were aligned and irreversibly bonded using oxygen plasma treatment (PDC-001, Harrick Plasma). Media reservoirs were generated using cloning cylinders (10 mm: Fisher Scientific) attached with PDMS to the inlet and outlet holes. Prior to cell seeding, all microfluidic devices were incubated with 2% Pluronic F-127 for at least 1 h to avoid interactions between cells and the PDMS surface and inducing cell-cell aggregation. Lastly, the devices were washed with PBS and sterilized with UV-light for 1 h.

2.3 HepG2 cell cultures

HepG2 cells were cultured in T-75 culture flasks in DMEM media supplemented with 1% (vol/vol) penicillin-streptomycin and 10% FBS, at 37 ºC with 5% CO_2. At 80% confluency, cells were passaged into a new T-75 flask or seeded into AggrewellTM400 plates and/or microfluidic devices. For seeding into AggrewellTM400 and microfluidic cultures, we ensured cell viability to be at least 90%.

2.3.1 Cell culture in standard large volume 3D plates

HepG2 cell spheroids were generated using commercial 24-well AggrewellTM400 plates following the manufacturer´s protocol. While there are other commercial products suitable for cell spheroid cultures (e.g. f- or u-shaped plates), they are designed to culture one spheroid per well and do not mimic a microfluidic device where an array of spheroids is cultured in the same volume of media. Conversely, Aggrewell plate is designed to create a high-density array of spheroids in the same well and therefore represents a better "large volume" comparison to microfluidic spheroid cultures. Within each well there are 1,200 v-bottom sub-wells 400×400 μm each. Spheroids form within individual sub-wells. Prior to seeding cells, a plate was first treated with 2 mL anti-adherence rinse solution (STEMCELL Technologies Inc., Vancouver, Canada) and then centrifugated at 1300g for 5 min. Subsequently, the anti-adherence rinse solution was aspirated and HepG2 cells were seeded at the density of 3.6 x 10^5 cells per well. The plates were centrifugated at 100g for 3 min to ensure uniform cell distribution within the microwells, and then incubated for 5 days at 37ºC with 5% CO_2 with daily media exchange. To prevent spheroid washout, 50% of the media volume was collected and exchanged during media exchanges. To analyze morphology of the spheroids, brightfield images were acquired of the wells during the spheroids culture.

2.3.2 Cell culture in microfluidic devices

HepG2 monoculture. To generate HepG2 spheroids in microfluidic devices, a total of 20,000 cells were seeded per device. We pipetted 100 μL of cell suspension at 2x10^7 cells/mL into the device inlet while keeping the outlet empty. The difference in hydro-static pressure between inlet and outlet drove

cells into the culture chamber and the microwells. Once the microwells were filled with cells, the leftover cells were removed from the media reservoirs and the cells outside of the microwells washed out. After-wards, 250 μL of media was added into each reservoir. To ensure spheroids formation, 1% matrigel was added to the media in the first 24 h of culture. Fresh media was ex-changed every 24 h. Compact spheroids were formed after 24-48 h of device seeding.

Co-culture of HepG2 and LX2 cells. The stellate cell line LX2 was cultured in DMEM media supplemented with 1% (vol/vol) penicillin-streptomycin and 2% FBS in a T-75 culture flask at 37 ºC with 5% CO_2. To generate HepG2-LX2 spheroids, we pre-pared a cell suspension containing 85% HepG2 and 15% LX2. This ratio was chosen based on the proportions of liver cell types *in vivo* [37]. The HepG2-LX2 cell suspension was seeded into microfluidic devices as previously described in the HepG2 monoculture section. Fresh media was exchanged every 24 h. Compact spheroids were formed after 24-48 h of device seeding. For LX2 identification in the HepG2-LX2 spheroids, LX2 cells were stained with Vybrant DiD dye prior to mixing with HepG2 cells.

2.4 T-2 toxicity in microfluidic devices

To determine the effects of T-2 in HepG2 and HepG2-LX2 spheroids, we added different concentrations of the toxin (0, 15, 30 and 60 nM) 3 days after seeding the cells. Then, the cells were treated for 24 h with the toxin by adding T-2 to the culture media with a final concentration of DMSO at 0.1%. Appropriate controls containing the same amount of solvent were included in each experiment. Four culture conditions were tested: (1) HepG2 spheroids without T-2, (2) HepG2 spheroids with T-2, (3) HepG2-LX2 spheroids without T-2, and (4) HepG2-LX2 spheroids with T-2.

2.5 Live/dead assay and analysis

An inverted fluorescence microscope (IX-83, Olympus) with a 10x objective lens was used to carry out a quantitative assay to evaluate the viability of HepG2 and HepG2-LX2 spheroids after 24 h of T-2 exposure. We used Calcein-AM (green) and ethidium homodimer (red) dyes, corresponding to live and dead cells, respectively. The staining solution was prepared in a 15 mL tube by mixing 1 μL calcein and 2 μL ethidium homodimer per 1 mL media. Then, 250 μL of staining solution was added to each culture chamber and incubated for 30 min at 37 ºC. After this incubation, we removed the media and washed with 250 μL PBS per device. At least 3 images with 6 spheroids each were acquired for each condition in brightfield and fluorescence channels for calcein (ex/em 494/517 nm) and ethidium homodimer (ex/em 528/617 nm). For each area, a Z-stack was acquired and then all fluorescence data compressed to a single image using the "full projection" feature.

Images were analyzed using a custom-made MATLAB script to determine cytotoxicity of T-2 in mono- and co-cultures. Briefly, images were grouped per condition and for each set of images (i.e., BF, green and red fluorescence channels); the green channel image was used to locate the spheroids. A circular area of 300 pixels was drawn surrounding each spheroid. Images were binarized using a consistent threshold per channel across all groups to obtain the area (A_{red} or A_{green}) of each fluorescence channel per spheroid. Cytotoxicity was calculated using the following equation: $\text{Cytotoxicity}\% = 100 \times A_{red} / (A_{green} + A_{red})$. Six spheroids per condition were analyzed.

2.6 Spheroid formation Image Analysis

2.6.1 Assessing area, solidity, and circularity of hepatic spheroids

HepG2 cells were cultured in commercial 3D plates and microfluidic devices as described in Methods section 2.3. Brightfield images were acquired immediately after cell seeding (0 h) and every 24 h for five days. For both culture conditions, at least five images containing six spheroids each were acquired at every time point (Fig. S1A). Acquired images were analyzed using Python and ImageJ to quantify and compare three metrics: 1) area of the spheroid, 2) solidity and 3) circularity (further description of methodology may be found in supplementary data). The Area of the spheroid is determined by detecting the number of pixels that the spheroid encompasses in the image. Solidity is a metric that indicates how regular (or "smooth") the surface of the spheroid is while. circularity is an indicator of how similar to a true circle a spheroid is [38–40]. Six spheroids per condition were analyzed.

2.6.2 HepG2 and HepG2-LX2 spheroids growth analysis

HepG2 and HepG2-LX2 spheroids were tracked for 4 days, and brightfield images were acquired at days 3 and 4 after seeding, corresponding with the addition of the mycotoxin (day 3) and 24 h after T-2 exposure (day 4). All spheroids in an image were measured using ImageJ to determine the area of spheroids at both days (before mycotoxin exposure and 24 h after treatment). The relative spheroid growth after 24 h of T-2 (day 4) was compared between HepG2 and HepG2-LX2 spheroids. Six spheroids per condition were analyzed.

2.7 Analysis of hepatic albumin production by ELISA

Albumin production of hepatocytes in vitro is typically analyzed to determine the hepatic function. Albumin secretion was measured for each culture format by ELISA of conditioned media using a human albumin kit and following the manufacturer's instructions.

The albumin ELISA was carried out for: (1) HepG2 spheroids cultured in Aggre-wellTM400 plates and microfluidic devices for 5 days with daily media exchange. The media from each well or microfluidic chamber was collected on days 3, 4 and 5, and the albumin secreted was measured by an ELISA assay. (2) HepG2 or HepG2-LX2 spheroids were cultured only in microfluidic devices for 4 days with daily media exchanges. Spheroids were treated with 15, 30, and 60 nM of T-2 on days 3 and 4. The media collected at these time points was analyzed for albumin secreted in HepG2 spheroid monocultures and HepG2-LX2 spheroid co-cultures. The medium is collected from 3 devices per condition, in each device there are 84 spheroids. Therefore, the content of albumin producing 252 spheroids in each condition is analyzed.

2.8 RT-PCR analysis of hepatic gene expression

HepG2 or HepG2-LX2 spheroids were cultured in microfluidic devices for 3 days and exposed to T-2 at 0, 15, 30 or 60 nM for 24 h, as described above. Total RNA was extracted from HepG2 spheroids at day 4 (24h after T-2 exposure) using the High Pure RNA Isolation kit and dissolved in nuclease-free water. The RNA concentration was quantified using the NanoDrop One Spectrophotometer (Thermo Fisher Scientific).

Complementary DNA (cDNA) synthesis was performed using the Transcriptor First Strand cDNA Synthesis kit. Gene expression level was

quantified using the SYBR master. RT-PCR was performed with 40 cycles. Relative gene expression level was determined through the Ct method using Glyceraldehyde 3-phosphate dehydrogenase (GAPDH) as a housekeeping gene. We carried out RT-PCR analysis for some of the most common enzymes of phase I (CYP1A1, CYP1A2, CYP2E1, CYP3A4) and phase II (UGT1A1) metabolism, and transporters of phase III metabolism (MDR1, MRP2) in the liver. The gene-specific primers used in this study are listed in Table 1. The spheroids of 3 devices per condition (252 spheroids per condition) were analyzed.

Table 1. Gene-specific primers for RT-PCR assays.

Gene symbol	**Gene name**	**Tm (ºC) Forward primer/Revers primer**	**Forward primer/Revers primer**
GAPDH	Glyceraldehyde 3-phosphate dehydrogenase	57.2/57.7	TGTTGCCATCAATGACCCCTT/ CTCCACGACGTACTCAGCG
CYP1A1	Cytochrome P450 1A1	59.4/57.4	CATTAACATCGTCTTGGACC/ TCTTGGATCTTTCTCTGTACC
CYP1A2	Cytochrome P450 1A2	52.5/56.4	GCTTCTACATCCCCAAGAAAT/ ACCACTTGGCCAGGACT
CYP2E1	Cytochrome P450 2E1	57.5/57.8	GACACCATTTTCAGAGGATAC/ TTCATTCAGGAAGTGTTCTG
CYP3A4	Cytochrome P450 3A4	50.1/51.8	ACTGCCTTTTTTGGGAAATA/ GGCTGTTGACCATCATAAAAG
UGT1A1	UDP Glucuronosyl transferase 1A1	54.8/56.7	TTGATCCCAGTGGATGGC/ ATGCTCCGTCTCTGATGTACAAC
MDR1	Multidrug resistance mutation 1	56.3/56.1	GTCATCGCTGGTTTCGATGATG/ ATTTCCTGCTGTCTGCATTGTG

Gene symbol	Gene name	Tm (ºC) Forward primer/Revers primer	Forward primer/Revers primer
MDR2	Multidrug resistance protein 2	53.1/53.1	TCCAACTGTGCTTCAAGC/ GGCATCCACAGACATCAG

Tm: melting temperature

2.9 Secretome analysis

HepG2 and HepG2-LX2 supernatants from spheroids in microfluidic cultures were collected and analyzed for inflammatory markers by Eve Technologies (Calgary, AB, Canada) using 15-plex assay. The medium is collected from 3 devices per condition after 24 h of T-2 exposure, in each device there are 84 spheroids. Therefore, the content of markers producing 252 spheroids in each condition is analyzed.

2.10 Statistical analysis

One-tailed unpaired t-test analysis with $p < 0.05$ was used for statistical analysis of results. The number of replicates in each assay is specified in Material and Methods section. Data were expressed as mean ± SD. The data was statistically analyzed using GraphPad Prism (ver. 7; GraphPad Software).

3. Results and Discussion

3.1. Cultivation of hepatic spheroids in microfluidic devices vs. standard large volume 3D plates

The microfluidic device design was described by us previously [27]. The PDMS device consists of a culture chamber with a height of 100 μm that is connected by two transport channels to the media reservoirs. A culture chamber

contains 84 cylindrical wells 350 μm in diameter and 300 μm in depth (See Figure 1A).

We compared spheroid formation in PDMS microwells inside the microfluidic devices vs. commercial 3D plate (Aggrewell). Both culture systems were seeded with ~250 cells per well and were maintained in the same media. Both culture systems are shown in Figure 1B and 1C. Importantly, spheroid formation proceeded faster in the microfluidic device compared to the conventional 3D plate. Time course images in Figure 1D and 1E demonstrate that in a microfluidic device, spheroid formation was nearly complete by day 2 with fully compacted spheroids appearing by day 3. In contrast, in an Aggrewell plate, spheroid formation only began at day 2 with compact spheroids appearing by day 5. Additional image analysis revealed significative differences between Aggrewell and microfluidic cultures in terms of circularity and solidity of spheroids over time ($p < 0.05$ for 24 h and $p < 0.005$ for all other time points). As ob-served in the scatter plots in Fig. 1F, the circularity and solidity of each group of spheroids is well differentiated. For example, with microfluidic spheroids reached solidity values of > 90% after 24 h of culture while spheroids in Aggrewell plate reached comparable levels after 5 days of culture. Similarly, circularity of spheroids was 60% after 48 h of culture in a microfluidic device vs. 50% after 120 h of culture in an Aggrewell plate. When comparing the area of the spheroids against its circularity (Fig. 1G), it is observed that the spheroids cultured in Aggrewell tended to be smaller and irregular even after 120 h of culture, suggesting that this culture format is not optimal for maintenance and growth of HepG2 spheroids. For microfluidic cultures, we observed that over time, the spheroids get more circular and their area increases, suggesting that the

spheroid is getting compact and growing, indicating a more suitable culture environment.

To further characterize the difference between culture platforms, hepatic function of the spheroids was assessed by albumin ELISA. As shown in Fig. 1H, albumin levels in Aggrewell 3D plate were ~2x lower than in microfluidic devices. Moreover, production of albumin declined for Aggrewell cultures of spheroids while it increased for microfluidic spheroid cultures.

The enhancement in hepatic cell function observed in microfluidic devices compared to standard large volume 3D plates can be attributed to several factors including: 1) improved oxygenation in PDMS-based microfluidic devices and 2) enhanced paracrine signaling due to small local volume of microfluidic devices.

The albumin production reported by us is comparable to albumin values reported by Choi et al. (1.35 $\mu g/1x10^4$ cells/day) who cultured primary rat hepatocyte spheroids in microfluidic devices and significantly better than those reported by Kurosawa et al. (0.014 $\mu g/1x10^4$ cells/day) who created hepatocyte monolayer cultures [27,41]. Taken together, our results highlight that microfluidic 3D hepatic cultures were superior to standard large volume 3D culture plates in terms of dynamics of spheroid formation and albumin production. Therefore, we proceeded to deploy microfluidic cultures for mycotoxin exposure experiments.

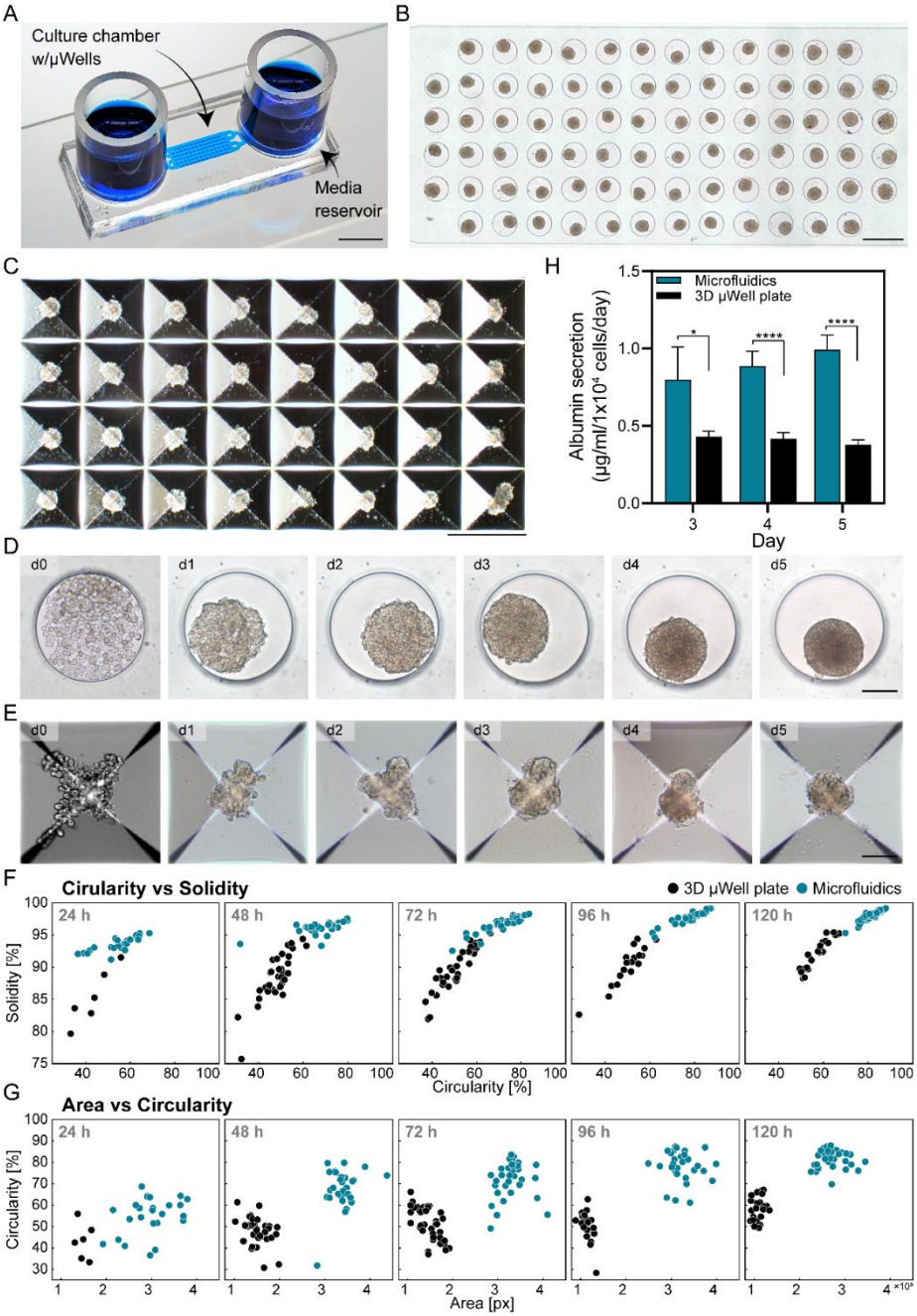

Figure 1. Formation of hepatic spheroids in microfluidic devices and conventional 3D plates. (A) Picture of the microfluidic device used for hepatic

spheroid cultures; the device contained two reservoirs connected to a cell culture chamber via transport channels. Scale bar: 5 mm. (B) Micrograph of the 84 microfluidic microwells with hepatic spheroids at day 5. Scale bar: 500 μm. (C) Micrograph of the pyramidal microwell array with HepG2 spheroids after 5 days of culture in conventional (Aggrewell) 3D plates. Scale bar: 500 μm. (D) Timelapse images of HepG2 cells aggregating into spheroids after 5 days of culture in a microfluidic device. Scale bar: 100 μm. (E) Timelapse images of HepG2 cells aggregating into spheroids after 5 days of culture in a conventional 3D plate. Scale bar: 100 μm. (F, G) Quantitative comparison of HepG2 spheroid formation measured by (F) circularity vs solidity and (G) area vs circularity in microfluidic device and conventional 3D plate throughout 5 days of culture. (H) Albumin ELISA of HepG2 spheroids in conventional 3D plates and microfluidic devices. Data are expressed as mean ± SD of 3 samples. Statistical significance was determined by one-tailed unpaired t-test, **p*-value < 0.05 and *****p*-value < 0.0001.

3.2. Creating microfluidic 3D co-cultures and assessing viability upon T-2 exposure

As noted above, nonparenchymal liver cells have been used in the past to enhance phenotype and function of hepatocyte cultures. We wanted to test a hypothesis that the presence of nonparenchymal liver cells would further enhance 3D hepatic cultures in microfluidic devices. We employed LX-2, a hepatic stellate cell line, to create co-cultures with HepG2 cells. The proportions of LX-2 cells (15%) and HepG2 cells (85%) were chosen based on cellular composition of the liver *in vivo*. LX2 cells were labeled with cell tracker (Vybrant DiD - magenta color). LX2 cells were aggregated to HepG2 cells to form the spheroids during the first 24 hours of culture. As may be appreciated from Fig. 2A, after 3 days of cultures, LX2 cells were homogeneously distributed in the hepatic spheroids. HepG2 and HepG2-LX2 spheroids were exposed for 24 h to

different concentrations of the T-2 mycotoxin (0, 15, 30, and 60 nM), with cell viability analyzed using live/dead staining. As shown in Fig. 2B and 2C, the presence of dead cells increased at higher T-2 concentrations in monocultures, however, this increase was not as pronounced in HepG2-LX2 spheroids. Quantification of live/dead fluorescence (see Fig. 2D) confirmed that monocultures experienced several fold higher cytotoxicity compared to co-cultures at all concentrations of T-2. Interestingly, the viability of co-culture spheroids at 0 nM T-2 was ~3 fold higher than monoculture spheroids at the same condition. This suggested that stellate cells improved viability and stability of hepatic cells.

The hepatic function of microfluidic 3D cultures was assessed using albumin ELISA (see Fig. 2E). HepG2-LX2 spheroids produced 2.153 μg/mL/1x10^4 cells/day, while HepG2 spheroids produced 1.702 μg/mL/1x10^4 cells/day, showing a tendency of in-creasing functionality in the co-culture, although the difference is not statistically significant. Albumin production decreased in a concentration-dependent manner in microfluidic monocultures and co-cultures after 24 h exposure to T-2 (15, 30, and 60 nM). In HepG2 spheroids, the albumin production decreased 68.3% (15 nM), 77.6% (30 nM) and 78.5% (60 nM) after 24 h, with respect to control (0 nM T-2). On the other hand, microfluidic co-cultures lost 40.8% (15 nM), 59.3% (30 nM) and 68.1% (60 nM) of albumin production when compared to control. Given that loss in albumin was more pronounced than decrease in cell viability (see Fig 2D), we conclude that, in addition to having direct cytotoxic effects, exposure to T-2 also attenuated hepatic phenotype.

HepG2 cells are capable of proliferation, and we assessed changes in spheroid diameter for monocultures and co-cultures in the presence of T-2. As shown in

Fig 2F, HepG2-LX2 spheroids were larger than HepG2 spheroids after 4 days of culture in the absence of T-2. The T-2 exposure caused a greater decline in spheroid growth for monoculture vs. co-culture spheroids.

Are stellate cells affected by exposure to T-2? To address this question, we carried out RT-PCR analysis for desmin, an intermediate filament protein present in stellate cells but not in hepatocytes (Nitou et al., 2000). This analysis (see Fig 2G) revealed that desmin expression did not change significantly with exposure to T-2, suggesting a minimal cytotoxic effect on these cells. Taken together, our results demonstrate that microfluidic spheroid co-cultures of hepatic cells and stellate cells exhibited better growth and albumin production and are more resistant to injury compared to 3D hepatic monocultures.

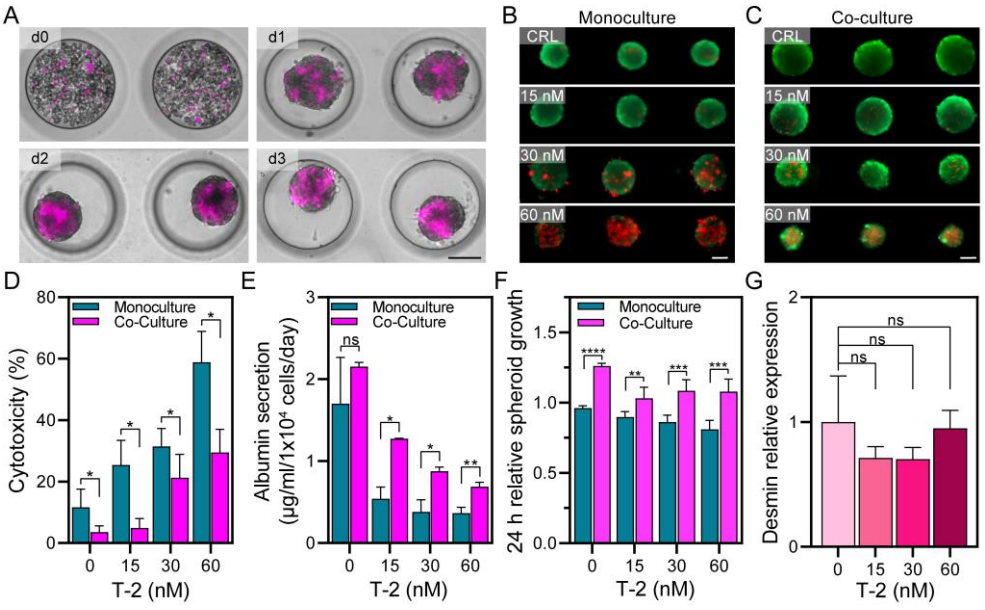

Figure 2. Formation of HepG2-LX2 spheroids and hepatic function assessment in microfluidic cultures. (A) Microscopy images of HepG2-LX2 spheroids after 0, 1, 2 and 3 days of culture. LX2 cells were stained with Vybrant DiD (magenta color). Scale bar: 100 µm. (B, C) Live/dead assay after 24 h of 0, 15, 30 and 60

nM T-2 in HepG2 (B) and HepG2-LX2 (C) spheroids in microfluidic devices. Live and dead cells took up Calcein-AM (green) and ethidium homodimer (red), respectively. Scale bar: 100 μm. (D) Cytotoxicity assessment of HepG2 and HepG2-LX2 spheroids in microfluidic cultures after 24 h exposure to T-2 mycotoxin. (E) Albumin ELISA of HepG2 and HepG2-LX2 spheroids in microfluidic cultures after 24 h of T-2 exposure. (F) Spheroid growth in monoculture and co-culture after 24 h of T-2 exposure. Changes in spheroid diameter were normalized to day 3 after seeding, corresponding with the addition of the mycotoxin. (G) RT-PCR analysis of desmin, a stellate cells marker, desmin gene expression in HepG2-LX2 spheroids after 24 h exposure to varying concentrations of T-2. Data are expressed as mean ± SD of 3 samples. Statistical significance determined by one-tail unpaired t-test, * p-value < 0.05, *** p-value < 0.001, ****p-value < 0.0001.

3.3. Evaluating the expression of hepatic enzymes in microfluidic spheroid cultures

The liver is the main organ for xenobiotic metabolism. For this reason, *in vitro* models used to investigate xenobiotic metabolisms often focus on hepatic cells or subcellular fractions, such as microsomes. The metabolism of xenobiotics can be classified in three phases [42–44]. Phase I is comprised of enzymes responsible for performing oxidation, hydrolysis, or hydroxylation reactions of xenobiotics. Phase II involves conjugation reactions of the oxidized xenobiotics with glucuronic or sulfuric acid, for example, increasing its hydrophilicity and thus enhancing the secretion through bile and urine. Phase III is formed by transporters, such as the multidrug resistance (MDR), that pump conjugated compounds out of the hepatocytes, leading to limited bioavailability of the substrates. Since the T-2 metabolic pathway is not yet fully understood, several phase I and II metabolic enzymes and phase III transporters have been linked to T-2 metabolism [45]. Previously, it was reported that T-2 is rapidly

metabolized and may contribute to the overall toxicity of the mycotoxin [46]. It is important to improve our understanding of T-2 metabolism to better understand its mechanism of action in causing liver and systemic toxicity.

In the present study, we used RT-PCR to assess expression of Phase I, II and III enzymes and transporters for HepG2 and HepG2-LX2 spheroids in microfluidic cultures after 24 h of T-2 exposure. As shown in Figure 3, expression of CYP1A1 (Fig. 3A), CYP1A2 (Fig. 3B), CYP2E1 (Fig. 3C), CYP3A4 (Fig. 3D), UGT1A1 (Fig. 3E), MDR1 (Fig. 3F) and MDR2 (Fig. G) was induced by T-2, confirming that this mycotoxin is metabolized and excreted by HepG2 cells. The choice of enzymes was guided by prior reports of liver metabolism of T-2 and other trichothecenes [47–49].

It was important to observe that microfluidic monocultures of hepatic spheroids responded to 24 h exposure of T-2 by upregulating expression of all tested enzymes with the exception of CYP3A4 and UGT1A1. Regarding the phase I metabolism enzymes, the expression levels of CYP1A1, CYP1A2, CYP2E1 and CYP3A4 increased 3.89, 6.17, 40.81 and 2.99-fold, respectively, compared to microfluidic spheroids not exposed to T-2. In terms of phase II metabolism enzymes, UGT1A1 increased 4.35-fold com-pared with the control. Lastly, the expression levels of MDR1 and MDR2 were 3.48 and 1.32-fold higher, respectively, compared with their controls. Of all the enzymes tested, CYP2E1 was induced the most (~41 fold compared to control) pointing to an important role played by this cytochrome in T-2 metabolism. An important role of CYP2E1 in T-2 metabolism was previously reported by Lin et al. [50]. Furthermore, CYP2E1 is involved in the metabolism of other mycotoxins produced by *Fusarium* fungi, for example, it is the main cytochrome involved in the metabolism of Zearalenone (ZEA) [49].

Expression of metabolizing enzymes in microfluidic 3D co-cultures was interesting and counterintuitive. We did observe induction of some metabolizing enzymes (e.g. CYP1A1 – 0.59 fold at 60 nM T-2, CYP1A2 – 2.14 fold at 60 nM T-2, CYP2E1 – 0.86 fold at 60 nM T-2). However, the levels of enzyme induction were much lower in co-cultures with stellate cells compared to monocultures of HepG2 cell spheroids, except in the case of MDR2 and CYP3A4, where the decrease of induction is not significant or only significant at 30 nM T-2. This observation is counterintuitive in light of the fact that co-cultures showed better, albeit marginally, production of albumin (see Figure 2). Thus, one could expect similar or better induction of metabolizing enzymes in co-cultures compared to monocultures. While the reasons for lower induction of metabolizing enzymes in co-cultures remain to be elucidated, there have been literature reports describing stellate cells sequestering mycotoxins in lipid droplets thus neutralizing their effects in the liver [51,52]. We hypothesize that something similar may be happening in microfluidic co-cultures and such sequestration of mycotoxin may explain lower cytotoxicity and better albumin production in co-cultures exposed to T-2 (see Figure 2).

The metabolism of T-2 is complicated because more than 10 metabolites have been identified [50]. According to Lin and colleagues, the CYP450 enzymes that contribute to T-2 metabolism include CYP3A4, CYP2E1, CYP1A2, CYP2C9, CYP2B6, CYP2D6 and CYP2C19, in decreasing order of contribution [50].

Phase III metabolism in HepG2 cells has not been widely studied under T-2 exposure, however, there are studies confirming the importance of this phase in HepG2 cells [53]. In this work, we demonstrate that MDR1 and MDR2 were engaged in T-2 excretion in microfluidic monocultures (Fig. 3F and 3G). Our

observations are corroborated by previous studies with intestinal epithelial cells that showed such mycotoxins as deoxynivalenol (DON), nivalenol (NIV), and ochratoxin A (OTA) to be substrates for MDR2 [54–56]. In summary, our results demonstrate that microfluidic hepatic spheroids expressed Phase I, II and III metabolizing enzymes/transporters and that these enzymes/transporters were induced by T-2. Microfluidic hepatic monocultures exhibited much higher enzyme induction compared to co-cultures with stellate cells. Our results highlight that microfluidic spheroid cultures represent an excellent model for investigating mycotoxin effects on liver metabolism. The mechanisms by which stellate cells attenuate induction of metabolizing enzymes may involve sequestration/neutralization of T-2 but require further investigation.

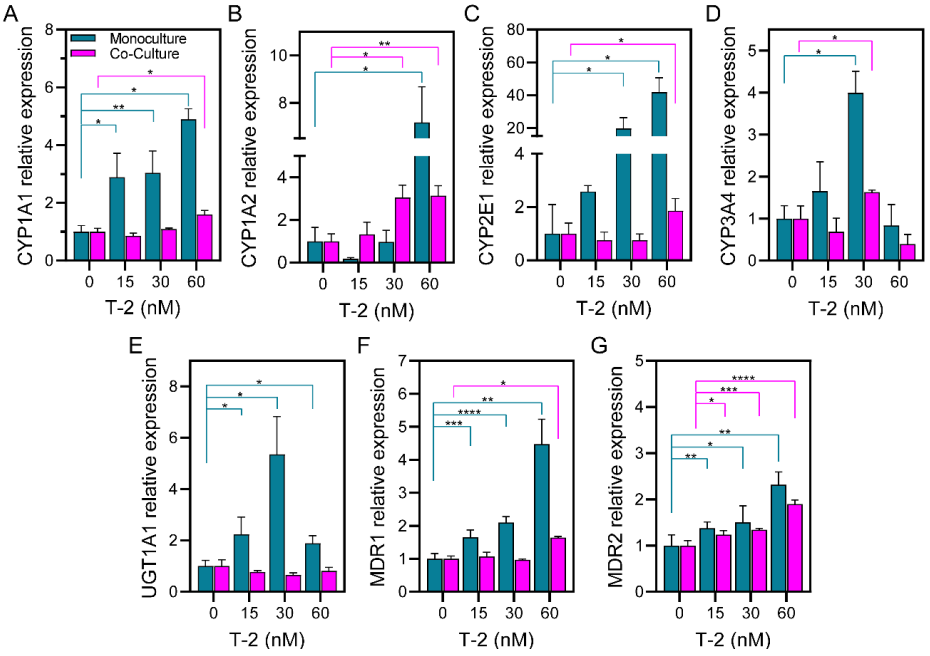

Figure 3. Assessing expression of genes associated with hepatic metabolic activity after exposure to T-2. RT-PCR analysis of phase I (A) CYP1A1, (B) CYP1A2, (C) CYP2E1, and (D) CYP3A4, phase II (E) UGTA1 and phase III (F) MDR1, and (G) MDR2 genes associated with the ability to metabolize or

transport the mycotoxin. Gene expression results are normalized by 0 h of T-2 expo-sure condition. Data are expressed as relative expression to the control as mean ± SD of 3 samples. Statistical significance determined by one-tail unpaired t-test, * *p*-value < 0.05, ** *p*-value < 0.005, *** *p*-value < 0.001, ****p-value < 0.0001. This is a table. Tables should be placed in the main text near to the first time they are cited.

3.4. Assessing inflammatory markers in microfluidic hepatic spheroid cultures

The exposure to T-2 has been shown to affect intestinal barrier function and may lead to pathogen infections, inflammatory bowel diseases (IBD), and mucinous adenocarcinomas [57]. To the best of our knowledge, inflammatory effects of T-2 have not been explored in liver cultures to date. However, other trichothecenes that also produce gastrointestinal inflammation, such as DON, have been associated with increased production of inflammatory cytokines (TNF-α and IL.6) in porcine hepatocytes and co-cultures of hepatocytes and Kupffer cells [58,59].

Therefore, in this study, we wanted to evaluate changes in production of inflammatory cytokines after T-2 exposure in microfluidic hepatic spheroid cultures. Both monoculture and co-culture formats were evaluated. Of 15 inflammatory biomarkers analyzed using commercial multiplexed immunoassay panel, we focused on 6 proteins (IL-1RA, GM-CSF, MCP-1, TNF-α, IL-8 and IL-6) that were significantly affected by exposure to 60 nM T-2 (See Figure 4A).

The IL-1RA acts as an anti-inflammatory cytokine by binding to and blocking access to the IL-1 receptor without causing downstream signaling [60]. Opposing trends for IL-1RA levels in monocultures and co-cultures in Fig. 4a may have several explanations. It is plausible that there are inflammatory

processes under way in spheroid monocultures in the absence of mycotoxin and that higher level of IL-1RA in monocultures may indicate anti-inflammatory response. This hypothesis is supported by the results in Fig. 2D that show much greater loss of viability in monocultures compared to co-cultures in the absence of mycotoxin exposure. The increase in IL-1RA levels in co-cultures after exposure to T-2 may point to a mounting anti-inflammatory response (Fig. 4B).

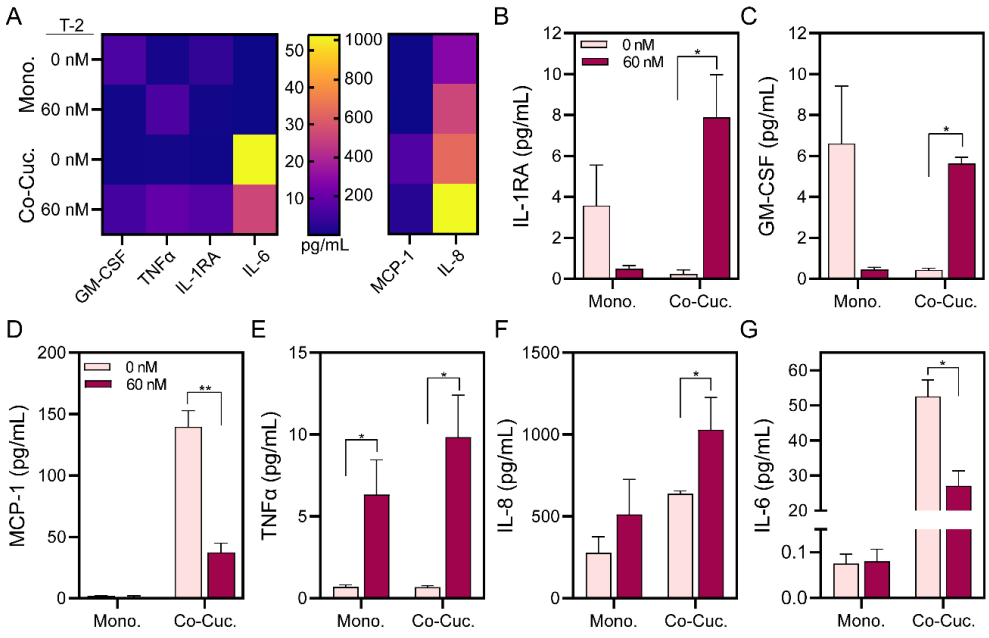

Figure 4. Secretome analysis of microfluidic hepatic spheroid cultures. (A) Heatmap of secreted signals, IL-1RA (B), GM-CSF (C), MCP-1 (D), TNF-α (E), IL-8 (F) and IL-6 (G) in monoculture and co-culture spheroids after 24 h of 60 nM T-2 exposure. Data are expressed as mean ± SD of 3 samples. Statistical significance was determined by one-tail unpaired t-test, * *p*-value < 0.05.

GM-CSF is a proinflammatory and regulatory cytokine associated with proliferation, differentiation and chemotaxis of immune cells, epithelial regeneration, and liver fibrosis [61]. Like IL-1RA, GM-CSF may function as a

regulatory cytokine during monoculture in the absence of mycotoxin, however in co-cultures with T-2 may be involved in a pro-inflammatory response orchestrated by stellate cells (Fig. 4C). This could explain the increase of IL-1RA levels in co-cultures with T-2 to counteract the pro-inflammatory response of GM-CSF (see Fig. 4A).

MCP-1 is a pleiotropic signal that may be produced by immune cells to promote migration and infiltration of other immune cells into injured site but may also be secreted by stellate cells [62]. Given that levels of MCP-1 were negligible in monocultures but robust in co-cultures (Fig. 4D), suggests that stellate cells may be a source of MCP-1 in our cultures [62,63]. Decline of MCP-1 levels in co-cultures exposed to T-2 may be attributed to injury or cell damage.

TNF-α and IL-8 are canonical pro-inflammatory cytokines that may be produced by epithelial, stromal, and immune cells during injury [64]. Production of both cytokines increased in mono- and co-cultures exposed to T-2 suggests that mycotoxin triggers inflammatory responses in hepatic cultures (Fig. 4E, F).

The IL-6 was another cytokine expressed at high levels in microfluidic spheroid cultures. It exhibited higher expression in co-cultures than in monocultures, with T-2 exposure causing no change in monocultures but a decrease in co-cultures (see Fig. 4G). IL-6 is a complex, pleiotropic molecule known to exhibit either pro- or anti-inflammatory effects depending on the context (type of injury, biological system etc.). In the liver, IL-6 may be produced by hepatocytes or stellate cells in response to toxicants. It is also a mitogen involved in liver regeneration-proliferation of hepatocytes after partial hepatectomy [65]. For example, Norris et al. demonstrated that levels of hepatic IL-6 *in vitro* and *in vivo*, after partial hepatectomy, were increased by exposure to hepatocyte growth factor (HGF) [65]. Stellate cells are an important source of

HGF in the liver [37]. Thus, higher levels of IL-6 observed in co-cultures may be the result of stellate cells signaling to hepatic cells via HGF or other morphogens. Another explanation is that stellate cells produce IL-6 directly and account for the difference in IL-6 levels between monocultures and co-cultures [66]. We therefore posit that in our case, IL-6 may function as a mitogen and an indicator of cell health. This would explain declining levels of IL-6 after exposure to T-2 in co-cultures.

Similar to our study, Liu and colleagues reported that T-2 induced the expression of the pro-inflammatory cytokine TNF-α in BRL cells (a rat liver cell line) [67]. Additionally, TNF-α, IL-8 and IL-6 increased after T-2 exposure in PC12 cells used as neuron model cells [64]. Other authors reported that DON exposure to porcine hepatocytes, hepatocytes-Kupffer cell co-cultures, porcine alveolar macrophages and U937 cells decreased IL-6 levels [58,68,69]. In addition, our observations are in line with those of Nagashima and colleagues that mycotoxins such as Rubratoxin B, do not induce MCP-1 secretion in HepG2 monocultures and leads to GM-CSF secretion in hepatic cultures [70].

Taken together, our results point to expression of pro- (TNF-α, IL-8, GM-CSF, MCP-1) and anti-inflammatory cytokines (IL-1RA) in microfluidic hepatic spheroid cultures. These results also underscore that increasing culture complexity makes it more challenging to discern cellular origins of signals and their mechanisms of action (e.g. discussion around IL-6). In the future, we are planning to explore the mechanism of activation of inflammatory cytokines. The Nicotinamide N-methyltransferase (NNMT) is an enzyme present in the liver that regulates pro-inflammatory cytokines [71]. Xu et al. reported that NNMT may be a therapeutic target for DON-induced inflammation, because NNMT

overexpression decreased the pro-inflammatory cytokines [72,73]. Therefore, NNMT may be a target for attenuating liver inflammation after T-2 exposure.

4. Conclusions

In this work, we stablished and characterized microfluidic hepatic spheroid cultures comprised of HepG2 cells alone or in co-culture with stellate cells (LX2 cells). We used microfluidic cultures to evaluate exposure to mycotoxin T-2. We first demonstrated that hepatic spheroids formed faster, were more viable and functional in microfluidic devices than in commercial 3D cultures (Aggrewell plate). Then, we assessed cytotoxicity, cell function, gene expression and cytokine production of our hepatic cultures when exposed to the mycotoxin T-2. Importantly, the effects of the toxin were compared in microfluidic spheroid cultures of HepG2 cells alone or in co-cultures with stellate cells (LX2 cells).

We demonstrated that T-2 induced cell injury in 3D hepatic cultures, decreased albumin synthesis, and increased production of inflammatory cytokines including TNF-α. We also observed that the extent of injury was diminished by the presence of stellate cells in microfluidic spheroid cultures. The mechanisms by which stellate cells attenuate T-2 toxicity are multifactorial and need further work. Our studies highlighted two potential roles. First, while the expression of metabolizing enzymes was similar between the two microfluidic culture formats, induction of these enzymes was significantly lower in microfluidic co-cultures compared to monocultures. This leads us to believe that hepatocytes in co-cultures may not experience the same levels of T-2. Whether this is due to T-2 partitioning into lipid droplets within stellate cells or whether transport of T-2 is inhibited in some way remains to be determined. Second, stellate cells may be the source of signals (e.g. IL-6) that promote hepatic

phenotype and function, making hepatocytes less susceptible to insult with toxicants.

In summary, microfluidic 3D hepatic cultures were well-suited for testing T-2 mycotoxin. In the future, we will use this culture platform to evaluate therapeutic strategies for attenuating mycotoxin-induced inflammatory response. The microfluidic culture platform may be enhanced further by including more liver cell types and by using primary liver cells instead of cell lines.

Supplementary Materials: The following supporting information can be downloaded at: www.mdpi.com/xxx/s1, Figure S1: Comparison of spheroid formation on Aggrewells vs Micro-fluidic devices. A) Brightfield images. B) Analysis of Aggrewell images. C) Analysis of microfluidic images. D) Metrics analyzed in both culture method for comparison.

Author Contributions: Conceptualization, M.T., J.M.H-V, A.R.; methodology, M.T., J.M.H-V., A.M.G.-S., K.G., S.R., A.D.R.-F.; software, M.T., J.M.H-V., A.M.G.-S., S.R., A.D.R.-F.; validation, M.T., J.M.H-V., A.M.G.-S., G.S., A.R., Y.R.-C., M.-J.R; formal analysis, M.T., J.M.H-V., A.M.G.-S., S.R., A.D.R.-F; investigation, M.T., J.M.H-V., A.M.G.-S., K.G., S.R., A.D.R.-F; resources, M.T., J.M.H-V., A.M.G.-S., K.G., S.R., A.D.R.-F; data curation, M.T., J.M.H-V., A.M.G.-S., K.G., S.R., A.D.R.-F; writing—original draft preparation, M.T., J.M.H-V.; writing—review and editing, M.T., J.M.H-V, G.S., Y.R.-C., M.-J.R., A.R.; visualization, J.M.H-V, G.S., Y.R.-C., M.-J.R, A.R.; supervision, J.M.H-V, A.R.; project administration, M.-J.R., A.R; funding acquisition, A.R. All authors have read and agreed to the published version of the manuscript.

Funding: This research was funded by Alexander Revzin, grant number P30DK084567, R01DK134661 and R21CA236612.

Institutional Review Board Statement: Not applicable.

Informed Consent Statement: Not applicable.

Data Availability Statement: Data is contained within the article.

Acknowledgments: This work is part of a research project funded by the Spanish Ministry of Science and Innovation PID2020-115871RB-I00,

MCIN/AEI/10.13039/501100011033. Mercedes Taroncher is grateful for the pre-doctoral grant PRE2021-096941 provided by the Spanish Ministry of Science and Innovation project. Additional funding was provided by the grants from the National Institutes of Health (P30DK084567, R01DK134661 and R21CA236612).

Conflicts of Interest: The authors declare no conflicts of interest.

5. References

1. EFSA 2017a. Human and Animal Dietary Exposure to T-2 and HT-2 Toxin. EFSA Journal 2017, 15, doi:10.2903/j.efsa.2017.4972
2. Pereira, V.L.; Fernandes, J.O.; Cunha, S.C. Mycotoxins in Cereals and Related Foodstuffs: A Review on Oc-currence and Recent Methods of Analysis. Trends Food Sci Technol 2014, 36, 96–136, doi: 10.1016/j.tifs.2014.01.005
3. Alshannaq, A.; Yu, J.H. Occurrence, Toxicity, and Analysis of Major Mycotoxins in Food. Int J Environ Res Public Health 2017, 14 (6), 632, doi: 10.3390/ijerph14060632
4. EFSA 2017b. Appropriateness to Set a Group Health Based Guidance Value for T2 and HT2 Toxin and Its Modified Forms. EFSA Journal 2017, 15(1), doi:10.2903/j.efsa.2017.4655.
5. EFSA 2011. Scientific Opinion on the Risks for Animal and Public Health Related to the Presence of T-2 and HT-2 Toxin in Food and Feed. EFSA Journal 2011, 9(12) 2481, doi:10.2903/j.efsa.2011.2481.
6. Steinkellner, H.; Binaglia, M.; Dall'Asta, C.; Gutleb, A.C.; Metzler, M.; Oswald, I.P.; Parent-Massin, D.; Alex-ander, J. Combined Hazard Assessment of Mycotoxins and Their Modified Forms Applying Relative Potency Factors: Zearalenone and T2/HT2 Toxin. Food and Chemical Toxicology 2019, 131, 110599, doi: 10.1016/j.fct.2019.110599
7. EFSA 2022. Assessment of Information as Regards the Toxicity of T-2 and HT-2 Toxin for Ruminants. EFSA Journal 2022, 20, doi:10.2903/j.efsa.2022.7564.
8. Kimura, H.; Sakai, Y.; Fujii, T. Organ/Body-on-a-Chip Based on Microfluidic Technology for Drug Discovery. Drug Metab Pharmacokinet 2018, 33, 43–48, doi: 10.1016/j.dmpk.2017.11.003
9. Goossens, J.; Pasmans, F.; Verbrugghe, E.; Vandenbroucke, V.; De Baere, S.; Meyer, E.; Haesebrouck, F.; De Backer, P.; Croubels, S. Porcine Intestinal Epithelial Barrier Disruption by the Fusarium Mycotoxins Deox-ynivalenol and T-2 Toxin Promotes Transepithelial Passage of Doxycycline and Paromomycin. BMC Vet Res 2012, 8, 1-10, doi:10.1186/1746-6148-8-245.
10. Jia, Z.; Cheng, Y.; Jiang, X.; Zhang, C.; Wang, G.; Xu, J.; Li, Y.; Peng, Q.; Gao, Y. 3D Culture System for Liver Tissue Mimicking Hepatic Plates for Improvement of Human Hepatocyte (C3A) Function and Polarity. Bio-med Res Int 2020, 2020, doi:10.1155/2020/6354183.
11. Martínez-Alonso, C.; Taroncher, M.; Rodríguez-Carrasco, Y.; Ruiz, M.J. Evaluation of the Bioaccessible Frac-tion of T-2 Toxin from Cereals and Its Effect on the

Viability of Caco-2 Cells Exposed to Tyrosol. Toxins (Basel) 2023, 15(8) 493, doi:10.3390/toxins15080493.
12. Mulac, D.; Lepski, S.; Ebert, F.; Schwerdtle, T.; Humpf, H.U. Cytotoxicity and Fluorescence Visualization of Ergot Alkaloids in Human Cell Lines. J Agric Food Chem 2013, 61, 462–471, doi:10.1021/jf304569q.
13. Yang, L.; Tu, D.; Wang, N.; Deng, Z.; Zhan, Y.; Liu, W.; Hu, Y.; Liu, T.; Tan, L.; Li, Y.; et al. The Protective Ef-fects of DL-Selenomethionine against T-2/HT-2 Toxins-Induced Cytotoxicity and Oxidative Stress in Broiler Hepatocytes. Toxicology in Vitro 2019, 54, 137–146, doi:10.1016/j.tiv.2018.09.016.
14. Taroncher, M.; Rodríguez-Carrasco, Y.; Ruiz, M.J. T-2 Toxin and Its Metabolites: Characterization, Cytotoxic Mechanisms and Adaptive Cellular Response in Human Hepatocarcinoma (HepG2) Cells. Food and Chemical Toxicology 2020, 145, 111654, doi:10.1016/j.fct.2020.111654.
15. Taroncher, M.; Halbig, F.; Rodríguez-Carrasco, Y.; Ruiz, M.J. Stressful Effects of T-2 Metabolites and Defense Capability of HepG2 Cells. Toxins (Basel) 2022, 14(12) 841, doi:10.3390/toxins14120841.
16. Martínez-Alonso, C.; Taroncher, M.; Castaldo, L.; Izzo, L.; Rodríguez-Carrasco, Y.; Ritieni, A.; Ruiz, M.-J. Ef-fect of Phenolic Extract from Red Beans (Phaseolus Vulgaris L.) on T-2 Toxin-Induced Cytotoxicity in HepG2 Cells. 2022, 11(7) 1033, doi:10.3390/foods.
17. Jensen, C.; Teng, Y. Is It Time to Start Transitioning From 2D to 3D Cell Culture? Front Mol Biosci 2020, 7, 33.
18. de Hoyos-Vega, J.M.; Hong, H.J.; Stybayeva, G.; Revzin, A. Hepatocyte Cultures: From Collagen Gel Sand-wiches to Microfluidic Devices with Integrated Biosensors. APL Bioeng 2021, 5 (4), doi: 10.1063/5.0058798
19. Mukundan, S.; Bell, J.; Teryek, M.; Hernandez, C.; Love, A.C.; Parekkadan, B.; Chan, L.L.Y. Automated As-sessment of Cancer Drug Efficacy On Breast Tumor Spheroids in AggrewellTM400 Plates Using Image Cy-tometry. J Fluoresc 2022, 32, 521–531, doi:10.1007/s10895-021-02881-3.
20. Dunn, J.C.Y.; Yarmush, M.L.; Koebe, H.G.; Tompkins, R.G. Hepatocyte Function and Extracellular Matrix Geometry: Long-Term Culture in a Sandwich Configuration. The FASEB journal 1989, 3(2) 174-177, doi: 10.1096/fasebj.3.2.2914628
21. Foster, E.; You, J.; Siltanen, C.; Patel, D.; Haque, A.; Anderson, L.; Revzin, A. Heparin Hydrogel Sandwich Cultures of Primary Hepatocytes. Eur Polym J 2015, 72, 726–735, doi:10.1016/j.eurpolymj.2014.12.033.
22. Vongchan, P.; Warda, M.; Toyoda, H.; Toida, T.; Marks, R.M.; Linhardt, R.J. Structural Characterization of Human Liver Heparan Sulfate. Biochim Biophys Acta Gen Subj 2005, 1721, 1–8, doi:10.1016/j.bbagen.2004.09.007.
23. Berthiaume, F., M.P.V., T.M., & Y.M.L. Effect of Extracellular Matrix Topology on Cell Structure, Function, and Physiological Responsiveness: Hepatocytes Cultured in a Sandwich Configuration. The FASEB 1996, 10, 1471–1484, doi: 10.1096/fasebj.10.13.8940293

24. Hughes, D.L.; Hughes, A.; Soonawalla, Z.; Mukherjee, S.; O'neill, E. Dynamic Physiological Culture of Ex Vivo Human Tissue: A Systematic Review. Cancers (Basel) 2021, 13(12) 2870, doi: 10.3390/cancers13122870
25. Zhang, Y.S.; Zhang, Y.N.; Zhang, W. Cancer-on-a-Chip Systems at the Frontier of Nanomedicine. Drug Discov Today 2017, 22, 1392–1399, doi: 10.1016/j.drudis.2017.03.011
26. Trujillo-de Santiago, G.; Flores-Garza, B.G.; Tavares-Negrete, J.A.; Lara-Mayorga, I.M.; González-Gamboa, I.; Zhang, Y.S.; Rojas-Martínez, A.; Ortiz-López, R.; Álvarez, M.M. The Tumor-on-Chip: Recent Advances in the Development of Microfluidic Systems to Recapitulate the Physiology of Solid Tumors. Materials 2019, 12(18), 2945, doi: 10.3390/ma12182945
27. Hoon Choi, J.; Loarca, L.; De Hoyos-Vega, J.M.; Neda Dadgar, X.; Loutherback, K.; Vijay Shah, X.H.; Styba-yeva, G.; Revzin, A.; Hoyos-Vega, D.J. Microfluidic Confinement Enhances Phenotype and Function of Hepatocyte Spheroids Microfluidic Confine-Ment Enhances Phenotype and Function of Hepatocyte Spheroids. Am J Physiol Cell Physiol 2020, 319 (3) C552-C560, doi:10.1152/ajpcell.00094.2020.-A.
28. Dadgar, N.; Gonzalez-Suarez, A.M.; Fattahi, P.; Hou, X.; Weroha, J.S.; Gaspar-Maia, A.; Stybayeva, G.; Revzin, A. A Microfluidic Platform for Cultivating Ovarian Cancer Spheroids and Testing Their Responses to Chemotherapies. Microsyst Nanoeng 2020, 6(1) 93, doi:10.1038/s41378-020-00201-6.
29. de Hoyos-Vega, J.M.; Hong, H.J.; Loutherback, K.; Stybayeva, G.; Revzin, A. A Microfluidic Device for Long-Term Maintenance of Organotypic Liver Cultures. Adv Mater Technol 2023, 8, 2201121, doi:10.1002/admt.202201121.
30. Fattahi, P.; de Hoyos-Vega, J.M.; Choi, J.H.; Duffy, C.D.; Gonzalez-Suarez, A.M.; Ishida, Y.; Nguyen, K.M.; Gwon, K.; Peterson, Q.P.; Saito, T.; et al. Guiding Hepatic Differentiation of Pluripotent Stem Cells Using 3D Microfluidic Co-Cultures with Human Hepatocytes. Cells 2023, 12(15) 1982, doi:10.3390/cells12151982.
31. Kane, B.J.; Zinner, M.J.; Yarmush, M.L.; Toner, M. Liver-Specific Functional Studies in a Microfluidic Array of Primary Mammalian Hepatocytes. Anal Chem 2006, 78, 4291–4298, doi:10.1021/ac051856v.
32. Clement, B.; Guguen-guillouzo, C.; Campion, J.; Glaise, D.; Bourel, M.; Guillouzo, A.; Guguen-Guillouzo, C. Long-Term Co-Cultures of Adult Human Hepatocytes with Rat Liver Epithelial Cells: Modulation of Albu-min Secretion and Accumulation of Extracellular Material. Hepatology 1984; Vol. 4(3) 373-380, doi: 10.1002/hep.1840040305
33. Khetani, S.R.; Bhatia, S.N. Microscale Culture of Human Liver Cells for Drug Development. Nat Biotechnol 2008, 26, 120–126, doi:10.1038/nbt1361.
34. Jang, K.-J.; Otieno, M.A.; Ronxhi, J.; Lim, H.-K.; Ewart, L.; Kodella, K.R.; Petropolis, D.B.; Kulkarni, G.; Rubins, J.E.; Conegliano, D.; et al. Reproducing Human and Cross-Species Drug Toxicities Using a Liver-Chip; 2019; 11(517) eaax5516, doi: 10.1126/scitranslmed.aax5516

35. Ukairo, O.; Kanchagar, C.; Moore, A.; Shi, J.; Gaffney, J.; Aoyama, S.; Rose, K.; Krzyzewski, S.; Mcgeehan, J.; Andersen, M.E.; et al. Long-Term Stability of Primary Rat Hepatocytes in Micropatterned Cocultures. J Bio-chem Mol Toxicol 2013, 27, 204–212, doi:10.1002/jbt.21469.
36. Zhou, Q.; Patel, D.; Kwa, T.; Haque, A.; Matharu, Z.; Stybayeva, G.; Gao, Y.; Diehl, A.M.; Revzin, A. Liver Injury-on-a-Chip: Microfluidic Co-Cultures with Integrated Biosensors for Monitoring Liver Cell Signaling during Injury. Lab Chip 2015, 15, 4467–4478, doi:10.1039/c5lc00874c.
37. Friedman, S.L. Hepatic Stellate Cells: Protean, Multifunctional, and Enigmatic Cells of the Liver. 2008, 88(1) 125-172, doi:10.1152/physrev.00013.2007.
38. Arzt, M.; Deschamps, J.; Schmied, C.; Pietzsch, T.; Schmidt, D.; Tomancak, P.; Haase, R.; Jug, F. LABKIT: Labeling and Segmentation Toolkit for Big Image Data. Front Comput Sci 2022, 4, 10, doi:10.3389/fcomp.2022.777728.
39. Amaral, R.L.F.; Miranda, M.; Marcato, P.D.; Swiech, K. Comparative Analysis of 3D Bladder Tumor Spheroids Obtained by Forced Floating and Hanging Drop Methods for Drug Screening. Front Physiol 2017, 8, 284532, doi:10.3389/fphys.2017.00605.
40. Mora, C.F.; Kwan, A.K.H. Sphericity, Shape Factor, and Convexity Measurement of Coarse Aggregate for Concrete Using Digital Image Processing. Cement and concrete research 2000, 30(3) 351-358, doi: 10.1016/S0008-8846(99)00259-8
41. Kurosawa, H.; Yasumoto, K.; Kimura, T.; Amano, Y. Polyurethane Membrane as an Efficient Immobilization Carrier for High-Density Culture of Rat Hepatocytes in the Fixed-Bed Reactor. Biotechnol Bioeng 2000, 70, 160–166, doi:10.1002/1097-0290(20001020)70:2<160::AID-BIT5>3.0.CO;2-C.
42. Bechmann, L.P.; Hannivoort, R.A.; Gerken, G.; Hotamisligil, G.S.; Trauner, M.; Canbay, A. The Interaction of Hepatic Lipid and Glucose Metabolism in Liver Diseases. Journal of hepatology 2012, 56(4) 952-964, doi: 10.1016/j.jhep.2011.08.025
43. Crettol, S.; Petrovic, N.; Murray, M. Pharmacogenetics of Phase I and Phase II Drug Metabolism; 2010; Vol. 16(2) 204-219, doi: 10.2174/138161210790112674
44. Guengerich, F.P. Cytochrome P450s and Other Enzymes in Drug Metabolism and Toxicity; 2006; Vol. 8, E101-E111.
45. Williams, J.A.; Hyland, R.; Jones, B.C.; Smith, D.A.; Hurst, S.; Goosen, T.C.; Peterkin, V.; Koup, J.R.; Ball, S.E. Drug-Drug Interactions for UDP-Glucuronosyltransferase Substrates: A Pharmacokinetic Explanation for Typically Observed Low Exposure (AUC 1/AUC) Ratios. Drug Metabolism and Disposition 2004, 32, 1201–1208, doi: 10.1124/dmd.104.000794
46. Taroncher, M.; Rodríguez-Carrasco, Y.; Ruiz, M.J. Interactions between T-2 Toxin and Its Metabolites in HepG2 Cells and in Silico Approach. Food and Chemical Toxicology 2021, 148, 111942, doi:10.1016/j.fct.2020.111942.
47. Lootens, O.; Vermeulen, A.; Croubels, S.; De Saeger, S.; Van Bocxlaer, J.; De Boevre, M. Possible Mechanisms of the Interplay between Drugs and Mycotoxins—

Is There a Possible Impact? Toxins (Basel) 2022, 14 (12) 873, doi: 10.3390/toxins14120873
48. Song, W.; Wang, Y.; Huang, T.; Liu, Y.; Chen, F.; Chen, Y.; Jiang, Y.; Zhang, C.; Yang, X. T-2 Toxin Metabolism and Its Hepatotoxicity: New Insights on the Molecular Mechanism and Detoxification. Environmental Pollu-tion 2023, 330, 121784, doi: 10.1016/j.envpol.2023.121784
49. Wen, J.; Mu, P.; Deng, Y. Mycotoxins: Cytotoxicity and Biotransformation in Animal Cells. Toxicol Res (Camb) 2016, 5, 377–387, doi: 10.1039/c5tx00293a
50. Lin, N.N.; Chen, J.; Xu, B.; Wei, X.; Guo, L.; Xie, J.W. The Roles of Carboxylesterase and CYP Isozymes on the in Vitro Metabolism of T-2 Toxin. Mil Med Res 2015, 2, 1-7, doi:10.1186/s40779-015-0041-6.
51. Trusal, L.R. Metabolism of T-2 mycotoxin by cultured cells. Toxicon 1986; 24(6) 597-603, doi: 10.1016/0041-0101(86)90180-7
52. Lindberg, L.A., G.Y., K.E. Massive Lipid Accumulation in Mink Liver Stellate Cells May Be Caused by Fusarium Mycotoxins in the Feed. Acta vet. scand 1985, 26, 423–424, doi: 10.1186/BF03546543
53. Stanley, L.A.; Wolf, C.R. Through a Glass, Darkly? HepaRG and HepG2 Cells as Models of Human Phase I Drug Metabolism. Drug Metab Rev 2022, 54, 46–62, doi: 10.1080/03602532.2022.2039688
54. Artursson, P.; Palm, K.; Luthman, K. Caco-2 Monolayers in Experimental and Theoretical Predictions q of Drug Transport; Advanced drug delivery reviews 2001; 46(1-3)27-43, doi: 10.1016/S0169-409X(00)00128-9
55. Kadota, T.; Furusawa, H.; Hirano, S.; Tajima, O.; Kamata, Y.; Sugita-Konishi, Y. Comparative Study of Deox-ynivalenol, 3-Acetyldeoxynivalenol, and 15-Acetyldeoxynivalenol on Intestinal Transport and IL-8 Secretion in the Human Cell Line Caco-2. Toxicology in Vitro 2013, 27, 1888–1895, doi:10.1016/j.tiv.2013.06.003.
56. Sergent, T.; Parys, M.; Garsou, S.; Pussemier, L.; Schneider, Y.J.; Larondelle, Y. Deoxynivalenol Transport across Human Intestinal Caco-2 Cells and Its Effects on Cellular Metabolism at Realistic Intestinal Concen-trations. Toxicol Lett 2006, 164, 167–176, doi:10.1016/j.toxlet.2005.12.006.
57. Kim, Y.S.; Ho, S.B. Intestinal Goblet Cells and Mucins in Health and Disease: Recent Insights and Progress. Curr Gastroenterol Rep 2010, 12, 319–330.
58. Döll, S.; Schrickx, J.A.; Dänicke, S.; Fink-Gremmels, J. Deoxynivalenol-Induced Cytotoxicity, Cytokines and Related Genes in Unstimulated or Lipopolysaccharide Stimulated Primary Porcine Macrophages. Toxicol Lett 2009, 184, 97–106, doi:10.1016/j.toxlet.2008.10.024.
59. Königs, M.; Schwerdt, G.; Gekle, M.; Humpf, H.U. Effects of the Mycotoxin Deoxynivalenol on Human Pri-mary Hepatocytes. Mol Nutr Food Res 2008, 52, 830–839, doi:10.1002/mnfr.200700439.
60. Volarevic, V.; Al-Qahtani, A.; Arsenijevic, N.; Pajovic, S.; Lukic, M.L. Interleukin-1 Receptor Antagonist (IL-1Ra) and IL-1Ra Producing Mesenchymal Stem Cells as

Modulators of Diabetogenesis. Autoimmunity 2010, 43, 255–263, doi: 10.3109/08916930903305641
61. Karmacharya, M.B.; Hada, B.; Park, S.R.; Kim, K.H.; Choi, B.H. Granulocyte-Macrophage Colony-Stimulating Factor (GM-CSF) Shows Therapeutic Effect on Dimethylnitrosamine (DMN)-Induced Liver Fibrosis in Rats. PLoS One 2022, 17(9) e0274126, doi:10.1371/journal.pone.0274126.
62. Maher, J.J. Interactions between Hepatic Stellate Cells and the Immune System; In seminars in liver disease 2001; 21 (3) 417-426, doi: 10.1055/s-2001-17555
63. Marra, F.; Romanelli, R.G.; Giannini, C.; Failli, P.; Pastacaldi, S.; Arrighi, M.C.; Pinzani, M.; Laffi, G.; Montalto, P.; Gentilini, P. Monocyte Chemotactic Protein-1 as a Chemoattractant for Human Hepatic Stellate Cells; Hepatology 1999; 29(1) 140-148, doi: 10.1002/hep.510290107
64. Pei, X.; Jiang, H.; Liu, X.; Li, L.; Li, C.; Xiao, X.; Li, D.; Tang, S. Targeting HMGB1 Inhibits T-2 Toxin-Induced Neurotoxicity via Regulation of Oxidative Stress, Neuroinflammation and Neuronal Apoptosis. Food and Chemical Toxicology 2021, 151, 112134, doi:10.1016/j.fct.2021.112134.
65. Norris, C.A.; He, M.; Kang, L.I.; Ding, M.Q.; Radder, J.E.; Haynes, M.M.; Yang, Y.; Paranjpe, S.; Bowen, W.C.; Orr, A.; et al. Synthesis of IL-6 by Hepatocytes Is a Normal Response to Common Hepatic Stimuli. PLoS One 2014, 9(4) e96053, doi:10.1371/journal.pone.0096053.
66. Kim, Y.; Fiel, M.I.; Albanis, E.; Chou, H.I.; Zhang, W.; Khitrov, G.; Friedman, S.L. Anti-Fibrotic Activity and Enhanced Interleukin-6 Production by Hepatic Stellate Cells in Response to Imatinib Mesylate. Liver Interna-tional 2012, 32, 1008–1017, doi:10.1111/j.1478-3231.2012.02806.x.
67. Liu, X.; Pan, Z.; Wang, Y. Ultrasound-Assisted Turbine Bead Milling for Disintegration of Nannochloropsis Oculata Cells. J Appl Phycol 2019, 31, 1651–1659, doi:10.1007/s10811-018-1702-0.
68. Döll, S.; Schrickx, J.A.; Dänicke, S.; Fink-Gremmels, J. Interactions of Deoxynivalenol and Lipopolysaccha-rides on Cytokine Excretion and MRNA Expression in Porcine Hepatocytes and Kupffer Cell Enriched Hepatocyte Cultures. Toxicol Lett 2009, 190, 96–105, doi:10.1016/j.toxlet.2009.07.007.
69. Sugita-Konishi, Y.; Pestka, J.J. Differential Upregulation of TNF-α, IL-6, and IL-8 Production by Deoxyniva-lenol (Vomitoxin) and Other 8-Ketotrichothecenes in a Human Macrophage Model. J Toxicol Environ Health A 2001, 64, 619–636, doi:10.1080/152873901753246223.
70. Nagashima, H.; Nakamura, K.; Goto, T. Rubratoxin B Induced the Secretion of Hepatic Injury-Related Colony Stimulating Factors in Human Hepatoma Cells. Toxicol Lett 2003, 145, 153–159, doi:10.1016/S0378-4274(03)00270-4.
71. Yang, D.; Zhang, X.; Yue, L.; Hu, H.; Wei, X.; Guo, Q.; Zhang, B.; Fan, X.; Xin, Y.; Oh, Y.; et al. Thiamethoxam Induces Nonalcoholic Fatty Liver Disease in Mice via Methionine Metabolism Disturb via Nicotinamide N-Methyltransferase Overexpression. Chemosphere 2021, 273, 129727, doi:10.1016/j.chemosphere.2021.129727.

72. Liu, A.; Guo, M.; He, L.; Martínez, M.A.; Martínez, M.; Lopez-Torres, B.; Martínez-Larrañaga, M.R.; Wang, X.; Anadón, A.; Ares, I. Nicotinamide N-Methyltransferase Protects against Deoxynivalenol-Induced Growth Inhibition by Suppressing pro-Inflammatory Cytokine Expression. Food and Chemical Toxicology 2022, 163, 112969, doi:10.1016/j.fct.2022.112969.
73. Xu, J.; Moatamed, F.; Caldwell, J.S.; Walker, J.R.; Kraiem, Z.; Taki, K.; Brent, G.A.; Hershman, J.M. Enhanced Expression of Nicotinamide N-Methyltransferase in Human Papillary Thyroid Carcinoma Cells. Journal of Clinical Endocrinology and Metabolism 2003, 88, 4990–4996, doi:10.1210/jc.2002-021843.

SUPPLEMENATRY INFORMATION

USING MICROFLUIDIC HEPATIC SPHEROID CULTURES TO ASSESS LIVER TOXICITY OF T-2 MYCOTOXIN

Mercedes Taroncher[1,2], Alan M. Gonzalez-Suarez[1], Kihak Gwon[1], Samuel Romero[3], Angel D. Reyes-Figueroa[3,4], Yelko Rodríguez-Carrasco[2], María-José Ruiz[2], Gulnaz Stybayeva[1], Alexander Revzin[1,*], Jose M. de Hoyos-Vega[1,*]

[1] Department of Physiology and Biomedical Engineering, Mayo Clinic, Rochester, MN, USA 55901

[2] Research Group in Alternative Methods for Determining Toxics Effects and Risk Assessment of Contami-nants and Mixtures (RiskTox). Laboratory of Food Chemistry and Toxicology, Faculty of Pharmacy, Uni-versity of Valencia, Av. Vicent Andrés Estellés s/n, 46100, Valencia, SPAIN

[3] Centro de Investigación en Matemáticas Unidad Monterrey, Apodaca, NL, MEXICO 66628

[4] Consejo Nacional de Ciencia y Tecnología, CDMX, MEXICO 03940

* Corresponding authors: dehoyos-vega.jose@mayo.edu; Revzin.alexander@mayo.edu

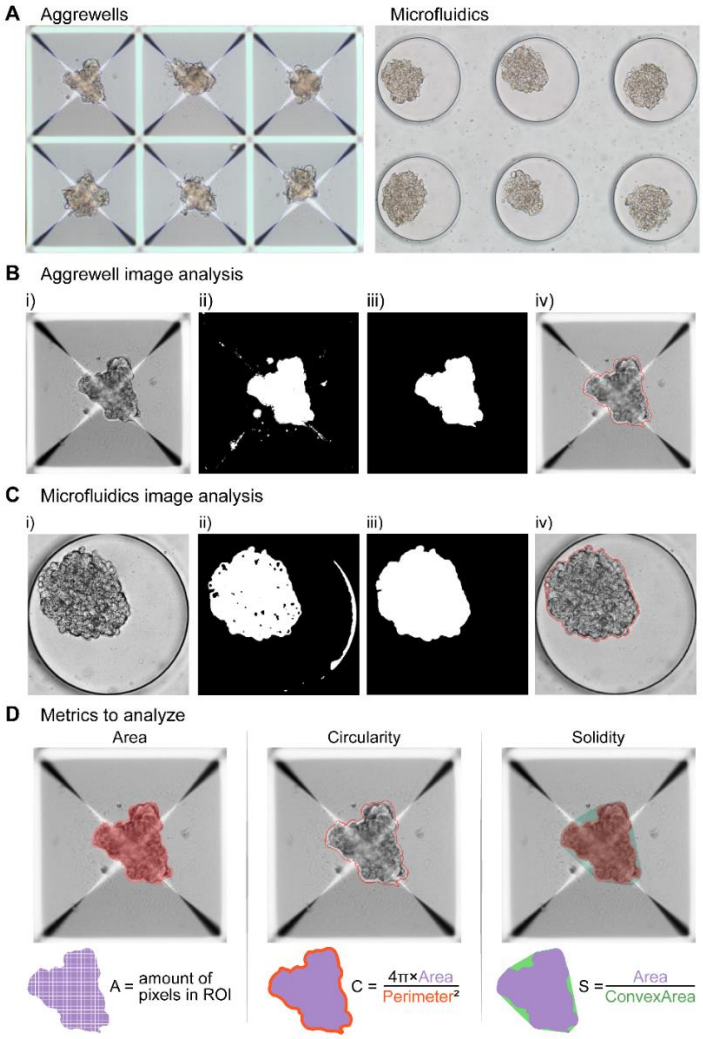

Figure S1. Comparison of spheroid formation on a microfluidic device and a commercial 3D plate. A) Brightfield images. B) Analysis of images in an Aggrewell plate. C) Analysis of microfluidic images. D) Metrics analyzed in both culture method for comparison.

Spheroid Formation Image Analysis

HepG2 cells were cultured in Aggrewell plate and in microfluidic devices as described in Methods section 2.3. Brightfield images were acquired just after cell seeding and then every 24 h for 5 days (Fig. S1A). Images were analyzed using Python and ImageJ for area, solidity, and circularity of each spheroid.

Image Analysis in Aggrewell Plate

Aggrewell images were segmented using Fiji (ImageJ) and the plugin Labkit [1] – Intuitive Pixel Classification [1]. The segmentation resulted in a binary image with the spheroid pixels localized (Fig. S1Bii), with some extra pixels. We then used Python (v3.11.5) with the OPENCV2 library (v4.8.1) to crop each well and maintain only the region of interest (largest element of the image), followed by binary transformations to remove extra pixels, dilate thin lines, and fill the object area if any black spots were found. The area of the spheroid in pixel was determined as the area of the white element in the binary image (Fig. S1Biii). Finally, we determined the perimeter of the spheroid by defining the contour of the white object in the binary image. Figure S1B shows the segmentation steps for aggrewell images.

Image Analysis in a Microfluidic Device

To segment the spheroids in the microfluidic device images we only used Python and OPENCV2. The images from microfluidic devices show a smoother background compared to the aggrewell images, making the determination of the spheroid simpler. We first detected each circle in the image corresponding to the

microwell walls, and deleted the pixels external to the circle. Then, we inverted the image color and applied a median blur filter to denoise the image and threshold to obtain the area of the spheroid as a binary image. We applied binary transformations to remove unwanted elements and filling black holes inside the spheroid to obtain the final spheroid area. Similarly to the aggrewell images, we determined the area and perimeter of the spheroid using the binary image. Fig. S1C shows the image segmentation steps for microfluidic cultures.

Metrics for Image Analysis

After image segmentation, we used two metrics to determine if the spheroid formation was different between Aggrewell and microfluidic cultures: circularity and solidity [2,3]. For each spheroid at each time point, we calculated its circularity and solidity. The circularity of the spheroid was calculated by following equation (1) [2]. A value of 1 (100%) would mean that the spheroid shape is closer to a circle.

$$Circularity = \frac{4\pi \cdot Area}{Perimeter^2} \qquad (1)$$

For solidity, we use the spheroid perimeter and the determined a convex area (Fig. S1D) that represents a smooth spheroid. We then compare the area of the actual spheroid vs the convex area. This comparison returns a value between 0-1, where a value closer to 1 (100%) would mean that the spheroid has a smooth surface. After calculating the circularity and solidity of each spheroid, we plotted the results in scatter plots to show the differences between culture conditions.

References:

1. Arzt, M.; Deschamps, J.; Schmied, C.; Pietzsch, T.; Schmidt, D.; Tomancak, P.; Haase, R.; Jug, F. LABKIT: Labeling and Segmentation Toolkit for Big Image Data. Front Comput Sci 2022, 4, 10, doi:10.3389/fcomp.2022.777728.

2. Amaral, R.L.F.; Miranda, M.; Marcato, P.D.; Swiech, K. Comparative Analysis of 3D Bladder Tumor Spheroids Obtained by Forced Floating and Hanging Drop Methods for Drug Screening. Front Physiol 2017, 8, 284532, doi:10.3389/fphys.2017.00605.

3. Mora, C.F.; Kwan, A.K.H. Sphericity, Shape Factor, and Convexity Measurement of Coarse Aggregate for Concrete Using Digital Image Processing; 2000, 30(3) 351-358, doi: 10.1016/S0008-8846(99)00259-8

4. Discusión

Discussion

4. DISCUSIÓN

En la presente Tesis Doctoral se han evaluado los efectos tóxicos y mecanismos de acción de la T-2 y sus metabolitos mediante modelos alternativos a la experimentación animal. Para ello, se determinó la predicción toxicocinética de dichas micotoxinas mediante modelos computacionales bien establecidos para simular los procesos ADME, la absorción gastrointestinal y penetración de la BHE. Para confirmar los datos de predicción obtenidos, posteriormente se evaluó el efecto citotóxico de la T-2 y sus principales metabolitos, HT-2, Neo, T2-triol y T2-tetraol, de forma individual y combinada, en la línea celular HepG2. A continuación, se determinó el tipo de interacción entre la T-2 y sus metabolitos. Se identificaron los productos de biotransformación de la T-2 intracelulares y en el medio extracelular durante un ciclo de 24 h en las células HepG2. Posteriormente, se evaluaron los mecanismos de toxicidad de la T-2 en las células HepG2. Concretamente, se determinó el estrés oxidativo producido mediante la generación de ROS y se observó un incremento del estrés oxidativo en las células HepG2 expuestas a T-2 y sus metabolitos. Por ello, el siguiente objetivo planteado fue evaluar el sistema de defensa intracelular enzimático (GPx, GST, CAT y SOD) y no enzimático (GSH) de las células HepG2 ante la exposición de dichas micotoxinas; así como el efecto protector de algunos alimentos de la dieta como son las judías rojas, microalgas e hidrolizados de pescado, que son fuentes importantes de aporte de compuestos antioxidantes en la dieta. Seguidamente, se determinaron otros posibles mecanismos de acción causantes de los efectos tóxicos de la T-2, tales como la proliferación celular, alteraciones en el ciclo celular, la inducción de apoptosis y necrosis y el daño al ADN. Por último, debido a que los cultivos en monocapa no reproducen con exactitud la respuesta fisiológica de los sistemas *in vivo* expuestos a los

compuestos tóxicos, se estudiaron los efectos tóxicos de la T-2 en modelos 3D (esferoides) dentro de dispositivos microfluídicos en monocultivo de células HepG2 y co-cultivo de células HepG2-LX2. Al introducir otra línea celular presente en los hepatocitos e incluir la microfluídica, se obtuvieron resultados de toxicidad más cercanos a los que se obtendrían en un sistema *in vivo*.

4.1. Determinación del perfil toxicológico y ADME de la T-2 y sus metabolitos

Los métodos computacionales pueden mejorar en gran medida la comprensión de las bases moleculares y biológicas de la toxicidad producida por las sustancias químicas, y ofrecen una mayor confianza respecto a los factores críticos para evaluar el riesgo por exposición a sustancias tóxicas. Además, son métodos más aceptables desde el punto de vista ético y con un enfoque sostenible respecto a las alternativas a los métodos *in vivo*.

La evaluación de los procesos toxicocinéticos (ADME/t) de la T-2, HT-2, Neo, T2-triol y T2-tetraol se predijo utilizando el programa de predicción libre AdmetSAR versión 2, y la predicción de la absorción gastrointestinal (HIA) y penetración de la BHE se evaluó con la herramienta SwissADME, mediante el método del BOILED-Egg.

Según la herramienta AdmetSAR, la mayoría de las micotoxinas presentan una buena solubilidad en disolventes orgánicos por su valor log*P* alto, excepto el T2-tetraol. Además, todas muestran buena penetración a través de la BHE. Según las reglas de Lipinski, tanto la T-2 como sus metabolitos muestran una buena absorción después de la exposición oral, aunque la T-2 mostró la mayor HIA, debido a que es altamente lipófila para atravesar las membranas celulares. Por otro lado, se predice que Neo, T2-triol y T2-tetraol son buenos sustratos de

la P-gp, una bomba de eflujo transmembrana, por lo que esta unión podría impedir la mayor absorción gastrointestinal humana en comparación con las otras micotoxinas (T-2 y HT-2). Todas las micotoxinas analizadas son sustrato de la isoenzima CYP3A4, implicada en la fase I del metabolismo oxidativo. Además, Neo, T2-triol y T2-tetraol son sustratos para el aclaramiento metabólico mediado por UDP-glucuronil transferasas (UGT). La T-2 y sus metabolitos inhiben los transportadores de los hepatocitos OATP1b1 y OATP1b3 y de la bomba de exportación de sales biliares BSEP. Esto es importante cuando se observan niveles elevados de ácidos biliares, debido a la inhibición de su exportación, puede provocar colestasis y hepatotoxicidad en sistemas *in vivo*. Por otra parte, los datos de genotoxicidad mostraron resultados negativos para todas las micotoxinas, a excepción del test de Ames para T-2 y HT-2. En resumen, como se esperaba, la T-2 y sus metabolitos indujeron daño hepático y mostraron alta toxicidad.

Según el método del BOILED-Egg, se predice una alta absorción intestinal y pobre absorción a nivel cerebral. Y de la misma manera que AdmetSAR, predice que T-2 y HT-2 no son buenos sustratos de la P-gp, al contrario que Neo, T2-triol y T2-tetraol.

Los modelos de predicción *in silico* presentan una gran variedad de resultados, dependiendo del software utilizado. Los modelos SwissADME y AdmetSAR se consideran adecuados para predecir el comportamiento de las micotoxinas, porque proporcionan datos sobre mecanismos de acción de las micotoxinas que presentan un posible riesgo tóxico potencial. Sin embargo, es necesario comprender cuándo y cómo se puede utilizar estos métodos. Además, se deberán realizar futuros estudios para mejorar la estandarización, armonización

y actualización de los métodos *in silico*. Sin embargo, no hay que olvidar que estos métodos predictivos requieren de la complementación de ensayos *in vitro* para verificar la predicción del perfil de toxicidad de T-2 y sus metabolitos.

Por tanto, un enfoque integrado usando modelos *in silico* e *in vitro* puede ser útil para la evaluación del riesgo por exposición a la T-2 y sus metabolitos. Así, el siguiente objetivo fue evaluar los efectos tóxicos por estas micotoxinas en células hepáticas y los mecanismos de acción por los que causan dichos efectos.

4.2. Viabilidad celular

4.2.1. Efectos tóxicos de la T-2 y sus metabolitos

Se evaluó la citotoxicidad de la T-2, HT-2, Neo, T2-triol y T2-tetraol en las células HepG2 tras 24 y 48 h de exposición. Los métodos que se utilizaron fueron el de la sal de tetrazolio (MTT) y el del contenido de proteínas totales (PT).

La T-2 disminuyó la viabilidad en las células HepG2 de manera dependiente de la concentración y del tiempo de exposición, con un rango de valores de IC_{50} de 61.9 ± 2,4 nM hasta 70,7 ± 7,4 nM tras 24 y 48 h de exposición, respectivamente, considerando ambos métodos. A concentraciones bajas se observó un aumento de la viabilidad celular. Esto puede ser debido a que los sistemas biológicos pueden adaptarse a una exposición crónica de niveles bajos de agentes tóxicos y protegerse frente a efectos negativos a dosis más altas, en un proceso llamado hórmesis. Por ello, se evalúa la posible adaptación de las HepG2 expuestas a la T-2. Con este objetivo, se hace un pretratamiento de T-2 con dosis bajas durante 2 h (0,25 y 2,5 nM, basadas en la cantidad de T-2 encontrada en cereales y la ingesta poblacional media de ellos) y posterior adición de dosis más altas (10, 15 y 20 nM) no observándose ningún aumento en la

viabilidad celular. Por tanto, se concluye que las células HepG2 no experimentan ninguna adaptación frente a la toxicidad de la T-2.

En cuanto al resto de metabolitos, los valores de IC_{50} durante 24 y 48 h de exposición por el método del MTT y PC abarcaron un rango desde 59,6 ± 1,1 nM hasta 68,2 ± 5,4 nM para la HT-2; desde 55,6 ± 13,7 nM hasta 121,1 ± 16,0 nM para el Neo; desde 870,0 ± 240,0 nM hasta 1240,0 ± 310,0 nM para el T2-triol y desde 1380,0 ± 340,0 nM hasta 2770,0 ± 80,0 nM para el T2-tetraol. El orden de citotoxicidad disminuye en el siguiente orden: T-2=HT-2 > Neo > T2-triol > T2-tetraol. Tanto la función mitocondrial (evaluada con el ensayo del MTT) como las proteínas (PT) disminuyeron con concentraciones crecientes de la T-2 y sus metabolitos y con el tiempo de exposición. Los resultados de IC_{50} obtenidos contribuyeron a la elección de las concentraciones seleccionadas para los ensayos posteriores. La disminución de la toxicidad de los metabolitos respecto a la T-2 puede deberse al aumento de grupos hidroxilo como consecuencia de la hidrólisis en los procesos de biotransformación.

Los resultados obtenidos en este trabajo, están en concordancia con los datos publicados en la bibliografía consultada. No obstante, se puede observar una gran variabilidad con respecto a la viabilidad celular, ya que los valores de IC_{50} dependen de la línea celular, el tiempo de exposición y el método utilizado.

4.2.2. Efectos tóxicos de las combinaciones de la T-2 y sus metabolitos

Debido a que los consumidores estamos expuestos de forma simultánea a varias micotoxinas a través de la dieta, o a una micotoxina y sus metabolitos, el siguiente paso fue evaluar los efectos citotóxicos de las combinaciones binarias de la T-2 y sus metabolitos. Para los estudios de las mezclas de micotoxinas se seleccionó el método del MTT y tiempo de exposición 24 h.

Las curvas de relación dosis-respuesta no muestran diferencias entre la citotoxicidad de las combinaciones binarias y las micotoxinas evaluadas individualmente en las células HepG2. Los valores de IC_{50} de las combinaciones fueron: 34,42 ± 0,58 nM para la combinación de T-2 + HT-2; 55,04 ± 14,24 nM para T-2 + Neo; 257,09 ± 25,21 nM para T-2 + T2-triol; 38,51 ± 16,83 nM para Neo + HT-2; 234,83 ± 8,65 nM para HT-2 + T2-triol; 460,77 ± 77,72 nM para Neo + T2-triol; 816,96 ± 167,43 nM para T2-triol + T2-tetraol; 713,66 ± 136,03 nM para T-2 + T2-tetraol; 709,59 ± 61,63 nM para HT-2 + T2-tetraol y 721,64 ± 38,97 nM para Neo + T2-tetraol.

La mezcla T-2 + HT-2 mostró el mayor potencial citotóxico con el valor más bajo de IC_{50} (34,42 nM), mientras que las combinaciones que mostraron el menor efecto citotóxico fueron las que incluían T2-tetraol en la mezcla.

Posteriormente, para determinar el tipo de interacción entre las micotoxinas en las combinaciones se aplicó el método de las isobolas de Chou (2006) y Chou and Talalay (1984) basado en el índice de combinación (IC). Los resultados obtenidos mostraron un efecto antagónico (IC > 1) en todas las fracciones afectadas de las combinaciones T-2 + T2-triol, T-2 + Neo, T2-triol + Neo, T2-tetraol + Neo y Neo + HT-2. Sin embargo, se observaron efectos antagónicos a fracciones afectadas bajas y aditivos (IC < 1) a fracciones afectadas altas en las combinaciones T-2 + HT-2, T-2 + T2-tetraol, T2-triol + HT-2, T2-triol + T2-tetraol y T2-tetraol + HT-2.

El efecto antagonista puede estar justificado por la estructura química similar entre las micotoxinas de la mezcla y, por lo tanto, ambas micotoxinas podrían competir por unirse al mismo receptor. Debido a su menor impedimento

estérico, los metabolitos de la T-2 pueden unirse al receptor más fácilmente que la T-2 y HT-2 y disminuir la respuesta tóxica.

El tipo de interacción producido entre las micotoxinas de una combinación es de gran importancia dado que proporciona información toxicológica sobre el riesgo real al que se exponen los consumidores por la ingestión de alimentos contaminados por micotoxinas; ya que un mismo hongo puede producir más de una micotoxina y los alimentos pueden estar contaminados por varias especies de hongos micotoxigénicos de forma simultánea. En este sentido, es importante conocer el tipo de metabolitos que se generan por procesos de biotransformación en los seres vivos y poder predecir sus efectos tóxicos.

4.3. Identificación de productos de biotransformación de la T-2

La identificación de metabolitos de T-2 en cultivos de células humanas proporciona información sobre sus rutas metabólicas y posibles efectos tóxicos. De esta manera, se puede conocer el daño real tras la exposición a la T-2.

En un primer estudio se adicionaron 60 nM de T-2 a las células HepG2 y tras 24 h de exposición se recogió medio de cultivo y una suspensión de células. Paralelamente, se fortificó medio de cultivo con una mezcla de T-2, HT-2, Neo, T2-triol y T2-tetraol, y se incubó durante 24 h en las mismas condiciones que las células HepG2 expuestas a T-2. Este medio de cultivo fortificado se utilizó como muestra control. Se realizó una extracción líquido-líquido, con lisis celular previa en el caso de la suspensión celular. Se cuantificó la T-2 y sus metabolitos a nivel extra e intracelular, mediante cromatografía líquida acoplada a espectrometría de masas de alta resolución con analizador de tiempo de vuelo (LC-HRMS-Q-TOF).

Los resultados de los cromatogramas obtenidos por LC-HRMS-Q-TOF en la muestra control revelaron un aducto de amonio estable y abundante [M + NH4]$^+$ con m/z 484.2541 y tiempo de retención (Rt) de 11,68 min correspondiente a la T-2. Ésto se confirmó con la presencia de los iones producto característicos (m/z 365, 305, 245 y 215) generados por fragmentación de los aductos de amonio, de acuerdo con la información disponible en la bibliografía (Yang et al., 2017). Por otra parte, no se detectó ni el aducto de amonio [M+NH4]$^+$ de la T-2 ni sus iones producto ni a nivel intracelular ni en el medio de cultivo después de 24 horas de exposición a la T-2

No obstante, tanto en el medio de cultivo como en las células se observaron picos que se identificaron como metabolitos de la T-2. Se identificó como HT-2 (Rt = 10,91 min) el pico que mostró un aducto de amonio estable y abundante [M+NH4]$^+$ a m/z 442.2439. T2-triol a m/z 383,2064 ([M+H]$^+$, Rt = 9,70 min) y Neo a m/z 400,1966 ([M+NH4]$^+$, Rt = 8,86 min).

Los resultados evidenciaron que la T-2 se metabolizada completamente por las células HepG2, siendo el principal metabolito la HT-2 (94,1 %), que se cuantificó en 56,40 nM, seguido del Neo (3,31 nM) y T2-triol (0,15 nM). Nuestros resultados confirman que la biotransformación de T-2 da lugar a metabolitos más polares y fáciles de eliminar, encontrándose cantidades mayores a nivel intracelular. Además, estos resultados confirman que la hidrólisis es la vía principal del metabolismo de T-2, en concordancia con los resultados reportados recientemente por otros autores (EFSA, 2017; Narváez et al., 2021).

En un segundo estudio, se adicionaron 30 y 60 nM de T-2 a las células HepG2, se recogió medio de cultivo y una suspensión con células a la 0, 1, 2, 3,

6, 8 y 24 h de exposición y se cuantificó la T-2 y sus metabolitos a nivel extra e intracelular mediante LC-HRMS-Q-TOF.

Los resultados revelaron una biotransformación rápida y completa de la T-2. La T-2 (aducto de amonio $[M+NH4]^+$, m/z 484,2539, −0,81 ppm) fue la única identificada a las 0 h en el medio de cultivo y cuantificada a 58,7 ± 1,7 nM. No se detectó ninguno de sus metabolitos a nivel intra ni extracelular, probablemente debido al corto tiempo de exposición que no fue suficiente para su metabolización.

Después de 1 h de exposición, la concentración de T-2 en el medio de cultivo disminuyó (18,3 ± 1,3 nM), no detectándose T-2 a nivel intracelular. Se detectó HT-2 (aducto de amonio $[M+NH4]^+$, a m/z 442,2435 e iones producto característicos m/z 323 y m/z 263). La HT-2 se cuantificó a 11,2 ± 2,1 nM y 27,4 ± 3,5 nM en medio de cultivo y fracción celular, respectivamente. Además, también se detectó T2-triol según su espectro de masas (aducto protonado $[M+H]^+$ a m/z 383,2064, −1,02 ppm). El T2-triol sólo se detectó a 0,82 ± 0,2 nM en la fracción celular después de 1 hora de exposición a T-2.

Tras 2 y 3 h de exposición de T-2, se observó una disminución de ésta en el medio de cultivo (5,5 ± 0,9 nM después de 2 h y 1,9 ± 0,3 nM después de 3 h de exposición). Se observó un aumento en la concentración de HT-2 tanto en la fracción celular (32,5 ± 2,8 nM a las 2 h y 36,0 ± 3,1 nM a las 3 h) como en el medio de cultivo (15,6 ± 2,0 nM a las 2 h y 18,2 ± 3,4 nM a las 3 h). Respecto al T2-triol, se observó una reducción tanto en la fracción celular (1,7 ± 0,4 nM *vs* 1,1 ± 0,3 nM) como en el medio de cultivo (0,5 ± 0,1 nM *vs* 0,2 ± 0,03 nM) a las 2 y 3 h, respectivamente). Después de 3 h de exposición, se detectó un nuevo pico en muestras de la fracción celular, siendo su valor de masa exacta (aducto

protonado $[M+H]^+$ a m/z 299,1495, −0,54 ppm), que coincidente con los valores del estándar de T2-tetraol. Por lo tanto, la reducción en los niveles de T2-triol podría deberse a su biotransformación a T2-tetraol, ya que este puede formarse después de la desalquilación del T2-triol o la desacetilación de metabolitos derivados del Neo (Yang et al., 2017).

A las 6 horas de exposición, ya no se detectó T-2 en el medio de cultivo y se cuantificó una reducción de HT-2. Paralelamente, se observó un aumento de HT-2 en la fracción celular a las 6 h (44,4 ± 3,9 nM) y posteriormente una reducción entre las 8 h y las 24 h (39,9 ± 2,1 nM). Respecto al T2-triol, los niveles encontrados en el medio de cultivo se redujeron a lo largo del tiempo de exposición y no se detectaron después de 24 h. De manera similar, en la fracción celular se observó una reducción de T2-triol entre las 3 h y las 24 h de exposición. Respecto al medio de cultivo, el T2-tetraol se detectó por primera vez a las 6 h de exposición (0,03 ± 0,01 nM) y su concentración aumentó hasta 1,05 ± 0,03 nM a las 24 h.

Finalmente, tras 24 h de exposición, se detectó una nueva pero débil señal tanto en el medio de cultivo como en la fracción celular. Este metabolito mostró un ion característico del aducto de amonio $[M+NH4]^+$ a m/z 400,1966 (−1,21 ppm) e iones producto a m/z 245 y 215, coincidiendo con los valores del estándar de Neo, que se cuantificó a 0,2 ± 0,02 nM y a 1,54 ± 0,61 nM en medio de cultivo y fracción celular, respectivamente. Este metabolito podría seguir metabolizándose aún más a 4-desacetil-neosolaniol y 15-deacetil-neosolaniol y posteriormente a T2-tetraol tras su desacetilación, como también lo evidenciaron Yang y colaboradores (Yang et al., 2018).

Además, se llevó a cabo un análisis retrospectivo de las muestras utilizando la base de datos de micotoxinas y metabolitos relacionados (PCDL) de Agilent. Los resultados mostraron que tentativamente se identificaron formas monohidroxiladas de T-2 ($C_{24}H_{38}NO_{10}^+$, Rt= 9,45 min, m/z 500,2487) y HT-2 ($C_{22}H_{36}NO_9^+$, Rt= 9,21 min, m/z 458,2371), tanto en el medio de cultivo como en las muestras de fracción celular, recolectadas tras 6 horas de exposición a T-2. Estos metabolitos se corresponderían con 3'-OH-T-2 y 3'-OH-HT-2, respectivamente (Narváez et al., 2021; Yang et al., 2017). Sin embargo, estas señales eran débiles en las muestras detectadas y no pudieron confirmarse debido a la falta de estándares analíticos.

Respecto a los resultados obtenidos tras exponer células HepG2 a 30 nM de T-2 y estudiar su biotransformación de 0 a 24 h, sólo se detectó HT-2 en cantidades cuantificables, desde su LOQ hasta 17,9 ± 2,3 nM. La evolución de los niveles de HT-2 reproduce la tendencia observada en el estudio realizado con 60 nM de T-2. El resto de los metabolitos identificados en el estudio dirigido con 60 nM de T-2 no se detectaron a 30 nM de T-2. Probablemente debido a los bajos niveles que estarían por debajo del LOQ del método, a pesar de mostrar buena sensibilidad.

4.4. Estrés oxidativo

Debido al efecto citotóxico observado tanto de la T-2 como de sus metabolitos en las células HepG2, los siguientes ensayos se centran en identificar cuáles son los mecanismos de acción que producen dicha citotoxicidad. Para ello, se eligen 3 concentraciones de cada micotoxina (30, 15 y 7,5 nM para la T-2; 50, 25 y 12,5 nM para el Neo; 0,45, 0,25 y 0,12 μM para el T2-triol y 1,7, 0,9 y 0,45 μM para el T2-tetraol) correspondientes a la $IC_{50}/2$, $IC_{50}/4$ y $IC_{50}/8$ de cada

una de ellas. Debido a que prácticamente toda la T-2 se transforma a HT-2 en organismos vivos en las primeras horas de exposición, la T-2 y HT-2 se estudian como un único compuesto, ya que no se pueden considerar de forma independiente.

En primer lugar, se estudió si la toxicidad inducida por las micotoxinas se debe a la capacidad de generar ROS. Los resultados obtenidos en las células HepG2 demostraron que tras 24 h de exposición, la T-2 produjo un aumento de ROS a las concentraciones más altas ensayadas, el T2-triol indujo un aumento sólo a la concentración más baja y el T2-tetraol produjo ROS a todas las concentraciones ensayadas. Sin embargo, el Neo no produjo un aumento de ROS a ninguna de las concentraciones ensayadas. Este efecto ha sido corroborado por otros autores en distintas líneas celulares hepáticas (con un rango de 10 a 100 nM), en células GH3 (de 10 a 40 nM), en PK-15 (1000 nM) y en células de neuroblastoma-2a (de 5 a 80 ng/mL) (Deyu et al., 2018; Li et al., 2021; Yang et al., 2016; Zhang et al., 2018).

Por lo tanto, el estrés oxidativo se puede considerar un mecanismo relacionado con la citotoxicidad producida por la T-2 y sus metabolitos en las células HepG2. El incremento de ROS intracelular puede activar diferentes rutas de señalización o destinos metabólicos a nivel celular, ya que una producción incontrolada puede conducir a daño al ADN, aumento de producción de citoquinas inflamatorias, afectación de la proliferación celular y en última instancia, apoptosis o necrosis. Por ello, el siguiente paso fue determinar si tras la exposición a estas micotoxinas, los sistemas de defensa se activan para eliminar las sustancias oxidantes generadas.

4.5. Sistemas de defensa antioxidantes

Tras el aumento del estrés oxidativo producido por la T-2 y sus metabolitos en las células HepG2, se procedió a evaluar el sistema de defensa intracelular (tanto no enzimático como enzimático) en líneas celulares hepáticas (HepG2) e intestinales (Caco-2) y el efecto antioxidante de diferentes sustancias bioactivas ingeridas de forma conjunta con estos compuestos en la dieta.

4.5.1. Sistemas no enzimáticos (glutatión)

Respecto al sistema no enzimático celular, se evaluó el GSH, ya que es la principal sustancia intracelular que protege a las células de las sustancias oxidantes. La disminución de GSH indica aumento de estrés oxidativo. El GSH también actúa como sustrato de algunas enzimas intracelulares.

En esta tesis, tras la exposición de la T-2 a las células HepG2, los niveles de GSH disminuyeron a las concentraciones más bajas (7,5 y 15 nM), y aumentaron en la más alta (30 nM). Este hecho puede deberse al intento celular de mantener el GSH en su estado reducido y evitar el estrés oxidativo a dosis altas. En lo referente a T2-tetraol, se observó un aumento de GSH a la concentración más baja (0,45 μM) y una disminución a la más alta (1,7 μM). Esto sugiere que la célula reduce la presencia de este metabolito a concentraciones bajas, pero el GSH se consume a las concentraciones altas, por lo que su efecto se verá disminuido. En cuanto a la exposición de Neo, los niveles de GSH disminuyeron en todas las concentraciones ensayadas (12,5, 25 y 50 nM), mientras que la T2-triol, produjo depleción de GSH únicamente a la concentración más alta (0,45 μM). En todos los casos, la deplección de GSH se acompaña de un incremento del GSSG.

Para confirmar el efecto citoprotector del GSH se llevó a cabo un pretratamiento con NAC (precursor de GSH) y con BSO (deplector del GSH) durante 24 h y posteriormente se expusieron las células a T-2 (7,5, 15 y 30 nM), Neo (12,5, 25 y 50 nM), T2-triol (0,12, 0,25 y 0,45 μM) y T2-tetraol (0,45, 0,9 y 1,7 μM). Al comparar los niveles de GSH en las células expuestas a las micotoxinas sin y con el pretratamiento, se observó un aumento de GSH tras el pretratamiento con NAC y una disminución con el pretratamiento con BSO. Este aumento de GSH en las células tratadas con NAC fue de hasta el 68,3% con respecto a las células no pretratadas; y una disminución del GSH de hasta el 88,5% en las células pretratadas con BSO respecto a las no pretratadas.

Este mismo efecto se observó para el resto de metabolitos. El pretratamiento con NAC aumentó los niveles de GSH intracelular para el Neo (197,6%), el T2-triol (34,7%) y el T2-tetraol (66,8%) respecto a las células no tratadas con NAC. Mientras que los niveles de BSO disminuyeron los niveles de GSH intracelular para el Neo (55,9%), T2-triol (38,7%) y T2-tetraol (58,9%) tras el pretratamiento con BSO respecto a las células no tratadas con este deplector.

De esta manera, se confirma que el NAC tiene un efecto citoprotector en las células HepG2 y que tras el pretratamiento con BSO, las células tienen más predisposición al daño oxidativo inducido por la T-2 y sus metabolitos debido a que los niveles de GSH disminuyen respecto a los niveles en las células sin pretratar.

Algunos autores relacionan que la generación de ROS y la deplección de GSH producida por algunas micotoxinas como la T-2, DON, citrinina y patulina con el daño al ADN (Liu et al., 2003; Wu et al., 2014). Por lo tanto, este será uno de nuestros objetivos posteriores.

4.5.2. Sistemas enzimáticos

En el sistema de defensa de primera línea frente a los radicales libres y ROS se incluyen la GPx, la GST, la CAT y la SOD. Por lo que a continuación, se determinan los sistemas de defensa enzimático en células HepG2 tras la exposición a T-2, Neo, T2-triol y T2-tetraol.

Los resultados obtenidos tras la exposición de T-2, Neo, T2-triol y T2-tetraol durante 24 h en las células HepG2 demostraron una gran variabilidad de respuesta en función de la micotoxina y la concentración ensayada.

En cuanto a la enzima GPx, se obtuvo una disminución (67,9%) tras la exposición a 30 nM de T-2. Mientras que se observó un aumento (39,2%) tras la exposición a 0,45 μM de T2-tetraol. El pretratamiento con NAC aumentó los niveles de GPx intracelular en células HepG2 tratadas con T-2 (hasta 326,4%), Neo (hasta 548,3%), T2-triol (hasta 68,8%) y T2-tetraol (hasta 108,4%) respecto a las células no tratadas. Por otro lado, los niveles de BSO disminuyeron los niveles de GPx intracelular en las células HepG2 expuestas al T2-tetraol (hasta 50,7%) tras el pretratamiento con BSO respecto a las células sin tratar.

Respecto a la enzima GST, se obtuvo un aumento de la actividad tras la exposición a 30 nM de T-2 (hasta 115,7%) y 0,45 μM de T2-triol (hasta 20,9%). El pretratamiento con NAC aumentó los niveles de GST intracelular para el T-2 (hasta 102,3%), el Neo (hasta 221,8%), el T2-triol (hasta 140,6%) y el T2-tetraol (hasta 227,7%) respecto a las células no tratadas. Por otro lado, los niveles de BSO disminuyeron los niveles de GPx intracelular para el T2-triol (hasta 83,7%) y para el T2-tetraol (hasta 80,6%) tras el pretratamiento con BSO respecto a las células no pretratadas.

La actividad de la CAT aumentó con las concentraciones más bajas de T-2 y T2-triol hasta 102,2% y 48,6%, respectivamente, frente al control. Por el contrario, a las concentraciones más bajas de Neo, la actividad de la CAT disminuyó al 49,3%, mientras que se detectó un aumento del 58,2% a la concentración más alta con respecto al control. Finalmente, con respecto a la actividad de la SOD en las células HepG2, se observó un aumento a todas las concentraciones ensayadas de Neo (hasta 445,9%), T2-triol (hasta 441,2%) y T2-tetraol (hasta 140,2%) en comparación con sus controles respectivos.

En nuestros resultados, se correlaciona la disminución de los niveles de GSH producidos por la T-2, con el aumento de la actividad de la GST. Sin embargo, la actividad de GPx se mantuvo sin cambios. Según Gouze y colaboradores, el grupo 12,13-epóxido, que caracteriza a todas las toxinas epoxi-tricoteceno (como la T-2, Neo, T2-triol y T2-tetraol), podría ser un sustrato para la conjugación con la GST, ya que GST es activa sobre el grupo epóxido. Estos autores demostraron que el tricoteceno DON tiene la capacidad de conjugarse con GST, ya que el DON es un sustrato de la GST (Gouze et al., 2006). Por tanto, en este trabajo el aumento de la actividad enzimática de la GST tras la exposición a T-2 nos sugiere que esta micotoxina podría ser un sustrato para la GST debido a la similitud estructural de ambos tricotecenos (DON y T-2). Así pues, la conjugación mediada por GST podría representar una vía de destoxicación para proteger a las células del daño causado por la T-2. Por otro lado, los resultados obtenidos respecto a la actividad de la GPx en las células HepG2, indica que no es la principal enzima implicada en la destoxicación de la T-2. Además, la GPx podría estar inactivada por la disminución de su propio sustrato (GSH). Por otra parte, la actividad de la SOD permanece sin cambios después de la exposición a T-2; mientras que la actividad enzimática de la CAT

aumentó. Esto puede deberse al hecho de que T-2 genera un aumento de las ROS, incluido el H_2O_2, y la CAT cataliza rápidamente el H_2O_2 en H_2O y O_2. Por lo tanto, nuestros resultados sugieren que las principales enzimas involucradas en la destoxicación de la T-2 en las células HepG2 son la GST y CAT. La actividad de la GST y los niveles de GSH permanecen altos a las concentraciones más altas de T-2, demostrando el papel protector del GSH en las células HepG2 sometidas a estrés oxidativo. De igual modo, la CAT es una enzima determinante en la disminución del estrés oxidativo tras la exposición a la T-2 en células HepG2, como demuestran nuestros resultados.

Otros autores observaron resultados similares a los de nuestro estudio respecto a la actividad de la SOD en células Hek-293 después de la exposición a DON y en las células SH-SY5Y después de la exposición a BEA, α-ZEL y β-ZEL (otras micotoxinas de Fusarium). Estos autores demostraron que la actividad de la SOD tiende a los niveles de actividad enzimática observados en el control (Tatay et al., 2017, 2016). Sin embargo, en la bibliografía se encuentran resultados contradictorios en cuanto a la actividad de las enzimas antioxidantes tras la exposición a micotoxinas. Yang y colaboradores observaron un aumento en las actividades de la CAT, la SOD y la GPx en hepatocitos de pollo de engorde después de la exposición de 10 a 100 nM de T-2 (Yang et al., 2016). Por el contrario, otros autores observaron una disminución en la actividad de CAT después de la exposición a 1 μM de T-2 en células de riñón porcino y células de Leydig (Li et al., 2021; Zhang et al., 2017). El aumento de las actividades de la CAT, GPx y SOD sugiere que las ROS generadas tras la exposición de T-2 en los hepatocitos son catalizadas por la SOD, y los altos niveles de H_2O_2, producidos como resultado de esta reacción, son destoxicados por la CAT y la GPx disminuyendo los niveles de GSH. Por el contrario, las enzimas SOD, GPx

y CAT no parecen ser las principales enzimas responsables de prevenir el estrés oxidativo causado por la T-2 en células de Leydig o de riñón porcino.

En este trabajo, con respecto a Neo, se observó una disminución significativa de GSH y un aumento de GSSG. Sin embargo, la disminución de los niveles de GSH no parece estar relacionado con la actividad de GPx, la cual permanece inalterada. Esto sugiere que el sistema enzimático celular no relacionado con el GSH (la CAT y la SOD), es el sistema de defensa enzimático más importante en las células HepG2 expuestas a Neo.

La disminución de GSH y el aumento de los niveles de GSSG con la concentración más alta de T2-triol observada en este trabajo, es similar a los efectos observados con ZEA y sus metabolitos (Tatay et al., 2016) y BEA (Mallebrera et al., 2014) en células CHO-K1. La disminución de los niveles de GSH va acompañada de un aumento de GST, indicando que la enzima detoxicante de T2-triol es principalmente GST. Por otro lado, el aumento de las ROS tras la exposición al T2-triol proporciona el estímulo para aumentar las actividades enzimáticas de la CAT y la SOD.

En las células HepG2, el GSH intracelular aumentó inmediatamente a la concentración más baja (0,45 μM) de T2-tetraol, acompañado por un aumento en la actividad de la GPx, actuando como un importante tampón redox como respuesta al daño oxidativo para mantener el GSH de las células en estado reducido. Sin embargo, a la concentración más alta (1,7 μM), el GSH se agota debido a los altos niveles de sustancias oxidantes generadas. Así, el principal mecanismo detoxicante enzimático implicado fue la enzima GPx. Por otro lado, los compuestos oxidantes producidos por el T2-tetraol fueron catalizados por la SOD, debido a que su actividad aumentó a todas las concentraciones ensayadas.

Respecto al pretratamiento celular con NAC y BSO, los niveles de GSH aumentaron en las células con pretratamiento con NAC porque el GSH está involucrado en el mecanismo de defensa celular cuando las células HepG2 se exponen a estas micotoxinas. Esto se demostró con el aumento de las actividades de la GPx y la GST tras el pretratamiento con NAC y posterior exposición a las micotoxinas. El tratamiento previo con el NAC suprimió el daño oxidativo inducido por T-2 y sus metabolitos en las células HepG2. Por el contrario, el pretratamiento con BSO mostró una disminución en los niveles de GSH en células expuestas a T-2, T2-triol y T2-tetraol, pero no tras la exposición a Neo, en comparación con las células sin tratamiento previo con BSO. Esto puede deberse a que las enzimas GPx y GST (dependientes de los niveles celulares de GSH) no participan en el mecanismo de destoxicación de Neo. De hecho, no se observaron cambios en las actividades de GPx (después de la exposición a Neo y T2-triol) y GST (después de la exposición a Neo) tras el pretratamiento con BSO en comparación con las células sin pretratamiento.

Estos resultados confirman que el GSH está involucrado en el mecanismo de defensa de las células HepG2 tras la exposición a T-2.

4.5.3. Antioxidantes exógenos

La ingesta de alimentos con compuestos antioxidantes permite reforzar el sistema de defensa antioxidantes endógeno. De esta manera, se evalúa el poder protector frente a la exposición de T-2 de las judías rojas, microalgas e hidrolizados de pescado. Las judías rojas, caracterizadas por su gran cantidad de compuestos fenólicos, se utilizaron para estudiar el posible efecto citoprotector frente a la exposición de la T-2 mediante ensayos de viabilidad celular. Las células HepG2 se pretrataron con extractos de judías rojas (dilución 1:8) durante 1 y 24

h y posteriormente se expusieron a 7,5, 15 y 30 nM de T-2 durante 24 h. Los resultados obtenidos mediante el ensayo del MTT mostraron que el pretratamiento con judías rojas no aumenta la viabilidad celular. A continuación se procedió a evaluar el posible efecto citoprotector del extracto de judías rojas con un tratamiento simultáneo entre las judías rojas y la T-2 (7,5, 15 y 30 nM) durante 24 h. En este caso, tampoco se observó un aumento de viabilidad con respecto a las células expuestas a T-2 con pretratamiento o respecto al control. Estos resultados pueden indicar que las judías rojas no previenen la citotoxicidad producida por la T-2 en las células HepG2 a las concentraciones ensayadas. Sin embargo, se estudió el efecto de la exposición simultánea de la T-2 con el extracto (dilución 1:8) de las judías rojas sobre la producción temprana de ROS intracelular (120 min) en las HepG2, y se demostró una disminución de ROS a la concentración de 7,5 nM de T-2.

Debido a la globalización de los mercados de alimentos, el consumo de las microalgas está aumentando considerablemente en nuestra gastronomía. Se estudió el posible efecto citoprotector de las microalgas *P. tricornutum* y *T. chuii* frente a la citotoxicidad de la T-2 en células HepG2 mediante ensayos de viabilidad celular (el MTT). Se compararon los resultados entre ambas microalgas (*P. tricornutum* y *T. chuii*), las cuales se sometieron a un proceso de disrupción celular (DR) y se compararon con las mismas no sometidas a dicho proceso. Se realizaron dos ensayos diferentes: en el primer ensayo, las células HepG2 se trataron simultáneamente con las microalgas liofilizadas (diluciones 1:16 y 1:32) y 7,5, 15 y 30 nM de T-2; y en el segundo ensayo, las células HepG2 se trataron simultáneamente con extractos etanólicos de las microalgas (con un rango de concentración de 0,1 a 100 μg/mL para *P. tricornutum* y de 2 a 400 μg/mL para *T. chuii*) y 7,5 nM de T-2.

Respecto a los liofilizados de microalgas, la exposición de 15 nM de T-2 junto con la dilución 1:32 de *T. chuii* con un 67% DR, aumentó la viabilidad celular entre un 17,2% (respecto al control) y un 20,0% (respecto a 15 nM de T-2). La T-2 adicionada a la dilución 1:64 de *T. chuii* con un 0 % DR, aumentó la viabilidad entre un 48,6% (respecto al control) y un 52,2 % (frente a 15 nM de T-2). Y la T-2 adicionada a la dilución 1:32 de *T. chuii* con un 0 % DR, aumentó la viabilidad un 32,6 % (frente al control) y en un 35,8 % (frente a 15 nM de T-2). No obstante, la mayor citoprotección se observó con el tratamiento simultáneo de 30 nM de T-2 y la dilución 1:64 de *T. chuii* con un 0 % DR (entre un 26,3% frente al control y un 81,6% frente a 30 nM de T-2).

Los datos obtenidos con la adición simultánea de la T-2 y los extractos etanólicos de las microalgas no mostraron ningún efecto citoprotector en las células HepG2. Este hecho podría explicarse debido a que en las microalgas también se encontraron metales como plomo (Pb), arsénico (As), cadmio (Cd) y mercurio (Hg), los cuales pueden contribuir a aumentar la toxicidad en las células HepG2, por lo que el efecto citoprotector cuando se adiciona la T-2 no se produce.

El efecto citoprotector de las microalgas ha sido observado previamente por otros autores. Sousa y colaboradores demostraron la actividad antifúngica de 54 mg/mL de extractos fenólicos de *Spirulina platensis* (1,15 mg compuesto fenólico/g) frente al hongo micotoxigenico *A. flavus* (Souza et al., 2011). Souza y colaboradores observaron que los extractos fenólicos comerciales de *Clorella* sp. son capaces de inhibir el crecimiento de *A. flavus* y la producción de sus AFs (Souza et al., 2011). Además, Pagnussatt y colaboradores mostraron la actividad antifúngica del extracto fenólico de *Spirulina* sp. frente a hongos del género

Fusarium. Y, el efecto antifúngico y antimicotoxigénico de los extractos fenólicos de *S. platensis* LEB 18 en forma libre y encapsulada frente a *F. graminearum* (Pagnussatt et al., 2016, 2014). De manera similar, Scaglioni y colaboradores mostraron el efecto inhibidor de los extractos fenólicos de *Nannochloropsis* sp. y *S. platensis* LEB 18 en cultivo de maíz. Además, en los campos de maíz, los autores encontraron una contaminación menor por *F. verticillioides* y su principal micotoxina, la FB1. De hecho, se comercializan extractos fenólicos de S. platensis LEB 18 para formular mezclas de cereales para alimentación institucional para niños (Scaglioni et al., 2018).

De manera similar, el efecto citoprotector de hidrolizados de espinas, cabezas y vísceras de salmón, caballa y lenguado fue evaluado en las células Caco2/TC7 expuestas 24 h a T-2. Los tres hidrolizados a la dilución 1:16 ejercieron efecto citoprotector frente a 60 nM de T-2, en orden creciente: espinas < cabezas < vísceras, con un incremento de viabilidad del 19,16%, 43,46% y 69,92%, respectivamente, comparado con la exposición de T-2 individualmente. Comparando entre las vísceras de los tres pescados, las de salmón son las que indujeron mayor efecto citoprotector frente a la T-2. Este efecto citoprotector podría deberse a la capacidad antioxidante de los hidrolizados de pescado para reducir la generación de ROS producidas por la exposición a la micotoxina.

Estos resultados sugieren que la microalga *T. chuii* y los hidrolizados de salmón, caballa y lenguado protegen a las células HepG2 y Caco-2 de la citotoxicidad producida por la generación de las ROS tras la exposición a la T-2, aunque se requieren más estudios para conocer el MoA de estos compuestos.

4.6. Proliferación celular

La proliferación celular es un indicador vital que nos indica la capacidad de replicación celular y, por tanto, el número de células sanas en una muestra biológica. Para determinar la proliferación celular se estudia la distribución de las células a lo largo del ciclo celular. Sin embargo, la progresión normal del ciclo celular podría verse afectada por eventos que dañan el ADN, los cuales son controlados por puntos de control, que determinan la progresión a la siguiente etapa del ciclo celular si no se detecta daño, o la detención del ciclo si se detecta daño en el ADN (Prosperini et al., 2013).

En este estudio, las células HepG2 se incubaron durante 24 h con 15, 30 y 60 nM de T-2. Los resultados mostraron un aumento significativo en la fase G_2/M (10,1%) a 15 nM de T-2 y una reducción del 12,5% a 60 nM con respecto al control. Además, a 60 nM de T-2, la fase subG_0/G_1 aumentó significativamente (11,8 veces mayor) frente al control. Mientras que la fase G_0/G_1 disminuyó 1,11 veces tras 30 nM de T-2. Por tanto, en nuestro estudio se observa que 60 nM de T-2 es capaz de alterar la progresión normal de la proliferación de las células HepG2.

La acumulación de células en la fase G_2/M tras 15 nM de T-2, puede indicar que concentraciones bajas de T-2 inducen la mitosis. Sin embargo, concentraciones altas de T-2 (60 nM) detienen el ciclo celular en la fase G_2/M, lo que podría deberse a daños en el ADN, deteniéndose la mitosis (como se observa al aumentar la fase subG_0/G_1).

El 5-Fu es un inhibidor de la timidilato sintetasa, por lo que bloquea la síntesis del nucleósido timidina, lo que afecta a la síntesis de ADN en la fase S. Por tanto, el 5-Fu interrumpe la replicación del ADN, daña al ADN y causa la muerte

celular. La T-2 en este estudio mostró un comportamiento similar al del 5-Fu en células HepG2. La perturbación del ciclo celular podría ser una respuesta al ADN dañado en el punto de control, o puede representar un proceso adaptativo por el que se retrasa o detiene el ciclo celular cuando se producen lesiones en el ADN para repararlo (Abid-Essefi et al., 2003; Prosperini et al., 2013).

La fase G_0/G_1 es una etapa en la que las células crecen y se preparan para replicar el ADN y completar el ciclo de división celular (Fernández-Blanco et al., 2016). Un comportamiento similar al de esta tesis ha sido observado por Lei y colaboradores. Estos autores encontraron que 0,02 nM de T-2 causa una detención en la fase G_0/G_1, acompañada de una disminución de células en la fase G_2/M en comparación con el control en las células C28/I2, L-02 y HK-2 (Lei et al., 2017). Por otra parte, Agrawal y colaboradores detectaron, de igual modo que en nuestro trabajo, en células de neuroblastoma humano (IMR-32) un aumento en la población de células en la fase $SubG_0/G_1$ tras la exposición a 60 nM de T-2. Dichos autores sugieren que podría ser una consecuencia de la proteína p21. Esta proteína regula la progresión del ciclo celular en la transición de la fase G_1 a S y, por tanto, detiene el ciclo en la fase G_1 en respuesta a estímulos de estrés que dañan al ADN. Además, estos autores indican que se produce la detención de la fase G_0/G_1 para reparar el ADN dañado, mediante la activación de la poli-ADP-ribosa-polimerasa-1 (PARP-1) evitando así la muerte celular por necrosis (Agrawal et al., 2015).

4.7. Muerte celular: apoptosis y necrosis

Considerando la disminución de viabilidad y la afectación de la proliferación y del ciclo celular generado tras la exposición de T-2 en las células HepG2, el siguiente objetivo fue determinar si estos efectos están implicados en los diferentes procesos de muerte celular. Para ello, se estudió la muerte celular por inducción de apoptosis y/o necrosis tras 2 y 24 h de exposición de las células HepG2 a la T-2. Tras 2 h de exposición a 15, 30 y 60 nM de T-2 no se observó ningún cambio comparado con el control. Por tanto, con las condiciones estudiadas no se activaron los mecanismos de muerte celular. Sin embargo, tras 24 h, se observó un aumento de la apoptosis temprana, tardía y necrosis de manera concentración-dependiente con respecto a las células control. La población de células en apoptosis temprana aumentó 18,97 ± 3,07% (30 nM T2) y 29,07 ± 3,25% (60 nM T2), respecto al control (11,03 ± 1,31%). La población de células apoptóticas tardías aumentó 12,27 ± 2,34% (30 nM) y 35,47 ± 8,24% (60 nM) en comparación con las células de control (5,30 ± 0,66%). Además, las células necróticas aumentaron únicamente a la concentración más alta (60 nM) un 5,43 ± 1,15% vs el control (1,60 ± 0,69%).

Como se ha mencionado en el apartado anterior, 60 nM de T-2 produjo la detención de la fase G_2/M, a la misma concentración a la que se observa que las células entran en apoptosis. Por otro lado, la disminución en la fase G_0/G_1 observada con 30 nM de T-2 se puede relacionar con la inducción de apoptosis en las células HepG2 a las 24 h de exposición. Además, se observó un aumento en la población de células en la fase $SubG_0/G_1$ tras 60 nM de T-2, lo que sugiere que el ciclo se detiene. Esto también está relacionado con el hecho de que esta concentración de T-2 da como resultado un aumento en el porcentaje de apoptosis celular temprana, tardía y necrosis. Estos resultados son consistentes

con los datos encontrados en la bibliografía (Agrawal et al., 2015; Weidner et al., 2012). La inducción de apoptosis por T-2 ha sido confirmada en varias líneas celulares (C28/I2, L-02 y HK-2) por Lei y colaboradores (Lei et al., 2017). De la misma manera, Wu y colaboradores y Agrawal y colaboradores informaron de un aumento en apoptosis total (temprana y tardía) en células L-02 e IMR-32 (Agrawal et al., 2014; Wu et al., 2019). Sin embargo, las diferencias entre los resultados de los autores mencionados vs los obtenidos en nuestro estudio podrían explicarse por los diferentes tiempos de exposición, líneas celulares involucradas, y por la sensibilidad de las pruebas aplicadas, las cuales podrían condicionar la respuesta.

Varios estudios han demostrado que la T-2 induce la apoptosis mediante la vía mitocondrial, mediada por las ROS en diferentes tipos de células (Fang et al., 2012; Ren et al., 2015; Wu et al., 2011). Estos resultados sugieren que la pérdida de viabilidad celular observada tras la exposición de T-2 en las células HepG2 se debe a la inducción de un proceso apoptótico y necrótico como consecuencia del aumento de estrés oxidativo inducido por las ROS generadas por la micotoxina. Además, se ha demostrado que el estrés oxidativo está asociado con la detención del ciclo celular dependiente de la proteína p53 (que controla la expresión de la proteína p21), la reparación del ADN y la apoptosis (Agrawal et al., 2015; Liu et al., 2008). Wu y colaboradores determinaron que las células L-02 tratadas con T-2 exhiben un aumento en la escisión de PARP-1 (implicado en la reparación del ADN) y el factor proapoptótico Bax que provoca la activación de la cascada de caspasas (implicado en la apoptosis) (Wu et al., 2019). En conclusión, la apoptosis y necrosis están involucradas en el daño celular inducido por la T-2 en células HepG2.

4.8. Daño al ADN: genotoxicidad y mutagenicidad

Teniendo en cuenta la disrupción del ciclo celular tras la exposición de las células HepG2 a la T-2 y su posible contribución al daño del ADN, se determinó el daño que podría producir esta micotoxina al material genético a través de diferentes mecanismos genotóxicos. Por una parte, la rotura de la doble hélice de ADN se analizó mediante el ensayo del cometa. Los resultados demostraron que las colas de cometa tras la exposición a la T-2 (15, 30 y 60 nM) en las células HepG2 causan la rotura de la doble hélice de ADN, de manera concentración-dependiente. Concretamente, se observó un aumento en el porcentaje de ADN de la cola de 13,94 % a 52,57 %, de la longitud de la cola de 9,98 % a 80,83 % y del momento de la cola de 1,90 % a 23,22 %. Por otra parte, las alteraciones en el reparto equitativo del material genético durante la división celular se evaluaron mediante el ensayo de micronúcleos (MN). Se confirma que la T-2 indujo daño al ADN por el ensayo de MN, ya que se observa un incremento de la frecuencia de MN (12,1 ± 1,2 %) a 60 nM de T-2 en comparación con el control (6,9 ± 0,9 %) tras 48 h de exposición.

En cuanto a los efectos mutagénicos, se estudió el ensayo de mutación inversa bacteriana y se analizó la exposición de T-2 en un rango de siete concentraciones (de 0,15 a 60 nM) en las cepas *S. typhimurium* TA98, TA100, TA1535 y TA1537, y *E. coli* WP2 con y sin fracción microsomal de hígado de rata (fracción S9). Los resultados obtenidos no mostraron diferencias significativas en el número de colonias revertidas respecto a las obtenidas en los controles negativos para todas las cepas ensayadas, con y sin fracción S9. Por lo tanto, nuestros resultados muestran que ni la T-2 ni sus metabolitos inducen mutaciones puntuales mediante sustituciones de pares de bases en el genoma de *S. typhimurium* ni en *E. coli* en las condiciones experimentales utilizadas.

Los datos disponibles en la bibliografía han demostrado que una alta proporción de MN está asociada con procesos de apoptosis. La apoptosis también podría estar relacionada con la detención del ciclo celular, especialmente cuando es producida por un genotóxico, para prevenir la transmisión de información genética dañada y promover la reparación del ADN. Además, la apoptosis podría estar relacionada con la generación de ROS, o con diferentes vías de señalización, como la vía MAP Kinasa (Wada and Penninger, 2004).

El aumento de MN y de cometas a 60 nM de T-2 coincide con la parada del ciclo celular en la fase G_2/M, la acumulación de células en la fase subG_0/G_1 y la apoptosis y necrosis a dicha concentración en las células HepG2. Todos estos resultados en conjunto podrían sugerir que la alteración del ciclo y la mitosis se deben a un mecanismo de reparación de daños en el ADN y que la T-2 causa daño al ADN mediante diversos mecanismos de acción.

Nuestros hallazgos son consistentes con otros estudios que publican que micotoxinas como la STE (a su IC_{50}, IC_{50}/2, y IC_{50}/4) es genotóxica por aumentar los MN y cometas en células SH-SY5Y (Zingales et al., 2021). Mamur y colaboradores publicaron un aumento en la intensidad de la cola del cometa tras la exposición durante 1 h a ENA (0,14, 0,29 y 1,15 μM) en linfocitos humanos (Mamur et al., 2018). También se ha detectado un daño significativo en el ADN mediante el ensayo del cometa con 1 y 12 μM de BEA en células CHO-K1 y Caco-2 tras 24 h de exposición (Mallebrera et al., 2016; Prosperini et al., 2013). Por otra parte, Somoskői y colaboradores informaron que 1,6 nM de T-2 aumentó los MN (33,3%) tras 96 h de exposición en blastocistos de embriones de ratón (Somoskői et al., 2016). El DON y su metabolito acetilado (3-ADON) también produjo aumento de MN en células TK6 humanas (25 μM,

3 h de exposición, incremento del 9,8%) y en células HepG2 (3 μM, 48 h de exposición, incremento del 13,1%), respectivamente (Juan-García et al., 2018; Takakura et al., 2014). BEA y OTA causaron una fuerte inducción de MN a 1,25 y 25 μM durante 48 h de exposición, en células HepG2, respectivamente (Juan-García et al., 2019).

Por otra parte, nuestros resultados mostraron ausencia de mutaciones puntuales en presencia o ausencia de la fracción S9. Estos hallazgos son consistentes con los resultados obtenidos por Alonso-Jauregui y colaboradores, los cuales evaluaron la genotoxicidad de 12 micotoxinas, incluida la T-2, con la prueba SOS/umu, un método que muestra una fuerte correlación con el ensayo de mutación inversa bacteriana (Alonso-Jauregui et al., 2022). Estos autores compararon los resultados obtenidos para cada micotoxina con una fracción S9 hepática y una fracción S9 alternativa procedente de riñones. Descubrieron que la T-2 mostraba una respuesta mutagénica negativa sin y con S9 hepático. Sin embargo, en presencia de la fracción S9 del riñón, se observó una respuesta mutagénica positiva a concentraciones superiores a 31 μg/mL. De manera similar, Smerák y colaboradores estudiaron la mutagenicidad de la combinación de T-2 y AFB_1, utilizando la prueba de Ames en las cepas TA98 y TA100. Estos autores encontraron que concentraciones de T-2 de 0,1, 0,25 y 1 μg/placa no causaron efecto mutagénico cuando se expusieron de forma individual, pero la exposición combinada produjo un efecto mutagénico mayor que el producido por la exposición individual de AFB1 (Smerák et al., 2001).

4.9. Citotoxicidad en modelos de cultivo 3D en dispositivos microfluídicos

En los cultivos 2D hay una carencia de interacciones apropiadas entre células y entre las células y las matrices propias de los organismos vivos. Los modelos tridimensionales (3D) de células se consideran un modelo óptimo para una mejor comprensión de la toxicidad real de una sustancia debido a la mayor organización celular. Además, los dispositivos microfluídicos representan modelos in vitro dinámicos y multiorgánicos (al poder co-cultivar células), acercándose aún más al entorno biológico in vivo.

En esta tesis, en primer lugar se comparó el cultivo de esferoides hepáticos en placas estándar 3D (Aggrewell) con dispositivos microfluídicos. El dispositivo fue de elaboración propia utilizando PDMS. Este dispositivo consta de una cámara de cultivo con una altura de 100 μm que está conectada por dos canales de transporte a los depósitos del medio de cultivo. La cámara de siembra contiene 84 pocillos cilíndricos de 350 μm de diámetro y 300 μm de profundidad. La formación de esferoides fue más rápida en el dispositivo microfluídico que en la placa convencional 3D. En el dispositivo, los esferoides estaban prácticamente formados el día 2 de la siembra y el día 3 estaban completamente compactados. Por el contrario, en la placa de Aggrewell, la formación de esferoides comenzó el día 2 y los esferoides compactos aparecen el día 5. El análisis de imágenes reveló diferencias significativas entre Aggrewell y los dispositivos microfluídicos en términos de circularidad y solidez de los esferoides a lo largo del tiempo. Con los dispositivos, los esferoides alcanzaron valores de solidez > 90% a las 24 h de siembra, mientras que los esferoides en placa Aggrewell alcanzaron niveles comparables después de 5 días de cultivo. De manera similar, la circularidad de los esferoides fue del 60 % después de 48 h de

siembra en el dispositivo microfluídico, y de 50 % después de 120 h de cultivo en una placa Aggrewell. Al comparar el área de los esferoides con su circularidad, se observa que los esferoides sembrados en Aggrewell tienden a ser más pequeños e irregulares incluso después de 120 h de cultivo, lo que sugiere que este formato de cultivo no es óptimo para el crecimiento de esferoides HepG2. En los dispositivos microfluídicos se observa que con el tiempo los esferoides se vuelven más circulares y su área aumenta, lo que sugiere que el esferoide es compacto y crece, indicando un entorno de cultivo más adecuado. A continuación, para una mejor caracterización de la diferencia entre las plataformas de cultivo, se evaluó la función hepática de los esferoides mediante la medición de albúmina con un kit ELISA. Los niveles de albúmina en la placa Aggrewell fueron 2 veces más bajos que en los dispositivos microfluídicos. Además, la producción de albúmina disminuyó en los cultivos de esferoides de Aggrewell, mientras que aumentó en los cultivos de esferoides de microfluidos. La mejora de la función de células hepáticas observada en los dispositivos microfluídicos en comparación con las placas 3D estándar de gran volumen se puede atribuir a varios factores que incluyen: la oxigenación mejorada en dispositivos microfluídicos debido al PDMS y la señalización paracrina mejorada debido al pequeño volumen local de dispositivos microfluídicos. La producción de albúmina que obtenemos es comparable a los valores de albúmina informados por Choi y colaboradores (1,35 μg/1x10^4 células/día) que sembraron esferoides de hepatocitos primarios de rata en dispositivos microfluídicos (Choi et al., 2020).

En conclusión, nuestros resultados mostraron que los cultivos de esferoides hepáticos en dispositivos microfluídicos tienen mejor dinámica de formación de esferoides y producción de albúmina que las placas convencionales Aggrewell.

Por lo tanto, la evaluación de los efectos de la T-2 en esferoides se llevó a cabo en dispositivos microfluídicos.

Las células hepáticas no parenquimatosas LX2 se utilizan para mejorar el fenotipo y la función de los cultivos de hepatocitos. En este estudio se evaluó si las LX2 presentan ventajas en la formación de los cultivos de esferoides hepáticos en dispositivos microfluídicos al adicionar la T-2. Se creó un co-cultivo con células HepG2 y LX2 a las proporciones de 85% (HepG2) y 15% (LX2), que se eligieron en función de la composición celular del hígado in vivo. Las células LX2 se marcaron con Vybrant DiD y se agregaron a las células HepG2 para formar esferoides durante las primeras 24 h de cultivo. Tras 3 días de cultivos, las células LX2 se distribuyeron homogéneamente en los esferoides hepáticos. Los esferoides HepG2 y HepG2-LX2 se expusieron durante 24 h a 15, 30 y 60 nM de T-2, y se analizó la viabilidad celular mediante tinción live/dead. La presencia de células muertas aumentó a las concentraciones más altas de T-2 en los esferoides de monocultivo. Sin embargo, este aumento no fue tan pronunciado en los esferoides HepG2-LX2. La cuantificación de la fluorescencia live/dead confirmó que los esferoides en monocultivos experimentaron una citotoxicidad varias veces mayor en comparación con los co-cultivos a todas las concentraciones de T-2. Además, la viabilidad de los esferoides de co-cultivo (HepG2-LX2) sin exposición a la micotoxina fue aproximadamente 3 veces mayor que la de los esferoides de monocultivo en las mismas condiciones. Esto sugiere que las células LX2 mejoran la viabilidad de las células hepáticas.

La función hepática de los esferoides en dispositivos microfluídicos se evaluó mediante la albúmina. Los esferoides de HepG2-LX2 produjeron 2,153

μg/mL/1x10^4 células/día, mientras que los esferoides HepG2 produjeron 1,702 μg/mL/1x10^4 células/día, mostrando una tendencia de funcionalidad creciente en el co-cultivo. La producción de albúmina disminuyó de manera concentración-dependiente en monocultivos y co-cultivos tras 24 h de exposición a 15, 30 y 60 nM de T-2. En los esferoides de HepG2, la disminución fue hasta un 78,5% tras 24 h de exposición, respecto al control; mientras que en los esferoides HepG2-LX2 disminuyó hasta el 68,1%, comparado con el control. Dado que la disminución de albúmina fue más pronunciada que la disminución de la viabilidad celular, se concluye que, además de tener efectos citotóxicos directos, la T-2 también atenuó el fenotipo hepático.

Por otra parte, se evaluó el crecimiento del esferoide en monocultivos y co-cultivos en presencia de T-2. Los resultados mostraron que los esferoides HepG2-LX2 fueron más grandes que los esferoides de HepG2 tras 4 días de cultivo en ausencia de T-2. Y, la exposición a T-2 provocó una mayor disminución en el crecimiento de esferoides en monocultivo que de los de co-cultivo.

La desmina es una proteína de filamento intermedio presente en las células LX2, pero no en los hepatocitos. Su expresión mantenida tras la exposición a las diferentes concentraciones de T-2 sugiere que las células LX2 del esferoide no se ven afectadas tras la adición de la T-2. En conjunto, nuestros resultados demuestran que los co-cultivos de esferoides de células hepáticas y LX2 en dispositivos microfluídicos mostraron un mejor crecimiento y producción de albúmina y fueron más resistentes al daño por T-2 en comparación con los monocultivos hepáticos 3D.

El siguiente objetivo fue evaluar la expresión de enzimas y transportadores de fase I, II y III del metabolismo para esferoides de células HepG2 y HepG2-LX2 en dispositivos microfluídicos tras 24 h de exposición a T-2 mediante la RT-qPCR. La expresión de CYP1A1, CYP1A2, CYP2E1, CYP3A, UGT1A1, MDR1 y MDR2 fue inducida por la T-2, lo que confirma que esta micotoxina es metabolizada y excretada por las células HepG2. Con respecto a las enzimas del metabolismo de fase I, en los esferoides de monocultivo de los dispositivos microfluídicos, los niveles de expresión de CYP1A1, CYP1A2, CYP2E1 y CYP3A4 aumentaron 3,89, 6,17, 40,81 y 2,99 veces, respectivamente, en comparación con los esferoides no expuestos a T-2. En cuanto a las enzimas del metabolismo de fase II, UGT1A1 aumentó hasta 4,35 veces en comparación con el control. Por último, los niveles de expresión de los transportadores de fase III MDR1 y MDR2 fueron 3,48 y 1,32 veces mayores, respectivamente, en comparación con sus controles. De todas las enzimas analizadas, CYP2E1 fue la que más se sobreexpresó (~41 veces en comparación con el control), lo que indica un papel importante desempeñado por este citocromo en el metabolismo de la T-2. De modo similar, Lin y colaboradores informaron previamente que el CYP2E1 tiene un papel importante en el metabolismo de la T-2 (Lin et al., 2015). Además, el CYP2E1 participa en el metabolismo de otras micotoxinas producidas por hongos de Fusarium, por ejemplo, se ha demostrado que es el principal citocromo implicado en el metabolismo de la ZEA (Wen et al., 2016).

Respecto a los esferoides de co-cultivo de los dispositivos microfluídicos, también se observó la inducción de algunas isoenzimas metabolizadoras de fase I tras la exposición a 60 nM de T-2. La sobreexpresión de CYP1A1 fue 0,59 veces mayor que el control, la del CYP1A2 2,14 veces y la del CYP2E1 0,86 veces. Sin embargo, los niveles de inducción enzimática fueron mucho menores

en co-cultivos con células LX2 en comparación con monocultivos de esferoides, excepto en el caso de la expresión del transportador MDR2 y de la isoenzima CYP3A4, donde la disminución de la inducción sólo fue significativa a 30 nM de T-2. La menor inducción de enzimas metabolizadoras en co-cultivos puede deberse a que las células LX2 secuestran micotoxinas en gotas de lípidos, neutralizando así sus efectos en el hígado. Trusal y colaboradores y Lindberg y colaboradores han observado este efecto con las células LX2 expuestas al DON (Lindberg, 1985; Trusal, 1986). Dicho "secuestro" de la T-2 puede explicar la menor citotoxicidad y la mejor producción de albúmina de los esferoides de co-cultivos expuestos a T-2 en los dispositivos microfluídicos.

Para finalizar, se evaluaron los cambios en la producción de citoquinas inflamatorias después de la exposición de esferoides hepáticos de mono y co-cultivo en dispositivos microfluídicos a 60 nM de T-2. Se analizaron la IL-1RA, GM-CSF, MCP-1, TNF-α, IL-8 y IL-6. La IL-1RA es una citoquina antiinflamatoria que se une y bloquea el acceso al receptor de IL-1 sin causar señalización posterior. Los niveles de IL-1RA tras la exposición de 60 nM de T-2 disminuyeron respecto al control en los esferoides de monocultivo; sin embargo, en el co-cultivo aumentaron. La disminución de los niveles de IL-1RA en monocultivos puede indicar una respuesta inflamatoria y su aumento en los esferoides en co-cultivos una respuesta antiinflamatoria creciente. Al igual que IL-1RA, los niveles de GM-CSF tras 60 nM de T-2 disminuyeron con respecto al control en los esferoides de monocultivo; sin embargo, en el co-cultivo aumentaron con respecto al control. La disminución de la expresión de GM-CSF del monocultivo indica una respuesta inflamatoria, sin embargo, su aumento en co-cultivos puede estar relacionado con una respuesta proinflamatoria.

Dado que los niveles de MCP-1 fueron insignificantes en monocultivos pero robustos en co-cultivos, se sugiere que las células LX2 pueden ser una fuente de MCP-1. La disminución de los niveles de MCP-1 en esferoides en co-cultivos expuestos a 60 nM de T-2 puede atribuirse a daño celular. El TNF-α e IL-8 son citoquinas proinflamatorias que pueden producirse durante una lesión. La producción de ambas citoquinas aumenta en esferoides en monocultivos y co-cultivos expuestos a 60 nM de T-2, comparada con el control, sugiriendo que la micotoxina desencadena respuestas inflamatorias en cultivos hepáticos. Esto podría explicar el aumento de los niveles de IL-1RA en esferoides en co-cultivos para contrarrestar la respuesta proinflamatoria tras la exposición a la T-2.

La IL-6 es una molécula compleja que exhibe efectos pro- o antiinflamatorios según el tipo de lesión y sistema biológico (Norris et al., 2014). La IL-6 mostró una mayor expresión en esferoides en co-cultivos que en monocultivos y la exposición a 60 nM T-2 no provocó cambios en los monocultivos, pero sí una disminución en los co-cultivos. Debido a que no se observó ningún cambio tras 60 nM de T-2 en el monocultivo con respecto al control, se considera que la IL-6 es secretada únicamente por las células LX2. Estudios anteriores revelan que el HGF es secretado en grandes cantidades cuando los esferoides se co-cultivan en dispositivos microfluídicos. Las grandes cantidades secretadas de HGF provocan una estimulación para secretar IL-6 en las células (Kim et al., 2012). Esto se confirma en este estudio, ya que se observó el incremento de IL-6 en esferoides de co-cultivo sin exposición a T-2. Sin embargo, disminuyó la expresión de la IL-6 al exponer las células a 60 nM de T-2, y esto puede deberse a que el esferoide se haya dañado y la secreción del HGF disminuya con la consiguiente disminución de IL-6.

De manera similar a nuestro estudio, Liu y colaboradores informaron que la T-2 inducía la expresión de la citoquina proinflamatoria TNF-α en la línea celular de hígado de rata (BRL) (Liu et al., 2019). Además, la expresión del TNF-α, IL-8 e IL-6 aumentaron después de la exposición a T-2 en células PC12 utilizadas como células modelo de neuronas (Pei et al., 2021). En resumen, nuestros resultados apuntan a la expresión de citoquinas proinflamatorias (TNF-α, IL-8, GM-CSF, MCP-1) y antiinflamatorias (IL-1RA) en cultivos de esferoides hepáticos en sistemas microfluídicos. Estos resultados también indican que la mayor complejidad de los cultivos de esferoides hace que sea más difícil identificar el origen de las vías de señalización de los mecanismos de acción, aunque también proporciona datos más reales frente a los modelos en 2D.

4.10. Referencias

Abid-Essefi, S., Baudrimont, I., Hassen, W., Ouanes, Z., Mobio, T.A., Anane, R., Creppy, E.E., Bacha, H., 2003. DNA fragmentation, apoptosis and cell cycle arrest induced by zearalenone in cultured DOK, Vero and Caco-2 cells: Prevention by Vitamin E. Toxicology 192, 237–248. https://doi.org/10.1016/S0300-483X(03)00329-9

Agrawal, M., Bhaskar, A.S.B., Rao, P.V.L., 2015. Involvement of Mitogen-Activated Protein Kinase Pathway in T-2 Toxin-Induced Cell Cycle Alteration and Apoptosis in Human Neuroblastoma Cells. Mol Neurobiol 51, 1379–1394. https://doi.org/10.1007/s12035-014-8816-4

Agrawal, Y.O., Sharma, P.K., Shrivastava, B., Ojha, S., Upadhya, H.M., Arya, D.S., Goyal, S.N., 2014. Hesperidin produces cardioprotective activity via PPAR-γ pathway in ischemic heart disease model in diabetic rats. PLoS One, 9(11), e111212. https://doi.org/10.1371/journal.pone.0111212

Alonso-Jauregui, M., González-Peñas, E., López de Cerain, A., Vettorazzi, A., 2022. Genotoxicity of 12 Mycotoxins by the SOS/umu Test: Comparison of Liver and Kidney S9 Fraction. Toxins 14 (6) 400. https://doi.org/10.3390/toxins14060400

EFSA, 2017. Human and animal dietary exposure to T-2 and HT-2 toxin. EFSA J 15 (8) e04972. https://doi.org/10.2903/j.efsa.2017.4972

Choi, J., Loarca, L., De Hoyos-Vega, J.M., Neda Dadgar, X., Loutherback, K., Vijay Shah, X.H., Stybayeva, G., Revzin, A., Hoyos-Vega, D.J., 2020. Microfluidic confinement enhances phenotype and function of hepatocyte spheroids Microfluidic confine-ment enhances phenotype and function of hepatocyte spheroids. Am J Physiol Cell Physiol 319(3), C552-C560. https://doi.org/10.1152/ajpcell.00094.2020.-A

Chou, T.C., 2006. Theoretical basis, experimental design, and computerized simulation of synergism and antagonism in drug combination studies. Pharmacol Rev 58(3), 621-681. https://doi.org/10.1124/pr.58.3.10

Chou, T.-C., Talalayi, P., 1984. Quantitative analysis of dose-effect relationships: the combined effects of multiple drugs or enzyme inhibitors. Adv Enzyme Regul 22, 27-55. https://doi.org/10.1016/0065-2571(84)90007-4

Deyu, H., Luqing, C., Xianglian, L., Pu, G., Qirong, L., Xu, W., Zonghui, Y., 2018. Protective mechanisms involving enhanced mitochondrial functions and mitophagy against T-2

toxin-induced toxicities in GH3 cells. Toxicol Lett 295, 41–53. https://doi.org/10.1016/j.toxlet.2018.05.041

Fang, H., Wu, Y., Guo, J., Rong, J., Ma, L., Zhao, Z., Zuo, D., Peng, S., 2012. T-2 toxin induces apoptosis in differentiated murine embryonic stem cells through reactive oxygen species-mediated mitochondrial pathway. Apoptosis 17, 895–907. https://doi.org/10.1007/s10495-012-0724-3

Fernández-Blanco, C., Juan-García, A., Juan, C., Font, G., Ruiz, M.J., 2016. Alternariol induce toxicity via cell death and mitochondrial damage on Caco-2 cells. Food Chem Toxicol 88, 32–39. https://doi.org/10.1016/j.fct.2015.11.022

Gouze, M.E., Laffitte, J., Rouimi, P., Loiseau, N., Oswald, I.P., Galtier, P., 2006. Effect of various doses of deoxynivalenol on liver xenobiotic metabolizing enzymes in mice. Food Chem Toxicol 44, 476–483. https://doi.org/10.1016/j.fct.2005.08.020

Juan-García, A., Taroncher, M., Font, G., Ruiz, M.J., 2018. Micronucleus induction and cell cycle alterations produced by deoxynivalenol and its acetylated derivatives in individual and combined exposure on HepG2 cells. Food Chem Toxicol 118, 719–725. https://doi.org/10.1016/j.fct.2018.06.024

Juan-García, A., Tolosa, J., Juan, C., Ruiz, M.J., 2019. Cytotoxicity, genotoxicity and disturbance of cell cycle in hepg2 cells exposed to OTA and BEA: Single and combined actions. Toxins 11 (6) 341. https://doi.org/10.3390/toxins11060341

Kim, Y., Fiel, M.I., Albanis, E., Chou, H.I., Zhang, W., Khitrov, G., Friedman, S.L., 2012. Anti-fibrotic activity and enhanced interleukin-6 production by hepatic stellate cells in response to imatinib mesylate. Liver Int 32, 1008–1017. https://doi.org/10.1111/j.1478-3231.2012.02806.x

Lei, Y., Guanghui, Z., Xi, W., Yingting, W., Xialu, L., Fangfang, Y., Goldring, M.B., Xiong, G., Lammi, M.J., 2017. Cellular responses to T-2 toxin and/or deoxynivalenol that induce cartilage damage are not specific to chondrocytes. Sci Rep 7 (1) 2231. https://doi.org/10.1038/s41598-017-02568-5

Li, X., Wang, X., Liu, S., Wang, J., Liu, X.Y., Zhu, Y., Zhang, L., Li, R., 2021. Betulinic acid attenuates T-2 toxin-induced cytotoxicity in porcine kidney cells by blocking oxidative stress and endoplasmic reticulum stress. Comp Biochem Physiol Part - C: Toxicol Pharmacol 249, 109124. https://doi.org/10.1016/j.cbpc.2021.109124

Lin, N.N., Chen, J., Xu, B., Wei, X., Guo, L., Xie, J.W., 2015. The roles of carboxylesterase and CYP isozymes on the in vitro metabolism of T-2 toxin. Mil Med Res 2, 1-7. https://doi.org/10.1186/s40779-015-0041-6

Lindberg, L.A., G.Y., K.E., 1985. Massive lipid accumulation in mink liver stellate cells may be caused by Fusarium mycotoxins in the feed. Acta Vet Scand 26, 423–424. https://doi.org/10.1186/BF03546543

Liu, B.H., Yu, F.Y., Wu, T.S., Li, S.Y., Su, M.C., Wang, M.C., Shih, S.M., 2003. Evaluation of genotoxic risk and oxidative DNA damage in mammalian cells exposed to mycotoxins, patulin and citrinin. Toxicol Appl Pharmacol 191, 255–263. https://doi.org/10.1016/S0041-008X(03)00254-0

Liu, X., Pan, Z., Wang, Y., 2019. Ultrasound-assisted turbine bead milling for disintegration of Nannochloropsis oculata cells. J Appl Phycol 31, 1651–1659. https://doi.org/10.1007/s10811-018-1702-0

Liu, Y.X., Wang, J., Guo, J., Wu, J., Lieberman, H.B., Yin, Y., 2008. DUSP1 is controlled by p53 during the cellular response to oxidative stress. Mol Cancer Res 6, 624–633. https://doi.org/10.1158/1541-7786.MCR-07-2019

Mallebrera, B., Font, G., Ruiz, M.J., 2014. Disturbance of antioxidant capacity produced by beauvericin in CHO-K1 cells. Toxicol Lett 226, 337–342. https://doi.org/10.1016/j.toxlet.2014.02.023

Mallebrera, B., Juan-Garcia, A., Font, G., Ruiz, M.J., 2016. Mechanisms of beauvericin toxicity and antioxidant cellular defense. Toxicol Lett 246, 28–34. https://doi.org/10.1016/j.toxlet.2016.01.013

Mamur, S., Yuzbasioglu, D., Yılmaz, S., Erikel, E., Unal, F., 2018. Assessment of cytotoxic and genotoxic effects of enniatin-A in vitro. Food Addit Contam Part A Chem Anal Control Expo Risk Assess 35, 1633–1644. https://doi.org/10.1080/19440049.2018.1486513

Narváez, A., Izzo, L., Pallarés, N., Castaldo, L., Rodríguez-Carrasco, Y., Ritieni, A., 2021. Human biomonitoring of t-2 toxin, t-2 toxin-3-glucoside and their metabolites in urine through high-resolution mass spectrometry. Toxins 13 (12) 869. https://doi.org/10.3390/toxins13120869

Norris, C.A., He, M., Kang, L.I., Ding, M.Q., Radder, J.E., Haynes, M.M., Yang, Y., Paranjpe, S., Bowen, W.C., Orr, A., Michalopoulos, G.K., Stolz, D.B., Mars, W.M., 2014. Synthesis of IL-6 by hepatocytes is a normal response to common hepatic stimuli. PLoS One 9 (4) e96053. https://doi.org/10.1371/journal.pone.0096053

Pagnussatt, F.A., De Lima, V.R., Dora, C.L., Costa, J.A.V., Putaux, J.L., Badiale-Furlong, E., 2016. Assessment of the encapsulation effect of phenolic compounds from Spirulina sp. LEB-18 on their antifusarium activities. Food Chem 211, 616–623. https://doi.org/10.1016/j.foodchem.2016.05.098

Pagnussatt, F.A., Del Ponte, E.M., Garda-Buffon, J., Badiale-Furlong, E., 2014. Inhibition of Fusarium graminearum growth and mycotoxin production by phenolic extract from Spirulina sp. Pestic Biochem Physiol 108, 21–26. https://doi.org/10.1016/j.pestbp.2013.11.002

Pei, X., Jiang, H., Liu, X., Li, L., Li, C., Xiao, X., Li, D., Tang, S., 2021. Targeting HMGB1 inhibits T-2 toxin-induced neurotoxicity via regulation of oxidative stress, neuroinflammation and neuronal apoptosis. Food Chem Toxicol 151, 112134. https://doi.org/10.1016/j.fct.2021.112134

Prosperini, A., Juan-García, A., Font, G., Ruiz, M.J., 2013. Beauvericin-induced cytotoxicity via ROS production and mitochondrial damage in Caco-2 cells. Toxicol Lett 222, 204–211. https://doi.org/10.1016/j.toxlet.2013.07.005

Ren, Z., Wang, Yachao, Deng, H., Deng, Y., Deng, J., Zuo, Z., Wang, Ya, Peng, X., Cui, H., Shen, L., 2015. Deoxynivalenol induces apoptosis in chicken splenic lymphocytes via the reactive oxygen species-mediated mitochondrial pathway. Environ Toxicol Pharmacol 39, 339–346. https://doi.org/10.1016/j.etap.2014.11.028

Scaglioni, P.T., Blandino, M., Scarpino, V., Giordano, D., Testa, G., Badiale-Furlong, E., 2018. Application of Fungicides and Microalgal Phenolic Extracts for the Direct Control of Fumonisin Contamination in Maize. J Agric Food Chem 66, 4835–4841. https://doi.org/10.1021/acs.jafc.8b00540

Smerák, P., Bárta, I., Polívková, Z., Bártová, J., Sedmíková, M., 2001. Mutagenic effects of selected trichothecene Mycotoxins and their combinations with Aflatoxin B1. Czech J Food Sci 19, 90–96.

Somoskői, B., Kovács, M., Cseh, S., 2016. Effects of T-2 mycotoxin on in vitro development and chromatin status of mouse embryos in preimplantation stages. Toxicol Ind Health 32, 1260–1265. https://doi.org/10.1177/0748233714555394

Souza, M.M.D., Prietto, L., Christ Ribeiro, A., Denardi de Souza, T., Badiale-Furlong, E., 2011. Assessment of the antifungal activity of Spirulina platensis phenolic extract against Aspergillus flavus. Cienc Agrotec 35, 1050-1058. https://doi.org/10.1590/S1413-70542011000600003

Takakura, N., Nesslany, F., Fessard, V., Le Hegarat, L., 2014. Absence of in vitro genotoxicity potential of the mycotoxin deoxynivalenol in bacteria and in human TK6 and HepaRG cell lines. Food Chem Toxicol 66, 113–121. https://doi.org/10.1016/j.fct.2014.01.029

Tatay, E., Espín, S., García-Fernández, A.J., Ruiz, M.J., 2017. Oxidative damage and disturbance of antioxidant capacity by zearalenone and its metabolites in human cells. Toxicol in Vitro 45, 334–339. https://doi.org/10.1016/j.tiv.2017.04.026

Tatay, E., Font, G., Ruiz, M.J., 2016. Cytotoxic effects of zearalenone and its metabolites and antioxidant cell defense in CHO-K1 cells. Food Chem Toxicol 96, 43–49. https://doi.org/10.1016/j.fct.2016.07.027

Trusal, L.R., 1986. Metabolism of T-2 mycotoxin by cultured cells. Toxicon 24(6), 597-603. https://doi.org/10.1016/0041-0101(86)90180-7

Wada, T., Penninger, J.M., 2004. Mitogen-activated protein kinases in apoptosis regulation. Oncogene, 23(16), 2838-2849. https://doi.org/10.1038/sj.onc.1207556

Weidner, M., Welsch, T., Hübner, F., Schwerdt, G., Gekle, M., Humpf, H.U., 2012. Identification and apoptotic potential of T-2 toxin metabolites in human cells. J Agric Food Chem 60, 5676–5684. https://doi.org/10.1021/jf300634k

Wen, J., Mu, P., Deng, Y., 2016. Mycotoxins: Cytotoxicity and biotransformation in animal cells. Toxicol Res 5(2), 377-387. https://doi.org/10.1039/c5tx00293a

Wu, J., Jing, L., Yuan, H., Peng, S. qing, 2011. T-2 toxin induces apoptosis in ovarian granulosa cells of rats through reactive oxygen species-mediated mitochondrial pathway. Toxicol Lett 202, 168–177. https://doi.org/10.1016/j.toxlet.2011.01.029

Wu, J., Zhou, Y., Yuan, Z., Yi, J., Chen, J., Wang, N., Tian, Y., 2019. Autophagy and apoptosis interact to modulate T-2 toxin-induced toxicity in liver cells. Toxins 11 (1) 45. https://doi.org/10.3390/toxins11010045

Wu, Q.H., Wang, X., Yang, W., Nüssler, A.K., Xiong, L.Y., Kuča, K., Dohnal, V., Zhang, X.J., Yuan, Z.H., 2014. Oxidative stress-mediated cytotoxicity and metabolism of T-2 toxin and deoxynivalenol in animals and humans: An update. Arch Toxicol 88, 1309–1326. https://doi.org/10.1007/s00204-014-1280-0

Yang, L., Yu, Z., Hou, J., Deng, Y., Zhou, Z., Zhao, Z., Cui, J., 2016. Toxicity and oxidative stress induced by T-2 toxin and HT-2 toxin in broilers and broiler hepatocytes. Food Chem Toxicol 87, 128–137. https://doi.org/10.1016/j.fct.2015.12.003

Yang, S., De Boevre, M., Zhang, H., De Ruyck, K., Sun, F., Zhang, J., Jin, Y., Li, Yanshen, Wang, Z., Zhang, S., Zhou, J., Li, Yi, De Saeger, S., 2017. Metabolism of T-2 Toxin in Farm Animals and Human in Vitro and in Chickens in Vivo Using Ultra High-Performance Liquid Chromatography- Quadrupole/Time-of-Flight Hybrid Mass Spectrometry Along with Online Hydrogen/Deuterium Exchange Technique. J Agric Food Chem 65, 7217–7227. https://doi.org/10.1021/acs.jafc.7b02575

Yang, S., Zhang, H., De Boevre, M., Zhang, J., Li, Yanshen, Zhang, S., De Saeger, S., Zhou, J., Li, Yi, Sun, F., 2018. Toxicokinetics of HT-2 Toxin in Rats and Its Metabolic Profile in Livestock and Human Liver Microsomes. J Agric Food Chem 66, 8160–8168. https://doi.org/10.1021/acs.jafc.8b02893

Zhang, X., Wang, Y., Velkov, T., Tang, S., Dai, C., 2018. T-2 toxin-induced toxicity in neuroblastoma-2a cells involves the generation of reactive oxygen, mitochondrial dysfunction and inhibition of Nrf2/HO-1 pathway. Food Chem Toxicol 114, 88–97. https://doi.org/10.1016/j.fct.2018.02.010

Zhang, Y. F., Yang, J. Y., Li, Y. K., & Zhou, W. (2017). Toxicity and oxidative stress induced by T-2 toxin in cultured mouse Leydig cells. Toxicol Mech Meth 27(2), 100-106. https://doi.org/10.1080/15376516.2016.1258747

Zingales, V., Fernández-Franzón, M., Ruiz, M.J., 2021. Sterigmatocystin-induced DNA damage triggers cell-cycle arrest via MAPK in human neuroblastoma cells. Toxicol Mech Meth 31, 479–488. https://doi.org/10.1080/15376516.2021.1916801

5. Conclusiones

Conclusions

5. CONCLUSIONES

1. La revisión bibliográfica realizada pone de manifiesto la toxicidad de la T-2. Sin embargo, la información sobre la toxicidad de sus metabolitos es limitada. Debido a la amplia variación en la concentración de la T-2 en los alimentos analizados en los últimos años y la reciente publicación de los límites máximos de T-2 y HT-2, se ha abierto un nuevo debate sobre la necesidad de una reevaluación de los mecanismos de acción de la T-2 para una mejor comprensión de su toxicocinética, efectos adversos y riesgos toxicológicos.

2. La aplicación de los métodos predictivos *in silico* AdmetSAR y SwissADME, muestran que la T-2 y sus metabolitos presentan buena absorción gastrointestinal y permeación de la BHE por sus propiedades lipófilas, a excepción del T2-tetraol. Todas las micotoxinas son sustrato de la P-gp (excepto T-2 y HT-2) y de la isoenzima CYP3A4, por lo que se predice la inducción de daño hepático y toxicidad, que debe confirmarse *in vitro*.

3. La T-2 y sus metabolitos reducen la viabilidad celular de manera concentración-dependiente en las células HepG2, en exposición individual y combinada. El orden de citotoxicidad individual disminuye como se muestra: T-2=HT-2 > Neo > T2-triol > T2-tetraol. Las combinaciones binarias producen efectos antagónicos en todas las fracciones afectadas. Sin embargo, se observaron efectos aditivos a fracciones afectadas altas en las combinaciones T-2 + HT-2, T-2 + T2-tetraol, T2-triol + HT-2, T2-triol + T2-tetraol y T2-tetraol + HT-2.

4. La biotransformación de la T-2 es rápida y completa en las células HepG2 y da lugar a metabolitos más polares y fáciles de eliminar. Se confirma que la hidrólisis es la principal vía metabólica de la T-2. Tras un ciclo de 24 h, los niveles

de T-2 y sus metabolitos fluctuaron tras la adición de 60 nM de T-2 en las células HepG2. A medida que disminuye la concentración de T-2 en función del tiempo, tanto a nivel intra como extracelular, aumenta la concentración de sus metabolitos HT-2, Neo, T2-triol y T2-tetraol, siendo HT-2 el mayoritario.

5. La T-2 (15 y 30 nM), el T2-triol (0,12 μM) y el T2-tetraol (a todas las concentraciones ensayadas) produjeron un aumento de las ROS en las células HepG2 tras 24 h de exposición. Sin embargo, el Neo no aumentó las ROS a ninguna de las concentraciones ensayadas.

6. El estrés oxidativo producido por la T-2 y sus metabolitos en las células HepG2 mostró una disminución en los niveles de GSH y una alteración en la actividad de enzimas antioxidantes. Las principales enzimas involucradas en la destoxicación de T-2 en las células HepG2 son la GST y CAT, en el caso del Neo, la CAT y la SOD, para el T2-triol la GST, CAT y SOD, y para el T2-tetraol la GPx y la SOD. El GSH y enzimas relacionadas (GPx y GST) muestran efecto citoprotector ya que la adición de NAC activó dichos sistemas de defensa, y la adición de BSO los disminuyó. El pretratamiento con los antioxidantes procedentes de la dieta como de las microalgas (*T. chuii*) y los hidrolizados de pescado (salmón, caballa y lenguado) protegen a las células HepG2 y Caco-2 de la citotoxicidad y el estrés oxidativo generado por la exposición a T-2.

7. La exposición de T-2 en células HepG2 desencadena el proceso de apoptosis y necrosis tras 24 h. Se observa disrupción del ciclo celular en la fase subG_0/G_1, G_0/G_1 y G_2/M. La parada en G_2/M está relacionada con daño en el ADN, que se confirma con la formación de colas de cometas en las células HepG2 a todas las concentraciones ensayadas de T-2, y micronúcleos a la concentración más

alta. Sin embargo, no se detecta efecto mutagénico de la T-2 por el ensayo del test de Ames.

8. La formación y caracterización de esferoides, evaluada mediante circularidad, solidez y producción de albúmina, demuestran que son más funcionales y proporcionan mejores resultados cuando se utilizan dispositivos microfluídicos que placas estándar.

9. Los resultados obtenidos al comparar los esferoides de monocultivo (HepG2) y co-cultivo (HepG2-LX2) en dispositivos microfluídicos ponen de manifiesto que la T-2 produce citotoxicidad y una disminución de albúmina de manera concentración-dependiente. Sin embargo, los esferoides de co-cultivo presentaron mayor viabilidad y nivel de albúmina que los esferoides de monocultivo. La T-2 se metaboliza y tansporta por las células hepáticas, tanto en los esferoides de monocultivo como co-cultivo, sin embargo, los niveles de inducción enzimática fueron menores en los co-cultivos. Los niveles de expresión de las citoquinas inflamatorias de esferoides hepáticos de mono y co-cultivo en dispositivos microfluídicos se vieron afectados tras la exposición de T-2.

10. La T-2 supone un riesgo tóxico potencial para el consumidor, al afectar a las células hepáticas. Por tanto, es importante realizar más estudios sobre los mecanismos de acción en modelos tridimensionales, ya que simulan mejor las condiciones *in vivo,* siguiendo las recomendaciones europeas del uso de métodos alternativos en la evaluación del riesgo toxicológico. De esta manera se puede prevenir los posibles riesgos asociados a la exposición de esta micotoxina y sus metabolitos a través de la dieta.

5. CONCLUSIONS

1. The literature review conducted highlights the toxicity of T-2. However, information on the toxicity of its metabolites is limited. The wide variation in the concentration of T-2 in foods tested in recent years and the recent publication of the maximum limits for T-2 and HT-2, have opened a new debate on the need to re-evaluate the mechanisms of action of T-2 in order to better understand its toxicokinetics, adverse effects and toxicological risks.

2. Application of the *in silico* predictive methods AdmetSAR and SwissADME shows that T-2 and its metabolites have good gastrointestinal absorption and blood brain barrier permeation due to their lipophilic properties, with the exception of T2-tetraol. All mycotoxins are substrates of P-gp (except T-2 and HT-2) and the CYP3A4 isoenzyme, so induction of liver damage and toxicity is predicted and needs to be confirmed *in vitro*.

3. The T-2 and its metabolites reduce cell viability in a concentration-dependent manner in HepG2 cells, in individual and combined exposure. The order of individual cytotoxicity decreases as shown: T-2=HT-2 > Neo > T2-triol > T2-tetraol. Binary combinations have antagonistic effects on all affected fractions. However, additive effects at high affected fractions were observed for the combinations T-2 + HT-2, T-2 + T2-tetraol, T2-triol + HT-2, T2-triol + T2-tetraol and T2-tetraol + HT-2.

4. Biotransformation of T-2 is rapid and complete in HepG2 cells, resulting in metabolites that are more polar and easier to eliminate. Hydrolysis is confirmed as the main metabolic pathway of T-2. After a 24 h cycle, the levels of T-2 and its metabolites fluctuated following the addition of 60 nM of T-2 in HepG2 cells.

As the concentration of T-2 decreases over time, both intracellularly and extracellularly, the concentration of its metabolites HT-2, Neo, T2-triol and T2-tetraol increases, with HT-2 being the major metabolite.

5. The T-2 (15 and 30 nM), T2-triol (0.12 μM) and T2-tetraol (at all concentrations tested) produced an increase in ROS in HepG2 cells after 24 h of exposure. However, Neo did not increase ROS at any of the concentrations tested.

6. Oxidative stress induced by T-2 and its metabolites in HepG2 cells showed a decrease in GSH levels and an alteration in the activity of antioxidant enzymes. The main enzymes involved in T-2 detoxification in HepG2 cells are GST and CAT; for Neo CAT and SOD; for T2-triol, GST, CAT and SOD; and for T2-tetraol, GPx and SOD. GSH and related enzymes (GPx and GST) show a cytoprotective effect, as the addition of NAC activated these defense systems and the addition of BSO decreased them. Pretreatment with dietary antioxidants such as microalgae (*T. chuii*) and fish hydrolysates (salmon, mackerel and herring) protects HepG2 and Caco-2 cells from cytotoxicity and oxidative stress induced by T-2 exposure.

7. The T-2 exposure in HepG2 cells induces the process of apoptosis and necrosis after 24 h. Cell cycle arrest is observed in the subG0/G1, G0/G1 and G2/M phase. The G2/M arrest is associated with DNA damage, as confirmed by the formation of comet tails in HepG2 cells at all tested concentrations of T-2 and micronuclei at the highest concentration. However, no mutagenic effect of T-2 was detected by the Ames test.

8. The formation and characterization of spheroids, evaluated by circularity, solidity and albumin production, demonstrate that they are more functional and give better results when using microfluidic devices than standard plates.

9. Results obtained by comparing monoculture (HepG2) and co-culture (HepG2-LX2) spheroids in microfluidic devices show that T-2 induces cytotoxicity and a concentration-dependent decrease in albumin. However, co-culture spheroids showed higher viability and albumin levels than monoculture spheroids. The T-2 is metabolized and transported by liver cells in both monoculture and co-culture spheroids, but enzymatic activities were lower in co-cultures. Inflammatory cytokines expression levels of monoculture and co-culture liver spheroids in microfluidic devices were affected after T-2 exposure.

10. The T-2 represents a potential toxic risk to consumers through its effects on liver cells. Therefore, it is important to carry out more studies on the mechanisms of action in three-dimensional models, which better simulate *in vivo* conditions, in accordance with the European recommendations on the use of alternative methods in toxicological risk assessment. In this way, possible risks associated with dietary exposure to this mycotoxin and its metabolites can be avoided.

ANEXO I

ARTÍCULOS PUBLICADOS

Food and Chemical Toxicology 145 (2020) 111654

Contents lists available at ScienceDirect

Food and Chemical Toxicology

journal homepage: www.elsevier.com/locate/foodchemtox

T-2 toxin and its metabolites: Characterization, cytotoxic mechanisms and adaptive cellular response in human hepatocarcinoma (HepG2) cells

Mercedes Taroncher *, Yelko Rodríguez-Carrasco, María-José Ruiz

Laboratory of Food Chemistry and Toxicology, Faculty of Pharmacy, University of Valencia, Av. Vicent Andrés Estellés s/n, 46100, Burjassot, Valencia, Spain

ARTICLE INFO

Keywords:
T-2 toxin
Metabolites
Adaptive response
Cell proliferation
Cellular damage
LC-Q-TOF MS

ABSTRACT

The T-2 toxin (T-2) is a type A trichothecene produced by *Fusarium* species, and the most cytotoxic mycotoxin of the group. A study was made to determine T-2 cytotoxicity in human hepatocarcinoma (HepG2) cells; evaluate whether there is an adaptive response of HepG2 cells exposed to low concentrations of T-2; identify the T-2 metabolites by LC-Q-TOF MS; and determine whether T-2 disrupts cell proliferation in HepG2 cells. The IC_{50} values obtained ranged from 61.9 ± 2.4 nM to 70.7 ± 7.4 nM. No adaptive response was observed. There was no evidence of extra- or intracellular accumulation of T-2 after 24 h of exposure as determined by LC-Q-TOF MS. However, some T-2 metabolites such as HT-2 toxin, neosolaniol and T-2 triol showed important (>75%) intracellular accumulation. Cell distribution was significantly increased in SubG0/G1 phase (11.8-fold higher) and decreased (12%) in G2/M phase at 60 nM T-2, versus the control. Simultaneously, increased necrosis (238%) and apoptosis/necrosis (up to 35.5%) were observed in HepG2 cells exposed to T-2. In conclusion, the results show that T-2 leads to loss of cell viability without an adaptive response, and that the metabolites generated play an important role in T-2 cytotoxicity, increasing HepG2 cell damage.

1. Introduction

Fusarium fungi produce various mycotoxins, including trichothecenes, with adverse effects upon humans and animals (Streit et al., 2012; Van der Fels-Klerx et al., 2012). Trichothecenes are subdivided into four types (A-D) according to the substituents of the tetracyclic ring system. These mycotoxins frequently occur in cereals worldwide, notably in wheat, barley, maize, oats, rye and rice (Fatima et al., 2018). In such contaminated crops, mycotoxins and/or their metabolites can be found together, and their toxicological activities could result in cumulative additive or synergistic effects (EFSA, 2016, EFSA, 2017a, EFSA, 2017b). Considerable attention has been paid to T-2 toxin (T-2), a type A trichothecene, owing to its high toxicity (Fatima et al., 2018). According to the EFSA, T-2 and/or its metabolites were present in grains for human consumption in a significant number of collected samples from European countries, with oat being the food matrix showing the highest concentrations (41.7 μg/kg) (EFSA, 2017a, EFSA, 2017b).

In vitro human liver microsomal incubations have been used in metabolic studies of mycotoxins, since liver microsomes contain a variety of enzymes that are involved in the formation of both phase I and phase II metabolites. Reactive metabolites can be broadly classified into electrophiles and radicals. Electrophilic reactive metabolites, formed in the presence of a toxic metabolizing system, are often able to form metabolites with small molecule trapping agents. In the scientific literature, several studies have revealed extensive metabolism of T-2 in the mammalian liver (Wu et al., 2014; Yang et al., 2017a, Yang et al., 2017b). Nowadays, state-of-the-art equipment such as liquid chromatography (LC) coupled to a tandem mass spectrometer (MS/MS) or a high-resolution mass spectrometer (HRMS) have become the standard in determining mycotoxins and/or their metabolites in biological matrices, and can provide indirect information on the structure of the reactive species from which they are formed (Rodríguez-Carrasco et al., 2018). Nonetheless, few data are currently available regarding the detection of T-2 and its biotransformation products in tissues and biological fluids, thus complicating evaluation of the potential risks related to exposure to this mycotoxin (EFSA, 2017b). In this line, improved understanding of the metabolic fate of T-2 is of great interest from a toxicological point of view.

T-2 toxicity is related to food refusal, and increases the risk of septicemia and hemorrhage due to molecular effects such as apoptosis of

* Corresponding author. Laboratory of Food Chemistry and Toxicology, Faculty of Pharmacy, University of Valencia, Av. Vicent Andrés Estellés, s/n, 46100, Burjassot, Valencia, Spain.
E-mail address: Mercedes.taroncher@uv.es (M. Taroncher).

https://doi.org/10.1016/j.fct.2020.111654
Received 12 June 2020; Received in revised form 25 July 2020; Accepted 28 July 2020
Available online 7 August 2020

Food and Chemical Toxicology 148 (2021) 111942

Contents lists available at ScienceDirect

Food and Chemical Toxicology

journal homepage: www.elsevier.com/locate/foodchemtox

Interactions between T-2 toxin and its metabolites in HepG2 cells and *in silico* approach

Mercedes Taroncher, Yelko Rodríguez-Carrasco *, María-José Ruiz

Laboratory of Food Chemistry and Toxicology, Faculty of Pharmacy, University of Valencia, Av Vicent Andrés Estellés s/n, 46100, Burjassot, Valencia, Spain

ARTICLE INFO

Keywords:
T-2 toxin
Cytotoxicity
Metabolites
Interaction
In silico
In vitro

ABSTRACT

The T-2 toxin (T-2) is commonly metabolized to HT-2 toxin (HT-2), Neosolaniol (NEO), T2-triol and T2-tetraol and they can modify the toxicity of T-2. In this study, T-2 and its modified forms were evaluated by *in vitro* and *in silico* methods. The *in vitro* cytotoxicity individually was evaluated by MTT and Total Protein Content (PC) assays in human hepatocarcinoma (HepG2) cells. The order of IC_{50} was T-2 tetraol > T-2 triol > NEO > T-2 = HT-2. The T-2 and HT-2 evidenced the highest cytotoxic effect in HepG2 cells individually. No differences were observed in binary combinations tested and the two mycotoxins in the mixture tested individually. The T-2+HT-2 combination showed the highest toxic potential with the lowest IC_{50} value of 34.42 ± 0.58 nM at 24 h. All binary combinations exhibited antagonistic interactions. The ADME and toxicity profile of mycotoxins were obtained by the *in silico* admetSAR predictive model which determines the metabolic and toxicological approaches in order to know if these mycotoxins might be taken into consideration to support a more realistic and adequate risk assessment.

1. Introduction

Human beings are exposed to different mycotoxins through their daily diet. The exposure to these mycotoxins is practically unavoidable due to their ubiquity, natural origin or production during food transformation. Food contamination is a major problem in Europe as demonstrated by the notifications system issued by "Rapid Alert System for Food and Feed" (RASFF) of the European Food Safety Authority (EFSA). In the last report (2019), mycotoxins are classified according to the hazard category in the first place in food products, with 534 notifications (RASFF, 2020). The mycotoxins may cause adverse effects in the short, medium and long term for consumers depending on the concentrations in the food and the exposure time. Toxic effects can range from mild to potentially toxic such as cancer or mutations. However, their toxicity can be increased when they are present in the diet simultaneously or as a consequence of metabolism. In fact, synergistic toxic effects have been described *in vivo* and *in vitro* for some mixtures of mycotoxins or metabolites originated from a parent compound (EFSA, 2014a; 2020a; Sultana Shaik et al., 2016; Kar and Leszczynski, 2019). Hence, these aspects should be considered when dealing with contaminants ingested simultaneously in the diet.

Mycotoxins cause significant toxic effects at cellular and organic levels; therefore, it is important to know the toxicity of those that have not been studied or their toxicity data is absent. Currently, food safety agencies (EFSA; Food and Agriculture Organization, FAO; World Health Organization, WHO/OMS; Food and Drug Administration, FDA) have set as a new challenge, "to evaluate the possible cumulative and synergistic effects of the different chemical substances to which consumers are usually exposed through the diet", since to date most of the published data are obtained from individual toxicity studies (unrealistic scenario) (EFSA, 2014b).

An additional challenge is to investigate the mechanisms of toxic action of alternative methods to animal experimentation for those substances whose mechanisms have not yet been fully elucidated (Directive, 2010/63/EU). Given the increased requirements and restrictions at legislative level alternative approaches, such as *in vitro* and *in silico* methods, are a cost-effective solution because of saving time, money and minimizing animal testing, and are also encouraged and promoted by the European authorities (European Chemicals Agency (ECHA) and EFSA) (EFSA, 2020b). Computational approaches have already been proven as efficient alternatives for assessing the chemical toxicity by regulatory authorities. To date, different tools have been developed *in silico* to predict modes of action (MoA) and mechanisms by which Adverse Outcome Pathways (AOP) of known chemical substances occur

* Corresponding author.
E-mail address: yelko.rodriguez@uv.es (Y. Rodríguez-Carrasco).

https://doi.org/10.1016/j.fct.2020.111942
Received 13 November 2020; Received in revised form 16 December 2020; Accepted 18 December 2020
Available online 28 December 2020

foods

MDPI

Article

Identification of Biotransformation Products of T-2 Toxin in HepG2 Cells Using LC-Q-TOF MS

Mercedes Taroncher [1,2], Veronica Zingales [1,2], Yelko Rodríguez-Carrasco [1,2,*] and María José Ruiz [1,2]

[1] Laboratory of Food Chemistry and Toxicology, Faculty of Pharmacy and Food Science, University of Valencia, Av. Vicent Andrés Estellés s/n, 46100 Burjassot, Spain; mercedes.taroncher@uv.es (M.T.); veronica.zingales@uv.es (V.Z.); m.jose.ruiz@uv.es (M.J.R.)

[2] Research Group Alternative Methods for Determining Toxic Effects and Risk Assessment of Contaminants and Mixtures (RiskTox; GIUV2021-513), University of Valencia, 46100 València, Spain

* Correspondence: yelko.rodriguez@uv.es; Tel./Fax: +34-96-3544-228

Abstract: The T-2 toxin (T-2) is a type A trichothecene found in cereals. The formation of metabolites is a frequent cause of mycotoxin-induced toxicity. In this work, the conversion of T-2 during biotransformation reactions in HepG2 cells was evaluated. For this, HepG2 cells were exposed to 30 ($IC_{50}/2$) and 60 (IC_{50}) nM of T-2 for 0, 1, 2, 3, 6, 8 and 24 h, and the concentrations of T-2 and its metabolites HT-2, T2-triol, T2-tetraol and neosolaniol were determined in both the cell fraction and culture medium through liquid chromatography coupled to high-resolution mass spectrometry–time of flight (LC-Q-TOF MS). Results showed a fast metabolization of T-2 (>90%) during the first 2 h, with HT-2 as its main (>95%) biotransformation product. The cell fraction showed higher levels ($p < 0.05$) of HT-2 (39.9 ± 2.1 nM) compared to the culture medium (12.53 ± 2.4 nM). This trend was also observed for the identified metabolites. T2-triol reached its maximum concentration (1.7 ± 0.4 nM) at 2 h, and at later times a time-dependent increase in the T2-tetraol and neosolaniol concentrations was observed. The identification of T-2 metabolites shows the need to continue combined toxicity studies of mycotoxins for a correct risk characterization of these natural contaminants.

Keywords: T-2; biotransformation; HepG2; in vitro; LC-Q-TOF MS

Citation: Taroncher, M.; Zingales, V.; Rodríguez-Carrasco, Y.; Ruiz, M.J. Identification of Biotransformation Products of T-2 Toxin in HepG2 Cells Using LC-Q-TOF MS. *Foods* **2024**, *13*, 1501. https://doi.org/10.3390/foods13101501

Academic Editor: Yun Wang

Received: 18 April 2024
Revised: 2 May 2024
Accepted: 8 May 2024
Published: 13 May 2024

1. Introduction

Field crops are naturally contaminated by several species of *Fusarium* fungi, which produce trichothecene mycotoxins. These mycotoxins have been frequently evaluated, and the European Food Safety Authority (EFSA) considers that due to toxicity following dietary exposure, there is a potential risk for acute and chronic adverse effects in humans and animals [1]. Therefore, there is a need to identify and quantify their levels in cereals to monitor and verify that the established maximum levels are not exceeded. The T-2 toxin (T-2) is one of the most common mycotoxins of the trichothecenes found mainly in oat, wheat and wheat byproducts [2]. The exposure of T-2 in the population was calculated considering the concentration reported in wheat and wheat-based products and the average consumption of cereals. The maximum level of T-2 found in breakfast cereals for adults and infants was 4.47 µg/kg and 0.11 µg/kg, respectively [1]. Moreover, the wheat and wheat-based products consumption according to data reported by the Food Agriculture Organization was 0.27 kg/day [3]. According to the above, adults are exposed to 2.59 nM T-2, while infants are exposed to 0.064 nM T-2.

As the most toxic trichothecene, T-2 is regarded as the main cause of alimentary toxic aleukia disease (ATA), a gastrointestinal disorder that affected World War II soldiers and people around the world after ingesting moldy food [4]. ATA is characterized by vomiting, diarrhea, gastroenteritis, leukopenia (aleukia), hemorrhages, skin inflammation and, in severe cases, death due to asphyxia [5]. ATA affected some people, especially those between the ages of 10 and 40, with a mortality rate of 60% in the former USSR from 1932 to 1947,

toxins

MDPI

Article

Stressful Effects of T-2 Metabolites and Defense Capability of HepG2 Cells

Mercedes Taroncher [1], Fiona Halbig [2], Yelko Rodríguez-Carrasco [1,*] and María-José Ruiz [1]

[1] Department of Preventive Medicine and Public Health, Food Science, Toxicology and Forensic Medicine, Faculty of Pharmacy, University of Valencia, 46100 Burjassot, Valencia, Spain
[2] Department of Pharmacy, Rheinische Friedrich-Wilhelms-Universität Bonn, 53115 Bonn, Germany
* Correspondence: yelko.rodriguez@uv.es

Abstract: The T-2 toxin (T-2), a mycotoxin produced by several species of *Fusarium* which belongs to group A of trichothecenes, is rapidly metabolized, and its main metabolites are HT-2, Neosolaniol (Neo), T2-triol and T2-tetraol. In this work, the antioxidant defense system of HepG2 cells against oxidative stress induced by T-2 and its metabolites was evaluated. The results obtained demonstrated that there is an overall decrease in glutathione (GSH) levels after all mycotoxins exposure. Moreover, the GSH levels and the enzymatic activities related to GSH (GPx and GST) increased with NAC pre-treatment (glutathione precursor) and decreased with BSO pre-treatment (glutathione inhibitor). The GPx activity is increased by T2-tetraol. The GST activity increased after T-2 and T2-triol exposure; however, T2-tetraol decreased its activity. Furthermore, CAT activity increased after T-2 and T2-triol; nevertheless, Neo decreased its activity. Finally, SOD activity is increased by all mycotoxins, except after T-2 exposure. So, the damage associated with oxidative stress by T-2 and its metabolites is relieved by the antioxidant enzymes system on HepG2 cells.

Keywords: T-2; metabolites; glutathione; antioxidant enzymes

Key Contribution: The role played by oxidative stress of T-2 and mainly its metabolites Neo, T2-triol, and T2-tetraol on HepG2 cells.

check for updates

Citation: Taroncher, M.; Halbig, F.; Rodríguez-Carrasco, Y.; Ruiz, M.-J. Stressful Effects of T-2 Metabolites and Defense Capability of HepG2 Cells. *Toxins* **2022**, *14*, 841. https://doi.org/10.3390/toxins14120841

Received: 24 October 2022
Accepted: 24 November 2022
Published: 1 December 2022

Publisher's Note: MDPI stays neutral with regard to jurisdictional claims in published maps and institutional affiliations.

1. Introduction

Mycotoxins are toxic secondary metabolites produced under favorable conditions by fungi that grow on food and feed worldwide [1]. Mycotoxin contamination is an aggravated problem in developing countries. The most detected mycotoxins in food are aflatoxins (AFs), fumonisins (FBs), ochratoxin A (OTA), patulin (PAT), zearalenone (ZEA), and trichothecenes. Among the trichothecenes, the T-2 toxin (T-2) is the most cytotoxic compound [1,2]. The T-2 is produced by various species of *Fusarium*, such as *F. sporotichioides*, *F. poae*, *F. equiseti*, and *F. acuminatum*. It is detected in field crops such as wheat, maize, barley, and oats and processed grains such as malt, beer, and bread [3]. Furthermore, T-2 has also been detected in drinking water in endemic areas of China, such as Qinghai, and in traditional Chinese medicines [4–6]. The most common route of T-2 exposure is through ingestion, although there are other routes. Farmers may be exposed via direct contact with contaminated grain dust and hay, and it could cause organ damage to the kidney, liver, skin, brain, and gut [7,8].

The T-2 is rapidly metabolized to HT-2, Neosolaniol (Neo), T2-triol, and T2-tetraol [1,9]. Consequently, the cytotoxic mechanism of T-2 in vivo and in vitro might be partly attributable to its metabolites [10]. Previously, the cytotoxicity of T-2 metabolites was studied individually and in combinations in various in vitro studies, and it was observed that T-2 showed the highest cytotoxic effect [9]. The T-2 is a predisposing factor in the Kashin–Beck disease (KBD), a chronic endemic type of osteochondropathy that was mainly distributed

foods

MDPI

Article

Effect of Phenolic Extract from Red Beans (*Phaseolus vulgaris* L.) on T-2 Toxin-Induced Cytotoxicity in HepG2 Cells

Carmen Martínez-Alonso [1,†], Mercedes Taroncher [1,†], Luigi Castaldo [2], Luana Izzo [2], Yelko Rodríguez-Carrasco [1,*], Alberto Ritieni [2] and María-José Ruiz [1]

[1] Department of Preventive Medicine and Public Health, Food Science, Toxicology and Forensic Medicine, Faculty of Pharmacy, University of Valencia, Burjassot, 46100 Valencia, Spain; carmar36@alumni.uv.es (C.M.-A.); mercedes.taroncher@uv.es (M.T.); m.jose.ruiz@uv.es (M.-J.R.)

[2] Department of Pharmacy, Faculty of Pharmacy, University of Naples "Federico II", Via Domenico Montesano 49, 80131 Naples, Italy; luigi.castaldo2@unina.it (L.C.); luana.izzo@unina.it (L.I.); alberto.ritieni@unina.it (A.R.)

* Correspondence: yelko.rodriguez@uv.es

† These authors contributed equally to this work.

Abstract: Red beans contain human bioactive compounds such as polyphenols. Several in vitro studies have proposed the natural compounds as an innovative strategy to modify the toxic effects produced by mycotoxins. Hence, in this work, a complete investigation of the polyphenolic fraction of red beans was performed using a Q-Orbitrap high-resolution mass spectrometry analysis. Notably, epicatechin and delphinidin were the most detected polyphenols found in red bean extracts (3.297 and 3.108 mg/Kg, respectively). Moreover, the red bean extract was evaluated against the T-2 toxin (T-2) induced cytotoxicity in hepatocarcinoma cells (HepG2) by direct treatment, simultaneous treatment, and pre-treatment assays. These data showed that T-2 affected the cell viability in a dose-dependent manner, as well as observing a cytotoxic effect and a significant increase in ROS production at 30 nM. The simultaneous treatment and the pre-treatment of HepG2 cells with red bean extract was not able to modify the cytotoxic T-2 effect. However, the simultaneous treatment of T-2 at 7.5 nM with the red bean extract showed a significant decrease in ROS production, with respect to the control. These results suggest that the red bean extract could modulate oxidative stress on HepG2 cells.

Keywords: beans; phenolic compounds; T-2 toxin; HepG2 cells; reactive oxygen species

Citation: Martínez-Alonso, C.; Taroncher, M.; Castaldo, L.; Izzo, L.; Rodríguez-Carrasco, Y.; Ritieni, A.; Ruiz, M.-J. Effect of Phenolic Extract from Red Beans (*Phaseolus vulgaris* L.) on T-2 Toxin-Induced Cytotoxicity in HepG2 Cells. *Foods* **2022**, *11*, 1033. https://doi.org/10.3390/foods11071033

Academic Editor: Paula C. Castilho

Received: 21 March 2022
Accepted: 28 March 2022
Published: 2 April 2022

1. Introduction

Red beans (*Phaseolus vulgaris* L.), in addition to being a great source of vegetable protein, fiber, and certain micronutrients in the human diet, contain a great variety of bioactive compounds. Bioactive compounds are simple substances that have biological activity, associated with their ability to modulate one or more metabolic processes, which results in the promotion of better health conditions. Different bioactive compounds have been studied for their positive effect on human health, such as the following: enzymes, probiotics, prebiotics, fibers, phytosterols, peptides, proteins, saponins, unsatured fatty acids, and phenolic compounds, among others [1]. Particularly, colored beans have significant amounts of phenolic compounds. Phenolic compounds are classified as flavonoids (flavones, flavonols, flavanones, isoflavones, anthocyanins, chalcones, dihydrochalcones, and catechins), phenolic acids (hydroxybenzoic, hydroxyphenyl acetic, hydroxyphenyl pentanoic, and cinnamic hydroxyl acids), tannins, stilbenes, and lignans. Phenolic acids, flavonoids, and anthocyanidins are the main phenolic compounds identified and characterized in beans [2,3]. Phenolic compounds determine the color of the seeds of these legumes; hence, in general, a higher phenolic content is observed in more pigmented beans [4]. Phenolic compounds, besides from contributing to the smell, taste, and color of food, have a long-term intake that could play a bioactive role due to their antioxidant activity,

Toxicology Mechanisms and Methods

ISSN: (Print) (Online) Journal homepage: https://www.tandfonline.com/loi/itxm20

Evaluation of cytotoxicity, analysis of metals and cumulative risk assessment in microalgae

Mercedes Taroncher, Yelko Rodríguez-Carrasco, Francisco J. Barba & María José Ruiz

To cite this article: Mercedes Taroncher, Yelko Rodríguez-Carrasco, Francisco J. Barba & María José Ruiz (2023) Evaluation of cytotoxicity, analysis of metals and cumulative risk assessment in microalgae, Toxicology Mechanisms and Methods, 33:5, 388-400, DOI: 10.1080/15376516.2022.2152514

To link to this article: https://doi.org/10.1080/15376516.2022.2152514

Published online: 05 Dec 2022.

antioxidants

MDPI

Article

Cytoprotective Effects of Fish Protein Hydrolysates against H_2O_2-Induced Oxidative Stress and Mycotoxins in Caco-2/TC7 Cells

Mercedes Taroncher [1], Yelko Rodríguez-Carrasco [1], Tone Aspevik [2], Katerina Kousoulaki [2], Francisco J. Barba [1,*] and María-José Ruiz [1]

[1] Department of Preventive Medicine and Public Health, Food Science, Toxicology and Forensic Medicine, Faculty of Pharmacy, University of Valencia, 46100 Burjassot, Valencia, Spain; mercedes.taroncher@uv.es (M.T.); yelko.rodriguez@uv.es (Y.R.-C.); M.jose.ruiz@uv.es (M.-J.R.)

[2] Department of Nutrition and Feed Technology, Nofima AS, 5141 Bergen, Norway; tone.aspevik@Nofima.no (T.A.); katerina.Kousoulaki@Nofima.no (K.K.)

* Correspondence: francisco.barba@uv.es; Tel.: +34-9-6354-4972

Abstract: Many studies report the potent antioxidant capacity for fish protein hydrolysates, including radical scavenging activity and inhibition ability on lipid peroxidation (LPO). In this study, the in vitro cytotoxicity of protein hydrolysates from different salmon, mackerel, and herring side streams fractions was evaluated in the concentration range from 1 to 1:32 dilution, using cloned human colon adenocarcinoma cells TC7 (Caco-2/TC7) by MTT and PT assays. The protein hydrolysates' antioxidant capacity and oxidative stress effects were evaluated by LPO and reactive oxygen species (ROS) generation, respectively. The antioxidant capacity for pure and bioavailable hydrolysate fraction was also evaluated and compared. Additionally, mycotoxin levels were determined in the fish protein hydrolysates, and their cytoprotective effect against T-2 toxin was evaluated. Both hydrolysates and their bioavailable fraction induced similar cell viability rates. The highest cytoprotective effect was obtained for the salmon viscera protein hydrolysate (HSV), which increased the cell viability by 51.2%. ROS accumulation induced by H_2O_2 and LPO was suppressed by all pure hydrolysates. The cytoprotective effect of hydrolysates was observed against T-2. Moreover, the different fish fraction protein hydrolysates contain variable nutrients and unique bioactive peptide composition showing variable bioactivity, which could be a useful tool in developing dietary supplements with different target functional properties.

Keywords: fish hydrolysates; cytotoxicity; oxidative stress; cytoprotective effect; bioavailability

Citation: Taroncher, M.; Rodríguez-Carrasco, Y.; Aspevik, T.; Kousoulaki, K.; Barba, F.J.; Ruiz, M.-J. Cytoprotective Effects of Fish Protein Hydrolysates against H_2O_2-Induced Oxidative Stress and Mycotoxins in Caco-2/TC7 Cells. *Antioxidants* **2021**, *10*, 975. https://doi.org/10.3390/antiox10060975

Academic Editors: Michał Swieca and Monica Rosa Loizzo

Received: 12 May 2021
Accepted: 16 June 2021
Published: 18 June 2021

1. Introduction

Synthetic antioxidants are commonly used to preserve food products, including butylated hydroxytoluene (BHT), tert-butyl hydroquinone (TBHQ) and butylated hydroxyanisole (BHA), but their use is limited due to the potential toxic effects in humans [1–3]. Therefore, there is an increasing consumer demand for natural antioxidants in order to delay food deterioration caused by oxidation, as well as to alleviate the oxidative stress caused by mitochondrial generation of reactive oxygen species (ROS) [4–7], proteins and peptides being of great interest [8–10].

Protein hydrolysates and peptides exhibit multiple physiological functionalities such as antimicrobial, antioxidant, antihypertensive, and cholesterol-lowering effects and immunomodulatory activities [11–13]. Moreover, in some recent studies, the ability of fish protein hydrolysates to suppress DSS-Induced colitis by modulating intestinal inflammation in mice, as well as to suppresses diabetes and modulates intestinal microbiome in a murine model of diet-induced obesity, has been observed [14,15].

Filleting fish generates large amounts of protein-rich side stream materials, such as heads, backbones, viscera, and trimmings, with potential use for human consumption when

Toxicology 501 (2024) 153712

Contents lists available at ScienceDirect

Toxicology

journal homepage: www.elsevier.com/locate/toxicol

Assessment of the genotoxic and mutagenic effects induced by T-2 mycotoxin in HepG2 cells

Mercedes Taroncher [a], Cristina Fuentes [a,b,*], Yelko Rodríguez-Carrasco [a], María-José Ruiz [a]

[a] Research Group in Alternative Methods for Determining Toxic Effects and Risk Assessment of Contaminants and Mixtures (RiskTox). Laboratory of Food Chemistry and Toxicology, Faculty of Pharmacy and Food Sciences, Universitat de València, Av. Vicent Andrés Estellés s/n, Burjassot, 46100 València, Spain
[b] Department of Food Technology, Universitat Politècnica de València, Camino de Vera s/n, 46022 València, Spain

ARTICLE INFO

Handling Editor: Dr. Mathieu Vinken

Keywords:
HepG2 cells
Micronucleus
Comet assay
Mutagenicity
Genotoxicity

ABSTRACT

The T-2 toxin is a mycotoxin produced by molds belonging to *Fusarium*. Among the *Fusarium* mycotoxins, trichothecenes are frequently reported in food and feed, being the T-2 toxin (T-2) the mycotoxin which possesses the highest toxicity. According to EFSA, T-2 is found in various cereal grains used in food and feed products, mainly in oats, and it has a high environmental impact due to its mechanisms of toxicity. However, recent information on its genotoxic and mutagenic effects is lacking. This work aimed to evaluate the genotoxic and mutagenic potential of T-2 in vitro. For this purpose, HepG2 cells were exposed to 15, 30, and 60 nM T-2 for 24 h, then the DNA damage was evaluated by the micronucleus and the comet assays. In addition, point mutation analysis was performed by the bacterial reverse mutation test using 0.15–60 nM of T-2 concentrations. The results showed chromosomal damage at 60 nM T-2 since significantly more MN appeared at this concentration than in the control samples. Regarding the comet assay, DNA double helix breaks appeared at all concentrations tested and, in a concentration-dependent manner. However, no mutagenic effects were observed at any of the concentrations tested for the *Salmonella typhimurium* (*S. Typhimurium*) strains TA98, TA100, TA1535, TA1537, or the *Escherichia coli (E. Coli)* WP2 strain in the absence or presence of a metabolic activation system. Therefore, these results showed that T-2 mycotoxin produced genotoxic effects by MN and comet assay, while no mutagenicity was observed. However, further research simulating different metabolic activation pathways and the combined exposure of this mycotoxin with other mutagenic chemicals that could be present in the diet is necessary to discard the mutagenic potential of T-2 fully. These results highlight the carcinogenic potential and danger associated with T-2 exposure and should be considered to prevent associated food risks for the human population.

1. Introduction

The increasing incidence of cancer is a public health concern and may be attributed to changes in the environment and lifestyle exposures, including diet (Lécuyer et al., 2022). During the last decades, several investigations have been carried out to study how the whole diet may cause point mutations, thus, increasing the risk of developing cancer (Agudo et al., 2018; Shivappa et al., 2014; Van Woudenbergh et al., 2013). Several dietary factors such as nitrites, coffee, tea, processed meat, or alcohol have been associated with cancer risk (IARC, 2023). Although the role of these factors in carcinogenesis is not clearly understood, evidence suggests that chronic diseases and carcinogenesis are promoted by inflammatory processes (Lécuyer et al., 2022; Mantovani et al., 2008). Some food contaminants, such as mycotoxins, to which we could be exposed through our daily diet have been classified by the International Agency for Research on Cancer (IARC) as carcinogenic.

Abbreviations: 2-AA, 2-aminoanthracene; 9-AC, 9-aminoacridine; 2-NF, 2-Nitrofluorene; AFB1, Aflatoxin B1; BEA, Beauvericin; CECT, Spanish Collection of Culture Strains; CRL, control; DMEM, Dulbecco's Modified Eagle's Medium; DMSO, Dimethyl sulfoxide; DON, Deoxynivalenol; EDTA, Ethylenediaminetetraacetic acid; EFSA, European Food Safety Agency; EMA, nucleic acid dye A; EtOH, ethanol; IARC, International Agency for Research on Cancer; IC_{50}, Mean inhibition concentration; LMA, Low Melting point Agarose; MeOH, methanol; MN, micronucleus; MTT, methylthiazol tetrazolium salt; NADP, Nicotinamide Adenine Dinucleotide Phosphate; NaN_3, sodium azide; NBCS, Newborn Calf Serum; OECD, Organisation for Economic Cooperation and Development; OTA, Ochratoxin A; PBS, Phosphate Buffered Saline; PI, Propidium Iodide; RNase A, ribonuclease A; S9, metabolic activation system fraction; SEM, Standard Error of the Mean; Trp, tryptophan.

* Corresponding author at: Department of Food Technology, Universitat Politècnica de València, Camino de Vera s/n, 46022 València, Spain.
E-mail address: crifuelp@upvnet.upv.es (C. Fuentes).

https://doi.org/10.1016/j.tox.2023.153712
Received 23 October 2023; Received in revised form 14 December 2023; Accepted 15 December 2023
Available online 19 December 2023

cells

MDPI

Article

Using Microfluidic Hepatic Spheroid Cultures to Assess Liver Toxicity of T-2 Mycotoxin

Mercedes Taroncher [1,2], Alan M. Gonzalez-Suarez [1], Kihak Gwon [1], Samuel Romero [3], Angel D. Reyes-Figueroa [3,4], Yelko Rodríguez-Carrasco [2], María-José Ruiz [2], Gulnaz Stybayeva [1], Alexander Revzin [1,*] and Jose M. de Hoyos-Vega [1,*]

1 Department of Physiology and Biomedical Engineering, Mayo Clinic, Rochester, MN 55901, USA; mercedes.taroncher@uv.es (M.T.); gonzalezsuarez.alan@mayo.edu (A.M.G.-S.); stybayeva.gulnaz@mayo.edu (G.S.)
2 Research Group in Alternative Methods for Determining Toxics Effects and Risk Assessment of Contaminants and Mixtures (RiskTox), Laboratory of Food Chemistry and Toxicology, Faculty of Pharmacy, University of Valencia, Av. Vicent Andrés Estellés s/n, 46100 Valencia, Spain; yelko.rodriguez@uv.es (Y.R.-C.); m.jose.ruiz@uv.es (M.-J.R.)
3 Centro de Investigación en Matemáticas Unidad Monterrey, Apodaca 66628, NL, Mexico; angel.reyes@cimat.mx
4 Consejo Nacional de Humanidades, Ciencias y Tecnologías, Ciudad de Mexico 03940, Mexico
* Correspondence: revzin.alexander@mayo.edu (A.R.); dehoyos-vega.jose@mayo.edu (J.M.d.H.-V.)

Abstract: The *Fusarium* fungi is found in cereals and feedstuffs and may produce mycotoxins, which are secondary metabolites, such as the T-2 toxin (T-2). In this work, we explored the hepatotoxicity of T-2 using microfluidic 3D hepatic cultures. The objectives were: (i) exploring the benefits of microfluidic 3D cultures compared to conventional 3D cultures available commercially (Aggrewell plates), (ii) establishing 3D co-cultures of hepatic cells (HepG2) and stellate cells (LX2) and assessing T-2 exposure in this model, (iii) characterizing the induction of metabolizing enzymes, and (iv) evaluating inflammatory markers upon T-2 exposure in microfluidic hepatic cultures. Our results demonstrated that, in comparison to commercial (large-volume) 3D cultures, spheroids formed faster and were more functional in microfluidic devices. The viability and hepatic function decreased with increasing T-2 concentrations in both monoculture and co-cultures. The RT-PCR analysis revealed that exposure to T-2 upregulates the expression of multiple Phase I and Phase II hepatic enzymes. In addition, several pro- and anti-inflammatory proteins were increased in co-cultures after exposure to T-2.

Keywords: T-2; HepG2 cells; microfluidic devices; spheroids; cytotoxicity

Citation: Taroncher, M.; Gonzalez-Suarez, A.M.; Gwon, K.; Romero, S.; Reyes-Figueroa, A.D.; Rodríguez-Carrasco, Y.; Ruiz, M.-J.; Stybayeva, G.; Revzin, A.; de Hoyos-Vega, J.M. Using Microfluidic Hepatic Spheroid Cultures to Assess Liver Toxicity of T-2 Mycotoxin. *Cells* **2024**, *13*, 900. https://doi.org/10.3390/cells13110900

Academic Editor: Alexander E. Kalyuzhny

Received: 27 April 2024
Revised: 10 May 2024
Accepted: 22 May 2024
Published: 24 May 2024

1. Introduction

Mycotoxins are secondary metabolites of low molecular weight produced by filamentous fungi that are often present in food. They may cause adverse effects in the short and long term for consumers depending on the concentrations present in aliments and the exposure time [1]. Mycotoxins are present worldwide in cereals—notably wheat, barley, maize, oats, rye, and rice—and animal feed [2]. Mycotoxins represent one of the most important categories of natural toxins relative to human and animal health. Mycotoxins produce significant economic losses around the world because the value of the crop is reduced when high levels of mycotoxins are detected in the grain [2]. According to the Food and Agriculture Organization (FAO), more than 300 different mycotoxins have been identified in food commodities and animal feed [3]. Among these, the T-2 toxin (T-2) is found in several cereals, predominantly oats [1]. The T-2 is a type A trichothecene (tetracyclic sesquiterpenoid compound characterized by a 12,13-epoxy group and a functional carbonyl group at C-8) produced by several species of *Fusarium* fungi [4]. Some of the described mechanisms of action of this toxin are inhibition of protein synthesis, activation